DIRECTORIO DE PROFESORES DEL CURSO SISMOLOGIA Y SISMICIDAD
1980.

1.- M. en I. Abraham Díaz Rodríguez
Jefe de la Sección de Mecánica de Suelos
División de Estudios de Posgrado
Facultad de Ingeniería
UNAM
550 52 15 Ext. 4490

2.- Dr. Luis Esteva Maraboto
Investigador
Instituto de Ingeniería
UNAM
548 97 94

3.- Dr. Octavio A. Rascón Chávez (Coordinador)
Investigador
Instituto de Ingeniería
UNAM
548 54 95

4.- Dr. Shri Krishna Singh
Profesor e Investigador
División de Estudios de Posgrado
Facultad de Ingeniería
UNAM

5.- Dr. Francisco Sánchez Sesma
Investigador
Instituto de Ingeniería
Cubículo B-106
UNAM
550 52 15 Ext. 3635

'edcs.

VI CURSO INTERNACIONAL DE INGENIERIA SISMICA SISMOLOGIA Y SISMICIDAD 1980

Fecha	Tema	Hora	Profesor
Julio 8	Origen de los temblores. Instrumentos para registrar temblores. Magnitud e intensidad. Sismicidad de la tierra. Predicción de Temblores.	17 a 20 h	Dr. Shri Krishna Singh
Julio 10	Propagación de ondas en un medio seminfinito o en uno estratificado.	17 a 18:30 h	Dr. Francisco Sánchez Sesma
Julio 10	Efectos sísmicos en suelos granulares .	18:30 a 20 h	M. en I. Abraham Díaz Rodríguez
" 15	" " " " "	17 a 18:30 h	
Julio 15	Influencia de las condiciones locales. Tipos de temblores.	18:30 a 20 h	Dr. Luis Esteva Maraboto
Julio 17	Nociones de teoría de probabilidades. El proceso estocástico de Poisson. Relaciones entre magnitud, intensidad y distancia focal. Propiedades estadísticas de los temblores.	17 a 20 h	Dr. Octavio A. Rascón Chávez .
Julio 22 y 24	Sismicidad local y regional Regionalización sísmica. Sismicidad de la República Mexicana. Microregionalización sísmica. Elaboración de espectros de diseño.	17 a 20 h c/día	Dr. Luis Esteva Maraboto

'edcs.

EVALUACION DEL PERSONAL DOCENTE

CURSO: VI CURSO INTERNACIONAL DE INGENIERIA SISMICA. SISMOLOGIA Y SISMICIDAD

FECHA: Del 8 de julio al 24, 1980.

CONFERENCISTA	DOMINIO DEL TEMA	EFICIENCIA EN EL USO DE AYUDAS AUDIOVISUALES	MANTENIMIENTO DEL INTERES. (COMUNICACION CON LOS ASISTENTES, AMENIDAD, FACILIDAD DE EXPRESION).	PUNTUALIDAD	
1. Dr. Shri Krishna Singh					
2. Dr. Francisco Sánchez Sesma					
3. M. en I. Abraham Díaz Rodríguez					
4. Dr. Luis Esteva Maraboto					
5. Dr. Octavio A. Rascón Chávez.					
6.					
7.					
8.					
9.					
ESCALA DE EVALUACION: 1 a 10					

EVALUACION DE LA ENSEÑANZA

SU EVALUACION SINCERA NOS AYUDARA A MEJORAR LOS PROGRAMAS POSTERIORES QUE DISEÑAREMOS PARA USTED.

TEMA	ORGANIZACION Y DESARROLLO DEL TEMA	GRADO DE PROFUNDIDAD LOGRADO EN EL TEMA	GRADO DE ACTUALIZACION LOGRADO EN EL TEMA	UTILIDAD PRACTICA DEL TEMA	
Origen de los temblores. Instrumentos para registrar temblores. Magnitud e					
Propagación de ondas en un medio semin finito o en uno estratificado.					
Efectos sísmicos en suelos granulares.					
Influencia de las condiciones locales. Tipos de temblores.					
Nociones de teoría de probabilidades. El proceso estocástico de Poisson.					
Sismicidad local y regional. Regionalización sísmica. Sismicidad de la Rép.					

ESCALA DE EVALUACION: 1 a 10

EVALUACION DEL CURSO

	CONCEPTO	EVALUACION
1.	APLICACION INMEDIATA DE LOS CONCEPTOS EXPUESTOS	
2.	CLARIDAD CON QUE SE EXPUSIERON LOS TEMAS	
3.	GRADO DE ACTUALIZACION LOGRADO CON EL CURSO	
4.	CUMPLIMIENTO DE LOS OBJETIVOS DEL CURSO	
5.	CONTINUIDAD EN LOS TEMAS DEL CURSO	
6.	CALIDAD DE LAS NOTAS DEL CURSO	
7.	GRADO DE MOTIVACION LOGRADO EN EL CURSO	

ESCALA DE EVALUACION DE 1 A 10

1. ¿Qué le pareció el ambiente en la División de Educación Continua?

MUY AGRADABLE	AGRADABLE	DESAGRADABLE

2. Medio de comunicación por el que se enteró del curso:

PERIODICO EXCELSIOR ANUNCIO TITULADO DI VISION DE EDUCACIÓN CONTINUA	PERIODICO NOVEDADES ANUNCIO TITULADO DI VISION DE EDUCACIÓN CONTINUA	FOLLETO DEL CURSO

CARTEL MENSUAL	RADIO UNIVERSIDAD	COMUNICACION CARTA, TELEFONO, VERBAL, ETC.

REVISTAS TECNICAS	FOLLETO ANUAL	CARTELERA UNAM "LOS UNIVERSITARIOS HOY"	GACETA UNAM

3. Medio de transporte utilizado para venir al Palacio de Minería:

AUTOMOVIL PARTICULAR	METRO	OTRO MEDIO

4. ¿Qué cambios haría usted en el programa para tratar de perfeccionar el curso?

_____

_____

_____

5. ¿Recomendaría el curso a otras personas?

SI	NO

6. ¿Qué cursos le gustaría que ofreciera la División de Educación Continua?

7. La coordinación académica fue:

EXCELENTE	BUENA	REGULAR	MALA

8. Si está interesado en tomar algún curso intensivo ¿Cuál es el horario más conveniente para usted?

LUNES A VIERNES DE 9 A 13 H. Y DE 14 A 18 H. (CON COMIDAS)	LUNES A VIERNES DE 17 A 21 H.	LUNES, MIERCOLES Y VIERNES DE 18 A 21 H.	MARTES Y JUEVES DE 18 A 21 H.

VIERNES DE 17 A 21 H. SABADOS DE 9 A 14 H.	VIERNES DE 17 A 21 H. SABADOS DE 9 A 13 Y DE 14 a 18 H.	O T R O

9. ¿Qué servicios adicionales desearía que tuviese la División de Educación Continua, para los asistentes?

10. Otras sugerencias:

VI CURSO INTERNACIONAL DE INGENIERIA SISMICA

SISMOLOGIA Y SISMICIDAD

EARTHQUAKES

S. KRISHNA SINGH

JULIO, 1980

Contents

References

A. Continental Drift and Plate Tectonics

H. Takeuchi, S. Uyeda, and H. Kanamori, 1967, Debate about the Earth, Freeman, Cooper & Company.

A. Cox, 1973, Plate Tectonics and Geomagnetic Reversals, W.H. Freeman Company.

X. Le Pichon, J. Francheteau, and J. Bonnin, 1973, Plate Tectonics, Elsevier.

B. Seismology

C. F. Richter, 1958, Elementary Seismology, W.H. Freeman Co.

Bruce. A. Bolt, 1978, Earthquake, A Primer, W.H. Freeman Co.

K.E. Bullen, 1959, An Introduction to the Theory of Seismology, Cambridge University Press

W. M. Ewing, W. S. Jardetzky, and F. Press; 1957, Elastic Waves in Layered Earth

M. Båth, 1967, Mathematical Aspects of Seismology, Elsevier.

K. Aki and P. Richards, Quantitative Seismology, Vol. I & II, W.H. Freeman, 1980

C. Structure of the Earth

H. Jeffreys, 1959, The Earth, Cambridge University Press

B. Gutenberg, 1959, Physics of the Earths Interior, Academic Press.

F. D. Stacey, 1969, Physics of the Earth, John Wiley & Sons

D. Prediction of Earthquakes

T. Rikitake, 1976, , Earthquake Prediction, Elsevier

C. Lomnitz and S.K. Singh (1976), Earthquakes and Earthquake Prediction, in C. Lomnitz and E. Rosenblueth (Editors), "Seismic Risk and Engineering Decisions", Elsevier

F. Press, 1975, Earthquake Prediction, Scientific American.

E. Attenuation

L. Knopoff, 1964, "Q", Revs. Geophys, vol. 2, 625.

F. Near-Field Ground Motion

J. N. Brune, 1976, The Physics of Earthquake Strong Motion, in C. Lomnitz and E. Rosenblueth (Editors), "Seismic Risk and Engineering Decisions", Elsevier.

Continental Drift, Sea Floor Spreading and Plate Tectonics

Continental drift proposed by Wegener in about 1910 was not accepted by geophysicists till the early 1960s. That all the continents were once (about 200 million years ago) together in a land mass, which Wegener called Pangea, and that they drifted to occupy their present positions, appeared physically not possible. The overwhelming evidence of geophysical data in 1960s, however, clearly showed that Wegener's hypothesis was essentially correct. A review of the subject is given in the (enclosed) reprint by Dietz and Holden. The following reprints by Dewey on Plate Tectonics and by James on the Evolution of the Andes would show the reader how the concept of plate tectonics has evolved and how it explains much of the geological and geophysical data.

SCIENTIFIC AMERICAN OFFPRINTS

2

THE BREAKUP OF PANGAEA

by Robert S. Dietz and John C. Holden

SCIENTIFIC AMERICAN
OCTOBER 1970
VOL. 223, NO. 4 PP. 30-41

PUBLISHED BY W. H. FREEMAN AND COMPANY 660 MARKET STREET, SAN FRANCISCO, CALIFORNIA 94104

THE BREAKUP OF PANGAEA

Pangaea is the single land mass that is believed to have given rise to the present continents. Its outline has now been plotted and its further disruption has been projected into the future

by Robert S. Dietz and John C. Holden

The history of science is replete with outrageous hypotheses. They are mostly forgotten, as best they should be, but from time to time one of them turns out to be true. So it was with the concept that the earth is a sphere spinning in space, supported by nothing at all. Now it also seems to be with the theory of continental drift, which in its extreme form holds that all the continents were once joined in a single great land mass. Named Pangaea, this universal continent was somehow disrupted, and its fragments—the continents of today—eventually drifted to their present locations.

Over the past three years geologists and geophysicists have been forced to abandon the old dogma that the crust of the earth is essentially fixed and to accept the new heresy that it is quite mobile. The notion that continents can drift thousands of kilometers in a few hundred million years is now generally accepted. Geology therefore finds itself in much the same position that astronomy was in at the time of Copernicus and Galileo. Textbooks are being rewritten to embrace the new mobilistic viewpoint.

Although the theory of continental drift has triumphed, many of its details remain uncertain. Advocates of drift are challenged to say exactly how the present continents fitted together to form Pangaea, or alternatively to reconstruct the two later supercontinents Laurasia and Gondwana, which some theorists prefer to a single all-embracing land mass. The original concept of Pangaea ("all lands") was proposed in the 1920's by Alfred Wegener. Most attempts to improve on his reconstruction have been rather generalized sketches showing how the continents might have been joined. A few workers have made jigsaw fits with considerable care but without taking advantage of the latest concepts in geotectonics. Recently British theorists have presented detailed reconstructions showing how land masses were juxtaposed before the opening of either the Atlantic or the Indian Ocean, but their solutions show only the relative motions of the masses involved.

In this article we present a reconstruction of Pangaea in which the continents are assembled with cartographic precision. For the first time Pangaea is positioned on the globe in absolute coordinates. This reconstruction is accompanied by four maps that show the breakup and subsequent dispersion of the continents by the end of the four major geologic periods covering the past 180 million years: the Triassic, the Jurassic, the Cretaceous and the Cenozoic.

The guiding rationale for our reconstruction is the drift mechanism associated with plate tectonics and sea-floor spreading [*see illustration on page 4*]. According to this concept the earth has a strong lithosphere, or outer shell of rock, about 100 kilometers thick. Presumably in response to forces generated in the asthenosphere, the weak upper mantle of rock underlying the lithosphere, the shell was broken up into a number of separate plates. There are now some 10 major plates, plus numerous additional subplates. The continents resting on these plates were rafted across the surface of the globe.

The mechanism of plate movement is not yet clear. The plates may be pushed, carried by convection cells in the mantle, driven by gravitational forces or pulled. We prefer a model based on pulling; we suspect that plates are colder and heavier at our boundary than elsewhere and they dive down into the earth's mantle along "subduction" zones. These zones usually show themselves as deep trenches, which are disposed principally around the periphery of the Pacific. As a result a tear, or rift, widens along the opposite boundary of the plate; this rift is filled by a solid flow of viscous mantle rock and by dikes of molten tholeiitic basalt (a differentiated partial melt of the mantle). Because the mantle rock and its basaltic derivative are both heavier than the granitoid rock of the continents they assume a level about four kilometers below sea level. Consequently such a pulled-apart region always becomes new ocean floor. As two adjacent plates continue to pull apart, basaltic dikes continue to pour into the suboceanic rift, which remains midway between the two plates. This highly symmetrical process, which creates new ocean basins or continuously repaves old ocean floors, is termed sea-floor spreading. The rate of spreading, measured from the mid-ocean rift to either plate, is from one centimeter per year (10 kilometers per million years) to several times that figure. This is remarkably rapid by geological standards, being many times faster than mountains are elevated by tectonism or leveled by erosion. For example, the North American plate is moving westward the length of one's body in a lifetime.

The discovery of a mid-ocean ridge system some 40,000 kilometers long, winding through all the ocean basins, was an important prelude to the sea-floor-spreading hypothesis. It was soon recognized that the ridge has a fossa, or axial depression, into which dikes of basalt are continuously being injected. This linear depression in the ridge marks the location of the rift. The term "mid-ocean," although appropriate for the part of the ridge system in the Atlantic

SUBCONTINENT OF INDIA, originally attached to what is now Antarctica, made the longest migration of all the drifting land masses: approximately 9,000 kilometers in 200 million years. This picture, taken at an altitude of 650 kilometers from *Gemini XI* in September, 1966, shows all of the subcontinent. The Himalayan mountains, 3,700 kilometers away, are just visible on the horizon.

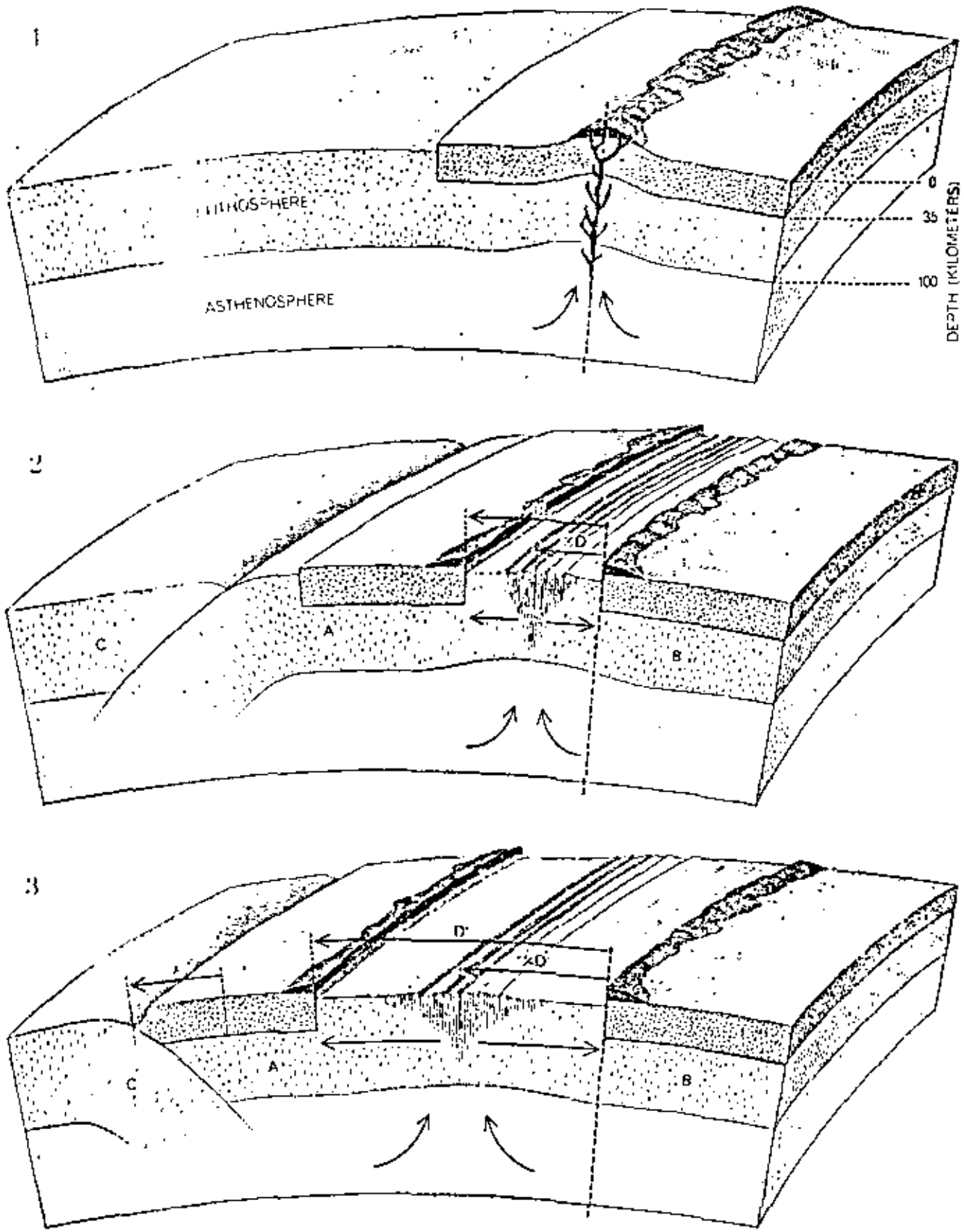

THEORY OF PLATE TECTONICS provides a mechanism for continental drift. The process begins (*1*) when a spreading rift develops under a continent (*color*) that is resting on a single crustal plate. Molten basalt from the asthenosphere spills out. The second simultaneous requirement for continental drift is the formation of a zone of subduction, or trench, into which oceanic crust of the new moving plate (*A*) is pulled and "consumed" (*2*). As the new continent carried by plate *A* is rafted to the left, a new ocean basin is created between the two land masses. In the third stage (*3*) the continent on plate *A* encounters and overrides the trench for some distance (*A'*) and eventually reverses, or flips, its direction from west-dipping to east-dipping. Because the continent on plate *B* is here arbitrarily fixed, the mid-ocean rift migrates to the left, remaining in the center of the new ocean basin, whose width is *D'*.

and the Indian Ocean, is a misnomer for the ridge in the Pacific. The Atlantic and the Indian Ocean are rift oceans, formed where continents were once split apart; therefore it is natural for the axis of spreading, marked by the ridge system, to remain in the center of these two oceans. The Pacific, on the other hand, is not a rift ocean; it is clearly the ancestral ocean, and it is becoming smaller as new ocean basins grow. Although the Pacific also has a ridge, it runs north-south well to the east of the ocean's center.

In reality the crustal motions are considerably more complex than the ones we have just outlined. The trenches and rifts apparently migrate, and the opposing plates are also subject to displacements produced by internal shears. The "megashears," the large zones of slippage along plate boundaries, also seem able to accommodate minor amounts of crustal extension or compression. Few of the plates are "ideal" in the sense of being rectilinear, of having a rift matched by an opposing trench and of having these two antithetical zones connected by a megashear. The Antarctic plate, for example, has no trench at all. Perhaps this anomaly is partly explained by the fact that a sphere cannot be covered with rectangles.

We can visualize the continents as being passively rafted over the surface of the globe as embedded plateaus of sialic (granite-like) rock resting on the even larger and thicker crustal plates. The continents have generally maintained their size and shape since the breakup of Pangaea. There have been some accretions with the formation of mountain belts, but these have been mostly confined to the sides of continents facing the Pacific. The sides of continents facing rift oceans (the Atlantic and the Indian Ocean) show little change; hence they can be fitted together almost as neatly as pieces of a jigsaw puzzle.

In contrast, the crustal plates can change in size or shape either by the addition of new ocean floor along the rifts or by the resorption of oceanic crust in trenches. Thus it has been possible for the North American and South American plates moving toward the Pacific to grow larger at first and then smaller as they passed over the great circle of the earth and now converge toward the central Pacific. An even more tortured history is reflected in the complex evolution of the Caribbean Sea region, caught as a "gore" between the North American and South Ameri-

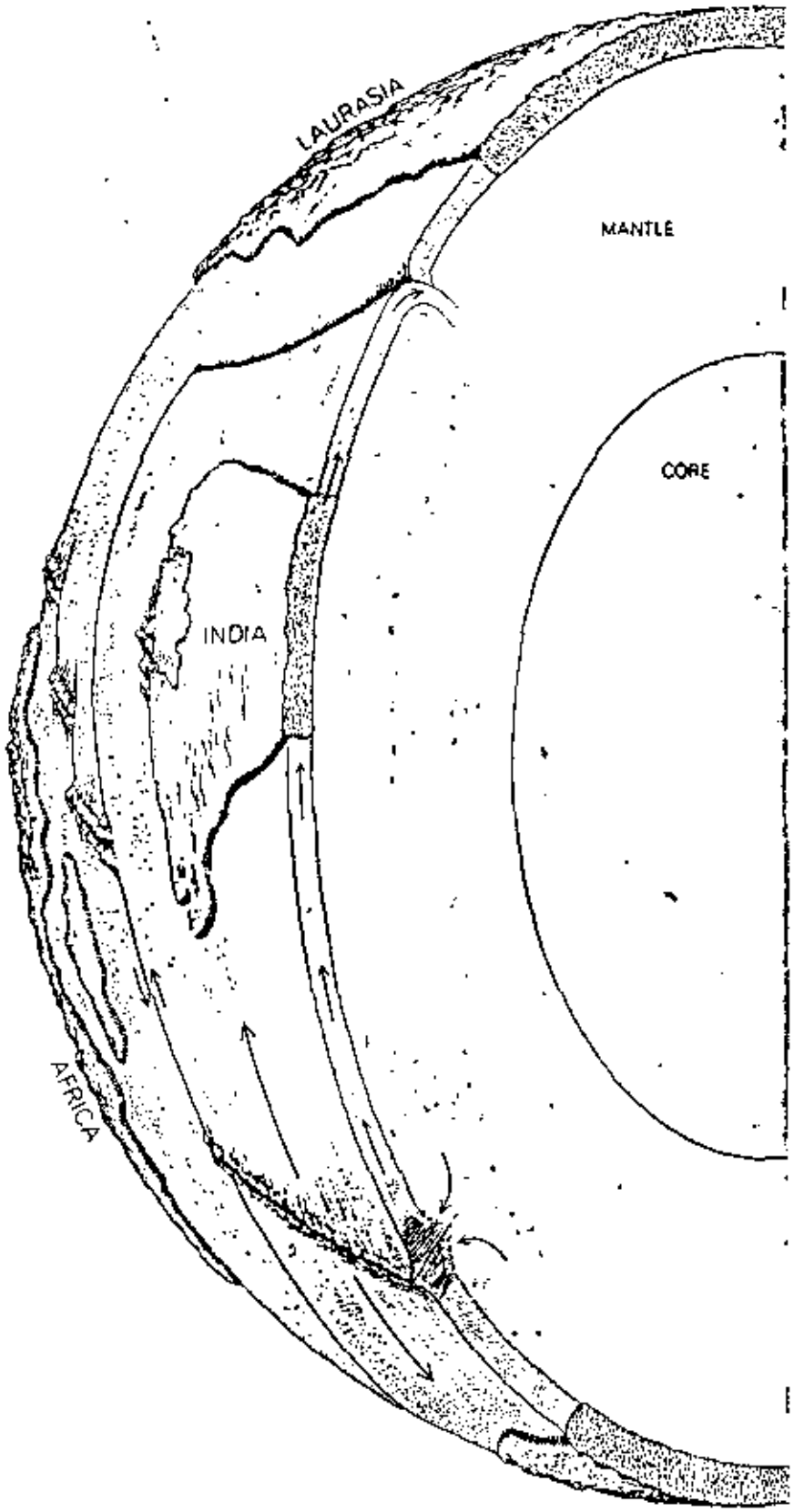

NORTHWARD DRIFT OF INDIA exemplifies how far a land mass can be carried when tectonic conditions are favorable. The plate carrying the Indian land mass is nearly a perfect rectangle, which was sliced away from Antarctica within the primitive universal continent of Pangaea. The plate that rafted India then migrated northward toward and subducted into the Tethyan trench, which ran east-west near the Equator. The plate evidently glided freely along parallel "megashears" on its eastern and western boundaries without interacting with the other crustal plates of the world. India finally collided with and underthrust the southeast margin of Asia, creating the Himalayas, which are thus two plates thick.

can plates, and the Scotia Sea region, similarly trapped between the South American and Antarctica plates. As we shall see, in at least one case two plates evidently collided, producing a mid-continent mountain range: the Himalayas.

In making our reconstruction of Pangaea we selected for fitting not the present coastlines of continents but the contour lines where the continental slope reaches a depth of 1,000 fathoms, or about 2,000 meters [*see illustration below*]. This isobath was selected because it is approximately halfway down the continental slope and thus marks roughly half the height of the vertical walls created when the continents first rifted. On the assumption that these walls subsequently slumped to a condition of stable repose, the 1,000-fathom isobath closely delineates the location of the original break.

For joining the two sides of the Atlantic we have followed, with some modification, the reconstruction proposed by Sir Edward Bullard, J. E. Everett and A. G. Smith of the University of Cambridge. For closing the Indian Ocean we have used the best-fit computer solutions of Walter P. Sproll, a colleague of ours in the Marine Geology and Geophysics Laboratory of the Environmental Science Services Administration. His studies provide precise fits between Australia and Antarctica and between Antarctica and Africa. The three continents together constitute most of Gondwana. Presumably India was also part of the Gondwana complex, but where it was attached remains unclear. Fortunately the pattern of fracture zones in the ocean floor provides crude but useful dead-reckoning tracks showing how the continents drifted. Using such tracks, we have placed the west coast of India against Antarctica rather than against western Australia, the fit that is often proposed.

Another difficult fit is presented by the bulge of Africa and the bight of North America. The areas of mismatch, particularly that caused by the Florida-Bahamas platform, are sufficiently large for one to reasonably argue that Africa and North America were never joined. On this assumption instead of Pangaea one obtains two unconnected supercontinents as the antecedent land masses: Laurasia in the Northern Hemisphere and Gondwana in the Southern. This version of the continental-drift theory has important adherents.

We nevertheless prefer the Pangaea reconstruction; in our view the areas of mismatch can reasonably be regarded as modifications that arose after Africa and North America began drifting apart. We regard the Florida-Bahamas platform as a sedimentary infilling of a small ocean basin that appeared when Africa

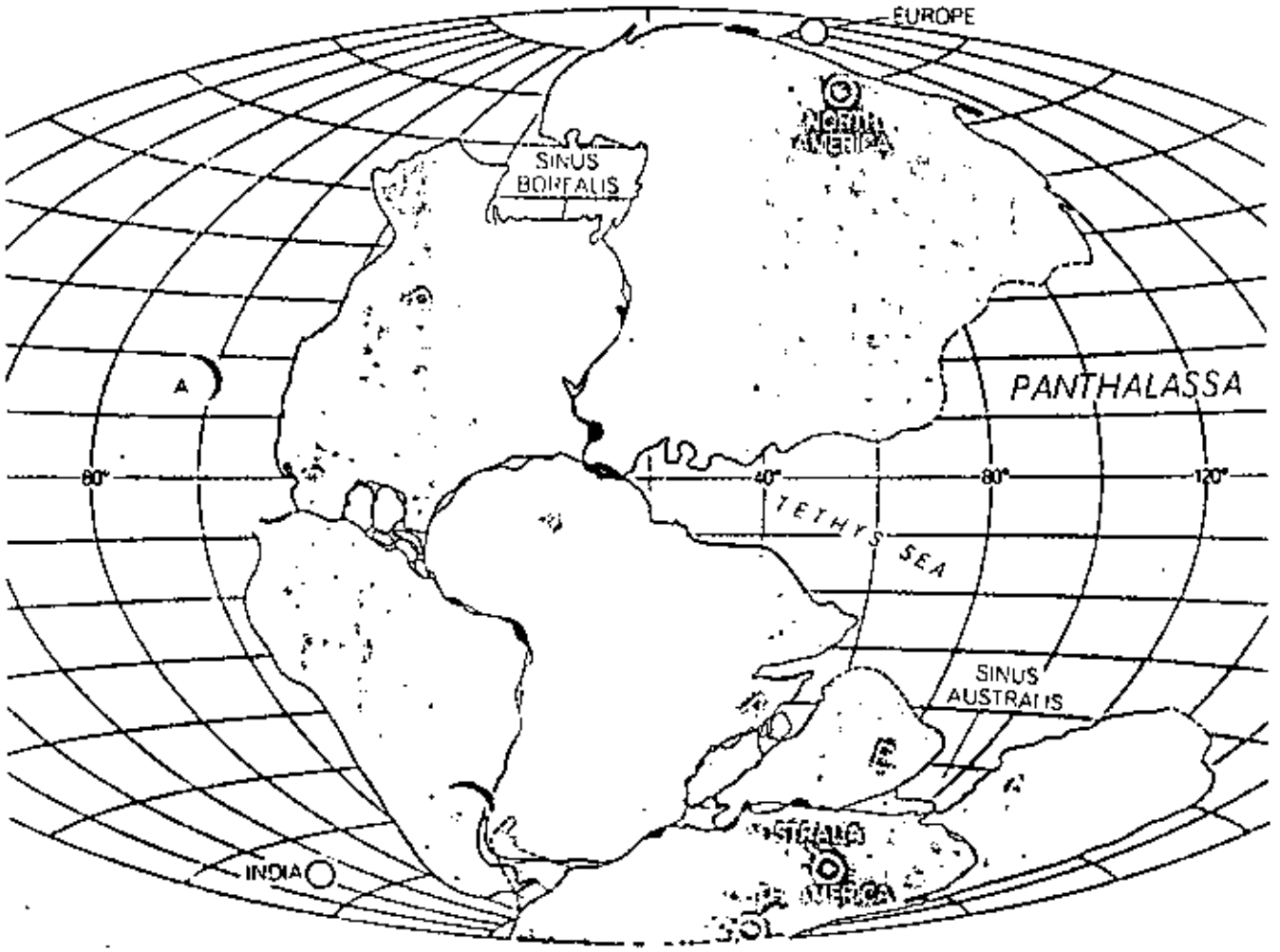

UNIVERSAL LAND MASS PANGAEA may have looked like this 200 million years ago. Panthalassa was the ancestral Pacific Ocean. The Tethys Sea (the ancestral Mediterranean) formed a large bay separating Africa and Eurasia. The relative positions of the continents, except for India, are based on best fits made by computer, using the 1,000-fathom isobath to define continental boundaries. When the continents are arranged as shown, the relative locations of the magnetic poles in Permian times are displaced to the positions marked by circles. Ideally these positions should cluster near the geographic poles. The hatched crescents (*A*) and (*B*) serve as modern geographic reference points; they represent the Antilles arc in the West Indies and Scotia arc in the extreme South Atlantic.

and North America first began to pull apart. Without this assumption the platform unaccountably overlaps a large portion of the bulge of Africa [*see illustration on page 12*].

According to our reconstruction, Pangaea was a land mass of irregular outline surrounded by the universal ocean of Panthalassa: the ancestral Pacific. The fit between North America and Africa provides the principal connection between the future block of northern continents and the future group of southern ones. On the east the Tethys Sea, a large triangular bight, separated Eurasia from Africa; the present Mediterranean Sea is a remnant of the Tethys. Other major indentations in the outline of Pangaea (adapting terminology from the moon) can be named Sinus Borealis, the ancestral Arctic Ocean, and Sinus Australis, a southern bay off the Tethys separating India from Australia. Our fully closed reconstruction of the Central American region is problematical. An alternate possibility is that the Gulf of Mexico is the remnant of an oceanic arm extending into the Americas from Panthalassa—a Sinus Occidentalis.

When measured down to the 1,000-fathom isobath, the total area of Pangaea was 200,000 square kilometers, or 40 percent of the earth's surface—equal to the area of the present continents measured to the same isobath. When the future continents were still part of Pangaea, they were generally to the south and east of their present location, so that the amount of land in the two hemispheres was almost equally balanced. (Today two-thirds of all the land lies north of the Equator.) The Y-shaped junction connecting North America, South America and Africa was located in the South Atlantic not far from the present position of Ascension Island. If New York had been in existence at the time, it would have been on the Equator and at longitude 10 degrees east (rather than 74 degrees west). Spain would also have been on the Equator, but it would have been near its present longitude. Japan would have been in the Arctic, well north of its position today. India and Australia would have bordered the Antarctic, far to the south of where they are now.

The great event that broke up Pangaea and set its fragments adrift evidently began no more than 200 million years ago, or in the last few percent of geologic time. There may have been—indeed, there probably was—"predrift drift" that assembled Pangaea from two or more smaller land masses. The evidence is still scanty, however, and does not bear directly on this discussion.

We take the immediate prelude to the breakup of Pangaea to be the first large outpourings of basaltic rock along the continental margins being es-

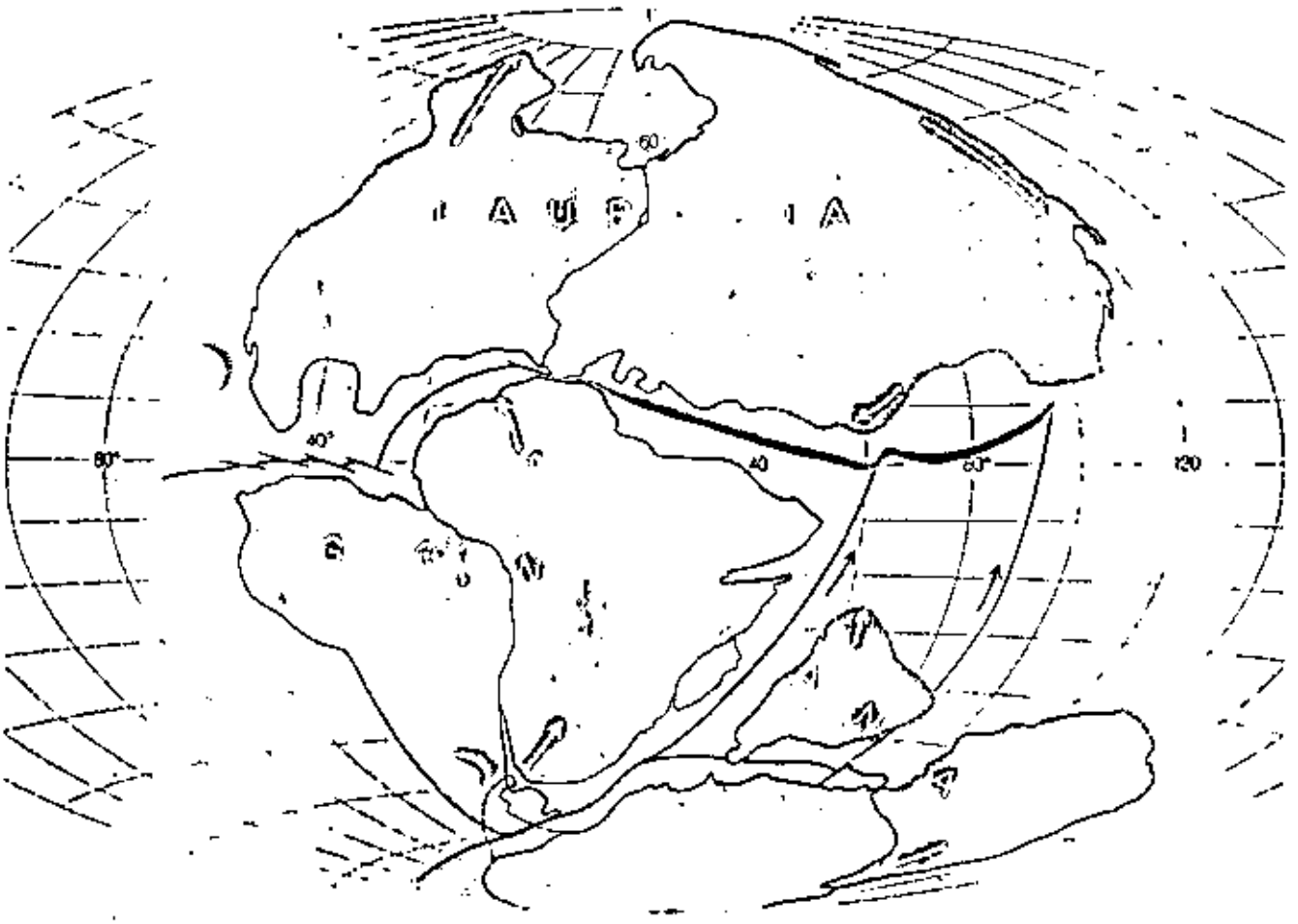

AFTER 20 MILLION YEARS OF DRIFT, at the end of the Triassic period 180 million years ago, the northern group of continents, known as Laurasia, has split away from the southern group, known as Gondwana. The latter has started to break up: India has been set free by a Y-shaped rift (*heavy line in color*), which has also begun to isolate the Africa South America land mass from Antarctica-Australia. The Tethyan trench (*hatched lines in black*), a zone of crustal uptake, runs from Gibraltar to the general area of Borneo. Black lines and black arrows denote megashears, zones of slippage along plate boundaries. The white arrows indicate the vector motions of the continents since drift began. Oceanic areas tinted in color represent new ocean floor created by sea-floor spreading.

tablished by rifting. The Triassic Newark series of basaltic flows along the east coast of the U.S. is a good example. Measurements of radioactivity indicate that the most ancient of these rocks are about 200 million years old, yielding a date that coincides with the middle of the Triassic period. As we interpret the evidence, two extensive rifts were initiated in Pangaea about 200 million years ago, which resulted in the opening of the Atlantic and the Indian Ocean by the end of the Triassic period 150 million years ago [*see illustration on preceding page*]. The northern rift split Pangaea from east to west along a line slightly to the north of the Equator and created Laurasia, composed of North America and Eurasia. The Laurasian land mass evidently rotated clockwise as a single plate around a pole of rotation that is now in Spain, creating a western "Mediterranean" that ultimately became part of the Gulf of Mexico and the Caribbean Sea. The southern rift split South America and Africa as a single land mass away from the remainder of Gondwana, consisting of Antarctica, Australia and India. Soon afterward (if not simultaneously) India was severed from Antarctica by a smaller rift to begin its rapid drift northward.

During the Jurassic period, from 150 to 135 million years ago, the direction of drift established by the Triassic rifts continued, further opening up the Atlantic and the Indian Ocean [*see illustration below*]. As North America drifted to the northwest, the Atlantic became more than 1,000 kilometers wide and probably remained fully connected to the Pacific. The east coast of the present U.S. ran almost east and west at a latitude of about 25 degrees north, so that coral reefs were able to grow all along the edge of the Atlantic continental shelf to the present Grand Banks, off Nova Scotia.

During the 45-million-year Jurassic period the Atlantic rift extended northward, blocking out the Labrador coastline and possibly initiating the opening up of the Labrador Sea between North America and Greenland. The interaction between the African and Eurasian plates forced the region of Spain to rotate counterclockwise 35 degrees, opening up the Bay of Biscay. The Tethys Sea, forerunner of the Mediterranean, continued to close at its eastern end. The Tethys was not only a zone of crustal subduction, or trench, but also a zone of shear along which Eurasia slid westward with respect to Africa. The compression associated with the Tethys trench raised bordering mountains composed of deep-water sediments.

At the close of the Jurassic an incipient rift began splitting South America away from Africa, entering from the south and working only as far north as where Nigeria is today. The tectonic situation first resembled the one now found in the rift zone along the backbone of high Africa (the region from Ethiopia to Tanzania) and then gradually opened farther to form a body of water resembling the Red Sea of today.

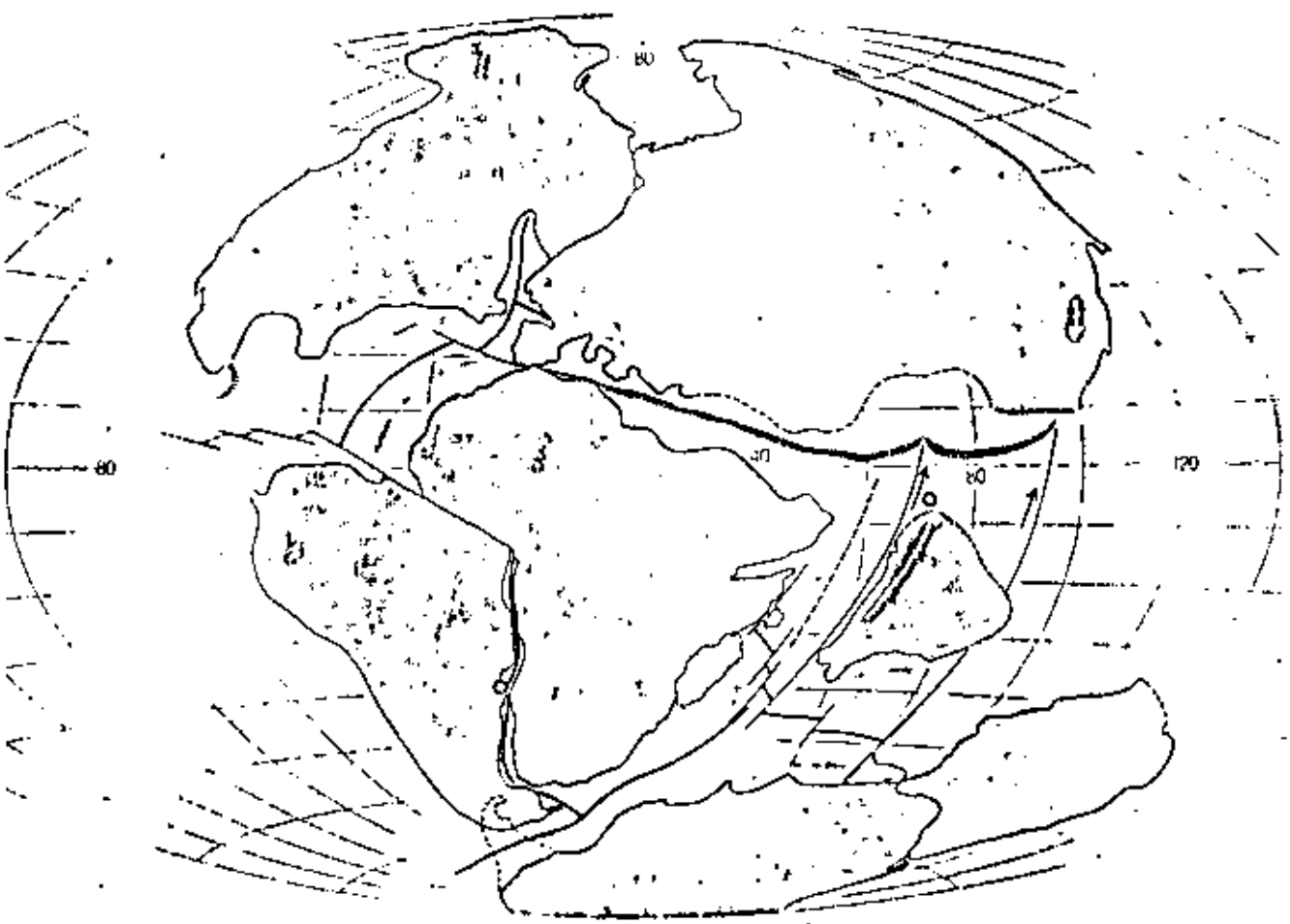

AFTER 65 MILLION YEARS OF DRIFT, at the end of the Jurassic period 135 million years ago, the North Atlantic and the Indian Ocean have opened considerably. The birth of the South Atlantic has been initiated by a rift. The rotation of the Eurasian land mass has begun to close the eastern end of the Tethys Sea. The Indian plate is about to pass over a thermal center (*colored dot*) that will soon pour out basalt to form the Deccan plateau. Later the hot spot will create the Chagos-Laccadive ridge in the Indian Ocean. Similarly, in the South Atlantic the Walvis thermal center (*colored dot*) will create the Walvis and Rio Grande "thread ridges."

At first freshwater sediments created thick deposits in pockets opened by faults; these sediments were overlain by deposits of salt.

By the end of the Cretaceous period, some 70 million years later (and 65 million years ago), the rupture of South America and Africa was complete, and the South Atlantic had widened rapidly to at least 3,000 kilometers [*see illustration below*]. Meanwhile the rift in the North Atlantic had switched from the west side of Greenland to the east side, blocking out its eastern margin (without, however, penetrating to the Arctic Ocean). Africa had drifted northward about 10 degrees and continued its counterclockwise rotation as the Eurasian plate rotated slowly clockwise. These two opposed motions nearly closed the eastern end of the Tethys Sea. The slow westward rotation of Antarctica continued. All the continents were now blocked out except for the remaining connection between Greenland and northern Europe and between Australia and Antarctica.

Although it is not shown on our maps, an extensive north-south trench system must have existed in the ancient Pacific to consume by subduction the rapid westward drift of the two plates carrying North and South America. North America presumably encountered this trench in the late Jurassic and early Cretaceous, with the result that the Franciscan fold belt, the predecessor of the California Coast Ranges, was accreted to the western margin of the continent. It appears that the trench was eventually overridden and "stifled" by North America's continued westward drift. Such trenches have the capacity to resorb ocean crust but not the lighter granitic crust of continents.

At about the same time, or soon afterward, South America first encountered the Andean trench and began to displace the trench westward, without ever overriding it. The early Andean fold belt resulted from this encounter. It seems likely that the trench originally dipped toward the west but was flipped over to its present eastward dip.

In the Cenozoic period (from 65 million years ago to the present) the continents drifted to the positions we observe today. The mid-Atlantic rift propagated into the Arctic basin, finally detaching Greenland from Europe [*see top illustration on next two pages*]. There were three other major developments during the Cretaceous: (1) the two Americas were rejoined by the Isthmus of Panama, created by volcanism and the arching upward of the earth's mantle, (2) the Indian land mass completed its remarkable journey northward by colliding with the underbelly of Asia and (3) Australia was rifted away from Antarctica and drifted northward to its present position.

In the collision of India with Asia the northern margin of the Indian plate was subducted below the Asiatic plate, creating the Himalayas. On India's passage to the north early in the Cenozoic its western margin crossed a fixed source of

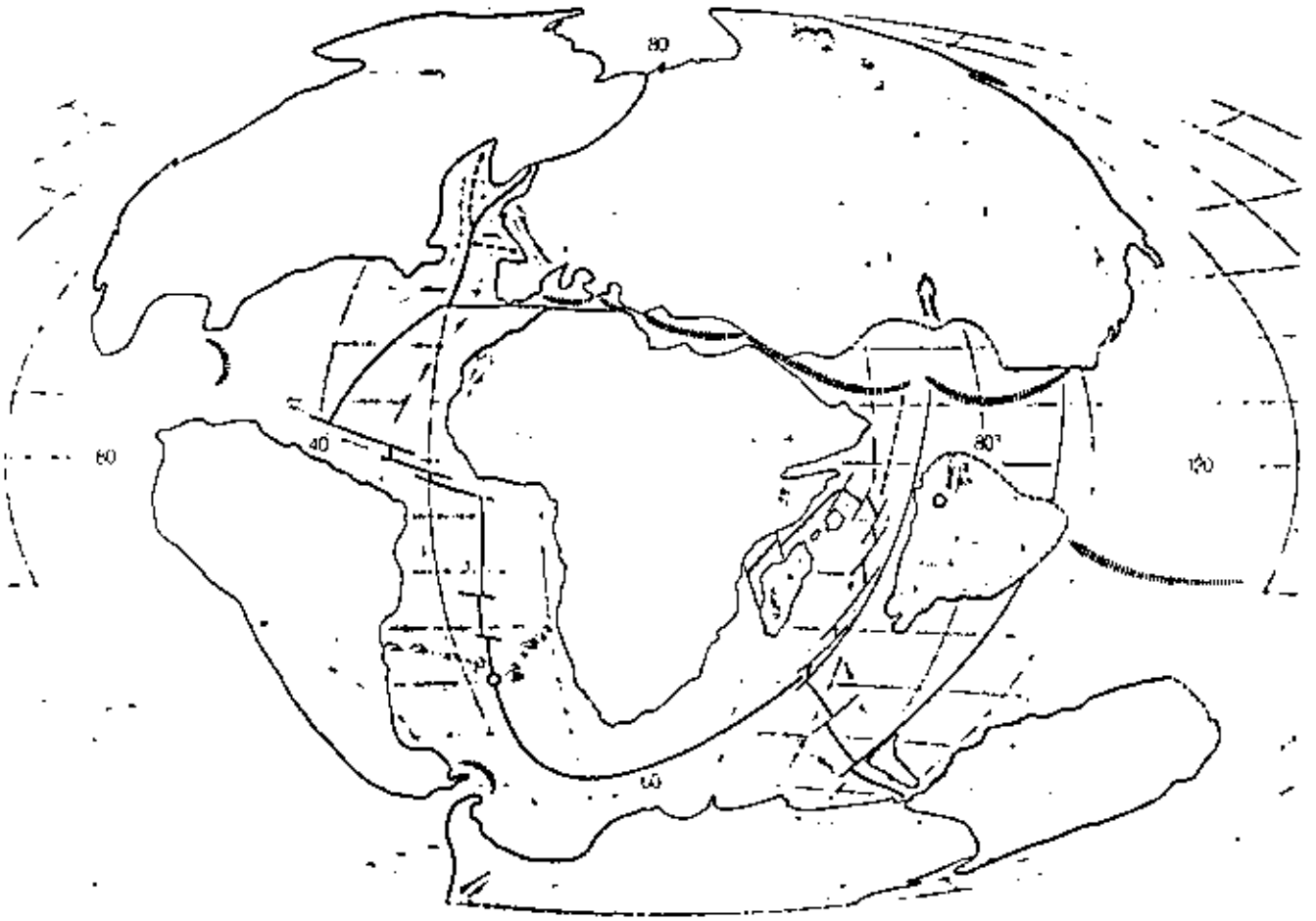

AFTER 135 MILLION YEARS OF DRIFT, 65 million years ago at the end of the Cretaceous period, the South Atlantic has widened into a major ocean. A new rift has carved Madagascar away from Africa. The rift in the North Atlantic has switched from the west side to the east side of Greenland. The Mediterranean Sea is clearly recognizable. Australia still remains attached to Antarctica. An extensive north-south trench (not shown) must also have existed in the Pacific to absorb the westward drift of the North American and South American plates. Note that the central meridian in all these reconstructions is 20 degrees east of the Greenwich meredian.

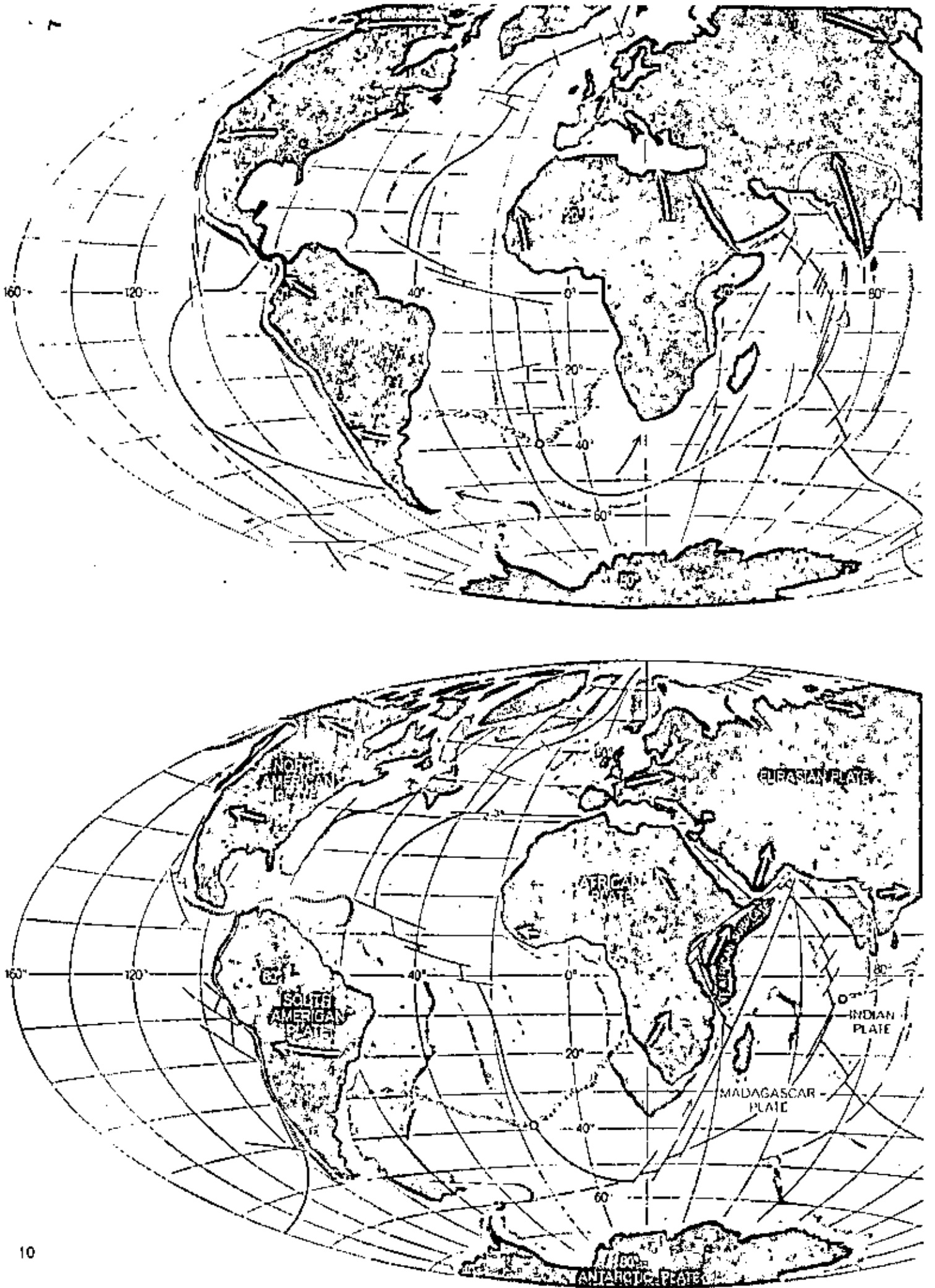
NORTH AMERICAN PLATE
EURASIAN PLATE
AFRICAN PLATE
SOUTH AMERICAN PLATE
INDIAN PLATE
MADAGASCAR PLATE
ANTARCTIC PLATE
160°
120°
40°
0°
20°
40°
60°
80°
60°

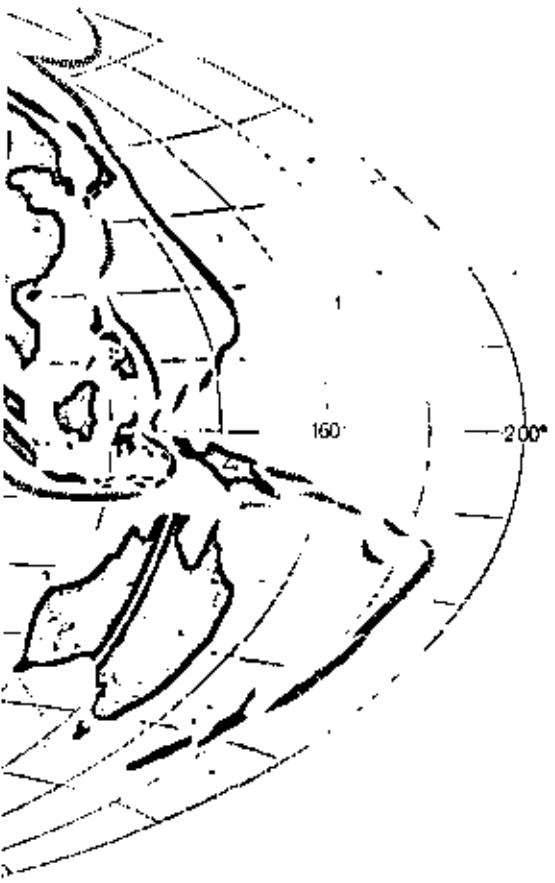

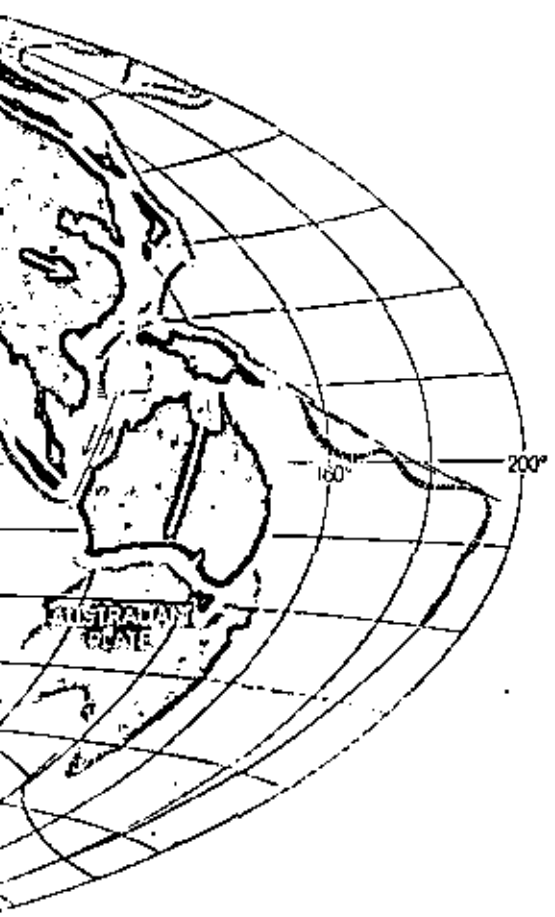

WORLD AS IT LOOKS TODAY was produced in the past 65 million years in the Cenozoic period. Nearly half of the ocean floor was created in this geologically brief period, as shown by the areas stippled in color. India completed its flight northward by colliding with Asia and a rift has separated Australia from Antarctica. The North Atlantic rift finally entered the Arctic Ocean, fissioning Laurasia. The widening gap between South America and Africa is closely traced by the thread ridges produced by the Walvis thermal center. The Antilles and Scotia arcs now occupy their proper positions with respect to neighboring land masses.

basaltic magma rising from the earth's upper mantle near the Equator. Molten rock erupted through the crust and poured onto the Indian subcontinent, laying down the basalts of the Deccan plateau. Even after India had left the hot spot behind, magma continued to stream out on the ocean floor, producing the Chagos-Laccadive ridge, which became covered with coral as it subsided into the Indian Ocean. Finally, a branch of the Indian Ocean rift split Arabia away from Africa, creating the Gulf of Aden and the Red Sea, and a spur of this rift meandered west and south into Africa.

Less pronounced changes during the Cenozoic period included the partial closing of the Caribbean region and the continued widening of the South Atlantic as new ocean crust was emplaced by sea-floor spreading. As the Atlantic continued to open in the far north the northwestward movement of the Eurasian land mass was halted and reversed, simultaneously reversing its sense of slippage with respect to Africa. The new direction of shear has been strongly impressed on the tectonic character of the Mediterranean and the Near East. The major north-south rift in the Indian Ocean largely ceased spreading and became instead a megashear that accommodated the counterclockwise and northward rotation of the African plate.

The reader will have observed that our maps of continental drift show more than relative positions and motions; the land masses, beginning with Pangaea itself, are assigned absolute geographic coordinates. Since this has not been attempted before we shall briefly describe how we arrived at our results. In the mobile world of plate tectonics one must assume that all parts of the crust are capable of moving and almost surely have moved.

After an extensive search for some absolute reference point, we finally concluded that the Walvis thermal center, or hot spot, might provide what we sought. In reaching this conclusion we accepted a hypothesis put forward by J. Tuzo Wilson of the University of Toronto. He had suggested that the Walvis ridge and the Rio Grande ridge in the South Atlantic are nematoths, or "thread ridges" of basalt, that had been poured onto the spreading ocean floor from a fixed lava orifice rising from a deep, stagnant region of the mantle. As new floor was carried past the orifice, lava would periodically pour out and form a small volcanic cone. By observing the location of succeeding cones as they merged into a ridge one can establish the absolute direction taken by the crust in that region. A study of the Walvis and Rio Grande ridges enabled us to establish not only the drift of the South American plate with respect to the African plate but also any motion the two plates may have had in some other direction [*see illustration on page 13*].

Unfortunately the Walvis hot spot did not exist earlier than about 140 million years ago, so that its usefulness as a fixed point does not go back earlier than the end of the Jurassic period. To trace crustal motions during the first 60 million years after the breakup of Pangaea one has to rely on dead reckoning. We have made the assumption that Antarctica has moved very little from its original location when it was part of Pan-

WORLD 50 MILLION YEARS FROM NOW may look something like this. The authors have extrapolated present-day plate movements to indicate how the continents will have drifted by the end of what they propose to call the Psychozoic era (the age of awareness). The Antarctic remains essentially fixed but may rotate slightly clockwise. The Atlantic (particularly the South Atlantic) and the Indian Ocean continue to grow at the expense of the Pacific. Australia drifts northward and begins rubbing against the Eurasian plate. The eastern portion of Africa is split off, while its northward drift closes the Bay of Biscay and virtually collapses the Mediterranean. New land area is created in the Caribbean by compressional uplift. Baja California and a sliver of California west of the San Andreas fault are severed from North America and begin drifting to the northwest. In about 10 million years Los Angeles will be abreast of San Francisco, still fixed to the mainland. In about 50 million years Los Angeles will start sliding into the Aleutian trench.

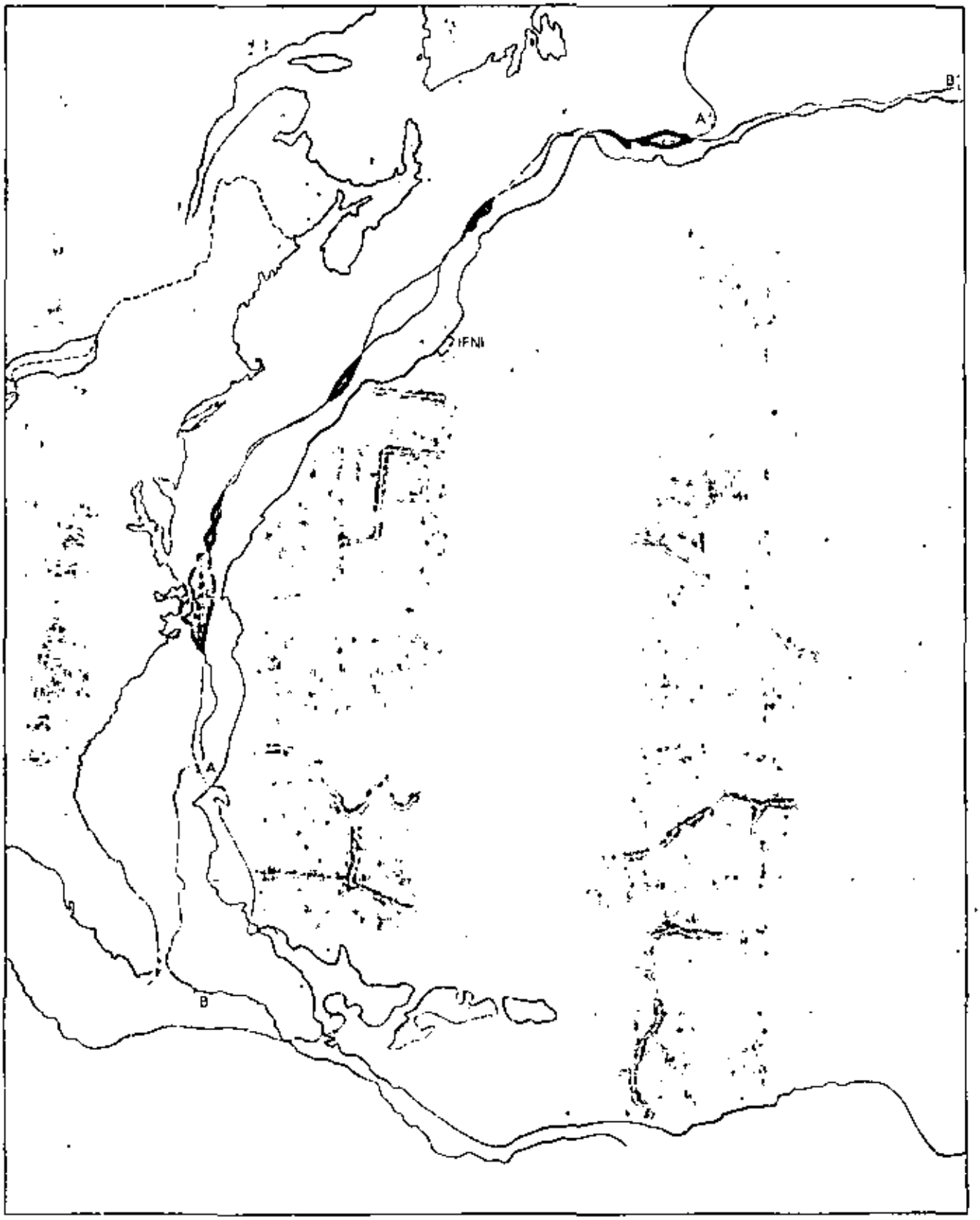

FIT OF AFRICA AGAINST NORTH AMERICA was made by the authors' colleague Walter P. Spruill with the aid of a computer. As in the reconstruction of Pangaea, it is assumed that each continent actually extends out into the ocean and halfway down the continental slope, where the ocean reaches a depth of 1,000 fathoms. The North American "coast" between *A* and *A'* was matched for best fit to the African "coast" between *B* and *B'*. White areas are gaps in the fit; black areas are overlaps. The overlap produced by the Bahamas platform, an enormous area half the size of Texas, is specially depicted in dark color. The authors propose that the platform represents an accumulation of sediments followed by coral growth after the two continents became separated. The largest gap in the proposed fit between the two continents is found off the Spanish enclave of Ifni. The Ifni gap may have been created when a small section of Africa split off and was translated 190 kilometers to the southwest, forming the eastern group of the Canary Islands.

gaea. This seems reasonable because the Antarctica plate is entirely surrounded by a system of rifts and megashears; there is no associated trench toward which the plate would tend to move away from its polar position.

Independent support for this assumption is obtained by plotting the position of the North and South poles before the dispersal of Pangaea. These positions are obtained by studying the direction of magnetization in rocks of the Permian period, as obtained by E. Irving of the Dominion Observatory in Canada and by other workers. We plotted the Permian pole positions with respect to each continent as it exists today and then rotated these pole positions as needed to assemble the continents into our version of Pangaea. By this method the pole positions should ideally cluster at one of the geographic poles. Actually there is some scatter, as can be seen in our reconstruction of Pangaea (*see illustration on page 6*), but all the positions do fall within either the Arctic Circle or the Antarctic Circle.

We can now summarize how the continents have moved in time and space. The two Americas have drifted a long way, generally westward. North America has drifted more than 8,000 kilometers west northwest; the tip of Florida once lay in the South Atlantic near the present position of Ascension Island. Moving toward the Tethyan trench system, India and Australia were carried far to the north. Africa rotated counterclockwise perhaps 20 degrees as the Eurasian land mass, similarly moving toward the Tethyan trench, rotated clockwise a roughly equal amount. India's remarkable flight is probably attributable to its being rafted on an "ideal" plate. Approximately rectangular, the Indian plate was sliced away from Pangaea by a rift along what is now India's east coast and then was free to move northward toward a major trench. This northward movement was facilitated by two parallel megashears.

Decades ago Wegener proposed that the drift of the continents was vectored by forces he termed *Westwanderung* (westward drift) and *Polarfluchtkraft* (flight from the poles). Although real, these forces are minuscule and not likely to be the underlying cause of drift. Our solution, however, does support Wegener's hypothesis of a westward flight, which, like the slip of the atmosphere, directly opposes the earth's rotation. We have also inferred a latitudinal drift, but from the South Pole only, or, paraphrasing Wegener's terminology, a *Sudpolarfluchtkraft*.

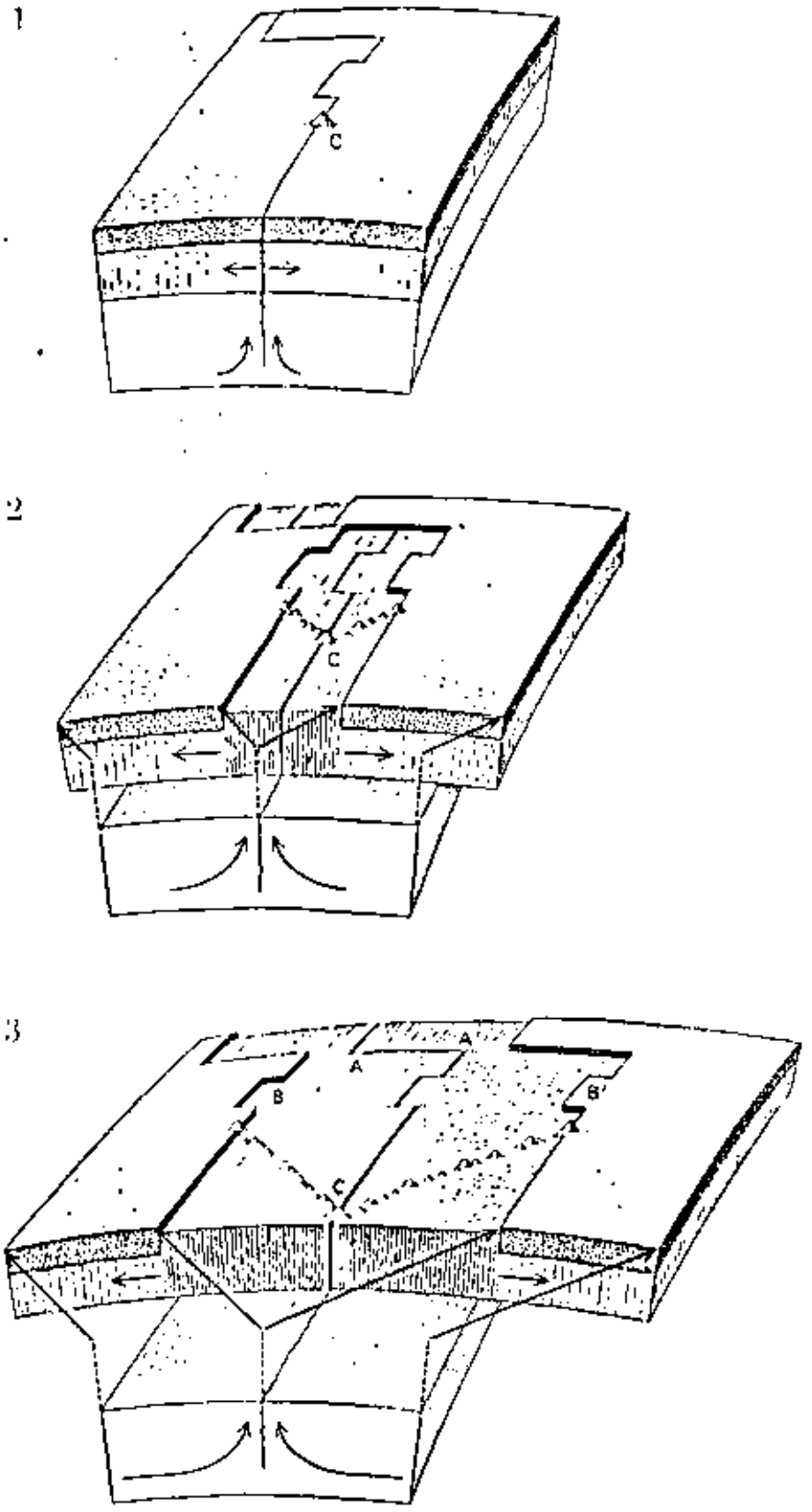

SEPARATION OF SOUTH AMERICAN AND AFRICAN PLATES can be traced in absolute geographic coordinates by observing the orientation of the thread ridges, a V-shaped stream of volcanoes, produced by the Walvis thermal center (*C*). The hot spot has evidently been pouring out magma from a source deep in the mantle for the past 140 million years. The three-part diagram illustrates a hypothesis first proposed by J. Tuzo Wilson of the University of Toronto. The thread ridges show that the South American and African plates have been not only drifting rapidly apart but also migrating northward. Features such as the strike of the ridge-ridge transform faults (*A–A'*) and matching indentations on opposing continents (*B–B'*) can do more than indicate the relative motion of two plates.

The Authors

ROBERT S. DIETZ and JOHN C. HOLDEN are marine geologists with the Environmental Science Services Administration, working at the Atlantic Oceanographic and Meteorological Laboratories in Miami. Dietz, who obtained his Ph.D. from the University of Illinois in 1941, has written extensively on geotectonics, geosynclines, continental drift (with the late Harry H. Hess of Princeton he was originator of the sea-floor-spreading concept that is now widely accepted as the underlying mechanism of continental drift), the morphology and structure of the ocean floor, the history of ocean basins, the evolution of continental shelves and slopes, marine mineral resources and astroblemes. Holden is completing work on his doctorate in micropaleontology at the University of California at Berkeley. "As a switch from the megathinking world of plate tectonics and continental drift," he writes, "I find solace in investigating the microcosmic world revealed by the microscope."

Bibliography

THE ORIGIN OF CONTINENTS AND OCEANS. Alfred Wegener. Methuen & Co. Ltd., 1924.

CONTINENT AND OCEAN BASIN EVOLUTION BY SPREADING OF THE SEA FLOOR. Robert S. Dietz in *Nature*, Vol. 190, No. 4779, pages 854–857; June 3, 1961.

HISTORY OF OCEAN BASINS. H. H. Hess in *Petrologic Studies: A Volume in Honor of A. F. Buddington*, edited by A. E. J. Engel, Harold L. James and B. F. Leonard. The Geological Society of America, 1962.

CONTINENTAL DRIFT. J. Tuzo Wilson in *Scientific American*, Vol. 208, No. 4, pages 86–100; April, 1963.

RISES, TRENCHES, GREAT FAULTS AND CRUSTAL BLOCKS. W. Jason Morgan in *Journal of Geophysical Research*, Vol. 73, No. 6, pages 1959–1982; March 15, 1968.

GEOTECTONIC EVOLUTION AND SUBSIDENCE OF BAHAMA PLATFORM. Robert S. Dietz, John C. Holden and Walter P. Sproll in *Geological Society of America Bulletin*, Vol. 81, No. 7, pages 1915–1927; July, 1970.

900
SCIENTIFIC AMERICAN OFFPRINTS

Knight 15

PLATE TECTONICS

by John F. Dewey

SCIENTIFIC AMERICAN
MAY 1972
VOL. 226, NO. 5 PP. 56-68

PUBLISHED BY W. H. FREEMAN AND COMPANY 660 MARKET STREET, SAN FRANCISCO, CALIFORNIA 94104

PLATE TECTONICS

The earth's surface is divided into a mosaic of rigid, shifting plates. As they move apart, slide past each other and converge, new crust is generated, continents drift and mountains are formed

by John F. Dewey

It has long been observed that mountains, volcanoes and earthquakes are not randomly distributed over the earth's surface but are found in distinct and usually narrow zones. To account for these evidences of instability in the earth's crust many hypotheses have been put forward. They have included such diverse notions as global expansion, global contraction, the effect of lunar tidal forces and wholesale uplift or foundering of large segments of the earth's crust. One other explanation—continental drift—was advanced from time to time but was unpalatable to most geophysicists because it seemed to violate what was known about the mechanical properties of the earth's crust. Nevertheless, continental drift seemed to explain geological similarities between continents thousands of miles apart. It also explained why some continental margins, for example those of South America and Africa, match each other so precisely.

Within the past 10 years continental drift has been placed on a firm foundation by the development of the concept of sea-floor spreading, originally proposed by the late Harry H. Hess of Princeton University. Sea-floor spreading involves the notion that the floor of the ocean is continuously being pulled apart along a narrow crack that is centered on a ridge that can be traced through the major ocean basins. Volcanic material (liquid basalt) rises from the earth's mantle to fill the crack and continuously create new oceanic crust.

The concept might have been difficult to confirm except for the fortunate fact that the polarity of the earth's magnetic field periodically reverses. It had been observed from magnetometer surveys that rocks of the ocean floor exhibit a zebra-stripe pattern in which the intensity of magnetization changes abruptly in linear ribbons parallel to the nearest oceanic ridge. In 1963 F. J. Vine and D. H. Matthews of the University of Cambridge proposed that the magnetic pattern was evidence of both sea-floor spreading and reversals of the earth's magnetic field. To many geologists the one seemed almost as improbable as the other. Vine and Matthews argued that as the basaltic liquid rose into the axial crack of the oceanic ridges and solidified it would become magnetized in the then prevailing direction of the earth's magnetic field. If new oceanic crust was continuously generated, as Vine and Matthews believed, one should find that each ridge axis is bordered symmetrically by pairs of parallel strips whose direction of magnetization is the same, that is, both normal or both antinormal. The hypothesis was strikingly confirmed in many traverses across oceanic ridges. Furthermore, a time scale of magnetic reversals has been developed showing that the rate of sea-floor spreading is between two and 18 centimeters per year.

It is now clear that virtually all of the present area of the oceans has been created by sea-floor spreading during the past 200 million years, or during the last 5 percent or so of the recorded geologic history of the earth. The creation of new surface area means either that the earth has expanded dramatically or that surface area is somewhere being destroyed at the same rate at which it is being created. There is good evidence that the earth has not expanded more than about 2 percent in the past 200 million years. Thus there must be, in general terms, a global conveyor-belt system or surface motion that links zones of surface creation and surface destruction.

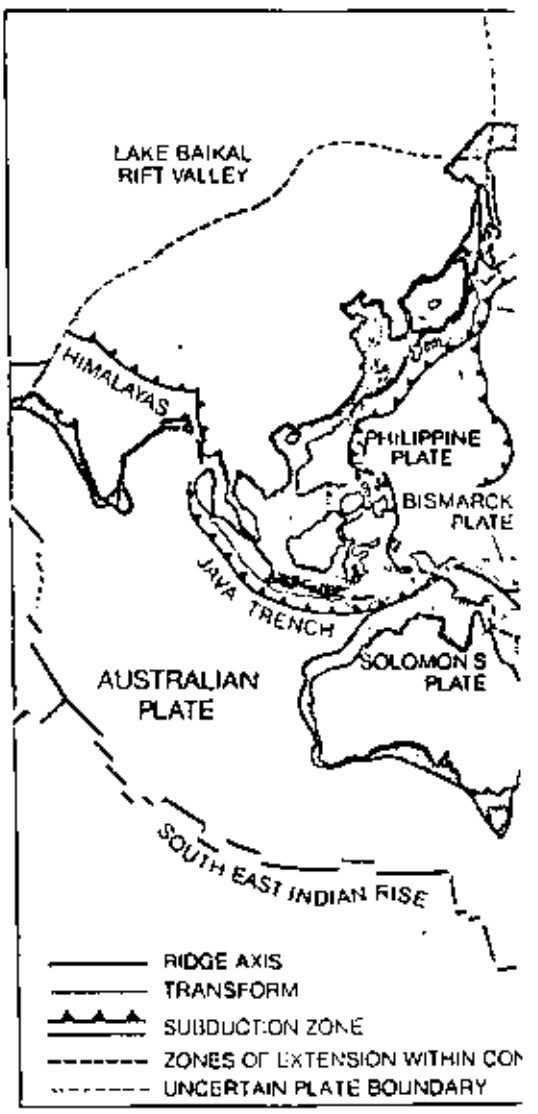

MOSAIC OF PLATES forms the earth's lithosphere, or outer shell. According to the recently developed theory of plate tectonics, the plates are not only rigid but also in constant relative motion. The boundaries of plates are of three types: ridge axes, where plates are diverging and new oceanic floor is generated; transforms, where plates slide past each other, and subduction zones, where plates converge and one plate dives under the leading edge of its neighbor. Triangles indicate the leading edge of a plate.

The concept of sea-floor spreading has now been joined to the earlier idea of continental drift in a single unifying theme called the theory of plate tectonics. The geometric part of the theory visualizes the lithosphere, or outer shell, of the earth as consisting of a number of rigid plates. The kinematic part of the theory holds that the plates are in constant relative motion: they can slide past each other, they can move apart on opposite sides of an oceanic ridge or they can converge, in which case one of the plates must be consumed. Let us now see how various instabilities in the earth's crust can be visualized in terms of plate tectonics.

Earthquakes

Most earthquakes occur in narrow zones that join to form a continuous network bounding regions that are seismically less active. The seismic network is associated with a variety of characteristic features such as rift valleys, oceanic ridges, mountain belts, volcanic chains and deep oceanic trenches [*see illustration below*]. The seismic areas mark the boundaries between plates, which are largely free of earthquakes. There appear to be four types of seismic zone, which can be distinguished by their characteristic morphology and geology.

The first type is represented by narrow zones of high surface heat flow and basaltic volcanic activity along the axes of mid-oceanic ridges where earthquakes are shallow (less than 70 kilometers deep). The axes of the ridges, of course, are the active sites of sea-floor spreading. In Iceland, where the Mid-Atlantic Ridge rises above sea level, the spreading rate has been measured at about two centimeters per year.

The second type of seismic zone is marked by shallow earthquakes in the absence of volcanoes. A good illustration is the region around the San Andreas fault in California and around the Anatolian fault in northern Turkey, along both of which large surface displacements parallel to the fault have been measured [see "The San Andreas Fault," by Don L. Anderson; SCIENTIFIC AMERICAN, November, 1971].

The third type of seismic zone is intimately related to deep oceanic trenches associated with volcanic island-arc systems, such as those around the Pacific Ocean. Earthquakes there can be shallow, intermediate (70 to 300 kilometers) or deep (300 to 700 kilometers), according to where they take place in the steeply plunging lithospheric plate that borders the trench. Thus the earthquake epicenters (the points on the surface above the initial break) define a geologic structure dipping down into the earth away from the trench. These inclined earthquake zones, called Benioff zones, underlie active volcanic chains and have a variety of complex shapes.

The fourth type of seismic zone is typified by the earthquake belt that extends from Burma to the Mediterranean Sea. It consists of a wide, diffuse continental zone within which generally shallow earthquakes are associated with high mountain ranges that clearly owe their existence to large compressive forces. Earthquakes of intermediate depth occur in some areas such as the Hindu Kush and Romania. Although deep-focus

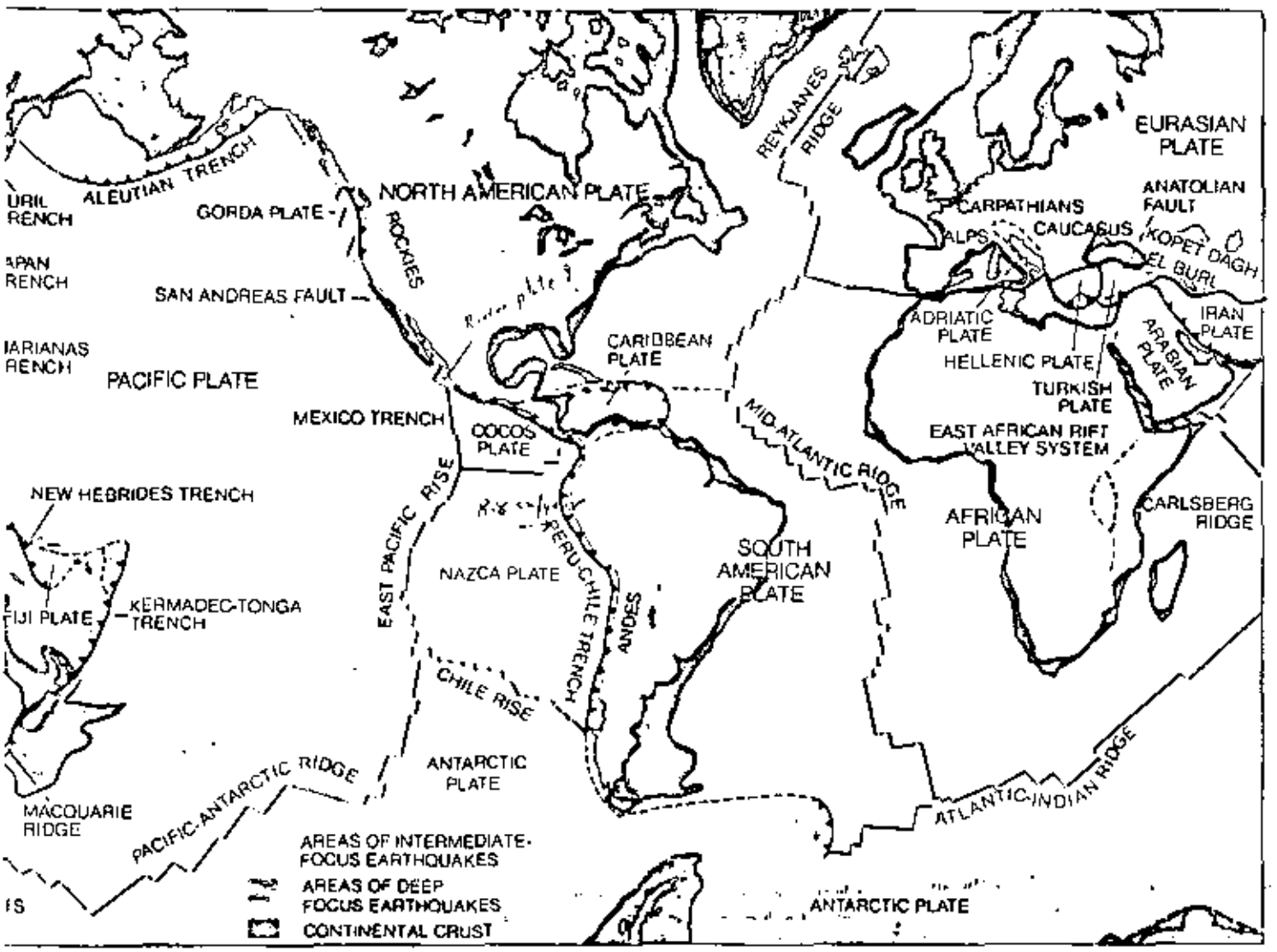

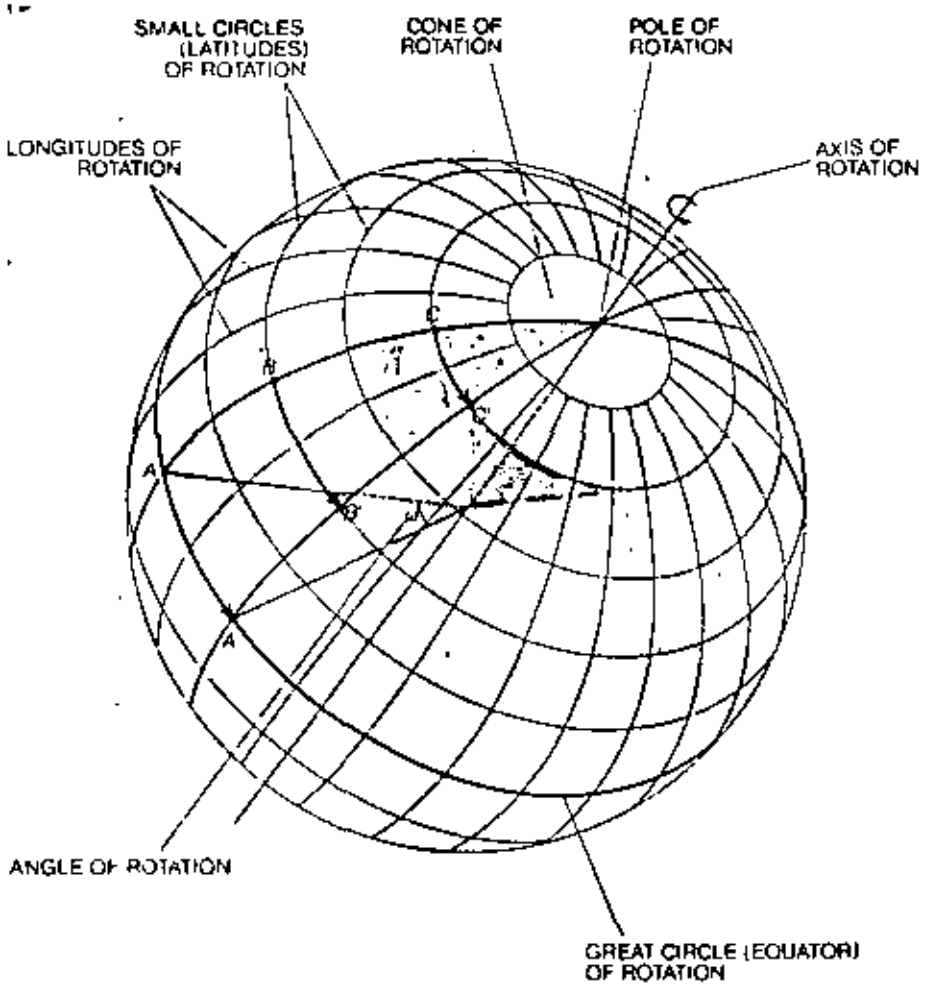

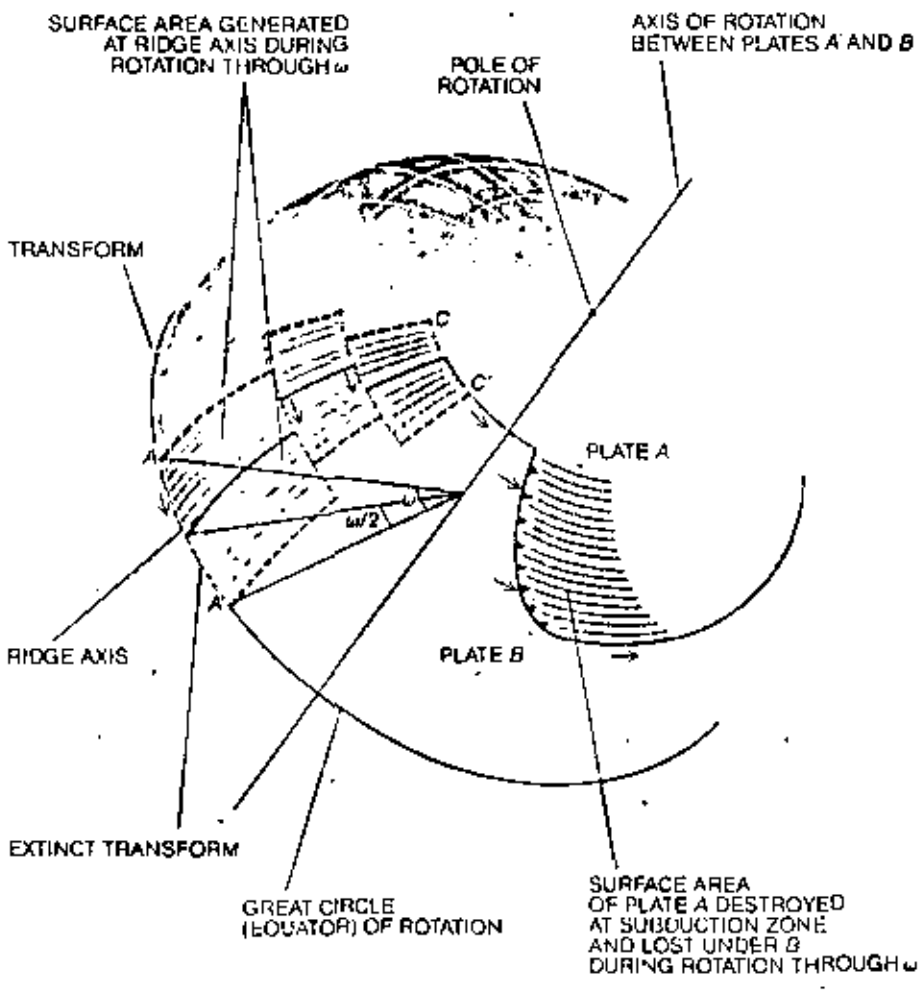

earthquakes are rare, they have been recorded in a few places, for example just north of Sicily under the Tyrrhenian volcanoes.

An earthquake results when stresses accumulate to the point that rocks in the earth's crust break. The breakage is the consequence of brittle failure of the rock (in contrast to plastic deformation, which can relieve stresses slowly). The first seismic waves to leave the region of the break (the hypocenter) are waves of alternate compression and rarefaction generated by the sudden release of elastic energy. After an earthquake one finds that the seismological stations that have received the first waves can be assigned to one of four geographic quadrants. In two of the quadrants, lying opposite each other, the first waves are compressional; in the other two quadrants the first waves are rarefactional.

The quadrants define the orientation of two nodal planes on one of which a sudden slip has presumably produced the earthquake. The intersection of the nodal planes is the null direction, or intermediate stress axis, parallel to which effectively no strain occurs. The line bisecting the quadrant in which the first motion is compressional defines the direction of least principal stress, parallel to which there is extensional strain. The bisector of the rarefaction quadrant defines the direction of the maximum principal stress along which there is compressional strain.

Lynn R. Sykes of the Lamont-Doherty Geological Observatory of Columbia University has applied this analysis to the seismic belts of the world and has shown systematically that the ridge axes are in tension, that there is lateral movement along the second type of seismic zone and that compression dominates the third and fourth types. Thus seis-

AXIS OF ROTATION can be selected in such a way (*top illustration at left*) that a set of two or more points lying on the surface of a sphere (*A, B, C*) can be moved by a rigid rotation around that axis to new positions (*A', B', C'*), preserving the original geometry of the set. A unique axis can be found only if the initial and final positions of two or more points are known. Similarly, the relative motion of two rigid plates can be described as a rigid rotation around a suitably selected axis of rotation (*bottom illustration at left*). Plate *A* is designated as fixed while plate *B* is rotated anticlockwise, as viewed down the axis of rotation. As plate *B* rotates through angle omega (ω), new surface area is added symmetrically to both plates at the ridge axis, which itself travels through an angle equal to one-half omega.

mology emphasizes that there are three kinds of plate boundary: boundaries across which plates are pulled apart, boundaries along which plates slide past each other and boundaries across which plates converge. Since rock material does not pile up indefinitely in the compressional zones, it follows that somewhere there must be zones in which plates are consumed.

The Plate Mosaic

One can therefore construct a model of global surface displacement involving a mosaic of plates each of which exhibits one or more of the three types of boundary. At ridge axes plates separate and new surface area is generated by the continuous accretion of new oceanic crust at the trailing edges of the plates. At transform faults plates slide past each other and surface area is neither created nor destroyed. At subduction zones one plate is consumed and slides down into the mantle under the leading edge of another plate.

Plates vary greatly in size from the six major plates, such as the plate that carries virtually the entire Pacific Ocean, down to very small plates, such as the plate that is essentially coextensive with Turkey. Moreover, plate boundaries do not always coincide with the margins of continents; many continental margins are peaceful earthquake-free nonvolcanic regions. Hence plates can be partly oceanic and partly continental or they can be entirely one or the other. This fact overcomes one of the traditional objections to continental drift, namely the mechanical difficulty of having a geologically weak continent plow its way across a strong ocean floor. According to the plate-tectonic view, continents and oceans are rafted along by the same crustal conveyor belt.

A look at the boundary around the African plate reveals two important consequences of plate motion. The greater part of the boundary is a ridge axis extending from the North Atlantic into the Indian Ocean and the Red Sea; thus the entire African plate must be growing in area. This behavior in turn means that plates elsewhere on the globe must be getting smaller. The second consequence of the growth of the African plate is that the Carlsberg Ridge in the Indian Ocean is moving away from the Mid-Atlantic Ridge, illustrating one of the essential corollaries of plate kinematics: plate motion is relative. There is no coordinate system within which absolute plate motion can be defined except a system defined in relation to a particular plate or plate boundary that is arbitrarily chosen as being "fixed."

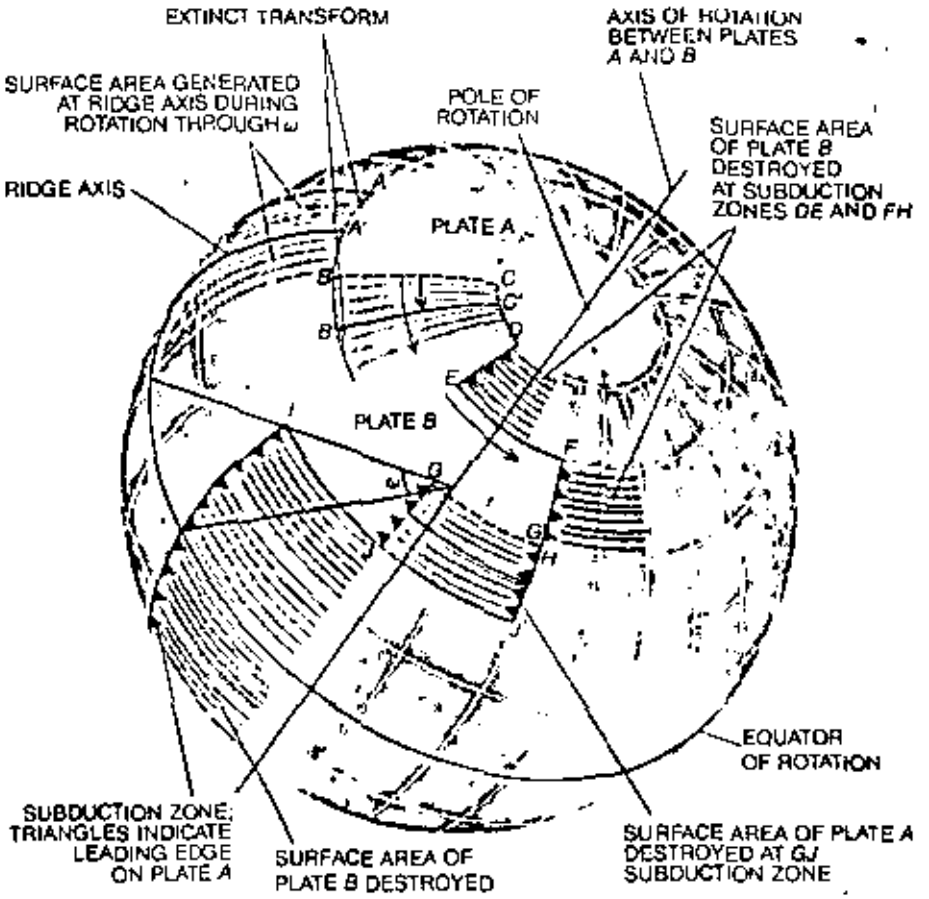

THREE KINDS OF TRANSFORM can exist as segments of a single plate boundary: ridge axis to ridge axis (*AB*), ridge axis to subduction zone (*CD*) and subduction zone to subduction zone (*EF, GH, IJ*). Plate *A* is again assumed to be fixed while plate *B* rotates anticlockwise. Ridge-axis-to-ridge-axis transforms (*AB, A'B'*) maintain a constant length because new surface area is generated symmetrically at ridge axes. Transforms joining ridge axes to subduction zones decrease or increase in length at half the transform slip rate. In the example depicted here *CD* shortens to *C'D*, but if the leading edge at subduction zone *DE* were on plate *A* (as in the case of *GJ*), *CD* would have lengthened. Transform *EF* maintains a constant length, whereas *GH* shortens to zero length and *IJ* lengthens to *IJ'*.

The basic assumption that plates are rigid is essential to plate tectonics and appears to be justified by the fact that excellent restorative fits can be made between many pairs of continental margins. (In making such a fit the margin is typically defined as the 1,000-fathom isobath on the continental shelf adjacent to the continent.) Similar fits can be made with even greater precision between pairs of magnetic anomalies symmetrically disposed on each side of a ridge axis. If plates had been distorted as they evolved, these fits could not be made. As further confirmation of rigidity, profiles produced by seismic reflection have shown that sediments laid down on the oceanic crust as it moves away from a ridge axis form undistorted flat layers.

The fact that rigid plates are in relative motion on a spherical earth means that a displacement between any two plates can be described by a rotation around an axis passing through the center of the earth. The intersection of this axis with the earth's surface is termed the pole of rotation (*see illustration on opposite page*). This concept was first applied by Sir Edward Bullard, J. E. Everett and A. G. Smith of the University of Cambridge to demonstrate the fit of the continental margins around the Atlantic Ocean. Relative surface motion between two plates proceeds along circles of rotation around the axis of rotation. The circles can be considered as latitudes of rotation from zero radius at the pole of rotation to a maximum at the equator of rotation. Relative plate motion is best described, however, as an angular velocity, since the velocity along rotation circles increases from zero at the pole of rotation to a maximum at the equator of rotation. The nature of displacement across a plate boundary is therefore entirely dependent on its orientation with respect to the circles of rotation.

Of particular interest are boundaries parallel to rotation circles. At these boundaries are faults where surface area is conserved; such faults are called trans-

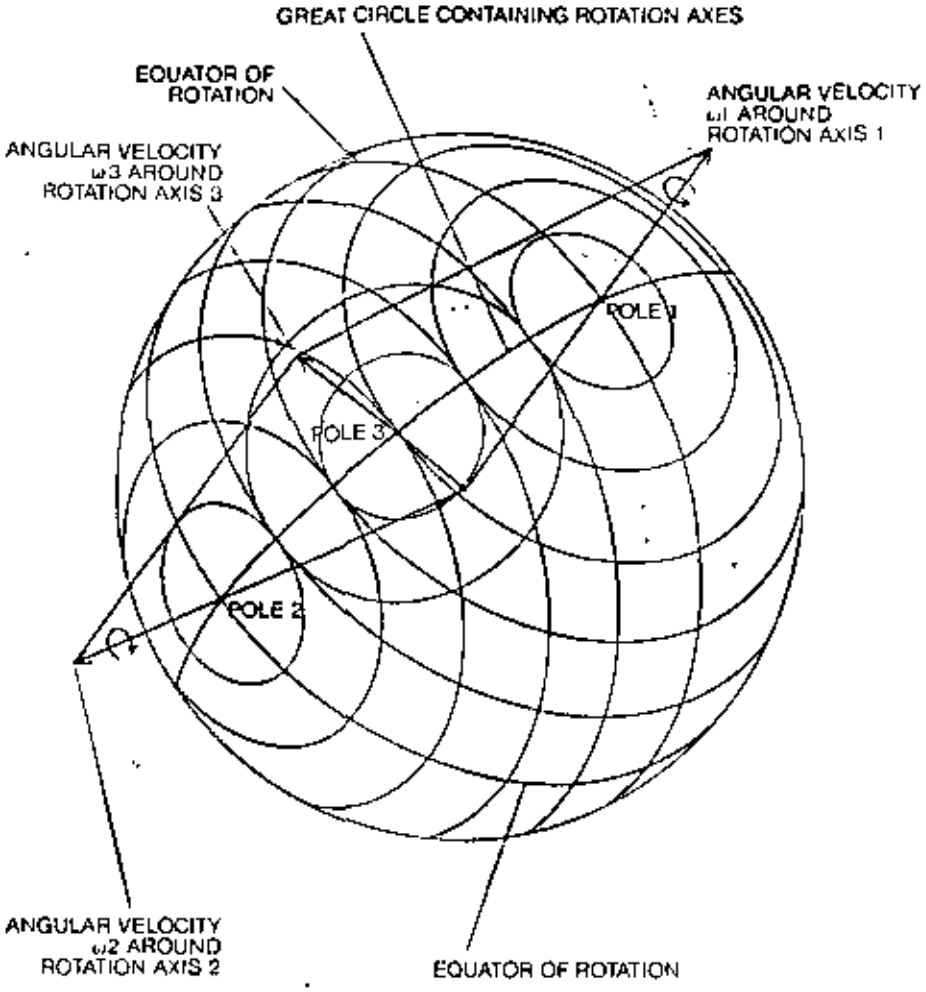

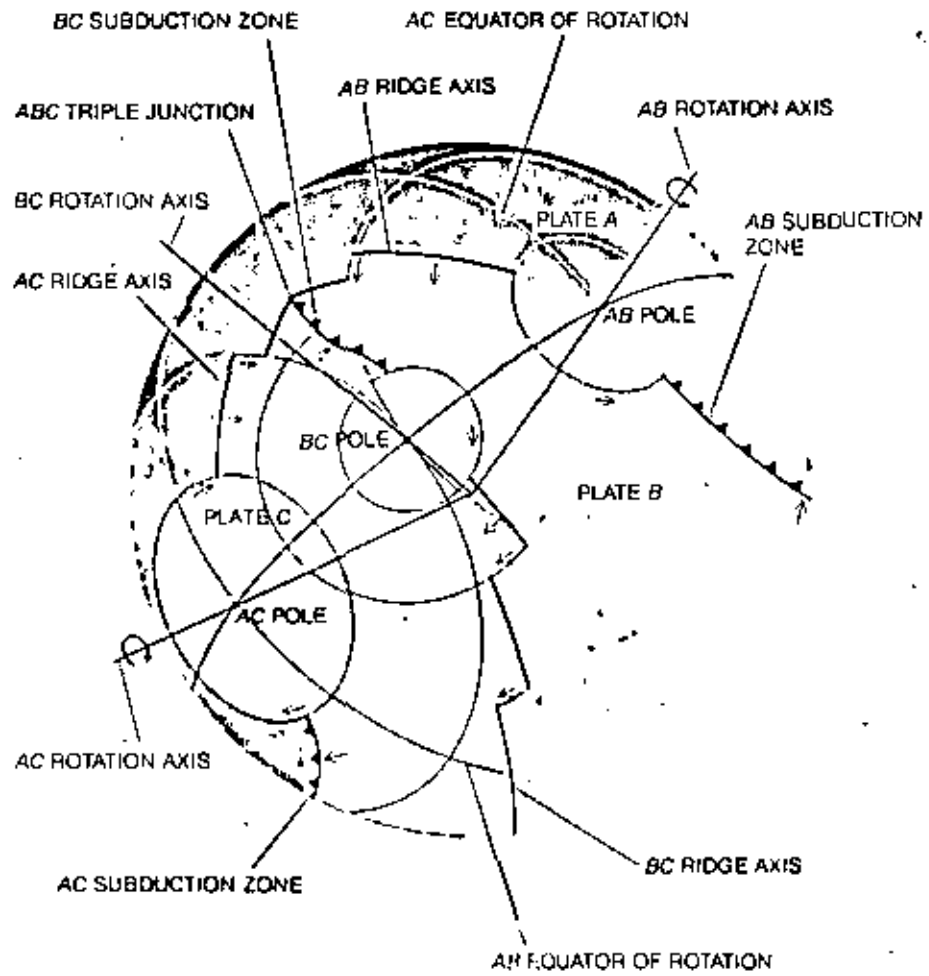

form faults. Great circles drawn perpendicularly to transform faults that are segments of one plate boundary will intersect to define the rotation pole. Plate boundaries oblique to circles of rotation are either ridges or subduction zones, depending on whether plates are separating or converging across them. The increasing rate of plate separation across ridge axes with increasing distance from the pole of rotation is reflected by a progressively increasing distance between particular magnetic anomalies and the ridge axis. Similarly, the rate of plate convergence at subduction zones increases away from the pole of rotation. A particularly good illustration is afforded by the New Zealand–Tonga seismic zone. That part of the zone south of New Zealand has only shallow earthquakes; intermediate-focus earthquakes start in New Zealand and deep-focus earthquakes north of New Zealand [*see illustration on pages 2 and 3*]. This suggests a progessive northward increase in convergence rate across the subduction zone, so that the downgoing plate reaches progressively deeper levels.

Separation rates across ridges where plates are moving apart can be directly deduced from magnetic-anomaly patterns, but there is no direct method for deducing convergence rates across subduction zones where one plate is diving under another and creating a trench. Close attention has therefore been given to plate boundaries where individual segments are a ridge, a transform fault and a subduction zone, because the angular velocity of relative motion deduced for a ridge segment also applies to a trench segment. The angular velocity can be directly translated into a circle-of-rotation velocity for any circle of rotation that crosses the subduction zone.

THIRD AXIS and angular velocity of rotation are defined (*top illustration at left*) as the vector sum of two others. If one knows the angular velocities of two rigid rotations around two axes (*1 and 2*) passing through the center of a sphere, one obtains their vector sum to determine the angular velocity around a third axis (*3*) lying in the same plane as the first two. In the example illustrated the poles of rotation axes *1* and *2* are 90 degrees apart and the angular velocities around them (*ω1 and ω2*) are equal, so that the pole of the third axis lies midway along a great circle between poles *1* and *2*. Similarly (*bottom illustration at left*), if one knows the axes of rotation and the angular velocities that describe the relative motion of plates *A* and *B* and plates *B* and *C*, one can ascertain the rotation axis (*AC*) that describes the relative motion of plates *A* and *C*.

depending on its "rotational latitude." Although there is no apparent geometric reason why ridges should lie parallel to longitudes of rotation, they appear in most cases to approximate this relation. Furthermore, the symmetrical distribution of paired matching magnetic anomalies with respect to the ridge axis where they were generated indicates that new crustal material is added symmetrically to the trailing edges of the diverging plates.

For some reason, perhaps one related to the driving mechanism for plate motion, straight ridge-transform boundaries are a mechanically stable configuration. Subduction zones are generally curved, perhaps also for mechanical reasons, and convergence directions can be right-angled or oblique to them, according to whether they are right-angled or oblique to rotation circles. One may pass in gradations from pure subduction to pure transform motion along a single plate boundary; therefore the orientation of a subduction zone, unlike the orientation of a ridge or a transform fault, is a poor guide to the relative direction of displacement.

The axial spreading zone of oceanic ridges is not a continuous feature. It is interrupted and offset by transform faults that in some places create high submarine cliffs. Transform faults were formerly thought to be lines along which the ridge axis had been displaced from a once continuous zone, since they continue as bathymetric features beyond the offset ends of the ridge axis. J. Tuzo Wilson of the University of Toronto argued, however, that they are simply offsets of the spreading axis and form an integral part of a single boundary. He coined the term transform fault to describe them because they merely transform relative motion between the two ridge segments. Seismic first-motion studies confirmed Wilson's prediction of transform motion; further support is provided by the observation that earthquakes are restricted to that portion between the offset ends of the ridge axis.

The active portion of a transform fault defines part of a circle of rotation. Similarly, the inactive continuation of a transform fault beyond the offset ridge axis defines circles of rotation for the previous history of plate divergence across the ridge axis; it represents earlier circles of rotation "frozen" into adjacent oceanic crust generated earlier. This is of fundamental importance for two reasons. First, the excellent circles-of-rotation lines described by inactive transform faults justify the assumption that relative motion between two plates can be described in

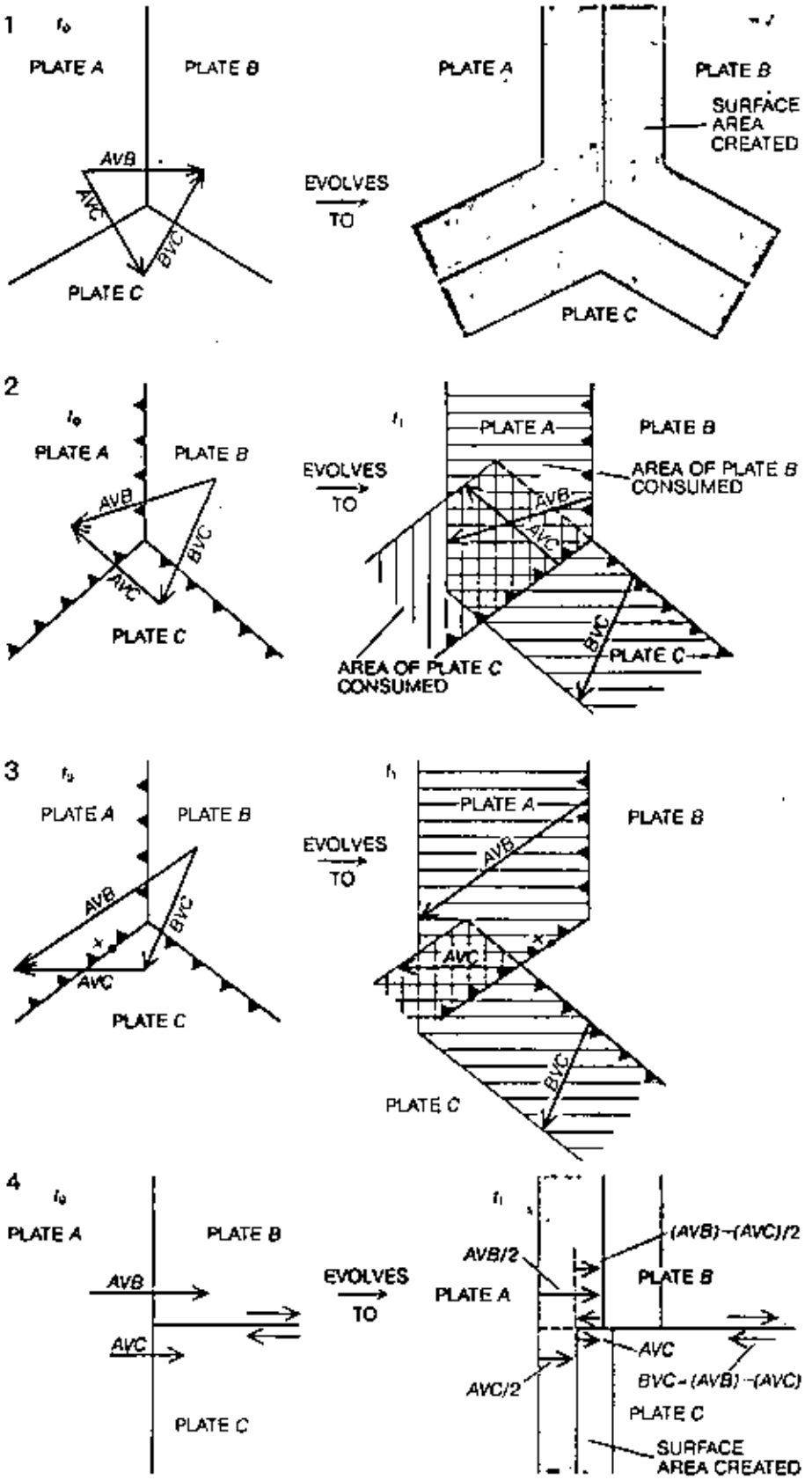

FOUR TRIPLE JUNCTIONS are depicted with their velocity triangles at time t_0 and their configuration at time t_1. Ridge axes are solid color; subduction zones are solid black; transforms are gray. A triple junction involving three ridges (*1*) is always stable. When three subduction zones meet (*2 and 3*) and two leading edges lying on plate *A* do not form a straight line, the triple junction is stable only when the *A* v. *C* velocity vector is parallel to the leading edge of plate *C* (*2*). Otherwise (*3*) the triple junction moves. Thus at some time between t_0 and t_1 the triple junction moves past point *X*. Before the time of movement the relative motion at *X* is *A* v. *C* and thereafter *A* v. *B*. The last diagram (*4*) depicts how it comes to pass that a triple junction involving two ridges and a transform can have the configuration at t_0 only instantaneously since the triple junction evolves immediately to t_1, in which plates *B* and *C* are separated by the transforms and the ridge is thus offset.

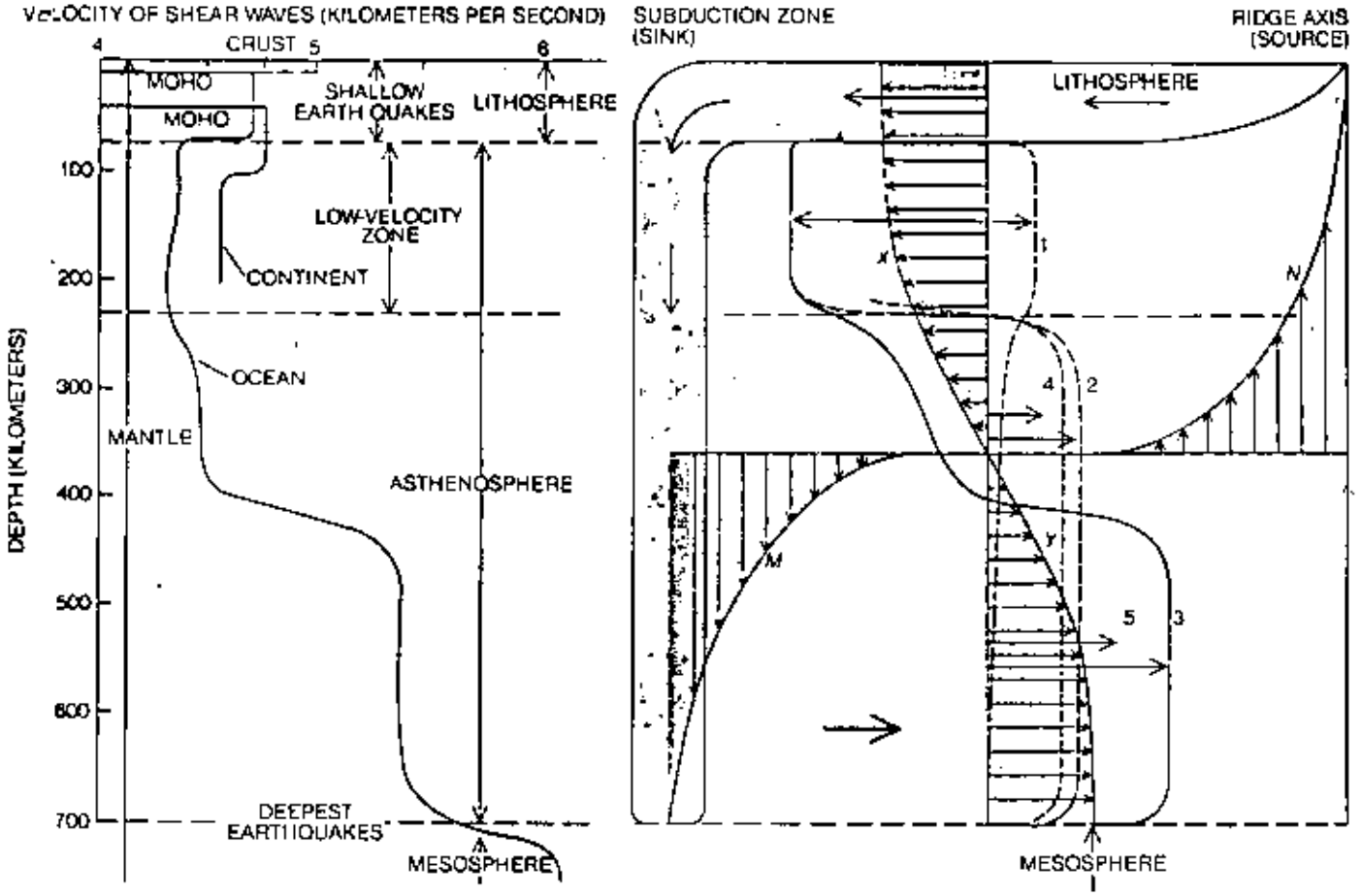

VARYING VELOCITY OF SHEAR WAVES in lithosphere and asthenosphere (*left*) suggests models showing how mass-transfer circuits (*right*) introduce new plate material at ridge axes and consume it at subduction zones. The velocity of shear waves decreases at 70 and 150 kilometers under oceans and continents respectively. Evidently mass-transfer circuits extend to a depth of at least 700 kilometers. Material descending at sinks (under curve *M*) must be balanced by material rising at sources (under *N*), and the upper lateral transfer (under *X*) must be balanced by return flow (under *Y*). Five shapes are suggested for lateral-transfer gradients.

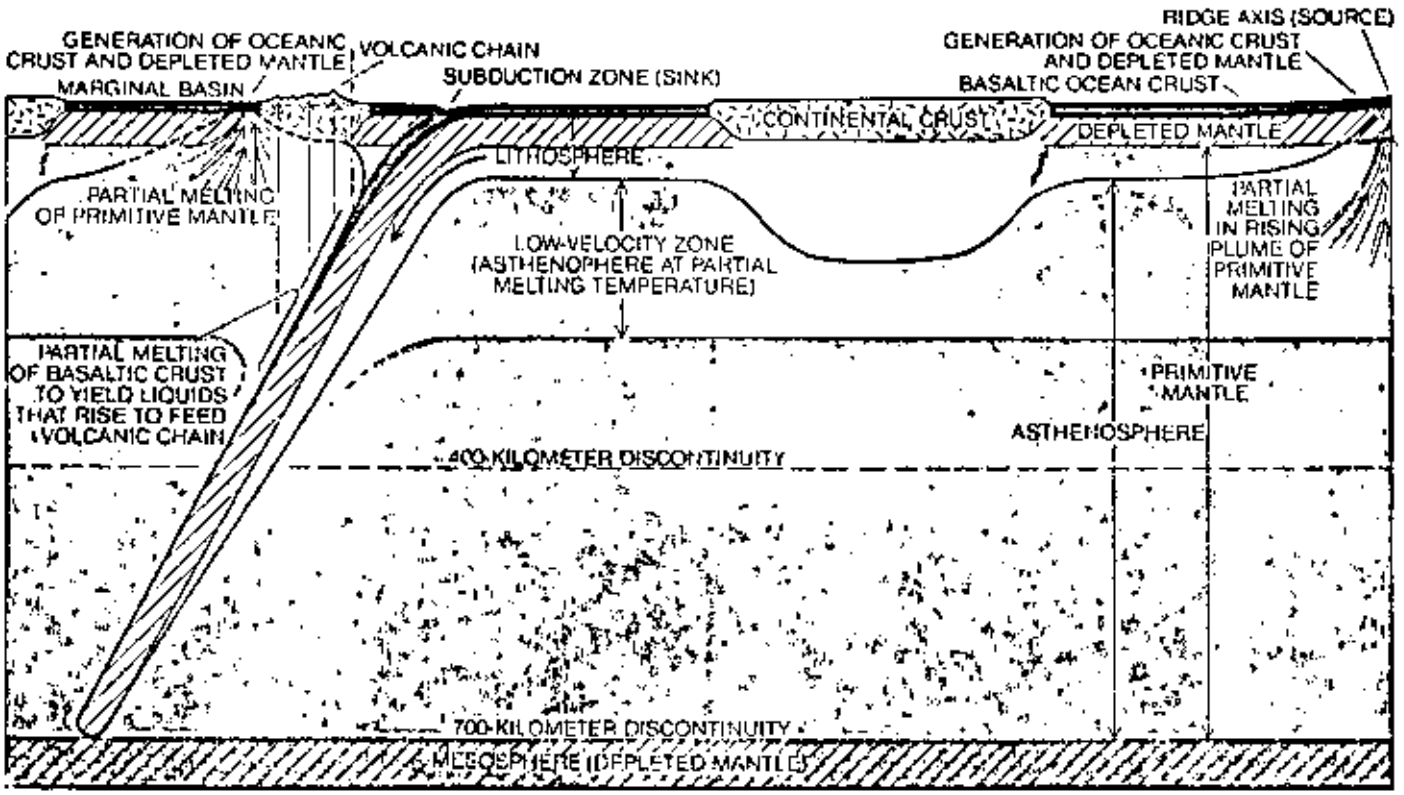

LITHOSPHERE PLATE of solidified rock serves as a thermal boundary conduction layer "floating" on molten or semimolten rock of the asthenosphere. In this schematic view the lithosphere is thicker under the continent it is rafting toward a subduction zone, where the plate descends into the mantle under leading edge of another plate. New oceanic crust is steadily being added at ridge axis.

terms of a rigid rotation around a fixed pole. Second, it provides the key to working out past plate motions. The inactive transform faults give the direction but not the rate of old displacements. Rates, however, can be deduced from the spacing of magnetic anomalies of known ages.

Walter C. Pitman III and Manik Talwani of the Lamont-Doherty Observatory have devised a simple but elegant technique using well-defined pairs of magnetic anomalies of known ages and fracture-zone orientations for computing plate displacements in the central Atlantic Ocean for the past 180 million years. First they assumed that successive pairs of magnetic anomalies were generated at the ridge axis and moved apart on rigid plates. They then found a series of rotation poles around which they could fit the pairs of progressively older magnetic anomalies; the series ended with a rotation that fitted the continental margins of Africa and North America. Reversing this sequence gives the kinematics of plate divergence that records the history of the opening of the central Atlantic Ocean.

A consequence of the symmetrical generation and asymmetric destruction of surface area, at ridge areas and subduction zones respectively, is that transform faults can retain a constant length or can change their length [*see illustration on page 5*]. Transform faults that join ridge axes, or subduction zones with leading edges on the same plate, stay the same length. Where transform faults join subduction zones with leading edges on different plates, they lengthen or shorten, depending on whether the leading edges face away from or toward one another. A transform fault that joins a ridge axis to a subduction zone increases or decreases in length depending on which plate the leading edge lies on.

If the axes and angular velocities of rotation between two pairs of plates (*A* and *B* and *A* and *C*) are known, the axis and angular velocity of rotation between the third pair (*B* and *C*) can be calculated [*see illustration on page 6*]. This means that if ridge-axis segments fall along the boundaries between *A* and *B* and *A* and *C*, the relative motion of *B* and *C* can be found. Xavier le Pichon of the Center for the Study of Oceanography and Marine Biology in Brittany developed this technique for computing the relative motions between the six largest plates and was thus able to work out convergence directions and rates across all the major subduction zones.

With the same technique Pitman has computed the relative motion of Africa and Europe for the past 80 million years. During this time North America and Africa have been parts of separate plates moving apart around a sequence of rotation axes as the central Atlantic has widened. North America and Europe have been similarly moving apart but around a different sequence of rotation axes. Therefore there has been relative motion between Africa and Europe. This motion has been complex but the net effect has been to nearly eliminate a formerly wide oceanic region between the two continents.

Since relative displacements are along circles of rotation, the relative motion between three plates cannot be described by the customary velocity vector triangle except instantaneously at a point. If, however, we are interested in relative motions in an area of the earth's surface so small that it may be regarded as a flat surface, with the result that circle-of-rotation segments are virtually straight lines, the velocity vector triangle is a convenient device for illustrating relative motion. A small area of great interest is one where three plate boundaries join to form a triple junction. Triple junctions are demanded by plate rigidity; this is the only way a boundary between two rigid plates can end. D. P. McKenzie of the University of Cambridge and W. Jason Morgan of Princeton University have analyzed all possible forms of triple junctions with velocity vector triangles and have shown that they can be stable or unstable depending on whether they are able or unable to maintain their geometry as they evolve [*see illustration on page 7*].

Plate Thickness and Composition

So far we have considered those essential aspects of plate geometry and evolution that can be treated from a surface point of view. We have not yet inquired into the thickness and composition of lithospheric plates. It has been known for many years from gravity and seismic-refraction measurements and from general considerations of mass balance that the continents are underlain by a relatively light "granitic" crust about 40 kilometers thick and the oceans by a denser "basaltic" crust only about seven kilometers thick. Both continental and oceanic crust are underlain by a mantle of denser material. The junction between crust and mantle is the "Moho," or Mohorovicic discontinuity. It was the goal of the now abandoned Mohole project to drill through the relatively thin oceanic crust into the mantle.

Plates must be at least as thick as the oceanic and continental crust because some plates have oceanic and continental portions between which there is no differential motion. It was thought for many years that the Moho might be an important physical discontinuity of mechanical decoupling on which large crustal displacements proceed. It is now clear that if there is a zone of decoupling between an outer rigid shell and a less viscous layer below, it is considerably deeper than the Moho.

The best evidence for the thickness of plates comes from seismology. The velocity of seismic waves is dependent on the density and flow properties of the rock through which they pass; it is high in rigid, dense rocks and low in less rigid, lighter rocks. Moreover, an increase in confining pressure increases the velocity of waves and an increase in temperature decreases it. Although confining pressure must increase with depth, recent studies indicate that the velocities of shear waves suddenly decrease below a surface about 70 kilometers under the oceans and about 150 kilometers under the continents [*see top illustration on opposite page*]. Shear-wave velocities then increase with depth, with marked increases between 350 and 450 kilometers and just above 700 kilometers.

These data suggest that an outer rigid layer 70 to 150 kilometers thick (the lithosphere) lies above a weaker and hotter layer (the asthenosphere) that becomes increasingly viscous with depth. The thickness of the lithosphere therefore probably constitutes the thickness of the rigid plates, and the lithosphere is discontinuous at plate boundaries. Earthquakes present a test of this hypothesis, since the cold, rigid lithosphere is probably their source. The distribution of earthquakes should thus provide a guide to the thickness of the lithosphere and to its distribution where it descends in subduction zones into the interior of the earth.

Ridges and transform faults are characterized by earthquakes whose depth extends to about 70 kilometers. The inclined zone of intermediate and deep-focus earthquakes indicates the descent of the lithosphere into the asthenosphere, where it is consumed at subduction zones.

Bryan L. Isacks and Peter Molnar of the Lamont-Doherty Observatory, working with seismic first-motion records, have analyzed the stresses in descending lithospheric plates. They find that the stresses are consistent with those that would be expected if a cold slab of bending lithosphere were to meet increasing resistance as it descended into

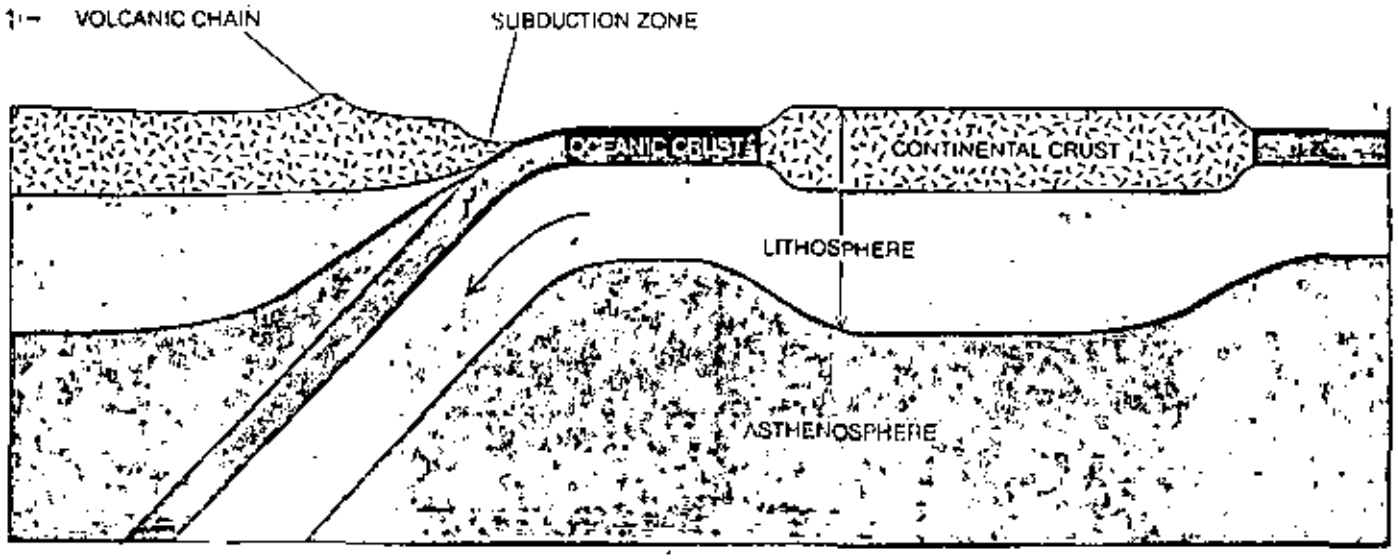

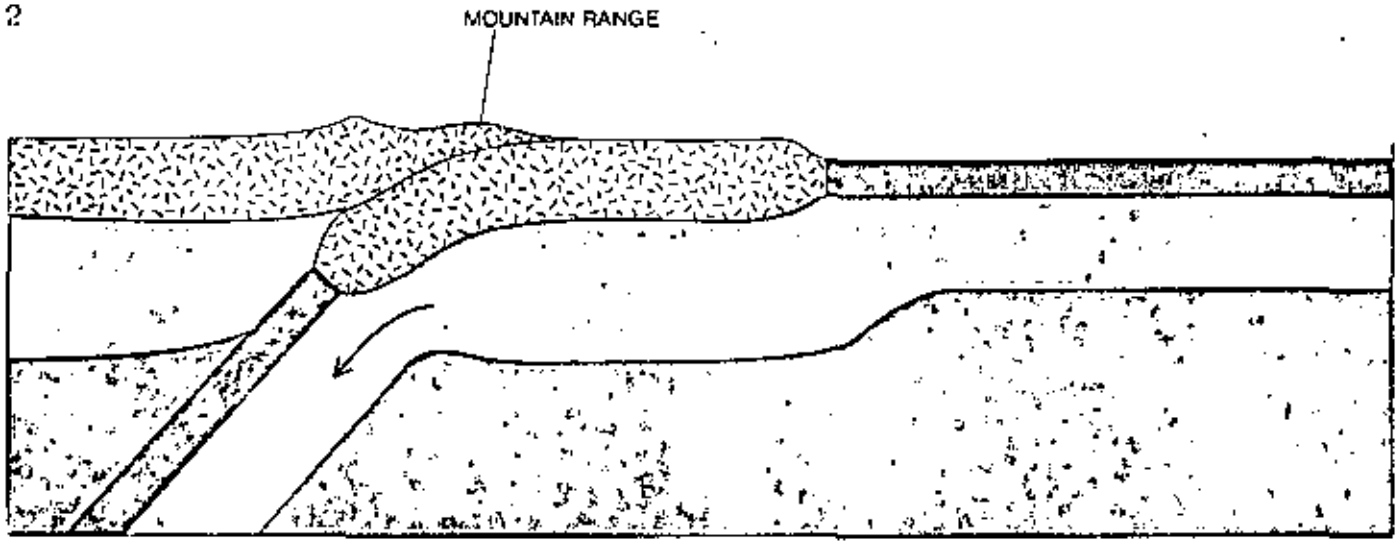

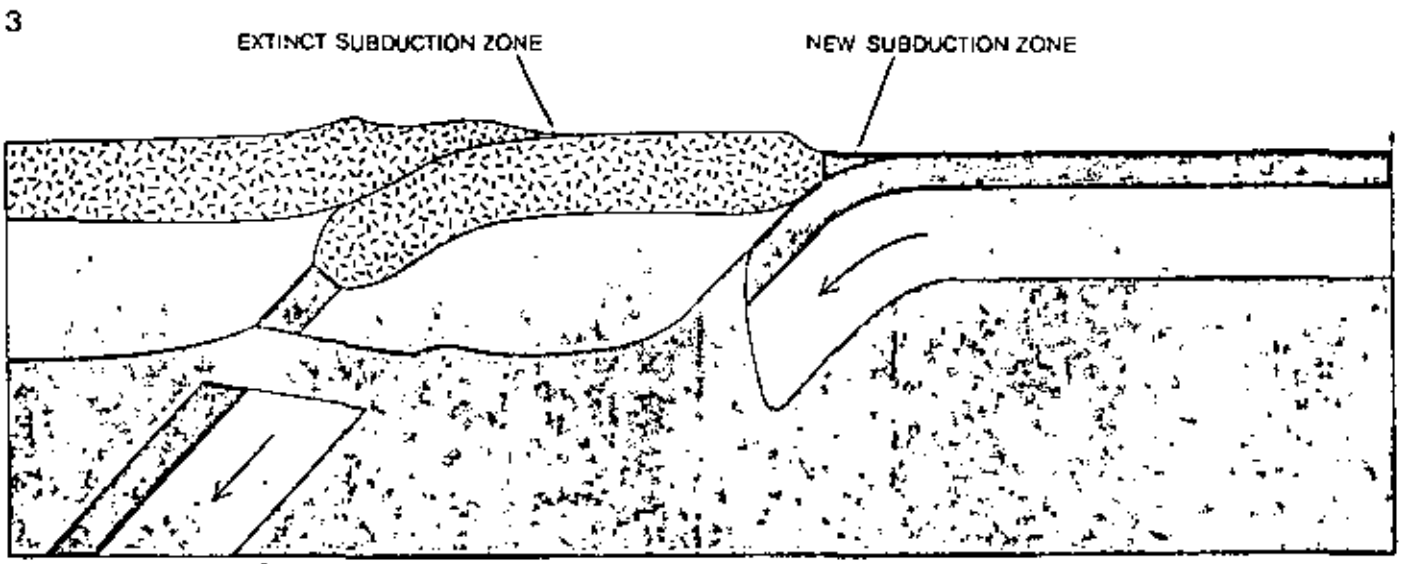

COLLISION OF CONTINENTS occurs when a plate carrying a continent is subducted at the leading edge of a plate carrying another continent (1). Since the continental crust is too buoyant to be carried down into the asthenosphere, the collision produces mountain ranges (2). The Himalayas evidently formed when a plate carrying India collided with the ancient Asian plate some 40 million years ago. The descending plate may break off, sink into asthenosphere and a new subduction zone may be started elsewhere (3).

an increasingly viscous asthenosphere. Where the cross section of the lithosphere is curved (at subduction zones) its upper part is under tension, suggesting elastic bending. Where the lithosphere has descended only a short distance into the asthenosphere it is under tension along its length, indicating low resistance to its descent. Continuously inclined seismic zones, representing slabs of lithosphere that have descended to lower parts of the asthenosphere, are characterized by compression along the slab. This fact suggests that the downgoing lithosphere is put into compression as it meets increasing resistance to its descent. An instructive case is where there is a gap in the inclined seismic zone, suggesting a discontinuity in the downgoing slab. Earthquakes above the gap indicate tension; earthquakes below it indicate compression. Evidently part of the slab has broken off and is descending at a faster rate than the remainder.

The general kinematics of plates—their growth and consumption—requires some form of mass convection, or mass-transfer circuits, in the mantle. Heat flow to the earth's surface is highest along ridge axes, it declines rapidly to a low plateau value across the plates and falls to a minimum at subduction zones. Therefore the lithosphere may represent a cold, rigid boundary conduction layer that is created at the hot ridge "sources" and destroyed at the cold subduction-zone "sinks." Any acceptable model for the geometry of the mass circuits in the earth's mantle must satisfy a number of conditions.

Conditions to Be Met

First, there must be a gross balance between vertical mass transfer at sources and sinks and lateral mass transfer by plate motion and motions in the asthenosphere. Second, the 700-kilometer limit on the depth of earthquakes and the abrupt increase in shear-wave velocity that marks the bottom of the asthenosphere imply that the mass-transfer circuits involve only the lithosphere and the asthenosphere. Third, the boundaries along which new crust is being generated on the earth exceed in length the boundaries where crust is being destroyed, so that plates are generally consumed at individual sinks faster than they are created at individual sources. Fourth, a simple geometric consequence of the fact that plates can change their surface area is that plate boundaries can move in relation to other plate boundaries. This fact implies that mass-transfer circuits must also change their geometry as the plates evolve. Fifth, mass-transfer circuits cannot take the form of simple, regular convection cells linking sources and sinks with an upper lateral transfer and a lower return flow because there is no simple one-to-one relation between sources and sinks.

There are several great circles around the earth along which one can cross two ridge axes without an intervening subduction zone or can cross two subduction zones without an intervening ridge axis. Circuits involving mass-transfer rates of up to 10 centimeters per year must be accompanied by convective heat transfer, because thermal inertia prevents the elimination by conduction of temperature differences between different parts of the circuit. This condition is reflected in the persistence of earthquakes in a plunging slab down to depths approaching 700 kilometers. It is not clear, however, whether convective mass transfer and heat transfer is the cause or a consequence of plate motion. The models for relative lithosphere-asthenosphere motion at the top of page 8 illustrate this difficulty. They are all certainly far too simplistic. Indeed, the relative surface motions of plates may not be a guide to motions in the asthenosphere.

Let us consider a model in which the crust, lithosphere and asthenosphere are linked in a simple source-to-sink system [*see bottom illustration on page 8*]. The lithosphere in this model acts as a cold boundary conduction layer to a hotter asthenosphere, the upper part of which (the low-velocity zone) is probably near its melting temperature. Tension induced by plate separation at the ridge axis reduces the confining pressure in the low-velocity zone under the ridges. Reduction of confining pressure causes partial melting of primitive mantle in the low-velocity zone and the rising of a mush of crystals and liquid, with the result that the ridges are broadly uplifted. As the column of partially molten material rises it undergoes further partial melting; eventually the basaltic liquid rises to fill the crack continuously generated by plate separation. The liquid cools and crystallizes to form the basaltic oceanic crust and leaves under it a depleted layer of mantle.

Where plates descend into the asthenosphere, their leading edge carries a chain of volcanoes; thus one infers that the volcanic rocks are linked in some way with the descending plate. Because the volcanic rocks are less dense than the basalts of the oceanic crust, it is likely that they are formed by partial fusion of the oceanic basalts with other material as the basalts are carried down into the hot asthenosphere. The depleted mantle in the plunging plate is denser than the primitive asthenosphere through which it sinks, both because it has had a lighter basaltic fraction removed from it under the ridge axis and because it is cooler. Therefore once a plate has begun to descend in a particular subduction zone it is likely to continue until the plunging plate meets increasing resistance deep in the asthenosphere.

Since continental crust is only about 40 kilometers thick, whereas plates are 70 kilometers or more thick, the continents ride as passengers on the plates. In the framework of plate tectonics continental drift is no more significant than "ocean-floor drift." Nevertheless, continents, unlike oceans, impose certain important restraints on plate motion. The narrow, sharply defined trenches and the regularly inclined earthquake zones sloping away from trenches indicate that oceanic lithosphere is easily consumed by subduction, probably because it has a thin, dense crust. Intracontinental seismic zones associated with mountain ranges exhibit compressional deformation over a wide area, which implies that continental lithosphere is hard to consume because it has a thick, relatively buoyant crust.

Within the Alpine-Himalayan mountain belt are narrow zones characterized by a distinctive assemblage of rocks, known as the ophiolite suite, whose composition and structure suggest that they are slices of oceanic crust and mantle. If they are, ophiolite zones mark the lines along which continents collided following the contraction of an ocean by plate consumption [*see illustration on opposite page*]. The small oceanic areas within the Alpine belt, such as the Mediterranean Sea and the Black Sea, may be remnants of larger oceans that once lay between Africa and Europe. Evidently lithosphere carrying light continental crust is difficult to consume, as is indicated by the marked scarcity of intermediate-focus and deep-focus earthquakes in zones where continents have collided. Thus it seems that continental collision terminates subduction along the collision zone. This implies that mass-transfer circuits must be drastically rearranged after the collision of continents, since a major sink is eliminated. As a result new sinks may form in oceans elsewhere.

As we have seen, any hypothetical driving mechanism for plate motion must meet a number of conditions. At present some form of thermal convec-

tion in the upper mantle seems to hold the most promise, but other mechanisms have been suggested that may play some role in plate dynamics. These mechanisms include the retarding effect of earth tides raised by the gravitational attraction of the moon, the possible pull exerted by a plate "dangling" in the asthenosphere and forces created by plates sliding down the slight grade between sources and sinks. It is also possible that some small plates are mechanically driven by the effects of relative motion between adjacent larger plates. For example, the westward motion of the wedge-shaped Turkish plate with respect to the Eurasian plate may be caused by its being squeezed like an orange seed between the Arabian and the Eurasian plate.

Extinct Plates

It is now certain that plate tectonics has operated for at least the past 200 million years of earth history. During this time virtually all the present oceans were created and others were destroyed. Two hundred million years ago the major continental masses were assembled into the single supercontinent Pangaea [*see illustration below*]. It is therefore legitimate to ask if the breakup of Pangaea some 180 million years ago marked the beginning of plate tectonics. Geologic studies of mountain belts older than 200 million years strongly indicate that they owe their origin to processes operating at plate boundaries that are now extinct. The Ural and Appalachian-Caledonian mountain belts, which lie within ancient Pangaea, have narrow zones where ophiolites are found. These old ophiolite zones, like those in the Alpine-Himalayan mountain belt, thus mark the sites of vanished oceans. This implies that the Urals, for example, were created by the collision of two conti-

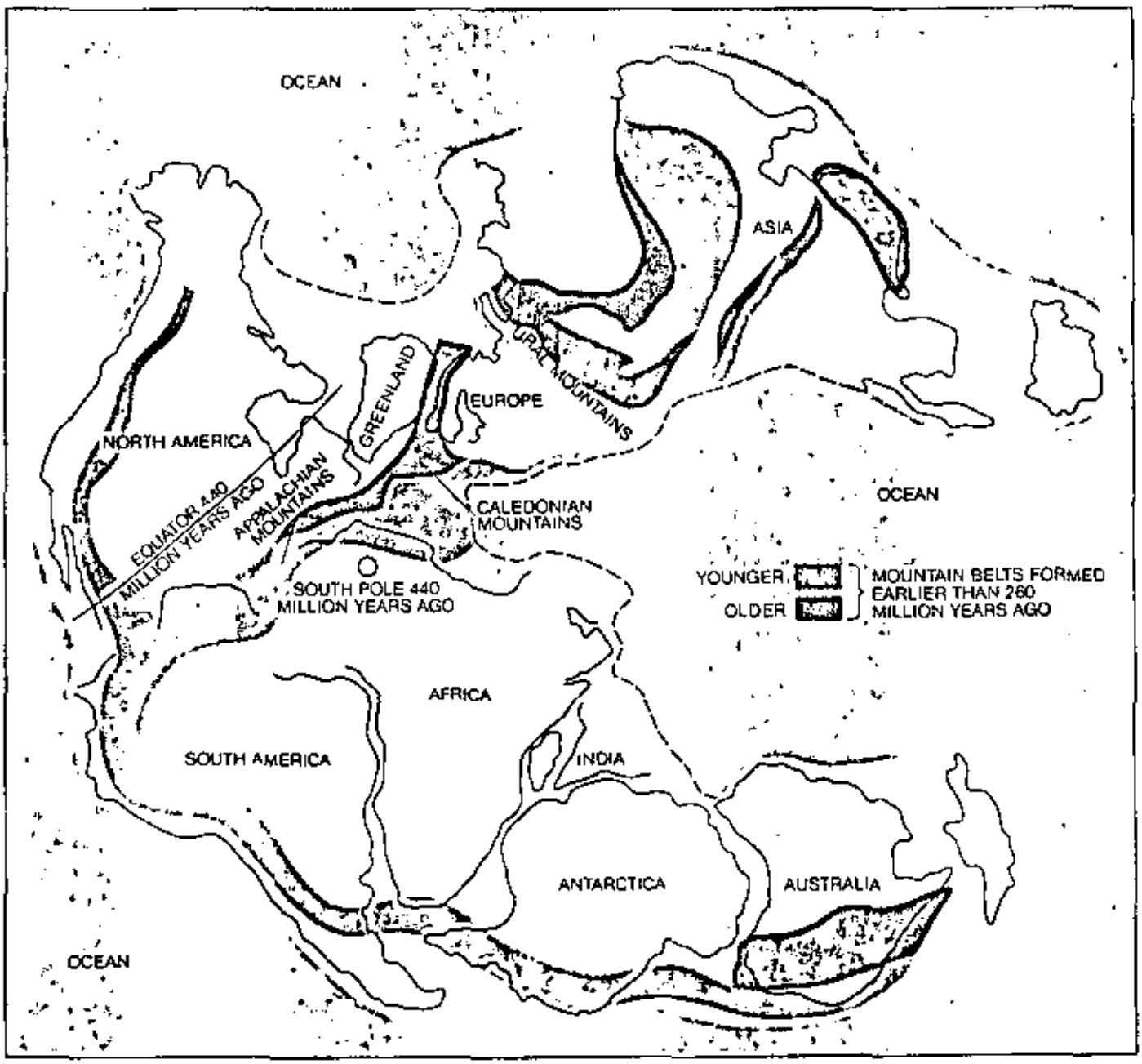

ANCIENT CONTINENT OF PANGAEA is reconstructed by fitting together the major continental land masses. Pangaea started to break up about 200 million years ago with a rift between Africa and Antarctica. Other rifts allowed South America, Australia and India to drift into their present positions. Mountain belts formed more than 260 million years ago are shown in shadings that distinguish younger and older belts. These mountain belts indicate lines of collision between continental fragments antedating Pangaea. Thus a prior collision of North America and Africa formed the younger part of the Appalachians 260 million years ago. Such a collision would explain how Equator and South Pole of 440 million years ago were brought close together after formation of Pangaea.

mental masses and that the ophiolites were generated by sea-floor spreading at a ridge axis before the continents were brought together.

Large-scale horizontal motions of continents before 200 million years ago are supported by other lines of reasoning. Glacial deposits and other data indicate that about 400 million years ago a south polar ice cap covered the Sahara. At the same time eastern North America lay near the Equator. On the Pangaea reconstruction these close polar and equatorial positions are incompatible: they indicate that Africa and North America were separated by an ocean some 10,000 kilometers wide. The contraction of this ocean and the resulting collision of North America and Africa were probably largely responsible for the growth of the Appalachian mountain belt [see "Geosynclines, Mountains and Continent-building," by Robert S. Dietz; SCIENTIFIC AMERICAN, March, 1972]. It seems a reasonable assumption that long, narrow, well defined zones of mountain-building were established along zones of plate convergence. If this is the case, plate tectonics has been operating for the past two billion years.

The absence of well-defined zones of mountain-building older than two billion years suggests, however, that some mechanism other than plate tectonics, at least as we know it at present, was responsible for the evolution of the earth's crust in earlier epochs. The ancient "shield" regions of the continents, which contain rocks older than 2.4 billion years, are characterized by rocks distributed in swirling patterns over areas so wide they can hardly be explained by processes arising at the boundaries of rigid plates. Evidently the shield areas were stabilized about 2.4 billion years ago, and by some 400 million years later a lithosphere with sufficient rigidity to crack into a plate mosaic had developed.

This does not necessarily mean that plate tectonics as we know it today began two billion years ago. Mountain belts older than 600 million years do not have ophiolite complexes like those of the younger mountain belts, indicating that sea-floor spreading before 600 million years ago generated a different type of oceanic crust and mantle. Geological data suggest that plates may have been getting thicker and that plate boundaries may have become more narrowly localized with time.

An exciting corollary of plate tectonics is that it provides a means whereby the total volume of continental crust can increase with time. We have seen that the primitive mantle of the asthenosphere undergoes partial melting to liberate a basaltic liquid that rises and cools to form the oceanic crust on the ridge axis, and that partial melting of the oceanic crust on a descending plate may yield the liquids that erupt to build the volcanic chains on the leading edge of plates. Volcanic rocks, with their deep-level intrusions of liquids that crystallized before they reached the surface, have the same bulk composition as that of the continental crust. The volcanic chains may therefore be sites where strips of embryonic continental crust are generated. Since they lie on the leading edge of plates, their destiny is to collide with other volcanic chains or with various kinds of continental margin. In this way new strips of light continental crust will be added to continental margins.

As we have seen, the arrival of a continental margin at a subduction zone blocks further plate consumption at that site. Thus the oceanic ridge provides an effective means of growing continental crust, but there is no means of destroying such crust. This implies that the total volume of continental crust has been increasing for the past two billion years. One should not conclude, however, that strips of new crust have been added to the continents as a succession of regular concentric rings. Rather, discontinuous strips have been added at different times, reflecting the complex interaction of continental margins with the plate-boundary mosaic.

Although there are geologic phenomena that plate tectonics does not yet obviously explain, and although the driving mechanism is obscure, these deficiencies do not constitute rational objections to the theory of plate tectonics. One of the serious mistakes that many earth scientists made in the past was to reject continental drift because it was not clear how or why it occurred. The remarkable success of plate tectonics has been not only that it provides a consistent logical framework that draws together such diverse phenomena as sea-floor spreading, continental drift, earthquakes, volcanoes and the evolution of mountain chains but also that it has been successfully quantified and tested to the point where its essential core can no longer be questioned.

The essential core of plate tectonics is the geometric evolution of plates and the kinematics of their relative motion. It is of paramount importance to fully explore all the geometric and kinematic aspects of plate evolution if we are ever to understand the dynamics of plate motion and the geologic corollaries of plate tectonics.

The Author

JOHN F. DEWEY is professor of geology at the State University of New York at Albany. Born in England, he received his bachelor's degree and his Ph.D. at the University of London. He taught at the University of Manchester from 1960 to 1964 and at the University of Cambridge from 1964 to 1970, taking up his position at Albany in 1971. His research interests include the role of plate tectonics in the earth's history, identification of criteria by which old plate margins can be recognized, the evolution of mountain belts, and field research in the Appalachians, mainly in Newfoundland. He lists his outside interests as "gymnastics and skiing."

Bibliography

SPECULATIONS ON THE CONSEQUENCES AND CAUSES OF PLATE MOTION. D. P. McKenzie in *Geophysical Journal of the Royal Astronomical Society*, Vol. 18, No. 1, pages 1–32; September, 1969.

MOUNTAIN BELTS AND THE NEW GLOBAL TECTONICS. John F. Dewey and John M. Bird in *Journal of Geophysical Research*, Vol. 75, No. 14, pages 2625–2647; May 10, 1970.

The Evolution of the Andes

The geology of the central Andes indicates that the history of the range can be understood in terms of the consumption of a plate of the earth's crust plunging under South America

by David E. James

A great series of mountain belts, the Andean cordillera, sweeps down the west coast of South America from Venezuela and Central America nearly to the southern tip of Chile. A long arc-shaped deep in the ocean floor, the Peru-Chile trench, is clearly allied with the mountain chain and runs roughly parallel to it from about four degrees north latitude to 40 degrees south. Some 15,000 meters (more than nine miles) of vertical relief separates the deepest part of the trench from the highest Andean peak. The Andean arc, comprised of both mountains and trench, is a living, evolving system. It is a part of the circumpacific "ring of fire," and the live volcanoes that dot the length of the cordillera and the devastating earthquakes that punctuate the flow of South American life are ever present reminders that the mountain-building processes that raised the Andean chain are still very active today.

Many earth scientists, of whom I am one, believe that the Andean arc is a modern analogue of many older mountain belts: that if we had lived in the region of the Sierra Nevada 100 million years ago or the northern Appalachians 450 million years ago, we would have witnessed mountain-building activity of a similar kind. Until recently this view was not widely accepted. It was generally supposed that the processes through which older mountain belts evolved are not being duplicated today. That supposition is rapidly giving way to the concept that mountain-building activity has proceeded in accordance with consistent geologic patterns that have been repeated over and over again during at least the past two billion years of earth history, and that it continues to do so today. In this view the Andean chain is the foremost modern example of those mountain-building processes at work, and so, by understanding the Andes, we seek to learn how ancient mountain belts were born, matured and in some cases died long before man arrived to record their origin or their passage.

Concepts of orogeny, or mountain building, have recently been revolutionized by the theory of plate tectonics [see "Plate Tectonics," by John F. Dewey; SCIENTIFIC AMERICAN, May, 1972]. This theory, which has been developed with startling rapidity over the past decade, holds that the outer rind of the earth, the lithosphere, consists of a mosaic of rigid plates that are in motion with respect to one another. These plates, some 100 kilometers (60 miles) thick, include not only the earth's solid crust but also part of the denser upper mantle. Plate boundaries, or junctions, rarely coincide with continental margins, and so the relative movements of parts of the earth's surface are now viewed in terms of plate motions rather than "continental drift." The proud continents, which were once thought to plow through oceanic crust like great ships, are now reduced to the status of passive passengers on the lithospheric plates. Volcanic magma welling up from deep within the earth's mantle creates the lithospheric plates along oceanic ridges. Newly generated lithosphere moves away from the ridges to yield to constantly replenished volumes of magma injected along the axes of the ridge. These spreading plates are consumed at trenches, where they bend down and plunge into the earth's mantle.

Most of the world's tectonic activity—earthquakes, volcanoes and mountain building—is concentrated along plate junctions. The west coast of South America is such a junction [*see illustration on next page*]. Here the oceanic Nazca plate, generated along the East Pacific Ridge, is consumed in the Peru-Chile trench, where it bends down and slides under the South American plate at a rate of about six centimeters per year. Examination of the structure and geology of the central Andes reveals that most of the present-day orogenic activity and the geologic evolution of the past 200 million years can be understood in terms of the subduction, or consumption, of the oceanic plate under South America. This interaction of the two plates accounts for the crumpling of the stable continental margin to form belts of fold mountains that now constitute the eastern ranges of the Andes, for the birth of the great Andean volcanic cordillera to the west and for the continental growth of western South America.

Lured by the sheer scale of the Andes mountains, the Carnegie Institution of Washington, in concert with a number of South American institutions, set out more than a decade ago to study the nature and evolution of the central Andes of southern Peru, Bolivia and northern Chile. Many years of work have led progressively to a rather complete

REGION OF THE ANDES near Lake Titicaca on the boundary between Peru and Bolivia is shown on the opposite page in a photograph made by the Earth Resources Technology Satellite. The lake is on the altiplano, or high plateau, nearly four kilometers above sea level. Rising above the altiplano to the west (*bottom*) are the volcanic mountains of the western cordillera; to the east (*top*) are the fold mountain belts of the eastern cordillera.

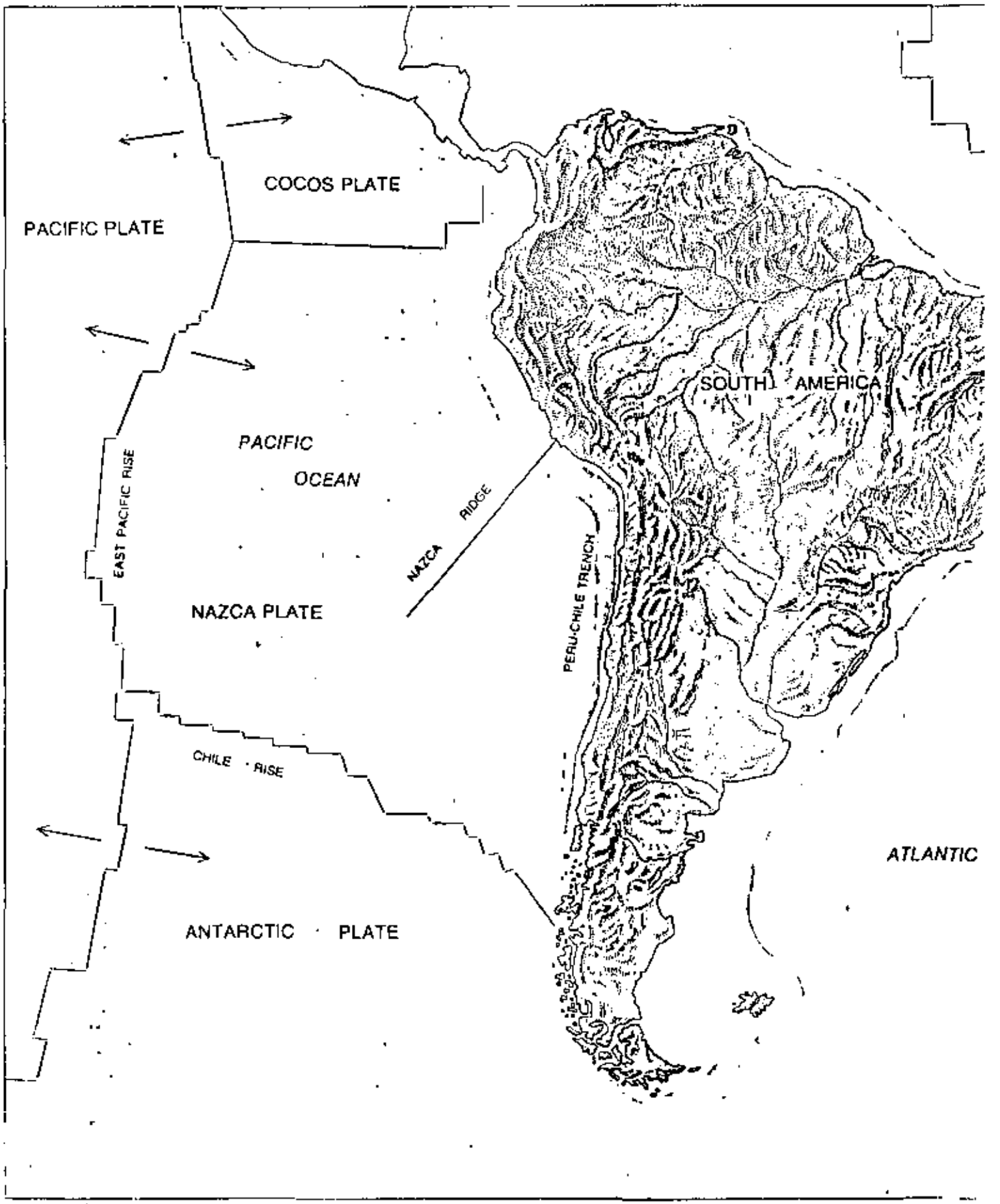

GEOPHYSICAL SETTING of the Andes is portrayed. According to the theory of plate tectonics, the lithosphere, or outer shell of the earth, consists of several rigid plates that are moving with respect to one another. The juncture between the Nazca plate and the South American plate represents the most important modern example of interaction of an oceanic and a continental plate. The Nazca plate is generated along the East Pacific Rise and consumed in the Peru-Chile trench. The interaction of the two plates at the trench

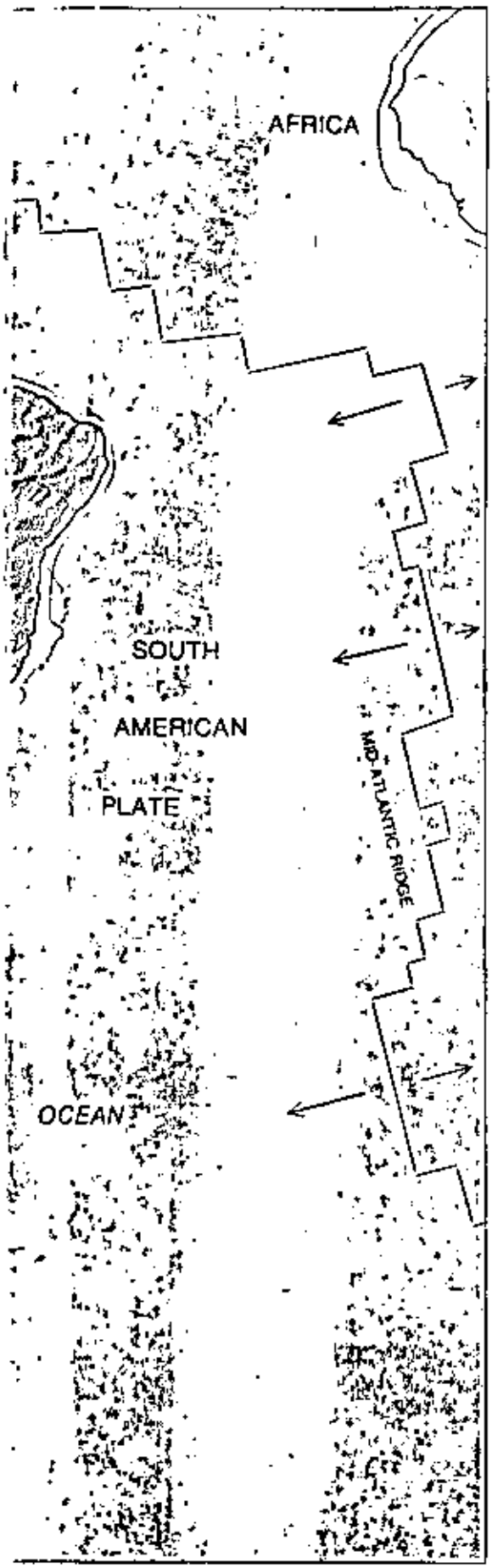

has caused deformation and growth of the continental margin of South America, thereby forming the Andean mountain system. Arrows indicate flow away from ridges.

understanding of the physical properties of the earth under the central Andes, but it is only recently that the conceptual tools have been available with which to understand the forces and sequences of orogenic events that produced the Andes and that continue to generate volcanism and seismicity along the Andean chain even today.

To understand the evolution of the central Andes it is necessary to draw on two distinct kinds of evidence, geophysical and geological. Important geophysical evidence includes the distribution of earthquakes and the distribution within the crust and upper mantle of certain physical properties: the velocity of seismic waves, the absorption of their energy (their attenuation) and the density of rock. From these properties one can deduce information on the kinds of rock in the earth's interior and whether they are rigid or mobile. Geological evidence derives from the study of rock types and their structures as observed on the earth's surface; it is only from geological evidence that one can read the history of past events. I shall consider the geophysical evidence first, since it provides the observational basis for most of our knowledge concerning the plate-tectonic framework of the juncture between the converging South American and Nazca plates.

Earthquake distribution provides key evidence regarding plate interactions. It is a general tenet of plate theory that the inclined earthquake zones (the Benioff zones, named for Hugo Benioff) that bend down under trenches and volcanic arcs define the upper part of the descending oceanic plates. Descending lithospheric plates are cooler and hence more rigid than the asthenosphere (the hot mantle) through which they sink, and it is widely supposed that only within the lithosphere are rocks rigid enough to support brittle fracture, or earthquakes. This supposition is supported by the observation that in most island arcs earthquakes appear to be confined almost entirely to the descending plate.

Under the central Andes, however, earthquakes occur not only in the descending plate but also in a continuous wedge between the earth's surface and the top of the sinking oceanic plate to a depth of from 200 to 300 kilometers (*see top illustration on page 68*). This observation leads one to suspect that the leading edge of the overriding South American lithosphere may be an abnormal 200 to 300 kilometers thick—much thicker than the usual 100 kilometers observed for most plates and in startling contrast to the 50-kilometer thickness measured seismically for the undersliding Nazca plate. More direct evidence that the Andean lithosphere is 200 to 300 kilometers thick derives from seismic results, which show that there is no low-velocity zone or zone of high seismic-wave attenuation in that region.

Both low-velocity zones and zones of high attenuation in the mantle are commonly interpreted as being regions of softer rock and are associated with the asthenosphere; conversely, the absence of these zones implies that the rock is comparatively rigid. An important consequence of the thick lithosphere under the Andes is that it precludes convective overturn in the mantle above the Benioff zone. It is this overturn that is believed to produce the secondary centers of seafloor spreading that develop behind island arcs but that are conspicuously absent behind the continental Andean arc.

A second important set of geophysical observations, on crustal thickness, provides an additional linkage between the present plate-tectonic regime of the Andes and the orogenic history of the Andes as it is read in the geologic record. Seismic data show that the crust of the central Andes is extremely variable in thickness. Over a distance of little more than 500 kilometers it varies from about 11 kilometers (including water) in the Pacific basin to 30 or 35 kilometers along the coast (a "normal" continental crust), more than 70 kilometers under the western-range volcanic crest, 50 to 55 kilometers under the eastern fold ranges and finally 35 kilometers under the Brazilian shield. Only in the Himalayas have crustal thicknesses of as much as 70 kilometers been observed elsewhere.

Yet one could have predicted these results obtained from seismic measurements simply on the basis of topography and the principle of isostasy. This principle states that mass excess above sea level—a mountain chain, for example—must be compensated by an equal mass deficiency at depth: the mountain chain's crustal root, which displaces mantle rock, must be less dense than the rock it displaces. It is evident, of course, that the reverse expression of the principle of isostasy is equally valid: Any mass deficiency at depth must be compensated by a mass excess at the surface; any growth or thickening of the crust, such as by the injection of magma into the crust from below, will result in surface uplift. From seismic studies of the crust it is known that areas that have long remained at sea level (and are thus presumed to be in isostatic balance) are underlain by "normal" continental crust 30 to 40 kilo-

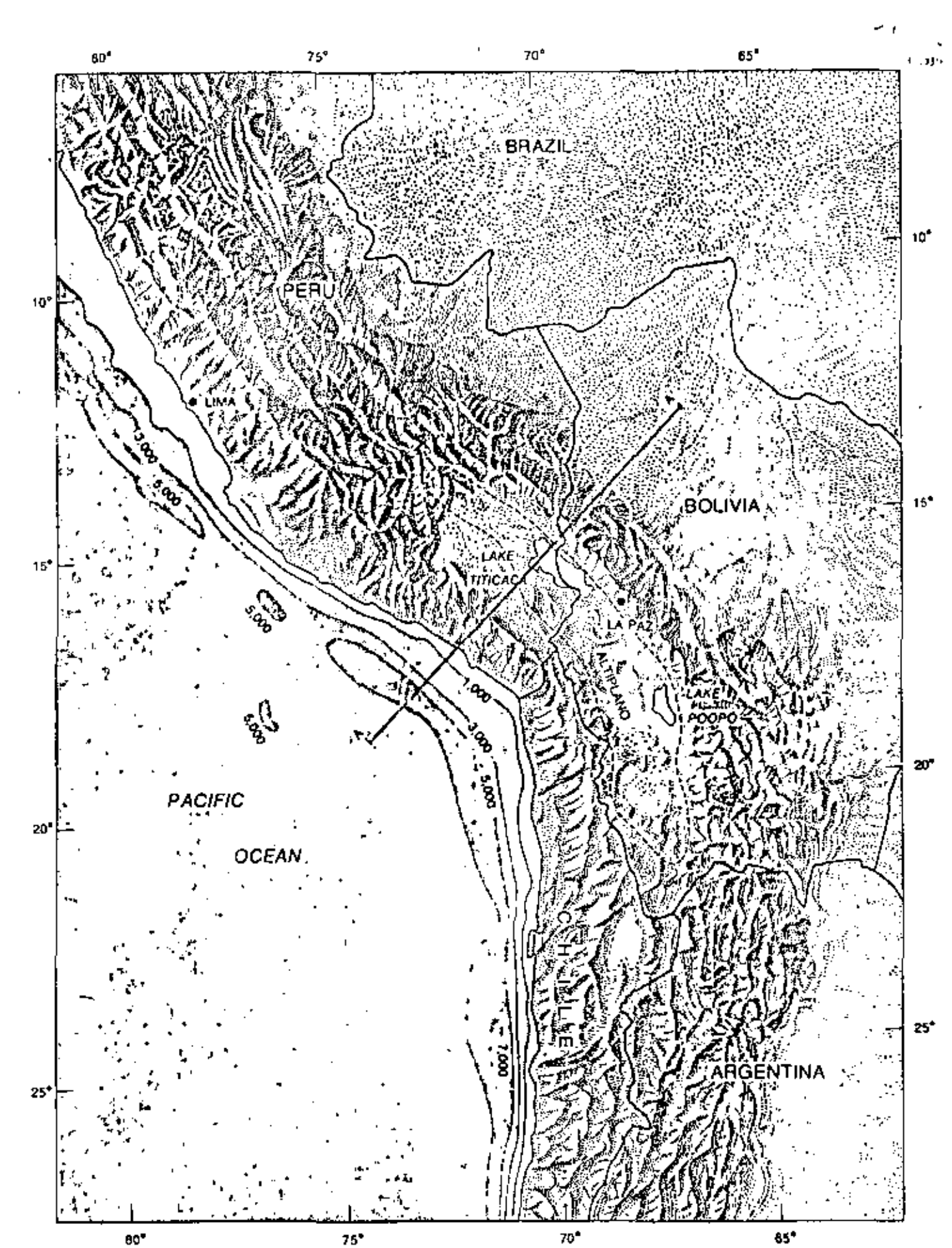

CENTRAL ANDES is a region where mountain-building forces appear to be still at work. North of Lima the Andes form a single belt of closely spaced mountain chains running parallel to the coast. South of Lima, however, the mountains branch, with the easterly fold belt running hundreds of kilometers inland and the westerly volcanic chain continuing parallel to the coast. Between these ranges lies the altiplano, a broad flat plain underlain by an enormous wedge of sedimentary debris eroded from the adjacent cordilleras. The two ranges merge again in northern Chile. Line *A*-*A'* shows region portrayed in several succeeding illustrations.

meters thick. Areas below sea level are underlain by thinner crust, those above by thicker crust. This fact becomes central when considering crustal evolution, since geology indicates that many of the highest parts of the Andes were once near sea level.

One additional line of geophysical evidence, seismic velocity, can be used for guessing the composition of the rocks within the Andean crust and the adjacent oceanic crust. In laboratory experiments the velocity of seismic waves in common rock types has been measured over a large range of temperature and pressure. Seismic velocities of rock in the lower oceanic crust are appropriate to rock of basaltic composition at that temperature and pressure. Interestingly, even though the pressure and the temperature in the crustal root under the Andes are much greater than in the lower oceanic crust, the seismic velocities of the rocks are the same. Yet it is known that if basaltic rock were subjected to the pressures and temperatures found in the deep continental crust, it would undergo metamorphic transformation to a rock type with higher seismic velocities and densities than are observed.

When different kinds of rock are examined in detail, only lighter crustal rocks, similar in composition to those observed at the surface, exhibit the appropriate seismic velocities at the temperature and pressure of the lower crust. This leads to the inference that the Andean crust is rather homogeneous vertically, the rocks in the Andean root being similar in composition to the volcanic and plutonic rocks that form the upper levels of the crust. Exceptions to vertical crustal homogeneity occur in the altiplano (the high plateau between the two great volcanic cordilleras) and the eastern cordilleras. Variations in seismic velocity show that the altiplano could be underlain by up to 30 kilometers of sedimentary rock, perhaps mixed with volcanic deposits, and that the eastern cordillera is underlain by at least five to 10 kilometers of sedimentary rock.

In order to reconstruct the progressive development of the Andean system one must turn to the information that can be read from the geologic record. Paleozoic sedimentary rocks laid down some 250 to 450 million years ago are among the oldest rocks of the central Andes. Time has not treated them kindly, and we find them collapsed and crumpled to form the fold mountains of the eastern ranges. These rocks, some 10 kilometers of monotonously repetitive muddy, sandy sedimentary beds, are called geosynclinal rocks [see "Geosynclines, Mountains and Continent-building," by Robert S. Dietz; SCIENTIFIC AMERICAN, March, 1972]; once they formed the quiet Paleozoic continental margin of western South America. (A modern analogue to the western seaboard of Paleozoic South America is the inactive continental margin of the east coast of North America, where a great sedimentary wedge some 250 kilometers wide and up to about 10 kilometers thick has formed between the continental shelf and the abyssal plain of the ocean.)

During Permian and Triassic time, between about 200 and 250 million years ago, the quiet of the western coast of South America gradually gave way to rumblings brought on by the incipient breakup of the supercontinent Pangaea and the onset of the plate-tectonic cycle that is still under way. The continental edge became unstable and the geosynclinal strata were warped and buckled upward. Magma, possibly derived from partial melting of deeply buried geosynclinal strata, invaded and poked through the sedimentary pile to form batholiths (bodies of intrusive igneous rock) at depth and volcanoes at the surface. The old volcanoes have long since disappeared, but volcanic rocks from this period are found interlayered with sedimentary beds. The intrusive rocks, probably representing the deeper feeder levels of the volcanoes, are commonly found today exposed in the cores of the eastern fold ranges, nestled among crumpled geosynclinal rocks.

About 190 million years ago, in earliest Jurassic time, the major axis of tectonic activity shifted several hundred kilometers oceanward, to the west. The lithosphere broke along the junction between the South American continent and the Pacific Ocean basin and the oceanic plate began its descent into the mantle under western South America. One can only speculate now on the reasons for the catastrophic rupture of the lithosphere, although there is some evidence that it may have been in response to the onset of sea-floor spreading along an ancestral East Pacific Rise. We do know that the South Atlantic Ocean had not yet begun to open and that South America and Africa were still one.

As the Pacific plate plunged under South America, andesitic magma welled to the surface, sweated out of the descending basaltic oceanic crust. Andesite is the characteristic volcanic rock of the Andes. It is richer in silica, and hence less dense, than basalt; its composition is what is termed intermediate, that is, between basalt and granite in chemical composition. These andesitic rocks of Jurassic age are well preserved all along the coastal regions of southern Peru and northern Chile. It is still somewhat problematical, however, whether the andesites were extruded on sialic (continental, shallow-water) crust or simatic (oceanic, deep-water) crust. The lavas themselves appear to have been extruded below water, since many have been highly altered by seawater.

One might infer from this that the volcanic arc of the central Andes began as an island arc in the ocean off the coast of ancestral southern Peru and northern Chile [*see illustration on next two pages*]. Yet the picture of the Jurassic arc is not simple, because Jurassic volcanic rocks in southern Peru are wedged in among crystalline metamorphic rocks at least 400 million years old. Just what these remnants of ancient sialic crust are doing some 300 kilometers west of the currently exposed geosynclinal rocks of the Paleozoic continental margin is not known. The presence of sialic rocks does not necessarily imply, however, that the Jurassic arc formed on continental crust. The rocks could be part of a Paleozoic microcontinent or peninsula that lay to the west of the South American coastline. Or they could be sialic flotsam swept into and plastered to the edge of South America, buoyant debris scraped from the top of the oceanic plate as it dived down at the trench.

These difficulties aside, formation of the Andean volcanic arc was well in progress during Jurassic time. The fact that Jurassic volcanic rocks are still widely preserved indicates that the Jurassic arc never stood much above sea level and consequently suffered little erosional destruction. Furthermore, it appears that the entire region to the east of the Jurassic arc, extending as far east as and encompassing the area of the present-day Andes, must have been near sea level, since marine sedimentary deposits are mapped throughout the area. This observation is important because it shows that the crust of the Andes was still thin, probably no more than 35 kilometers thick.

I have noted that the Jurassic arc formed during a period when South America and Africa were still a single continent. Dating of the magnetic pattern of the South Atlantic by Walter C. Pitman III and others at the Lamont-Doherty Geological Observatory of Columbia University indicates that it was only about 135 million years ago that the South Atlantic began to open by spreading along the Mid-Atlantic Ridge. For-

mation of the Jurassic arc inaugurated the impressive series of mountain-building episodes that produced the Andean belt, but it was not until sometime after the break-off of South America from Africa that Andean orogeny began in earnest.

About 100 million years ago, during Cretaceous time, a second major volcanic arc began to form parallel to and continentward of the Jurassic arc. (My treatment of Andean development as a series of a few distinct episodes is an oversimplification, but it serves to trace the growth of the mountain system; igneous activity has actually been rather continuous from about 200 million years ago to the present day.) The lavas of this volcanic chain were extruded above sea level—clear evidence that the volcanoes developed astride continental crust. Activity along the Cretaceous arc reached maximum intensity about 50 to 60 million years ago with the invasion of the crust by massive amounts of magma. The invading magmas crystallized to form enormous batholiths that now lie exposed all along the western flanks of the western ranges.

The contemporaneous volcanoes, which must have towered far above sea level, have long since been stripped off by erosion, exposing the intrusive underpinnings of the volcanic arc: the Andean batholith. In some areas, such as southern Peru, erosion has not eaten as deeply, so that small batholiths are mantled by volcanic debris of similar age and composition. These small intrusive bodies are probably parts of the feeder pipes that supplied the volcanoes. In time the volcanic roofs of the batholiths will be further stripped away, leaving only the deep-seated intrusive foundation of the vanished Cretaceous volcanic arc exposed to view.

The crustal swelling that accompanied the invasion of magma produced major traumas in the easily deformed geosynclinal rocks of the eastern ranges. Upwelling magmas dilated the crust along the line of the Cretaceous arc. The geosynclinal rocks were alternately sloughed off and pushed aside by the growing orogenic welt and were crumpled and thrown up into the fold mountains of the eastern ranges. Enormous volumes of sediments were eroded from the flanking mountain ranges and dumped into the intervening altiplano basin; some places in the altiplano received up to seven kilometers of sediment in Cretaceous time alone.

It is significant that the Cretaceous arc lies on the continent side of the older Jurassic arc because it has usually been supposed that, as debris from the oceanic crust is stuffed under volcanic arcs, the trench and arc will migrate oceanward. Quite the contrary is true in the Andean region: during the course of Andean evolution the axis of the volcanic arc has marched ever inland, away from the sea. Even on a fine scale one finds successive intrusions of the Andean batholith shifted continentward. One can only speculate on the reasons for the eastward mi-

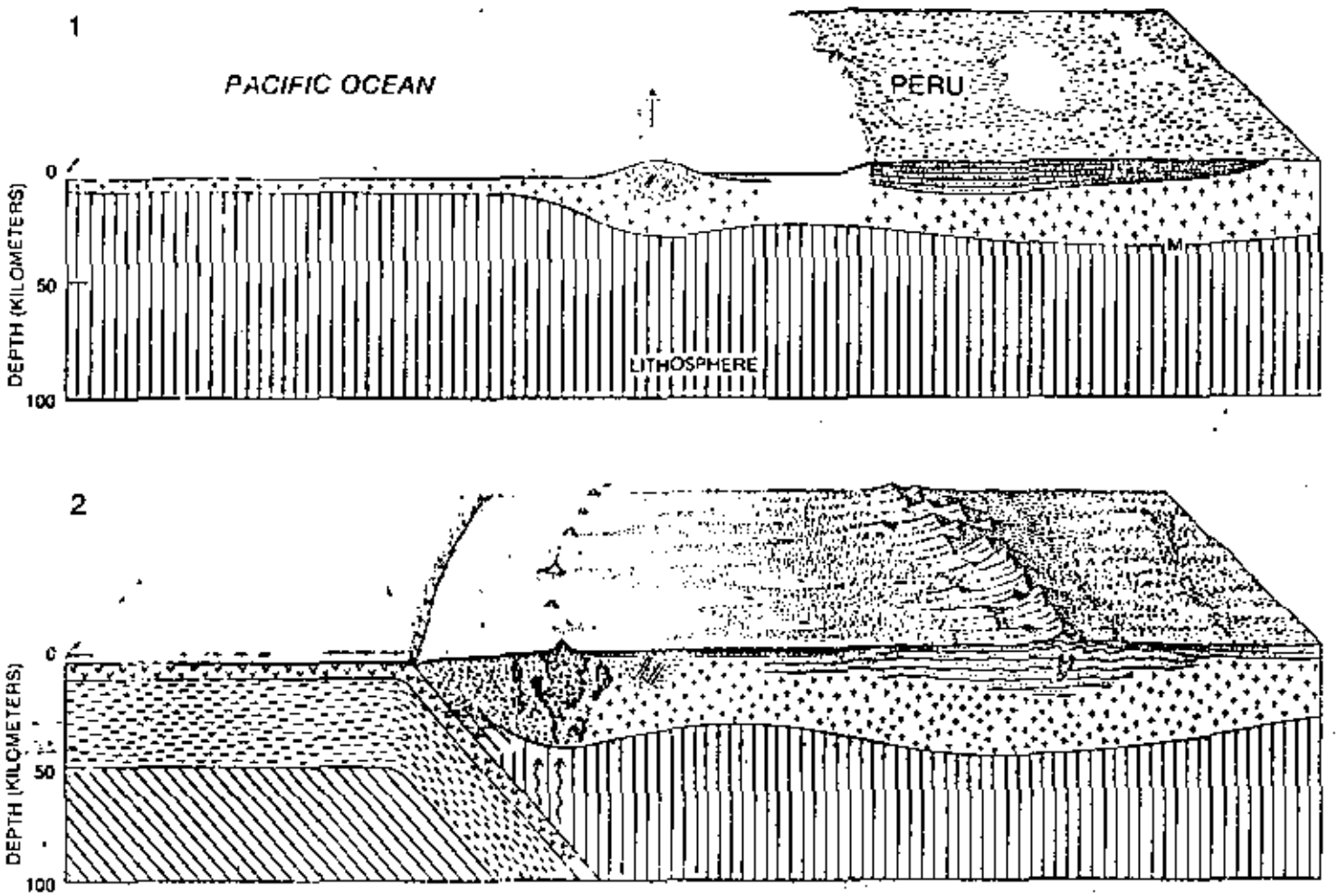

ANDEAN EVOLUTION is shown in views northwesterly from line *A–A'* in map on page 64. Late in Paleozoic period (*1*), some 250 million years ago, sedimentary deposits blanketed the present coastline, and there were no mountains. In Triassic and Jurassic times (*2*), about 200 million years ago, underthrusting of the lithosphere began, buckling the sedimentary rocks and pushing them upward

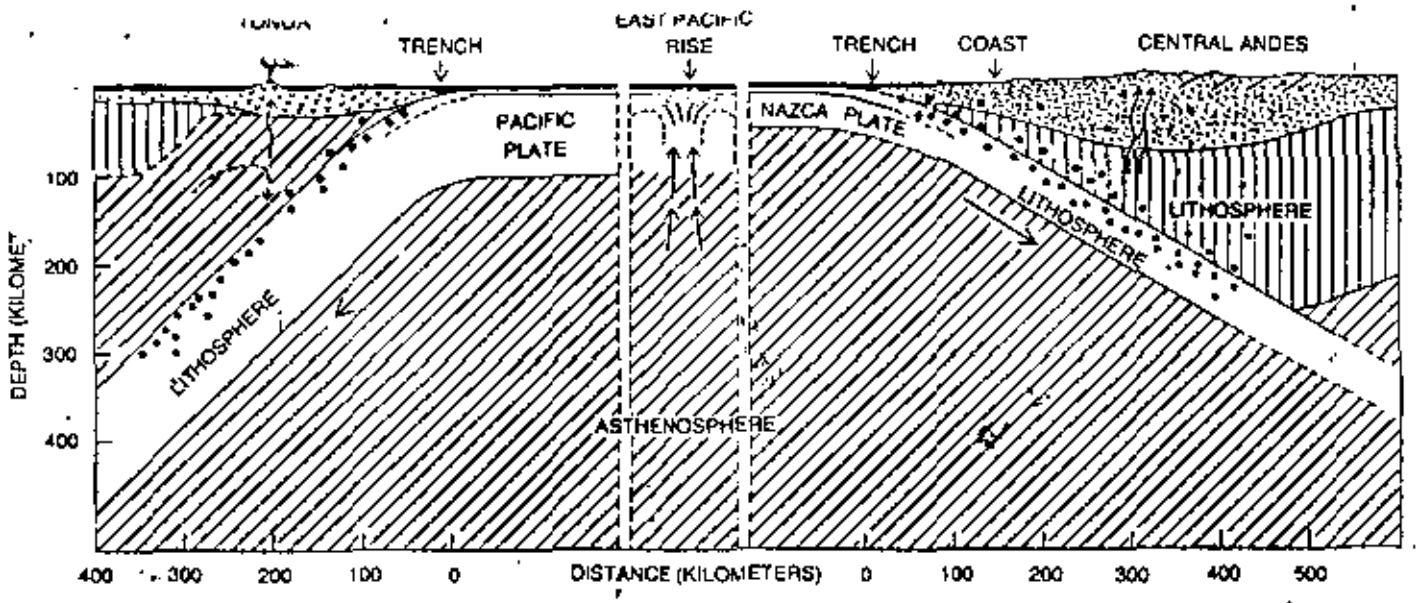

STRUCTURAL CONTRASTS between the Andean volcanic arc and the Tonga-Fiji island arc account for differences in physiographic settings and earthquake distributions. In the Tonga arc most earthquakes occur within the descending slab, which has mobile asthenosphere material above it and below it. There is also evidence of minor sea-floor spreading west of the arc. These observations suggest that drag from the sinking plate causes convective overturn (*arrows*) in the overlying asthenosphere, which in turn causes the spreading behind the arc. Earthquakes in the Andes are not confined to the descending plate, nor is there any evidence of crustal spreading east of the volcanic arc. Evidently the thick lithosphere under the leading edge of South America prevents convection and secondary spreading, and the forces generated by the descending slab produce earthquakes rather than convection above the slab. The intensity of earthquake activity under the Andes is indicated by the density of dots. Few dots show lighter activity.

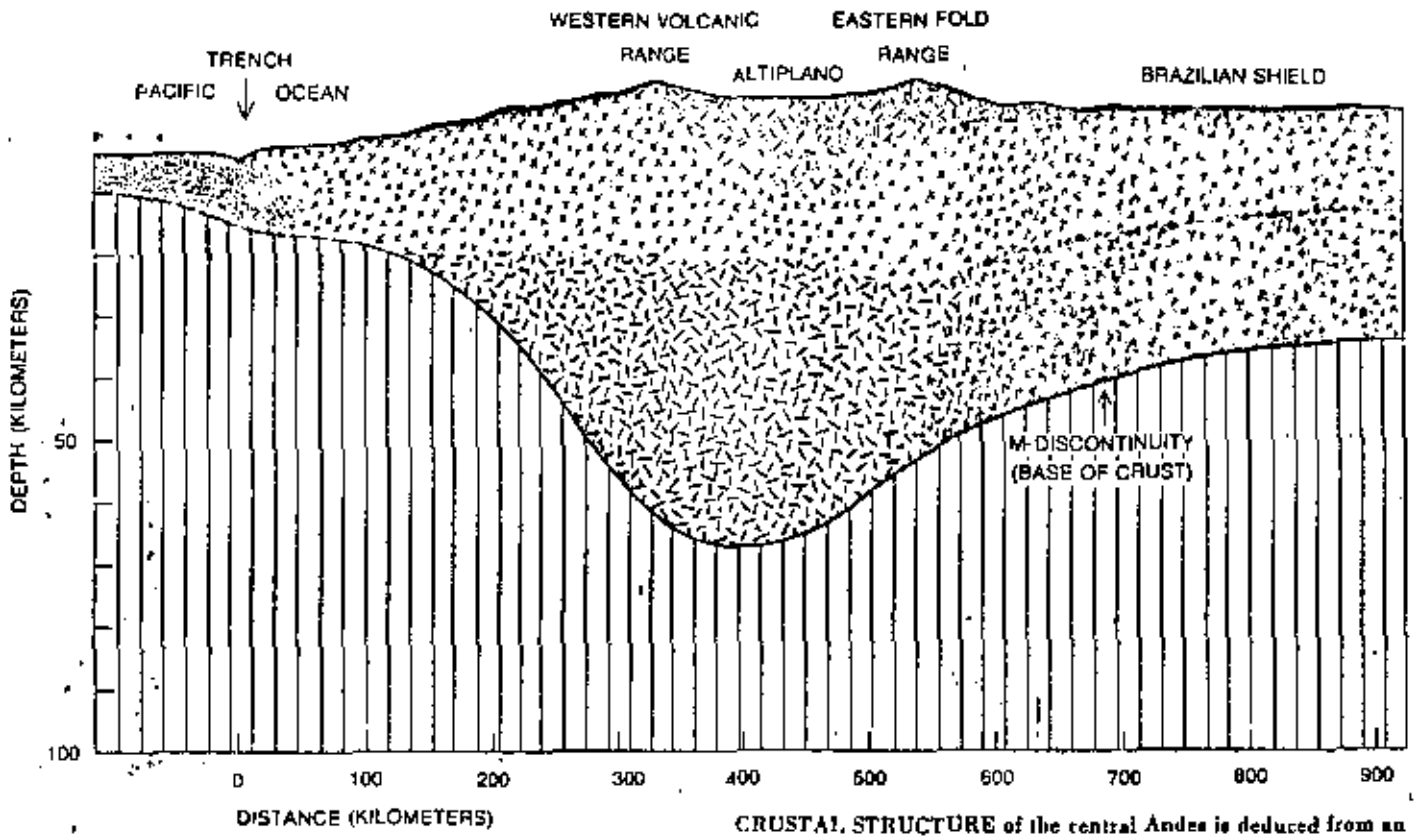

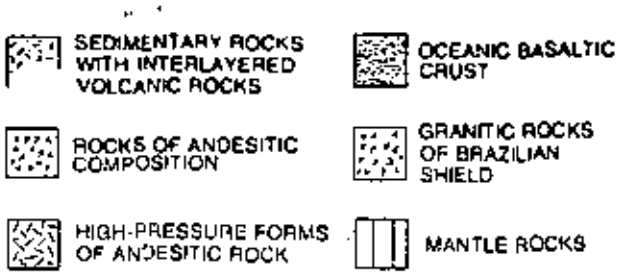

CRUSTAL STRUCTURE of the central Andes is deduced from an analysis of the propagation of seismic waves through the various kinds of rock underlying the region. Light color indicates a seismic velocity of about five kilometers per second, medium color a velocity of about six kilometers per second and dark color about 6.6 kilometers per second. The thickest parts of the crust underlie the western cordillera and the western part of the altiplano, where large quantities of magma have entered the crust from below. The crust of the eastern fold range has been crumpled and compressed to a thickness of 50 kilometers. Some 30 kilometers of sediment eroded from earlier flanking mountains underlies the altiplano.

gration, but I shall return to this question when I consider the origins of the volumes of magma that have built the Andean crust.

The present-day Andean volcanic edifice began to emerge about 15 million years ago. In northern Chile and southern Peru huge volumes of silicic volcanic ash exploded out of fissures and flowed out from eruptive centers, eventually to blanket hundreds of thousands of square kilometers. Even now, when most of these ash deposits have long since been eroded away, it has been estimated that their remnants cover some 100,000 to 150,000 square kilometers to an average depth of 500 meters. The ash eruptions continued steadily until about four million years ago, when they ended abruptly and were followed closely by the outpouring of andesitic lavas from volcanic vents. These later lavas form the great stratovolcanoes, some still active, that dominate the Andean chain and rise to well over six kilometers in the central Andes.

The massive influx of magma into the crust under the modern Andean volcanic crest swelled the crust and produced extensive folding and thrust-faulting in the altiplano and the eastern ranges. The geosynclinal sediments were further pushed aside by the expanding magmatic welt and the eastern ranges were jammed up to form narrow, high mountain chains. Sedimentary debris flooding in from both the eastern and the western range during Tertiary time piled up in the altiplano to thicknesses as great as 15 kilometers. We are now witnessing at least a temporary waning of activity, and through the relaxation of compressive stresses some extensional features have formed in the altiplano. Lake Titicaca is a notable site of one such feature: a graben, a long depression between fault lines.

So far I have considered Andean evolution from the point of view of surface geology, describing the inland march of the volcanic arc, the resulting progressive crumpling of the Paleozoic geosyncline and the gradual uplift of the Andean chain. I have not yet inquired in detail into the growth of the crust and the origin of the crustal rocks below the surface.

Classical concepts of mountain building, formulated long before the advent of plate tectonics, held that geosynclinal rocks formed in elongated basins of deep subsidence and that these basins were necessary precursors of later mountain belts, which were presumed to form through the deformation and melting of the thick geosynclinal sedimentary strata. The tectonic mechanics whereby these sedimentary rocks were melted and deformed was always a mystery, as was the origin of the subsiding basin itself. A number of problems are posed by classical concepts of geosynclines when they are applied to the central Andes. The crust under the volcanic crest is more than 70 kilometers thick, and yet no sedimentary basin can ever sit for long on crust more than about 35 or 40 kilo-

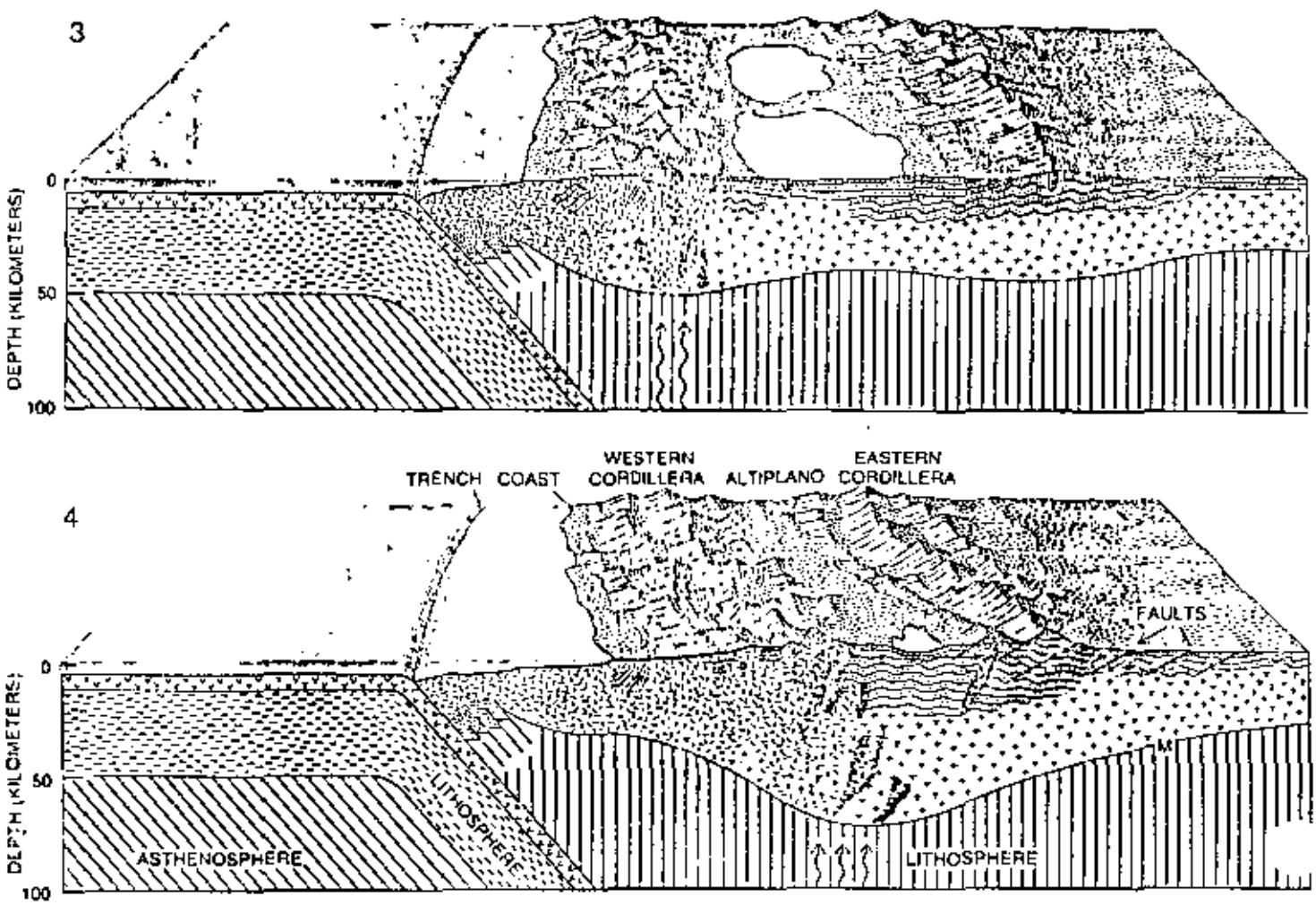

and eastward. Rising magma from the descending oceanic plate formed an arc of volcanoes in the coastal waters of western South America. Some batholiths, or bodies of intrusive igneous rock, formed in the sedimentary layers of the eastern ranges. In Cretaceous and early Cenozoic times (130 to 60 million years ago) a second volcanic arc began to form eastward of the Jurassic arc. Upwelling magma swelled the crust, pushing aside the ancient sedimentary rocks, which crumpled to form the fold mountains of the eastern cordillera. Material eroded from these mountains poured into altiplano region. Formation of the present volcanic range began 10 to 15 million years ago, reaching by Pliocene or Pleistocene time (5 million years ago, the present structure.

meters thick without bobbing above sea level and thus ending sedimentation.

If remobilized geosynclinal rocks are to make up the crust of the western cordillera, they must therefore have undergone twofold foreshortening to produce a doubling in crustal thickness. Yet in the volcanic chain we find few tectonic patterns such as thrust faults and tightly compressed folds that would suggest crustal shortening. On the contrary, studies of seismic earthquake mechanisms and modes of faulting indicate that the deformational style is extensional: the earth under the volcanic arc is swelling rather than contracting. Clearly knowledge of the Andean crust could not be easily mated with classical concepts of geosynclinal mountain building.

Only the advent of plate-tectonic theory has adjusted this unhappy mismatch between mountains and mountain-building theory, and it has done so by providing mountain-building mechanisms and processes that bear a clear relation to the Andean orogenic belt. It now appears to be evident (although some rearguard scientific battles still rage) that the geosynclinal sedimentary rocks are simply victims trapped at the continental margins and caught up in the tectonic processes that accompany subduction. The geosynclinal wedge must participate in, but can never be a prime mover of, the mountain-building process itself. If this analysis is correct, it follows that the magmas that built the central Andean volcanic arc were derived from below the crust and that the great volumes of rock that solidified from these magmas have produced crustal thickening and massive uplift of the arc.

We are left, then, with the question of the sources of magma below the crust. There are two principal possibilities: partial melting of the dense mantle rocks in the wedge between the crust and the top of the underthrust plate, or partial melting of the basalts and sediments of the oceanic crust riding down into the mantle on the lithospheric conveyor belt. Most observations argue against a mantle source for the andesitic rocks of the Andes. If the thickness of the crust in the volcanic arc had been doubled by the addition of magma from below, then some 20 percent partial melting of mantle rock between the crust and the subduction zone would be required to provide the necessary volume of additions to the crust. Experimental studies of the partial melting of probable mantle materials do not readily support the extraction of this quantity of andesitic magma from dense mantle rocks. A source in the mantle for the Andean rocks seems possible only if mantle flow provides a constant supply of rock undepleted in its low-melting-point fraction. Yet we have already seen that the upper mantle under the Andes is rigid lithosphere to a depth of from 200 to 300 kilometers, and therefore probably quite immobile.

An alternate proposition, that the magmas are derived from the descending oceanic crust, is currently most in favor and is a theory that I believe provides a viable explanation of Andean crustal genesis. Rocks of the oceanic crust have melting temperatures several hundred degrees Celsius below those of mantle rocks. As the cold oceanic crust descends into the mantle it is heated by the hot mantle in which it is enveloped, and at depths of about 100 to 150 kilometers the basaltic crust may well reach its melting point. The partly melted fraction of oceanic crust would be less dense than either the parent rock or the surrounding mantle rocks and would migrate upward into the crust. Most of the magma would be trapped and would solidify at the lower and intermediate levels of the crust; only a small fraction would ever make its way to the surface to come out through volcanoes, and so the volcanic pile on the earth's surface represents only a small part of the total increase in crustal volume.

A phenomenon related to the origins of the crustal rocks is the eastward migration of igneous activity. Assuming that the rocks originate through partial melting of the descending plate, there are a number of ways to explain the migration. If, for example, the depth in the earth at which melting occurs remains constant, then either a progressive decrease in the dip of the descending plate or a progressive continentward migration of the trench could cause an eastward migration of igneous activity. Or, if the position of the descending plate remains constant, the depth at which melting occurs on the slab may increase with time, thus pushing the source of magma deeper and eastward. A critical consideration here is the position and dip of the descending plate since the onset of subduction. Has the dip of the Benioff zone changed or has the trench migrated over the past 200 million years?

Examination of the chemistry of the rocks themselves provides a partial answer to this question. William R. Dickinson of Stanford University and Trevor Hatherton of the New Zealand Department of Scientific and Industrial Research have demonstrated a clear positive correlation between the amount of potash (K_2O) in modern volcanic rocks and the depth to the underlying Benioff zone. For particular rock types such as andesite collected from island arcs all over the world, the potash content is a more or less linear function of the depth to the underlying Benioff zone. By the inverse corollary of this relation one should be able to estimate the depth to defunct Benioff zones by measuring the potash content in older rocks.

We have just begun to apply this technique in the Andes. The data are by no means complete, but as we proceed from rocks of the Jurassic arc to those of the Cretaceous arc and on to those of the modern arc we find a progressive increase in potash content. This progressive increase, of course, is also correlated with increasing depth to the present Benioff zone. We find similar variations for strontium content, another chemical variable that has been shown to exhibit a positive correlation with the depth to the Benioff zone.

It is therefore possible to speculate with some basis in fact that the position of the Benioff zone has not changed greatly with time. If that is so, the eastward migration of the arc over the past 200 million years implies that the position in the mantle at which the oceanic crust melts has been pushed to progressively greater depths. It may well be that in the Andes the continued underthrusting of the cold oceanic slab into the mantle under the continent has gradually cooled the surrounding mantle rocks, so that the temperature at which melting occurs in the descending plate is attained only at greater and greater depths. If such a process accounts for the migration of igneous activity ever inland from the trench, then as long as subduction continues under the central Andes the volcanic chains of the future will impinge ever more on the old geosynclinal rocks, driving them even farther inland.

One day, however, Andean orogeny will end. The volcanic chain will stop growing and the inevitable destruction by erosion will set in. To reduce the Andes to sea level, some 35 kilometers of crust will have to be stripped away, exposing the center of the earth's crust. The sedimentary debris removed from the mountain edifice will be dumped on the continental shelf, the continental slope and the oceanic abyssal plain of the Pacific. There the sediments will pile up to await the next tectonic cycle, in which they will be crumpled, buckled upward and swept aside to give way to the next great volcanic mountain belt.

The following Fig. gives 12 plates. The relative displacements at selected points are given in the following Table.

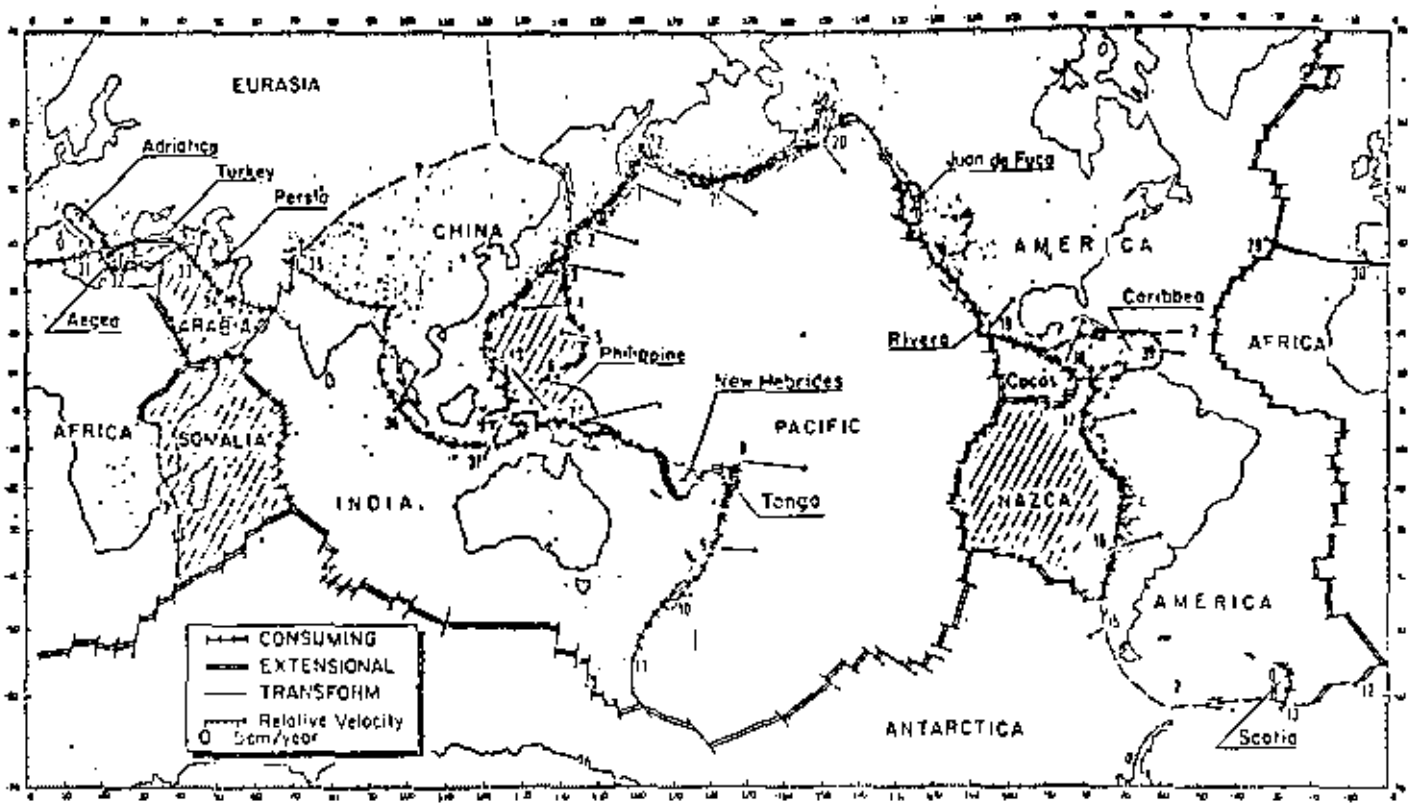

Fig.27. Present worldwide plate kinematic pattern at the surface of the earth. Seismicity after Barazangi and Dorman (1969). In addition to the six large plates used by Le Pichon (1968), six additional plates (shown hachured) are used in a twelve-plate model after Morgan (1971b). Vectors of differential motions are shown at selected points. See text and Table IV, V.

TABLE 1 38

Computed differential movements along consuming plate boundaries (except for southwest Atlantic) as given in Fig.27 using Morgan's (1971b) poles

No.	Lat.	Long.	Plates in Le Pichon (1968)	Plates in Morgan (1971b)	Rate (cm/year)	Azimuth	Location
1	51	160	EU/PA	AM/PA	7.2	114	Kurile Trench
2	43	148	EU/PA	AM/PA	7.5	107	Kurile Trench
3	35	142	EU/PA	EU/PA	8.6	101	Japan Trench
4	27	143	EU/PA	PA/PH	7.5	265	Japan Trench
5	19	148	EU/PA	PA/PH	4.9	282	Mariana Trench
6	11	142	EU/PA	PA/PH	2.3	243	Mariana Trench
7	−3	142	IN/PA	IN/PH	14.5	78	New Guinea
8	−13	−172	IN/PA	IN/PA	9.9	97	north Tonga Trench
9	−34	−178	IN/PA	IN/PA	5.8	95	south Kermadec Trench
10	−45	169	IN/PA	IN/PA	3.5	72	south New Zealand
11	−55	159	IN/PA	IN/PA	2.6	29	Macquarie Island
12	−58	−7	AM/AN	AM/AN	1.1	255	southwest Atlantic
13	−61	−26	AM/AN	AM/AN	1.3	232	south Sandwich Trench
15	−50	−75	AM/AN	AM/AN	3.1	240	Cape Horn
16	−35	−74	AM/AN	NZ/AM	8.7	74	south Chile Trench
17	−4	−82	AM/AN	NZ/AM	8.8	77	north Peru Trench
18	7	−79	AM/AN	NZ/AM	8.3	75	Panama Gulf
19	20	−106	AM/AN	CO/AM	6.4	39	north Middle America Trench
20	57	−150	AM/PA	AM/PA	5.6	144	east Aleutian Trench
21	50	−178	AM/PA	AM/PA	6.9	126	west Aleutian Trench
22	54	162	AM/PA	AM/PA	7.0	115	west Aleutian Trench
29	40	−31	AF/EU	AF/EU	1.0	294	Azores
30	36	−6	AF/EU	AF/EU	1.6	345	Gibraltar
31	38	15	AF/EU	AF/EU	2.3	358	Sicily
32	35	25	AF/EU	AF/EU	2.6	6	Crete
33	37	45	IN/EU	AR/EU	4.3	13	Turkey
34	30	53	IN/EU	AR/EU	4.9	22	Iran
35	35	72	IN/EU	IN/EU	4.5	4	Tibet
36	0	97	IN/EU	IN/EU	6.9	31	west Java Trench
37	−12	120	IN/EU	IN/EU	7.1	28	east Java Trench
38	11	−86		CO/CR	7.4	24	Middle America Trench
39	15	−61		CR/AM	4.0	97	Lesser Antilles
40	13	126		EU/PH	9.5	140	Philippine Trench

was determined by Larson and Chase (1970) from a favorable distribution of fracture zones. The linear rate of separation increases very rapidly to the south and is as high as 7.5 cm/year of half-rate near the equator (Larson and Chase, 1970). The Galapagos triple junction at the intersection of the Galapagos and the East Pacific ridges, and the Easter Island triple junction at the intersection of the Chile and East Pacific ridges provide important checks of the kinematic determinations (Hey et al., 1972). The Caribbean plate, which is adjacent to the Cocos plate, is also well-defined by the seismic activity along its borders, except along the southwestern border in Colombia (Molnar

EARTHQUAKE PREDICTION

Note:

- Most earthquakes occur on the plate boundaries.
- Plate movement does not change in short time.
- All areas on the boundaries of plates are potentially sites of earthquakes.
- Recurrence period of large earthquakes ($M \geq 7.0$) along segments of boundary is highly variable (from 30 to 400 yrs or more).
- If the recurrence time is approximately known (e.g. in Mexico it appears to be from 30 to 60 years) the likelyhood of a having an earthquake is directly proportional to the time elapsed after the last large earthquake in the area.
- Kelleher et.al. (1973, J. Geophys. Res.,) basing on Fedotov, Mogi and Sykes's work prepared a 'seismic gap' map of the circum Pacific belt. The areas, which had not ruptured in the last 30 years were called a seismic gap. Recently McCann et.al (1979, in press) have updated the seismic gap map. In the following 3 figures of seismic gaps (Middle America, S. America, and the Caribean) are given. For middle America the gaps are marked ; for the other 2 regions these gaps could be inferred from the map.
- Seismic gap maps are useful in deciding where earthquake prediction effort should be channelized. It may be called part of long range prediction.

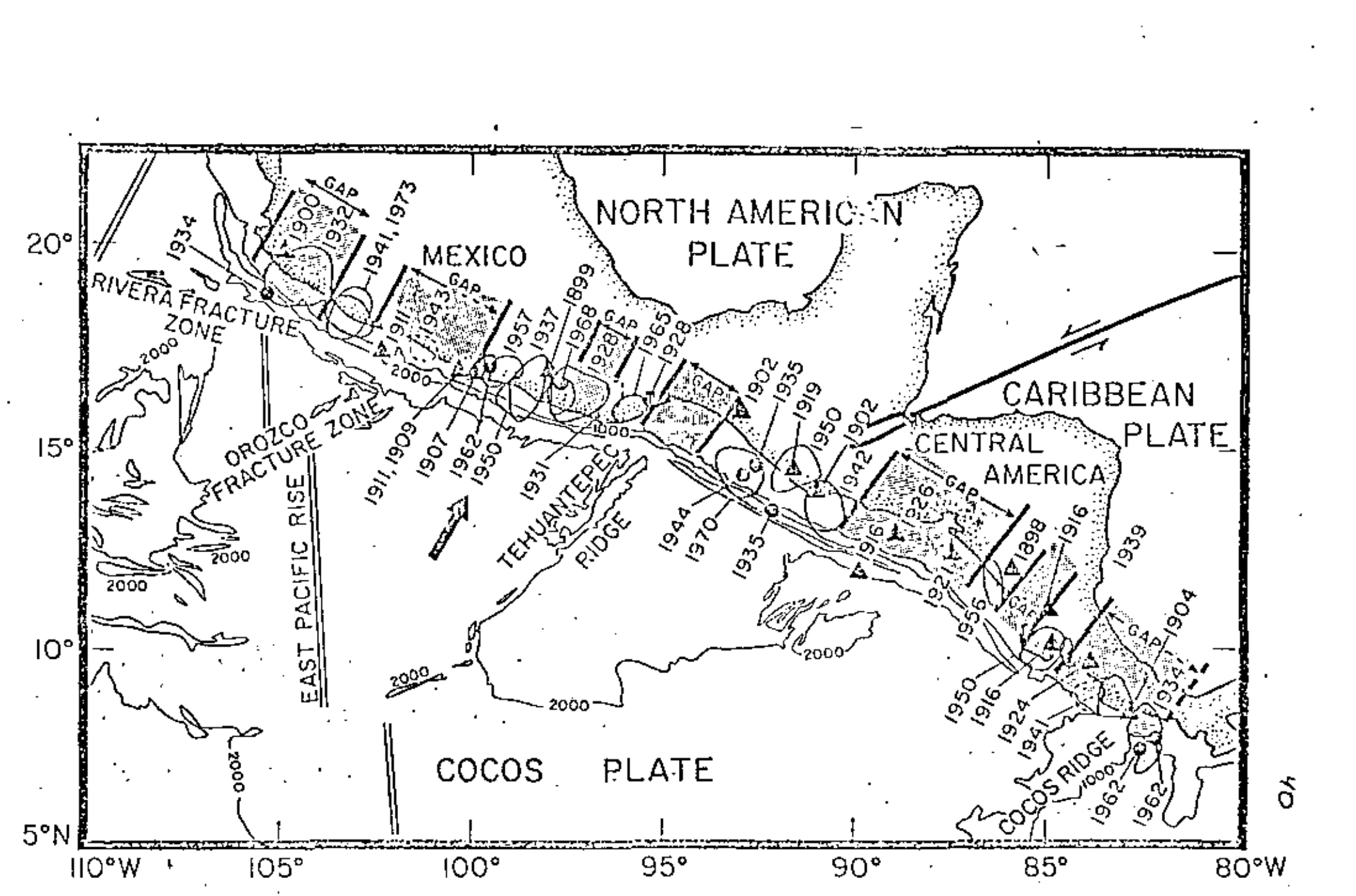
NORTH AMERICAN PLATE
MEXICO
CARIBBEAN PLATE
CENTRAL AMERICA
COCOS PLATE
RIVERA FRACTURE ZONE
OROZCO FRACTURE ZONE
EAST PACIFIC RISE
TEHUANTEPEC RIDGE
COCOS RIDGE
GAP
1900
1932
1934
1941, 1973
1911
1943
1957
1937
1899
1968
1928
1965
1928
1902
1935
1919
1950
1902
1942
1926
1916
1898
1916
1939
1956
1950
1916
1924
1941
1904
1934
1962
1962
1911, 1909
1907
1962
1950
1931
1944
1970
1935
2000
1000
20°
15°
10°
5°N
110°W
105°
100°
95°
90°
85°
80°W

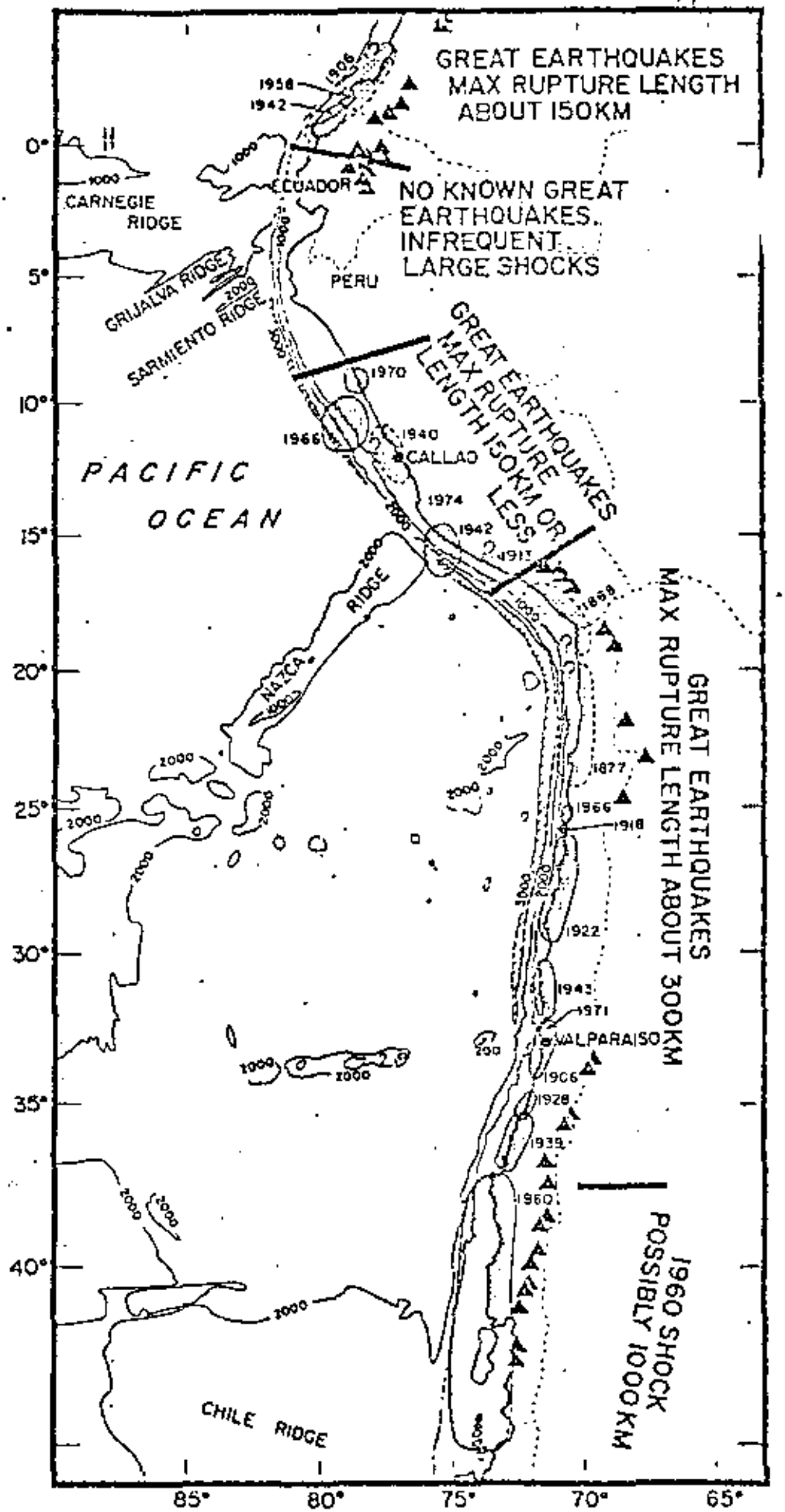
GREAT EARTHQUAKES
MAX RUPTURE LENGTH
ABOUT 150KM
1958
1942
1906
ECUADOR
NO KNOWN GREAT
EARTHQUAKES.
INFREQUENT
LARGE SHOCKS
CARNEGIE
RIDGE
GRIJALVA RIDGE
SARMIENTO RIDGE
PERU
GREAT EARTHQUAKES
MAX RUPTURE
LENGTH 150KM OR
LESS
1970
1966
1940
CALLAO
1974
1942
1911
PACIFIC
OCEAN
NAZCA
RIDGE
1868
GREAT EARTHQUAKES
MAX RUPTURE LENGTH ABOUT 300KM
1877
1966
1918
1922
1943
1971
VALPARAISO
1906
1928
1939
1960
1960 SHOCK
POSSIBLY 1000 KM
CHILE RIDGE
0°
5°
10°
15°
20°
25°
30°
35°
40°
85°
80°
75°
70°
65°

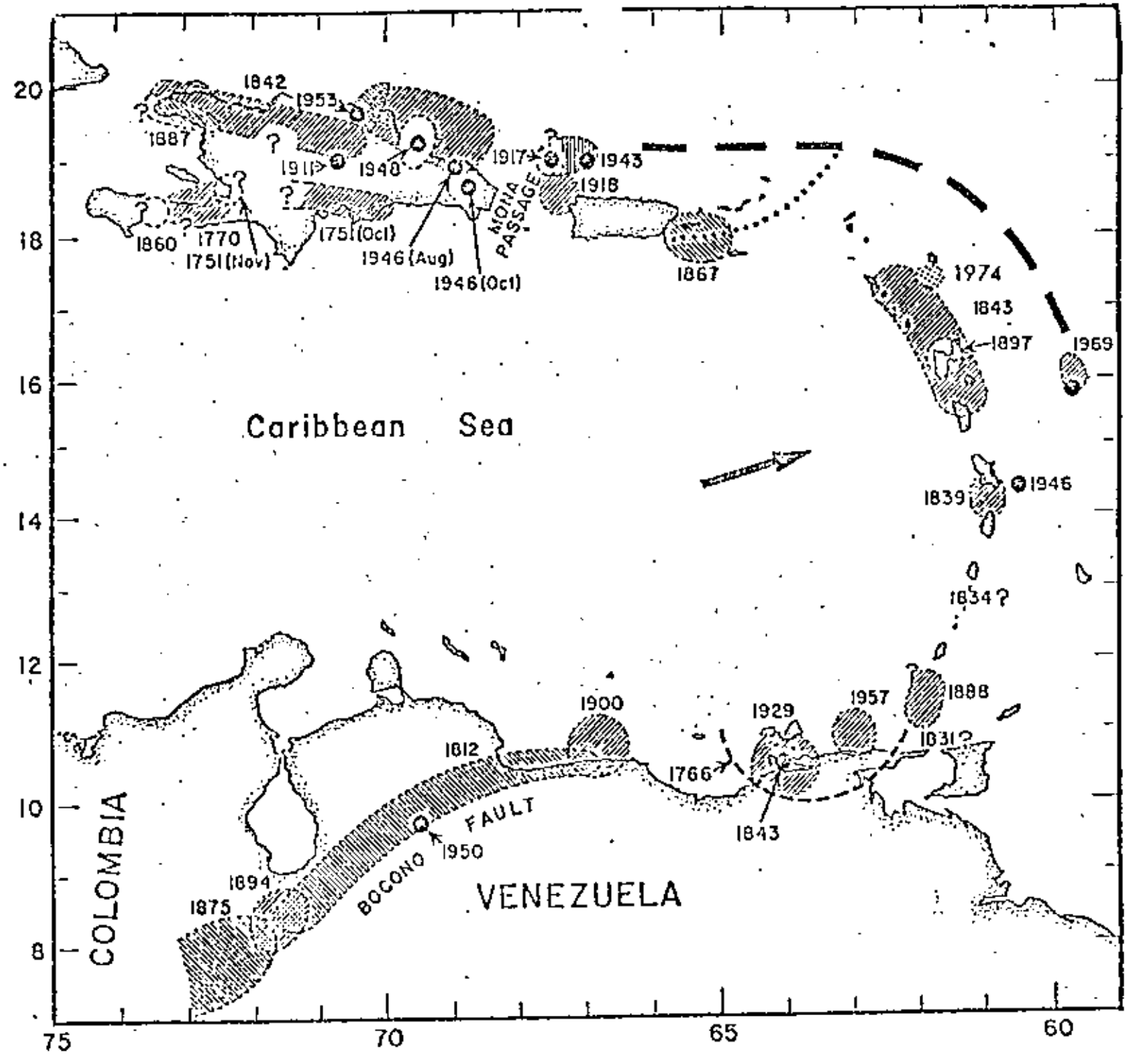
Caribbean Sea
COLOMBIA
VENEZUELA
MONA PASSAGE
BOCONO FAULT
1842
1953
1887
1911
1940
1917
1943
1918
1860
1770
1751 (Nov)
1751 (Oct)
1946 (Aug)
1946 (Oct)
1867
1974
1843
1897
1969
1946
1839
1834?
1900
1929
1957
1888
1831?
1812
1766
1843
1950
1894
1875
20
18
16
14
12
10
8
75
70
65
60

The monitoring of a seismic gap for precursors of an earthquake involves measurements of anomalous changes in geophysical and geochemical fields. Two models (dilatancy - diffusion model and dilatancy - - instability model) attempt to explain some of the observed precursory data. It is difficult to distinguish between the two models since data are few. It may be that the attempts to find a single model may be doomed ; regions may exhibit different anomalous behaviour. The following reprint by Press summarizes the state of knowledge on earthquake prediction.

SCIENTIFIC AMERICAN
Established 1845 May, 1975 Volume 232 Number 5

Earthquake Prediction

Recent technical advances have brought this long-sought goal within reach. With adequate funding several countries, including the U.S., could achieve reliable long-term and short-term forecasts in a decade

by Frank Press

The forecasting of catastrophe is an ancient and respected occupation. It is only in recent years, however, that earthquake prediction has parted company with soothsaying and astrology to become a scientifically rigorous pursuit. At present hundreds of geophysicists and geologists, mainly in the U.S., the U.S.S.R., Japan and China, are engaged in research with earthquake prediction as the direct goal. Most of these investigators believe that the goal is attainable. Some are more pessimistic. A few actually think that the side effects of prediction might be worse than the benefits and that the goal should be abandoned. Research on earthquake prediction therefore exemplifies many of the problems that face modern society: technology assessment, the design and organization of a massive mission-oriented project, the competition for funds and the political niceties of an undertaking involving admittance to previously inaccessible regions of another country.

I share the view of most of my colleagues that earthquake prediction is a highly desirable goal. Because of the large increase of population density in the earthquake-prone sections of the U.S., the potential loss from an earthquake as strong as the San Francisco shocks of 1906 could be as high as tens of thousands dead and hundreds of thousands injured, with property damage measured in the billions of dollars. A catastrophe on this scale would be unprecedented in the history of the country, yet it is an event that most seismologists expect to occur sooner or later. The seismic-risk map of the U.S. shows the most probable locations of strong earthquakes [*see illustration at left*]. The map is based primarily on earthquake history; it does not take into account the frequency of occurrence. Hence Boston is shown to be as risky as Los Angeles (mainly because of a single great quake that occurred in the Boston area in 1755), even though tremors are 10 times less frequent on the East Coast than on the West Coast. It is a sobering thought that a third of the nation's population live in the two regions of highest risk.

Preliminary results of current investigations indicate that predictions of strong earthquakes could be made many years in advance. It also appears likely that a method for making short-term

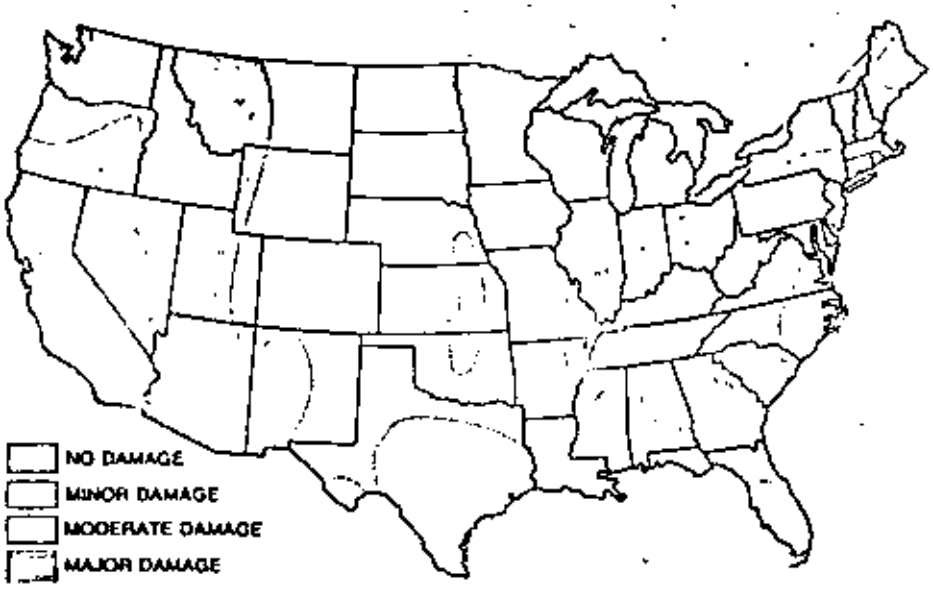

RISK OF DAMAGE FROM EARTHQUAKES is assessed in a broad, climatological sense in this map of the U.S., based on information compiled by the Coast and Geodetic Survey. The map is based primarily on historical records of destructive earthquakes and does not take into account the fact that earthquake tremors are much more frequent in the Western states than elsewhere. A third of the nation's population live in two darkest-colored regions.

predictions, as short as weeks or even days, will be developed. With this dual capability it should become possible to devise a remedial strategy that could greatly reduce casualties and lower property damage. For example, the long-range prediction of a specific event could spur the strengthening of existing structures in the threatened area and motivate authorities there to enforce current building and land-use regulations and to revise such codes for new construction. A public-education campaign on safety procedures could also be instituted.

Short-term prediction could mobilize disaster-relief operations and set in motion procedures for the evacuation of weak structures or particularly flammable or otherwise hazardous areas. The shutdown of special facilities, such as nuclear power plants and gas pipelines, and the evacuation of low-lying coastal areas subject to tsunamis, or "tidal waves," could also follow a short-term forecast.

The problem of how one communicates an earthquake prediction to the public and the consequences that flow from such warnings (and from possible false alarms) are now being examined. Research into the social aspects of earthquake prediction will presumably advance along with progress toward a physical solution of the problem. For these reasons most experts consider the ability to predict earthquakes to be justifiable on both humanitarian and economic grounds.

With the advent of the theory of plate tectonics the distribution of earthquake belts around the world became understandable. According to this view, the earth's lithosphere, or outer shell, is divided into perhaps a dozen rigid plates that move with respect to one another. Most of the large-scale active processes of geology—vulcanism, mountain-building, the formation of oceanic trenches, earthquakes—are concentrated at or near plate boundaries [*see illustration on next two pages*]. It is easy to see why stresses build up along plate boundaries, where the relative motion of the plates is resisted by frictional forces. When the stress increases to the point where it exceeds the strength of the rocks of the lithosphere or overcomes the frictional forces at the boundary of a plate, fracturing occurs and an earthquake results. The plate-tectonic model combined with earthquake statistics already makes it possible to predict earthquakes in the climatological sense of identifying particularly dangerous areas

HOUSING TRACTS constructed within the San Andreas Fault zone near San Francisco appear in the aerial photograph at bottom, made by Robert E. Wallace of the Geological Survey in 1966; the photograph at top shows the same scene approximately 10 years earlier. Solid white line in each view traces the approximate position of fault along which the ground ruptured and slipped some two metres during the great earthquake of 1906. Broken white lines give approximate boundaries of main fault zone. Pacific Ocean is at lower left.

and estimating the relative degree of danger. What is needed, however, is prediction more akin to weather forecasting: Where and when is the next earthquake likely to take place?

A combination of laboratory and field experiments over the past five years has led to a breakthrough in thinking about the problem of earthquake prediction. When a rock is squeezed, it deforms and eventually breaks. Just before it breaks it swells, owing to the opening and extension of tiny cracks. This inelastic increase in volume, a phenomenon long known to laboratory experimenters as dilatancy, begins when the stress reaches about half the breaking strength of the rock. In the mid-1960's William F. Brace and his colleagues at the Massachusetts Institute of Technology showed that measurable physical changes accompany dilatancy in laboratory experiments; such effects include changes in the electrical resistivity of the rock and in the velocity at which elastic waves travel through the rock. Brace suggested that dilatancy and its effects might be detectable in the earth's crust and provide a basis for earthquake prediction; his suggestion generated much excitement at the time because it opened up the possibility that premonitory physical changes could be observed in advance of earthquakes.

In the late 1960's two Russian investigators, A. N. Semenov and I. L. Nersesov, startled the seismological world with a report that unusual variations in the velocity of seismic waves appeared just before earthquakes in the Garm region of Tadzhikistan. Subsequently the Russians announced that in earthquake-epicenter regions in Garm, Tashkent and Kamchatka they had detected changes both in electrical resistivity and in the content of the radioactive gas radon in the water of deep wells.

These reports triggered a flurry of activity in the U.S. American seismologists went to the U.S.S.R. to see the data firsthand. They also began arranging their own experiments in order to observe the precursory phenomena. Technical papers on these phenomena authored by Russian, American and Japanese workers began to be presented in increasing numbers at scientific meetings and in journals. Last year a group of American geologists and geophysicists visited China and found a large-scale earthquake-prediction program under way, with important results that had not yet been reported at international meetings or in publications.

It is fortunate that a number of earthquake precursors have been found, each

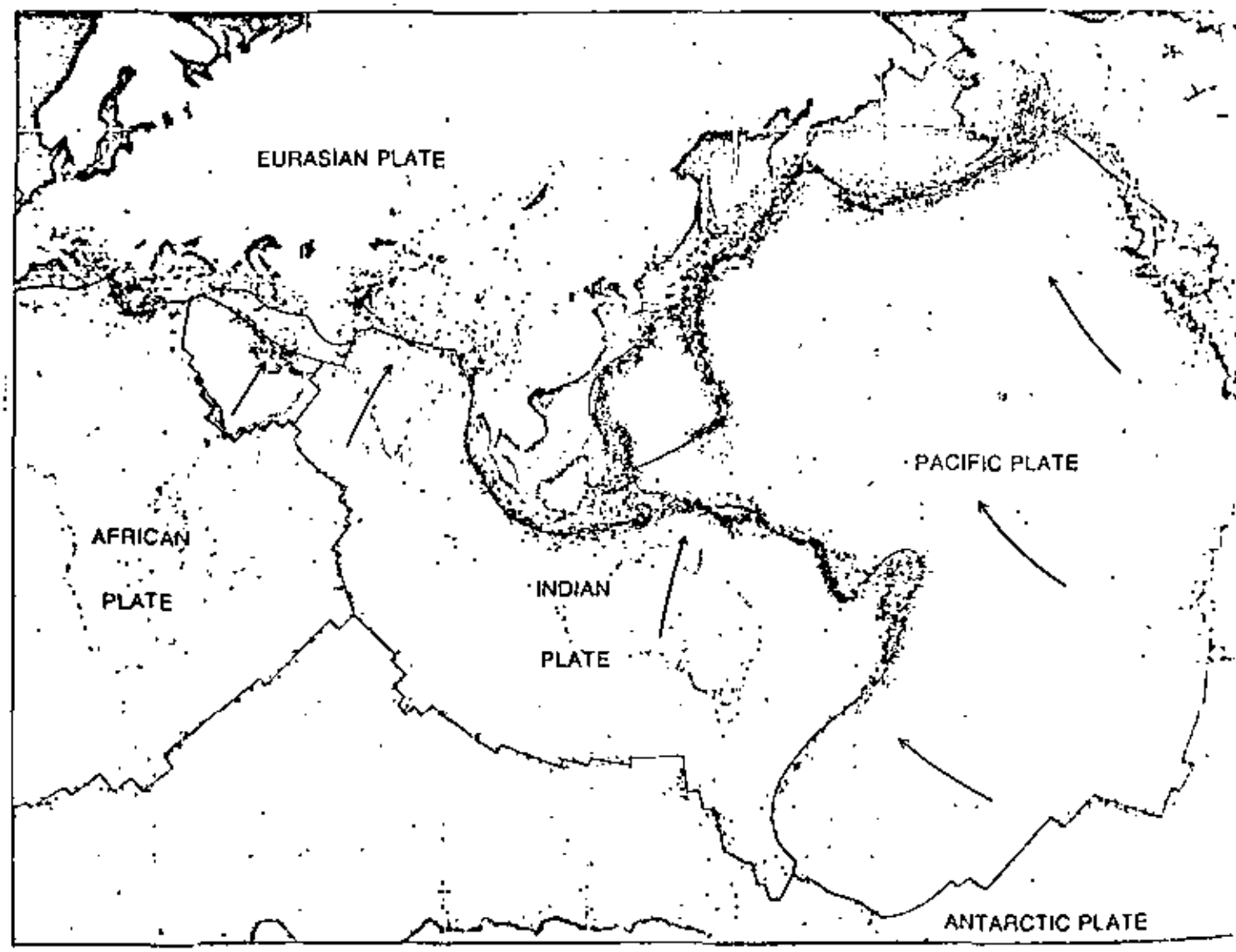

EPICENTERS OF 30,000 EARTHQUAKES recorded between 1961 and 1967 are indicated on this world map plotted by M. Barazangi and B. J. Dorman of Columbia University on the basis of information supplied by the Coast and Geodetic Survey. Also shown are the dozen or so moving plates that, according to the modern theory of plate tectonics, comprise the earth's rigid outer shell. Most earthquakes take place at or near plate boundaries, where the relative motion of the plates is resisted by frictional sticking until the stress builds up to the point where the rock fractures, causing an earthquake. Intraplate earthquakes, such as those that appear in the

based on a different physical measurement. Confidence in a prediction is enhanced when it is based on several independent lines of evidence, each with its distinctive "noise" history and its distinctive anomaly signaling an earthquake. How are the precursory anomalies observed?

An array of seismographs can be used to sense precursory changes in the velocity of compressional waves and shear waves in the focal region of an earthquake [*see illustration on next page*]. The seismic waves originate in smaller earthquakes within the focal region, in larger earthquakes outside the focal region or in artificial sources such as explosions or mechanical devices. Such anomalous changes have been observed in several parts of the U.S., the U.S.S.R. and China.

Seismically active regions have many more small earthquakes than large ones. This "background" of small tremors varies in time. Periods of calm before a strong shock are frequently observed; the background activity appears to go through a minimum and then to increase just before the main shock. The pattern of radiation of seismic waves reflects the stress field in the crust. In central Asia Russian investigators have found that the stress pattern shown by the small tremors is random during the calm period but becomes highly organized beginning three or four months before the main shock. The compressional stresses become aligned in the same direction as that of the forthcoming main shock.

Another approach is to measure anomalous changes in the volume of crustal rock in the focal region. The changes can be observed by tiltmeters, by devices for monitoring changes in sea level (corrected for oceanographic and meteorological effects) and by repeated surveying. In parts of Japan and China historical records of precursory changes in the level of lakes, rivers or the sea, sometimes dating back hundreds of years, may be related to the same phenomena [*see illustration on page 19*].

Precursory changes in water level, water turbidity and temperature in deep wells can be observed visually or with instruments. Observing the radon content of well water, a technique used extensively in the U.S.S.R. and China, also seems to be a sensitive indicator of forthcoming seismic activity [*see top illustration on page 21*].

If an electric current is fed into the earth's crust between two points several kilometers apart, voltage changes between two other points will show up if the resistivity of the intervening crustal rocks changes. Such precursory fluctuations have been reported in the U.S., the U.S.S.R. and China [*see bottom illustration on page 21*].

Magnetometers on the earth's surface can detect changes in magnetic field with a strength of about a hundred-thousandth of the earth's natural field. By subtracting the changes sensed by "standard" instruments removed from the epicentral region, noise introduced by fluctuations in the stream of electrically charged particles from the sun (the "solar wind") can be reduced and anomalous changes in the focal region can be detected. Precursory magnetic signals have also been observed in the U.S., the U.S.S.R. and China.

Although one can conceive of an earthquake-prediction strategy based purely on empirical observations such as these, it is highly desirable to have a physical model that explains the observations. A model not only enhances confidence in the basic notion of predictability but also makes for more efficient research procedures.

Two principal models have been proposed, both growing out of laboratory experiments. The dilatancy-diffusion theory, proposed by Amos M. Nur of Stanford University in 1972 and extended by Christopher H. Scholz, Lynn R. Sykes and Y. P. Aggarwal of Columbia University in 1973, is supported by most American specialists. Another model, which might be called the dilatancy-instability theory, was proposed in 1971 by workers at the Institute of Physics of the Earth in Moscow. It also has a few American and Japanese adherents. The models have a common feature: the growth of cracks as stress builds up in the crust just before an earthquake [*see illustration on page 23*].

Both models begin with a stage in which elastic strain builds up in the earth's crust. In the next stage small cracks open in the strained portion of the crust and dilatancy becomes a dominant factor. In the Russian view the development of cracks "avalanches" in this stage. In both models it is the second stage that marks the real beginning of precursory phenomena, since the open cracks change the physical properties of the rock. Seismic velocity (the ratio of compressional-wave velocity to shear-wave velocity) drops. Electrical resistivity increases if the rock is dry and decreases if it is wet. Water flow through the rock increases (and therefore more radon enters the water from the rock). Volume in the dilatant zone increases. In the American model the number of small tremors decreases in this stage because the cracks become undersaturated in water as they increase in number; as a result sliding friction increases and inhibits faulting.

The two models differ markedly in the third stage. In the American model water diffuses into the undersaturated dilatant region. The main effect of this inflow is to increase the seismic velocity and to raise the pore pressure in the cracks, weakening the rock to the point where small earthquakes increase in number and the main shock follows. In the Russian model water plays no re in the third stage. Instead the avalanche-like growth of cracks leads to instability and rapid deformation in the vicinity of the main fault. The stress load drops partially in the region surrounding the zone of unstable deformation, cracks partially close and the rock recovers some of

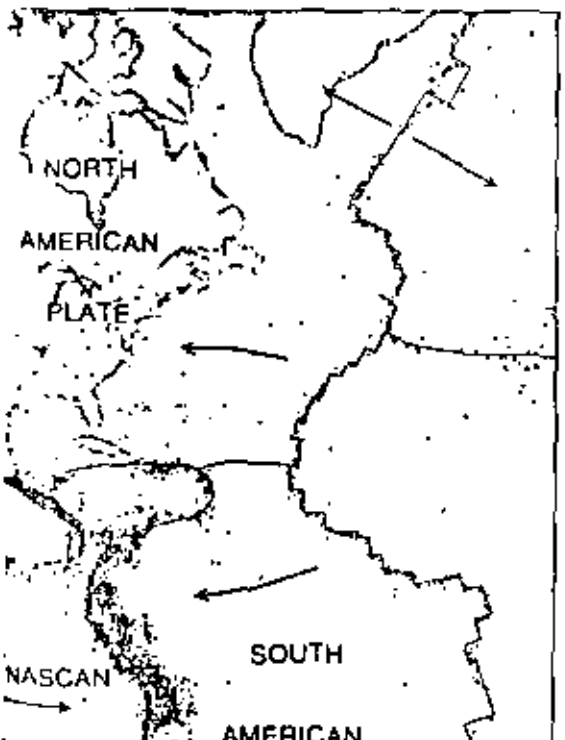

eastern U.S., are rare but can be destructive. China, squeezed by large plates on the south and the east, has a high level of seismic activity, which may be attributable to the [illegible] in central Asia.

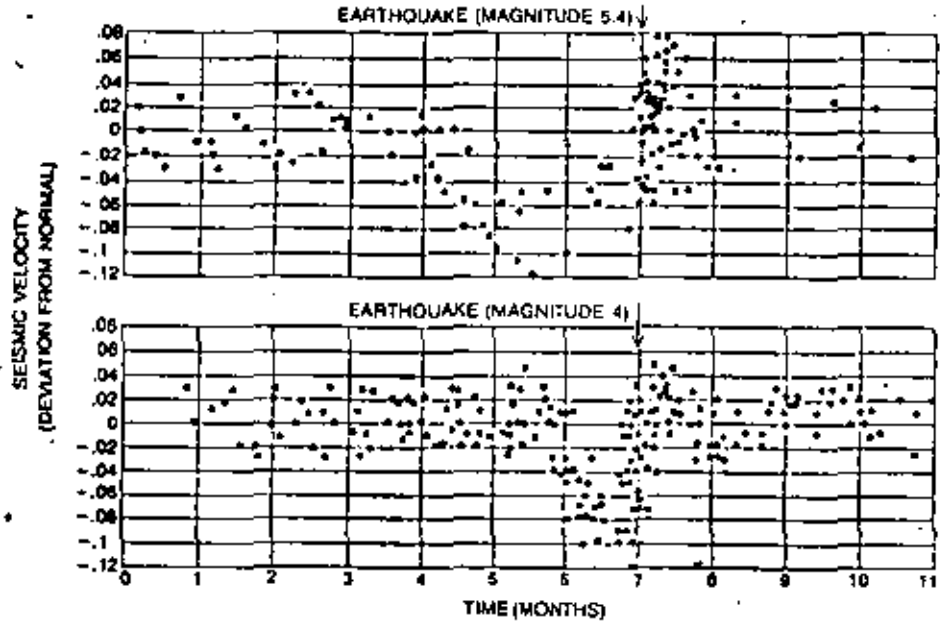

PREMONITORY CHANGES in seismic velocity (the ratio of compressional-wave velocity to shear-wave velocity) were observed in the late 1960's just before two fairly large earthquakes in the Garm region of Tadzhikistan by A. N. Semenov and I. L. Nersesov of the Institute of Physics of the Earth in Moscow. These composite diagrams, drawn from their work, are based on a number of smaller earthquakes in the region. Each point represents a deviation of the seismic velocity from the normal regional value and is derived by measuring the travel times of compressional waves and shear waves from each small earthquake to a local network of seismograph stations. The colored bands indicate the statistical scatter of the observations. The duration of the calm period preceding the main earthquake appears to increase with the magnitude of the forthcoming event. (The two earthquakes shown measured 5.4 and 4 on the Richter scale.) Seismic-velocity anomalies of this type have been observed about 18 times in U.S.S.R., 10 times in U.S. and several times in China.

its original characteristics. This sequence of events accounts for the increase in seismic velocity, the decrease in volume and the other changes typically observed in the third stage. The developing instability finally gives way to faulting, and the main shock ensues. In both models stress is released by the earthquake, and the crustal rock recovers most of its original properties.

An empirical formula, derived by James H. Whitcomb, J. D. Garmany and Don L. Anderson of the California Institute of Technology, connects the duration of the precursory anomaly with the magnitude of the predicted earthquake. For example, an event with a magnitude of 5 on the Richter scale has an anomaly lasting for about four months, whereas a major earthquake, with a magnitude of 7, say, would be preceded by an anomaly beginning some 14 years before the event. The formula is still rough, particularly in the high-magnitude range, but it appears that the large earthquakes will provide warning times on the order of 10 years. The discovery that the size of an earthquake, as well as its location and timing, is predictable should hold important implications for the design of an earthquake-mitigation strategy. Fortunately the larger the magnitude of the forthcoming quake, the longer the lead time available for making plans to combat its effects.

What is most needed now to bring earthquake-prediction technology to the point of implementation is a larger number of examples of successful prediction. So far only about 10 earthquakes have been predicted before the fact. Perhaps three times as many have been "predicted" after the fact by going back to the data and finding precursory signals. It is difficult to know how many formal predictions, based on the methods described above, have failed. The number is probably less than 10, which is not bad for the rudimentary research networks now in operation. That is still too small a sample to eliminate unreliable methods and to design a comprehensive, operating prediction system. Although the major earthquake belts extend for tens of thousands of kilometers, only a small fraction of that distance is instrumented adequately to test prediction methods. With the pooling of the data being gathered in various countries, however, the number of case histories should grow rapidly in the next few years, and statistically valid tests of prediction methods should be forthcoming. Seismologists of different nationalities, like workers in any other field of science, need to combine their results in order to advance toward a common goal.

The leading agency for earthquake-prediction research in the U.S. is the Geological Survey, which runs a strong program centered in California and supports a research program in several universities. In central California, the region where the San Andreas Fault is most active, the Geological Survey has installed a network of stations equipped with seismometers and tiltmeters. Magnetic and electrical observations are also conducted but to a much lesser degree. In southern California a large number of instruments are being installed in a joint effort involving the Geological Survey and Cal Tech. Data from these arrays are mostly telemetered into Menlo Park and Pasadena on telephone and microwave circuits. This growing ability to pinpoint earthquake locations and monitor precursory velocity changes, tilts, magnetic fluctuations and changes in electrical resistivity is beginning to pay out. Recently workers associated with the Geological Survey found that 10 California earthquakes were preceded by tilt changes in the vicinity of the epicenter [*see illustrations on page 20*]. Precursory changes in seismic velocity have been reported for about 10 earthquakes in California and New York.

Perhaps the most significant new data were gathered on November 28, 1974, when a magnitude-5 earthquake struck about 10 miles north of Hollister in central California. The tremor was preceded by distinct tilt changes and magnetic fluctuations convincingly above the noise level, and with indications of seismic-velocity changes. John H. Healy of the Geological Survey chided his colleagues the night before the quake for not publicly announcing the forthcoming event.

In spite of these interesting results the U.S. program is still not sufficiently supported to make prediction a reality within the next decade. It is simply a matter of too few methods being tested in too few places. With the present level of support many potentially important methods cannot be tested, such as arrays of wells monitoring water level and radon content, networks of resistivity sensors, sea-level gauges, advanced surveying techniques and so forth. Even now more data are being accumulated than can be digested, a situation that could easily be rectified if a large computer were provided to scan and automatically analyze the incoming stream of data. Universities and industries with much

research talent are insufficiently involved because of the lack of funds. Few studies are being conducted outside California. An additional $30 million per year could make prediction within a decade a realistic goal. The cost-effectiveness of such an investment is obvious when one remembers that the relatively modest San Fernando tremor (magnitude 6.6) that struck just north of Los Angeles in 1971 resulted in damage of more than $500 million.

The earthquake-prediction program of the U.S.S.R. is centered in the Institute of Physics of the Earth in Moscow. A program involving laboratory and field measurements, comparable in level to our own, is being carried out. The Russian field experiments form the longest series so far, having been started nearly 20 years ago. The impressive discovery of anomalous precursors stems from these efforts. The strategy of the Russian investigators is somewhat different from our own in that several experimental sites are being monitored in central Asia and Kamchatka with a lower density of instruments compared with our heavier emphasis on specific areas in California. Moreover, the Russians are exploring more methods than we are. Nevertheless, it appears that in the absence of a major new initiative, operat-

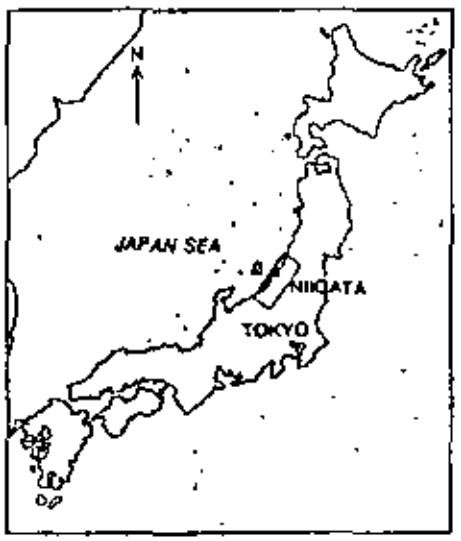

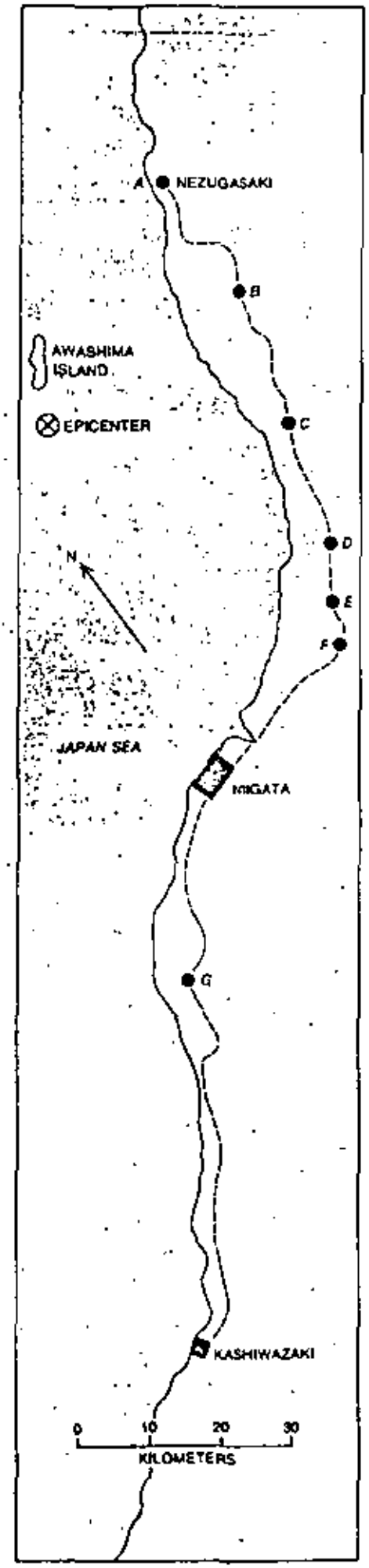

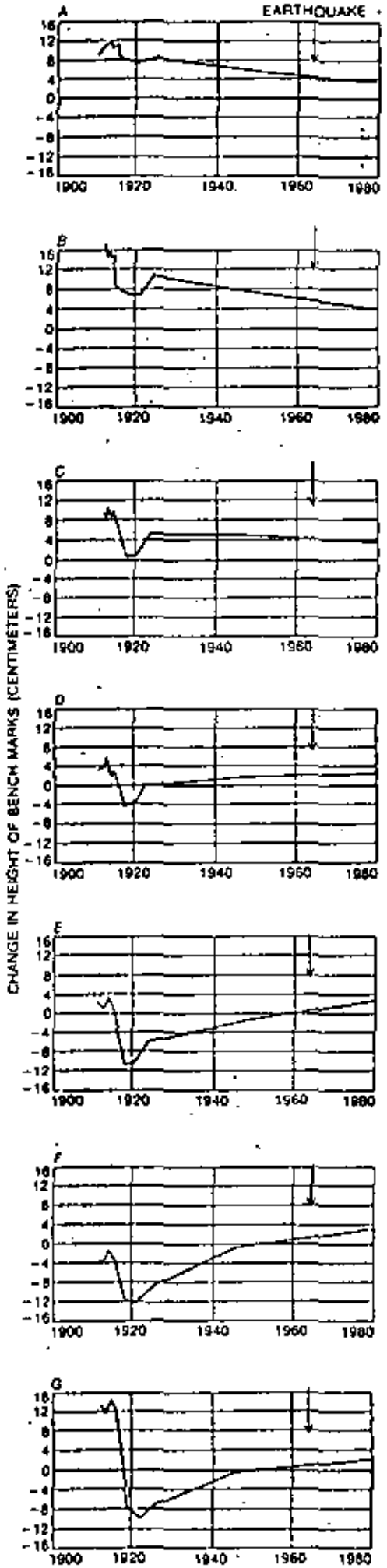

ANOMALOUS UPLIFT of the earth's crust in the vicinity of Niigata in Japan was observed for about 10 years before the disastrous 7.5-magnitude earthquake there in 1964, according to the Japanese investigator T. Dambara. The uplift was detected by plotting changes in the height of bench marks measured in repeated land surveys. The graphs at right correspond to the lettered benchmark sites (*black dots*) shown on the detailed map. Evidence of the crustal uplift was also obtained from records showing a precursory drop in mean sea level observed by a tide-gauge station at Nezugasaki.

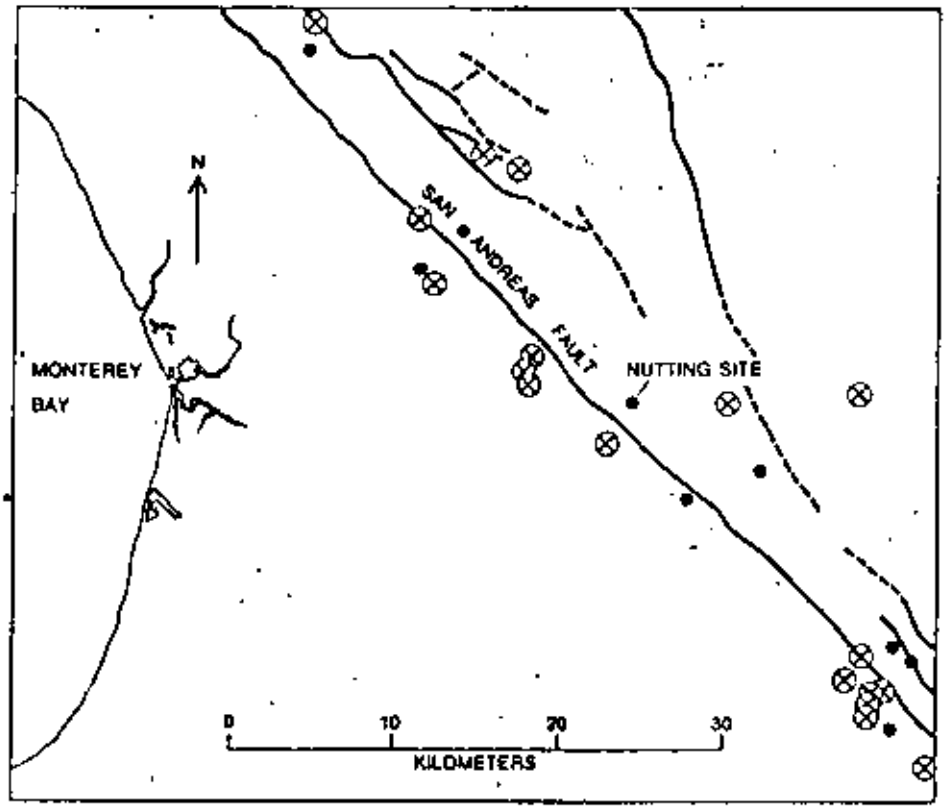

TILTING OF EARTH'S CRUST just before earthquakes has been observed by investigators associated with the Geological Survey using an array of sensitive tiltmeters (*black dots*) installed along 85 kilometers of the San Andreas Fault east of Monterey Bay. Circled crosses denote epicenters of all earthquakes with a magnitude greater than 2.5 recorded in the region between July, 1973, and March, 1974. Data summarized in illustration below were obtained at Nutting tiltmeter site, seven kilometers southwest of the town of Hollister.

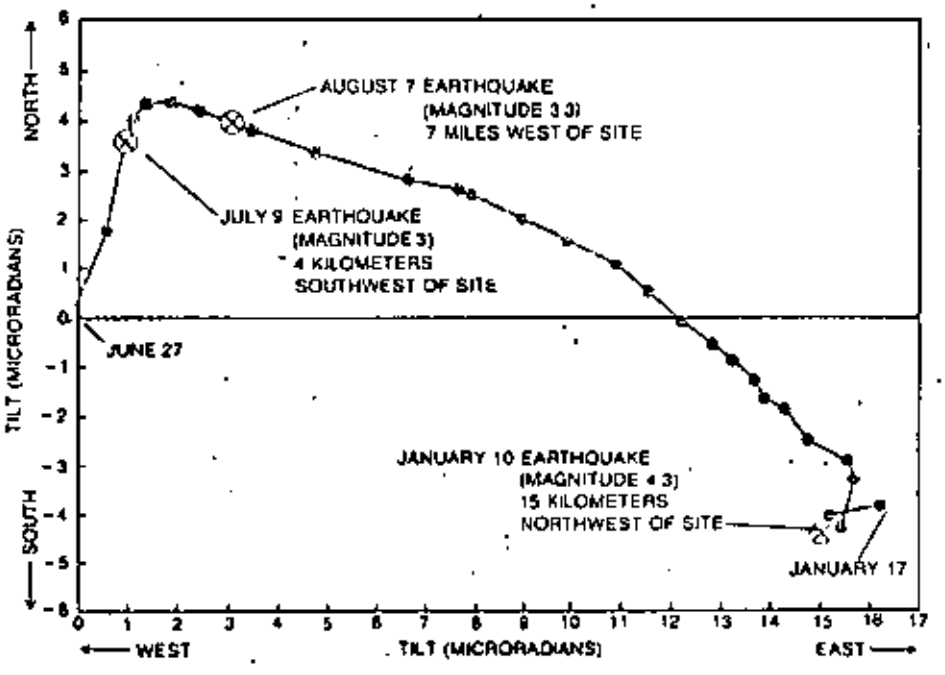

SEVEN-MONTH RECORD of crustal tilting was made during parts of 1973 and 1974 with the aid of a tiltmeter located in a shallow hole at the Nutting site. The colored dots represent the weekly mean tilt direction and magnitude. Several major local earthquakes are indicated; each is preceded by clear precursory change in tilt direction. M. J. S. Johnston and C. F. Mortensen of the Geological Survey report that precursory anomalies of this type have been detected on at least 10 occasions; the largest such event was on November 28, 1974, when a magnitude-5 earthquake struck about 10 miles north of Hollister. So far no comparable tilt change has been recorded that has not been followed by an earthquake.

ing prediction systems covering large areas will not be forthcoming in the U.S.S.R. either in this decade. As part of the environmental treaty between the U.S. and the U.S.S.R. there has been a rewarding exchange of ideas and personnel in the fields of earthquake prediction and seismic engineering. A formal bilateral working group has been established. In this way both American and Russian workers are kept informed of the latest unpublished developments; joint experiments are under way, and there is healthy criticism of each side's efforts by the other. This kind of close cooperation would have been unthinkable a few years ago.

Although Japanese earth scientists have been devoted to the notion of earthquake prediction since the turn of the century, a formal research program dedicated to this goal did not get under way until 1965. For years reports of anomalous sea-level changes and tilts prior to earthquakes have emanated from Japan, but the data were sparse and of uneven quality, and the world community of geophysicists was unimpressed. It now seems that some of these reports must have described true precursory phenomena. In any case the Japanese workers include some of the world's best geophysicists. It is therefore a tragedy that a strike has crippled the Earthquake Research Institute in Tokyo for several years.

The Japanese are currently emphasizing surveys every five years extending more than 20,000 kilometers. So far 17 observatories have been equipped with strain detectors and tiltmeters. Observations of the level of seismicity, of changes in the velocity of seismic waves and of magnetic and electrical phenomena are also under way. Cooperation between the U.S. and Japan in this field is quite close.

This just October I had the good fortune to participate in a month-long trip to China as a member of a group of 10 American earthquake specialists. This tour of Chinese research facilities followed a visit by 10 Chinese earthquake experts to the U.S. earlier last year. Since scholarly publication in China was suspended during the "cultural revolution," almost everything we saw in China was new to us. Following the destructive Hsing-Tai earthquake of 1966 the Chinese embarked on a major effort in the field of earthquake prediction. Chairman Mao and Premier Chou En-lai issued statements charging Chinese scientists with achieving this goal. At present some 10,000 scientists, engi-

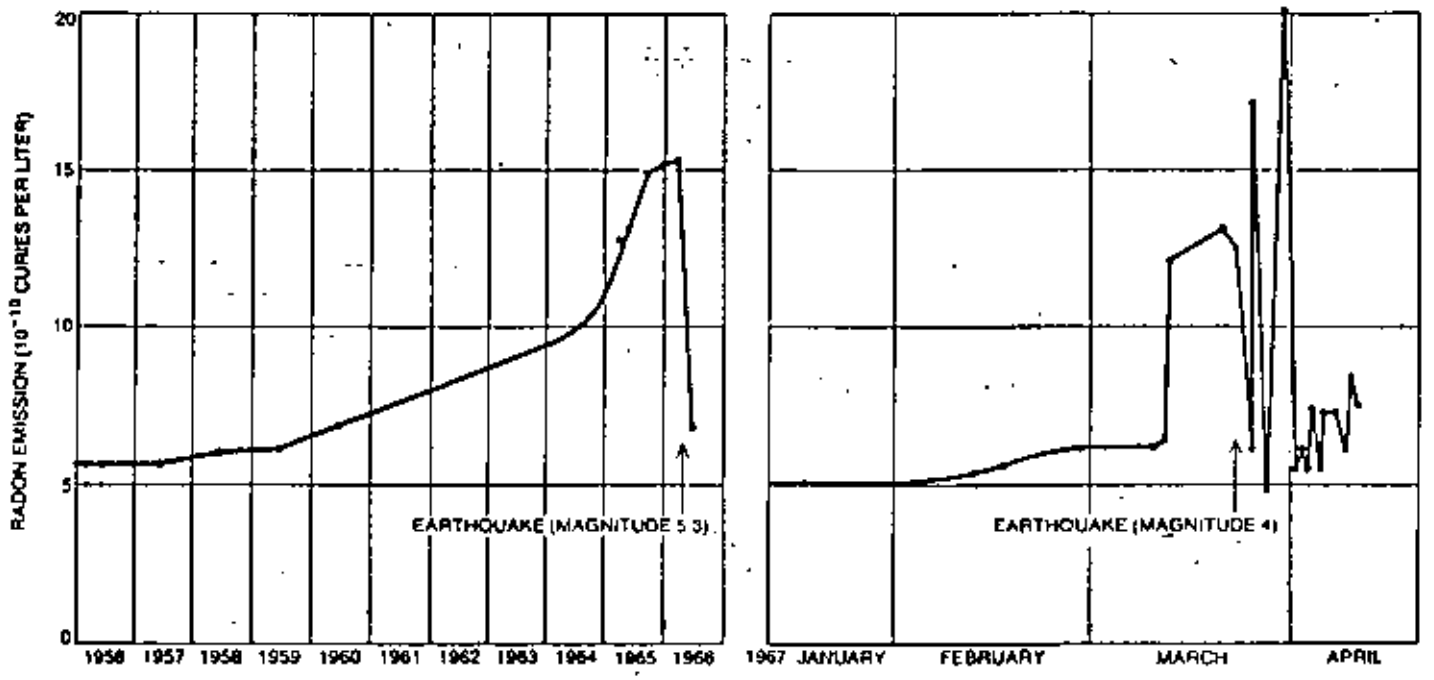

AMOUNT OF RADIOACTIVE GAS RADON dissolved in the water of deep wells has been found by Russian researchers to increase significantly in the period preceding an earthquake. The two examples shown here were recorded before two major earthquakes in the vicinity of Tashkent. The 1966 event (*left*) had a magnitude of 5.3; the 1967 aftershock (*right*) had a magnitude of 4. This promising observational technique is used extensively in both the U.S.S.R. and China, but it has not yet been tried in U.S.

neers, technicians and other workers are engaged in the program—more than 10 times the number of such workers in the U.S.

A unique feature of the Chinese approach is the use of an even larger number of amateurs, mostly students and peasants, who build their own equipment, operate professional instruments in remote areas and educate the local people about earthquakes. So far 17 fully equipped seismograph stations and 250 auxiliary stations have been installed. Data pertinent to earthquake prediction are being obtained at a total of 5,000 points. Every method described in this article is being tested in China. The Chinese say that they have made successful predictions, involving the evacuation of people from their homes and a consequent saving of lives. They also admit to false alarms and failures, chalking these up to the fact that their program is new and they are still in a learning phase. The motivation for success is strong. The high population density, the nature of rural construction and the high degree of seismicity make China particularly vulnerable to earthquakes.

Although it is difficult to gauge the quality of the Chinese program from a brief visit, there is no question that the potential is great. In a few years the Chinese will probably be gathering more data than anyone else, owing to the size of their program and the more frequent

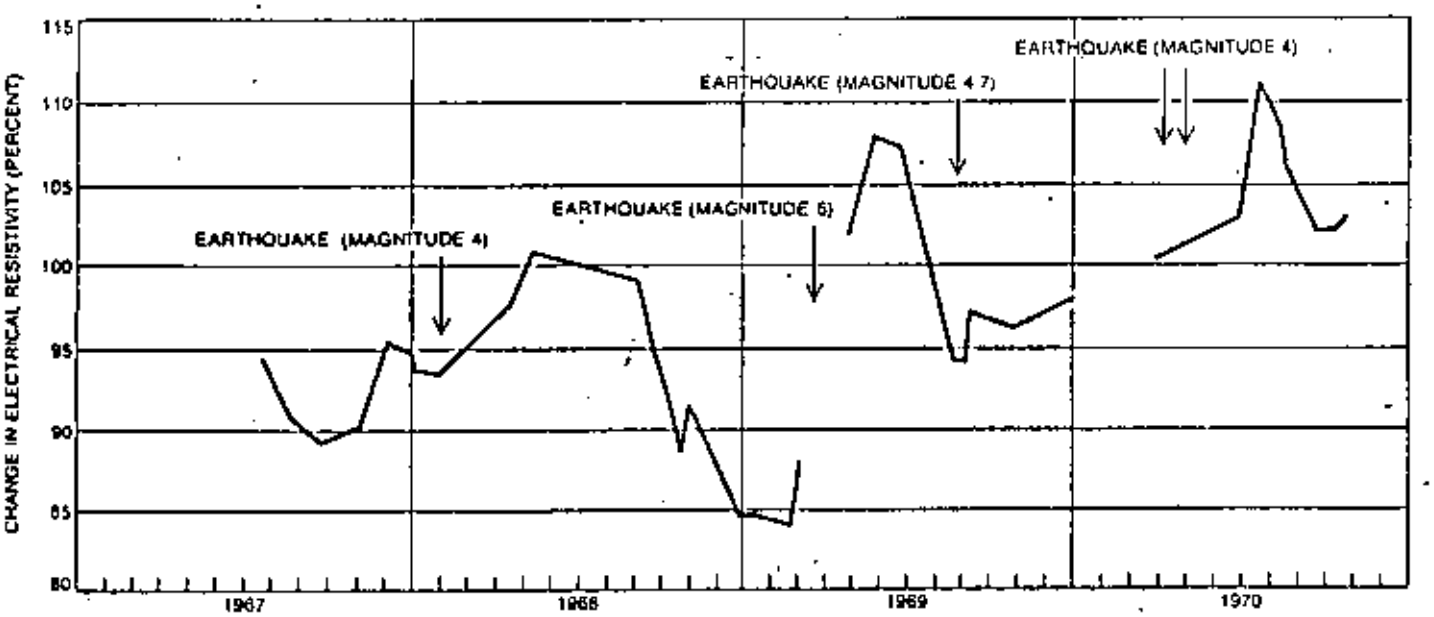

CHANGES IN ELECTRICAL RESISTIVITY of the earth's crust prior to earthquakes have been reported in the U.S.S.R., China and the U.S. The data for this graph were obtained by G. A. Sobolev and O. M. Barsukov for a series of earthquakes monitored in the U.S.S.R. between 1967 and 1970. Measurements of this type are made by feeding an electric current into the ground and observing voltage changes a few kilometers away. In general it has been found that earthquakes are preceded by a decrease in crustal resistivity.

incidence of earthquakes in their country. It may well be that the first statistical validation of prediction methods will come from China. It would be a pity if political considerations were to inhibit close international cooperation on this score, because joint projects with China could pay out in a more rapid achievement of a mutually desirable goal.

Although the prediction of earthquakes has been emphasized in this account, a comprehensive program to reduce vulnerability to destructive earthquakes includes progress in other areas: earthquake engineering, risk analysis, land-use regulation, building codes and disaster preparedness. Unlike earthquake prediction, about which there is a good deal of optimism but (so far at least) no guarantee of success, research and development in these other areas is bound to result in reduced casualties and lowered economic losses. Earthquake engineering deals with the efficient and economic design of structures that may have to withstand the shaking of earthquakes. The alteration of existing structures to improve their performance is included. Not only are residences, commercial buildings, schools, hospitals, dams, bridges and power plants examined individually but also the interaction of all these elements in the system we call a community is considered. This developing technology can serve its purpose only if it is transferred from the investigators to the professional practitioners and to the regulatory bodies that draft building codes.

The damage caused by recent earthquakes in Japan and Alaska dramatized the fact that structures that could withstand the shaking were nevertheless toppled by foundation failure. Severe ground-shaking can cause soils to settle or liquefy and thereby lose their ability to support structures. Research on this poorly understood phenomenon is an important aspect of earthquake engineering. When it is better understood, it might be possible to take countermeasures or to institute land-use regulations that would limit construction on vulnerable soils as well as along active faults, in potential landslide areas or in coastal zones subject to tsunamis.

Some regions suffer major earthquakes frequently, others suffer them infrequently. In some places the potential for severe ground-shaking is higher because seismic waves propagate with less attenuation or because the soil resonates and amplifies the ground motion. In one city the problem following a quake is fire; in another it is flooding. Construction practices differ from region to region. Some of these factors are known explicitly; some can only be described in probabilistic terms. All of them, and other factors as well, must be combined into an overall assessment of risk on which decisions must be based. Risk assessment is a new and important part of earthquake research. Also helping to provide a rational basis for decision making about land use and construction in earthquake regions is economic analysis of such questions as to what degree, in an area with a given probability of strong earthquakes, the added costs of safer construction are offset by the potential saving of life, property and productivity.

The possibility of controlling or modifying earthquakes arose a few years ago as the result of a chance discovery. The injection of wastewater into a deep well near Denver was found to have triggered small earthquakes. Since that time both laboratory and field experiments have shown that the injection of a fluid in a fault zone reduces friction resistance by decreasing the effective normal stress across the fault. In a sense fluid injection serves to weaken the fault whereas fluid withdrawal can strengthen it. If a preexisting stress is present, an earthquake could result if a fault were unlocked by fluid injection. In a remarkable field test of these ideas workers from the Geological Survey injected and withdrew fluids in a water-injection well of the Rangeley oil fields in Colorado and found that in this way they could switch seismicity on and off.

The extension of these results to the control of a major active fault such as the San Andreas Fault is unlikely in the near future. Some future generation, however, may be able to modify earthquakes by the injection of fluid and the controlled, gradual release of crustal strain. Science often advances more rapidly than is expected, of course, and in any case research on the possibility of modifying earthquakes should be encouraged for the sake of the next generation, if not of our own.

Although the number of case histories is still too small to make a positive statement about the feasibility of earthquake prediction, most seismologists would agree that prediction is an achievable goal in the not too distant future. Unfortunately the level of present effort in the U.S. is below that required to move rapidly to an operating prediction system. If a major earthquake were to

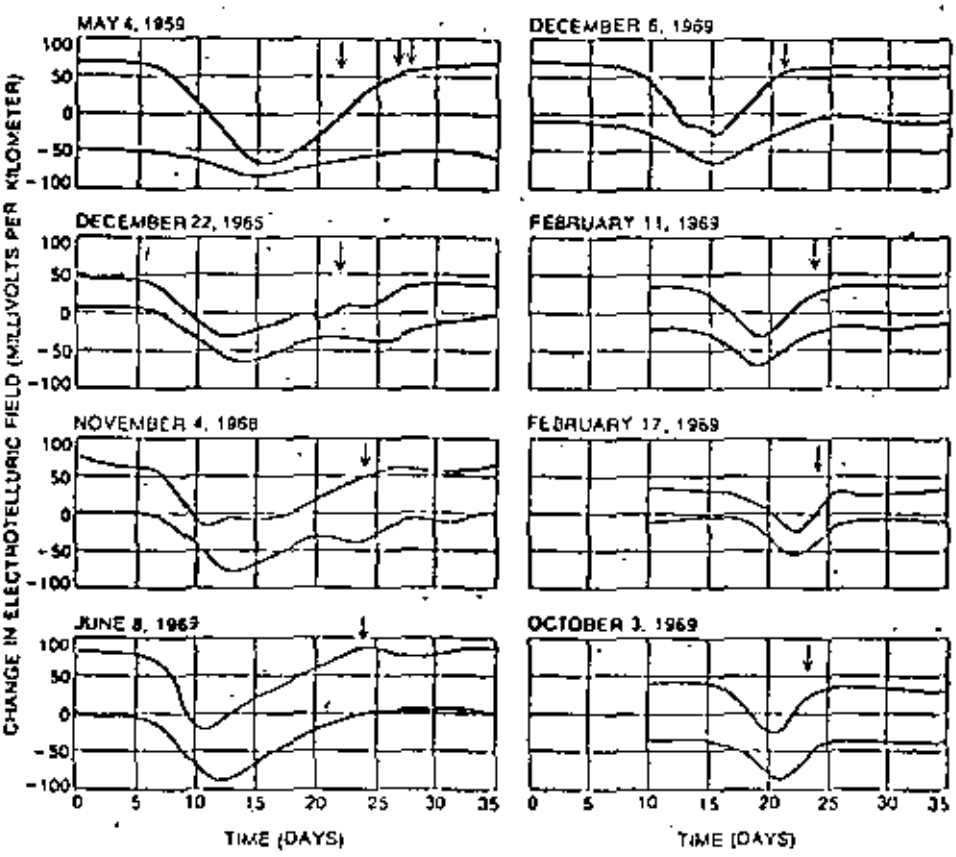

REDUCTION IN NATURAL ELECTRIC CURRENTS inside the earth just before an earthquake has also been observed by the Russian investigators. Data were obtained by recording voltage changes between points a few kilometers apart. Arrows denote earthquakes.

strike the U.S., the following day would almost certainly see abundant resources made available for a large-scale earthquake-mitigation program. (The earthquake-prediction programs of China and the U.S.S.R. were launched after severe earthquakes in each of those countries.) How does one sell preventive medicine for a future affliction to government agencies beleaguered with current illnesses?

It is proper, I believe, for scientists to assume an advocate role when they perceive an inadequate government response to some new opportunity or to some future danger. Earth scientists have a case to make. They can point to housing tracts placed in fault zones or on unstable hillside slopes. They can cite a newly built hospital that collapsed when shaken by the moderate San Fernando earthquake. The same tremor caused a dam to be stressed to near the failure point. A slightly larger shock would have resulted in casualties in the tens of thousands in the floodplain below the dam. Scientists can question the policy of a government that spends billions in construction but is unable to support research that would safeguard its own investment. They can question the wisdom of budgeting less than a tenth of a percent of the total construction investment for research on possible hazards. They can show how a research dollar invested today can yield an enormous return in lives saved and property preserved tomorrow. At a time when basic research budgets have not kept pace with the growth of the economy as a whole, earth scientists can point up the practical value to society of their new comprehension of the forces that have shaped the earth.

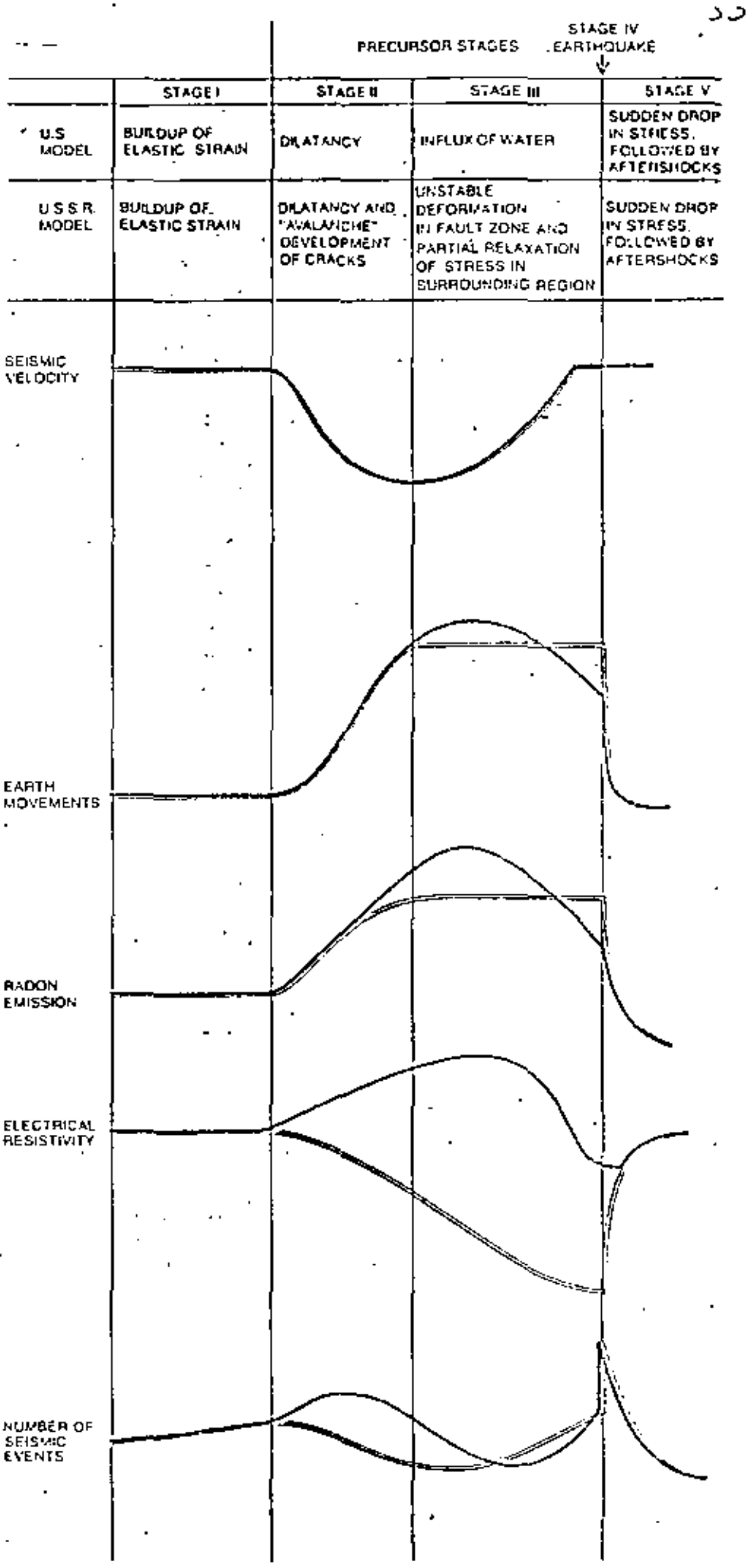

TWO MODELS of the mechanism responsible for earthquakes have been proposed in an attempt to put earthquake prediction on a sound theoretical basis. One view, called the dilatancy-diffusion model, was developed mainly in the U.S. The alternative, sometimes known as the dilatancy-instability model, was formulated in the U.S.S.R. The black-outlined curves show the expected precursory signals according to the American model; the colored curves show the expected precursory signals according to the Russian model. (Dilatancy is the technical term used to describe the inelastic increase in volume that begins when the stress on a rock reaches half the breaking strength of the rock.) The illustration is based on the work of Christopher H. Scholz, Lynn R. Sykes and Y. P. Aggarwal of the U.S. and V. I. Myachkin and G. A. Sobolev of the U.S.S.R.

Seismic Waves

A. Within the body of an elastic solid two types of elastic waves can propagate: Compressional or longitudinal (P-wave) and transverse or shear (S-wave). If λ and μ are the Lamé's constant then

$$\alpha \text{ (the P-wave velocity)} = \sqrt{\frac{\lambda+2\mu}{\rho}}$$

$$\beta \text{ (the S-wave velocity)} = \sqrt{\frac{\mu}{\rho}} \qquad \rho = \text{the density}$$

For a Poisson solid ($\lambda=\mu$):

$$\alpha = \sqrt{3}\,\beta$$

B. Along the free surface of an elastic solid two surface elastic waves can propagate:

Rayleigh waves (Half space), velocity $c_R < 0.92\beta$

Love waves (for a layered solid), velocity c_L, $\beta_1 < c_L < \beta_2$

The movement of the particle for each type of the wave is shown in the following Fig.

Velocity of surface waves depend on the wave length λ. Waves with large λ sample deeper in the earth and propagate faster. Thus the waves are dispersed in real earth. The dispersion of the waves can be used to infer crustal and upper mantle structure. In fact dispersion of such waves provides a very powerful tool for such studies.

Reference on Elastic Waves:

Ewing, M., Jardetzky, W. S., and Press, F., Propagation of Elastic Waves in Layered Media, McGraw-Hill, 1957

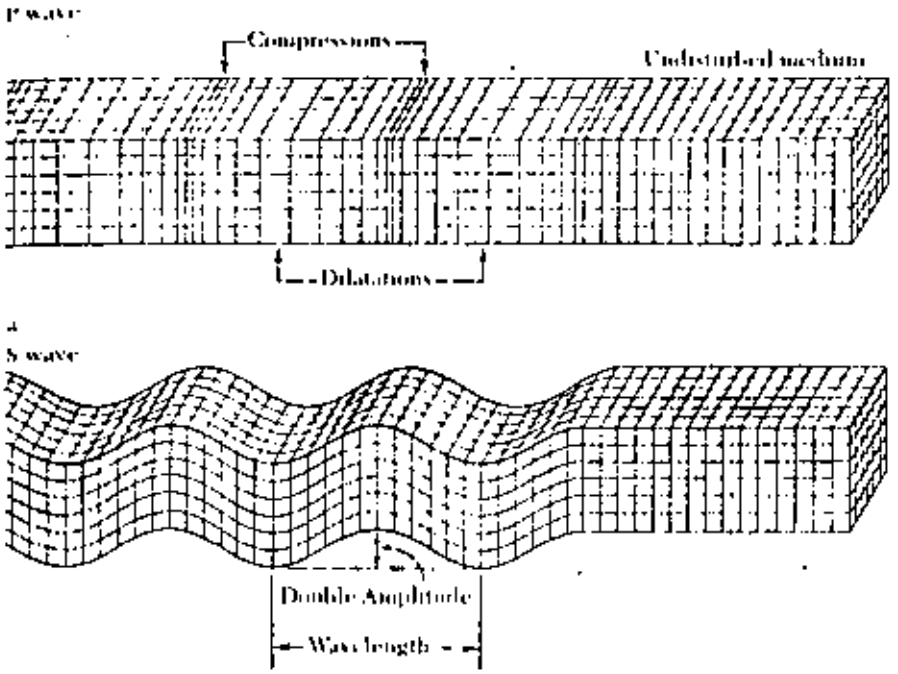

Diagram illustrating the forms of ground motion near the ground surface in four types of earthquake waves. [From Bruce A. Bolt, *Nuclear Explosions and Earthquakes*. W. H. Freeman and Company. Copyright © 1976.]

Waves on encountering a boundary are reflected, refracted, and diffracted. A plane P wave incident on a plane boundary gives rise to four phases:

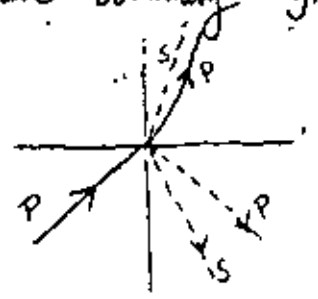

{ reflected and refracted P
reflected and refracted S

Since earth is layered the seismogram contains many phases.

Based on observed travel times of different waves all over the world, standard travel-time curves have been constructed by Jeffreys and Bullen and Gutenberg. The Jeffreys-Bullen travel time curves are shown in the following Fig.

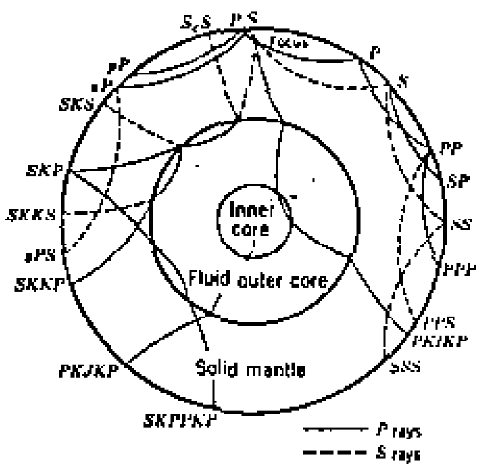

Nomenclature of different seismic phases

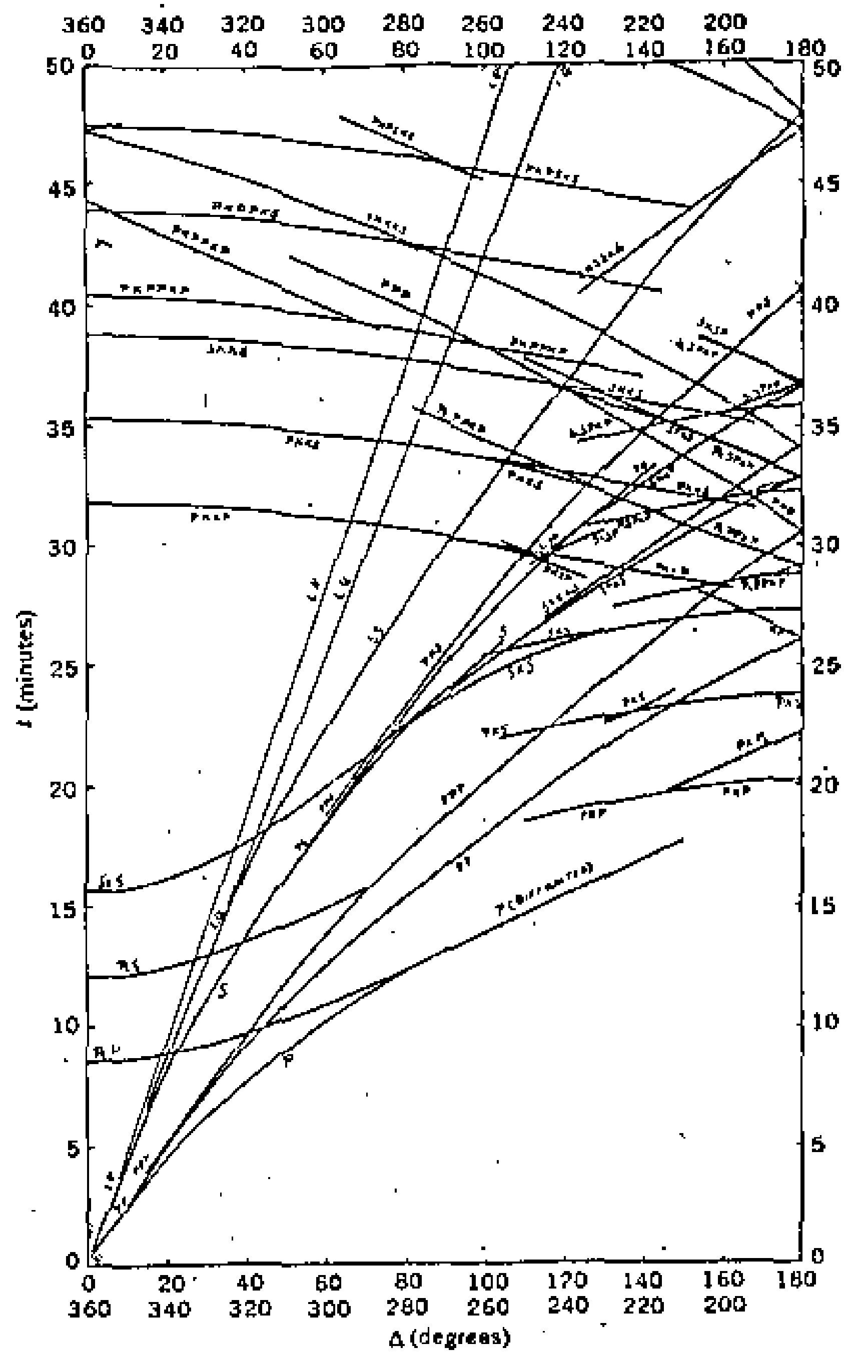

The Jeffreys-Bullen travel time curves. Reproduced, by permission, from Jeffreys and Bullen (1940).

Selected wave paths and lines of equal travel times in minutes (wave fronts) for P waves through the earth are shown in the following Fig.

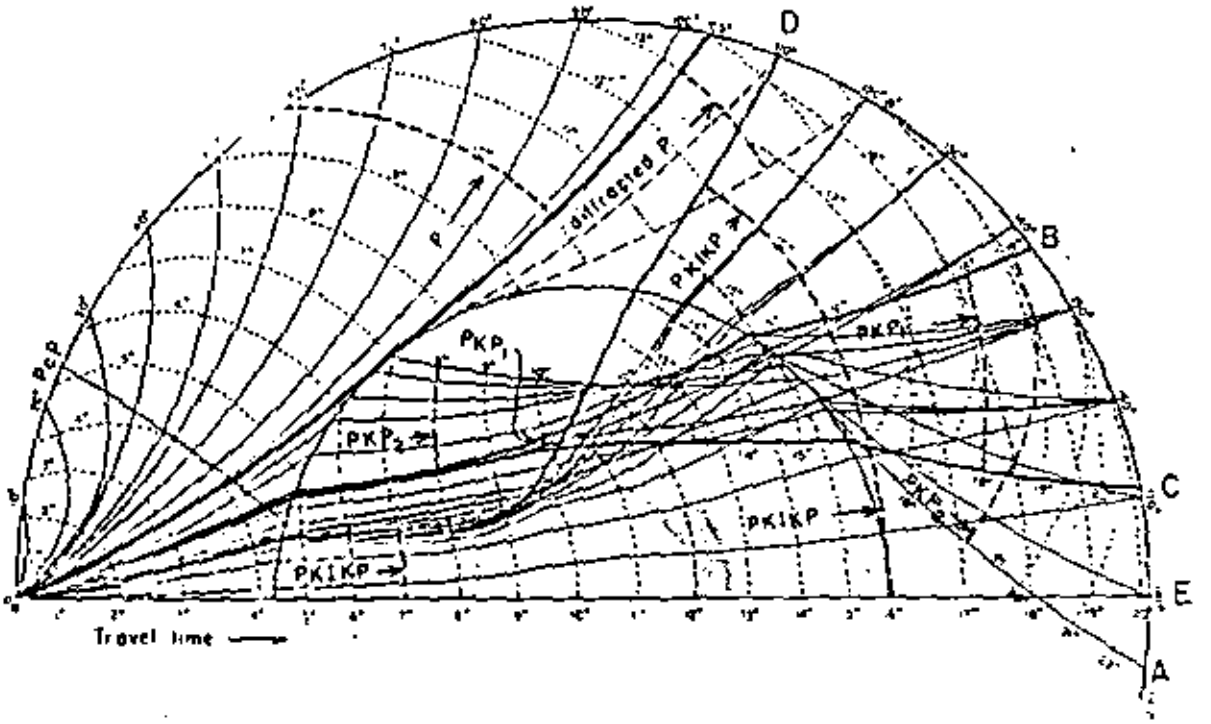

Thus the seismogram contains many phases. These phases can be identified by a trained observer. It is obviously useful to know which phase is expected to arrive at what time at a given epicentral distance. Usually when a phase arrives there is a change of frequency and/or amplitude.

Since the time it takes a wave to arrive a distance depends on the velocity, data on travel time is inverted to obtain the velocity structure of the earth.

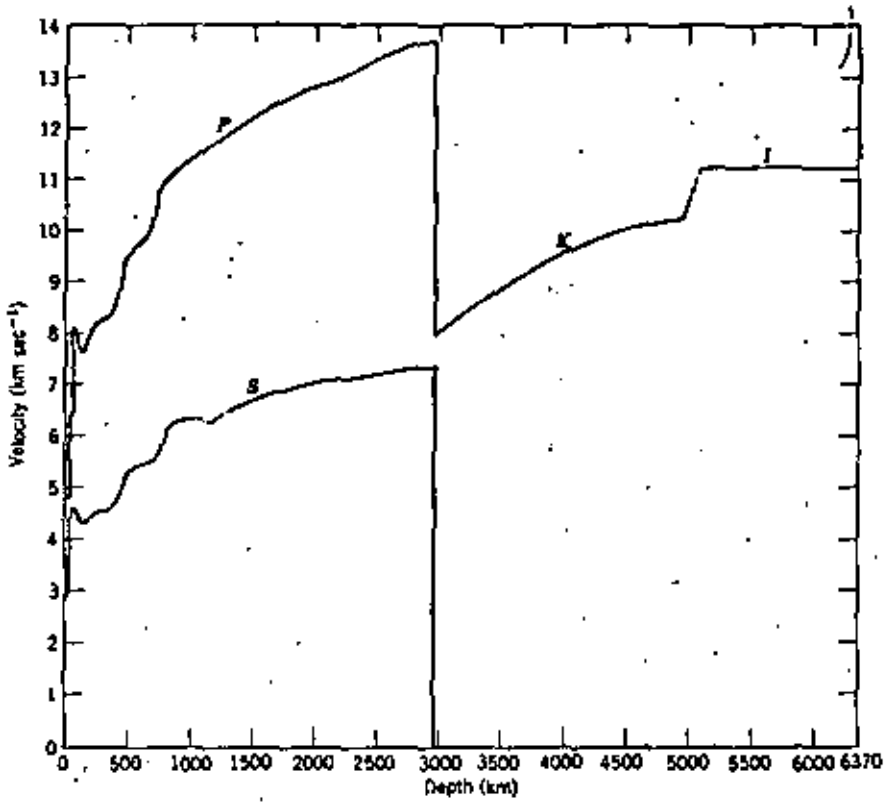

Velocities of P and S waves within the Earth. Mantle velocities are based on data by Gutenberg (1958a), Toksöz et al. (1967) and Anderson (1967b).

Intensity Scale

First intensity scale was developed by Rossi and Forel in 1880's. Values ranging from I to X were used in this scale. Mercalli in 1902 introduced a more refined scale ranging from I to XII. A modified and abridged Mercalli Intensity Scale is given below which has been adopted for California condition. Intensity at a site is measured in terms of damage to the works of man, amount of disturbances to the surface of the ground and extent of animal reaction to the shaking. Based on this a value is assigned on the intensity scale. From the data collected isoseismal maps are prepared. Clearly near the source (epicenter) the intensity values are highest.

There are several advantages in the use of intensity scale:

(1) In many areas there are no local instruments to measure the ground motion.

(2) For historical earthquakes; when there were no instruments, the isoseismal maps may be prepared and a magnitude and epicentral location (although approximately) can be estimated.

(3) Effect of local geology may be reflected in the damage. It is helpful in microregionalization.

Disadvantages are obvious:

(a) A subjective scale. Reports may be exaggerated. There are other difficulties. For example, land slide gives X on modified Mercalli scale but in some regions land slides can result from small shaking.

(b) In unpopulated areas and for off-shore earthquakes no isoseismal maps can be constructed.

A relation between magnitude M, distance R, and intensity I based on data from Mexico has been given by Esteva (1968, Reports to I.I. 182)

$$I = 1.45\,M - 5.7 \log_{10} R + 7.9$$

Abridged Modified Mercalli Intensity Scale

Note: The mean maximum acceleration and velocity values for the wave motion are for firm ground, but vary greatly depending on the type of earthquake source.

AVERAGE PEAK VELOCITY (CENTIMETERS PER SECOND)	INTENSITY VALUE AND DESCRIPTION	AVERAGE PEAK ACCELERATION (g IS GRAVITY = 980 CENTIMETERS PER SECOND SQUARED)
	I. Not felt except by a very few under especially favorable circumstances. (I Rossi-Forel Scale.)	
	II. Felt only by a few persons at rest, especially on upper floors of buildings. Delicately suspended objects may swing. (I to II Rossi-Forel Scale.)	
	III. Felt quite noticeably indoors, especially on upper floors of buildings, but many people do not recognize it as an earthquake. Standing motorcars may rock slightly. Vibration like passing of truck. Duration estimated. (III Rossi-Forel Scale.)	

1–2	IV. During the day felt indoors by many, outdoors by few. At night some awakened. Dishes, windows, doors disturbed; walls make cracking sound. Sensation like heavy truck striking building. Standing motorcars rocked noticeably. (IV to V Rossi Forel Scale.)	0.015g–0.02g
2–5	V. Felt by nearly everyone; many awakened. Some dishes, windows, and so on broken; cracked plaster in a few places; unstable objects overturned. Disturbances of trees, poles, and other tall objects sometimes noticed. Pendulum clocks may stop. (V to VI Rossi Forel Scale.)	0.03g–0.04g
5–8	VI. Felt by all, many frightened and ran outdoors. Some heavy furniture moved; a few instances of fallen plaster and damaged chimneys. Damage slight. (VI to VII Rossi-Forel Scale.)	0.06g–0.07g
8–12	VII. Everybody runs outdoors. Damage negligible in buildings of good design and construction; slight to moderate in well built ordinary structures; considerable in poorly built or badly designed structures; some chimneys broken. Noticed by persons driving cars. (VII Rossi-Forel Scale.)	0.10g–0.15g
20–30	VIII. Damage slight in specially designed structures; considerable in ordinary substantial buildings with partial collapse; great in poorly built structures. Panel walls thrown out of frame structures. Fall of chimneys, factory stacks, columns, monuments, walls. Heavy furniture overturned. Sand and mud ejected in small amounts. Changes in well water. Persons driving cars disturbed. (VIII + to IX Rossi-Forel Scale.)	0.25g–0.30g

45–55	IX. Damage considerable in specially designed structures; well designed frame structures thrown out of plumb; great in substantial buildings, with partial collapse. Buildings shifted off foundations. Ground cracked conspicuously. Underground pipes broken. (IX+ Rossi-Forel Scale.)	0.50g–0.55g
More than 60	X. Some well built wooden structures destroyed; most masonry and frame structures destroyed with foundations; ground badly cracked. Rails bent. Landslides considerable from river banks and steep slopes. Shifted sand and mud. Water splashed, slopped over banks. (X Rossi-Forel Scale.)	More than 0.60g
	XI. Few, if any, (masonry) structures remain standing. Bridges destroyed. Broad fissures in ground. Underground pipelines completely out of service. Earth slumps and land slips in soft ground. Rails bent greatly.	
	XII. Damage total. Waves seen on ground surface. Lines of sight and level distorted. Objects thrown into the air.	

Modified Mercalli Intensity Scale (1956 version)*

Masonry A, B, C, D. To an aid ambiguity of language, the quality of masonry, brick otherwise, is specified by the following lettering.

Masonry A. Good workmanship, mortar, and design; reinforced, especially lateral and bound together by using steel, concrete, etc.; designed to resist lateral forces.

Masonry B. Good workmanship and mortar; reinforced, but not designed in detail to resist lateral forces.

Masonry C. Ordinary workmanship and mortar; no extreme weaknesses like failing to tie in at corners, but neither reinforced nor designed against horizontal forces.

Masonry D. Weak materials, such as adobe; poor mortar; low standards of workmanship; weak horizontally.

*Original 1931 version in Wood, H. O., and Neumann, F., 1931, Modified Mercalli intensity scale of 1931: Seismological Society of America Bulletin, v. 21, no. 5, p. 277–283.
1956 version prepared by Charles F. Richter, in Elementary Seismology, 1958, pp. 137–138. W. Freeman and Company.

INTENSITY VALUE	DESCRIPTION

I. Not felt. Marginal and long-period effects of large earthquakes.

II. Felt by persons at rest, on upper floors, or favorably placed.

III. Felt indoors. Hanging objects swing. Vibration like passing of light trucks. Duration estimated. May not be recognized as an earthquake.

IV. Hanging objects swing. Vibration like passing of heavy trucks; or sensation of a jolt like a heavy ball striking the walls. Standing cars rock. Windows, dishes, doors rattle. Glasses clink. Crockery clashes. In the upper range of IV, wooden walls and frame creak.

V. Felt outdoors; direction estimated. Sleepers wakened. Liquids disturbed, some spilled. Small unstable objects displaced or upset. Doors swing, close, open. Shutters, pictures move. Pendulum clocks stop, start, change rate.

VI. Felt by all. Many frightened and run outdoors. Persons walk unsteadily. Windows, dishes, glassware broken. Knickknacks, books, etc. off shelves. Pictures off walls. Furniture moved or overturned. Weak plaster and masonry D cracked. Small bells ring (church, school). Trees, bushes shaken visibly, or heard to rustle.

VII. Difficult to stand. Noticed by drivers. Hanging objects quiver. Furniture broken. Damage to masonry D, including cracks. Weak chimneys broken at roof line. Fall of plaster, loose bricks, stones, tiles, cornices also unbraced parapets and architectural ornaments. Some cracks in masonry C. Waves on ponds, water turbid with mud. Small slides and caving in along sand or gravel banks. Large bells ring. Concrete irrigation ditches damaged.

VIII. Steering of cars affected. Damage to masonry C; partial collapse. Some damage to masonry B; none to masonry A. Fall of stucco and some masonry walls. Twisting, fall of chimneys, factory stacks, monuments, towers, elevated tanks. Frame houses moved on foundations if not bolted down; loose panel walls thrown out. Decayed piling broken off. Branches broken from trees. Changes in flow or temperature of springs and wells. Cracks in wet ground and on steep slopes.

IX. General panic. Masonry D destroyed; masonry C heavily damaged, sometimes with complete collapse; masonry B seriously damaged. General damage to foundations. Frame structures, if not bolted, shifted off foundations. Frames racked. Serious damage to reservoirs. Underground pipes broken. Conspicuous cracks in ground. In alluviated areas sand and mud ejected, earthquake fountains, sand craters.

X. Most masonry and frame structures destroyed with their foundations. Some well-built wooden structures and bridges destroyed. Serious damage to dams, dikes, embankments. Large landslides. Water thrown on banks of canals, rivers, lakes, etc. Sand and mud shifted horizontally on beaches and flat land. Rails bent slightly.

XI. Rails bent greatly. Underground pipelines completely out of service.

XII. Damage nearly total. Large rock masses displaced. Lines of sight and level distorted. Objects thrown into the air.

Magnitude Scales

- Intensity reported of an earthquake depends on the density of population, type of construction etc. It is subjective.
- If an earthquake occurs in the sea or an uninhabited area no intensity can be assigned to it.
- A 'measure' of the earthquake, which can be determined by seismic observatories all over the world, and be assigned a single number representing its 'strength' is needed.
- Wadati in Japan (1931) and Richter in California (1935) decided on a scheme which depended upon the wave amplitude measured by a seismograph.
- The earthquake size varies enormously, the amplitudes of the waves differ by factors of thousands from earthquake to earthquake.
- Richter defined the magnitude of a local earthquake (M_L) as the logarithm (base 10) of maximum seismic wave amplitude (in thousandths of a millimeter) recorded on a standard seismograph at 100 km distance from the epicenter. Since earthquake epicentral distance would be different than 100 km, Richter applied a correction for distance to take into account the attenuation: An example of how to calculate M_L is shown in the Figure.
- Type of wave for determining M_L is not specified. It is simply the largest amplitude. The wave could be P, S, or surface wave.
- Other magnitudes in common use are the body wave magnitude (m_b) and the surface wave magnitude (M_s)

EXAMPLE OF THE CALCULATION OF THE RICHTER MAGNITUDE (M_L) OF A LOCAL EARTHQUAKE

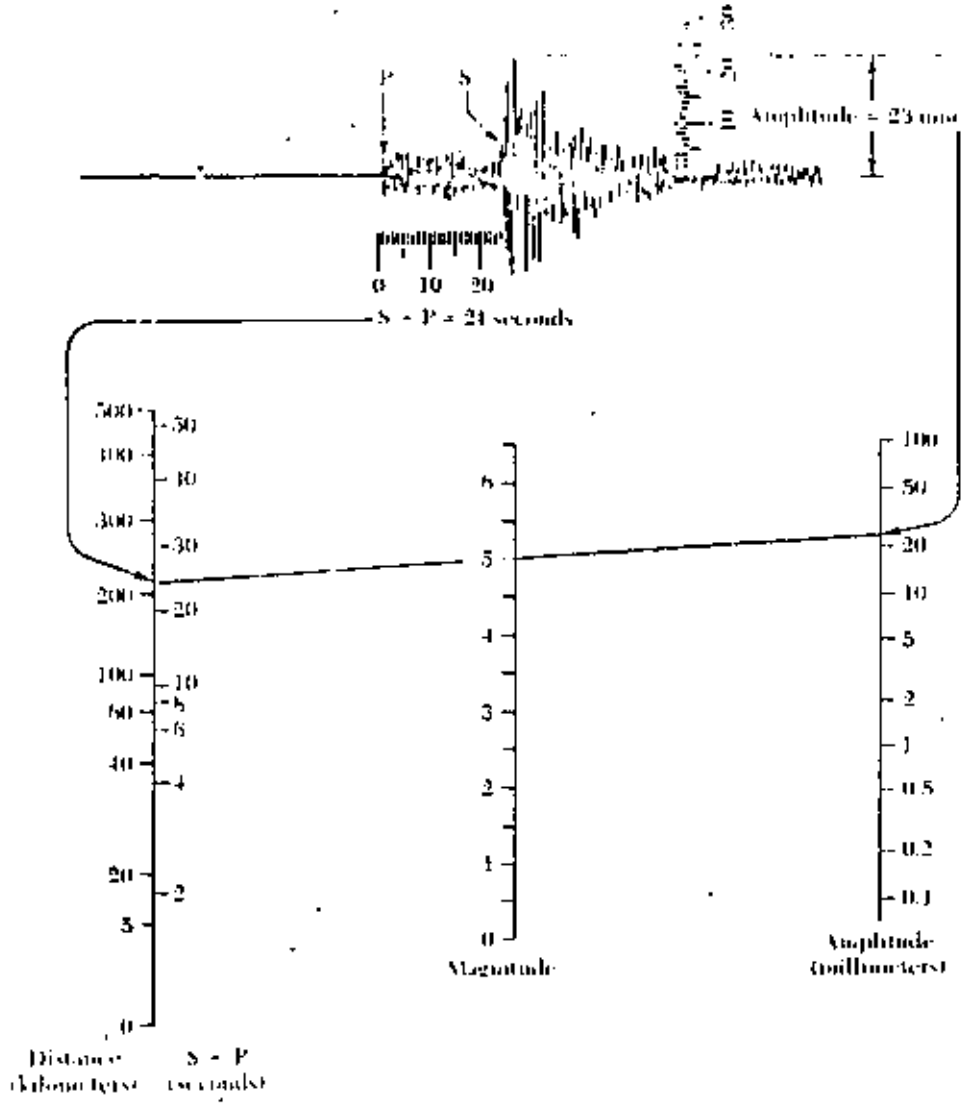

Procedure for calculating the local magnitude, M_L

1. Measure the distance to the focus using the time interval between the S and the P waves (S - P = 21 seconds).
2. Measure the height of the maximum wave motion on the seismogram (23 millimeters).
3. Place a straight edge between appropriate points on the distance (left) and amplitude (right) scales to obtain magnitude M_L = 5.0.

M_S was defined by Gutenberg in 1945 for shallow earthquakes

$$M_S = \log A_H + 1.656 \log \Delta + 1.818 + C \qquad (15^\circ < \Delta < 130^\circ)$$

where A_H = horizontal component of maximum ground motion (zero to peak, in microns) during surface wave having a period T of about 20 sec.

$$A_H = (A_N^2 + A_E^2)^{1/2}$$

A_N = max^m amplitude on N-S

A_E = max^m amplitude on E-W

- A modern version of the formula which has been adopted by International Association for Seismology and Physics of the Earth's Interior (IASPEI) is.

$$M_S = \log (A/T)_{max} + 1.66 \log \Delta + 3.3$$

For $T = 20$ the formula reduces to

$$M_S = \log A_{20} + 1.66 \log \Delta + 2.0$$

which is close to original Gutenberg formula, For details see Geller and Kanamori (Bull. Seism. Soc. Am., vol. 67, 1977, pp. 587-598.

- m_b, the body wave magnitude, is calculated from

$$m_b = \log (A/T) + Q$$

where Q is an empirically determined term which depends on Δ and source depth. A is the maximum amplitude (in micron) of P wave. In modern practice T, in general, is about 1 sec. (Other waves, such as PP or SH, are also sometimes used).

- Note that for the same earthquake M_L, m_b, and M_S magnitudes are, in general, different. This is to be expected since they are determined from different waves and at different periods. M_S and m_b are approximately related by $m_b = 2.5 + 0.63 M_S$
- Seismic energy E_S is empirically related to M_S by

$$\log E_S = 1.5 M_S + 11.8$$

- It has been shown (recently) that for large earthquakes (maximum dimension of rupture $\gtrsim 100$ km), M_S begins to get saturated. Thus although the seismic energy may keep on increasing, M_S does not increase.

To circumvent the problem of saturation of M_S

another magnitude called the minimum strain energy magnitude (M_W) has been introduced (Kanamori, J. Geophys. Res., vol 82, 1977, pp. 1981-1987). Total energy released in an earthquake can be written as

$$E_t = \bar{\sigma}\,\bar{u}\,A$$

where $\bar{\sigma} = (\sigma_1+\sigma_2)/2$ = average stress
σ_1 = initial stress
σ_2 = final stress
$\bar{u}$ = average dislocation on the fault surface
A = fault area.

The total energy release E_t is the sum of energy lost in friction, E_f, and energy radiated as seismic waves. Thus

$$E_t = E_f + E_S$$

$$\therefore \quad E_S = -E_f + E_t$$

$$= -\sigma_f\,\bar{u}\,A + \bar{\sigma}\,\bar{u}\,A = \bar{u}A\left(\frac{\sigma_1+\sigma_2}{2} - \sigma_f\right)$$

If $\sigma_f = \sigma_2$, which is called Orowan model, then

$$E_S = \bar{u}\,A\,\frac{(\sigma_1-\sigma_2)}{2}$$

$$= \frac{\bar{u}\,A\,\Delta\sigma}{2} \quad \text{where } \Delta\sigma = \text{stress drop} = \sigma_1-\sigma_2$$

$$= \frac{\Delta\sigma\, M_0}{2\mu} \quad \text{where } M_0 = \mu A \bar{u} = \text{Seismic moment}$$

Experience shows that Orowan's model is reasonable. μ = rigidity

$$\therefore \quad \log E_S = \log M_0 + \log\left(\frac{\Delta\sigma}{2\mu}\right)$$

Since $\frac{\Delta\sigma}{\mu} \simeq 1\times10^{-4}$ for large interplate earthquakes, then

$$\log E_S = \log M_0 - 4.3$$

Thus if we can estimate M_0 (and it is possible to do so if we know the area of rupture from aftershocks etc.), we

can estimate E_s. Since Gutenberg-Richter magnitude-energy relation, valid for max^m rupture length $\lesssim 100$ km, is

$$\log E_s = 1.5\, M_s + 11.8$$

and

$$\log E_s = \log M_0 - 4.3 \quad \text{for all earthquakes,}$$

magnitude M_w can be defined such that

$$1.5\, M_w + 11.8 = \log M_0 - 4.3$$

or, $$M_w = \frac{2}{3} \log M_0 - 10.73$$

This M_w would be nearly equal to M_s for max^m rupture length $\lesssim 100$ km but for larger earthquake it would not suffer from saturation. For example Chile earthquake (May 22, 1960) $M_s = 8.3$ but $M_w = 9.5$. On the M_w scale this earthquake turns out to be the largest earthquake of this century! The following Table taken from Kanamori (1977)

Sample Calculation of Magnitudes and Energy of an Earthquake

The following calculations are for an Alaskan earthquake recorded at Oroville, California. The energy factor (equation 4) allows us to get an idea of the scale of energy release that is possible for earthquakes of different magnitude. For instance, we would need 30 earthquakes of magnitude 6 to release the equivalent amount of energy in the Earth's crust as released by just one magnitude 7 earthquake, and we would need 900 magnitude 5 earthquakes to produce the same energy. It follows, therefore, that even if small earthquakes occur in swarms in a particular area, they do very little to reduce the reservoir of strain energy needed for a major earthquake. But tectonic energy is drained away into heat and seismic waves in a truly gigantic way by a major earthquake like that of 1906 along the San Andreas fault with a magnitude M_s of 8¼. That earthquake released about 10^{24} ergs of strain energy within 60 seconds! (Only a fraction went into ground shaking.)

It is well known that, as the threshold of earthquake size being considered in a seismic region is lowered, the number of earthquakes above that magnitude rapidly increases [illegible]. The rate of occurrence of shocks above a given magnitude is again logarithmic and is measured by a parameter b (see equation 5). The smaller b is the more numerous are the earthquakes in a given time span. When b is determined for a seismically active region, the total seismic energy released over a period can be calculated by using the energy factor.

Magnitude is also sometimes roughly estimated from the length of surface fault rupture L (in kilometers—see equation 6).

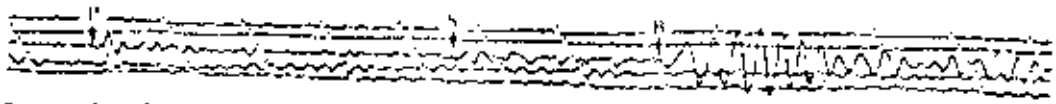

Let A be the amplitude, and T the period of a wave measured at a distance Δ from the source. One minute between gaps.

Measured values (reduced to ground motion)

P wave, A = 1.4 microns, T = 12 sec

Rayleigh wave, A = 4.3 microns, T = 20 sec

$\Delta = 28°$

Body wave magnitude m_b ($25° < \Delta < 90°$)

$$m_b = \log A - \log T + 0.01\,\Delta + 5.9 \qquad (1)$$

$$= 0.15 - 1.08 + 0.28 + 5.9$$

$$= 5.3$$

Surface wave magnitude M_s ($25° < \Delta < 90°$)

$$M_s = \log A + 1.66 \log \Delta + 2.0 \quad (2)$$
$$= 0.63 + 2.40 + 2.0$$
$$= 5.0$$

Relation between m_b and M_s (approximate)

$$m_b = 2.5 + 0.63\, M_s \quad (3)$$
$$= 2.5 + 3.2 \text{ (above earthquake)}$$
$$= 5.7 \text{ (compared with 5.3 calculated directly)}$$

Seismic energy E

$$\log E = 11.8 + 1.5\, M_s \quad (4)$$
$$= 19.3$$
$$E = 2.0 \times 10^{19} \text{ ergs}$$

Relation between n and M_L

$$\log n = a - b\, M_L \quad (5)$$

Relation between M_s and L (worldwide data)

$$M_s = 6.03 + 0.76 \log L \quad (6)$$

Relation between M_s and S the area of rupture (Worldwide data)

$$M_S = 3.21 + 1.92 \log S - 0.18 (\log S)^2 \quad (7).$$

For a theoretical basis for empirical relations in seismology see Kanamori and Anderson (Bull. Seism. Soc. Am., vol. 65, 1975) and Geller (Bull. Seism. Soc. Am., vol. 66, 1976).

LIST OF GREAT EARTHQUAKES WITH M_S, M_o, AND M_W VALUES.
(H. Kanamori, J. Geophys. Res., v. 82, 1977)

TABLE . Great Earthquakes

Date	Region	M_s	M_o 10^{27} dyn cm	M_w	Source for M_o Value*
June 25, 1904	Kamchatka	8.0			
June 25, 1904	Kamchatka	8.1			
April 4, 1905	East Kashmir	8.0			
July 9, 1905	Mongolia	8¼	50	8.4	*Okal* [1977].
July 23, 1905	Mongolia	8¼	50	8.4	*Okal* [1977].
Jan. 31, 1906	Ecuador	8.6	204	8.8	From the aftershock area.
April 18, 1906	San Francisco	8¼	10	7.9	Estimated from fault length of 500 km, width of 15 km, and dislocation of 5 m.
Aug. 17, 1906	Rat Islands	8.0			
Aug. 17, 1906	Central Chile	8.4	29	8.2	From the aftershock area.
Sept. 14, 1906	New Britain	8.1			
April 15, 1907	Mexico	8.1			
Oct. 21, 1907	Afghanistan	8.0			
Jan. 3, 1911	Turkestan	8.4	4.9	7.7	*Chen and Molnar* [1977]
May 23, 1912	Burma	8.0			
May 1, 1917	Kermadec	8.0			
June 26, 1917	Samoa	8.3			
Aug. 15, 1918	Mindanao	8¼			
Sept. 7, 1918	Kurile	8¼			
April 30, 1919	Tonga	8.3			
June 5, 1920	Taiwan	8			
Sept. 20, 1920	Loyalty Islands	8			
Dec. 16, 1920	Kansu, China	8.5	6.6	7.8	*Chen and Molnar* [1977].
Nov. 11, 1922	Central Chile	8.3	69	8.5	From the aftershock area.
Feb. 3, 1923	Kamchatka	8.3	37	8.3	From the aftershock area.
Sept. 1, 1923	Kanto	8.2	8.5	7.9	
April 14, 1924	Philippine	8.3			
May 22, 1927	Tsinghai, China	8.0	3.0	7.6	*Chen and Molnar* [1977].
June 17, 1928	Guerrero, Mexico	7.8	12	8.0	From the aftershock area.
Dec. 1, 1928	Central Chile	8.0	3	7.6	From the aftershock area.
March 7, 1929	Fox Islands (Aleutian)	8.1	6.7	7.8	*Kanamori* [1972b].
Aug. 10, 1931	Sinkiang, China	8.0	12	8.0	*Chen and Molnar* [1977].
May 14, 1932	Molucca	8.0	1.5	7.4	From the 100-s magnitude
June 3, 1932	Jalisco, Mexico	8.1	15	8.1	Average of value from the aftershock area and value from the 100-s magnitude.
March 2, 1933	Sanriku	8.5	43	8.4	
Jan. 15, 1934	India-Nepal	8.3	16	8.1	*Chen and Molnar* [1977]
July 18, 1934	Santa Cruz Islands	8.2	0.8	7.2	From the 100-s magnitude based on one station.
Feb. 1, 1938	Banda Sea	8.2	70	8.5	From the 100-s magnitude.
Nov. 10, 1938	Alaska	8.3	28	8.2	Average of value from the aftershock area and value from the 100-s magnitude.
April 30, 1939	Solomon Islands	8.0			
Dec. 26, 1939	Turkey	8.0			
May 24, 1940	Peru	8.0	25	8.2	From the aftershock area.
June 26, 1941	Andaman Islands	8.1	3	7.6	From the 100-s magnitude.
Nov. 25, 1941	North Atlantic	8.3			
Aug. 24, 1942	Peru	8.1	27	8.2	From the aftershock area.
April 6, 1943	Chile	7.9	28	8.2	From the aftershock area.
Dec. 7, 1944	Tonankai	8.0	15	8.1	
Nov. 27, 1945	West Pakistan	8¼			
Aug. 4, 1946	Dominican Republic	8.1			
Dec. 20, 1946	Nankaido	8.2	15	8.1	
Jan. 24, 1948	Philippine	8.2			
Aug. 22, 1949	Alaska	8.1	15	8.1	From the aftershock area.
Aug. 15, 1950	Assam	8.6	100	8.6	Average of values from *Ben-Menahem et al* [1974], *Chen and Molnar* [1977], and G. S. Stewart (personal communication, 1977).
Nov. 18, 1951	Tibet	8.0	1.9	7.5	*Chen and Molnar* [1977].
March 4, 1952	Tokachi-oki	8.3	17	8.1	
Nov. 4, 1952	Kamchatka	8¼	350	9.0	*Kanamori* [1976b].
March 9, 1957	Aleutian Islands	8¼	585	9.1	From the aftershock area.
Dec. 4, 1957	Mongolia	8.3	18	8.1	*Okal* [1976].
July 10, 1958	Alaska	7.9	29	8.2	From the aftershock area.
Nov. 6, 1958	Kurile Islands	8.7	40	8.3	Y. Fukao (personal communication, 1977).
May 4, 1959	Kamchatka	8¼	26	8.2	From the aftershock area.
May 22, 1960	Chile	8.3	2000	9.5	
Oct. 13, 1963	Kurile Islands	8.1	67	8.5	
March 28, 1964	Alaska	8.4	820	9.2	
Feb. 4, 1965	Aleutian Islands	7¾	125	8.7	
Oct. 17, 1966	Peru	7.5	20	8.1	
May 16, 1968	Tokachi-oki	7.9	28	8.2	
Feb. 28, 1969	North Atlantic	8.0	6	7.8	
Aug. 11, 1969	Kurile Islands	7.8	22	8.2	

TABLE - (Continued)

Date	Region	M_S	M_o 10^{27} dyn cm	M_W
May 31, 1970	Peru	7.8	10	7.9
Jan. 10, 1971	West New Guinea	8.1	–	–
Oct. 3, 1974	Peru	7.6	15	8.1
May 26, 1975	North Atlantic	7.9	5	7.7
July 27, 1976	China	8.0	2	7.5
Aug. 16, 1976	Mindanao	8.2	19	8.1

SOURCE PARAMETERS

Description of the Earthquake Source

Apart from the hypocentral location and magnitude of an earthquake there are several other source parameters (which require special study) which shed light on the details of the earthquake process, give important data on the current tectonics of the area, and may help in future earthquake predictions.

Earthquake: When two sides of an earthmass suddenly move with respect to one another, seismic waves are generated and earthquake is said to have occurred. Reid studying 1906 San Francisco earthquake proposed the "Elastic Rebound Theory."

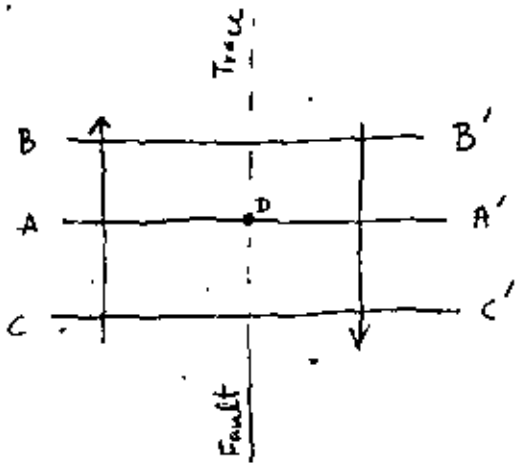

Initially

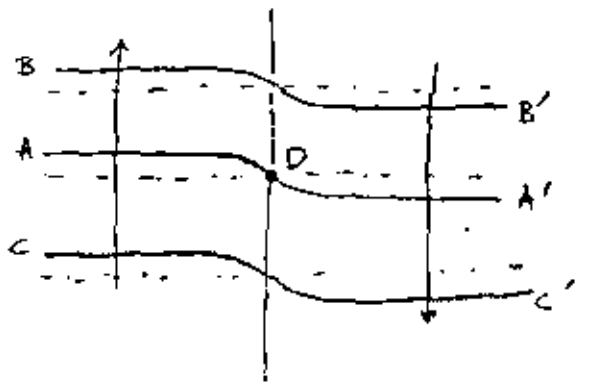

Strained state:

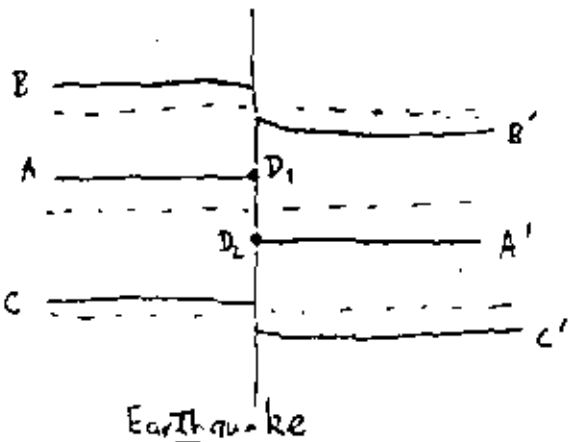

Earthquake

Imagine 3 parallel lines AA', BB', CC'. Due to tectonic forces these lines are deformed (strained state) till the rock breaks at a point D: This breakage at D along the fault trace is an earthquake (The breakage is not limited to point D only but to points adjacent to it as well). Since the tectonic forces causing the strain change very slowly the cycle is repeated. Reid's theory works well for atleast shallow earthquakes. Summarizing then an earthquake is a sudden dislocation in an earth mass. The following Fig. gives a schematic drawing of how a rupture may nucleates at focus & the dislocation propagates on the fault plane. Dislocation, in general, does not reach the surface although there are exceptions such as 1906 San Francisco earthquake and the recent Motagua, Guatemala earthquake. The rupture velocity in large earthquakes

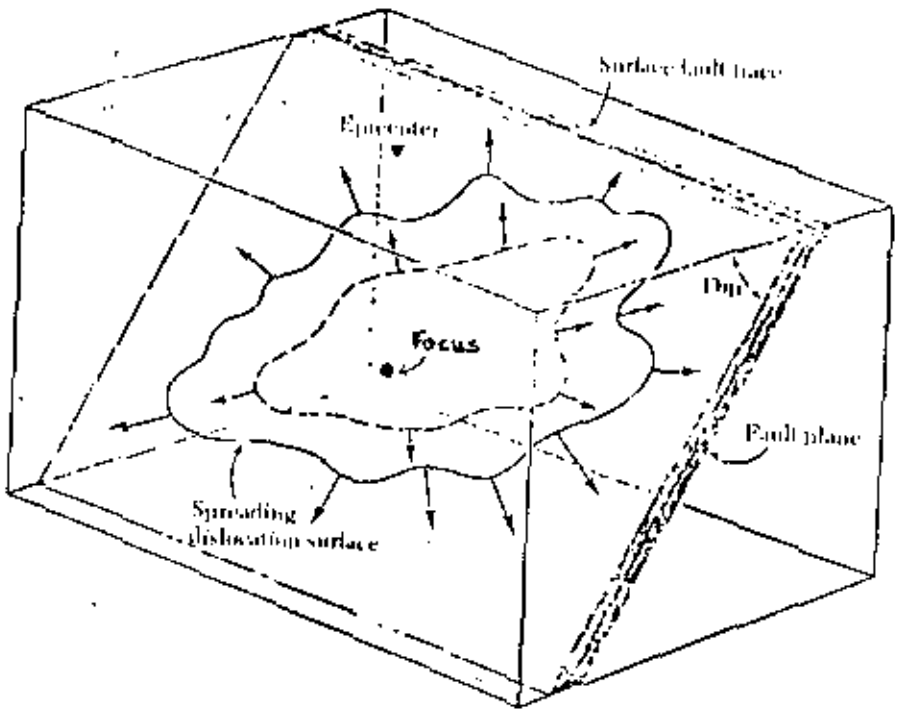

may vary; the rupture may be rather complex. The details of rupture are reflected in recorded seismic waves.

Focal Mechanism: P-wave arrives first at a seismic station. For the same earthquake at some stations the polarity of P wave is found to be up (compressional), at others down (dilatational). Moreover distribution of compressions and dilatations forms a systematic pattern.

Remembering that an earthquake is a dislocation and that it can be shown that a dislocation can be represented by a double couple system of forces (without moment), it.

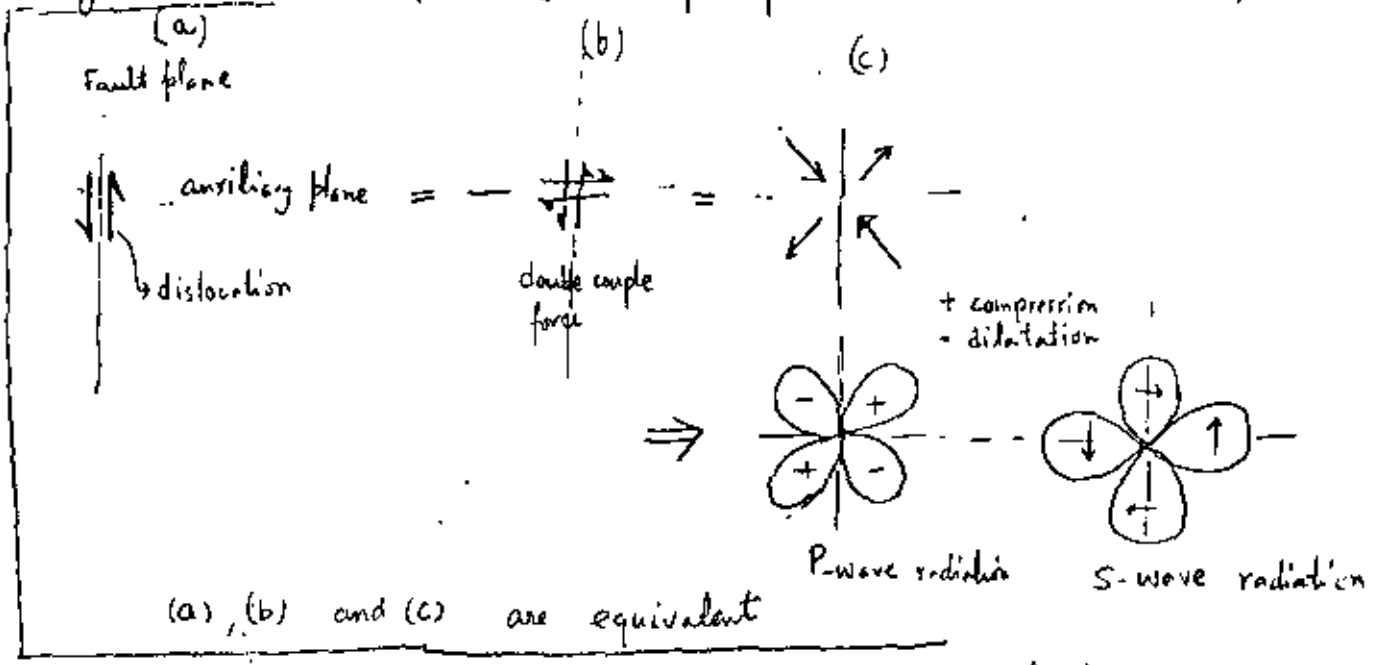

follows from the above Fig. that from the polarity of P waves (and from the polarization of S waves) 2 planes can be determined; one of which is the fault plane. It is not possible to know, however, which of these 2 planes is the fault plane, except from geological information. However geological constraints, in most cases, are sufficient to ascertain the fault plane. This information is of great importance in tectonic studies. Also the fault plane orientation is needed for recovering other source parameter from the seismograms. From the focal mechanism study, the type of

faulting (there are 3 types of faulting : normal, strike-slip, and reverse ; see next Fig.) is thus determined.

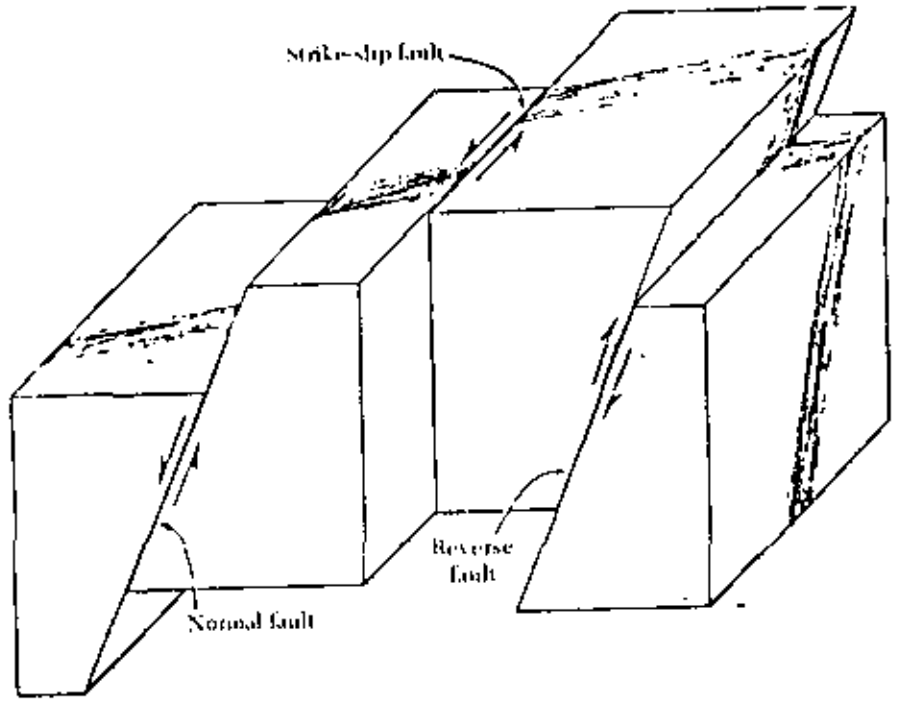

Diagram showing the three main types of fault motion.

The problem of determination of focal mechanism of an earthquake from world-wide data is complicated by the fact that the earth is spherical and the velocity with depth (which causes rays to bend). The procedure consists of imagining a sphere surrounding the source. The rays arriving at different distances (Δ) are traced back to the focal sphere. A stereographic projection of the sphere is made : From the distribution of compression and dilatation on this projection, the 2 planes are determined.

Just as the distribution of seismicity defines the boundary of the plate, the focal mechanism defines the type of the boundary (accreting, transform or subducting) as well as the direction of motion of adjacent plates.

The next Fig. shows, schematically, how the focal mechanism is determined.

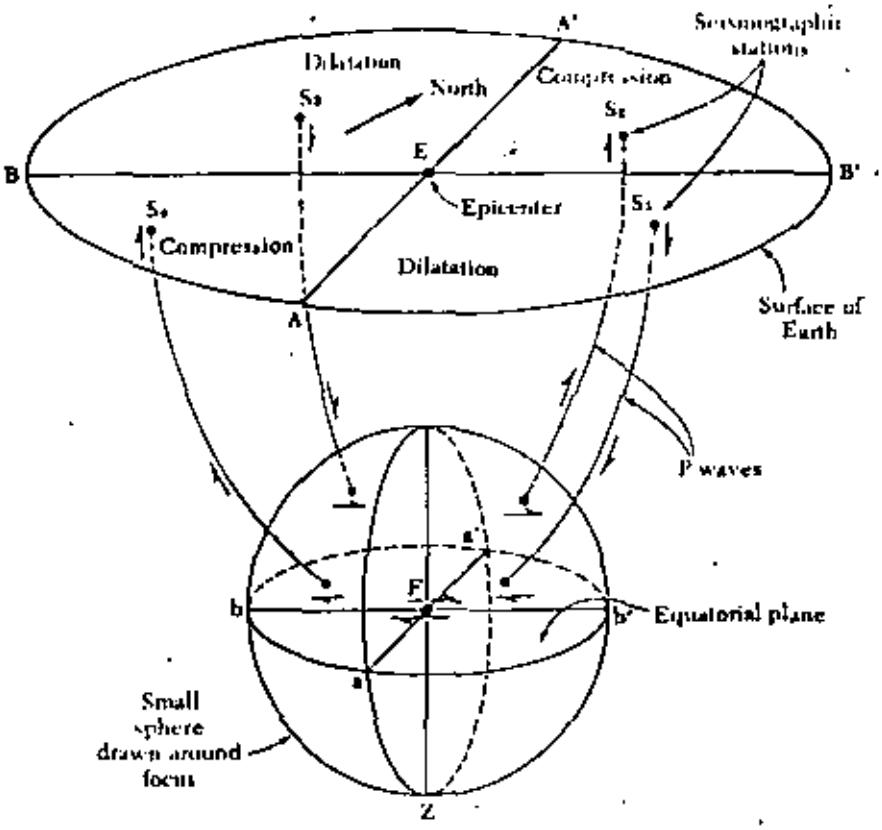

The diagram below is a plan view looking down on the circle A'B'AB. For this earthquake, a quadrantal pattern of compressions and dilatations would be observed at the surface. One of the lines A'EA' or BEB' that separate the different motions will indicate the strike and dip of the fault plane. (In this case, BEB' corresponds to the direction of the fault.)

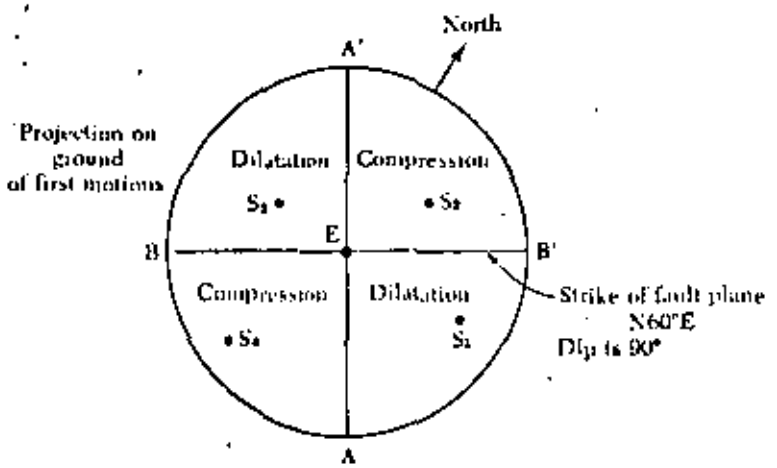

Seismic Moment:

In recent years the seismic moment M_0 has become one of the most important source parameters since it measures the 'size' of an earthquake at very low frequencies ($\omega \to 0$) and thus measures the gross nature of the earthquake (the details of the dislocation does not affect M_0) and M_0 does not suffer from saturation problem of M_S and m_b magnitudes. M_0, the seismic moment, is defined by

$$M_0 = \mu A \bar{u}$$

where μ = rigidity, A = rupture area, and $\bar{u}$ = average dislocation. M_0 can be estimated from geodetic measurements (for surface faulting), free oscillation data, spectra of P and S waves and surface waves. Consistent value of M_0 is found from the different methods.

At long wavelengths and large distance as compared to the source dimension and at periods greater than the duration of rupture an earthquake may be viewed as point shear dislocation acting as a step function of time. (As mentioned before a point dislocation is equivalent to a double couple point source). Spectra of displacement components are given by

$$\Omega_P(\omega) = \frac{1}{4\pi r} \frac{M_0}{\rho \alpha^3} R_P(\theta, \phi) \quad : \text{P-wave}$$

$$\Omega_S(\omega) = \frac{1}{4\pi r} \frac{M_0}{\rho \beta^3} R_S(\theta, \phi) \quad : \text{S-wave}$$

where r = distance from source to observation point, α, β = P and S wave velocity, $R_{P,S}(\theta, \phi)$ = radiation pattern of P and S waves, ρ = density. Since point source approximation is valid for wave lengths > source dimension, we note that

the low frequency spectral amplitudes are independent of frequency and details of the rupture process. Thus the low frequency level of spectra gives M_0. Clearly the result given above is for an elastic, homogeneous, isotropic infinite space. For real earth several corrections to the observed spectra are made. In recent years seismic moment M_0 is being determined from synthetic modelling of earthquakes. The procedure consist of fitting observed seismograms to the computed seismograms in a realistic earth.

Stress Drop: Let the initial and final shear stresses be σ_1 and σ_2. Stress drop $\Delta\sigma$ is defined as

$$\Delta\sigma = \sigma_1 - \sigma_2$$

Let us consider a circular fault over which the stress drops from σ_1 to σ_2. It can be shown that (Singh, Bull. Seism. Soc. Am. 1977)

$$\Delta\sigma = \frac{7\pi}{16}\mu\frac{\bar{u}}{a}, \quad a = \text{radius of the fault}$$

Since $M_0 = \mu A \bar{u}$, it follows that

$$\Delta\sigma = \frac{7}{16}\frac{M_0}{a^3} = \frac{7\pi^{3/2}}{16}\frac{M_0}{A^{3/2}}$$

Thus if we know M_0 and the radius of the fault a, we can compute $\Delta\sigma$. Similar relations for other type of fault geometries can be derived.

Area of Rupture: Area of rupture associated with an earthquake can be determined from aftershock

observed in this field (only a few earthquakes). Aftershock area, generally, grows with time. and it seems that 1 to 2 day aftershock locations define the rupture are well.

From above,

$$M_0 = \frac{16}{7\pi^{3/2}} \Delta\sigma \; A^{3/2}$$

$$\therefore \log M_0 = \frac{3}{2} \log A + \log\left(\frac{16\,\Delta\sigma}{7\pi^{3/2}}\right)$$

Good quality data on well studied earthquakes are shown in the following Fig:

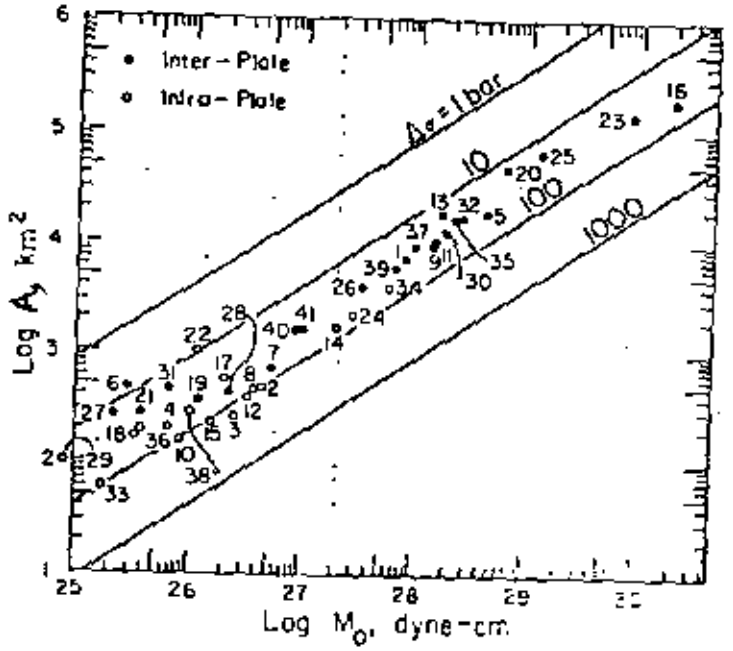

Data show that remarkable linearity with a slope of 2/3 between log A and log M_0. The linearity is explained in terms of constant stress drop. The stress $\Delta\sigma$ for interplate (boundary of plates) earthquakes is about 30 bars and for intraplate earthquakes $\Delta\sigma \simeq 75$ bars. The stress drop is nearly independent of the size of the earthquake. That $\Delta\sigma$ lies between

10^3 to 100 bars is surprising since the estimated stresses in the plates are of the order of a kilobar.

(1 bar = 10^6 dyne/cm^2 ≃ 1 atmosphere)

If $\Delta\sigma = 30$ bars then

$$M_0 \simeq 1.23 \times 10^{22} A^{3/2} \text{ dyne cm} \quad (A \text{ in km}^2).$$

Thus an estimate of M_0 can be made for an earthquake from the above relation if we know A. Example: Chile earthquake of May 22, 1960, A = 200,000 km^2. Thus from above relation $M_0 = 1.1 \times 10^{30}$ dyne-cm. The moment determined from study of seismic waves is $M_0 = 2 \times 10^{30}$ dyne-cm, about a factor of 2 more.

As mentioned in the section of magnitudes, knowing M_0 we can compute the minimum strain energy magnitude M_W.

Equivalent radius of the fault: Spectra of teleseismic P and S waves is schematically shown below. The spectra

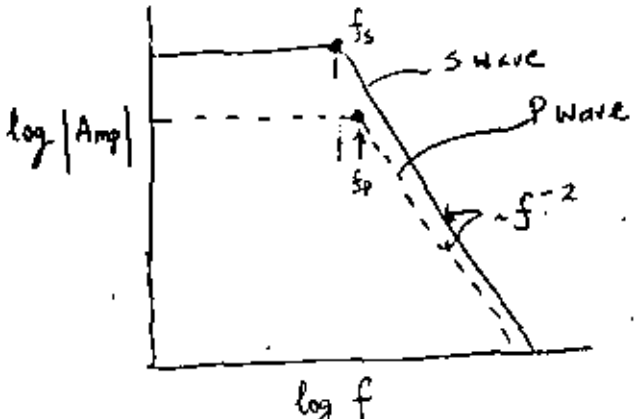

are flat at low frequencies and then decays $\sim f^{-2}$. The corner frequency f_s (or f_p) is defined by the intersection of the 2 slopes. Theoretically it has been shown that

$$f_s \simeq 0.37\beta/a \qquad f_p \simeq 0.37\alpha/a$$

a = radius of fault
α = P wave velocity
β = S wave velocity

From observed spectra f_s and f_p, and thus a, can be estimated.

Near-Field Ground Motion: Just what ground motion can be expected near the source of an earthquake is important question in seismic engineering and is difficult question to answer. Regressions on M (magnitude), distance and recorded strong motion (say acceleration) has been carried out by several authors but since the data near the surface are very few, extrapolation of the regression curves at short distances is of dubious value. Recourse to more deterministic models is preferable.

Given a dislocation on a fault surface it is not difficult to compute the near-field ground motion but since we don't know the likely dislocation, the exercise is somewhat futile. Also the stresses associated with the dislocation may not be realistic. A simple physical argument of Brune (J. Geophys. Res., vol. 75, 1970, pp. 4997-5009) leads to some interesting results.

Assume that stress drop occurs instantaneously over the fault surface. For points near the fault and for short time after the stress drop the fault can be thought as infinite.

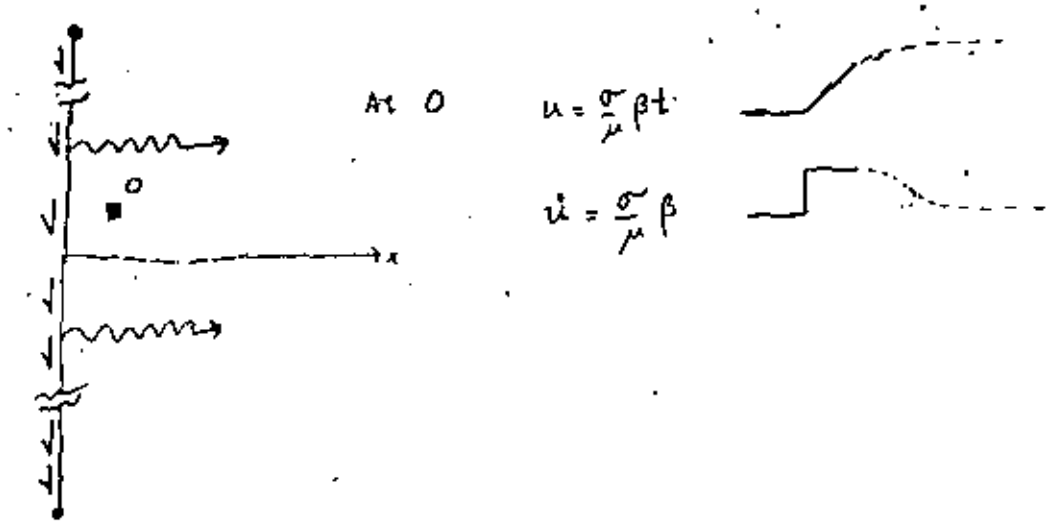

Thus $\sigma(x,t) = \sigma H(t - x/\beta)$ where $H(t)$ is unit step function

$$\sigma = \mu \frac{\partial u}{\partial x}$$

$\therefore$ At $x=0$ $\quad u = 0 \quad , t<0$

$u = \left(\frac{\sigma}{\mu}\right)\beta t \quad , 0<t<T$, where T is the time required for elastic waves to propagate from the ends of the ruptured surface.

$$\dot{u} = \frac{\sigma\beta}{\mu}$$

$= 100$ cm/sec if $\sigma = 100$ bars (10^8 dyn/cm^2), $\mu = 3\times10^{11}$ dyn/cm^2, $\beta = 3$ km/sec.

Thus the initial velocity is directly proportional to the stress drop. A max^m of 150 cm/sec appears reasonable. Although acceleration is infinite as the wave arrives, it can be calculated for any finite band of frequency.

$$\ddot{u}(t) = \frac{\sigma\beta}{\mu}\delta(t) = \frac{\sigma\beta}{\mu}\frac{1}{2\pi}\int_{-\infty}^{\infty} e^{i\omega t}\, d\omega$$

If we consider a finite frequency band from 0 to ω_s then

$$\ddot{u}(t) = \frac{\sigma\beta}{\mu}\frac{1}{2\pi}\int_{-\omega_s}^{\omega_s} e^{i\omega t}\, d\omega$$

$$= \frac{1}{\pi}\frac{\sigma}{\mu}\beta\,\omega_s\left(\frac{\sin\omega_s t}{\omega_s t}\right)$$

If the cut off frequency is 10 Hz and $\sigma = 100$ bars, then

$$\ddot{u}(t) \simeq 2g$$

The largest observed acceleration observed to date is about 1.25 g, for the San Fernando earthquake of 1971.

Attenuation :

A plane wave propagating in earth decreases in amplitude due to attenuation by internal friction. The decrease in amplitude can be roughly approximated by

$$A(f,t) = A_0 e^{-\pi f t/Q} = A_0 e^{-\pi f R/Qv}$$

where A_0 = initial amplitude, f = frequency, t = travel time, Q = attenuation coefficient, R = distance and v = wave velocity (α or β). Larger the Q less is the attenuation. Even if Q were constant (independent of frequency), at high frequencies the wave would be attenuated rapidly. There are many definitions of Q. An excellent review paper on Q is by Knopoff (Rev. Geophys., Vol. 2, 1964, pp 625-660).

Generally it has been assumed that Q is constant over a broad frequency range. However recent work based on coda analysis of local earthquakes suggest that for a range of 1 to 25 Hz, $Q \propto f^n$ where $0.5 \leq n \leq 0.8$. Thus Q increases with frequency. The following fig. shows results on Q_β (for shear waves), from Aki (1979, preprint). The result is important since the frequency range of 1 to 10 Hz is of interest in seismic engineering. $Q_\beta \simeq 500$ at $f \leq 0.06$ ($T \geq 20$ sec). It appears to reach at minimum at $f \simeq 0.5$ ($T \simeq 2$ sec) afterwhich it increases ...

$A(f,t) = A_0 e^{-\pi f t/Q} = A_0 e^{-\pi f R/Qv}$

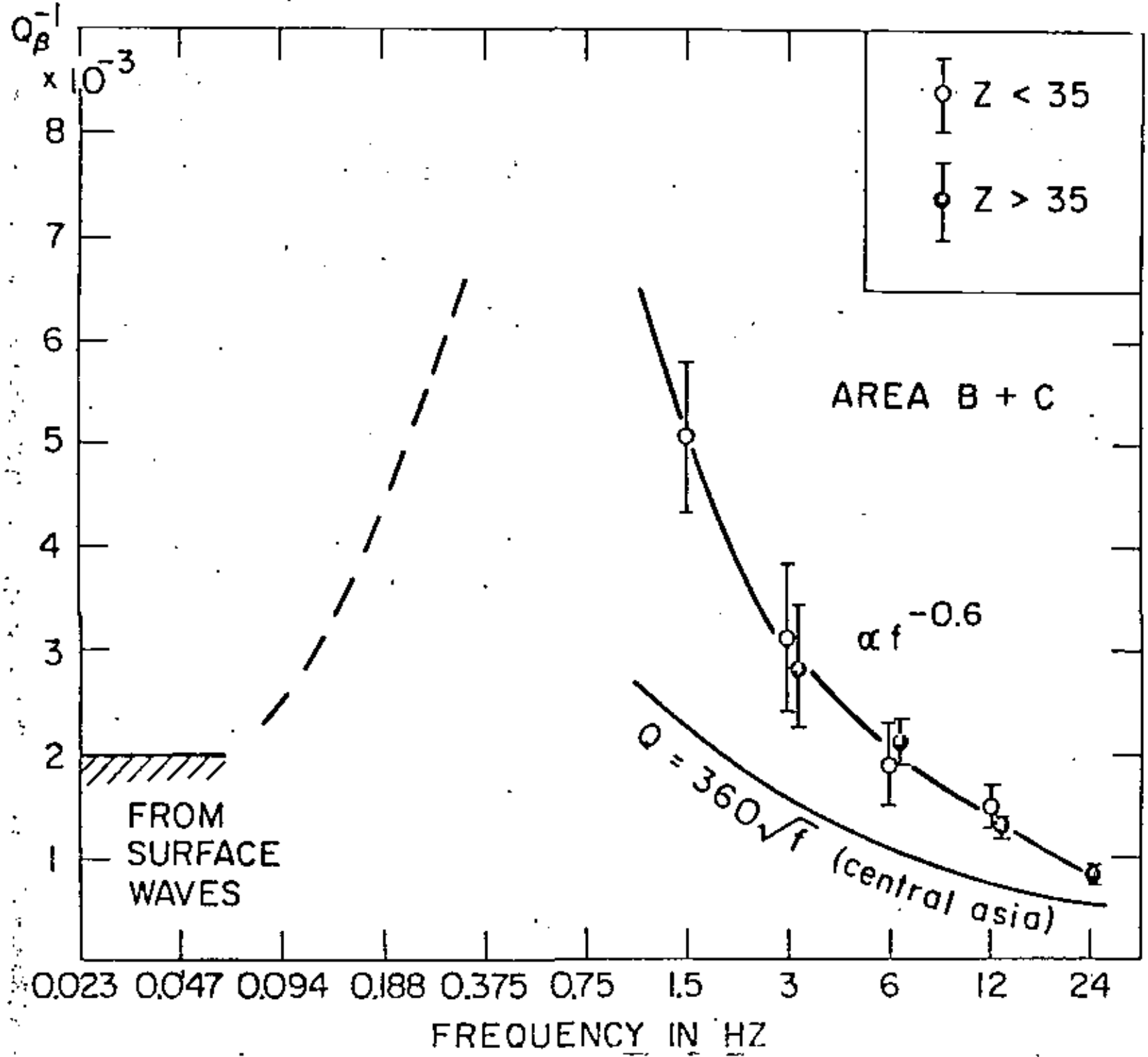

Coming back to near-field ground motion, since the peak accelerations are associated with high frequency seismic waves (3–10 Hz), Q, along with scattering, plays an important role in determining the pattern of strong motion. High frequencies would be attenuated at short distances, independent of fault size. Geometrical spreading in the nearfield is ofcourse governed by the fault size. The effect of Q is accentuated by the fact that large amplitude waves (near the source) may act nonlinearly and drastically lower the effective Q. Q near the source may be as low as 50. For Q = 50 at 5 Hz, e^{-1} distance is 10 km. Uncertainty in Q is the greatest source of error in estimating upper limits for particle velocity and acceleration.

An excellent reference on near-field ground motion is:

Brune, J. N. (1976) "The Physics of Earthquake Ground Motion" in C. Lomnitz and E. Rosenblueth (Editors) "Seismic Risk and Engineering Decisions", Elsevier Pres.

Seismicity:

As mentioned earlier seismicity, mostly, is confined to the plate boundaries. In fact some of the boundaries of the plates (and thus their number) is defined by the seismicity. At the accretion boundary, where hot material unwells, only small earthquakes occur. It is at transform faults and subduction zones where large and great earthquakes occur. Subduction zones are, by far, the largest contributors to the energy release.

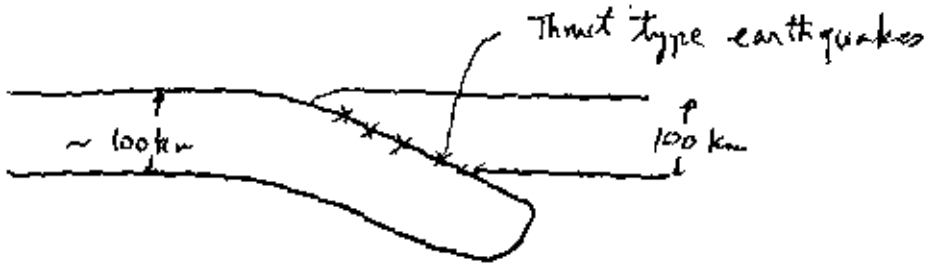

The earthquakes which occur on the plate boundaries are called <u>interplate</u> earthquakes and those which occur in the plates are called <u>intraplate</u> earthquakes. Note that in plate tectonics (the plates are assumed rigid) no <u>intraplate</u> earthquakes are assumed to occur.

About 75% of the shallow focus seismic energy is released along the circum Pacific belt. About 23% is released around the trans-Asiatic or Alpide belt which extends from Indonesia through Himalayas to the Mediterranean. The intermediate (70-300 km) and deep-focus (>300 km) earthquake energy release is even more pronounced for the Pacific belt.

Table . (Data from Bäth and Duda, 1979)
Average annual frequency and energy for given magnitudes for the interval 1905 - 1977.

Magnitude M	Annual frequency $\Sigma N/yr$	Annual energy - $\Sigma EN/year, 10^{25}$ ergs
≥ 6.0	209	0.63
≥ 6.5	63	0.61
≥ 7.0	19	0.57
≥ 7.5	6	0.52
≥ 8.0	2	0.42
≥ 8.5	0.4	0.26

Recall the Energy - magnitude relation

$$\log E = 1.5\,M + 11.8$$

Thus a magnitude 7 earthquake releases about 30 times as much energy as a magnitude 7 earthquake. It is the large earthquakes that contribute heavily to the energy. It also follows that small earthquakes can not act as 'valves' in releasing accumulated strain energy.

Frequency - magnitude relations for the interval 1905 - 1977 (world wide) ($M \geq 7.0$) are shown in the following Figure. Dots: Single frequency N (M intervals of 0.1 unit) and Stars refer to cumulative frequency ΣN.

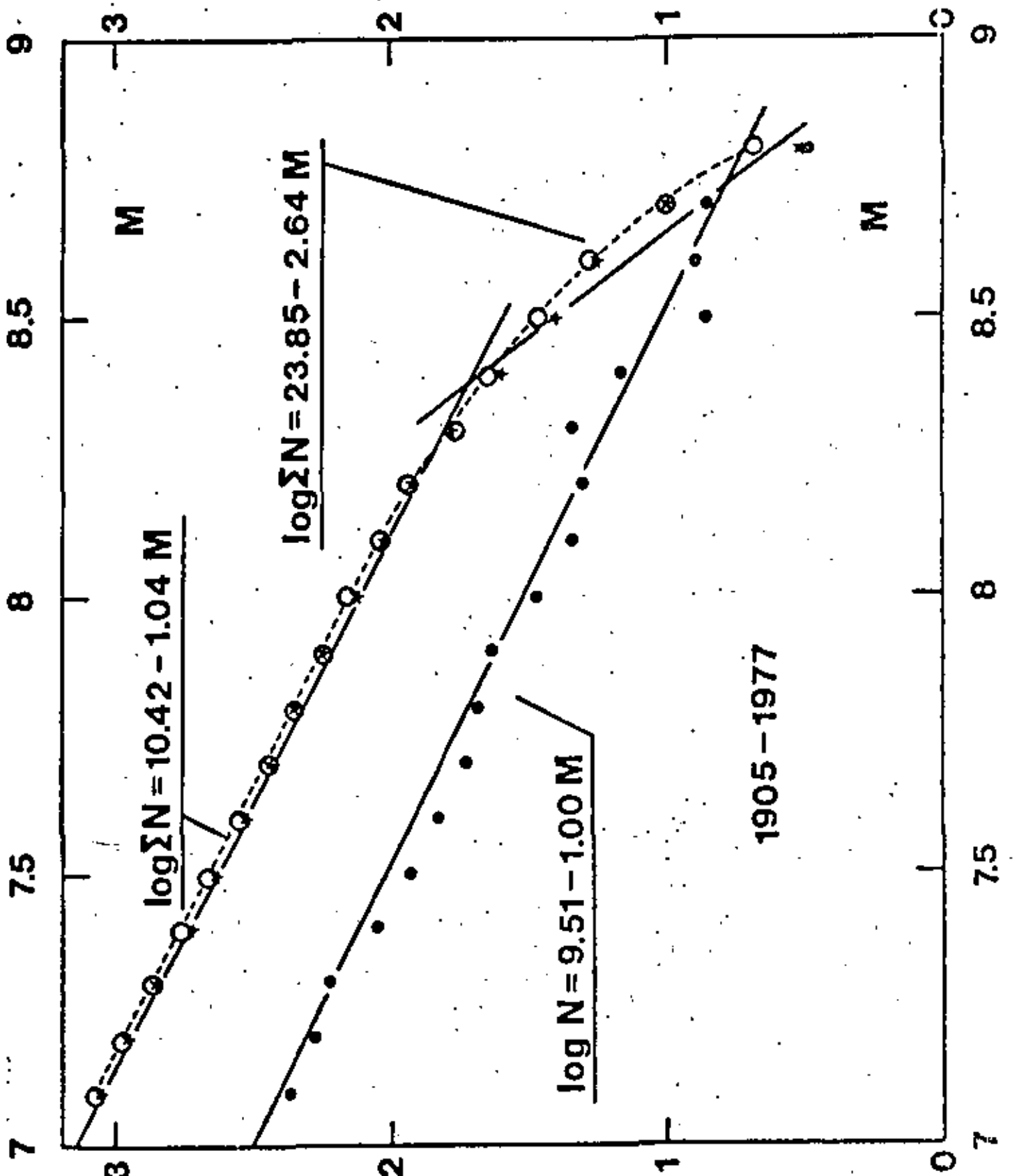

Cumulative Energy Release and number of Earthquakes (M≥7.0) since 1897

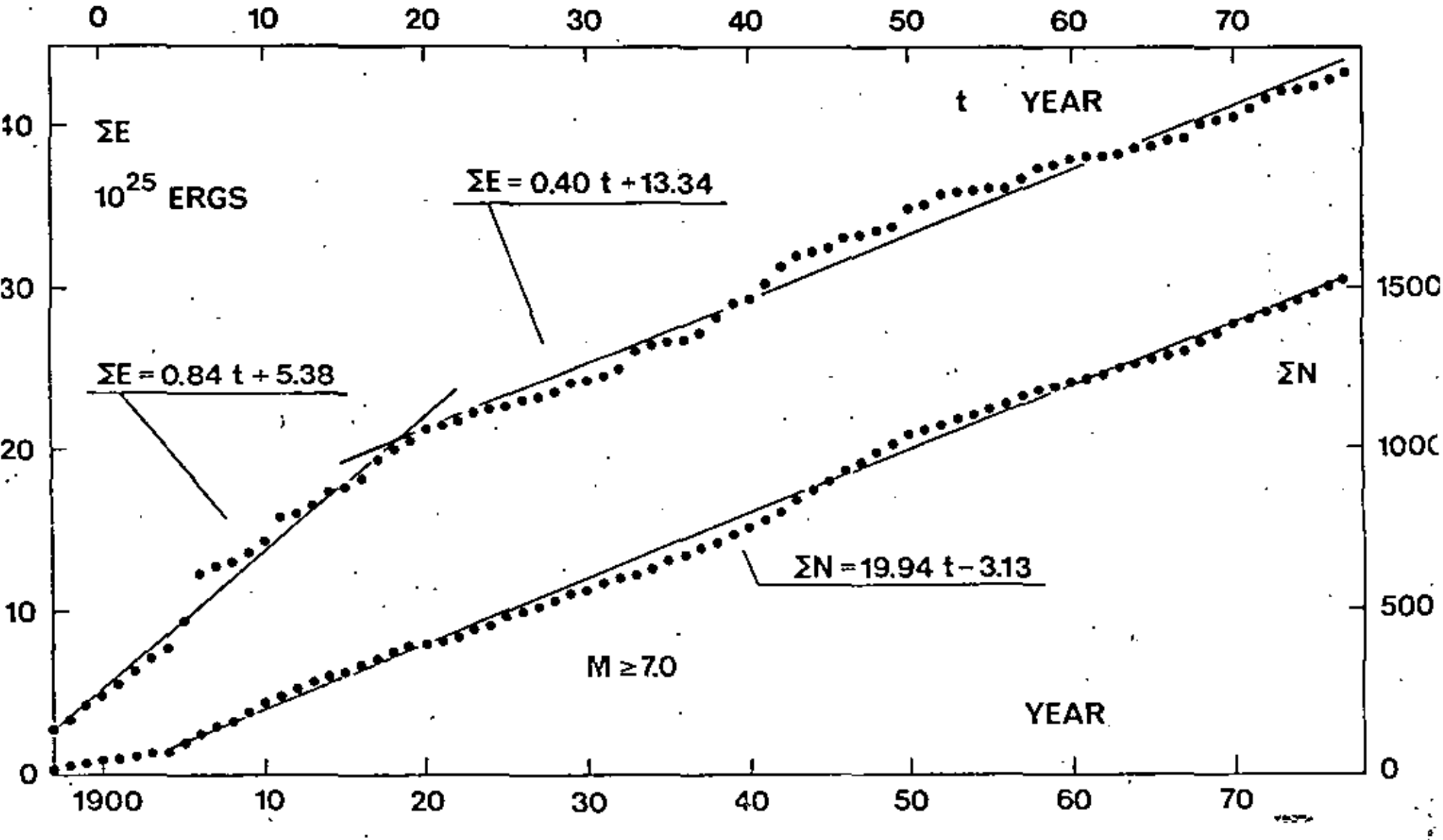

For seismic risk calculation of an area, statistics on local seismicity to smaller values of M might be needed. Data of $M \geq 5.5$ before 1965 or so are not uni... Data of $M \geq 7.0$ since 1918 is reliable. A regi... analysis of seismicity from 1897 to 1964 (inclusive) given by S. Duda (1965, Tectonophysics, vol. 2, pp. 409–452) also gives a catalog of earthquakes ($M \geq 7.0$). A list of destinctive earthquakes is given the following. These are not necessarily great earthquakes.

Notable World Earthquakes and Seismicity.

YEAR	DATE (GMT)	REGION	DEATHS	MAGNITUDE	COMMENTS
856	December	Greece, Corinth	45,000		
1038	January 9	China, Shensi	23,000		
1057		China, Chihli	25,000		
1268		Asia Minor, Silicia	60,000		
1290	September 27	China, Chihli	100,000		
1293	May 20	Japan, Kamakura	30,000		
1531	January 26	Portugal, Lisbon	30,000		
1556	January 23	China, Shensi	830,000		
1663	February 5	Canada, St. Lawrence River			Max. intensity X Chimneys broken in Massachusetts.
1667	November	Caucasia, Shemaka	80,000		
1693	January 11	Italy, Catania	60,000		
1737	October 11	India, Calcutta	300,000		
1755	June 7	Northern Persia	40,000		
1755	November 1	Portugal, Lisbon	70,000		Great tsunami.
1783	February 4	Italy, Calabria	50,000		
1797	February 4	Ecuador, Quito	40,000		
1811	December 16	Missouri, New Madrid	Several		Intensity XI. Also Jan. 23, Feb. 7, 1812.
1812	December 21	California, off-shore Santa Barbara	Several injuries		Max. intensity X. Reported tsunami uncertain
1819	June 16	India, Cutch	1,543		
1822	September 5	Asia Minor, Aleppo	22,000		

Year	Date (GMT)	Region	Deaths	Magnitude	Comments
1828	December 18	Japan, Echigo	30,000		
1857	January 9	California, Fort Tejon			San Andreas fault rupture. Intensity X-XI
1868	August 13	Peru and Bolivia	25,000		
1868	August 16	Ecuador and Colombia	Ecuador 40,000 Colombia 30,000		
1872	March 26	California, Owens Valley,	About 50		Large-scale faulting.
1886	August 31	South Carolina, Charleston-Summerville	About 60		
1891	October 28	Japan, Mino-Owari	7,000		
1896	June 15	Japan, Riku-Ugo	22,000		Tsunami.
1897	June 12	India, Assam	1,500	8.7	
1899	September 3 & 10	Alaska, Yakutut Bay		7.8 & 8.6	
1906	April 18	California, San Francisco	700	8.25	
1908	December 28	Italy, Messina	120,000	7.5	
1915	January 13	Italy, Avezzano	30,000	7	
1920	December 16	China, Kansu	180,000	8.3	
1923	September 1	Japan, Kwanto	143,000	8.2	Great Tokyo fire.
1932	December 26	China, Kansu	70,000	7.6	
1935	May 31	India, Quetta	60,000	7.5	
1939	January 24	Chile, Chillan	30,000	7.75	
1939	December 27	Turkey, Erzincan	23,000	8.0	
1948	June 28	Japan, Fukui	5,131		
1949	August 5	Ecuador, Pelileo	6,000		
1960	February 29	Morocco, Agadir	14,000	5.9	
1960	May 21–30	Southern Chile	5,700	8.5	
1962	September 1	Northwest Iran	14,000	7.3	
1963	July 26	Yugoslavia, Skopje	1,200	6.0	
1964	March 28	Alaska	131	8.6	Prince William Sound, Tsunami.
1968	August 31	Iran	11,600	7.4	Surface faulting.
1970	May 31	Peru	66,000	7.8	$530,000,000 damage. Great rock slide.
1971	February 9	California, San Fernando	65	6.5	$550,000,000 damage.
1972	December 23	Nicaragua, Managua	5,000	6.2	
1975	February 4	China, Liaoning Province	few	7.4	Predicted.
1976	February 4	Guatemala	22,000	7.9	200-kilometer rupture Motagua fault.
1976	May 6	Italy, Friuli (Gemona)	965	6.5	Extensive damage. No surface faulting.
1976	July 27	China, Tangshan	About 650,000	7.6	Great economic damage, also perhaps 780,000 injured. Not predicted.
1977	March 4	Romania, Vrancea	2,000	7.2	Damage in Bucharest.

Source: U.S. National Oceanic and Atmospheric Administration.

Instruments :

The theory of damped seismographs is very simple and is given, for example, in Richter (pp 28 – 230). Principle

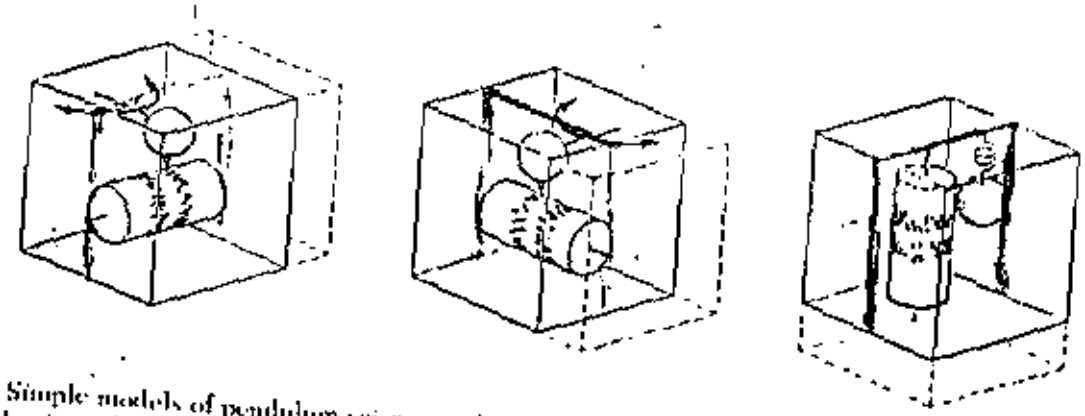

Simple models of pendulum seismographs recording vertical and two horizontal directions of ground motion. The pendulum must be damped in order to separate seismic pulses. [From Bruce A. Bolt, *Nuclear Explosions and Earthquakes*. W. H. Freeman and Company. Copyright © 1976.]

of pendulum seismographs is schematically shown above. The ground motion moves the frame but the pendulum more or less remains at the same point due to the inertia of the mass. The relative motion is magnified (mechanically or electronically) from 100 to 100,000 times or more. The oscillation of the pendulum when the wave has passed needs to be avoided; this is accomplished by damping (mechanical or electronic). It is of great importance to know the response of the seismograph so that from the records, the precise ground motion can be determined.

A seismic record which lacks precise time marks is not very useful. Modern seismographs have internal crystal clocks which puts a time signal on the record. An ideal situation is when the seismic data from many stations are telemetered to a central station where all the data is recorded on paper (and/or magnetic tape) and a single clock puts the time marks. Modern observatories keep time to

better than 1/1000 sec accuracy.

A strong motion seismograph is designed such that even near the epicenter it does not go off the scale. Typically the magnification of such instruments is between 1 to 20. Often a continuous record is not desired. The system triggers when a 'strong motion' occurs and is recorded on a photographic paper. Such records are very important from engineering point since they provide ground motion near the source of an earthquake. Ordinary seismographs (with their high magnification) go off the scale if a large earthquake occurs nearby.

In the following the seismic instrumentation of important large structures (strong motion seismograph and microseismic networks) is given.

Seismic Instrumentation of Important Large Structures

Stronig Motion Instrumentation

Instrument Characteristics. The first requirement for strong-motion instrumentation is insensitivity—the strongest possible earthquake ground motions should stay on scale. In addition, a wide dynamic range is advantageous, since valuable information can be obtained from small nondamaging earthquakes. To study the dynamic response of the engineering structure, a wide frequency response range is also needed. Such a range requires high recording speeds that make continuous recording impracticable. An inertia trigger operated by the initial portion of the earthquake ground motion has been found to be a satisfactory solution to this problem.

Accelerograph Location. Completely adequate definition of input ground motions and structural response would require a large number of accelerographs at carefully selected points. For major projects, in highly seismic regions, detailed studies of the optimum number and location of accelerographs would be expected for the special conditions of the particular site. For minimum recommendations, however, questions of location are secondary to the prime object of ensuring that at least some information of engineering value will be obtained for all strong shaking.

For this purpose, it is recommended that not fewer than four strong motion accelerographs be installed. Two of these should be located to record earthquake motions in the foundation, and two to measure structural response. For dams, the foundation instruments can often be mounted on abutments, or at an appropriate site in the immediate vicinity of the dam that is not obviously influenced in a major way by local geologic structural features. The instruments to measure dam response can usually be mounted at two different locations on the crest, or in upper galleries should they exist; they should not be mounted on special superstructures that may introduce localized dynamic behavior.

The purpose of requiring two instruments for each function is to give some indication of the uniformity of conditions, and to ensure some useful information in the event of instrument malfunction.

Accelerograph Installation and Maintenance. It is essential that the instruments be well protected from such environmental conditions as flooding or excessive summer temperatures, and from tampering or vandalism. The accelerograph, which is about 20 centimeters by 20 centimeters by 40 centimeters in size, can often be conveniently installed in the corner of a basement office, storage room, or gallery of a dam. If no space of this type is available near a suitable site, an insulated metal enclosure sealed against weather and interference can usually be provided by the instrument manufacturer at a reasonable cost. The accelerograph should be firmly bolted down to a concrete foundation, as specified by the instructions of the instrument manufacturer.

Checking, maintenance, and servicing of the accelerographs should be carried out on a regular schedule according to the instructions of the instrument manufacturer. Routine maintenance can usually be carried out by a regular member of the technical staff, if he is given a small degree of special training. Similarly, instructions in the proper preservation of records and their transmittal for data processing can be given, so that they are not lost during or after an earthquake.

Accelerograph Cost Estimates. Accelerographs meeting the necessary requirements are commercially available at 1978 prices in the $2,000 to $2,500 range. A suitable protective housing can usually be provided, if necessary, for $500 to $1,000. The only additional cost of installation will be the provision of standard electric lines or solar panels for battery trickle charging. The total 1978 cost of a typical recommended system will thus be about $12,000.

Local Seismograph Networks

Network Requirements. Sensitive seismographs to measure local earthquakes are sometimes advisable in the vicinity of projects such as large dams and nuclear reactors before major construction begins. The purposes of such instrumentation are to (1) determine the frequency of local earthquakes (if any); (2) determine the location of seismic activity and its depth; (3) determine the magnitude and some indication of focal mechanisms of the earthquakes; (4) allow prediction of the course of earthquake occurrence.

Reasonably precise location of an earthquake focus requires that the onset of P waves (and also S waves where feasible) be recorded to an accuracy of ±0.1 second or better, at a minimum of four nearby seismographs. There must be a common time base for all seismographs, and they should ideally surround the region of earthquake activity. For dams, the overall aims can be accomplished in two stages. In the preclosure stage, where the main purpose is to establish if any local earthquakes at all occur normally, a minimum network of three short-period vertical-component seismometers may be sufficient. With such a network a rough but adequate assessment of background earthquake frequency, location (using P and S waves), and magnitude can be made. If local earthquakes are prevalent the network should be expanded to at least four seismographs with the additional seismometer as near as possible to the active area.

After dam closure, it is advisable, at the least, to operate a four-station network for a period extending some years beyond the time when maximum impounding is complete. If a sequence of earthquakes does occur, then the network should be densified. Such studies of reservoir induced seismicity usually warrant special research. The requirement then is to obtain an accuracy in the location of earthquake foci of about 1 kilometer, so that correlations with geological faults can be made.

Network Location. The selection of sites for the sensitive seismographs often depends on practical considerations such as accessibility and avoidance of construction work. However, several general considerations should govern the configuration to the greatest extent practically possible. First, the sites should be uniformly spread in azimuth around the project.

The interstation distance should not be more than about 30 kilometers or less than 5 kilometers. Individual site selection should depend upon the local tectonic structures. It is best to locate the instruments on outcrops of basement rock, and they should be as remote as possible from construction activities, streams, quarrying, spillways, and so on. Normally, sites should be chosen so that they do not have to be shifted throughout the life of the project. It is also helpful to make field surveys of the relative background microseismic noise at prospective sites, with the use of a portable seismographic recorder before locations are finalized.

It has been found adequate to place the seismometers in shallow pits (about 1 meter deep) in the surficial rock. A generally adequate housing is a steel drum, with a watertight cover, that is set on concrete poured at the bottom of the pit.

Seismographic Characteristics. A variety of suitable components for a reliable high-gain seismographic system is now commercially available. Thus numerous systems can be designed to meet the aims previously established. The following two alternative systems—A and B—meet the minimum requirement and have been field tested. In both, the response of the overall seismographic system should be between 5 hertz and 50 hertz.

Seismographic System A. The system makes use of available portable seismometers and visual recording units. The network stations are not connected, and depend on separate crystal clocks at each recorder. Recording is normally on smoked paper and the paper records must be changed every day. This can be done by a member of the maintenance staff without special training.

The portable system for each site is in four parts: (1) seismometer; (2) waterproof single-packaged recording unit with batteries (size approximately 50 centimeters by 50 centimeters by 25 centimeters); (3) radio receiver; (4) power source such as solar battery charger.

Seismographic System B. This system telemeters the signals from individual seismometers of the network to a central recording room by

hard-wire connections. Power is needed at the individual seismometers for the amplifiers and voltage-controlled oscillators. At the recording station, additional power is needed for the signal discriminators, amplifiers, and drum and tape recorders. The system is costlier than System A because of the cost of land lines. Its great advantage is the centralization of recording at one convenient accessible location. Maintenance personnel would rarely need to visit the seismometers in the field. Components of the telemetered system are now all commercially available.

Network Operation and Analysis. Operation of either network A or B should not require instrumentation specialists or a staff seismologist. The critical requirements in all such studies of seismicity are continuity of operation and minimum system adjustments.

For either system, an operator would need to change the paper records each day of the week at about the same hour. He would need to mark the date and location on each seismogram. Any absolutely essential changes in system characteristics would need to be logged. It may be necessary, from time to time, to readjust and calibrate the seismometers in accord with the procedures specified by the equipment manufacturers.

For the telemetry system B, the discriminators, radio, clock, and recording drums can usually be located in a small room in the engineering quarters. The ac power is usually available. Seismograms can often be examined and stored in the same facility. All seismographic instrumentation should be bolted to the building structure to prevent movement and damage in the case of an earthquake.

The analysis side of the high-gain system often requires some seismological expertise. Special arrangements are not needed, of course, if no or very few local earthquakes are recorded. However, if the region is seismic or, at a dam, if the local seismicity increases on closure, or both, it is recommended that some special advice be obtained on analysis from a consultant seismologist.

Cost Estimates. The components in systems A and B are now commonly available and widely used by seismologists. At 1978 prices, the seismometers in System A cost about $1,000. A complete portable recording system can be obtained for $4,000. A suitable solar cell unit is about $500 or $600. The total cost of a four-station network of System A type is thus about $20,000. No cost is included for preparation of pits or housing.

The cost of installation of the preferred System B is somewhat higher. The seismometer-amplifier-oscillator package at each site is

listed at about $1,800 in 1978. At the central recording facility, each discriminator-amplifier-recorder package costs about $2,500. A suitable crystal clock is about $1,500 and a WWV radio receiver $500. The estimated total cost of the instrumentation at current prices is thus again about $20,000. In addition, however, there is the cost of the overland telemetry lines. In some areas commercial telephone lines may be available for rental. (In certain locations, RF radio telemetry links may be suitable.)

centro de educación continua
división de estudios de posgrado
facultad de ingeniería unam

VI CURSO INTERNACIONAL DE INGENIERIA SISMICA

SIMOLOGIA Y SISMICIDAD

PROPAGACION DE ONDAS ELASTICAS EN UN MEDIO SEMINFINITO

FRANCISCO J. SANCHEZ-SESMA

JULIO, 1980

PROPAGACION DE ONDAS ELASTICAS EN UN MEDIO SEMINFINITO

por

Francisco J Sánchez-Sesma

Instituto de Ingeniería, Universidad Nacional Autónoma de México

1. INTRODUCCION

Las ondas sísmicas se propagan desde la fuente de acuerdo con las propiedades mecánicas del medio en que viajan y, por supuesto, dependen también de las características de la fuente. La descripción del fenómeno ha podido hacerse de forma satisfactoria al recurrir a simplificaciones e hipótesis que llevan a la formulación de modelos que representan los aspectos más importantes de la propagación de ondas en la tierra. Es usual aceptar que la tierra es un medio elástico lineal, homogéneo e isotrópico. En un medio de esta naturaleza con extensión ilimitada se pueden propagar dos tipos de ondas elásticas; las ondas P o de compresión y las ondas S o de cortante. Las primeras se propagan con mayor velocidad y por eso se les suele llamar primarias mientras que las segundas reciben el nombre de secundarias. Existen diversas soluciones para las ecua-

ciones que gobiernan el fenómeno de propagación. Así, para una fuente puntual se podría hablar de ondas esféricas, que a grandes distancias de la fuente se pueden representar como ondas planas. En algunos casos se modela el problema de propagación como bidimensional y las soluciones para una fuente se dan en términos de ondas cilíndricas, que también a grandes distancias son aproximadamente planas. Un buen número de soluciones de las ecuaciones fundamentales puede encontrarse en el excelente texto de Ewing, Jardetzky y Press (1957).

La existencia de una superficie libre introduce reflexiones de las ondas al llegar a esta. Para estudiar la naturaleza de las reflexiones dicha superficie debe considerarse libre de esfuerzos. Dado que a grandes distancias de la fuente las ondas pueden suponerse planas y que para las longitudes de onda de interés la curvatura de la tierra es, comparativamente, pequeña se estudiará el problema de reflexión de ondas planas por la superficie de un medio elástico seminfinito. Dicha superficie se supondrá plana.

A continuación se presentan algunos aspectos de la propagación de ondas en un medio elástico de extensión ilimitada y se expresan las ecuaciones que gobiernan el fenómeno en términos de potenciales de desplazamiento. Posteriormente se discute la reflexión de ondas planas por la

frontera libre de un semiespacio elástico, homogeneo e isotrópico. La incidencia de ondas P y SV armónicas se estudia con detalle. Finalmente se presentan las ondas superficiales de Rayleigh y de Love, las primeras como caso límite en que la velocidad aparente es menor que las velocidades de propagación de las ondas de cuerpo y las segundas como ejemplo de propagación en el caso más simple de un medio estratificado.

2. PROPAGACION DE ONDAS EN UN MEDIO ELASTICO

Puede demostrarse que en un sólido elástico, homogéneo e isotrópico las ecuaciones de movimiento están dadas por

$$(\lambda+2\mu)\frac{\partial^2 u}{\partial x^2} + \mu\left(\frac{\partial^2 u}{\partial y^2}+\frac{\partial^2 u}{\partial z^2}\right)+(\lambda+\mu)\left(\frac{\partial^2 v}{\partial x\partial y}+\frac{\partial^2 w}{\partial x\partial z}\right) = \rho\,\frac{\partial^2 u}{\partial t^2}$$

$$(\lambda+2\mu)\frac{\partial^2 v}{\partial y^2} + \mu\left(\frac{\partial^2 v}{\partial x^2}+\frac{\partial^2 v}{\partial z^2}\right)+(\lambda+\mu)\left(\frac{\partial^2 u}{\partial x\partial y}+\frac{\partial^2 w}{\partial y\partial z}\right) = \rho\,\frac{\partial^2 v}{\partial t^2} \qquad (1)$$

$$(\lambda+2\mu)\frac{\partial^2 w}{\partial z^2} + \mu\left(\frac{\partial^2 w}{\partial x^2}+\frac{\partial^2 w}{\partial y^2}\right)+(\lambda+\mu)\left(\frac{\partial^2 u}{\partial x\partial z}+\frac{\partial^2 v}{\partial y\partial z}\right) = \rho\,\frac{\partial^2 w}{\partial t^2}$$

donde u, v, w = desplazamientos en las direcciones x, y, z, respectivamente; λ, μ = constantes de Lamé, ρ = densidad del medio y t = tiempo. Estas ecuaciones pueden escribirse de una manera compacta en notación vectorial, esto es

$$\mu\nabla^2\vec{u} + (\lambda+2\mu)\,\nabla\nabla\cdot\vec{u} = \rho\,\ddot{\vec{u}} \qquad (2)$$

donde $\bar{u} = (u, v, w)$ = vector desplazamiento, ∇^2 = operador Laplaciano y ∇ = operador gradiente.

Antes de considerar soluciones generales de las ecuaciones de movimiento dos ejemplos simples permitirán ilustrar las principales características de las ondas planas en un sólido elástico de extensión ilimitada.

Supongase que $u \neq 0$, $v = w = 0$ y que u es solo función de x y del tiempo. Las ecs 1 se reducen a la expresión

$$(\lambda+2\mu) \frac{\partial^2 u}{\partial x^2} = \rho \frac{\partial^2 u}{\partial t^2} \qquad (3)$$

una solución de esta ecuación es

$$u = f(t - x/\alpha) + g(t + x/\alpha) \qquad (4)$$

donde $\alpha^2 = (\lambda+2\mu)/\rho$ y f,g son funciones de *una sola variable* que pueden describir una forma de onda arbitraria. Un simple análisis de los argumentos de f y g permite establecer que $f(t-x/\alpha)$ representa una onda que viaja en la dirección positiva de x con velocidad α y $g(t+x/\alpha)$ describe una onda que viaja en la dirección negativa. Debe notarse que $f(t-x/\alpha)$ puede representar una onda armónica estacionaria, $\exp[i\omega(t-x/\alpha)]$ donde $i = \sqrt{-1}$ y ω = frecuencia circular del movimiento. Puede demostrarse que la ec 4 representa ondas de compresión o P.

Un segundo ejemplo simple se obtiene si se supone que $u = w = 0$ y que $v = v(x,t)$. De las ecs 1 se obtiene que

$$\mu \frac{\partial^2 v}{\partial x^2} = \rho \frac{\partial^2 v}{\partial t^2} \qquad (5)$$

y la solución tiene la misma forma que la ec 4 pero representa ondas que viajan con una velocidad β, donde $\beta^2 = \mu/\rho$. Debe notarse que el movimiento es perpendicular a la dirección de avance. Puede demostrarse que las soluciones de la ec 5 representan ondas de cortante, sin cambio de volumen.

Las ecuaciones de movimiento pueden resolverse de una manera más general por medio de *potenciales de desplazamiento*.

Si el vector desplazamiento se expresa como

$$\bar{u} = \nabla\phi + \nabla \times \bar{\psi}, \text{ con } \nabla \cdot \bar{\psi} = 0 \qquad (6)$$

donde ϕ es un potencial escalar y $\bar{\psi}$ es un potencial vectorial, puede demostrarse que la ec 6 representa una solución de la ec 2 (o de la ec 1 en coordenadas rectangulares) si ϕ y $\bar{\psi}$ satisfacen, respectivamente, las ecuaciones de onda:

$$\nabla^2\phi = \frac{1}{\alpha^2} \frac{\partial^2 \phi}{\partial t^2} \qquad (7)$$

$$\nabla^2\bar{\psi} = \frac{1}{\beta^2}\frac{\partial^2\bar{\psi}}{\partial t^2} \qquad (8)$$

Así, por ejemplo, una solución de la ec 7 que representa una onda plana de compresión que viaja en una dirección arbitraria está dada por

$$\phi = f\left(t - \frac{x\ell + ym + zn}{\alpha}\right) \qquad (9)$$

donde ℓ, m, n = cosenos de los ángulos formados por la dirección de viaje y los tres ejes coordenados, respectivamente. Si $\bar{r} = (x, y, z)$ y $\bar{n} = (\ell, m, n)$ donde $\bar{r}$ = vector de posición y $\bar{n}$ = vector unitario que da la dirección de propagación, la ec 9 puede escribirse como

$$\phi = f(t - \bar{r}\cdot\bar{n}/\alpha) \qquad (10)$$

Es evidente que soluciones similares pueden encontrarse para los tres componentes del potencial vectorial y representarían ondas de cortante viajando con una velocidad β.

En coordenadas rectangulares la ec 6 se desarrolla como

$$\begin{aligned} u &= \frac{\partial\phi}{\partial x} + \frac{\partial\psi_z}{\partial y} - \frac{\partial\psi_y}{\partial z} \\ v &= \frac{\partial\phi}{\partial y} - \frac{\partial\psi_z}{\partial x} + \frac{\partial\psi_x}{\partial z} \\ w &= \frac{\partial\phi}{\partial z} + \frac{\partial\psi_y}{\partial x} - \frac{\partial\psi_x}{\partial y} \end{aligned} \qquad (11)$$

donde $\bar{\psi} = (\psi_x, \psi_y, \psi_z)$.

Los potenciales de desplazamiento ϕ y $\overline{\psi}$ permiten especificar ondas planas de compresión y cortante, respectivamente, que viajen en cualquier dirección y con cualquier forma. Además, dado el caracter lineal de las ecuaciones involucradas, cualquier combinación de soluciones sigue satisfaciendo las ecuaciones de movimiento de un sólido elástico, homogéneo e isotrópico de extensión ilimitada. La utilidad de este hecho se hace evidente cuando se hace necesario seleccionar una combinación particular de ondas planas que satisfaga una cierta condición de frontera o que describa una fuente. Tal es el caso en el problema que se aborda a continuación.

3. REFLEXION DE ONDAS PLANAS POR LA FRONTERA LIBRE DE UN SEMIESPACIO ELASTICO

Considérese que la frontera libre es el plano yz como se muestra en la fig 1. Además, sin perder generalidad, supóngase que las direcciones de avance de las ondas están alojadas en el plano xz.

Para describir el movimiento debido a ondas de cortante se introduce el concepto de planos de polarización. Así, se descompone el movimiento en la dirección de la coordenada y (ondas polarizadas horizontalmente o SH) y en la

dirección perpendicular a la dirección de avance en el plano vertical xz (ondas polarizadas verticalmente o SV). En la propagación de ondas P el movimiento es en la dirección de avance de la onda. Esto se ilustra en la fig 2.

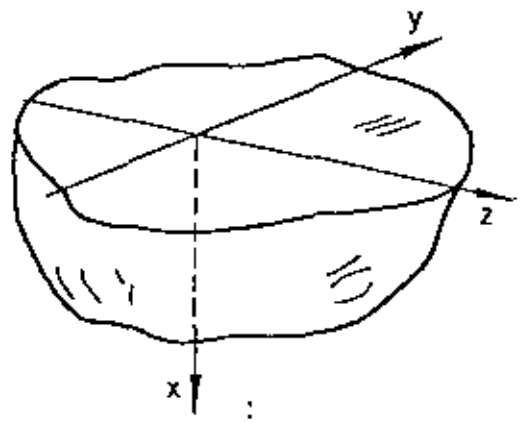

Fig 1. Sistema de coordenadas en el semiespacio elástico

La propagación de ondas SH está gobernada por la ecuación

$$\frac{\partial^2 v}{\partial x^2} + \frac{\partial^2 v}{\partial z^2} = \frac{1}{\beta^2} \frac{\partial^2 v}{\partial t^2} \qquad (12)$$

Que es precisamente la ecuación de onda en dos dimensiones, en este caso no es necesario recurrir a la formulación del problema en términos de los potenciales de desplazamiento. Puede demostrarse que, en la reflexión de una onda SH plana por una frontera libre, el ángulo de incidencia es igual al ángulo de reflexión y la onda reflejada mantiene la forma de la onda incidente. Si la onda incidente está dada

por

$$v^{(i)} = f\left(t + \frac{x \cos\gamma - z \operatorname{sen}\gamma}{\beta}\right) \qquad (13)$$

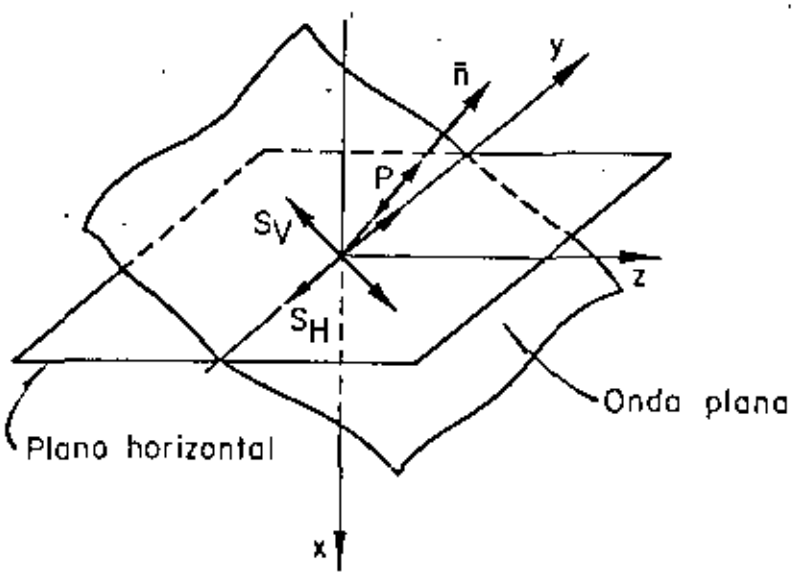

Fig 2. Nomenclatura para ondas planas

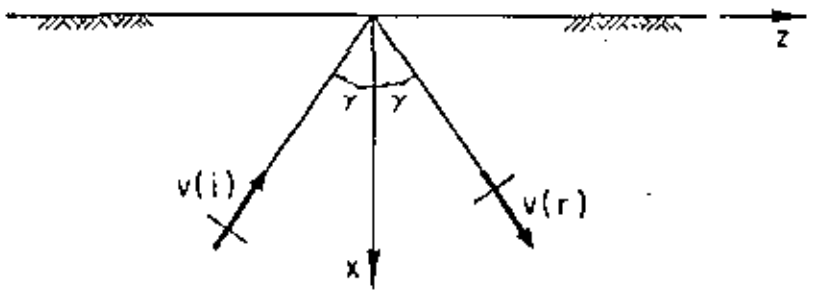

Fig 3. Ondas SH incidente y reflejada

la onda reflejada está dada simplemente por

$$v^{(r)} = f(t - \frac{x \cos\gamma + z \operatorname{sen}\gamma}{\beta}) \qquad (14)$$

aquí γ = ángulo de incidencia. Puede verificarse que $v = v^{(i)} + v^{(r)}$ satisface la ec 12 y la condición de que el plano $x = 0$ esté libre de esfuerzo pues los únicos esfuerzos relevantes están dados por

$$\tau_{xy} = \mu \frac{\partial v}{\partial x} , \quad \tau_{yz} = \mu \frac{\partial v}{\partial z} \qquad (15)$$

y combinando las ecs 13, 14 y 15 resulta que $\tau_{xy} = 0$ en $x = 0$. Debe observarse que en estas condiciones el movimiento en $x = 0$, la superficie libre, se puede escribir como

$$v_{x=0} = 2\, f(t - \frac{z \operatorname{sen}\gamma}{\beta}), \qquad (16)$$

por lo que el factor de amplificación es dos.

En la propagación de ondas P y SV el movimiento está en el plano xz, es decir $u = u(x,z,t)$, $w = w(x,z,t)$ y $v = 0$. En este caso las ecuaciones de onda que deben satisfacer los potenciales, si $\psi = \psi_y$, son

$$\frac{\partial^2\phi}{\partial x^2} + \frac{\partial^2\phi}{\partial z^2} = \frac{1}{\alpha^2} \frac{\partial^2\phi}{\partial t^2} \qquad (17)$$

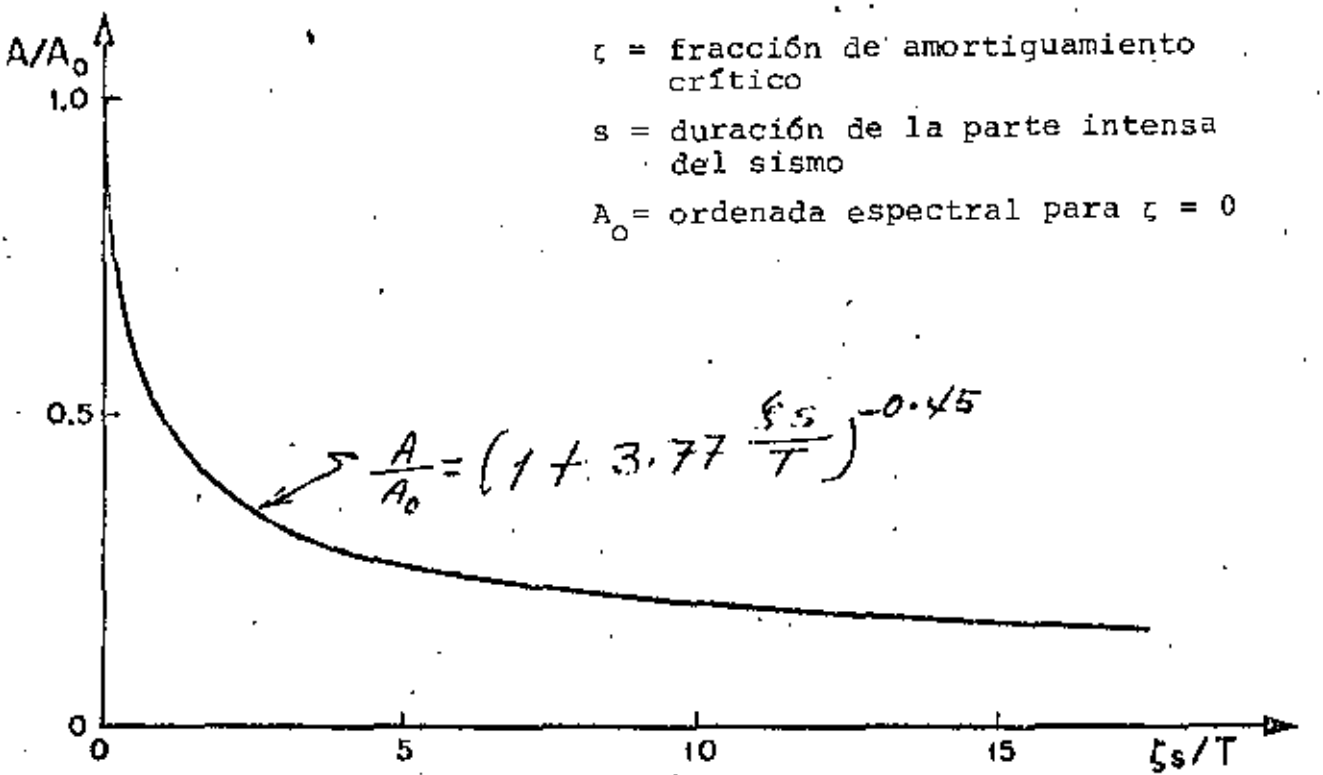

Fig. 15 Factor de reducción por el amortiguamiento

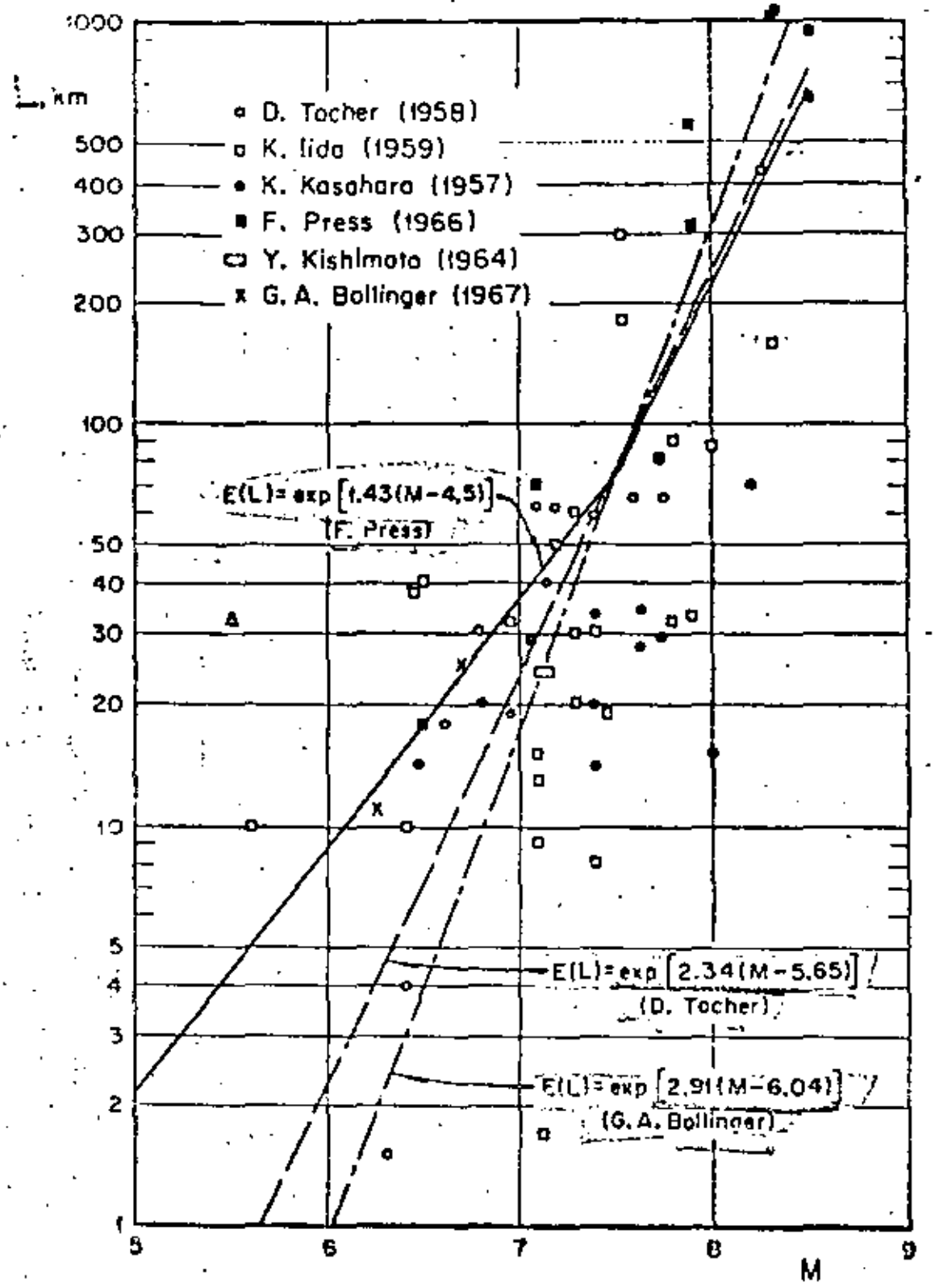

Fig. 3.1 Correlación entre la longitud de la falla y la magnitud del sismo

(Según G.A. Bollinger)

motion accelerograms versus the corresponding data computed using equation (8). For this data sample, although there is considerable scatter, equation (8) generally underestimates the mean of the data by about a factor of two. The reason for this discrepancy is not known and requires further study. However, analysis of the data and the fact that the discrepancy between the data and equation (8) is approximately a constant factor suggests that the scaling of peak displacement with magnitude and focal distance is not substantially in error. The discrepancy may be due to an inaccurate determination of the

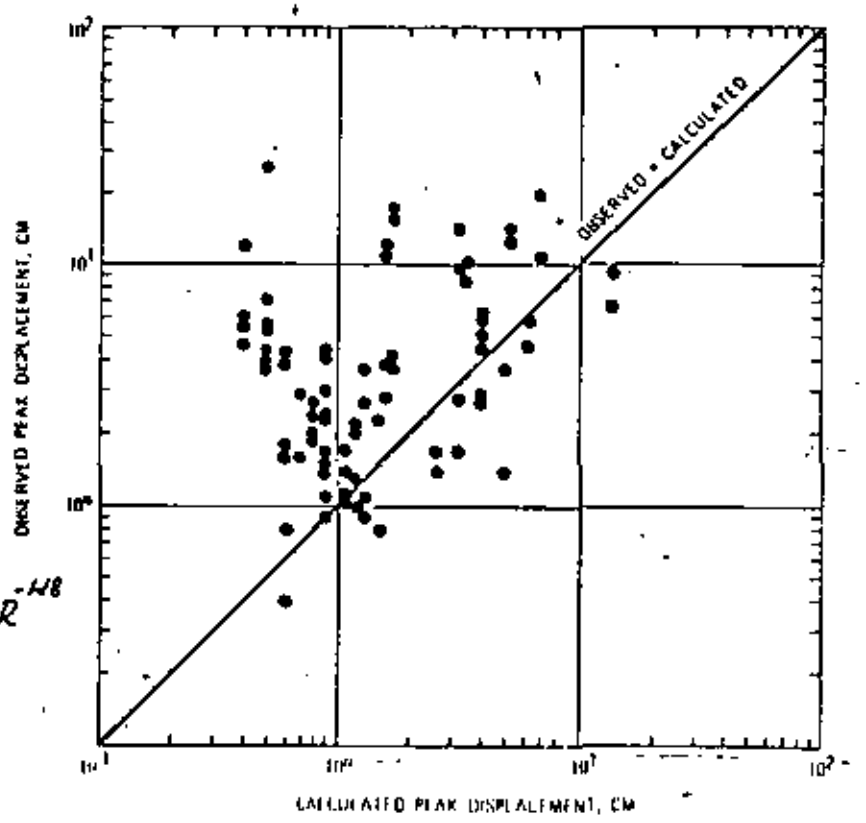

FIG. 9. Comparison between peak displacements derived from the CALTECH strong-motion accelerograms and corresponding calculations using equation (8).

constant factor in equation (8) or to the influence of local site amplification effects in the CALTECH data, an effect not included in this analysis.

Discussion

It is of interest to examine equations (6), (7), and (8) in terms of the classical correlations between earthquake magnitude and epicentral intensity, radius of perceptibility, and maximum epicentral acceleration.

Gutenberg and Richter (1956) suggested that earthquake intensity is best related to peak ground acceleration. Using the Gutenberg-Richter intensity-acceleration equation and equation (6), assuming a focal depth of 15 km, one derives an equation relating magnitude and epicentral intensity. The equation so derived differs significantly from Gutenberg and Richter's empirical relationship. This suggests that earthquake intensity may not be closely related to peak acceleration, a suggestion that has been made previously by many researchers.

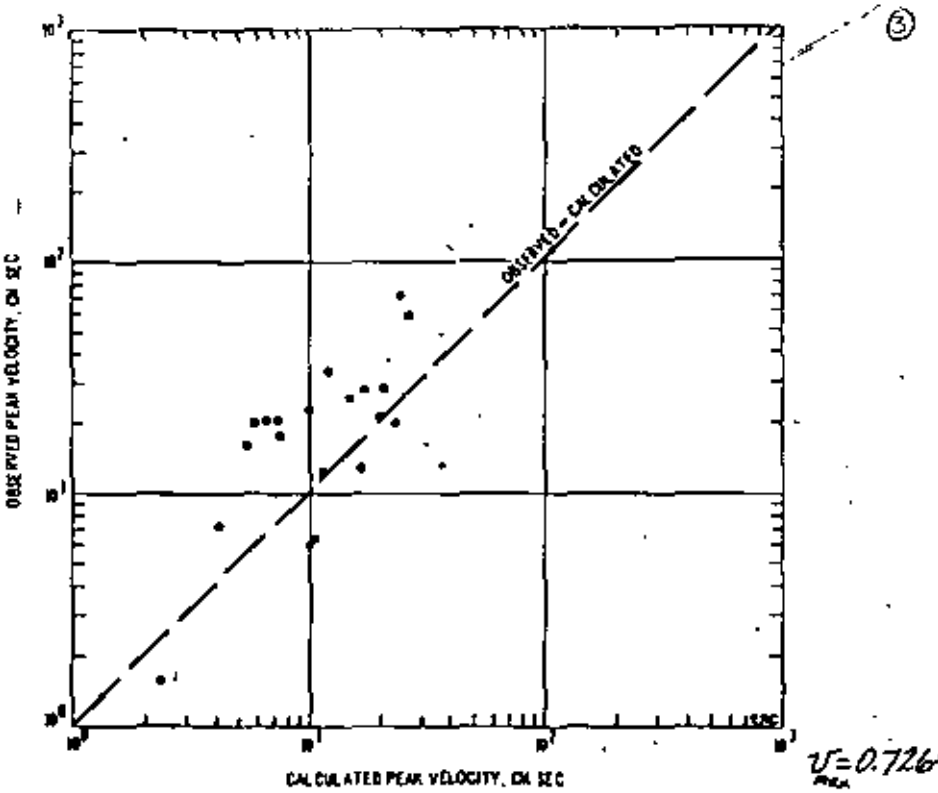

FIG. 7. Comparison between 20 recorded peak velocities (Ambraseys, 1969) and corresponding calculations using equation (7).

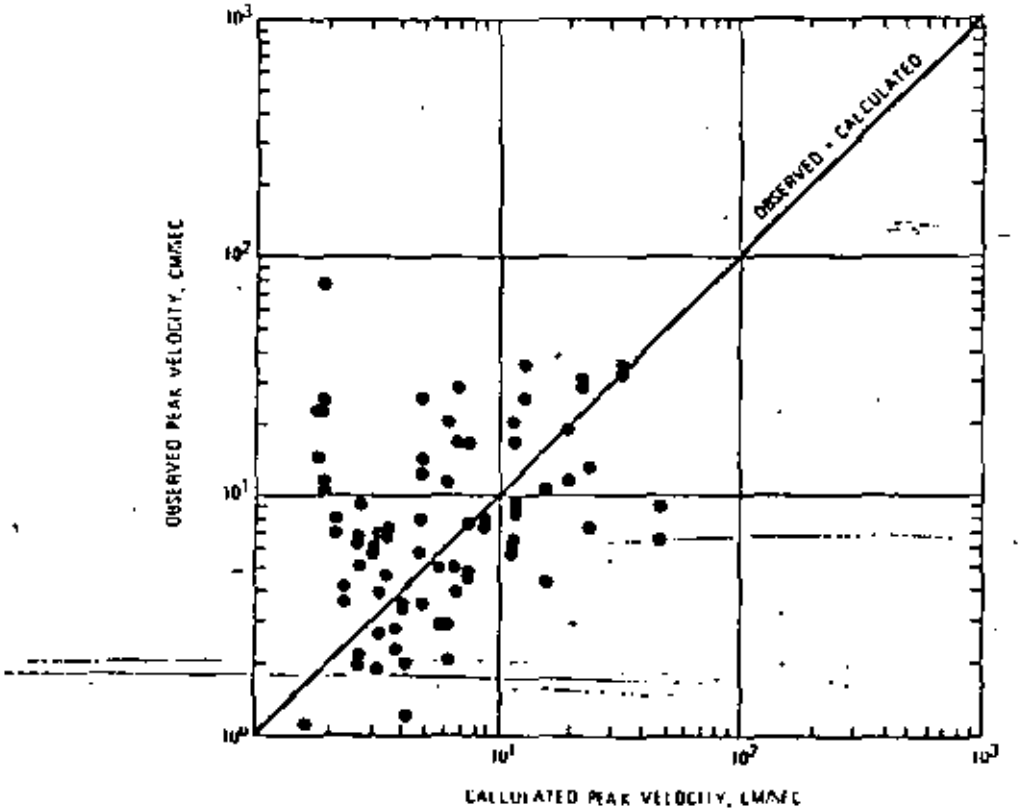

FIG. 8. Comparison between peak velocities derived from the CALTECH strong-motion accelerograms and corresponding calculations using equation (7).

Bulletin of the Seismological Society of America (Oct., 1974)

Tomado de:

Por D.L. Orphal y J.A. Lahoud

between the reported observations and calculations is good. The two measurements deviating most from the calculations were recorded at Lima and Koyna. It is noted that peak accelerations measured at Lima have been interpreted by Cloud and Perez (1971) to be anomalously high.

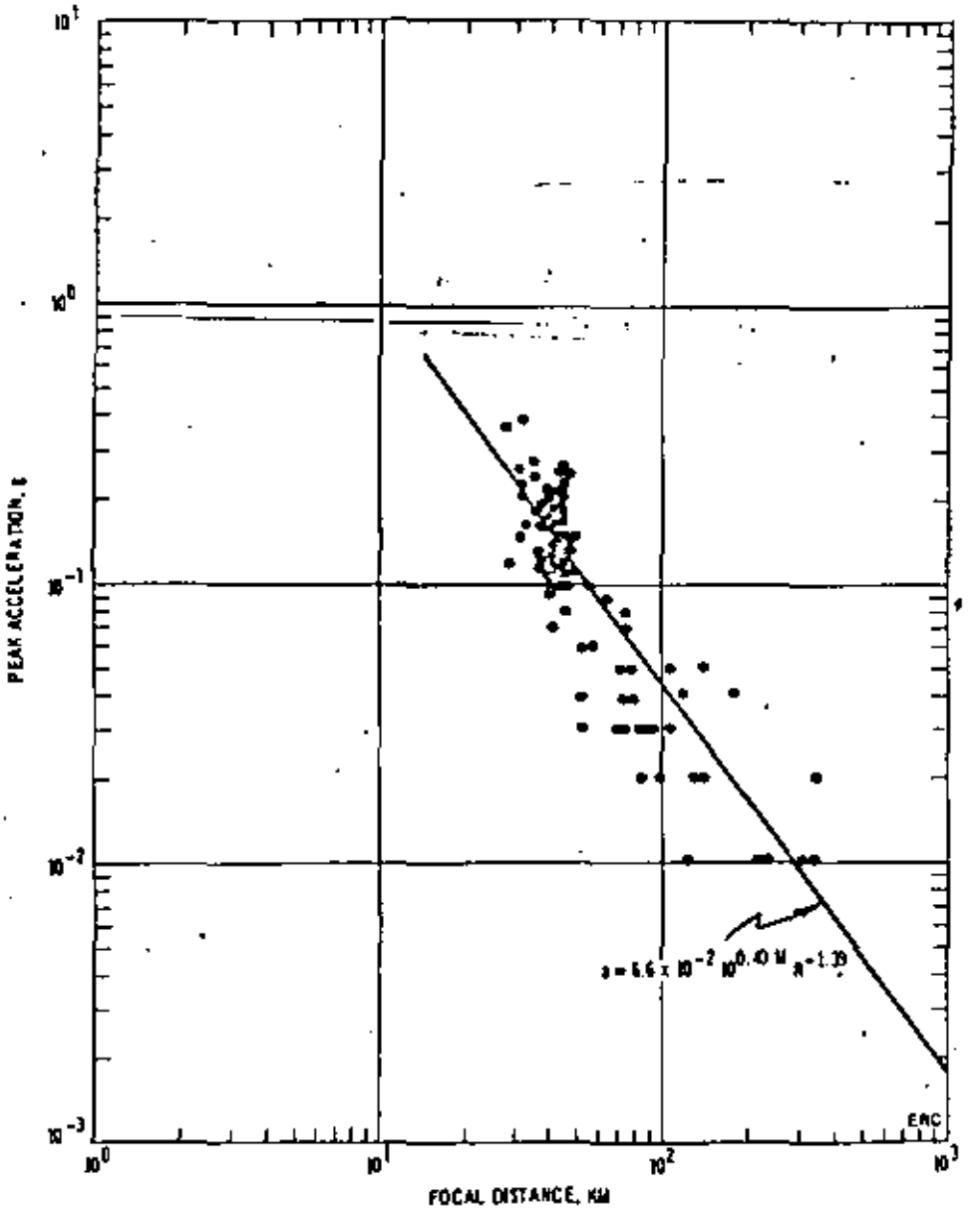

FIG. 3. Comparison between peak acceleration versus distance observed from San Fernando earthquake and calculated from equation (6).

The comparisons shown in Figures 3 through 5 are encouraging and suggest that equation (6) may be useful in predicting peak earthquake accelerations for a reasonably wide range of magnitudes, epicentral locations, focal depths and focal distances. As new earthquake ground-motion data are recorded, it is hoped that more extensive analyses will confirm the usefulness of equation (6) as well as delineate its range of validity.

CORRELACIONES ENTRE DIVERSOS PARAMETROS DE LOS TEMBLORES

POR
DR. OCTAVIO A. RASCON CH.

M = MAGNITUD EN LA ESCALA DE RICHTER

R = DISTANCIA FOCAL (EN KM)

$v_{máx}$ = VELOCIDAD MAXIMA DEL TERRENO (CM/SEG)

$a_{máx}$ = ACELERACION MAXIMA DEL TERRENO (CM/SEG^2)

$V_{máx}$ = VELOCIDAD ESPECTRAL MEDIA MAXIMA, CM/SEG (PARA $\zeta=0$)

$A_{máx}$ = ACELERACION ESPECTRAL MEDIA MAXIMA, EN CM/SEG^2 (PARA $\zeta=0$)

I = INTENSIDAD EN ESCALA DE MERCALLI MODIFICADA

W = ENERGIA DISIPADA, EN ERGS

$$v_{máx} = 32e^{M}(R + 25)^{-1.7}$$

$$a_{máx} = 5600\ e^{0.8M}(R + 40)^{-2}$$

$$V_{máx} = 250e^{M}(R + 60)^{-1.7}$$

$$A_{máx} = 69{,}600e^{0.8M}(R + 70)^{-2}$$

NOTA: ESTAS CORRELACIONES CORRESPONDEN A LAS COMPONENTES HORIZONTALES DE TEMBLORES REGISTRADOS EN TERRENO DURO.

$$I = 1.45M - 5.7\ LOG_{10}\ R + 7.9$$

$$I = \frac{LOG\ 14\ v_{máx}}{LOG\ 2}$$

APROPIADA PARA $I \leq 10$. PARA $I > 10$ SE SOBRESTIMA I.

$$LOG_{10}W = 11.4 + 1.5M$$

centro de educación continua
división de estudios de posgrado
facultad de ingeniería unam

VI CURSO INTERNACIONAL DE INGENIERIA SISMICA

SISMOLOGIA Y SISMICIDAD

CORRELACIONES ENTRE DIVERSOS PARAMETROS DE LOS TEMBLORES

DR. OCTAVIO A. RASCON CHAVEZ

JULIO, 1980

Esteva, L., 1969, Seismicity prediction: a bayesian approach. *Proc. 4th World Conf. Earthquake Eng. Santiago.*

Esteva, L., 1970. Consideraciones prácticas en la estimación bayesiana de riesgo sísmico. *Natl. Univ. Mexico, Inst. Eng., Rep.* 248.

Esteva, L., 1974. Geology and probability in the assessment of seismic risk. *Proc. 2nd Int. Congr. Int. Assoc. Eng. Geol., Sao Paulo.*

Esteva, L. and Villaverde, R., 1973. Seismic risk, design spectra and structural reliability. *Proc. 5th World Conf. Earthquake Eng., Rome*, pp. 2586–2597.

Figueroa, J., 1963. Isosistas de macrosismos mexicanos. *Ingeniería*, 33 (1): 45–68.

Gaisky, V.N., 1966. The time distribution of large, deep earthquakes from the Pamir–Hindu-Kush. *Dokl. Akad. Nauk Tadjik S.S.R.*, 9 (8): 18–21.

Gaisky, V.N., 1967. On similarity between collections of earthquakes, the connections between them, and their tendency to periodicity. *Fiz. Zemli*, 7: 20–28 (English transl., pp. 432–437).

Gajardo, E. and Lomnitz, C., 1960. Seismic provinces of Chile. *Proc. 2nd World Conf. Earthquake Eng., Tokyo*, pp. 1529–1540.

Gutenberg, B. and Richter, C.F., 1954. *Seismicity of the Earth*. Princeton University Press, Princeton.

Gzovsky, M.G., 1962. Tectonophysics and earthquake forecasting. *Bull. Seismol. Soc. Am.*, 52 (3): 485–505.

Herrera, I., Rosenblueth, E. and Rascón, O.A., 1965. Earthquake spectrum prediction for the Valley of Mexico. *Proc. 3rd Int. Conf. Earthquake Eng., Auckland and Wellington*, 1: 61–74.

Housner, G.W., 1969. Engineering estimates of ground shaking and maximum earthquake magnitude. *Proc. 4th World Conf. Earthquake Eng., Santiago.*

Hudson, D.E., 1971. *Strong Motion Instrumental Data on the San Fernando Earthquake of February 9, 1971*. California Institute of Technology, Earthquake Engineering Research Laboratory.

Hudson, D.E., 1972a. Local distributions of strong earthquake ground shaking. *Bull. Seismol. Soc. Am.*, 62 (6).

Hudson, D.E., 1972b. *Analysis of Strong Motion Earthquake Accelerograms, III, Response Spectra, Part A*. California Institute of Technology, Earthquake Engineering Research Laboratory.

Hudson, D.E. and Vdwadia, F.E., 1973. Local distribution of strong earthquake ground motions. *Proc. 5th World Conf. Earthquake Eng., Rome*, pp. 691–700.

Kaila, K.L. and Narain, H., 1971. A new approach for preparation of quantitative seismicity maps as applied to Alpide Belt–Sunda Arc and adjoining areas. *Bull. Seismol. Soc. Am.*, 61 (5): 1275–1291.

Kaila, K.L., Gaur, V.K. and Narain, H., 1972. Quantitative seismicity maps of India. *Bull. Seismol. Soc. Am.*, 62 (5): 1119–1132.

Kaila, K.L., Rao, N.M. and Narain, H., 1974. Seismotectonic maps of southwest Asia region comprising eastern Turkey, Caucasus, Persian Plateau, Afghanistan and Hindukush. *Bull. Seismol. Soc. Am.*, 64 (3): 657–669.

Kelleher, J., Sykes, L. and Oliver, J., 1973. Possible criteria for predicting earthquake locations and their application to major plate boundaries of the Pacific and the Caribbean. *J. Geophys. Res.*, 78 (14): 2547–2585.

Knopoff, L., 1964. The statistics of earthquakes in southern California. *Bull. Seismol. Soc. Am.*, 54: 1871–1873.

Lomnitz, C., 1966. Magnitude stability in earthquake sequences. *Bull Seismol. Soc. Am.*, 56: 247–249.

Lomnitz, C. and [illegible]ox, A., 1966. Clustering in aftershock sequences. In: J.S. Steinhart and T. Jefferson [illegible]th (editors), *The Earth Beneath the Continents*. Am. Geophys. Union, pp. 502–508.

McGuire, R.K., 1974. Seismic structural response risk analysis incorporating peak response regressions on earthquake magnitude and distance. *Mass. Inst. Technol., Dep. Civ. Eng.*, R74-51.

Metz, H.A. and Cornell, C.A., 1973. Seismic risk analysis based on a quadratic magnitude–frequency law. *Bull. Seismol. Soc. Am.*, 63 (6): 1999–2006.

Milne, W.G. and Davenport, A.G., 1969. Earthquake probability. *Proc. 4th World Conf. Earthquake Eng., Santiago.*

Mogi, K., 1962. Study of elastic shocks caused by the fracture of heterogeneous materials and its relations to earthquake phenomena. *Bull. Earthquake Res. Inst. Tokyo*, 40: 125–173.

Molnar, P. and Sykes, L.R., 1969. Tectonics of the Caribbean and Middle America regions from focal mechanisms and seismicity. *Geol. Soc. Am. Bull.*, 80: 1639.

Newark, N.M. and Rosenblueth, E., 1971. *Fundamentals of Earthquake Engineering*. Prentice-Hall, Englewood Cliffs.

Omori, F., 1894. On the aftershocks of earthquakes. *J. Coll. Sci. Imp. Univ. Tokyo*, 7: 111–200.

Parzen, E., 1962. *Stochastic Processes*. Holden Day, San Francisco.

Petrushevsky, B.A., 1966. *The Geological Fundamentals of Seismic Zoning*. Scientific Translation Service, order 5032, Ann Arbor, USA.

Raiffa, H. and Schlaifer, R., 1968. *Applied Statistical Decision Theory*, MIT Press.

Rosenblueth, E., 1964. Probabilistic design to resist earthquakes. *Am. Soc. Civ. Eng., J. Eng. Mech. Div.*, 90 (EM5): 189–249.

Rosenblueth, E., 1969. Seismicity and earthquake simulation. *Rep. NSF-UCEER Conf. Earthquake Eng. Res., Pasadena*, pp. 47-64.

Rosenblueth, E., 1975. *Point Estimates for Probability Moments*. National University of Mexico, Institute of Engineering, Mexico City.

Rosenblueth, E., in preparation. Optimum design for infrequent disturbances.

Rukos, E., 1974. *Análysis dinamico de la margen izquierda de Chicoasén*. National University of Mexico, Institute of Engineering, Mexico City.

Salt, P.E., 1974. Seismic site response. *Bull. N. Z. Natl. Soc. Earthquake Eng.*, 7 (2): 63–77.

Scholz, C.H., 1968. The frequency–magnitude relation of microfracturing and its relation to earthquakes. *Bull. Seismol. Soc. Am.*, 58: 399–417.

Shlien, S. and Toksöz, M.N., 1970. A clustering model for earthquake occurrences. *Bull. Seismol. Soc. Am.*, 60 (6): 1765–1787.

Singh, S.K., 1975. *Mexican Volcanic Belt: Some Comments on a Model Proposed by F. Mooser*. National University of Mexico, Institute of Engineering, Mexico City.

Trifunac, M.D., 1973. Characterization of response spectra by parameters governing the gross nature of earthquake source mechanisms. *Proc. 5th World Conf. Earthquake Eng.*, Rome, pp. 701–704.

Tsuboi, C., 1958. Earthquake province. Domain of sympathetic seismic activities. *J. Phys. Earth.*, 6 (1): 35–49.

Utsu, T., 1961. A statistical study on the occurrence of aftershocks. *Geophys. Mag., Tokyo*, 30: 521–605.

Utsu, T., 1962. On the nature of three Alaska aftershock sequences of 1957 and 1958. *Bull. Seismol. Soc. Am.*, 52: 179–297.

Veneziano, D. and Cornell, C.A., 1972. Earthquake models with spatial and temporal memory for engineering seismic risk analysis. *Mass. Inst. Technol., Dep. Civ. Eng.*

Vere-Jones, D., 1970. Stochastic models for earthquake occurrence. *J. R. Stat. Soc.*, 32 (1): 1–45.

Wallace, R.E., 1970. Earthquake recurrence intervals on the San Andreas Fault. *Geol. Soc. Am. Bull.*, 81: 2875–2890.

Yegulalp, T.M. and Kuo, J.T., 1974. Statistical prediction of the [illegible]rences of maximum magnitude earthquakes. *Bull. Seismol. Soc. Am.*, 64 (2): 393–[illegible]14.

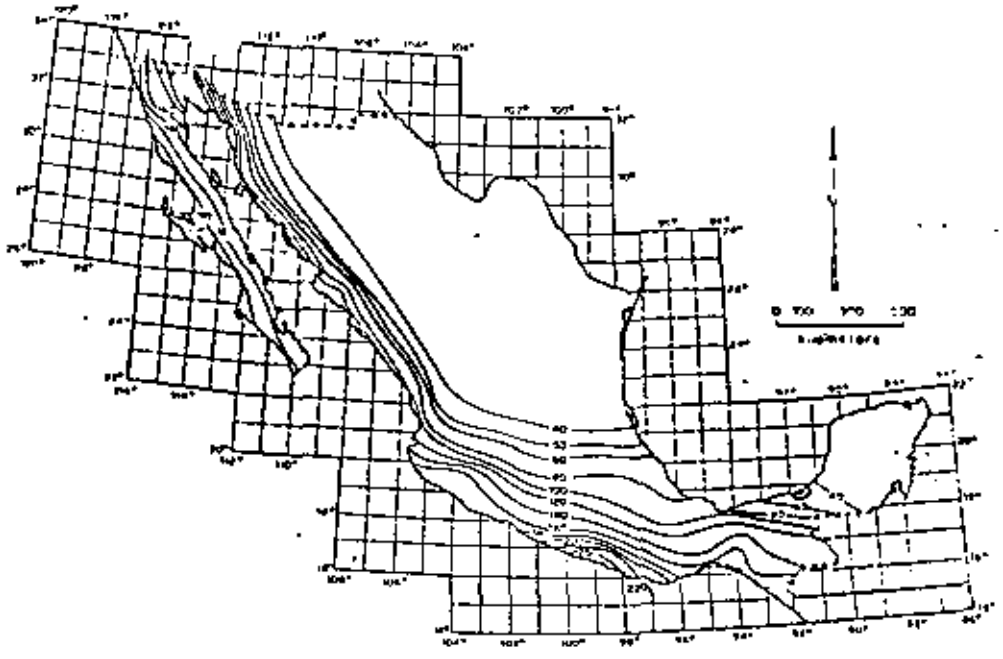

Fig. 6.20. Peak ground accelerations with return period of 100 years (cm/sec^2).

ratio of actual to predicted intensities; and geological details may significantly alter local seismicity in a small region, as well as energy radiation patterns, and hence regional seismicity in the neighbourhood. These systematic deviations are the matter of microzoning, that is, of local modification of risk maps similar to Figs. 6.19 and 6.20.

Most of the effort invested in microzoning has been devoted to study of the influence of local soil stratigraphy on the intensity and frequency content of earthquakes (see Chapter 4). Analytical models have been practically limited to response analysis of stratified formations of linear or nonlinear soils to vertically traveling shear waves. The results of comparing observed and predicted behavior have ranged from satisfactory (Herrera et al., 1965) to poor (Hudson and Udwadia, 1972). Topographic irregularities, as hills or slopes of firm ground formations underlying sediments, may introduce significant systematic perturbations in the surface motion, as a consequence of wave focusing or dynamic amplification. The latter effect was probably responsible for the exceptionally high accelerations recorded at the abutment of Pacoima dam during the 1971 San Fernando earthquake.

Present practice of microzoning determines seismic intensities or design parameters in two steps. First the values of those parameters on firm ground are estimated by means of suitable attenuation expressions and then they are amplified according to the properties of local soil; but this implies an arbitrary decision to which seismic risk is very sensitive: selecting the boundary between soil and firm ground. A specially difficult problem stems when trying to fix that boundary for the purpose of predicting t motion at the top of a hill or the slope stability of a high cliff (Rukos, 1974).

It can be concluded that rational formulation of microzoning for seismic risk is still in its infancy and that new criteria will appear that will probably require intensity attenuation models which include the influence of local systematic perturbations. Whether these models are available or the two-step process described above is acceptable, intensity-recurrence expressions can be obtained as for the unperturbated case, after multiplying the second member of eq. 6.34 by an adequate intensity-dependent corrective factor.

REFERENCES

Aki, K., 1963. *Some Problems in Statistical Seismology*. University of Tokyo, Geophysical Institute.

Allen, C.R., 1969. Active faulting in northern Turkey. *Calif. Inst. Tech., Div. Geol. Sci., Contrib.* 1577.

Allen, C.R., St. Amand, P., Richter, C.F. and Nordquist, J.M., 1965. Relationship between seismicity and geologic structure in the southern California region. *Bull. Seismol. Soc. Am.*, 55 (4): 753—797.

Ambraseys, N.N., 1973. Dynamics and response of foundation materials in epicentral regions of strong earthquakes. *Proc. 5th World Conf. Earthquake Eng., Rome.*

Ananiin, I.V., Bune, V.I., Vvedenskaia, N.A., Kirillova, I.V., Reisner, G.I. and Sholpo, V.N., 1968. *Methods of Compiling a Map of Seismic Regionalization on the Example of the Caucasus.* C. Yu. Schmidt Institute of the Physics of the Earth, Academy of Sciences of the USSR, Moscow.

Benjamin, J.R. and Cornell, C.A., 1970. *Probability, Statistics and Decision for Civil Engineers.* McGraw-Hill, New York.

Ben-Menahem, A., 1960. Some consequences of earthquake statistics for the years 1918—1955. *Gerlands Beitr. Geophys.*, 69: 68—72

Bollinger, G.A., 1973. Seismicity of the southeastern United States. *Bull. Seismol. Soc. Am.*, 63: 1785—1808.

Bolt, B.A., 1970. Causes of earthquakes. In: R.L. Wiegel (editor), *Earthquake Engineering.* Prentice-Hall, Englewood Cliffs.

Brune, J.N., 1968. Seismic moment, seismicity and rate of slip along major fault zones. *J. Geophys. Res.*, 73: 777—784.

Burridge, R. and Knopoff, L., 1967. Model and theoretical seismicity. *Bull. Seismol. Soc. Am.*, 57: 341—371.

Cornell, C.A. and Vanmarcke, E.H., 1969. The major influences on seismic risk. *Proc. 4th World Conf. Earthquake Eng. Santiago.*

Crouse, C.B., 1973. Engineering studies of the San Fernando earthquake. *Calif. Inst. Technol., Earthquake Eng. Res. Lab.* Rep. 73-04.

Cox, D.F. and Lewis, P.A.W., 1966. *The Statistical Analysis of Series of Events.* Methuen, London.

Davenport, A.G., 1972. A statistical relationship between shock amplitude, magnitude and epicentral distance and its application to seismic zoning. *Univ. Western Ontario, Faculty Eng. Sci.*, BLWT-4-72.

Davies, G.F. and Brune, J.N., 1971. Regional and global fault slip rates from seismicity. *Nature*, 229: 101—107.

Drakopoulos, J.C., 1971. A statistical model on the occurrence of aftershocks in the area of Greece. *Bull. Int. Inst. Seismol. Earthquake Eng.*, 8: 17—39.

Esteva, L., 1968. Bases para la formulación de decisiones de diseño sísmico. *Natl. Univ. Mexico, Inst. Eng. Rep.* 182.

$$Y = \epsilon Y_p = \epsilon b_1 \exp(b_2 M) g(R) \tag{6.33}$$

(see eqs. 6.4 and 6.5), where ϵ is a random factor and Y and Y_p stand for actual and predicted intensities, b_1 and b_2 are given constants, and $g(R)$ is a function of hypocentral distance. The probability that an earthquake originating at the source will have an intensity greater than y is equal to the probability that $\epsilon Y_p > y$. If Y_p is expressed in terms of M and randomness in ϵ is accounted for, one obtains:

$$\nu(y) = \int_{\alpha_U}^{\alpha_L} \nu_p(y/u) f_\epsilon(u) du \tag{6.34}$$

where ν and ν_p are respectively mean rates at which actual and predicted intensities exceed given values, $\alpha_U = y/y_U$, $\alpha_L = y/y_L$, y_U, and y_L are the predicted intensities that correspond to M_U and M_L, and f_ϵ the probability-density function of ϵ. If eq. 6.33 is assumed to hold:

$$\nu_p(y) = K_0 + K_1 y^{-r_1} - K_2 y^{-r_2} \tag{6.35}$$

where:

$$K_i = [b_1 g(R)]^{r_i} A_i \lambda_L dV \quad (i = 0, 1, 2) \tag{6.36}$$

$$r_0 = 0, \quad r_1 = \beta/b_2, \quad r_2 = (\beta - \beta_1)/b_2 \tag{6.37}$$

Substitution of eq. 6.35 into 6.34, coupled with the assumption that ln ϵ is normally distributed with mean m and standard deviation σ leads to:

$$\nu(y) = c_0 K_0 + c_1 K_1 y^{-r_1} - c_2 K_2 y^{-r_2} \tag{6.38}$$

where:

$$c_i = \exp(Q_i) \left[\phi\left(\frac{\ln \alpha_L - u_i}{\sigma}\right) - \phi\left(\frac{\ln \alpha_U - u_i}{\sigma}\right) \right] \tag{6.39}$$

ϕ is the standard normal cumulative distribution function, $Q_i = 1/2\ \sigma^2 r_i^2 + m r_i$, and $u_i = m + \sigma^2 r_i$. Similar expressions have been presented by Merz and Cornell (1973) for the special case of eq. 6.8 when $\beta_1 \to \infty$ and for a quadratic form of the relation between magnitude and logarithm of exceedance rate. Closed-form solutions in terms of incomplete gamma functions are obtained when magnitudes are assumed to possess extreme type-III distributions (eq. 6.9).

Intensity-recurrence curves at given sites are obtained by integration of the contributions of all significant sources. Uncertainties in local seismicities can be handled by describing regional seismicity in terms of means and variances of $\nu(y)$ and estimating these moments from eq. 6.34 and suitable first- and second-mor approximations. Influence of these uncertainties in design decisions has been discussed by Rosenblueth (in preparation).

6.5.2 Seismic probability maps

When intensity-recurrence functions are determined for a number of sites with uniform local ground conditions the results are conveniently represented by sets of seismic probability maps, each map showing contours of intensities that correspond to a given return period. For instance, Figs. 6.19 and 6.20 show peak ground velocities and accelerations that correspond to 100 years return period on firm ground in Mexico. These maps form part of a set that was obtained through application of the criteria described in this chapter. Because the ratio of peak ground accelerations and velocities does not remain constant throughout a region, the corresponding design spectra will not only vary in scale but also in shape (frequency content); in other words, seismic risk will usually have to be expressed in terms of at least the values of two parameters (for instance, as in this case, peak ground accelerations and velocities that correspond to various risk levels (return periods)).

6.5.3 Microzoning

Implicit in the above criteria for evaluation of regional seismicity is the adoption of intensity attenuation expressions valid on firm ground. Scatter of actual intensities with respect to predicted values was ascribed to differences in source mechanisms, propagation paths, and local site conditions; at least the latter group of variables can introduce systematic deviations in the

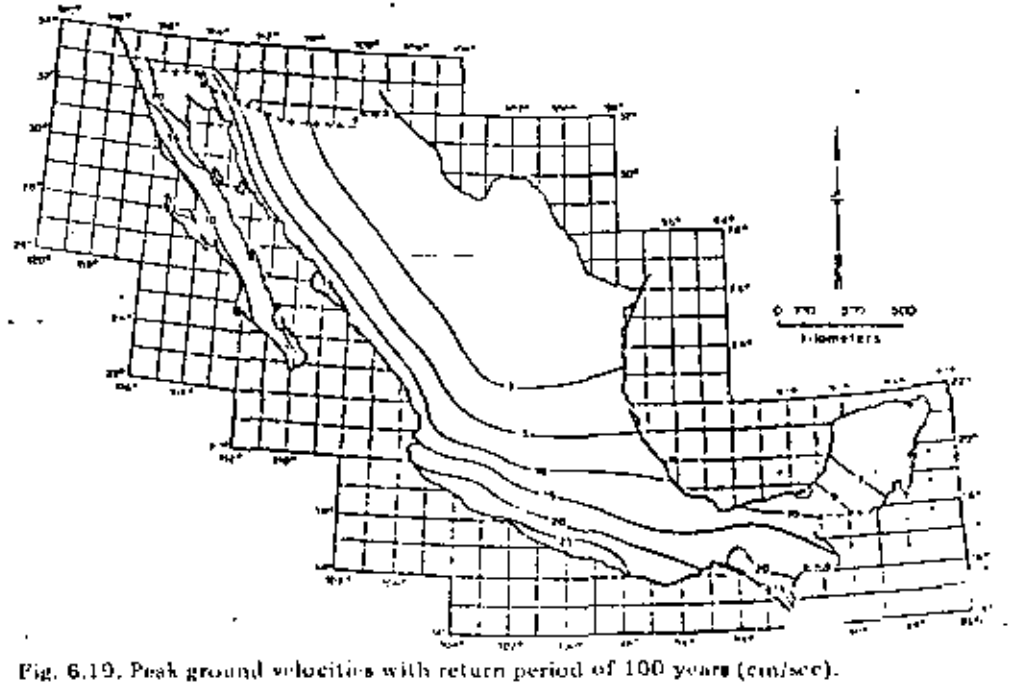

Fig. 6.19. Peak ground velocities with return period of 100 years (cm/sec).

ν_{L_i} can be expressed in terms of an initial probability distribution of p_i and of the correlation among p_i and p_j for any i and j. Because $\Sigma\nu_{L_i} = \nu_L$, one obtains $\Sigma p_i = 1$. This imposes two restrictions on the initial joint probability distribution of the p_i's: $E'(p_i) = 1$, $\text{var}'\ \Sigma p_i = 0$. If all p_i's are assigned equal expectations and all pairs p_i, p_j, $i \neq j$ are assumed to possess the same correlation coefficient $\rho_{ij} = \rho'$, the restrictions mentioned lead to $E'(p_i) = 1/s$ and $\rho' = -1/(s-1)$. Posterior values of $E(p_i)$ and ρ_{ij} are obtained according to the same principles that led to eqs. 6.25—6.28. Statistical evidence is in this case described by N, the total number of earthquakes generated in the system, and n_i ($i = 1, \ldots, s$) the corresponding numbers for the subzones. Given the p_i's, the probability of this event is the multinomial distribution:

$$P[A|p_1, \ldots, p_s] = \frac{N!}{n_1!, \ldots, n_s!}\, p_1^{n_1} \ldots p_s^{n_s} \tag{6.31}$$

If the correlation coefficients among seismicities of the various subzones can be neglected, each p_i can be separately estimated. Because p_i has to be comprised between 0 and 1, it is natural to assign it a beta initial probability distribution, defined by its parameters n_i' and N_i', such that $E'(p_i) = n_i'/N_i'$ and $\text{var}'(p_i) = n_i'(N_i' - n_i')/[N_i'^2(N_i' + 1)]$ (Raiffa and Schlaifer, 1968). The parameters of the posterior distribution will be:

$$n_i'' = n_i' + n_i, N_i'' = N_i' + N$$

Take for instance a zone whose prior distribution of λ_L is assumed gamma with expected value $\bar{\lambda}_L'$ and coefficient of variation V_L'. Suppose that, on the basis of geological evidence and of the dimensions involved, it is decided to subdivide the zone into four subzones of equal dimensions; a-priori considerations lead to the assignment of expected values and coefficients of variation of p_i for those subzones, say $E'(p_i) = 0.25$, $V'(p_i) = 0.25$ ($i = 1, \ldots, 4$). From previous considerations for $s = 4$ take $\rho_{ij}' = -1/3$ for $i \neq j$. Suppose now that, during a given time interval t, ten earthquakes were observed in the zone, of which 0, 1, 3, and 6 occurred respectively in each subzone. If the Poisson process model is adopted, $\bar{\lambda}_L'$ and V_L' can be expressed in terms of a fictitious number of events $n' = V_L'^{-2}$ occurred during a fictitious time interval $t' = n'/\bar{\lambda}_L'$; after observing n earthquakes during an interval t, the Bayesian mean and coefficient of variation of λ_L will be $\bar{\lambda}_L'' = (n' + n)/(t' + t)$, $V_L'' = (n' + n)^{-1/2}$ (Esteva, 1968). Hence:

$$\bar{\lambda}_L'' = (V_L'^{-2} + 10)/(V_L'^{-2}\bar{\lambda}_L'^{-1} + t), \qquad V_L'' = (V_L'^{-2} + 10)^{-1/2}$$

Local deviations of seismicity in each subzone with respect to the average λ_L can be analyzed in terms of p_i ($i = 1, \ldots, 4$); Bayesian analysis of the proportion in which the ten earthquakes were distributed among the subzones proceeds according to:

$$E''(p_i|A) = \frac{E'[p_i P(A|p_i, \ldots, p_4)]}{E'[P(A|p_i, \ldots, p_4)]} \tag{6.32}$$

The expectations that appear in this equation have to be computed with respect to the initial joint distribution of the p_i's. In practice, adequate approximations are required. For instance, Benjamin and Cornells' (1970) first-order approximation leads to $E''(p_1) = 0.226$, $E''(p_4) = 0.294$.

If correlation among subzone seismicities is neglected, and statistical information of each subzone is independently analyzed, when the p_i's are assigned beta probability-density functions with means and coefficients of variation as defined above, one obtains $E''(p_1) = 0.206$, $E''(p_4) = 0.313$, which are not very different from those formerly obtained; however, when $E'(p_i) = 0.25$ and $V'(p_i) = 0.5$, the first criterion leads to $E''(p_i) = 0.206$, $E''(p_4) = 0.314$, while the second produces 0.131 and 0.416, respectively. Part of the difference may be due to neglect of ρ_{ij}', but probably a significant part stems from inaccuracies of the first-order approximation to the expectations that appear in eq. 6.32; alternate approximations are therefore desirable.

Incomplete data. Statistical information is known to be fairly reliable only for magnitudes above threshold values that depend on the region considered, its level of activity, and the quality of local and nearby seismic instrumentation. Even incomplete statistical records may be significant when evaluating some seismicity parameters; their use has to be accompanied by estimates of detectability values, that is, of ratios of the numbers of events recorded to total numbers of events in given ranges (Esteva, 1970; Kaila and Narain, 1971).

6.5 REGIONAL SEISMICITY

The final goal of local seismicity assessment is the estimation of regional seismicity, that is, of probability distributions of intensities at given sites, and of probabilistic correlations among them. These functions are obtained by integrating the contributions of local seismicities of nearby sources, and hence their estimates reflect Bayesian uncertainties tied to those seismicities. In the following, regional seismicity will be expressed in terms of mean rates of exceedance of given intensities; more detailed probabilistic descriptions would entail adoption of specific hypotheses concerning space and time correlations of earthquake generation.

6.5.1 Intensity-recurrence curves

The case when uncertainty in seismicity parameters is neglected will be discussed first. Consider an elementary seismic source with volume dV and local seismicity $\lambda(M)$ per unit volume, distant R from a site S, where intensity-recurrence functions are to be estimated. Every time that a magnitude M shock is generated at that source, the intensity at S equals:

Bayesian uncertainty tied to the joint distribution of all seismicity parameters (λ_L, B_1, ..., B_r) can be included in the computation of the probability of occurrence of a given event Z by taking the expectation of that probability with respect to all parameters:

$$P(Z) = E_{\lambda_L, B}[P(Z); \lambda_L, B_1, ..., B_r)] \tag{6.29}$$

When the joint distribution of λ_L, B stems from Bayesian analysis of an initial distribution and an observed event, A, this equation adopts the form:

$$P''(Z) = \frac{E'_{\lambda_L, B}[P(Z|\lambda_L, B)P(A|\lambda_L, B)]}{E'_{\lambda_L, B}[P(A|\lambda_L, B)]} \tag{6.30}$$

where ' and " stand for initial and posterior, respectively.

Spatial variability. Figure 6.17 shows a map of geotectonic provinces of Mexico, according to F. Mooser. Each province is characterized by the large-scale features of its tectonic structure, but significant local perturbations to the overall patterns can be identified. Take for instance zone 1, whose seismotectonic features were described above, and are schematically shown in Fig. 6.18 (Singh, 1975): the Pacific plate underthrusts the continental block and is thought to break into several blocks, separated by faults transverse to the coast, that dip at different angles. The continental mass is also

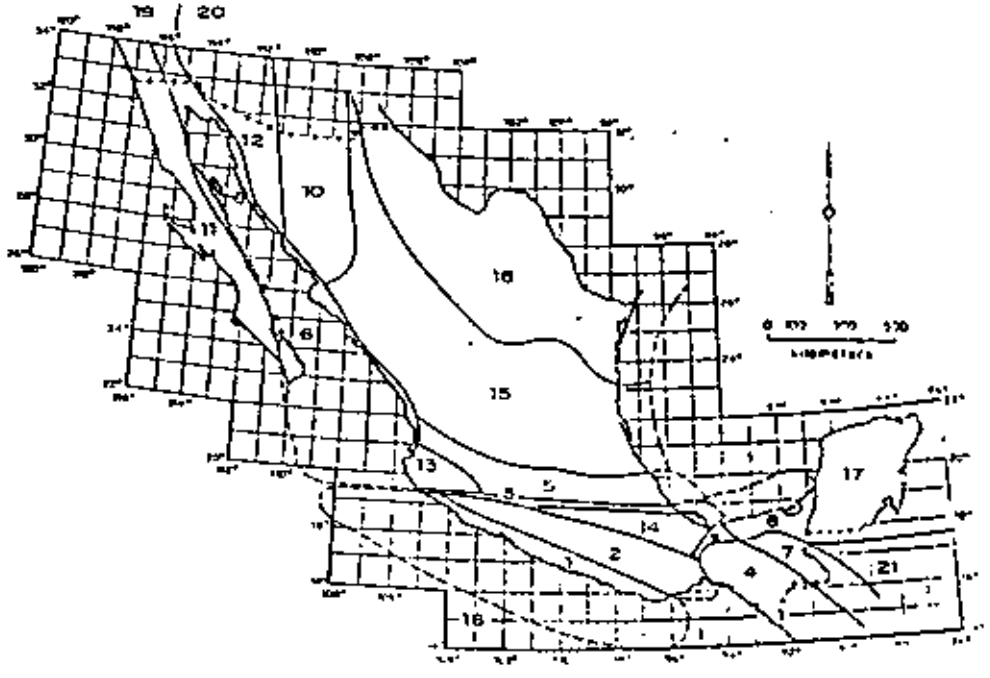

Fig. 6.17. Seismotectonic provinces of Mexico. (After F. Mooser.)

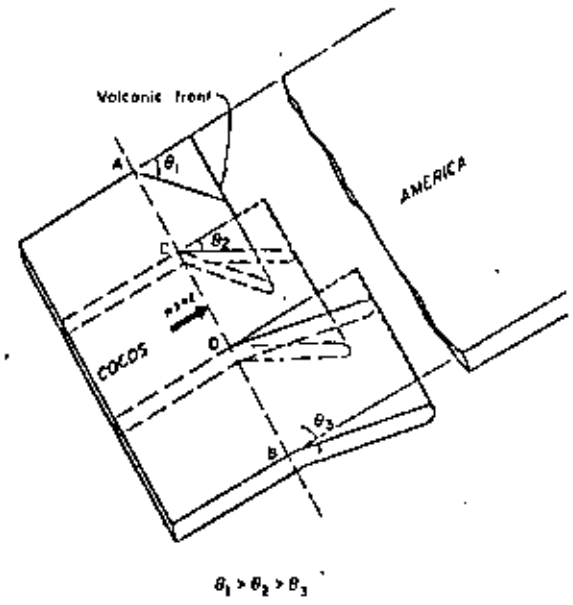

Fig. 6.18. Schematic drawing of the segmenting of Cocos plate as it subducts below American plate. (After Singh, 1974.)

made up of several large blocks. Seismic activity at the underthrusting plate or at its interface with the continental mass is characterized by magnitudes that may reach very high values and by the increase of mean hypocentral depth with distance from the coast; small and moderate shallow shocks are generated at the blocks themselves. Variability of statistical data along the whole tectonic system was discussed above and is apparent in Fig. 6.10. Bayesian estimation of local seismicity averaged throughout the system is a matter of applying eq. 6.21 or any of its special forms (eqs. 6.22 and 6.23), taking as statistical evidence the information corresponding to the whole system. However, seismic risk estimates are sensitive to values of local seismicity averaged over much smaller volumes of the earth's crust; hence the need to develop criteria for probabilistic inference of possible patterns of space variability of seismicity along tectonically homogeneous zones.

On the basis of seismotectonic information, the system under consideration can first be subdivided into the underthrusting plate and the subsystem of shallow sources; each subsystem can then be separately analyzed. Take for instance the underthrusting plate and subdivide it into s sufficiently small equal-volume subzones. Let ν_L be the rate of exceedance of magnitude M_L throughout the main system, ν_{L_i} the corresponding rate at each subzone, and define p_i as ν_{L_i}/ν_L, with p_i independent of ν_L (p_i is equal to the probability that an earthquake known to have been generated in the o l system originated at subzone i). Initial information about possible space variability of

probabilit· ·nsity function for ν was adopted such that the expected v· · of $\lambda(6.5)$ .he region coincided with its average throughout the com| seismic province. Two values of ρ were considered: 2 and 10, which correspond to coefficients of variation of 0.71 and 0.32, respectively. Values in Table 6.III were obtained for the ratio of the final to the initial expected values of ν, in terms of u_0.

The last two columns in the table contain the ratios of the computed values of $E''(T_1)$ and $E'(T)$ when ν is taken as equal respectively to its initial or to its posterior expected value. This table shows that, for $\rho = 10$, that is, when uncertainty attached to the geologically based assumptions is low, the expected value of the time to the next event keeps decreasing, in accordance with the conclusions of Kelleher et al. (1973). However, as time goes on and no events occur, the statistical evidence leads to a reduction in the estimated risk, which shows in the increased conditional expected values of T_1. For $\rho = 2$, the geological evidence is less significant and risk estimates decrease at a faster rate

6.4.1.3 Bayesian estimation of jointly distributed parameters

In the general case, estimation of B will consist in the determination of the posterior Bayesian joint probability function of its components, taking as statistical evidence the relative frequencies of observed magnitudes. Thus, if event A is described as the occurrence of N shocks, with magnitudes $m_1, ..., m_N$, and b_i ($i = 1, ..., r$) are values that may be adopted by the components of vector B being estimated, eq. 6.21 becomes:

$$f''_B(b_1, ..., b_r|A) = \frac{f'_B(b_1, ..., b_r)P(A|b_1, ..., b_r)}{\int ... \int f'_B(u_1, ..., u_r)P(A|u_1, ..., u_r)\mathrm{d}u_1, ..., \mathrm{d}u_r} \quad (6.25)$$

where $P(A|u_1, ..., u_r)$ is proportional to:

$$\prod_{i=1}^{N} g(m_i|u_1, ..., u_r)$$

and $g(m) = -\partial G^*(m)/\partial m$.

Closed-form solutions for f'' as given by eq. 6.25 are not feasible in general. For the purpose of evaluating risk, however, estimates of the posterior first and second moments of f'' can be obtained from eq. 6.25, making use of available first-order approximations (Benjamin and Cornell, 1970; Rosenblueth, 1975). Thus, the posterior expected value of B_i is given by $\int f''_{B_i}(u)\, u\, \mathrm{d}u$, where $f''_{B_i}(u_i) = \int ... \int f''_B(u_1, ..., u_r)\, \mathrm{d}u_1, ..., \mathrm{d}u_n$ and the multiple integral is of order $r - 1$, because it is not extended to the dominion of B_i. Hence:

$$E''(B_i) = \frac{E'_B[B_iP(A|B_1, ..., B_r)]}{E'_B[P(A|B_1, ..., B_r)]} \quad (6.26)$$

TABLE 6.III

Bayesian estimates of seismicity in one seismic gap

$u_0 = t_0/E'(T)$	$E''(\nu)/E'(\nu)$		$E''(T_1\|T_1 > t_0)/E'(T)$	
	$\rho = 2$	$\rho = 10$	$\rho = 2$	$\rho = 10$
0	1.0	1.0	0.75	0.75
0.1	0.95	0.99	0.76	0.74
0.5	0.75	0.94	0.91	0.71
1	0.58	0.87	1.14	0.73
5	0.20	0.54	3.11	1.05
10	0.11	0.36	5.47	1.55
20	0.06	0.22	10.50	2.48

where E' and E'' stand for initial and posterior expectation, and subscr... means that expectation is taken with respect to all the components of B. Likewise, the following *posterior moments* can be obtained:

Covariance of B_i and B_j

$$\mathrm{Cov}''(B_i, B_j) = \frac{E'_B[B_iB_jP(A|B_1, ..., B_r)]}{E'_B[P(A|B_1, ..., B_r)]} - E''(B_i)E''(B_j) \quad (6.2\ldots)$$

Expected value of $\lambda(M)$

$$E''[\lambda(M)] = E''(\lambda_1)E''[G^*(M; B)]$$

$$= E''(\lambda_1)\frac{E'_B[G^*(M; B)P(A|B_1, ..., B_r)]}{E'_B[P(A|B_1, ..., B_r)]} \quad (6.2\ldots)$$

Marginal distributions. The posterior expectation of $\lambda(M)$ is in some cas... all that is required to describe seismicity for decision-making purposes. O... ten, however, uncertainty in $\lambda(M)$ must also be acounted for. For instanc... the probability of exceedance of a given magnitude during a given time inte... val has to be obtained as the expectation of the corresponding probabiliti... over all alternative hypotheses concerning $\lambda(M)$. In this manner it can b... shown that, if the occurrence of earthquakes is a Poisson process and t... Bayesian distribution of λ_L is gamma with mean $\bar{\lambda}_L$ and coefficient of var... tion V_L, the marginal distribution of the number of earthquakes is negati... binomial with mean $\bar{\lambda}_L$. In particular, the marginal probability of ze... events during time interval t — equivalently, the complementary distributi... function of the waiting time between events — is equal to $(1 + t/t'')^{-\ldots}$ where $r'' = V_L^{-2}$ and $t'' = r''/\bar{\lambda}_L$. The marginal probability-density function... the waiting time, that should be substituted in eq. 6.20, is $\lambda_L(1 + t/t'')^{-r''-\ldots}$ which tends to the exponential probability function as r'' and t'' tend... infinity (and $V_L \to 0$) while their ratio remains equal to $\bar{\lambda}_L$.

progress is expected in the study of accumulation of stresses in the crust.

Knowledge of the geological structure can serve to formulate initial probability distributions of seismicity even when quantitative use of geophysical information seems beyond reach. Initial probability distributions of local seismicity parameters λ_L, B in the small volumes of the earth's crust that contribute significantly to seismic risk at a site, can be assigned by comparison with the average seismicity observed in wider areas of similar tectonic characteristics, or where the extent and completeness of statistical information warrant reliable estimates of magnitude-recurrence curves (Esteva, 1969). In this manner we can, for instance, use the information about the average distribution of the depths of earthquakes of different magnitudes throughout a seismic province to estimate the corresponding distribution in an area of that province, where activity has been low during the observation interval, even though there might be no apparent geophysical reason to account for the difference. Similarly, the expected value and coefficient of variation of λ_L in a given area of moderate or low seismicity (as a continental shield) can be obtained from the statistics of the motions originated at all the supposedly stable or aseismic regions in the world.

The significance of initial probabilities in seismic risk estimates, against the weight given to purely statistical information, becomes evident in the example of Fig. 6.16: if Kelleher's theory about activation of seismic gaps is true, risk is greater at the gaps than anywhere else along the coast; if Poisson models are deemed representative of the process of energy liberation, the extent of statistical information is enough to substantiate the hypothesis of reduced risk at gaps. Because both models are still controversial, and represent at most two extreme positions concerning the properties of the actual process, risk estimates will necessarily reflect subjective opinions.

6.4.1.2 Significance of statistical information

Estimation of λ_L. Application of eq. 6.23 to estimate λ_L independently of other parameters will be first discussed, because it is a relatively simple problem and because λ_L is usually more uncertain than M_0 and much more so than β.

A model as defined by eq. 6.19 will be assumed to apply. If the possible assumptions concerning the values of λ_L constitute a continuous interval, the initial probabilities of the alternative hypotheses can be expressed in terms of a probability-density function of λ_L. If, in addition, a certain assumption is made concerning the form of this probability-density function, only the initial values of $E(\lambda_L)$ and $V(\lambda_L)$ have to be assumed. It is advantageous to assign to $\nu = k/E(T)$ a gamma distribution. Then, if ρ and μ are the parameters of this initial distribution of ν, if k is assumed to be known, and if the observed outcome is expressed as the time t_n elapsed during $n + 1$ consecutive

6.23 leads t

also gamma, now with parameters $\rho + nk$ and $\mu + t_n$. The initial and the posterior expected values of ν are respectively equal to ρ/μ, and to $(\rho + nk)/(\mu + t_n)$. When initial uncertainty about ν is small, ρ and μ will be large and the initial and the posterior expected values of ν will not differ greatly. On the other hand, if only statistical information were deemed significant, ρ and μ should be given very small values in the initial distribution, and $E(\nu)$, and hence λ_L, will be practically defined by n, k, and t_n. This means that the initial estimates of geologists should not only include expected or most probable values of the different parameters, but also statements about ranges of possible values and degrees of confidence attached to each.

In the case studied above only a portion of the statistical information was used. In most cases, especially if seismic activity has been low during the observation interval, significant information is provided by the durations of the intervals elapsed from the initiation of observations to the first of the $n + 1$ events considered, and from the last of these events until the end of the observation period. Here, application of eq. 6.23 leads to expressions slightly more complicated than those obtained when only information about t_n is used.

The particular case when the statistical record reports no events during *at least* an interval $(0, t_0)$ comes up frequently in practical problems. The probability-density function of the time T_1 from t_0 to the occurrence of the first event must account for the corresponding shifting of the time axis. Furthermore, if the time of occurrence of the last event before the origin is unknown, the distribution of the waiting time from $t = 0$ to the first event coincides with that of the *excess life* in a renewal process at an arbitrary value of t that approaches infinity (Parzen, 1962). For the particular case when the waiting times constitute a gamma process, T_1 is measured from $t = 0$, T is the waiting time between consecutive events, and it is known that $T_1 \geq t_0$, the conditional density function of $\tau_1 = (T_1 - t_0)/E(T)$ is given by eq. 6.24 (Esteva, 1974), where $u_0 = t_0/E(T)$:

$$f_{\tau_1}(u|T_1 \geq t_0) = \frac{\sum_{m=1}^{k} \frac{k}{(m-1)!} [k(u+u_0)]^{m-1}}{\sum_{m=1}^{k} \sum_{n=1}^{m} \frac{1}{(n-1)!} (ku_0)^{n-1}} e^{-ku} \qquad (6.24)$$

Consider now the implications of Bayesian analysis when applied to one of the seismic gaps in Fig. 6.16, under the conditions implicit in eq. 6.24. An initial set of assumptions and corresponding probabilities was adopted as described in the following. From previous studies referring to all the southern coast of Mexico, local seismicity in the gap area (measured in terms of λ for $M_L \geq 6.5$) was represented by a gamma process with

Let H_i ($i = 1, ..., n$) be a comprehensive set of mutually exclusive assumptions concerning a given, imperfectly known phenomenon and let A be an observed outcome of such a phenomenon. Before observing outcome A we assign an initial probability $P(H_i)$ to each hypothesis. If $P(A|H_i)$ is the probability of A in case hypothesis H_i is true, then Bayes' theorem (Raiffa and Schlaifer, 1968) states that:

$$P(H_i|A) = P(H_i)\frac{P(A|H_i)}{\Sigma_j P(H_j)P(A|H_j)} \tag{6.21}$$

The first member in this equation is the (posterior) probability that assumption H_i is true, given the observed outcome A.

In the evaluation of seismic risk, Bayes' theorem can be used to improve initial estimates of $\lambda(M)$ and its variation with depth in a given area as well as those of the parameters that define the shape of $\lambda(M)$ or, equivalently, the conditional distribution of magnitudes given the occurrence of an earthquake. For that purpose, take $\lambda(M)$ as the product of a rate function $\lambda_L = \lambda(M_L)$ by a shape function $G^*(M,B)$, equal to the conditional complementary distribution of magnitudes given the occurrence of an earthquake with $M \geq M_L$, where M_L is the magnitude threshold of the set of statistical data used in the estimation, and B is the vector of (uncertain) parameters $B_1, ..., B_r$ that define the shape of $\lambda(M)$. For instance, if $\lambda(M)$ is taken as given by eq. 6.8, B is a vector of three elements equal respectively to β, β_1, and M_U; if eq. 6.9 is adopted, B is defined by k and M_U.

The initial distribution of seismicity is in this case expressed by the initial joint probability density function of λ_L and B: $f(\lambda_L, B)$. The observed outcome A can be expressed by the magnitudes of all earthquakes generated in a given source during a given time interval. For instance, suppose that N earthquakes were observed during time interval t and that their magnitudes were $m_1, m_2, ..., m_N$. Bayes' expression takes the form:

$$f'(\lambda_L, B|m_1, ..., m_N; t) = f(\lambda_L, B)\frac{P[m_1, m_2, ..., m_N; t|\lambda_L, B]}{\int\int P[m_1, m_2, ..., m_N; t|l, b]f(l,b)\mathrm{d}l\mathrm{d}b} \tag{6.22}$$

where $f'(.)$ is the posterior probability density function, and l and b are dummy variables that stand for all values that may be taken by λ_L and B, respectively. Estimation of λ_L can usually be formulated independently of that of the other parameters. The observed fact is then expressed by N_L, the number of earthquakes with magnitude above M_L during time t, and the following expression is obtained, as a first step in the estimation of $\lambda(M)$:

$$f'(\lambda_L|N_L; t) = f(\lambda_L)\frac{P(N_L; t|\lambda_L)}{\int P(N_L; t|l)f(l)\mathrm{d}l} \tag{6.23}$$

6.4.1.1 Initial probabilities of hypothetical models

Where statistical information is scarce, seismicity estimates will be very sensitive to initial probabilities assigned to alternative hypothetical models. the opinions of geologists and geophysicists about probable models, about the parameters of these models, and the corresponding margins of uncertainty should be adequately interpreted and expressed in terms of a function f as required by equations similar to 6.22 and 6.23. Ideally, these opinions should be based on the formulation of potential earthquake sources and on their comparison with possibly similar geotectonic structures. This is usually done by geologists, more qualitatively than quantitatively, when they estimate M_U. Initial estimates of λ_L are seldom made, despite the significance of this parameter for the design of moderately important structures (see Chapter 9).

Analysis of geological information must consider local details as well as general structure and evolution. In some areas it is clear that all potential earthquake sources can be identified by surface faults, and their displacements in recent geological times measured. When mean displacements per unit time can be estimated, the order of magnitude of creep and of energy liberated by shocks and hence of the recurrence intervals of given magnitudes can be established (Wallace, 1970; Davies and Brune, 1971), the corresponding uncertainty evaluated, and an initial probability distribution assigned. The fact that magnitude-recurrence relations are only weakly correlated with the size of recent displacements is reflected in large uncertainties (Petrushevsky, 1966).

Application of the criterion described in the foregoing paragraph can be unfeasible or inadequate in many problems, as in areas where the abundance of faults of different sizes, ages, and activity, and the insufficient accuracy with which focal coordinates are determined preclude a differentiation of sources. Regional seismicity may then be evaluated under the assumption that at least part of the seismic activity is distributed in a given volume rather than concentrated in faults of different importance. The same situation would be faced when dealing with active zones where there is no surface evidence of motions. Hence, consideration of the overall behavior of complex geological structures is often more significant than the study of local details.

Not much work has been done in the analysis of the overall behavior of large geological structures with respect to the energy that can be expected to be liberated per unit volume and per unit time in given portions of the structures. Important research and applications should be expected, however, since, as a result of the contribution of plate-tectonics theory to the understanding of large-scale tectonic processes, the numerical values of some of the variables correlated with energy liberation are being determined, and can be used at least to obtain orders of magnitude of expected activity along plate boundaries. Far less well understood are the occurrence of shocks in apparently inactive regions of continental shields and the behavior of complex continental blocks or regions of intense folding, but even there some

For the purpose of illustration, let it be assumed that a fixed and deterministically known damage D_0 occurs whenever a magnitude above a given value is generated at a given source. If $f(t)$ is the probability-density function of the waiting time to the occurrence of the damaging event, and if the risk level is sufficiently low that only the first failure is of concern, the expected value of the actualized cost of damage is (see Chapter 9):

$$\bar{D} = D_0 \int_0^\infty e^{-\gamma t} f(t) dt \qquad (6.20)$$

where γ is the discount (or compound interest) coefficient and the overbar denotes expectation. If the process is Poisson with mean rate ν, then $f(t)$ is exponential and $\bar{D} \cong D_0 \ \nu/\gamma$; however, if damaging events take place in clusters and most of the damage produced by each cluster corresponds to its first event, the computation of $\bar{D}$ should make use of the mean rate ν corresponding to the clusters, instead of that applicable to individual events. Table 6.11 shows a comparison of seismic risk determined under the alternative assumptions of a Poisson and a gamma model ($k = 2$), both with the same mean return period, k/ν (Esteva, 1974). Three descriptions of risk are presented as functions of the time t_0 elapsed since the last damaging event: T_1, the expected time to the next event, measured from instant t_0; the expected value of the present cost of failure computed from eq. 6.20, and the hazard function (or mean failure rate). Since clustering is neglected, risk of aftershock occurrence must be either included in D_0 or superimposed on that displayed in the table.

This table shows very significant differences among risk levels for both processes. At small values of t_0, risk is lower for the gamma process, but it

TABLE 6.11

Comparison of Poisson and gamma processes

$t_0\,\nu/k$	$\bar{T}_1\,\nu/k$	Poisson process, $k = 1$		$h k/\nu$	$T_1\,\nu/k$	Gamma process, $k = 2$		$h k/\nu$
		D/D_0				D/D_0		
		$\gamma k/\nu = 10$	$\gamma k/\nu = 100$			$\gamma k/\nu = 10$	$\gamma k/\nu = 100$	
0					1.0	0.0278	0.0004	0
0.1					0.92	0.0511	0.0036	0.367
0.2					0.86	0.0675	0.0059	0.667
0.5					0.75	0.0973	0.0100	1.333
1	1.0	0.0909	0.0099	1.0	0.67	0.120	0.0132	2.000
2					0.60	0.139	0.0156	2.667
5					0.54	0.154	0.0179	3.33
10					0.52	0.160	0.0187	3.8
					0.50	0.167	0.0196	4.0

grows with time, until it outrides that for the Poisson process, which remains constant. The differences shown clearly affect engineering decisions.

6.4 ASSESSMENT OF LOCAL SEISMICITY

Only exceptionally can magnitude-recurrence relations for small volumes of the earth's crust and statistical correlation functions of the process of earthquake generation be derived exclusively from statistical analysis of recorded shocks. In most cases this information is too limited for that purpose and it does not always reflect geological evidence. Since the latter, as well as its connection with seismicity, is beset with wide uncertainty margins, information of different nature has to be evaluated, its uncertainty analyzed, and conclusions reached consistent with all pieces of information. A probabilistic criterion that accomplishes this is presented here: on the basis of geotectonic data and of conceptual models of the physical processes involved, a set of alternate assumptions can be made concerning the functions in question (magnitude recurrence, time, and space correlation) and an initial probability distribution assigned thereto; statistical information is used to judge the likelihood of each assumption, and a posterior probability distribution is obtained. How statistical information contibutes to the posterior probabilities of the alternate assumptions depends on the extent of that information and on the degree of uncertainty implied by the initial probabilities. Thus, if geological evidence supports confidence in a particular assumption or range of assumptions, statistical information should not greatly modify the initial probabilities. If, on the other hand, a long and reliable statistical record is available, it practically determines the form and parameters of the mathematical model selected to represent local seismicity.

6.4.1 Bayesian estimation of seismicity

Bayesian statistics provide a framework for probabilistic inference that accounts for prior probabilities assigned to a set of alternate hypothetical models of a given phenomenon as well as for statistical samples of events related to that phenomenon. Unlike conventional methods of statistical inference, Bayesian methods give weight to probability measures obtained from samples or from other sources; numbers, coordinates and magnitudes of earthquakes observed in given time intervals serve to ascertain the probable validity of each of the alternative models of local seismicity that can be postulated on the grounds of geological evidence. Any criterion intended to weigh information of different nature and different degrees of uncertainty should lead to probabilistic conclusions consistent with the degree of confidence attached to each source of information. This is accomplished by Bayesian methods.

6.3.3.3 Re· ·al process models

The trigge. odels described are based on information about earthquake with magnitudes above relatively low thresholds recorded during time intervals of at most ten years. The degrees of clustering observed and the distributions of times between clusters cannot be extrapolated to higher magnitude thresholds and longer time intervals without further study.

Available information shows beyond doubt that significant clustering is the rule, at least when dealing with shallow shocks. However, there is considerable ground for discussion on the nature of the process of cluster origins during intervals of the order of one century or longer. While lack of statistical data hinders the formulation of seismicity models valid over long time intervals, qualitative consideration of the physical processes of earthquake generation may point to models which at least are consistent with the state of knowledge of geophysical sciences. Thus, if strain energy stored in a region grows in a more or less systematic manner, the hazard function should grow with the time elapsed since the last event, and not remain constant as the Poisson assumption implies. The concept of a growing hazard function is consistent with the conclusions of Kelleher et al. (1973) concerning the theory of periodic activation of *seismic gaps*. This theory is partially supported by results of nearly qualitative analysis of the migration of seismic activity along a number of geological structures. An instance is provided by the southern coast of Mexico, one of the most active regions in the world. Large shallow shocks are generated probably by the interaction of the continental mass and the subductive oceanic Cocos plate that underthrusts it and by compressive or flexural failure of the latter (Chapter 2). Seismological data show significant gaps of activity along the coast during the present century and not much is known about previous history (Fig. 6.16). Along these gaps, seismic-risk estimates based solely on observed intensities are quite low, although no significant difference is evident in the geological structure of these regions with respect to the rest of the coast, save some transverse faults which divide the continental formation into several blocks. Without looking at the statistical records a geophysicist would assign equal risk throughout the area. On the basis of seismicity data, Kelleher et al. have concluded that activity migrates along the region, in such a manner that large earthquakes tend to occur at seismic gaps, thus implying that the hazard function grows with time since the last earthquake. Similar phenomena have been observed in other regions; of particular interest is the North Anatolian fault where activity has shifted systematically along it from east to west during the last forty years (Allen, 1969).

Conclusions relative to activation of seismic gaps are controversial because the observation periods have not exceeded one cycle of each process. Nevertheless, those conclusions point to the formulation of stochastic models of seismicity that reflect plausible features of the geophysical processes.

These considerations suggest the use of renewal-process models to represent sequences of individual shocks or of clusters. Such dels are characterized because times between events are independen d identically distributed. The Poisson process is a particular renewal model for which the distribution of the waiting time is exponential. Wider generality is achieved, without much loss of mathematical tractability, if inter-event times are supposed to be distributed in accordance with a gamma function:

$$f_T(t) = \frac{\nu}{(k-1)!}(\nu t)^{k-1}\, e^{-\nu t} \tag{6.19}$$

which becomes the exponential distribution when $k = 1$. If $k < 1$, short intervals are more frequent and the coefficient of variation is greater than in the Poisson model; if $k > 1$, the reverse is true. Shlien and Toksöz (1970) found that gamma models were unable to represent the sequences of individual shocks they analyzed; but these authors handled time intervals at least an order of magnitude shorter than those referred to in this section.

On the basis of hazard function estimated from sequences of small shocks in the Hindu-Kush, Vere-Jones (1970) deduces the validity of 'branching renewal process' models, in which the intervals between cluster centers, as well as those between cluster members, constitute renewal processes.

Owing to the scarcity of statistical information, reliable comparisons between alternate models will have to rest partially on simulation of the process of storage and liberation of strain energy (Burridge and Knopoff, 1967; Veneziano and Cornell, 1973).

6.3.4 Influence of the seismicity model on seismic risk

Nominal values of investments made at a given instant increase with time when placing them at compound interest rates, i.e. when capitalizing them. Their real value — and not only the nominal one — will also grow, provided the interest rate overshadows inflation. Conversely, for the purpose of making design decisions, nominal values of expected utilities and costs inflicted upon in the future have to be converted into present or actualized values, which can be directly compared with initial expenditures. Descriptions of seismic risk at a site are insufficient for that purpose unless the probability distributions of the times of occurrence of different intensities — or magnitudes at neighbouring sources — are stipulated; this entails more than simple magnitude-recurrence graphs or even than maximum feasible magnitude estimates.

Immediately after the occurrence of a large earthquake, seismic risk is abnormally high due to aftershock activity and to the probability that damage inflicted by the main shock may have weakened natural or man-made structures if emergency measures are not taken in time. When aftershock activity has ceased and damaged systems have been repaired, a normal risk level is attained, which depends on the probability-density functions of the waiting times to the ensuing damaging earthquakes.

and $1 - [c/(c + t)]^{\delta}$ for $t \geq 0$, and as zero for $t < 0$, where λ, c, and δ are positive parameters. In Figs. 6.13–6.15, $\delta = 0.25$, $c = 2.3$ days, and $\lambda = 0.061$ shocks/day. The significance of clustering is evidenced by the high value of Poisson's dispersion index in Fig. 6.13, while no significant periodicity can be inferred from Fig. 6.14. Both figures show that the power-law model provides the best fit to the statistics of the samples. A similar analysis for New Zealand's deep shocks shows much less clustering: Poisson's dispersion index equals 2, and the hazard function is nearly constant with time.

Still, data reported by Gaisky (1967) have hazard functions that suggest models where the cluster origins as well as the clusters themselves may be represented by renewal processes. Mean return periods are of the order of several months, and hence these processes do not correspond, at least in the time scale, to the process of alternate periods of activity and quiescense of some geological structures cited by Kelleher et al. (1973), which have led to the concept of 'temporal seismic gaps', discussed below.

Simplified trigger models. Shlien and Toksöz (1970) proposed a simple particular case of the Neyman-Scott process; they lumped together all earthquakes taking place during non-overlapping time intervals of a given length and deemed them as clusters for which $\lambda(t)$ was a Dirac delta function. Working with one-day intervals, they assumed the number of events per cluster to be distributed in accordance with the discrete Pareto law and applied a maximum-likelihood criterion to the information consisting of 35 000 earthquakes reported by the USCGS from January 1971 to August 1968. The model proposed represents reasonably well both the distribution of the number of earthquakes in one-day intervals and the dispersion index. However, owing to the assumption that no cluster lasts more than one day, the model fails to represent the autocorrelation function of the daily numbers of shocks for small time lags. The degree of clustering is shown to be a regional function, and to diminish with the magnitude threshold value and with the focal depth.

Aftershock sequences. The trigger processes described have been branded as reasonable representations of regional seismic activity, even when aftershock sequences and earthquake swarms are suppressed from statistical records, however arbitrary that suppression may be. The most significant instances of clustering are related, however, to aftershock sequences which often follow shallow shocks and only rarely intermediate and deep events. Persistence of large numbers of aftershocks for a few days or weeks has propitiated the detailed statistical analysis of those sequences since last century. Omori (1894) pointed out the decay in the mean rate of aftershock occurrence with t, the time elapsed since the main shock; he expressed that rate as inversely proportional to $t + q$, where q is an empirical constant. Utsu (1961) proposed a more general expression, proportional to $(t + c)^{-\zeta}$, where ζ is a constant; Utsu's proposal is consistent with the power-law expression for $\Lambda(t)$ presented above.

Lomnitz and Hax (1966) proposed a clustering model to represent aftershock sequences; it is a modified version of Neyman and Scott's model, where the process of cluster origins is non-homogeneous Poisson with mean rate decaying in accordance with Omori's law, the number of events in each cluster has a Poisson distribution, and $\Lambda(t)$ is exponential. All the results and methods of analysis described by Vere-Jones (1970) for the stationary process of cluster origins can be applied to the nonstationary case through a transformation of the time scale. Fitting of parameters to four aftershock sequences was accomplished through use of the second-order information of the sample defined on a transformed time scale. By applying this criterion to earthquake sets having magnitudes above different threshold values it was noticed that the degree of clustering decreases as the threshold value increases.

The magnitude of the main shock influences the number of aftershocks and the distribution of their magnitudes and, although the rate of activity decreases with time, the distribution of magnitudes remains stable throughout each sequence (Lomnitz, 1966; Utsu, 1962; Drakopoulos, 1971). Equation 6.6 represents fairly well the distribution of magnitudes observed in most aftershock sequences. Values of β range from 0.9 to 3.9 and decrease as the depth increases. Since values of β for regular (main) earthquakes are usually estimated from relatively small numbers of shocks generated throughout crust volumes much wider than those active during aftershock sequences, no relation has been established among β-values for series of both types of events. The parameters of Utsu's expression for the decay of aftershock activity with time have been estimated for several sequences, for instance those following the Aleutian earthquake of March 9, 1957, the Central Alaska earthquake of April 7, 1958, and the Southeastern Alaska earthquake of July 10, 1958 (Utsu, 1962), with magnitudes equal to 8.3, 7.3, and 7.9, respectively; c (in days) was 0.37, 0.40, and 0.01, while ζ was 1.05, 1.05 and 1.13, respectively. The relationship of the total number of aftershocks whose magnitude exceeds a given value with the magnitude of the main shock was studied by Drakopoulos (1971) for 140 aftershock sequences in Greece from 1912 to 1968. His results can be expressed by $N(M) = A \exp(-\beta M)$, where $N(M)$ is the total number of aftershocks with magnitude greater than M, and A is a function of M_0, the magnitude of the main shock:

$$A = \exp(3.62\,\beta + 1.1 M_0 - 3.46) \qquad (6.18)$$

Formulation of stochastic process models for given earthquake sequences is feasible once this relationship and the activity decay law are available for the source of interest. For seismic-risk estimation at a given site the spatial distribution of aftershocks may be as significant as the distribution of magnitudes and the time variation of activity, particularly for sources of relatively large dimensions.

resent local micity processes was discussed in a comprehensive paper by Vere-Jones (1970), who calibrated them mainly against records of seismic activity in New Zealand. In addition to simple and compound Poisson processes (Parzen, 1962), he considered Neyman-Scott and Bartlett-Lewis models, both of which assume that earthquakes occur in clusters and that the number of events in each cluster is stocastically independent of its origin time. In the Neyman-Scott model, the process of clusters is assumed stationary and Poisson, and each cluster is defined by p_N, the probability mass function of its number of events, and $\Lambda(t)$, the cumulative distribution function of the time of an event corresponding to a given cluster, measured from the cluster origin. The Bartlett-Lewis model is a special case of the former, where each cluster is a renewal process that ends after a finite number of renewals. In these models the conditional probability of an event taking place during the interval $(t, t + dt)$, given that the cluster consists of N shocks, is equal to $N\lambda(t)dt$, where $\lambda(t) = \partial\Lambda(t)/\partial t$.

Because clusters overlap in time they cannot easily be identified and separated. Estimation of process parameters is accomplished by assuming different sets of those parameters and evaluating the corresponding goodness of fit with observed data.

Various alternative forms of Neyman-Scott's model were compared by Vere-Jones with observed data on the basis of first- and second-order statistics: hazard functions, interval distributions (in the form of power spectra) and variance time curves. The statistical record comprises about one thousand New Zealand earthquakes with magnitudes greater than 4.5, recorded from 1942 to 1961. Figures 6.13—6.15 show results of the analysis for shallow New Zealand shocks as well as the comparison of observed data with several alternative models. The process of cluster origins is Poisson in all cases, but the distributions of cluster sizes (N) and of times of events within clusters differ among the various instances: in the Poisson model no clustering takes place (the distribution of N is a Dirac delta function centered at $N = 1$) while in the exponential and in the power-law models the distribution of N is extremely skewed towards $N = 1$, and $\Lambda(t)$ is taken respectively as $1 - e^{-\lambda t}$

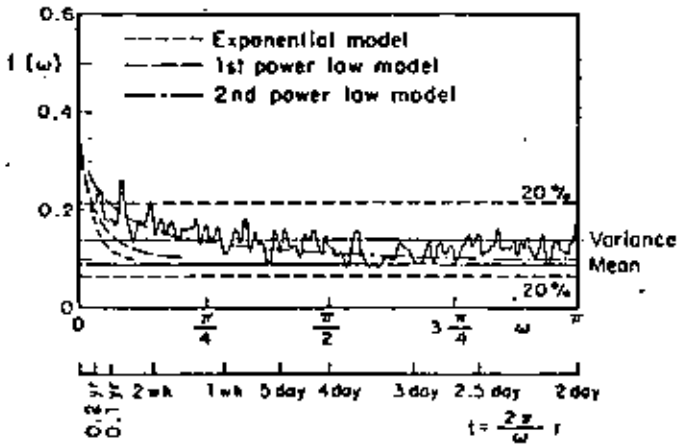

Fig. 6.14. Smoothed periodogram for New Zealand shallow shocks. (After Vere-Jones, 1966.)

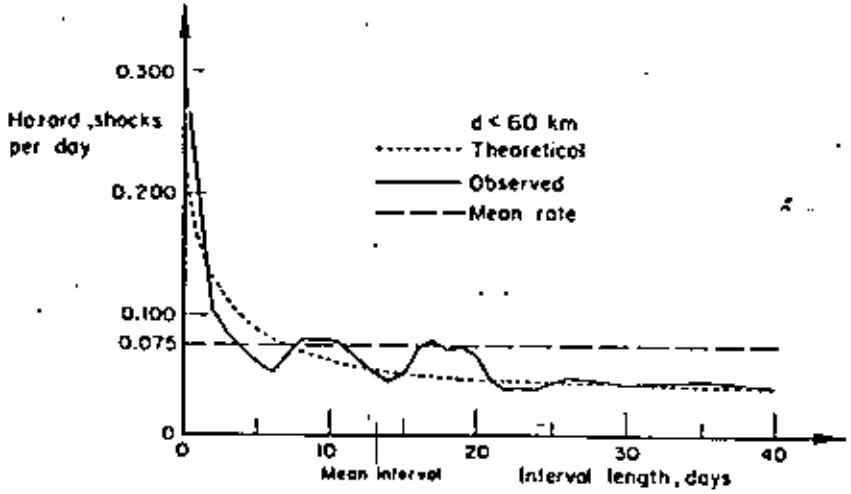

Fig. 6.15. Hazard function for New Zealand shallow shocks. (After Vere-Jones, 1970.)

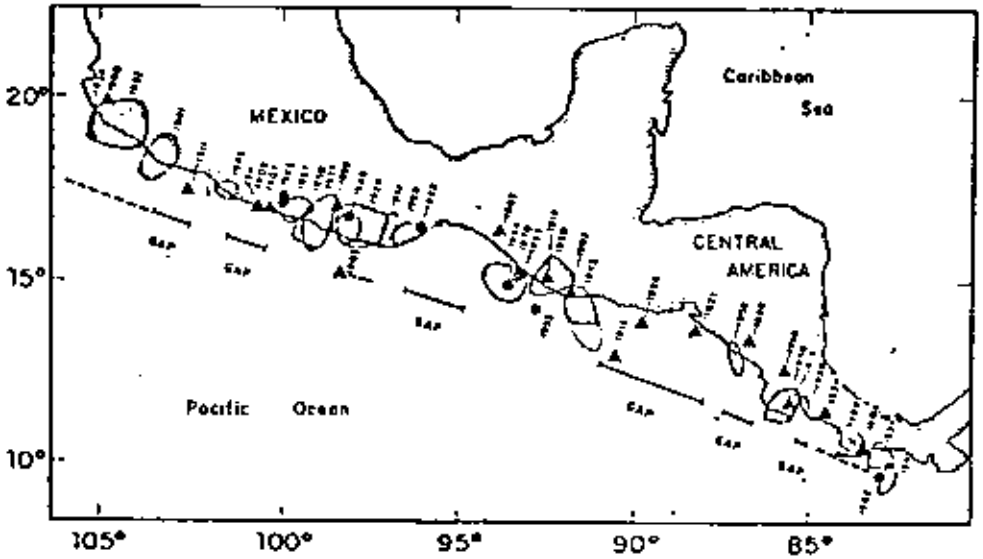

Fig. 6.16. Rupture zones and epicenters of large shallow Middle American earthquakes of this century. (After Kelleher et al., 1973.)

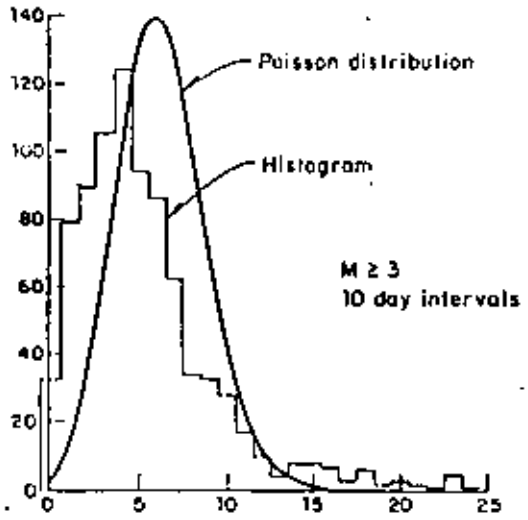

a) Including swarms

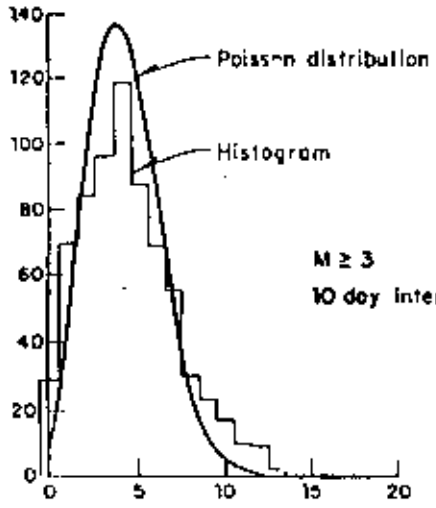

b) Eliminating swarms

Fig. 6.12. Evaluation of Poisson process assumption. (After Knopoff, 1964.)

$$\text{var}\,(N) = \nu \int_0^t E[W^2(t, \tau)]\mathrm{d}\tau \qquad (6.14)$$

Parzen (19[illegible] gives also an expression for the probability generating function $\psi_N(Z; t)$ [illegible] the distribution of N in terms of $\psi_W(Z; t, \tau)$, the generating function of each of the component processes:

$$\psi_N(Z; t) = \exp\left[-\nu t + \nu \int_0^t \psi_W(Z; t, \tau)\mathrm{d}\tau\right] \qquad (6.15)$$

where:

$$\psi_W(Z; t, \tau) = \sum_{n=0}^{\infty} Z^n \, P\{W(t, \tau) = n\} \qquad (6.16)$$

and the probability mass function of N can be obtained from $\psi_N(Z; t)$ by recalling that:

$$\psi_N(Z; t) = \sum_{n=0}^{\infty} Z^n P\{N = n\}$$

expanding ψ_N in power series of Z, and taking $P\{N = n\}$ equal to the coefficient of Z^n in that expansion. For instance, if it is of interest to compute $P\{N = 0\}$, expansion of $\psi_N(Z; t)$ in a Taylor's series with respect to $Z = 0$ leads to:

$$\psi_N(Z; t) = \psi_N(0; t) + Z\psi'_N(0; t) + \frac{Z^2}{2!}\psi''_N(0; t) + \ldots \qquad (6.17)$$

where the prime signifies derivative with respect to Z. From the definition of ψ_N, $P\{N = 0\} = \psi_N(0; t)$.

Because the component processes of 'trigger'-type time series appear overlapped in sample histories, their analytical representation usually entails study of a number of alternative models, estimation of their parameters, and comparison of model and sample properties — often second-order properties [illegible]ox and Lewis, 1966).

Vere-Jones models. Applicability of some general 'trigger' [illegible]dels to rep-

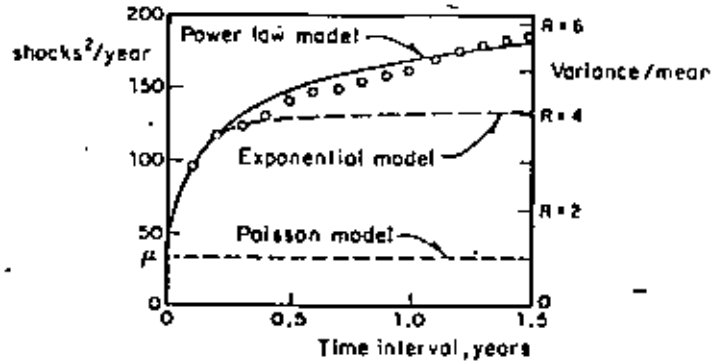

Fig. 6.13. Variance–time curve for New Zealand shallow shocks. (After Vere-Jones, 1966.)

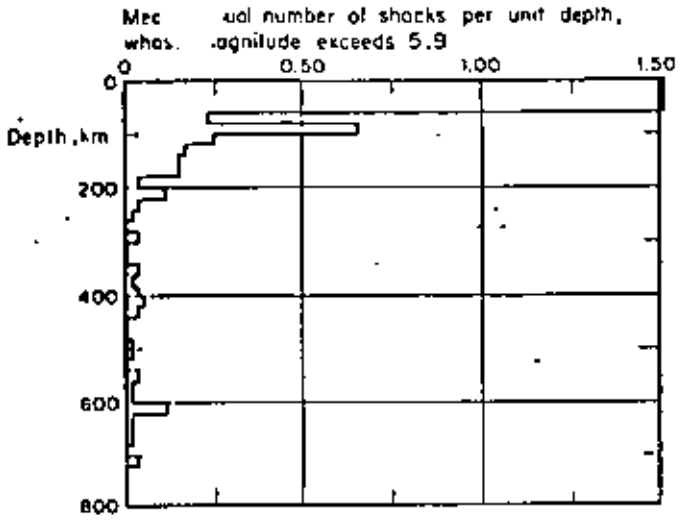

Fig. 6.11. Variation of seismicity with depth. Circum-Pacific Belt, (After Newmark and Rosenblueth, 1971.)

For the Poisson model, $h(t)$ is a constant equal to the mean rate of the process.

6.3.3.1 Poisson model

Most commonly applied stochastic models of seismicity assume that the events of earthquake occurrence constitute a Poisson process and that the M_i's are independent and identically distributed. This assumption implies that the probability of having N earthquakes with magnitude exceeding M during time interval $(0, t)$ equals:

$$p_N = [\exp(-\nu_M t)(\nu_M t)^N]/N! \qquad (6.11)$$

where ν_M is the mean rate of exceedance of magnitude M in the given volume. If N is taken equal to zero in eq. 6.11, one obtains that the probability distribution of the maximum magnitude during time interval t is equal to $\exp(-\nu_M t)$. If ν_M is given by eq. 6.6, the extreme type-I distribution is obtained.

Some weaknesses of this model become evident in the light of statistical information and of an analysis of the physical processes involved: the Poisson assumption implies that the distribution of the waiting time to the next event is not modified by the knowledge of the time elapsed since the last one, while physical models of gradually accumulated and suddenly released energy call for a more general renewal process such that, unlike what happens in the Poisson process, the expected time to the next event decreases as time goes on (Esteva, 1974). Statistical data show that the Poisson assumption may be acceptable when dealing with large shocl roughout the world (Ben-Menahem, 1960), implying lack of correlation between seismicities of different regions; however, when considering small volumes of the earth, of the order of those that can significantly contribute to seismic risk at a site, data often contradict Poisson's model, usually because of clustering of earthquakes in time: the observed numbers of short intervals between events are significantly higher than predicted by the exponential distribution, and values of Poisson's index of dispersion are well above unity (Figs. 6.12 and 6.13). In some instances, however, deviations in the opposite direction have been observed: waiting times tend to be more nearly periodic. Poisson's index of dispersion is smaller than one, and the process can be represented by a renewal model. This condition has been reported, for instance, in the southern coast of Mexico (Esteva, 1974), and in the Kamchatka and Pamir—Hindu Kush regions (Gaisky, 1966 and 1967). The models under discussion also fail to account for clustering in space (Tsuboi, 1958; Gajardo and Lomnitz, 1960), for the evolution of seismicity with time, and for the systematic shifting of active sources along geologic accidents (Allen, Chapter 3 of this book). On account of its simplicity, however, the Poisson process model provides a valuable tool for the formulation of some seismic-risk-related decisions, particularly of those that are sensitive only to magnitudes of events having very long return periods.

6.3.3.2 Trigger models

Statistical analysis of waiting times between earthquakes does not favor the adoption of the Poisson model or of other forms of renewal processes, such as those that assume that waiting times are mutually independent with lognormal or gamma distributions (Shlien and Toksöz, 1970). Alternative models have been developed, most of them of the 'trigger type' (Vere-Jones 1970), i.e. the overall process of earthquake generation is considered as the superposition of a number of time series, each having a different origin where the origin times are the events of a Poisson process. In general, let N be the number of events that take place during time interval $(0, t)$, τ_m = origin time of the mth series, $W_m(t, \tau_m)$ the corresponding number of event up to instant t_1 and n_t the random number of time series initiated in the interval $(0, t)$. The total number of events that occur before instant t is then

$$N = \sum_{m}^{n_t} W_m(t, \tau_m) \qquad (6.12$$

If origin times are distributed according to a homogeneous Poisson process with mean rate ν, and all W_m's are identically distributed stochastic processes with respect to $(t - \tau_m)$, it can be shown (Parzen, 1962) that the mean and variance of N can be obtained from:

$$E(N) = \nu \int_0^t E[W(t, \tau)]\mathrm{d}\tau \qquad (6.13$$

the amount of available information and their adoption offers significant advantages in the evaluation of regional seismicity, as shown later.

6.3.2 *Variation with depth*

Depth of prevailing seismic activity in a region depends on its tectonic structure. For instance, most of the activity in the western coast of the United States and Canada consists of shocks with hypocentral depths in the range of 20—30 km. In other areas, such as the southern coast of Mexico, seismic events can be grouped into two ensembles: one of small shallow shocks and one of earthquakes with magnitudes comprised in a wide range, and with depths whose mean value increases with distance from the shoreline (Fig. 6.10). Figure 6.11 shows the depth distribution of earthquakes with magnitude above 5.9 for the whole circum-Pacific belt.

6.3.3 *Stochastic models of earthquake occurrence*

Mean exceedance rates of given magnitudes are expected averages during long time intervals. For decision-making purposes the times of earthquake occurrence are also significant. At present those times can only be predicted within a probabilistic context.

Let t_i ($i = 1, \ldots, n$) be the unknown times of occurrence of earthquakes generated in a given volume of the earth's crust during a given time interval, and let M_i be the corresponding magnitudes. For the moment it will be assumed that the risk is uniformly distributed throughout the given volume, and hence no attention will be paid to the focal coordinates of each shock.

Classical methods of time-series analysis have been applied by different researchers attempting to devise analytical models for random earthquake sequences. The following approaches are often found in the literature:

(a) Plotting of histograms of waiting times between shocks (Knopoff, 1964; Aki, 1963).

(b) Evaluation of Poisson's index of dispersion, that is of the ratio of the sample variance of the number of shocks to its expected value (Vere-Jones, 1970; Shlien and Toksöz, 1970). This index equals unity for Poisson processes, is smaller for nearly periodic sequences, and is greater than one when events tend to cluster.

(c) Determination of autocovariance functions, that is, of functions representing the covariance of the numbers of events observed in given time intervals, expressed in terms of the time elapsed between those intervals (Vere-Jones, 1970; Shlien and Toksöz, 1970). The autocovariance function of a Poisson process is a Dirac delta function. This feature is characteristic for the Poisson model since it does not hold for any other stochastic process.

(d) The hazard function $h(t)$, defined so that $h(t)\,dt$ is the condition[al] probability that an event will take place in the interval $(t, t + dt)$ given that no events have occurred before t. If $F(t)$ is the cumulative probability distribution of the time between events:

$$h(t) = f(t)/[1 - F(t)] \tag{6.10}$$

where $f(t) = \partial F(t)/\partial t$.

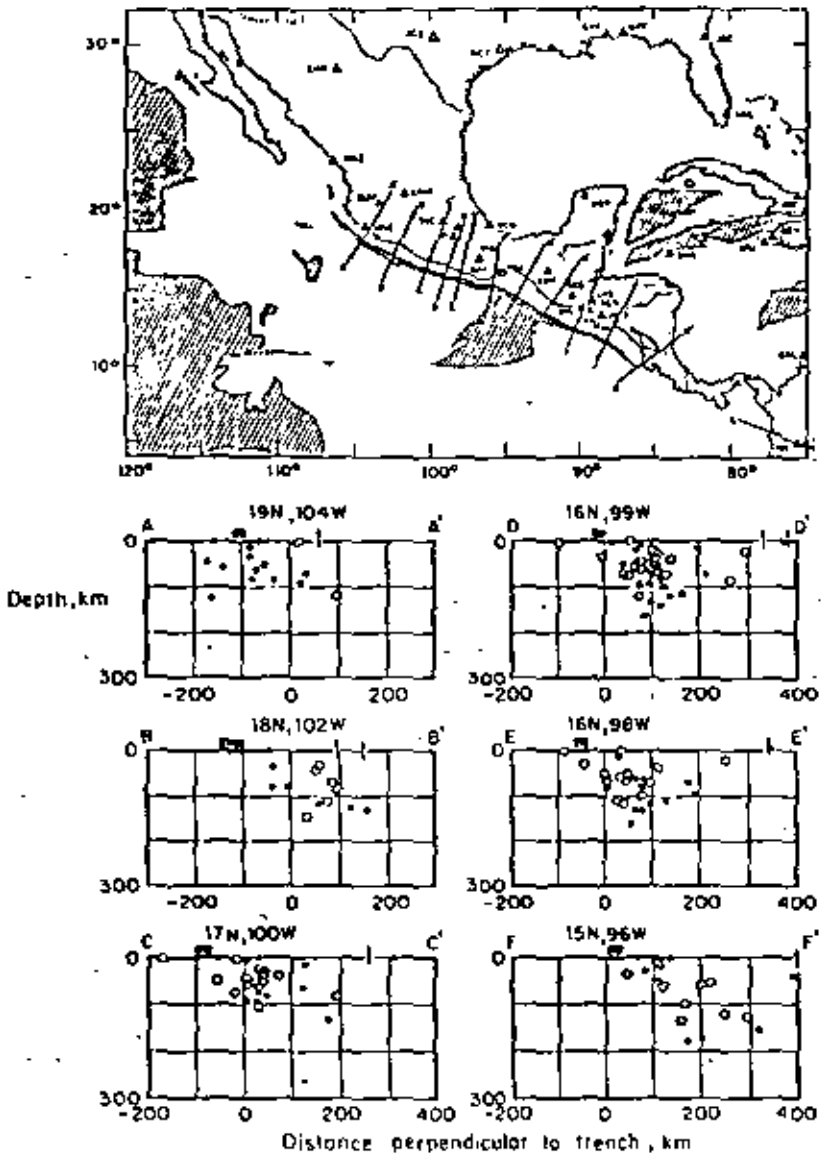

Fig. 6.10. Earthquake hypocenters projected onto a series of vertical sections through Mexico (After Molnar and Sykes, 1969.)

= maximum feasible magnitude, and $G^*(M)$ = complementary cumulative probability distribution of magnitudes every time that an event ($M \geq M_L$ occurs. A particular form of $G^*(M)$ that lends itself to analytical derivations is:

$$G^*(M) = A_0 + A_1 \exp(-\beta M) - A_2 \exp[-(\beta - \beta_1)M] \qquad (6.8)$$

where:

$$A_0 = A\beta_1 \exp[-\beta(M_U - M_L)]$$

$$A_1 = A(\beta - \beta_1) \exp(\beta M_L)$$

$$A_2 = A_0 \exp(-\beta_1 M_U + \beta M_L)$$

$$A = [\beta\{1 - \exp[-\beta_1(M_U - M_L)]\} - \beta_1\{1 - \exp[-\beta(M_U - M_L)]\}]^{-1}$$

As M tends to M_L from above, eq. 6.7 approaches eq. 6.6. Adoption of adequate values of M_U and β_1 permits satisfying two additional conditions: the maximum feasible magnitude and the rate of variation of λ in its vicinity. When $\beta_1 \to \infty$, eq. 6.8 tends to an expression proposed by Cornell and Vanmarcke (1969).

Yegulalp and Kuo (1974) have applied the theory of extreme values to estimating the probabilities that given magnitudes are exceeded in given time intervals. They assume those probabilities to fit an extreme type-III distribution given by:

$$F_{M_{max}}(M|t) = \exp[-C(M_U - M)^K t] \quad \text{for } M \leq M_U$$
$$= 0 \quad \text{for } M > M_U \qquad (6.9)$$

Here $F_{M_{max}}(M|t)$ indicates the probability that the maximum magnitude observed in t years is smaller than M, M_U has the same meaning as above, and C and K are zone-dependent parameters. This distribution is consistent with the assumption that earthquakes with magnitudes greater than M take place in accordance with a Poisson process with mean rate λ equal to $C(M_U - M)^K$. Equation 6.9 produces magnitude recurrence curves that fit closely the statistical data on which they are based for magnitudes above 5.2 and return periods from 1 to 50 years, even though the values of M_U that result from pure statistical analysis are not reliable measures of the upper bound to magnitudes, since in many cases they turn out inadmissibly high.

For low magnitudes, only a fraction of the number of shocks that take place is detected. As a consequence, λ-values based on statistical information lie below those computed according to eqs. 6.6 and 6.8 for M smaller than about 5.5. In addition, Fig. 6.9, taken from Yegulalp and Kuo (1974), shows that the numbers of detected shocks fit the extreme type III in eq. 6.9 better than the extreme type-I distribution implied by eq. 6.6., coupled with the assumption of Poisson distribution of the number of events. It is not

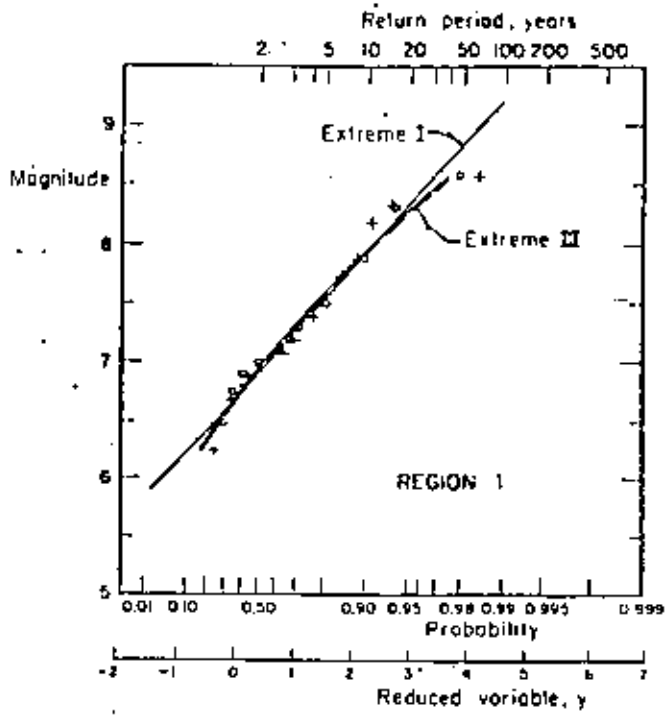

Fig. 6.9. Magnitude statistics in the Aleutian Islands region. (After Yegulalp and Kuo, 1974.)

clear what portion of the deviation from the extreme type-I distribution is due to the low values of the detectability levels and what portion comes from differences between the actual form of variation of λ with M and that given by eq. 6.6. The problem deserves attention because estimates of expected losses due to nonstructural damage may be sensitive to the values of λ for small magnitudes (say below 5.5) and because the evaluation of the level of seismic activity in a region is often made to depend on the recorded numbers of small magnitude shocks and on assumed detectability levels, i.e. of ratios of numbers of detected and occurred earthquakes (Kaila and Narain 1971; Kaila et al., 1972, 1974).

None of the expressions for λ presented in this chapter possess the desirable property that its applicability over a number of non-overlapping regions of the earth's crust implies the validity of an expression of the same form over the addition of those regions, unless some restrictions are imposed on the parameters of each λ. For instance, the addition of expressions like 6.6 gives place to an expression of the same form only if β is the same for all terms in the sum. Similar objections can be made to eq. 6.8. In what follows these forms will be preserved, however, as their accuracy is consistent with

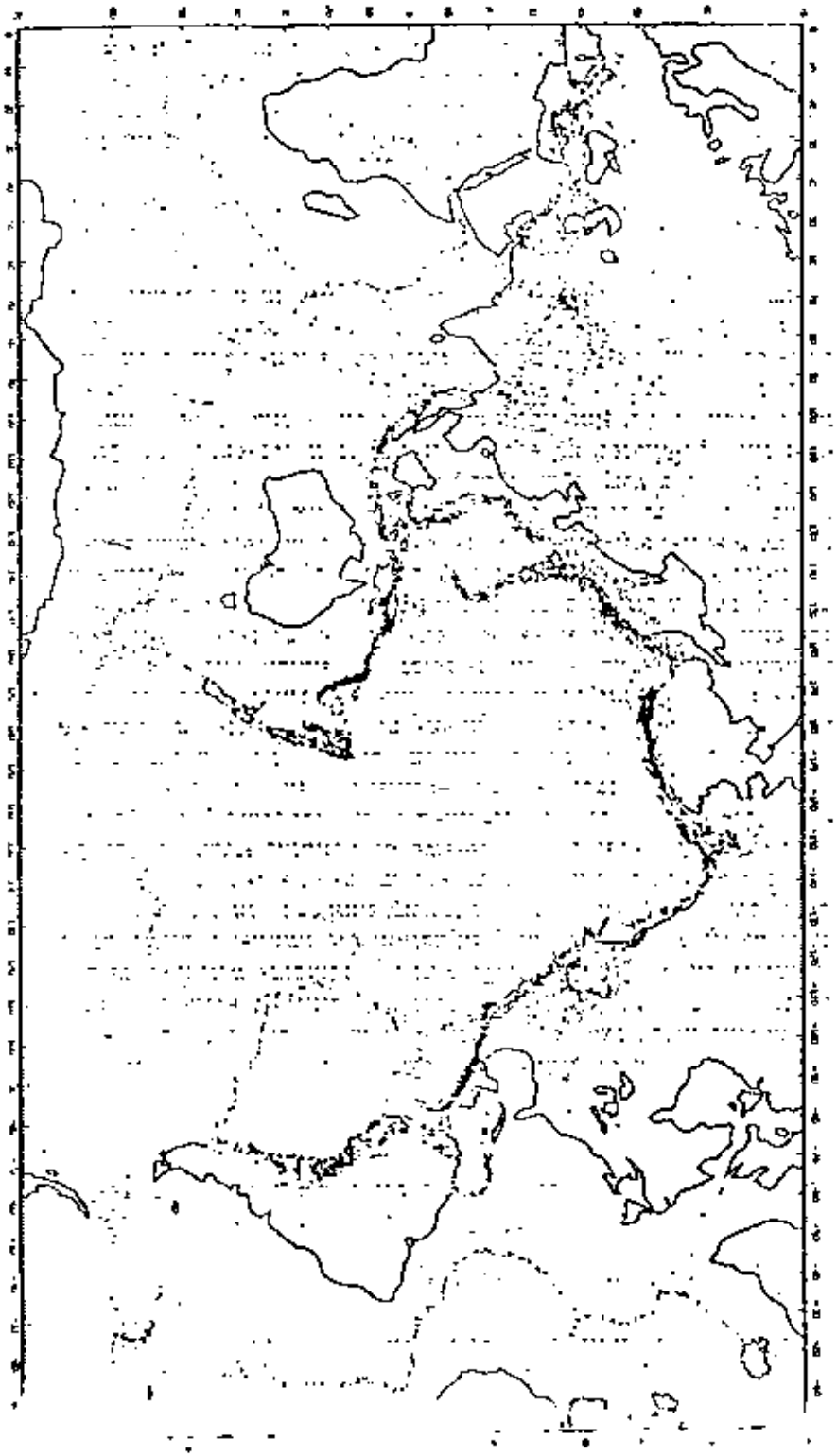

Fig. 6.7. Map showing epicenters for the interval 1961–1967. (After Newmark and Rosenblueth, 1971.)

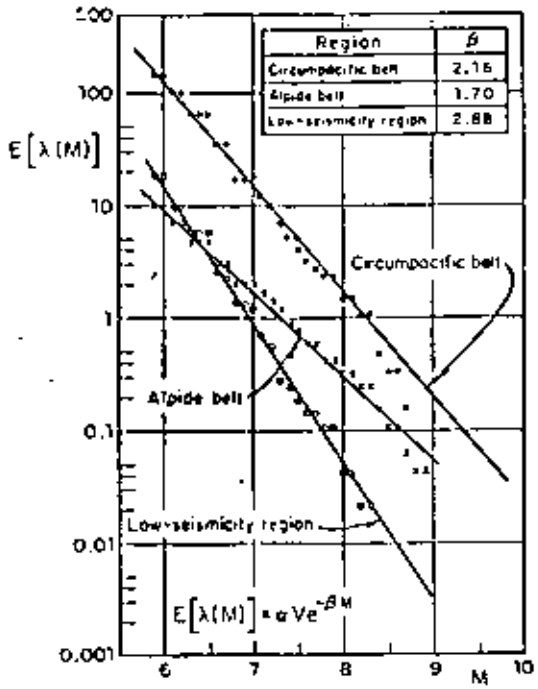

Fig. 6.8. Seismicity of macrozones. (After Esteva, 1968.)

tice of seismic zoning in the Soviet Union has been based on this concept (Gzovsky, 1962; Ananiin et al., 1968) and in many countries design spectra for very important structures, such as nuclear reactors or large dams, are usually derived from the assumption of a maximum credible intensity at a site; that intensity is ordinarily obtained by taking the maximum of the intensities that result at the site when at each of the potential sources an earthquake with magnitude equal to the maximum feasible value for that source is generated at the most unfavourable location within the same source. When this criterion is applied no attention is usually paid to the uncertainty in the maximum feasible magnitude nor to the probability that an earthquake with that magnitude will occur during a given time period. The need to formulate seismic-risk-related decisions that account both for upper bounds to magnitudes and for their probabilities of occurrence suggests adoption of magnitude recurrence expressions of the form:

$$\begin{aligned} \lambda &= \lambda_L G^*(M) && \text{for } M_L \leqslant M \leqslant M_U \\ &= \lambda_L && \text{for } M < M_L \\ &= 0 && \text{for } M > M_U \end{aligned} \qquad (6.7)$$

ere M_L = lowest magnitude whose contribution to risk is ; ficant, M_U .

TABLE 6.1

McGuire's attenuation expressions $y = b_1\, 10^{b_2 M}(R + 25)^{-b_3}$

y	b_1	b_2	b_3	$V(y)$ = coeff. of var. of y
a gals	472.3	0.278	1.301	0.548
v cm/sec	5.64	0.401	1.202	0.696
d cm	0.393	0.434	0.885	0.683
Undamped spectral pseudovelocities				
T = 0.1 sec	11.0	0.278	1.346	0.941
0.5	3.05	0.391	1.001	0.636
1.0	0.631	0.378	0.549	0.768
2.0	0.0768	0.469	0.419	0.989
5.0	0.0834	0.564	0.897	1.344
5% damped spectral pseudovelocities				
T = 0.1 sec	10.09	0.233	1.341	0.651
0.5	5.74	0.356	1.197	0.591
1.0	0.432	0.399	0.704	0.703
2.0	0.122	0.466	0.675	0.941
5.0	0.0706	0.557	0.938	1.193

natural period of 1 sec and a damping ratio of 2% attenuates in proportion to $(R + 25)^{-0.59}$. These results stem from the way that frequency content changes with R and lead to the conclusion that the ratio of spectral velocity should be taken as a function of M and R.

Table 6.1 summarizes McGuire's attenuation expressions and their coefficients of variation for ordinates of the pseudovelocity spectra and for peak ground acceleration, velocity and displacement. Similar expressions were derived by Esteva and Villaverde (1973), but they are intended to predict only the maxima of the expected acceleration and velocity spectra, regardless of the periods associated with those maxima. No analysis has been performed of the relative validity of McGuire's and Esteva and Villaverde's expressions for various ranges of M and R.

6.3 LOCAL SEISMICITY

The term *local seismicity* will be used here to designate the degree of seismic activity in a given volume of the earth's crust; it can be quantitatively described according to various criteria, each providing a different amount of information. Most usual criteria are based on upper bounds to the magnitudes of earthquakes that can originate in a given seismic source, on the amount of energy liberated by shocks per unit volume and unit time or on more detailed statistical descriptions of the process.

6.3.1 Magnitude-recurrence expressions

Gutenberg and Richter (1954) obtained expressions relating earthquake magnitudes with their rates of occurrence for several zones of the earth. Their results can be put in the form:

$$\lambda = \alpha e^{-\beta M} \tag{6.6}$$

where λ is the mean number of earthquakes per unit volume and per unit time having magnitude greater than M and α and β are zone-dependent constants; α varies widely from point to point, as evidenced by the map of epicenters shown in Fig. 6.7, while β remains within a relatively narrow range, as shown in Fig. 6.8. Equation 6.6 implies a distribution of the energy liberated per shock which is very similar to that observed in the process of microfracturing of laboratory specimens of several types of rock subjected to gradually increasing compressive or bending strain (Mogi, 1962; Scholz, 1968). The values of β determined in the laboratory are of the same order as those obtained from seismic events, and have been shown to depend on the heterogeneity of the specimens and on their ability to yield locally. Thus, in heterogeneous specimens made of brittle materials many small shocks precede a major fracture, while in homogeneous or plastic materials the number of small shocks is relatively small. These cases correspond to large and small β-values, respectively. No general relationship is known to the writer between β and geotectonic features of seismic provinces: complexity of crustal structure and of stress gradients precludes extrapolation of laboratory results; and statistical records for relatively small zones of the earth are not, as a rule, adequate for establishing local values of β. Figure 6.8 shows that for very high magnitudes the observed frequency of events is lower than predicted by eq. 6.6. In addition, Rosenblueth (1969) has shown that β cannot be smaller than 3.46, since that would imply an infinite amount of energy liberated per unit time. However, Fig. 6.8 shows that the values of β which result from fitting expressions of the form 6.6 to observed data are smaller than 3.46; hence, for very high values of M (above 7, approximately) the curve should bend down, in accordance with statistical evidence.

Expressions alternative to eq. 6.6 have been proposed, attempting to represent more adequately the observed magnitude-recurrence data (Rosenblueth, 1964; Merz and Cornell, 1973). Most of these expressions also fail to recognize the existence of an upper bound to the magnitude that can be generated in a given source. Although no precise estimates of this upper bound can yet be obtained, recognition of its existence and of its dependence on the geotectonic characteristics of the source is inescapable. Indeed, the prac-

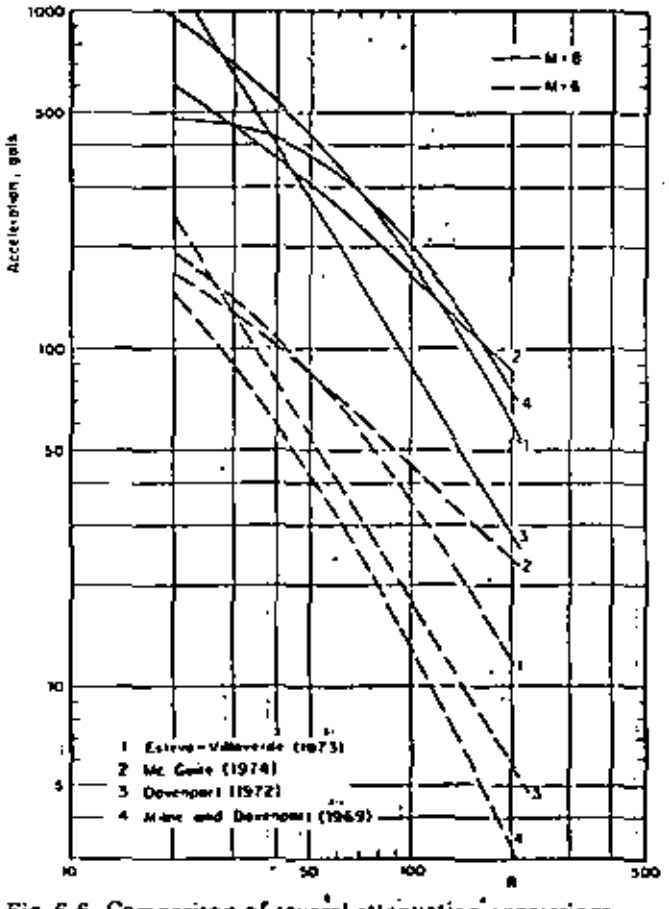

Fig. 6.6. Comparison of several attenuation expressions.

pared with R, is inadequate when dealing with earthquake sources whose dimensions are of the order of moderate hypocentral distances, and often greater than them. Although equation errors (probability distributions of the ratio of observed to predicted intensities) have been evaluated by Davenport (1972) and Esteva and Villaverde (1973), their dependence on M and R has not been analyzed. Because seismic risk estimates are very sensitive to the attenuation expressions in the range of large magnitudes and short distances, more detailed studies should be undertaken, aiming at improving those expressions in the mentioned range, and at evaluating the influence of M and R on equation error. Information on strong-motion records will probably be scanty for those studies, and hence they will have to be largely based on analytical or physical models of the generation and propagation of seismic waves. Although significant progress has been lately attained in this direction (Trifunac, 1973) the results from such models have hardly influenced the practice of seismic risk estimation because they have remained either unknown to or imperfectly appreciated by engineers in charge of the corresponding decisions.

6.2.1.3 Response spectra

Peak ground acceleration and displacement are fairly good indicators of the response of structures possessing respectively very high and very small natural frequencies. Peak velocity is correlated with the response of intermediate-period systems, but the correlation is less precise than that tying the former parameters; hence, it is natural to formulate seismic risk evaluation and engineering design criteria in terms of spectral ordinates.

Response spectrum prediction for given magnitude and hypocentral or site-to-fault distance usually entails a two-step process, according to which peak ground acceleration, velocity and displacement are initially estimated and then used as reference values for prediction of the ordinates of the response spectrum. Let the second step in the process be represented by the operation $y_s = \alpha y_g$, where y_s is an ordinate of the response spectrum for a given natural period and damping ratio, and y_g is a parameter (such as peak ground acceleration or velocity) that can be directly obtained from the time-history record of a given shock regardless of the dynamic properties of the systems whose response is to be predicted. For given M and R, y_g is random and so is $y_s/y_g = \alpha$; the mean and standard deviation of y_s depend on those of y_g and α and on the coefficient of correlation of the latter variables. As shown above, y_g can only be predicted within wide uncertainty limits, often wider than those tied to y_s (Esteva and Villaverde, 1973). The coefficient of variation of y_s given M and R can be smaller than that of y_g only if α and y_g are negatively correlated, which is often the case: the greater the deviation of an observed value of y_g with respect to its expectation for given M and R, the lower is likely to be α. In other words, it seems that in the intermediate range of natural periods the expected values of spectral ordinates for given damping ratios can be predicted directly in terms of magnitude and focal distance with narrower (or at most equal) margins of uncertainty than those tied to predicted peak ground velocities. For the ranges of very short or very long natural periods, peak amplitudes of ground motion and spectral ordinates approach each other and their standard errors are therefore nearly equal.

McGuire (1974) has derived attenuation expressions for the conditional values (given M and R) of the mean and of various percentiles of the probability distributions of the ordinates of the response spectra for given natural periods and damping ratios. Those expressions have the same form as eqs. 6.4 and 6.5, but their parameters show that the rates of attenuation of spectral ordinates differ significantly from those of peak ground accelerations or velocities. For instance, McGuire finds that peak ground velocity attenuates in proportion to $(R + 25)^{-1.20}$, while the mean of the pseudovelocity for a

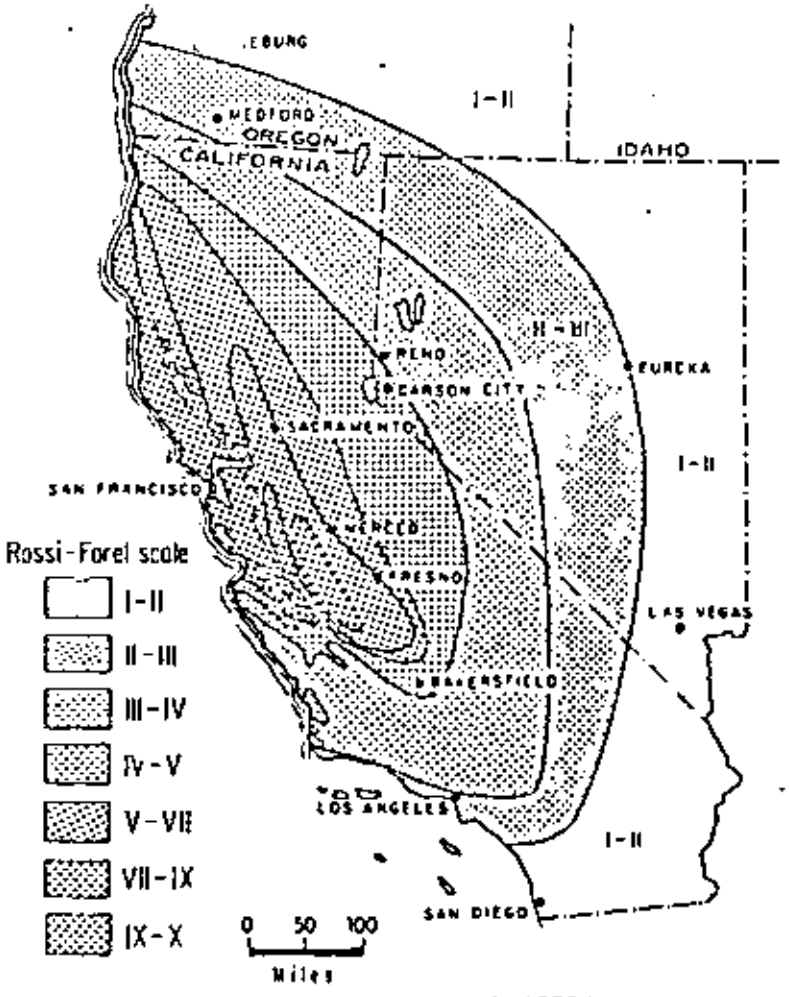

Fig. 6.3. Isoseismals in California. (After Bolt, 1970.)

He showed that intensities attenuate faster with distance on the west coast than in the rest of the country. This comparison is in agreement with Milne and Davenport (1969), who performed a similar analysis for Canada. From observations of strong earthquakes in California and in British Columbia, they developed the following expression for a, the peak ground acceleration, as a fraction of gravity:

$$a/g = 0.0069\, e^{1.6M}/(1.1\, e^{1.1M} + R^2) \qquad (6.2)$$

Here, R is epicentral distance in kilometers. The acceleration varies roughly as $e^{1.6M}R^{-2}$ for large R, and as $e^{0.6M}$ where R approaches zero. This reflects to some extent the fact that energy is released not at a single point but from a finite volume. A later study by Davenport (1972) led him

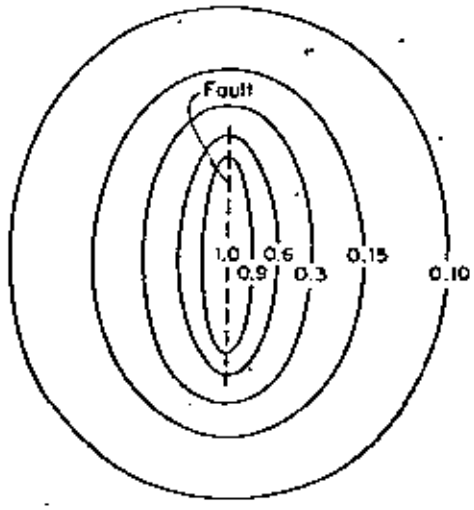

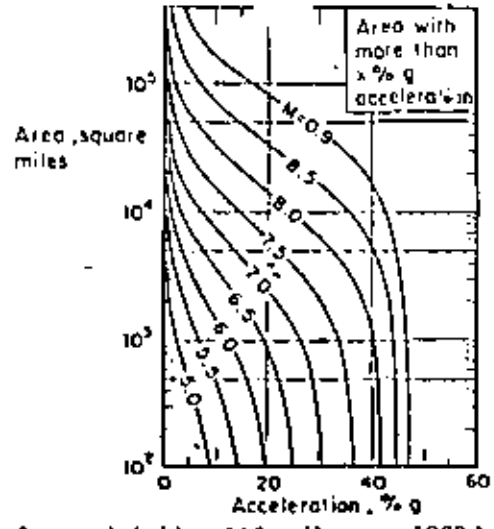

Fig. 6.4. Idealized contour lines of intensity of ground shaking. (After Housner, 1969.)

Fig. 6.5. Area in square miles experiencing shaking of x %g or greater for shocks of different magnitudes. (After Housner, 1969.)

to propose the expression:

$$a/g = 0.279\, e^{0.6M}/R^{1.64} \qquad (6.3)$$

The statistical error of this equation was studied by fitting a lognormal probability distribution to the ratios of observed to computed accelerations. A standard deviation of 0.74 was found in the natural logarithms of those ratios.

Esteva and Villaverde (1973), on the basis of accelerations reported by Hudson (1971, 1972a,b), derived expressions for peak ground accelerations and velocities, as follows:

$$a/g = 5.7\, e^{0.8M}/(R + 40)^2 \qquad (6.4)$$

$$v = 32\, e^{M}/(R + 25)^{1.7} \qquad (6.5)$$

Here v is peak ground velocity in cm/sec and the other symbols mean the same as above. The standard deviation of the natural logarithm of the ratio of observed to predicted intensity is 0.64 for accelerations and 0.74 for velocities. If judged by this parameter, eqs. 6.3 and 6.4 seem equally reliable. However, as shown by Fig. 6.6, their mean values differ significantly in some ranges.

With the exception of eq. 6.2, all the foregoing attenuation expressions are products of a function of R and a function of M. This form, which is acceptable when the dimensions of the energy-liberating source are small com-

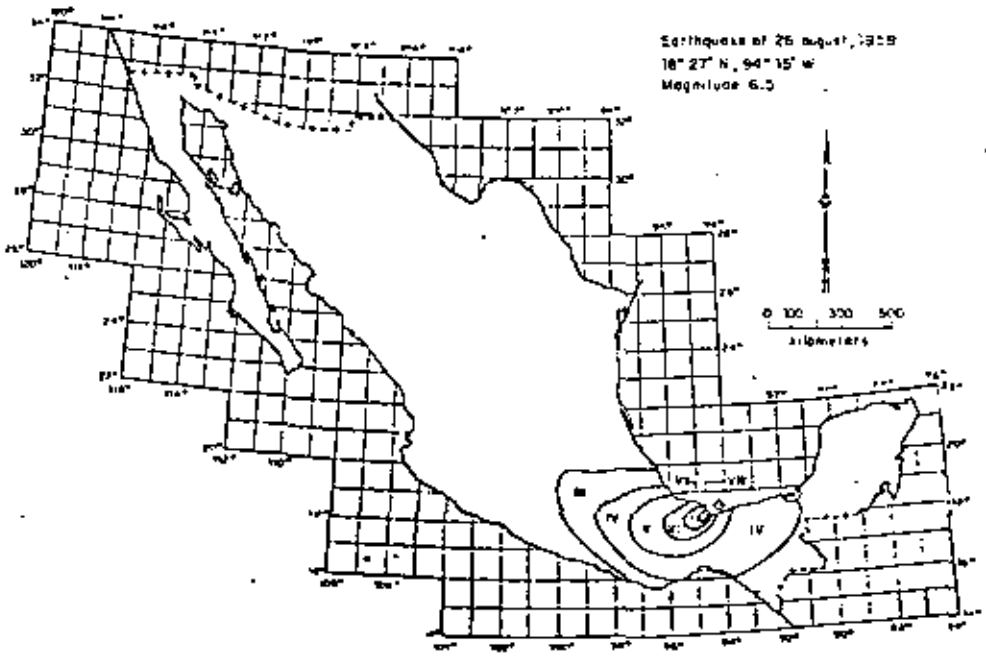

Fig. 6.1. Isoseismals of an earthquake in Mexico. (After Figueroa, 1963.)

central coordinates (Bollinger, 1973; Figueroa, 1963). In that case, intensity should be expressed as a function of magnitude and coordinates of source and site. For most areas in the world, intensity has to be predicted in terms of simple — and cruder — expressions that depend only on magnitude and distance from site to instrumental hypocenter. This stems from inadequate knowledge of geotectonic conditions and from limited information concerning the volume where energy is liberated in each shock.

A comparison of the rates of attenuation of intensities on firm ground for shocks on western and eastern North America has disclosed systematic differences between those rates (Milne and Davenport, 1969). This is the source of a basic, but often unavoidable, weakness of most intensity-attenuation expressions, because they are based on heterogeneous data, recorded in different zones, and the very nature of their applications implies that the less is known about possible systematic deviations in a given zone, as a consequence of the meagerness of local information, the greater weight is given to predictions with respect to observations.

6.2.1.1 Modified Mercalli intensities

An analys[illegible] the Modified Mercalli intensities on firm ground reported for earthquakes occurring in Mexico in the last few decades leads to the following expression relating magnitude M, hypocentral distance R (in kilometers) and intensity I (Esteva, 1968):

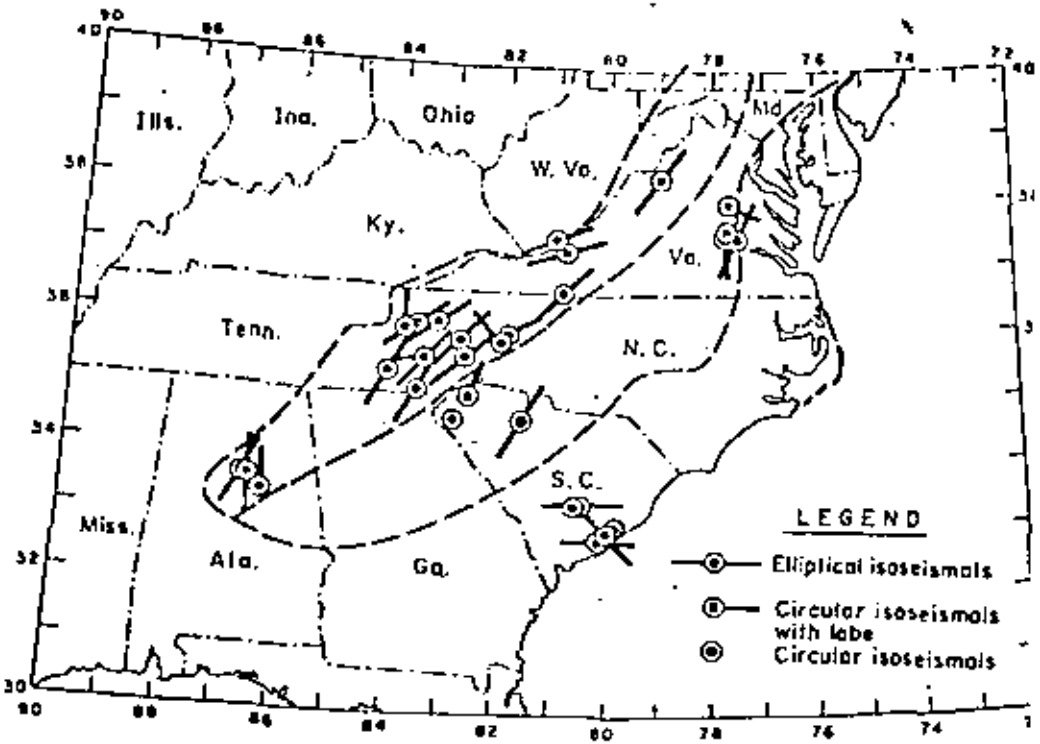

Fig. 6.2. Elongation of isoseismals in the southeastern United States. (After Bollinger, 1973.)

$$I = 1.45\,M - 5.7\,\log_{10} R + 7.9 \qquad (6.1)$$

The prediction error, defined as the difference between observed and computed intensity, is roughly normally distributed, with a standard deviation of 2.04, which means that there is a probability of 60% that an observed intensity is more than one degree greater or smaller than its predicted value.

6.2.1.2 Peak ground accelerations and velocities

A few of the available expressions will be described. Their comparison will show how cautiously a designer intending to use them should proceed.

Housner studied the attenuation of peak ground accelerations in several regions of the United States and presented his results graphically (1969) in terms of fault length (in turn a function of magnitude), sha[illegible] of isoseismals and areas experiencing intensities greater than given values (Fig. 6.4 and 6.5).

eral extremely large: some studies relating fault rupture area, stress drop, and magnitude (Brune, 1968) show that, considering not unusually high stress drops, it does not take very large source dimensions to get magnitudes 8.0 and greater, and those studies are practically restricted to the simplest types of fault displacement. It is not clear, therefore, that realistic bounds can always be assigned to potential magnitudes in given areas or that, when this is feasible, those bounds are sufficiently low, so that designing structures to withstand the corresponding intensities is economically sound, particularly when occurrence of those intensities is not very likely in the near future. Because uncertainties in maximum feasible magnitudes and in other parameters defining magnitude-recurrence laws can be as significant as their mean values when trying to make rational seismic design decisions, those uncertainties have to be explicitly recognized and accounted for by means of adequate probabilistic criteria. A corollary is that geophysically based estimates of seismicity parameters should be accompanied with corresponding uncertainty measures.

Seismic risk estimates are often based only on statistical information (observed magnitudes and hypocentral coordinates). When this is done, a wealth of relevant geophysical information is neglected, while the probabilistic prediction of the future is made to rely on a sample that is often small and of little value, particularly if the sampling period is short as compared with the desirable return period of the events capable of severely damaging a given system.

The criterion advocated here intends to unify the foregoing approaches and rationally to assimilate the corresponding pieces of information. Its philosophy consists in using the geological, geophysical, and all other available non-statistical evidence for producing a set of alternate assumptions concerning a mathematical (stochastic process) model of seismicity in a given source area. An initial probability distribution is assigned to the set of hypotheses, and the statistical information is then used to improve that probability assignment. The criterion is based on application of *Bayes theorem*, also called the *theorem of the probabilities of hypotheses*. Since estimates of risk depend largely on conceptual models of the geophysical processes involved, and these are known with different degrees of uncertainty in different zones of the earth's crust, those estimates will be derived from stochastic process models with uncertain forms or parameters. The degree to which these uncertainties can be reduced depends on the limitations of the state of the art of geophysical sciences and on the effort that can be put into compilation and interpretation of geophysical and statistical information. This is an economical problem that should be handled, formally or informally, by the criteria of decision making under uncertainty.

Available criteria for the evaluation of the contribution of potential seismic sources to the risk at a site make use of *intensity attenuation* expressions that relate intensity characteristics with magnitude and distance from the source. Depending on the application envisaged, the intensity characteristic to be predicted can be expressed in a number of manners, ranging from a subjective index, such as the *Modified Mercalli intensity*, to a combination of one or more quantitative measures of ground shaking (see Chapter 1).

A number of expressions for attenuation of various intensity characteristics with distance have been developed, but there is little agreement among most of them (Ambraseys, 1973). This is due in part to discrepancies in the definitions of some parameters, in the ranges of values analyzed, in the actual wave propagation properties of the geological formations lying between source and site, in the dominating shock mechanisms, and in the form of the analytical expressions adopted a priori.

Most intensity-attenuation studies concern the prediction of earthquake characteristics on rock or firm ground, and assume that these characteristics, properly modified in terms of frequency-dependent soil amplification factors, should constitute the basis for estimating their counterparts on soil ground. Observations about the influence of soil properties on earthquake damage support the assumption of a strong correlation between type of ground and intensity in a given shock. Attempts to analytically predict characteristics of motions on soil given those on firm ground or on bedrock have not been too successful, however (Crouse, 1973; Hudson and Udwadia, 1973; Salt, 1974), with the exception of some peculiar cases, like Mexico City (Herrera et al., 1965), where local conditions favor the fulfillment of the assumptions implied by usual analytical models. The following paragraphs concentrate on prediction on intensities on firm ground; the influence of local soil is discussed in Chapter 4.

6.2.1 Intensity attenuation on firm ground

When isoseismals (lines joining sites showing equal intensity) of a given shock are based only on intensities observed on homogeneous ground conditions, such as *firm ground* (compact soils) or bedrock, they are roughly elliptical and the orientations of the corresponding axes are often correlated with local or regional geological trends (Figs. 6.1—6.3). In some regions — for instance near major faults in the western United States — those trends are well defined and the correlations are clear enough as to permit prediction of intensity in the near and far fields in terms of magnitude and distance to the generating fault or to the centroid of the energy liberating volume. In other regions, such as the eastern United States and most of Mexico, isoseismals seem to elongate systematically in a direction that is a function of the

Chapter 6

SEISMICITY

LUIS ESTEVA

Instituto de Ingeniería, Universidad Nacional Autónoma de México, Mexico

6.1 ON SEISMICITY MODELS

Rational formulation of engineering decisions in seismic areas requires quantitative descriptions of seismicity. These descriptions should conform with their intended applications: in some instances, simultaneous intensities during each earthquake have to be predicted at several locations, while in others it suffices to make independent evaluations of the probable effects of earthquakes at each of those locations.

The second model is adequate for the selection of design parameters of individual components of a regional system (the structures in a region or country) when no significant interaction exists between response or damage of several such individual components, or between any of them and the system as a whole. In other words, it applies when the damage — or negative utility — inflicted upon the system by an earthquake can be taken simply as the addition of the losses in the individual components.

The linearity between monetary values and utilities implied in the second model is not always applicable. Such is the case, for instance, when a significant portion of the national wealth or of the production system is concentrated in a relatively narrow area, or when failure of life-line components may disrupt emergency and relief actions just after an earthquake. Evaluation of risk for the whole regional system has then to be based on seismicity models of the first type, that is, models that predict simultaneous intensities at several locations during each event; for the purpose of decision making, nonlinearity between monetary values and utilities can be accounted for by means of adequate scale transformations. These models are also of interest to insurance companies, when the probability distribution of the maximum loss in a given region during a given time interval is to be estimated.

Whatever the category to which a seismic risk problem belongs, it requires the prediction of probability distributions of certain ground motion characteristics (such as peak ground acceleration or velocity, spectral density, response or Fourier spectra, duration) at a given site during a single shock or of maximum values of some of those characteristics in earthquakes occurring during given time intervals. When the reference interval tends to infinity, the probability distribution of the maximum value of a given characteristic approaches that of its maximum *possible* value. Because different systems or subsystems are sensitive to different ground motion characteristics, the term *intensity characteristic* will be used throughout this chapter to mean a particular parameter or set of parameters of an earthquake motion, in terms of which the response is to be predicted. Thus, when dealing with the failure probability of a structure, intensity can be alternatively measured — with different degrees of correlation with structural response — by the ordinate of the response spectrum for the corresponding period and damping, the peak ground acceleration, or the peak ground velocity.

In general, local instrumental information does not suffice for estimating the probability distributions of maximum intensity characteristics, and use has to be made of data on subjective measures of intensities of past earthquakes, of models of *local seismicity*, and of expressions relating characteristics with magnitude and site-to-source distance. Models of local seismicity consist, at least, of expressions relating magnitudes of earthquakes generated in given volumes of the earth's crust with their return periods. More often than not, a more detailed description of local seismicity is required, including estimates of the maximum magnitude that can be generated in these volumes, as well as probabilistic (stochastic process) models of the possible histories of seismic events (defined by magnitudes and coordinates).

This chapter deals with the various steps to be followed in the evaluation of seismic risk at sites where information other than direct instrumental records of intensities has to be used: identifying potential sources of activity near the site, formulating mathematical models of local seismicity for each source, obtaining the contribution of each source to seismic risk at the site and adding up contributions of the various sources and combining information obtained from local seismicity of sources near the site with data on instrumental or subjective intensities observed at the site.

The foregoing steps consider use of information stemming from sources of different nature. Quantitative values derived therefrom are ordinarily tied to wide uncertainty margins. Hence they demand probabilistic evaluation, even though they cannot always be interpreted in terms of relative frequencies of outcomes of given experiments. Thus, geologists talk of the maximum magnitude that can be generated in a given area, assessed by looking at the dimensions of the geological accidents and by extrapolating the observations of other regions which available evidence allows to brand as similar to the one of interest; the estimates produced are obviously uncertain, and the degree of uncertainty should be expressed together with the most probable value. Following nearly parallel lines, some geophysicists estimate the energy that can be liberated by a single shock in a given area by making quantitative assumptions about source dimensions, dislocation amplitude and stress drop, consistent with tectonic models of the region and, again, with comparisons with areas of similar tectonic characteristics.

Uncertainties attached to estimates of the type just described are in gen-

centro de educación continua
división de estudios de posgrado
facultad de ingeniería unam

VI CURSO INTERNACIONAL DE INGENIERIA SISMICA

SISMOLOGIA Y SISMICIDAD

SISMICIDAD

DR. OCTAVIO A. RASCON CHAVEZ

JULIO, 1980

Las condiciones de frontera son que $v_1 = v_2$ y $(\tau_{xy})_1 = (\tau_{xy})_2$ en $x=0$ y que $\tau_{xy} = 0$ en $x=-H$. Estas condiciones conducen a un sistema de ecuaciones homogéneo en A, B y C. Para que se tenga solución diferente de cero el determinante del sistema debe anularse. Así, se tiene que

$$\tan k\gamma_1 H = I \frac{\mu_2\gamma_2}{\mu_1\gamma_1} = \frac{\mu_2(1 - c^2/\beta_2^2)^{1/2}}{\mu_1(c^2/\beta_1^2 - 1)^{1/2}} \qquad (51)$$

es la ecuación para obtener la velocidad de las ondas de Love.

Si $\beta_1 < \beta_2$ la ec 51 da valores reales de c, en el intervalo $\beta_1 < c < \beta_2$, que dependen de k y H. Pueden obtenerse ondas de Love de forma general superponiendo ondas de Love del tipo de la ec 49 con diferentes k.

La dependencia de la velocidad de propagación de la frecuencia ocasiona el fenómeno de *dispersión* y, en general, esto es el caso en medios estratificados.

6. BIBLIOGRAFIA

Ewing, W M, Jardetzky, W S y Press, F, *Elastic waves in layered media*, Mc Graw-Hill Book Co, Nueva York, 1957

White, J E, *Seismic waves: radiation transmission and attenuation*, Mc Graw-Hill Book Co., Nueva York, 1965

Fung, Y C, *Foundations of solid mechanics*, Prentice-Hall, Inc, Englewood Cliffs, Nueva Jersey, 1965

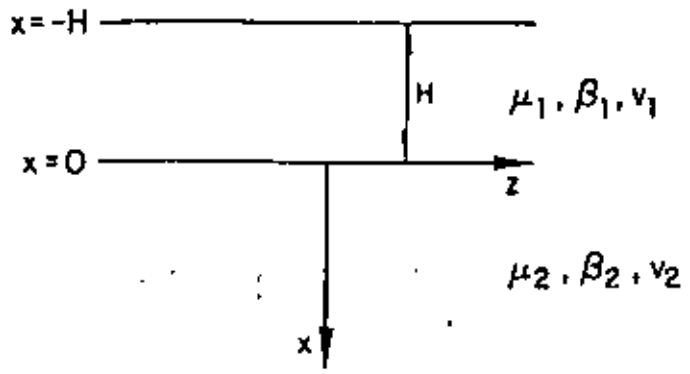

Fig 10. Notación para un estrato sobre un semiespacio elástico

para el estrato y

$$\frac{\partial^2 v_2}{\partial x^2} + \frac{\partial^2 v_2}{\partial z^2} + k_{\beta_2}^2 \, v_2 = 0 \qquad (48)$$

donde $k_{\beta_i} = \omega/\beta_i$, $i = 1,2$ para el semiespacio.

Haciendo uso de soluciones del tipo de las ecs 23 y 24 se puede escribir que

$$v_1 = (A\, e^{-k\gamma_1 x} + B\, e^{k\gamma_1 x})\, e^{Ik(z-ct)} \qquad (49)$$

$$v_2 = C\, e^{-k\gamma_2 x}\, e^{Ik(z-ct)} \qquad (50)$$

donde $\gamma_1 = (1-c^2/\beta_1^2)^{1/2}$ y $\gamma_2 = (1-c^2/\beta_2^2)^{1/2}$. Se observa que si $c < \beta_2$, $v_2 \to 0$ cuando $x \to \infty$.

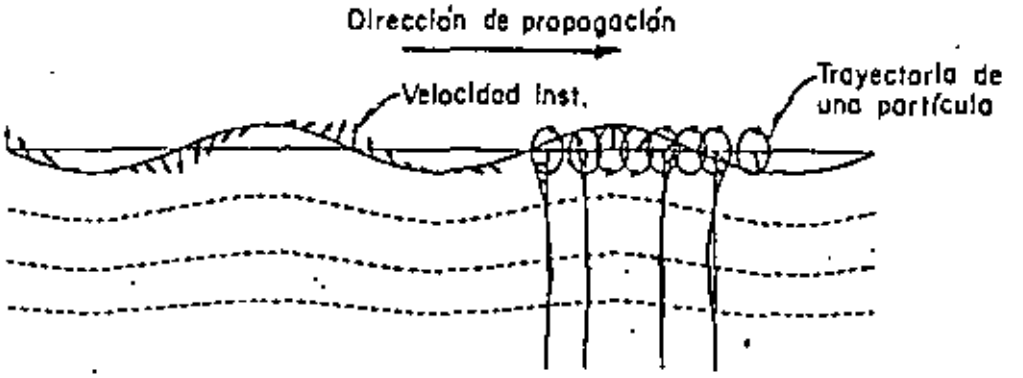

Fig 9. Ondas de Rayleigh

5. ONDAS DE LOVE

Puede demostrarse que la propagación de ondas superficiales (que se atenúen con la profundidad) del tipo SH es imposible en un semiespacio homogéneo. No obstante, las ondas SH superficiales se observan en la superficie de la tierra. Love demostró que una teoría suficiente para explicar las ondas SH superficiales puede desarrollarse si se tiene un estrato homogéneo de espesor uniforme H con propiedades μ_1 y β_1 sobre un semiespacio de propiedades μ_2 y β_2 como se muestra en la fig 10. Supóngase que los desplazamientos son independientes de la coordenada y, y además que la variación con el tiempo está dada por $e^{i\omega t}$. El plano $x = -H$ representa la superficie libre. Las ecuaciones de movimiento (ecs 1) se reducen a

$$\frac{\partial^2 v_1}{\partial x^2} + \frac{\partial^2 v_1}{\partial z^2} + k_{\beta_1}^2 v_1 = 0 \qquad (47)$$

distintos valores del módulo de Poisson ν. Las ondas de Rayleigh son ondas *superficiales* y debido a ello sufren

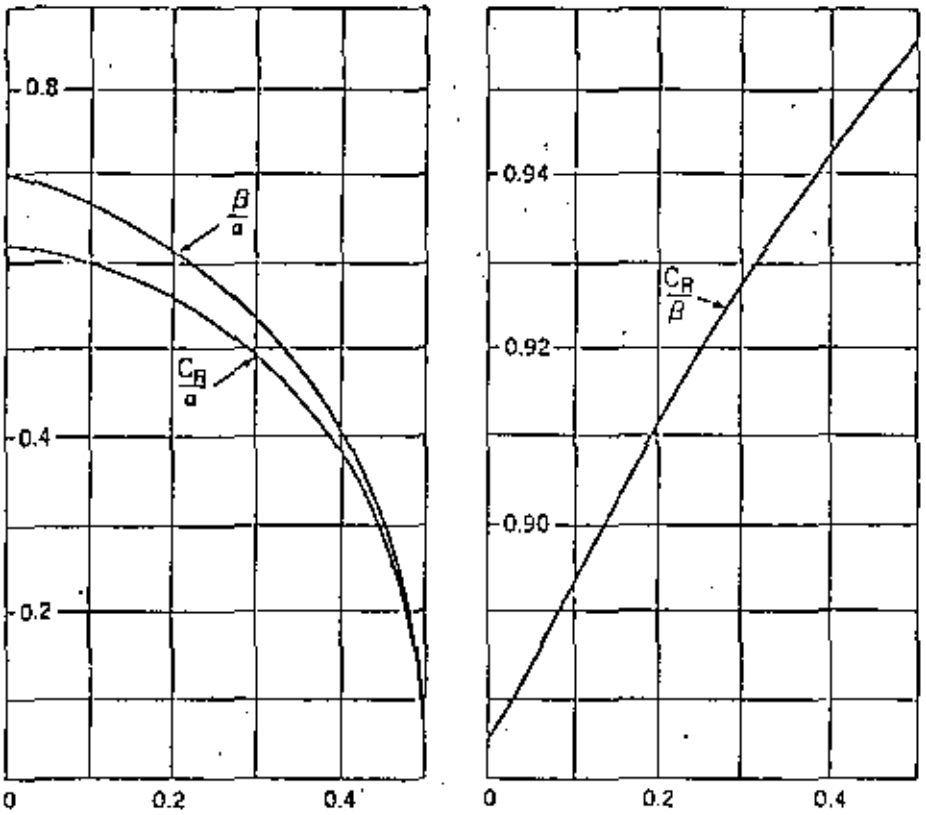

Fig 8. Relaciones β/α, c_R/α y c_R/β como funciones del módulo de Poisson ν

menor atenuación geométrica. Puede demostrarse que el movimiento generado por ondas de Rayleigh hace que las partículas describan trayectorias elípticas con ciclos retrógrados, a diferencia de los ciclos progresivos que se presentan en las ondas superficiales en líquidos. La fig 9 muestra un dibujo esquemático de las ondas superficiales de Rayleigh.

4. ONDAS DE RAYLEIGH

Para el tercer caso, $|c| < \beta < \alpha$, se tiene que

$$\phi = A_2 \, e^{-mx} \, e^{-i\ell z} \, e^{i\omega t} \tag{42}$$

$$\psi = B_2 \, e^{-kx} \, e^{-i\ell z} \, e^{i\omega t} \tag{43}$$

donde $m = |\omega|(1/c^2 - 1/\alpha^2)^{1/2}$ y $k = |\omega|(1/c^2 - 1/\beta^2)^{1/2}$. Se han eliminado A_1 y B_1 pues no representan ondas incidentes con potenciales finitos. Las ecuaciones de esfuerzos nulos en $x = 0$ conducen a

$$\frac{A_2}{B_2} = \frac{2i(1-c^2/\beta^2)^{1/2} \operatorname{sgn}\omega}{2 - c^2/\beta^2} \tag{44}$$

$$\frac{A_2}{B_2} = \frac{2 - c^2/\beta^2}{2i(1-c^2/\alpha^2)^{1/2} \operatorname{sgn}\omega} \tag{45}$$

como las ecs 44 y 45 deben ser iguales se obtiene que la velocidad de fase, c, debe satisfacer la siguiente ecuación:

$$(2 - \frac{c^2}{\beta^2})^2 - 4(1 - \frac{c^2}{\alpha^2})^{1/2} \, (1 - \frac{c^2}{\beta^2})^{1/2} = 0 \tag{46}$$

La raiz real de esta ecuación, c_R, encontrada por vez primera por Rayleigh, da la velocidad de las llamadas ondas de Rayleigh. En la fig 8 se presentan valores de c_R para

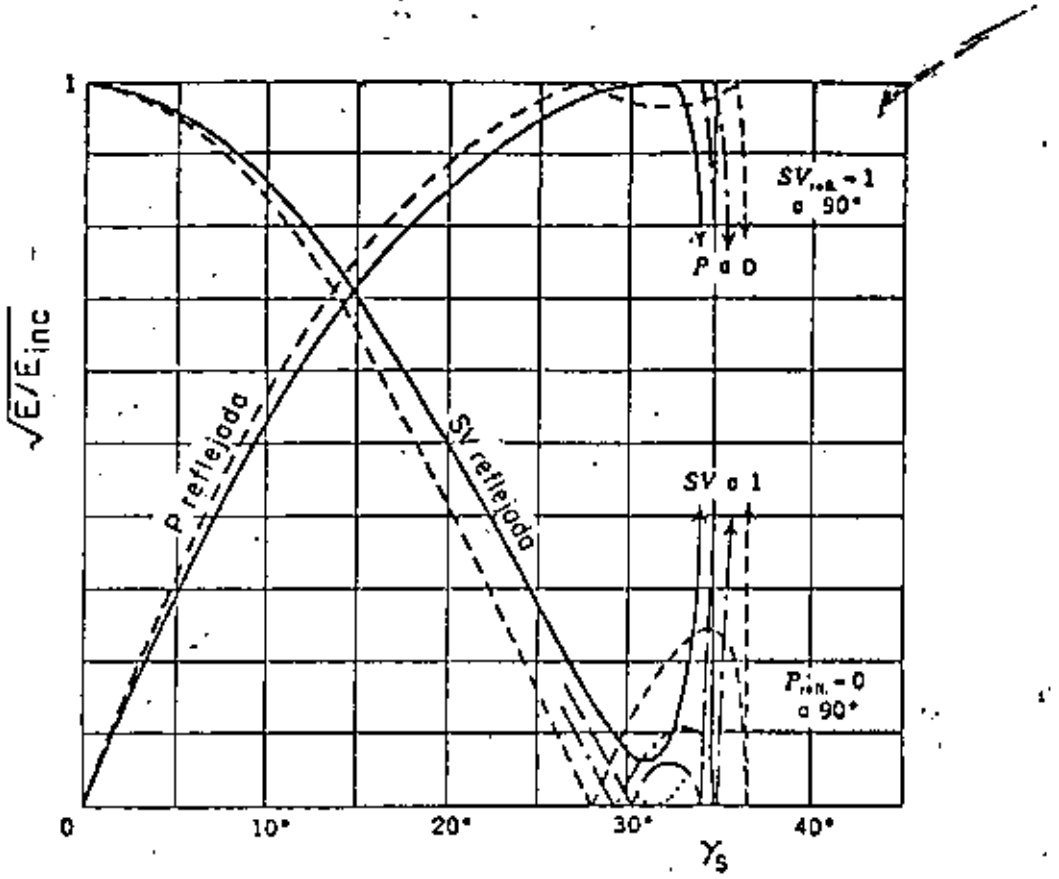

Fig 7. Raiz cuadrada de la relación de energía reflejada a energía incidente para una onda SV incidente en una superficie libre

$$\frac{A_2}{B_1} = -\frac{4\cot\gamma_S(\cot^2\gamma_S-1)}{(\cot^2\gamma_S-1)^2-4i(1-c^2/\alpha^2)^{1/2}\cot\gamma_S\ \mathrm{sgn}\,\omega} \qquad (40)$$

$$\frac{B_2}{B_1} = -\frac{(\cot^2\gamma_S-1)^2+4i(1-c^2/\alpha^2)^{1/2}\cot\gamma_S\ \mathrm{sgn}\,\omega}{(\cot^2\gamma_S-1)^2-4i(1-c^2/\alpha^2)^{1/2}\cot\gamma_S\ \mathrm{sgn}\,\omega} \qquad (41)$$

donde sgn ω =(-1 si $\omega<0$ o 1 si $\omega>1$). En este caso, la incidencia de ondas SV con ángulos de incidencia γ_S mayores que $\mathrm{sen}^{-1}(\beta/\alpha)$ genera ondas P no homogéneas que se atenuan con la profundidad.

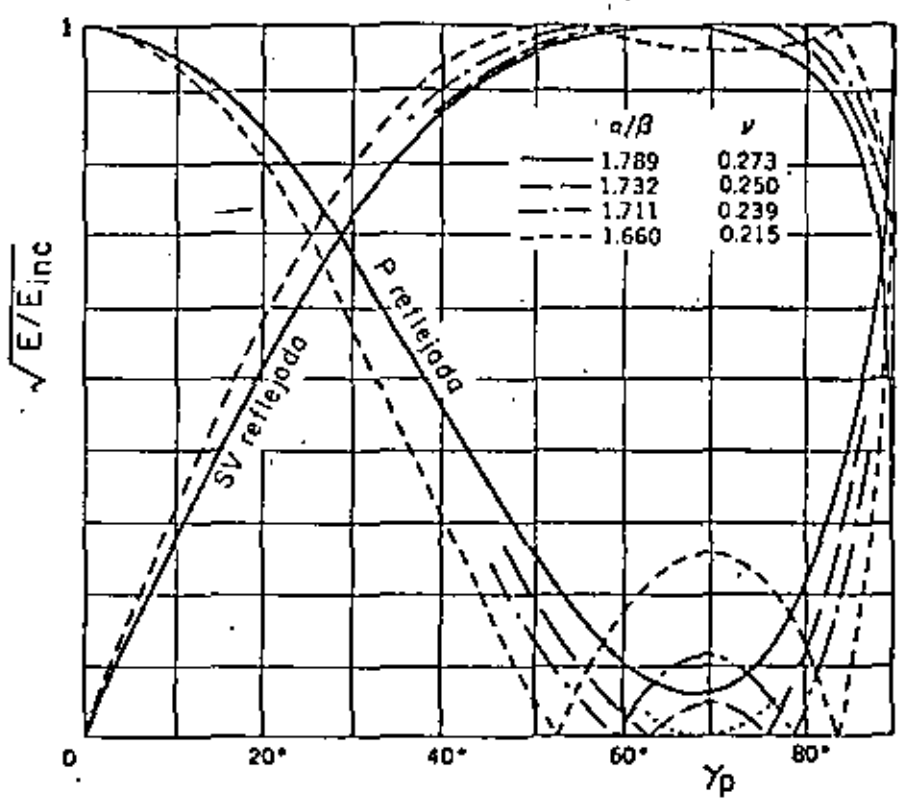

Fig 6. Raiz cuadrada de la relación de energía reflejada a energía incidente para una onda P incidente en una superficie libre

Para el segundo caso, $\beta < |c| < \alpha$, se tienen los potenciales

$$\phi = (A_1 e^{mx} + A_2 e^{-mx})\, e^{-i\ell z}\, e^{i\omega t} \qquad (38)$$

$$\psi = (B_1 e^{ikx} + B_2 e^{-ikx}) e^{i\ell z}\, e^{i\omega t} \qquad (39)$$

donde $\ell = \omega/c$, $m = |\omega|(1/c^2 - 1/\alpha^2)^{1/2}$ y $k = \omega(1/\beta^2 - 1/c^2)^{1/2}$. Para evitar que ϕ crezca indefinidamente al aumentar x se hace que $A_1 = 0$ por lo que *no hay* onda P incidente en este caso. Mediante un proceso análogo al del caso anterior se obtiene que

La incidencia de una onda P puede variar de vertical (c infinita) a horizontal ($c = \alpha$) y las ecs 33 y 34 permiten calcular las amplitudes de los potenciales de las ondas reflejadas. Para la incidencia de una onda SV se tiene que $0 \leq \gamma_S \leq \text{sen}^{-1}(\beta/\alpha)$.

Si se toma la energía cinética por unidad de volumen como $\frac{1}{2}\rho(\dot{u}^2 + \dot{\omega}^2)$, puede calcularse el flujo de energía mediante el producto de la energía cinética por la velocidad de propagación y el área del frente de onda considerado. Para incidencia de una onda P puede demostrarse que las fracciones de energía reflejada como ondas P y SV están dadas, respectivamente, por

$$\frac{A_2^2}{A_1^2} \quad y \quad \frac{B_2^2 \tan \gamma_P}{A_1^2 \tan \gamma_S}$$

y, similarmente, para incidencia de una onda SV se tiene que

$$\frac{A_2^2 \tan \gamma_S}{B_1^2 \tan \gamma_P} \quad y \quad \frac{B_2^2}{B_1^2}$$

En las figs 6 y 7 se presentan valores de $\sqrt{E/E_{inc}}$ para incidencia de ondas P y SV, respectivamente, en función del ángulo de incidencia y con diferentes relaciones α/β.

$$\psi = (B_1 e^{lkx} + B_2 e^{-lkx}) e^{-l\ell z} e^{l\omega t} \qquad (32)$$

donde $\ell = \omega/c$, $m = \omega(1/\alpha^2 - 1/c^2)^{1/2}$ Y $k = \omega(1/\beta^2 - 1/c^2)^{1/2}$. Si $B_1 = 0$ se tiene el caso mostrado en la fig 4 de incidencia de ondas P. En cambio si $A_1 = 0$ se tendrá incidencia de ondas SV. Sustituyendo las ecs 31 y 32 en las ecs 21 y 22, haciendo que $\sigma_x = \tau_{xz} = 0$ en x=0 y resolviendo el sistema de ecuaciones resultante se obtiene que

a) Para $B_1 = 0$

$$\frac{A_2}{A_1} = \frac{4 \cot \gamma_P \cot \gamma_S - (\cot^2 \gamma_S - 1)^2}{4 \cot \gamma_P \cot \gamma_S + (\cot^2 \gamma_S - 1)^2} \qquad (33)$$

$$\frac{B_2}{A_1} = \frac{4 \cot \gamma_P (\cot^2 \gamma_S - 1)}{4 \cot \gamma_P \cot \gamma_S + (\cot^2 \gamma_S - 1)^2} \qquad (34)$$

donde γ_P = ángulo de incidencia y de reflexión de la onda P y γ_S = ángulo de reflexión de la onda SV. Debe recordarse que la velocidad aparente está dada por

$$c = \frac{\alpha}{\operatorname{sen} \gamma_P} = \frac{\beta}{\operatorname{sen} \gamma_S} \qquad (35)$$

b) Para $A_1 = 0$

$$\frac{A_2}{B_1} = -\frac{4 \cot \gamma_S (\cot^2 \gamma_S - 1)}{4 \cot \gamma_P \cot \gamma_S + (\cot^2 \gamma_S - 1)^2} \qquad (36)$$

$$\frac{B_2}{B_1} = \frac{4 \cot \gamma_P \cot \gamma_S - (\cot^2 \gamma_S - 1)^2}{4 \cot \gamma_P \cot \gamma_S + (\cot^2 \gamma_S - 1)^2} \qquad (37)$$

que los potenciales sean finitos. Al definir ℓ como imaginario negativo con $\ell = \omega/c$ se observa que el producto

$$e^{-i\ell z}\, e^{i\omega t} = e^{i\omega(t-z/c)} \tag{27}$$

representa una onda armónica que viaja en la dirección positiva de z con una velocidad de fase c, si c es negativa la dirección de viaje es en la dirección negativa de z. En términos de los ángulos de las figs 4 y 5 se tiene que

$$c = \frac{\alpha}{\operatorname{sen} \gamma_P} = \frac{\beta}{\operatorname{sen} \gamma_S} \tag{28}$$

Con estas definiciones M y K deben ser o reales o imaginarios pues, de las ecs 25 y 26, se tiene que

$$M^2 = \ell^2 - \omega^2/\alpha^2 = \omega^2(1/c^2 - 1/\alpha^2) \tag{29}$$

y

$$K^2 = \ell^2 - \omega^2/\beta^2 = \omega^2(1/c^2 - 1/\beta^2) \tag{30}$$

Así, para $\beta < \alpha < |c|$, M y K son imaginarios; para $\beta < |c| < \alpha$, M es real y K imaginario; para $|c| < \beta < \alpha$, M y K son reales.

Para el primer caso, $\beta < \alpha < |c|$, se tienen los potenciales

$$\phi = (A_1 e^{imx} + A_2 e^{-imx}) e^{-i\ell z}\, e^{i\omega t} \tag{31}$$

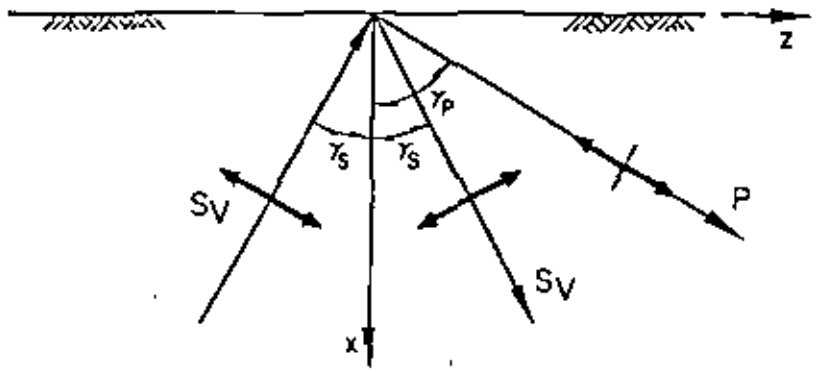

Fig 5. Incidencia de ondas SV

Mediante la técnica de separación de variables se puede demostrar que las soluciones de las ecs 17 y 18 son de la forma

$$\phi = A_o \, e^{Mx} \, e^{Lz} \, e^{\Omega t} \tag{23}$$

$$\psi = B_o \, e^{Kx} \, e^{Lz} \, e^{\Omega t} \tag{24}$$

donde

$$M^2 + L^2 = \frac{\Omega^2}{\alpha^2} \quad y \quad K^2 + L^2 = \frac{\Omega^2}{\beta^2} \tag{25}$$

Hasta ahora K, L, M y Ω con valores complejos son posibles soluciones, pero para los actuales propósitos basta hacer

$$\Omega = i\,\omega \quad y \quad L = -\,ik \tag{26}$$

pues al tener a Ω como número imaginario puro se garantiza

$$\frac{\partial^2\psi}{\partial x^2} + \frac{\partial^2\psi}{\partial z^2} = \frac{1}{\beta^2}\ \frac{\partial^2\psi}{\partial t^2} \qquad (18)$$

Los desplazamientos quedan como

$$u = \frac{\partial\phi}{\partial x} - \frac{\partial\psi}{\partial z} \qquad (19)$$

$$w = \frac{\partial\phi}{\partial z} + \frac{\partial\psi}{\partial x} \qquad (20)$$

Los esfuerzos que al valuarse en la superficie deben anularse son

$$\sigma_x = \lambda\left(\frac{\partial^2\phi}{\partial x^2} + \frac{\partial^2\psi}{\partial z^2}\right) + 2\mu\left(\frac{\partial^2\phi}{\partial x^2} - \frac{\partial^2\psi}{\partial x\partial z}\right) \qquad (21)$$

$$\tau_{xz} = \mu\left(2\ \frac{\partial^2\phi}{\partial x\partial z} + \frac{\partial^2\psi}{\partial x^2} - \frac{\partial^2\psi}{\partial z^2}\right) \qquad (22)$$

ya que $\tau_{xy} = 0$.

Considérense los casos mostrados en las figs 4 y 5, la incidencia de ondas P y de ondas SV, respectivamente.

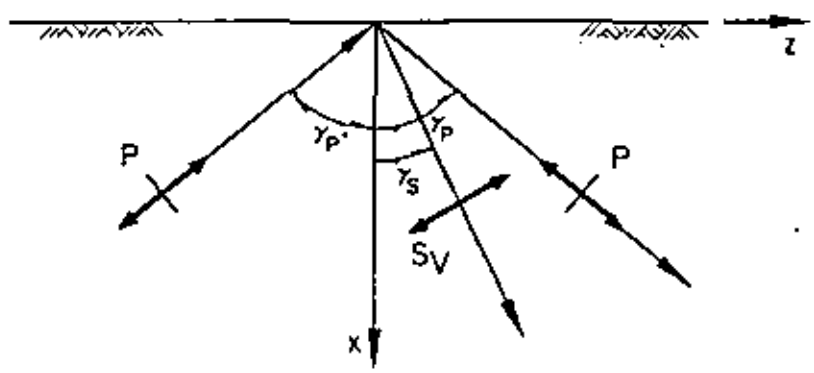

Fig 4. Incidencia de ondas P

centro de educación continua
división de estudios de posgrado
facultad de ingeniería unam

VI CURSO INTERNACIONAL DE INGENIERIA SISMICA

SISMOLOGIA Y SISMICIDAD

EFECTOS SISMICOS EN SUELOS GRANULARES

M. EN I. ABRAHAM DIAZ RODRIGUEZ

JULIO, 1980

EFECTOS SISMICOS EN SUELOS GRANULARES

por

Abraham Díaz Rodríguez*

INTRODUCCION

El comportamiento adecuado de los suelos y las cimentaciones durante la ocurrencia de temblores es esencial para evitar daños severos a toda clase de estructuras.

Las condiciones bajo las cuales los suelos (como parte de la cimentación o como material de construcción) pierden una parte significativa de su resistencia, conduciendo a fallas inducidas por temblores, no son, al menos hasta la fecha (junio, 1977) completamente entendidas y constituyen un campo fertil de investigación y de gran utilidad para la práctica profesional de la Ingeniería Civil.

La importancia de los efectos que los sismos pueden inducir en los suelos granulares se debe a los graves daños que se han observado en numerosas ocasiones durante los temblores pasados.

---

* Jefe de la Sección de Mecánica de Suelos y profesor de la División de Estudios de Posgrado, Facultad de Ingeniería, UNAM

APENDICE A

REVISION DE INVESTIGACIONES PASADAS

A.1 *INTRODUCCION*

El comportamiento adecuado de los suelos y las cimentaciones durante la ocurrencia de temblores es esencial para evitar daños severos a toda clase de estructuras.

Las condiciones bajo las cuales los suelos (como parte de la cimentación o como material de construcción) pierden una parte significativa de su resistencia, conduciendo a fallas inducidas por temblores, no son, al menos hasta la fecha (abril, 1980) completamente entendidas y constituyen un campo fértil de investigación y de gran utilidad para la práctica profesional de la Ingeniería Civil.

La importancia de los efectos que los sismos pueden inducir en los suelos granulares se debe a los graves daños que se han observado en numerosas ocasiones durante los temblores pasados.

De 1881 a 1946 se ha informado de 229 deslizamientos, que causaron el desplazamiento total de 25 millones de m^3 de arena. En Holanda, a orillas de los numerosos estrechos que existen, ha habido gran cantidad de deslizamientos que han provocado el rompimiento de diques y, por tanto, la inundación de grandes extensiones de terreno.

En México existen evidencias de que durante el sismo de 1959 (Marsal, 1961), un gran tramo de la margen izquierda del río Coatzacoalcos tuvo desplazamientos verticales y horizontales de importancia. Muchas instalaciones de la zona de astilleros sufrieron hundimientos bajo la cimentación y el asentamiento general fue notable después del sismo. Algunos tramos de los muelles cimentados sobre pilotes metálicos de 10 m de longitud sufrieron desplazamientos apreciables en dirección horizontal. Uno de los muelles se desplazó hacia el río más de 1/2 m. Tales movimientos se han atribuido al fenómeno de licuación en los mantos arenolimosos y limoarenosos que allí se encuentran entre 0 y 8 m de profundidad. En vista de las altas relaciones de vacíos y de la granulometría uniforme de dichos suelos, no puede descartarse esta posibilidad.

Durante el temblor de Chile, en 1960, se formaron extensas zonas de falla. La tierra fue arrastrada hacia el mar a lo largo de la costa de 600 m, llevando consigo todas las estructuras de retención; las paredes del muelle con secciones de 5 m de concreto reforzado fueron abatidas y luego arrastradas. En este mismo temblor, falló una presa debido a la licuación del suelo de cimentación.

En Alaska, en 1964 (Seed, 1969), se produjo un deslizamiento debido a la licuación del suelo que movió 70 millones de m^3 de material, destruyendo muchas de las instalaciones de la bahía de Anchorage. La superficie del terreno fue completamente devastada por los desplazamientos, produciéndose una nueva superficie irregular (fig 1). El 40 por ciento de las casas y edificios comerciales fueron seriamente dañados debido a las fisuras que se extendían bajo las construcciones, (fig 2).

Durante junio de 1964, en Niigata, Japón (Seed y Lee, 1966), hubo daños muy graves causados por licuación de la arena. Muchas estructuras se asentaron más de 1 m y se inclinaron notablemente; hubo un edificio que giró 80°(fig 3), quedando prácticamente tendido en el suelo. Además de estas fallas, hubo otras evidencias físicas de licuación. Poco después del sismo se observó que brotaba agua del suelo por grietas que se formaron, en las cuales llegaron a hundirse casas y automóviles; al mismo tiempo, se veía emerger a la superficie estructuras que debían permanecer bajo el suelo, como fué el caso de un tanque para tratamiento de aguas negras.

Durante este sismo, en la extensa zona licuada se produjeron daños en edificios, puentes, caminos, muelles, vías de ferrocarril, etc. Debido al asentamiento que se produjo, la parte de la ciudad cercana al río quedó completamente inundada. Se estima que en este sismo 2,130 edificios sufrieron falla total, 6,200 fueron seriamente dañados y 31,200 sufrieron daños ligeros (Seed y Lee, 1967).

A.2. FENOMENOS INDUCIDOS POR SISMOS

El comportamiento dinámico de los suelos granulares constituye, dentro de la dinámica de suelos, uno de los problemas que actualmente está lejos de ser comprendido totalmente y es mucho lo que falta por dilucidar en torno a ello, al grado que es posible ver interpretaciones diferentes y aún contradictorias de los hechos experimentales disponibles, y por tanto, constituye un campo fertil para la investigación en ingeniería sísmica.

Dos de los principales fenómenos que la ocurrencia de temblores pueden inducir en depósitos de suelos granulares son:

1. Cambios de volumen (densificación→asentamientos)
2. Reducción de la resistencia al esfuerzo cortante (Aumento de la presión de poro→licuación)

En lo que sigue se tratará de dar un breve panorama del estado de conocimiento que guardan estos dos temas. No se ha pretendido en este trabajo hacer un análisis exahustivo y completo. Para mayores detalles se ha elaborado una lista de referencias actualizada (junio de 1979) para que sirva de guía a aquellas personas que estén interesadas en profundizar en el tema.

A.3 ESTUDIOS DE DENSIFICACION

Es un hecho bien establecido que la aplicación de carga cíclica a una muestra de arena, da como resultado un decrecimiento progresivo de volumen, aún en el caso de arenas densas, las cuales se comportarían dilatantes bajo carga unidireccional o monotónica. Varias técnicas, tanto de laboratorio como de campo, se han desarrollado (Broms y Forssblad, 1969).

El uso de vibraciones verticales para producir la densificación de muestras de arena se ha utilizado en el pasado (D'Appolonia y D'Appolonia, 1967; Whitman y Ortigosa, 1968), estos estudios han mostrado que los cambios de peso volumétrico de las muestras son pequeños para aceleraciones menores de 1 g (figs 4 y 5).

Los cambios tanto de volumen como de características friccionantes de arenas secas inducidas por grandes aceleraciones horizontales y un gran número de ciclos de pequeña amplitud se han investigado utilizando cajas de corte colocadas sobre mesas vibradoras (Barkan, 1962; Youd, 1970), ver fig 6.

Otros estudios basados en ensayes de corte simple y mesas vibradoras, con niveles de aceleración y amplitudes de deformación semejantes a los esperados en temblores intensos, han mostrado que: la amplitud de deformación, compacidad relativa y número de ciclos de carga son los principales factores que gobiernan la densificación de suelos granulares secos o saturados bajo condiciones drenadas (Silver y Seed, 1969; Youd, 1972), ver fig 7.

Seed, Pyke y Martin (1975), realizaron una serie de ensayes de corte simple tanto en una (x) como en dos (x,y) direcciones. Se utilizaron dos patrones básicos de movimiento, en los ensayes bidireccionales.

Los resultados de los ensayes utilizando movimientos aleatorios se resumen en la fig 8, en donde se encuentra el asentamiento para 10 ciclos de carga como función de la relación, τ_h/σ_v , en donde τ_h , es el máximo esfuerzo cortante horizontal y, σ_v , es el esfuerzo vertical aplicado. Estas pruebas confirmaron las conclusiones de Silver y Seed (1971), que para un nivel de deformaciones cortantes el asentamiento inducido es independiente del esfuerzo vertical. Sin embargo, si se realiza una prueba bajo condiciones de esfuerzo controlado, las deformaciones cortantes cíclicas, y por tanto los asentamientos, se incrementan con el incremento de la relación de esfuerzos. Para un valor dado de la relación de esfuerzos se puede ver que el asentamiento causados por dos componentes de movimiento es aproximadamente igual a la suma de los asentamientos causados por cada una de los componentes.

Sobre la base de estos resultados parece razonable postular que para arenas saturadas ensayadas bajo condiciones no drenadas, el incremento de la presión de poro será aproximadamente dos veces mayor bajo dos componentes de movimiento que bajo una sola.

Tomando en cuenta todo lo anterior, se puede concluir que los aspectos más importantes relacionados con los cambios de volumen de suelos granulares, son los siguientes:

a) Los esfuerzos cortantes cíclicos constituyen el medio más efectivo de densificación.

b) Para un peso volumétrico dado, la amplitud de las deformaciones cortantes es el parámetro más importante que afecta la velocidad y magnitud de la densificación.

c) A mayores esfuerzos de sobrecarga la velocidad de densificación generalmente resulta menor.

d) La densificación es independiente de la frecuencia del movimiento.

A.3.1 CALCULO DE ASENTAMIENTO

La acción de los sismos puede causar asentamientos considerables en depósitos de suelos granulares. Durante el temblor de San Fernando, ocurrido el 9 de febrero de 1971, se tuvieron asentamientos de edificios, los cuales variaron de 10 a 15 cm (aprox. 4 a 6 pulgadas).

Mayores asentamientos, más espectaculares, e incluso inclinación de edificios pueden ocurrir debido a la licuación de los depósitos de arena saturada, pero este problema se tratará en el inciso siguiente.

Los asentamientos de depósitos de arena seca, resultantes del movimiento del terreno son rara vez uniformemente distribuídos, y, en general causan asentamientos diferenciales en las estructuras, los cuales, en algunos casos, pueden llegar a clasificarse como daños mayores. Daños severos de grandes estructuras en Skopje durante el temblor de 1963, fueron atribuidos a los asentamientos diferenciales causados por la densificación de lentes de arena suelta bajo las cimentaciones (Seed y Silver, 1972).

Los asentamientos de edificios cimentados sobre arena seca, considerando la acción de cargas estáticas, se estima empíricamente y generalmente, se pone poca atención a los posibles asentamientos debidos a los movimientos del terreno inducidos por sismos.

Se han propuesto dos procedimientos semi-empíricos para estimar los asentamientos provocados por temblores. Uno de éstos propuesto por Seed y Silver (1972) permite estimar el asentamiento de arenas secas, Pyke et al (1974) ampliaron el método para tomar en cuenta movimientos multi-direccionales. Lee y Albaisa (1974) propusieron un método aplicable a arenas saturadas.

El procedimiento de Seed y Silver (1972) para estimar el asentamiento de un estrato de arena debido a carga sísmica, consiste de los siguientes pasos:

a) Calcular la historia de deformaciones de cortante en varias capas del estrato, usando un método de análisis dinámico lineal.

b) Convertir la historia de deformaciones de cortante de cada capa a un número equivalente de ciclos de deformación cortante de amplitud constante.

c) Aplicar el número de ciclos de deformación cortante, determinado en (b) a muestras de arena ensayadas bajo condiciones de corte simple y determinar las deformaciones volumétricas y a partir de éstas conocer las deformaciones verticales resultantes.

d) Repetir el procedimiento de (c) para cada capa del estrato e integrar las deformaciones verticales para obtener el asentamiento total.

El paso (b) involucra una aproximación. Martin et al (1975) ha demostrado que el efecto de una historia irregular de deformaciones de cortante depende no únicamente de la magnitud de los pulsos en el registro, como también del orden en que ellos son aplicados. El procedimiento para determinar el número equivalente de ciclos no toma en cuenta el hecho antes mencionado.

Al expresar analíticamente la relación entre deformaciones de cortante y los cambios de volumen, se pueden eliminar los pasos b, c y d como sucede con el método de Martin et al (1975), el cual es aplicable al cálculo de asentamientos de estratos de arena seca o parcialmente saturada.

A.4. PERDIDA DE RESISTENCIA DE SUELOS GRANULARES→LICUACION DE ARENAS

Probablemente uno de los efectos más costosos y espectaculares que se puedan encontrar en ingeniería sísmica se deban al fenómeno de la licuación de arenas.

El fenómeno es complejo y aún no es claro y completamente comprendido, al grado que es posible encontrar interpretaciones diferentes y aún contradictorias de los hechos experimentales existentes.

La discrepancia empieza con la propia definición del término licuación. Mientras que para Seed (1966) el término "*licuación inicial*" es la condición de una muestra de arena en la cual la presión de poro inducida por la aplicación de carga cíclica alcanza el valor de la presión de confinamiento y el término "*licuación total*" es la condición correspondiente para que la muestra alcance una amplitud de deformación del 20%; Casagrande en 1969, utiliza los términos licuación y movilidad cíclica que después modifica (Casagrande, 1976) definiendo por "*licuación real*" a la respuesta de una muestra de arena suelta y saturada cuando se le somete a deformaciones o impactos que dan como resultado una pérdida sustancial de resistencia y en casos extremos a flujo de taludes, y por "*licuación cíclica*" la respuesta de un espécimen dilatante de arena cuando se le ensaya en cámara triaxial cíclica y la presión de poro se eleva en forma incremental hasta igualar la presión de confinamiento.

En este trabajo entenderemos por *"licuación de arenas"* al fenómeno mediante el cual una muestra de arena saturada pierde una gran parte de su resistencia al esfuerzo cortante (debido a carga monotónica o cíclica) y fluye o se comporta como un líquido hasta que los esfuerzos cortantes actuantes en la masa de suelo disminuyen a valores compatibles con la resistencia del suelo licuado, el movimiento se detiene, y el suelo recupera su resistencia y estabilidad.

Por tanto, un talud que se licúa llega a estabilizarse, cuando la pendiente se ha reducido a pocos grados.

A.4.1 DESCRIPCION DEL FENOMENO

El fenómeno de licuación de arenas es causado por el desarrollo de grandes presiones en el agua que ocupa los poros del suelo. Estas grandes presiones de poro son inducidas cuando se aplican a la masa de suelo esfuerzos o deformaciones de cortante, en condiciones tales que no se permite su disipación inmediata, es decir prácticamente a volumen constante. La forma de aplicación de los esfuerzos cortantes puede ser monotónica, cíclica o transitoria.

A.4.2 FACTORES QUE INFLUYEN EN LA OCURRENCIA DE LICUACION

Los factores más importantes que influyen en la ocurrencia de licuación son:

a) Tipo de suelo

Los suelos uniformemente graduados son más susceptibles de sufrir licuación que los suelos bien graduados; dentro de los primeros, las arenas finas se licúan más fácilmente que las gravas o suelos arcillosos aluviales. En el temblor de Alaska se observó que las estructuras de puentes cimentadas sobre arena sufrieron grandes desplazamientos, mientras que las cimentadas en grava no tuvieron daños.

En la fig 9 se muestran las envolventes de las curvas granulométricas de los suelos que se han licuado.

b) Compacidad relativa (C_r) o relación de vacíos (e)

Un depósito de arena suelta es más susceptible de sufrir licuación que un depósito de arena densa.

En el temblor de Niigata hubo licuación en zonas cuya C_r era del orden del 50 por ciento, o menor, en tanto que en las zonas con una $C_r > 70$ por ciento no se presentó ningún daño.

En la fig 10 se ilustra el concepto de compacidad relativa.

c) Esfuerzo confinante inicial

La susceptibilidad de licuación disminuye al aumentar el esfuerzo confinante. Ensayes de laboratorio han mostrado que para una relación de vacíos inicial, el esfuerzo cortante requerido para comenzar la licuación bajo condiciones de carga repetida, se incrementa con el aumento de la presión de confinamiento.

d) Magnitud del esfuerzo repetido

Cualquier depósito con una relación de vacíos mayor que su $e_{mín}$ es susceptible de sufrir pérdida parcial o total de resistencia, si la excitación es de intensidad suficiente.

Evidencias de campo demuestran que depósitos de arena suelta han resistido sismos de poca intensidad (0.005 g) y se han licuado ante la acción de sismos intensos (0.16 g), (Seed e Idriss, 1971).

La resistencia a la licuación decrece al aumentar la magnitud del esfuerzo.

e) Número de ciclos de esfuerzo

Todos los estudios de laboratorio indican que en una muestra sujeta a carga repetida, con un nivel de esfuerzo o deformación prescrito, el inicio de la licuación dependerá de la aplicación de un número requerido de ciclos de esfuerzo.

Esto se confirmó en Anchorage, durante el temblor de 1964, ya que los deslizamientos ocurrieron después de 90 seg de iniciado el movimiento.

Recientes investigaciones (1973 a la fecha) han aportado nuevos datos de los factores que influyen en el fenómeno de licuación de arenas, como son:

f) Estructura

Pyke (1974), Ladd (1974 y 1976) y Mulilis et al (1975), han encontrado que el método de preparación de la muestra (estructura)

afecta la relación de esfuerzos $(\frac{\sigma_{dc}}{2\sigma_3})$ que provoca la licuación hasta en un 200% .

g) Lapso de esfuerzo sostenido

Experiencias de laboratorio indican que muestras idénticas sometidas a cargas sostenidas por períodos que variaron de 0.1 a 100 días antes del ensaye, se vieron afectadas en la relación de esfuerzos hasta en un 25%. Estos resultados permiten suponer que el efecto de la edad del depósito es un factor importante. Debido a la enorme diferencia de escalas de tiempo entre laboratorio y campo se puede suponer una mayor diferencia que la del 25% mencionada arriba.

h) Historia previa de deformaciones

Este importante factor fue señalado por Finn et al en 1970, demostrando que las características de licuación de las arenas son influenciadas por la historia previa de deformaciones, él concluyó:

> *"La dependencia de la resistencia a la licuación para una arena con la historia de deformaciones conduce a la conclusión de que la resistencia de un depósito no puede ser determinada en una forma confiable mediante el ensaye de muestras formadas en el laboratorio aún y cuando se tenga la misma relación de vacíos que el depósito. Parece que la resistencia a la licuación sólo puede ser confiablemente determinada en muestras inalteradas"*

Seed et al (1975) realizaron experimentos en los cuales muestras de arena se sometieron a unas cuantas sacudidas de pequeña intensidad, los resultados indicaron que el efecto de la historia sísmica es incrementar considerablemente la resistencia a la licuación. En otras palabras para un número de ciclos las muestras de arena sometidas a sacudidas que inducen esfuerzos o deformaciones de bajo nivel requieren una relación de esfuerzos para provocar la licuación 45% mayor que aquellas muestras que no tenían historia previa (ver fig 11).

Debe de notarse que las características señaladas por los últimos tres factores se alteran durante el muestreo y que por lo tanto, el ensaye de muestras "*inalteradas*" no reflejará claramente su influencia.

A.4.3 TRABAJOS EXPERIMENTALES

Desde el punto de vista experimental, el fenómeno de licuación ha sido estudiado por varios investigadores utilizando diversos aparatos (triaxial, triaxial cíclica, corte simple cíclico, torsión cíclica y mesa vibradora).

El concepto de relación de vacíos crítica

La evidencia experimental ha demostrado que las arenas "*sueltas*" disminuyen su volumen bajo la acción de esfuerzos cortantes y que, por el contrario las arenas "*densas*" lo aumentan.

Tomando en cuenta lo anterior, A. Casagrande llegó a la conclusión de que el decremento de volumen de una arena suelta y el incremento de volumen de una arena densa tenderían a la misma relación de vacíos, en la cual la arena puede deformarse sin cambio de volumen, a la cual denominó "relación de vacíos crítica".

Dibujando los resultados de varios ensayes se obtiene una curva de relación de vacíos crítica, esta curva que divide el comportamiento dilatante (bajo la curva) y contractivo (arriba de la curva), Casagrande la propuso como una medida para investigar la susceptibilidad de licuación de una arena.

Posteriormente Casagrande al analizar la falla de la presa de Fort Peck se dio cuenta que la curva de relación de vacíos crítica no dividía realmente el comportamiento contractivo y dilatante de las arenas.

Castro (1969) modificó el concepto de relación de vacíos crítica y obtuvo, a partir de resultados de pruebas triaxiales consolidadas-no drenadas con medición de presión de poro (pruebas $\overline{cu}$), la curva de estado crítico. En la fig 12 se muestran las líneas e_f de estado crítico para varias arenas.

Ensaye triaxial cíclica

Seed y Lee (1966) fueron los primeros en utilizar cámara triaxial cíclica, con objeto de reproducir la condición de esfuerzos a que se haya sujeto un elemento de suelo durante un tem-

blor (atribuyendo el estado de deformaciones del suelo a la propagación de ondas de cortante).

Para un depósito de suelo con superficie horizontal, antes del temblor, el estado de esfuerzos puede ser idealizado como se muestra en la fig 13.a . Durante el sismo los esfuerzos cortantes generados superpuestos a los esfuerzos normales se muestran en la fig 13.b .

La cámara triaxial cíclica trata de simular las condiciones idealizadas descritas. Un espécimen saturado de forma cilíndrica se consolida a un esfuerzo $\bar{\sigma}_c$ y posteriormente con el drenaje cerrado se somete a un esfuerzo axial cíclico de magnitud $\pm \Delta\sigma_a$ (fig 14), este procedimiento proporciona esfuerzos cortantes cíclicos τ_{hv} en un plano a 45°.

Son varias las limitaciones de la cámara triaxial cíclica y éstas se mencionan en la literatura, siendo una de las principales la falta de entendimiento de la condición de campo que representa.

El comportamiento de las muestras de arena suelta, sometidas al ensaye con cámara triaxial cíclica, se caracteriza por un aumento gradual de la presión de poro sin que haya deformación axial apreciable, hasta que se produce el incremento que eleva la presión de poro hasta el valor de la presión confinante, momento a partir del cual la muestra se deforma súbitamente más del 20%. Las arenas en estado compacto exhiben un comportamiento similar al de las arenas sueltas, pero al llegar a la

"*Licuación inicial*" no se presenta una deformación grande en forma súbita, sino que la deformación se incrementa gradualmente.

Según el concepto de Seed y Lee (1966), cualquier espécimen de arena es susceptible de licuarse no importando su compacidad relativa. Los parámetros más importantes según estos investigadores son: el número de ciclos de esfuerzo $(Na)_\ell$ para alcanzar la condición $u = \bar{\sigma}_3$, la relación entre el esfuerzo cortante máximo y el esfuerzo confinante, $(\frac{\sigma_a}{2\bar{\sigma}_c})$ y la relación de vacíos.

Castro (1969) al realizar sus ensayes en cámara triaxial cíclica observó que durante la prueba se desarrollan heterogeneidades en las muestras, de manera especial en la zona superior. Atribuye a estas heterogeneidades, inducidas por el ensaye, el que especímenes densos alcancen la condición $u = \bar{\sigma}_3$

Ensaye de corte simple cíclico

La prueba de corte simple cíclico se desarrolló con la idea de conseguir mayor aproximación a las condiciones de campo que la lograda con cámara triaxial.

Uno de los primeros aparatos de corte simple fue el desarrollado por *Swedish and Norwegian Geotechnical Institutes* (Kjellman, 1951). Sin embargo, este aparato tenía el inconveniente de utilizar muestras cilíndricas (los esfuerzos cortantes en una sección horizontal no pueden ser uniformes).

En la Universidad de California, en Berkeley, Peacock y Seed (1968) desarrollaron un aparato de corte simple, que utilizaron para examinar la tendencia a licuarse de una muestra de arena sometida a este tipo de esfuerzo. También en la Universidad de British Columbia, Pickering y Finn (1969), Finn et al (1970 y 1971) han utilizado corte cíclico simple para el estudio de licuación.

En la figura 15 se ilustran los resultados obtenidos por Peacock y Seed.

Ensaye de Mesa Vibradora

Este tipo de ensayes generalmente consiste en colocar un recipiente o caja con arena saturada, sobre una mesa vibradora y medir la aceleración de la emsa a la cual ocurre la licuación.

Whitman (1970) menciona los factores que afectan los resultados y su influencia en la interpretación de los mismos:

1. Frecuencia de vibración
2. Duración de vibración
3. Tamaño y geometría del recipiente
4. Características de deformación del recipiente
5. Método de colocación de la muestra
6. Control del drenaje
7. Aparatos de medición de deformaciones
8. Presión confinante

Finn, Emery y Gupta (1971) mencionan las ventajas de usar grandes muestras y mesa vibradora.

Tal vez la principal objeción al uso de recipientes rígidos sobre mesa vibradora es que no representan las condiciones de campo.

Con objeto de superar esta dificultad Díaz, Weckmann e Iturbe (1973) proponen combinar la utilidad de las condiciones de corte simple y la ventaja de utilizar muestras grandes (30 x 60 x 90 cm) en un recipiente de paredes móviles para ensayar arena saturada en mesa vibradora.

METODOS PARA EVALUAR LA SUSCEPTIBILIDAD A LA LICUACION DE LOS SUELOS

En relación a la predicción de la susceptibilidad a la licuación de depósitos de suelos granulares saturados una considerable cantidad de investigación se ha dirigido hacia el desarrollo de mejores métodos de predicción y técnicas de ensaye.

Los métodos se pueden clasificar en tres categorías:

1. Métodos empíricos, basados en la comparación de las condiciones de los sitios en donde ocurrió o no licuación con las condiciones del sitio que se desea analizar.

   Dentro de esta categoría se clasifican los siguientes cuatro métodos:

Criterio del WES (Waterways Experimental Station)

Este criterio fue desarrollado para analizar la estabilidad de terraplenes a lo largo del Río Mississipi, en el que se produ-

cen flujos de material producidos por el incremento de la presión de poro originada por los cambios del nivel del río.

Criterio de Florin e Ivanov

Este criterio desarrollado en Rusia, en 1973, permite estimar la susceptibilidad a la licuación de suelos por medio de pruebas de campo. Se investigan los 10 m superiores de suelo haciendo explotar sucesivamente tres cargas de dinamita de 5 Kg. colocadas a una profundidad media de 4.5 m y determinando después de cada explosión, el asentamiento promedio de la superficie dentro de un radio de 4.5 m. La cantidad y profundidad a la que se coloca el explosivo se eligen de forma que no haya expulsión de suelo durante la explosión. Si el asentamiento promedio es menor de 8 a 10 cm y la relación de asentamientos entre explosiones sucesivas es menor que 0.6 se puede afirmar que ese suelo no es susceptible a licuación.

Criterio de Kishida

Este criterio está basado en el análisis de las condiciones del suelo de 3 sitios en los que ocurrió licuación, (Kishida, 1969). Bajo sismos de igual magnitud, puede ocurrir licuación si el nivel freático está cerca de la superficie, si las características granulométricas satisfacen las relaciones:

$$2mm > D_{50} > .074 \text{ mm}; \quad C_u < 10 \text{ y}$$

además si se cumplen las siguientes condiciones:

- El espesor del estrato de suelo no licuable, arriba del estrato, licuable es menor que 8 m.
- La relación de los espesores del estrato no licuable al

licuable es menor que 1.

Kishida también concluye que los suelos no son susceptibles a la licuación si:

- La presión efectiva de confinamiento es superior a 2 Kg/cm^2 o,
- La compacidad relativa es superior a 75%.

Criterio de Oshaki

Este criterio (Oshaki, 1969) establece que los suelos con nivel freático cercano a la superficie pueden licuarse si se presentan las siguientes características granulométricas:

$$2mm > D_{60} > 0.2\ mm;\ D_{10} < 0.1\ mm$$

Adicionalmente, establece que estos suelos tendrán poca probabilidad de licuarse si el número de golpes N_{sp} en prueba de penetración estándar es mayor que 2z, en que z es la profundidad en metro.

2. Métodos simplificados. Consisten básicamente en comparar la resistencia obtenida en pruebas de laboratorio, con los esfuerzos que provocará el sismo, calculados en forma simplificada.

   En esta categoría se clasifican los métodos propuestos por Seel e Idriss (1970) y por Casagrande (1976).

Método de Seed e Idriss

Este método consiste en comparar los esfuerzos inducidos por

el sismo en los estratos licuables con los que puede resistir el suelo sin que ocurra licuación. Para determinar los esfuerzos inducidos in situ, debe contarse con el acelerograma del sismo de diseño, la estratigrafía y las propiedades índice y mecánicas de los suelos. Seed e Idriss proponen un procedimiento simplificado para estimar la magnitud de los esfuerzos que origina el sismo. La magnitud de los esfuerzos que pueden provocar licuación en el suelo se obtiene a partir de pruebas de laboratorio, tanto triaxiales como de corte simple, con esfuerzos repetidos o bien se estima con gráficas de diseño obtenidas por Seed e Idriss. La comparación de los esfuerzos inducidos por el sismo con los que provocan licuación del suelo permite juzgar la susceptibilidad de un suelo a sufrir este fenómeno.

El esfuerzo cortante máximo ($\tau_{máx}$) a una profundidad z, conocida la aceleración máxima ($a_{máx}$) en la superficie del terreno, y suponiendo que la masa de suelo se comporta como un cuerpo rígido, se calcula mediante la expresión:

$$\tau_{máx} = \frac{\gamma z}{g} a_{máx}$$

$a_{máx}$ aceleración máxima en la superficie del terreno

γz presión vertical total a la profundidad z

g aceleración de la gravedad

$\tau_{máx}$ esfuerzo cortante máximo a la profundidad z

Como el terreno es deformable, en general se tendrá que:

$$\tau_{máx} = \frac{\gamma z}{g} \; a_{máx} \; r_d$$

siendo r_d un factor de corrección, menor que 1.

El análisis de varios sismos en sitios que presentan un estrato de arena en los 15 m superiores ha mostrado que r_d cae dentro del intervalo de valores de la fig. 16.

Seed e Idriss proponen calcular el esfuerzo cortante promedio τ_p que, para un número determinado de ciclos, produce el mismo efecto que el sismo con la expresión:

$$\tau_p = 0.65 \; \frac{\gamma z}{g} \; a_{máx} \; r_d$$

Por su parte, el número de ciclos significativos en el comportamiento del material dependerá de la duración del sismo. Para fines prácticos se puede usar la siguiente tabla:

Magnitud del sismo	N° de ciclos significativos, N
7	10
7 1/2	20
8	30

Previamente a la realización de pruebas de laboratorio, es preciso conocer la compacidad relativa del material in-situ. Para ello se utilizan los resultados de las investigaciones hechas por Holtz y Gibbs. En la fig 17 se presenta una gráfica modificada por Seed e Idriss (19) que permite conocer la compacidad relativa.

Los esfuerzos que provocarán la licuación en un suelo a una compacidad relativa dada, se pueden deducir en forma aproximada de los experimentos llevados a cabo por diversos investigadores, tanto en cámaras triaxiales como en aparatos de corte simple. A partir de pruebas en cámaras triaxiales se han obtenido gráficas que permiten estimar si ocurrirá licuación en un suelo sometido a un determinado número de ciclos (10 o 30 usualmente) para una relación de esfuerzos $(\frac{\sigma_{dc}}{2\sigma_c})$ dada y determinado tamaño de las partículas (representado por el D_{50}). En las figs 18 y 19 se presentan estas gráficas para una compacidad relativa de 50%.

Para determinar la relación de esfuerzos correspondiente a otra compacidad relativa se usa el hecho experimental de que la relación de esfuerzos $(\frac{\sigma_{dc}}{2\sigma_c})$ es aproximadamente proporcional a la compacidad relativa (fig 18 y 19). En las mismas figuras, se observa que el material menos resistente corresponde a un $D_{50} = 0.074$ mm.

Tomando en cuenta que el esfuerzo más significativo, en la licuación de un suelo bajo la acción de un temblor, es el esfuerzo cortante actuante en el plano horizontal; la prueba de corte simple es la que mejor asemeja las condiciones de deformación in-situ. Es por tanto importante correlacionar los resultados anteriores, obtenidos en cámaras triaxiales, con los obtenidos en pruebas de corte. Las investigaciones llevadas a cabo por Seed e Idriss, permitieron concluir que, para fines prácticos:

$$(\frac{\tau_{xy}}{\sigma_y}) \text{ corte simple} \quad C_o(\frac{\sigma_{dc}}{2\sigma_c}) \text{ triaxial}$$

en que C_o depende de la compacidad relativa (fig 20).

Comparando los esfuerzos producidos en el terreno por un temblor y los esfuerzos que el material es capaz de soportar, es posible determinar si el suelo presentará o no el fenómeno de licuación, para las condiciones particulares supuestas.

Seed e Idriss presentan un procedimiento simplificado que permite aplicar el método anterior en forma expedita mediante gráficas de penetración estándar contra la profundidad, elaboradas para 2 profundidades típicas del nivel freático y para 2 aceleraciones máximas del terreno (figs 21 y 22). En estas gráficas se delimitan tres zonas: una, en la cual no habrá licuación; otra, en la que podría o no presentarse licuación dependiendo de las características granulométricas del material y de la magnitud del temblor; y la tercera en la cual es muy probable que el material se licúe. Las fronteras entre las zonas anteriores se determinaron para una compacidad relativa de 50% y corresponden a condiciones extremas en cuanto al número de ciclos significativos producidos por un temblor y a la granulometría del material. La frontera a la izquierda de la cual se concluye que habrá licuación fue obtenida usando el mínimo número de ciclos razonable (N_{sp} = 10) combinado con la granulometría del material menos susceptible a la licuación (D_{50} = 2 mm); la frontera a la derecha de la cual se dice no habrá licuación se obtuvo combinando el máximo número de ciclos razonable (N_{sp} = 30) con

la granulometría del material más susceptible (D_{50} = .074 mm).

Método de Casagrande

En esencia el procedimiento consta de los siguientes pasos:

1. Se ejecutan pruebas triaxiales con aplicación de carga monotónica (o cíclica, dependiendo de la compacidad relativa de la arena), en muestras inalteradas labradas de bloques obtenidos manualmente, y se determina su respuesta.. De preferencia las pruebas deben ejecutarse en un equipo que disponga de extremos lubricados y los especímenes deben estar consolidados con una relación de esfuerzos principales de 2.
2. Se determina la línea de estado crítico, línea e_f, si es que los resultados de las pruebas lo permiten.
3. A partir de pruebas de compresión unidimensional, se estiman las combinaciones de esfuerzos efectivos y compacidad relativa (relación de vacíos) susceptibles de desarrollarse en el campo.
4. Se compara la posición de los puntos estimados en el paso anterior con la posición de la línea e_f. Los puntos situados arriba y a la derecha de la línea e_f son susceptibles de experimentar licuación. Puntos situados a la izquierda de y sobre la línea e_f, no son susceptibles de experimentar licuación
5. En suelos no susceptibles de experimentar licuación por su posición en relación con la línea e_f, es posible estimar el incremento de presión de poro inducido por la aplicación de

cargas cíclicas para un cierto número de ciclos. A. Casagrande estima que el número de ciclos necesario para inducir presiones de poro superiores al 50% de la presión de confinamiento in situ, es superior a cuatro veces el número de ciclos observados en el laboratorio (valor a partir del cual la influencia del fenómeno de movilidad cíclica en los resultados, es muy importante).

6. Si se requiere una estimación de las deformaciones inducidas por carga cíclica en el campo, es necesario ejecutar mediciones precisas de las deformaciones en el laboratorio, hasta que la presión de poro alcance el 50% de la presión de confinamiento, y utilizar estas mediciones como una guía de las posibles deformaciones in situ, teniendo en cuenta que solo una fracción de las deformaciones medidas en el laboratorio son causadas por el mecanismo que controla el desarrollo de presiones de poro y deformaciones en el campo.

3. Métodos de análisis basados en el cálculo de la respuesta del terreno. Un número creciente de modelos numericos para análisis de la respuesta dinamica de suelos granulares sujetos a cargas sísmicas se encuentran actualmente (1980) en uso.

Los modelos difieren entre sí en:

a) Las hipótesis de partida

b) la representación de las relaciones esfuerzo-deformación

c) la generación de la presión poro

d) los métodos para integrar las ecuaciones de movimiento.

Modelos desarrollados en la Universidad de California, Berkeley

Los modelos desarrollados en la Universidad de California, tiene las características principales:

1) Establece las ecuaciones de movimiento en función de esfuerzos totales .
2) Consideran el problema de desplazamientos pequeños.
3) El comportamiento no-lineal de los suelos se trata ya sea mediante un procedimiento lineal equivalente o mediante un criterio tipo Masing, que puede ser un Ramberg- Osgood o un Martín-Davidenkov.
4) La generación de la presión de poro se calcula a partir de resultados de pruebas triaxiales cíclicas consolidadas-no drenadas (Lee y Albaese, 1974), cuyas variables son:
   - σ'_o , *esfuerzo de consolidación*
   - σ_{dp} , *esfuerzo desviador cíclico*
   - $(u_g)_N$, *presión de poro generada para N ciclos*
   - N_ℓ , *número de ciclos para provocar la licuación*

   Al representar las relaciones N/N_ℓ vs $\frac{u_g}{\sigma'_o}$ se obtiene una franja angosta de forma peculiar que se representa mediante

$$\frac{N}{N_\ell} = \left| \frac{1}{2}\left(1 - \cos \frac{u_g}{\sigma'_o}\right) \right|^\alpha$$

   α es un parámetro que depende del tipo de arena y de las condiciones de prueba. Al aplicar la expresión para una historia irregular de ciclos de esfuerzos es necesario transformar dicha historia en un número de ciclos equivalentes, de amplitud constante, según el criterio descrito

por Seed et al 1975.

5) Las ecuaciones de movimiento se integran con el método del elemento finito ya sea con el criterio del método lineal equivalente o bien en forma incremental. La integración respecto al tiempo se lleva a cabo mediante un esquema que utilice el dominio de la frecuencia; o bien uno directo, paso a paso en el dominio del tiempo.

6) El amortiguamiento considerado es el lineal equivalente (Seed e Idriss, 1970) o bien el que resulta de considerar un modelo histerético.

7) La disipación de la presión de poro se calcula con base en la generación de la presión de poro conocida y la Teoría de Consolidación Unidimensional.

8) Para problemas bidimensionales la respuesta dinámica se cuantifica con el método lineal equivalente, mientras que para los problemas no lineales incrementales se considera únicamente el caso unidimensional.

El método exhibe las características de la respuesta dinámica elástica, como la de que el sistema regrese a su posición de equilibrio y no se tengan distorsiones angulares permanentes al cesar la excitación.

La solución exhibe marcados efectos de resonancia cuando el período predominante del acelerograma corresponde con el período fundamental del depósito.

Modelo desarrollado en la Universidad de Michigan, Ann Arbor

Wilie y Streeter (1976) y Liou et al (1977) describen el procedimiento seguido para el desarrollo del modelo en cuestión, cuyas características principales son:

1) Las ecuaciones de movimiento se establecen en función de los esfuerzos efectivos.

2) Considera el problema de desplazamientos pequeños.

3) Utiliza como ecuación constitutiva para el esqueleto un modelo Ramberg-Osgood modificado con ablandamiento por deformación, de la forma siguiente:

$$\gamma = \frac{\tau}{G_o(\bar{\sigma}_z)} \left[1 + \alpha \left| \frac{\tau}{C_1 \tau_m(\bar{\sigma}_z)} \right|^{R-1} \right] \qquad (2.12)$$

donde

τ *es el esfuerzo cortante*

γ *la deformación angular y*

$\bar{\sigma}_z$ *el esfuerzo vertical efectivo*

Los valores de G_o y τ_m corresponden al módulo de rigidez al cortante para deformaciones infinitesimales y al esfuerzo cortante asociado, respectivamente y se calculan de acuerdo con la ref 23, para el problema unidimensional. Los parámetros del modelo de Ramberg-Osgood en cuestión son α, C_1 y R. Para definir las trayectorias de carga y descarga se utiliza el criterio de Masing (ref 26).

4) La generación de presión de poro se considera al acoplar el movimiento del agua. El acoplamiento se efectúa al considerar

el flujo vertical del agua y utilizar la ley de Darcy.

5) Las ecuaciones de movimiento se establecen en forma de ecuaciones de ondas de cortante y de compresión. La solución de las ecuaciones de movimiento se obtienen con el método de las características y el acoplamiento de las ecuaciones se establece en el proceso de solución.

6) La disipación de la presión de poro se considera en forma implícita al modelar el movimiento del agua.

7) El amortiguamiento implícito en el modelo es el histerético y el provocado por el movimiento del agua.

8) El modelo es unidimensional.

Modelo desarrollado en la Universidad de British Columbia, Vancouver

Este modelo tienen las siguientes características:

1) Establece las ecuaciones de movimiento en función de esfuerzos efectivos.

2) Considera el problema de desplazamientos pequeños.

3) La curva esfuerzo-deformación para el esqueleto es del tipo hiperbólico.

$$\tau = G_{mo}\,\gamma/(1 + G_{mo}\,\gamma/\tau_{mo})$$

donde

G_{mo} es el módulo tangente inicial máximo, y

τ_{mo} es el esfuerzo cortante máximo sin provocar la falla

G_{mo} y τ_{mo} se determina según Harden y Drnevich (1972).

Las trayectorias de descarga y recarga se describen mediante el criterio tipo Masing (Pyke, 1979)

$$\frac{\tau-\tau_r}{2} = \frac{G_{mn}\,(\gamma-\gamma_r)}{2} \Big/ \left\{ 1 + \frac{G_{mn}\,|(\gamma-\gamma_r)|}{2\tau_{mn}} \right\}$$

donde

γ_r y τ_r son la deformación cortante y esfuerzo cortante del punto donde ocurre la inversión de esfuerzo

G_{mn} y τ_{mn} son el módulo al cortante y el efuerzo cortante respectivamente para el civlo N, expresados por:

$$G_{mn} = G_{mo}\left[1 + \frac{\varepsilon_{vd}}{H_1 + H_2\,\varepsilon_{vd}}\right] \left(\frac{\sigma'_v}{\sigma'_{vo}}\right) 1/2$$

$$\tau_{mn} = \tau_{mo}\left[1 + \frac{\varepsilon_{vd}}{H_3 + H_4\,\varepsilon_{vd}}\right] \left(\frac{\sigma'_v}{\sigma_{vo}}\right)\ 1/2$$

donde

ε_{vd} es la deformación volumética acumulada

H_1, H_2, H_3 y H_4 son constantes experimentales

σ'_v y σ'_{vo} son los esfuerzos verticales efectivos en el ciclo N e inicial respectivamente

4) La generación de la presión de poro se calcula mediante el cambio de volumen acumulado, obtenido experimentalmente. La expresión del incremento del cambio de volumen es:

$$\Delta\varepsilon_{vd} = C_1\,(\gamma - C_2\,\varepsilon_{vd}) + \frac{C_3\,\varepsilon_{vd}^2}{\gamma + C_4\,\varepsilon_{vd}}$$

C_1, C_2, C_3 y C_4 son constantes experimentales que toman en cuenta el tipo de arena y la compacidad relativa.
En condiciones no-drenadas y completa saturación, el incremento de la presión de poro durante cada intervalo de tiempo de integración se calcula mediante

$$\Delta u = \overline{E}_r \, \Delta \varepsilon_{vd}$$

donde

$\overline{E}_r$ es el módulo de recuperación elástica unidemensional

5) Las ecuaciones de movimiento se resuelven con el método de diferencias finitas y la integración se lleva a cabo con el método beta de Newmark.
6) Además del amortiguamiento histerético, se puede incluir amortiguamiento viscoso, de acuerdo con el criterio de Rayleigh.
7) La disipación de la presión de poro se calcula con base en la Teoría de la Consolidación Unidimensional.
8) El modelo es unidimensional y las ecuaciones de movimiento y las de disipación de la presión de poro se integran en forma independiente.

El modelo permite realizar análisis para tres condiciones diferentes de drenaje.

a) no permitiendo redistribución de la presión de poro
b) permitiendo redistribución pero no permitiendo disipación de la presión de poro
c) permitiendo disipasión

Los resultados obtenidos muestran claramente la influencia de las condiciones de drenaje sobre el desarrollo de la presión de poro.

El método permite calcular:

a. la historia de aceleraciones ($\ddot{x}$), deformaciones de cortante (γ) y los esfuerzos cortantes (τ) en cada capa.

b) El desarrollo de la presión de poro (u).

c) El inicio de la licuación

Para conocer las características de otros modelos se puede consultar el artículo de Porras, Díaz y Cervantes (1979).

PROCEDIMIENTOS PARA ESTABILIZAR DEPOSITOS DE ARENA SUSCEPTIBLES DE LICUARSE

En lo anteriormente tratado se bosquejaron los métodos para conocer si un depósito de arena es o no susceptible de experimentar licuación.
Conociendo que el fenómeno se puede presentar, el siguiente paso será tratar de evitar su ocurrencia. De acerdo con los factores que afectan el fenómeno se ocurre dos precodimientos:

1. Aumentar la compacidad relativa (C_r) → DENSIFICACION

2. Facilitar la disipación de la presión de poro → DRENAR

Dentro del primer grupo se pueden presentar varias alternativas para densificar el depósito hasta la profundidad que indique los cálculos (como mínimo):

VIBROFLOTACION

El principio de la densificación de depósitos de arena suelta mediante vibroflotación fue aplicado primeramente en Rusia, después en Alemania y en 1939 fue introducido en los Estados Unidos de Norteamérica.
La vibroflotación es una técnica que consiste en la aplicación simultánea de flujo de agua a presión y vibración.
El equipo consiste de: un vibroflot, una grúa, un sistema de bombeo, una fuente de potencia y un cargador frontal.
Las dimensiones aproximadas del vibraflot (componente principal del sistema) son:

diámetro ≈ 15"
longitud ≈ 6'
peso ≈ 2 ton
fuerza centrífuga horizontal ≈ 10 ton

El sistema de bombeo requiere entregar un gasto de ≈ 80gpm a una presión de 80psi. La velocidad aproximada de densificación es de 30 cm/min, el área de influencia tiene un radio de 2.7m.
El proceso de vibroflotación es ilustrado en la fig

PILOTES DE COMPACTACION

Los pilotes de compactación son hincados con el propósito de densificar arenas sueltas mediante dos efectos:

a. Desplazamiento de material de un volumen igual al del pilote
b. vibración debida al hincado

En este procedimiento generalmente se usan tubos metálicos llenos de material granular compacto que tienen una etapa falsa en la punta que permite su extracción una vez que se alcanza la profundidad deseada.
El efecto de la densificación se extiende de 3 a 4 diámetros, lateralmente y de 2 a 3 diámetros en la punta.
En el segundo grupo el objetivo es facilitar la disipación de la presión de poro generada mediante un sistema de drenaje eficiente.

DRENES VERTICALES DE GRAVA

Como se dijo anteriormente, si la presión de poro generada por carga cíclica puede ser disipada, tan rápidamente como es generada, entonces el peligro de licuación puede ser evitado.
Por tanto, un procedimiento para estabilizar un depósito susceptible de licuarse es instalar un sistema de drenes de grava como el mostrado en la fig
El diseño y análisis de tal sistema se puede hacer mediante alguno de los programas de computadora que hay para tal efecto como por

ejemplo, el LARF (*liquefaction analysis for radial flow*) desarrollado por Seed y Booker (1976).

REFERENCIAS

Ambraseys, N.N., 1970
"Factors controlling the earthquake response of foundation materials", Proc. Third European Symp. Earthq. Engrg., Sofia, Bulgaria, pp 309-323

Ambraseys, N.N., 1973.
"Dynamics and response of foundation materials in epicentral regions of strong earthquakes", Proc. Fifth World Conf. Earthq. Engrg., Rome, Italy, pp CXXVI-CXLVIII

Ambraseys, N.N., and Sarma, S., 1969
"Liquefaction of soils induced by earthquakes", Bull. Seism. Soc. Am., 59:651-664

Barkan, D.D., 1962
"Dynamics of Bases and Foundations", McGraw-Hill, New York, pp 434

Bazaraa, A., 1967
"Use of the standard penetration test for estimating settlements of shallow foundations on sand", Doctoral thesis, Dept. of Civil Engrg., University of Illinois, Urbana, Illinois

Broms, B. B. and Forssblad, L., 1969
"Vibratory compaction of cohesionless soils", Proc. Specialty Session No. 2, Seventh Interntl. Conf. Soil Mech. Found. Engrg., Mexico City, pp 101-118

Casagrande, A., 1936
"Characteristics of cohesionless soils affecting the stability of slopes and earth fills", J. of the Boston Society of Civil Engineers, January, pp 257-276

Casagrande, A., 1938
"The Shearing Resistance of Soils and its Relation to the Stability of Earth Dams", Proc. Soils and Foundation Conference of the U.S. Engineer Department, Boston, Mass.

Casagrande, A. and Shannon, W.L., 1948
"Stress-deformation and strength characteristics of soils under dynamic loads", Proc. Second Interntl. Conf. Soil Mech., Rotterdam, Holland, V, pp 29-34

Casagrande, A., 1965
"Role of the Calculated Risk in Earthwork and Foundation Engineering", Journal of the Soil Mechanics and Foundation Engineering Division, ASCE

Casagrande, A. y Rendón, F., 1976
"Reciprocating and Gyratory Shear Apparatus-Design, Testing Procedures and Tests on Saturated Sand", Report to Waterways Experimental Station, Vicksburg, Miss.

Casagrande, A., 1976
"Liquefaction and Cyclic Deformation of Sands: A Critical Review", Harvard Soil Mechanics Series No. 88, Harvard University, Cambridge, Mass.

Castro, G., 1969
"Liquefaction of sands", Report 81, Harvard Soil Mechanics Series, Harvard University, Cambridge, Mass.

Castro, G., 1975
"Liquefaction and Cyclic Mobility of Saturated Sands", Proc. ASCE, J. Geotechnical Engrg., Div., Vol. 101

Castro, G. and Christian, J.T., 1976
"Shear Strength of Soils and Cyclic Loading", Proc. ASCE, 102 (GT9): 887-894.

Castro, G. and Poulos, S.J., 1977
"Factors Affecting Liquefaction and Cyclic Mobility", Proc. ASCE, 103 (GT6): 501-506

Cervantes, R., Esteva, L., and Alduncin, G., 1973
"Riesgo sísmico en formaciones estratificadas", Internal Report, Instituto de Ingeniería, Universidad Nacional Autónoma de México, Mexico City

Corps of Engineers, U.S. Department of the Army, 1939
"*Report on the Slide of a Portion of the Upstream Face at Fort Peck Dam*", U.S. Government Printing Office, Washington, D. C.

Cuellar, V., Bazant, Z.P., Krizek, R.J., and Silver, M.L., 1977
"*Densification and Hysteresis of Sand Under Cyclic Shear*", Proc. ASCE, 103 (GT5): 399-416

D'Appolonia, D J. and D'Appolonia, E., 1967
"*Determination of the Maximum Density of Cohesionless Soils*", Proc. Third Asian Regional Conf. on Soil Mech. and Foundation Engrg., Haifa, Israel, pp 266-268

De Alba, P., Chan, C.K., and Seed, H.B., 1975
"*Determination of Soil Liquefaction Characteristics by Large-Scale Laboratory Tests*", Report No. EERC 75-14, University of California, Berkeley, Calif.

Díaz, S., Weckmann, O. Iturbe, R., 1973
"*Licuación de Arenas, Primera Parte*", Instituto de Ingeniería, UNAM, Informe 319

Donovan, N.C., 1971
"*A Stochastic Approach to the Seismic Liquefaction Problem*", Presented at First Interntl. Conf. on Applications of Statistics and Probability to Soil and Structural Engineering, Hong Kong

Faccioli, E. and Reséndiz, D., 1975
"*Soil Dynamics Behavior Including Liquefaction*", Report E15, Instituto de Ingeniería, UNAM, México

Finn, W.D.L., Pickering, D.J., and Bransby, P.L., 1969
"*Sand Liquefaction in triaxial and simple shear tests*", Report 11, Soil Mechanics Series, Dept. of Civil Engrg., University of British Columbia, Vancouver, Canada

Finn, W.D.L., Bransby, P.L., and Pickering, D.J., 1970
"*Effect of strain history of liquefaction of sand*", Journal of the Soil Mechanics and Foundations Division, ASCE, Vol. 96, No. SM6

Finn, W.D.L., Emery, J.J., and Gupta, Y.P., 1971
"*Liquefaction of Large Samples of Saturated Sand on A Shaking Table*", Proc. First Canadian Conf. on Earthq. Engrg., Vancouver, Canada, pp 97-110

Finn, W.D.L. and Byrne, P.M., 1976
"*Estimating Settlement in Dry Sands During Earthquakes*", Canadian Geotechnical J., Vol. 13, Number 4: 355-363

Finn, W.D.L., Lee, K.W., and Martin, G.R., 1977
"*An Effective Stress Model for Liquefaction*", Proc. ASCE, 103 (GT6): 517-533

Floring, V.A. and Ivanov, E.L., 1973
"*Liquefaction of Saturated Sandy Soils*", Proc. 5th Interntl. Conf. on Soil Mechanics and Foundations Engineering, Paris, France

Gibbs, H.J. and Holtz, W.G., 1957
Research on Determining the Density of Sands by Spoon Penetration Testing", Proc. Fourth Interntl. Conf. Soil Mech. Found. Engrg., London, England, 1, pp 35-39

Hardin, B.O. and Drnevich, V.P., 1972a
"*Shear Modulus and Damping in Soils: Measurement and Parameter Effects*", Proc. ASCE, 98 (SM6): 603-624

Hardin, B.O. and Drnevich, V.P., 1972b
"*Shear Modulus and Damping in Soils: Design Equation and Curves*", Proc. ASCE, 98 (SM7): 667-692

Huang, Wen-Xi, 1961
"Investigations on Stability of Saturated Sand Foundations and Slopes Against Liquefaction", Proc, 5th ICSMFD, Vol, 2

Idriss, I.M. and Seed, H.B., 1968b
"Seismic Response of Horizontal Soil Layers", Proc. ASCE, 94 (SM4): 1003-1031

Ishibashi, I. and Sherif, M.A., 1974
"Soil Liquefaction by Torsional Simple Shear Device", Proc. ASCE, 100 (GT8): 871-888

Ishihara, K. and Li, S., 1972
"Liquefaction of Saturated Sand in Triaxial Torsion Shear Test" Soils and Foundations, 12(2): 19-40

Ishihara, K. and Yasuda, S., 1972
"Sand Liquefaction Due to Irregular Excitation", Soil and Foundations, Vol 12, No. 4

Ishida, H., 1970
"Characteristics of Liquefaction of Level Sandy Ground During the Tokachioki Earthquake", Soil and Foundations, 10(2): 103-111

Ladd, R.S., 1976
"Effects of Specimen Preparation on the Cyclic Structural Stability of Sands", Symposium on Soil Liquefaction, ASCE National Convention, Philadelphia

Ladd, R.S., 1977
"Specimen Preparation and Cyclic Stability of Sand", Proc. ASCE, 103 (GT6): 535-547

Lee, K.L, and Seed, H.B., 1967
"Cyclic Stress Conditions Causing Liquefaction of Sand", Proc. ASCE, 93 (SM1): 47-70

Lee, K.L. and Fitton, J.A., 1968
"*Factors Affecting the Cyclic Loading Strength of Soil*", In: Symposium on Vibration Effects of Earthquakes on Soils and Foundations, ASTM Spec. Techn. Publ. 450, pp 71-95

Lee, K.L. and Albaisa, A., 1974
"*Earthquake Induced Settlements in Saturated Sands*", Proc. ASCE, 100 (GT4): 387-406

Liou, C.P. Streeter, V.L., and Richart, F.E., Jr., 1977
"*Numerical Model for Liquefaction*", Proc. ASCE, 103 (GT6): 589-606

Marsal, R.J., 1961
"*Behavior of a Sandy Uniform Soil During the Jaltipan Earthquake, Mexico*", Proc. 5h Interntl. Conf. on Soil Mech. and Foundation Engineering, Vol. I, pp 224-233

Martin, G.R., Fenn, W.D., and Seed, H.B., 1975
"*Fundamentals of Liquefaction Under Cyclic Loading*", Journal of the Geotechnical Engineering Division, No. GT5

Martin, R.E., 1977
"*Estimating Foundation Settlements in Residual Soils*", Proc. ASCE, 103 (GT3): 197-212

Middlebrooks, T.A., 1942
"*Fort Peck Slide*", ASCE Transactions, Vol. 107

Mulilis, J.P., Chan, C.K., and Seed, H.B., 1975
"*The Effects of Method of Sample Preparation on the Cyclic Stress-Strain Behavior of Sands*", Report No. EERC 75-18, University of California, Berkeley

Mulilis, J.P., Seed, H.B., Chan, C.K., Mitchell, J.K., and Arulanandan, K., 1977
"*Sample Preparation Sand Liquefaction*", Proc. ASCE, 103 (GT2): 91-108

Ohsaki, Y., 1966
"Niigata Earthquake, 1964, Building Damage and Soil Condition", Soils and Foundations, 6(2): 14-37

Ohsaki, Y., 1970
"Effects of Sand Compaction on Liquefaction During the Tokachioki Earthquake", Soils and Foundations, 10(2): 112-128

Papadakis, C.N., 1973
"Soil Transients by Characteristics Method", Doctoral thesis, Dept. of Civil Engrg., University of Michigan, Ann Arbor, Michigan

Peacock, W.H. and Seed, H.B., 1968
"Sand Liquefaction Under Cyclic Loading Simple Shear Conditions", Proc. ASCE, 94 (SM3): 689-708

Poulos, S.J., 1971
"The Stress-Strain Curves of Soils", Mimeographed pamphlet

Pyke, R., Chan, C.K., and Seed, H.B., 1974
"Settlement and Liquefaction of Sands Under Multi-directional Shaking", Report EERC 74-2, Earthq. Engrg. Res. Center, University of California, Berkeley, Calif.

Porras, V., Díaz, A., y Cervantes, R., 1979
"Modelos Numéricos para Analizar el Problema de Licuación", 5° Congreso Nacional de Ingeniería Sísmica, Guadalajara, Jal., Octubre 31 - Noviembre 3, 1979

Schnabel, P.B., Lysmer, J., and Seed, H.B., 1972b
"SHAKE: A Computer Program for Earthquake Response Analysis of Horizontal Layered Sites", Report EERC 72-12, Earthq. Engrg. Res. Center, University of California, Berkeley, Calif.

Seed, H.B., 1960
"Soil Strength During Earthquakes", Proc. Second World Conf. Earthq. Engrg., Tokyo and Kyoto, Japan, I, pp 183-194

Seed, H.B., 1969
"*The Influence of Local Soil Conditions on Earthquake Damage*", Soil Dynamics Speciality Conference, VII ICSMFD, Mexico

Seed, H.B., 1970
"*Soil Problems and Soil Behavior*", In: R.L. Wiegel (Editor), Earthquake Engineering, Prentice-Hall, Englewood Cliffs, New Jersey, pp 227-252

Seed, H.B. and Lee, K.L., 1966
"*Liquefaction of Saturated Sands During Cyclic Loading*", Proc. ASCE, 92 (SM6): 105-134

Seed, H.B. and Idriss, I.M., 1967
"*An Analysis of the Soil Liquefaction in the Niigata Earthquake*", Proc. ASCE, 93 (SM3): 83-108

Seed, H.B. and Idriss, I.M., 1969
"*Influence of Soil Conditions on Ground Motions During Earthquake*", Proc. ASCE, 95 (SM1): 99-137

Seed, H.B. and Idriss, I.M., 1970b
"*A Simplified Procedure for Evaluating Soil Liquefaction Potential*", Report EERC 70-9, Earthq. Engrg. Res. Center, University of California, Berkeley, Calif.

Seed, H.B. and Idriss, I.M., 1970c
"*Soil Moduli and Damping Factors for Dynamic Response Analyses*", Report EERC 70-10, Earthq. Engrg. Res. Center, University of California, Berkeley, Calif.

Seed, H.B. and Silver, M.L., 1972
"*Settlement of Dry Sands During Earthquakes*", Proc. ASCE, 98 (SM4): 381-397

Seed, H.B., Lee, K.L., Idriss, I.M., and Makdisi, F.I., 1973
"*Analysis of the Slide in the San Fernando Dams During the Earthquake of Feb. 9, 1971*", EERC, Report No. EERC 73-2, University of California, Berkeley, Calif.

Seed, H.B., Mori, K., and Chan, C.K., 1975
"*Influence of Seismic History on the Liquefaction Characteristics of Sands*", Report No. 75-25, University of California, Berkeley, Calif.

Seed, H. B., Indress, I. M., Makdasi, F. y Banerjee, N., 1975 *"Representative of irregular Stress Time Histories by Equivalent Uniform Stress. Series in Liquefaction Analysis"*. Report No.EERC 75-29, University of California, Berkeley, Calif.

Seed, H.B., Martin, P.P., and Lysmer, J., 1975 *"The Generation and Dissipation of Pore Water Pressures During Soil Liquefaction"*, Report No. EERC 75-26, University of California, Berkeley, Calif.

Seed, H.B., Arango, I., and Chan, C.K., 1975 *"Evaluation on Soil Liquefaction Potencial During Earthquakes"*, Report No. EERC 75-28, University of California, Berkeley, Calif.

Seed, H.B., Pyke, R., and Martin, G.R., 1975 *"Effect of Multi-directional Shaking on Liquefaction of Sands"* Report No. EERC 75-41, University of California, Berkeley, Calif.

Seed, H.B. and Booker, J.R., 1976 *"Stabilization of Potentially Liquefiable Sand Deposits Using Gravel Drain Systems"*, Report No. EERC 76-10, University of California, Berkeley, Calif.

Shannon & Wilson, Inc., and Agbabian-Jacobsen Associates, 1971 *"Soil Behavior Under Esathquake Loading Conditions"*, Report Prepared for U.S.A.E.C., Contract W-7405-eng-26

Shockley, W.C. and Ahluin, R.C., 1960 *"Non-Uniform Conditions in Traixial Test Specimens"*, Research Conference on Shear Strengh of Cohesive Soils, ASCE, Boulder, Colorado

Silver, M.L. and Sees, H.B., 1969 *"The Behavior of Sands Under Seismic Loading Conditions"*, Report EERC 60-16, Earthq. Engrg. Res. Center, University of California, Berkeley, Calif.

Streeter, V.L., Wylie, E.B., and Richart, F.E., 1973 *"Soil Motion Computations by Characteristics Method"*, ASCE, Natl. Struct. Engrg. Meeting, San Francisco, California, Preprint 1952

Thiers, G.R. and Seed, H.B., 1968a
"*Cyclic Stress-Strain Characteristics of Clay*", Proc. ASCE, 94 (SM2): 555-569

Valera, J.E. and Donovan, N.C., 1977
"*Soil Liquefaction Procedures-A REview*", Proc. ASCE 103 (GT6): 607-625

Watson, J.D., 1970
"*Stress-Deformation Characteristics of Cohesionless Soils From Triaxial Compression Tests*", Doctoral Thesis, Harvard University, Cambridge, Mass.

Whitman, R.V. and Ortigosa, P., 1968
"*Densification of Sand by Vertical Vibrations*", Technical Paper T68-5, Dept. of Civil Engrg., Massachusetts, Institute of Technology, Cambridge, Mass.

Wyle, E.B., and Streeter, V.L., 1976
"*Characteristics Methods for Liquefaction of Soils*", 2nd International Conference on Numerical Methods in Geomechanics, Blacksburg, Va.

Yegian, M.K., 1976
"*Resk Analysis for Earthquake-Induced Ground Failure by Liquefaction*", M.I.T., Publication No. R76-22

Youd, T.L.; 1970
"*Densification and Shear of Sand During Vibration*", Proc. ASCE, 96 (SM3): 863-880

Youd, T.L., 1972
"*Compaction of Sands by Repeated Shear Straining*", Proc. ASCE, 98 (SM7): 709-726

Youd, T.L. and Hoose, S.N., 1976
"*Liquefaction During 1906 San Francisco Earthquake*", Proc. ASCE, 102 (GT5): 425-439

Zeevaert, L., 1967
"*Free Vibration Torsion Test to Determine Shear Modulus of Elasticity of Soils*", Proc. Third Panamerican Conf. Soil Mech. and Found. Engrg., Caracas, Venezuela, I. 111-129

Fig 1. Area de deslizamientos en Anchorage (1964)

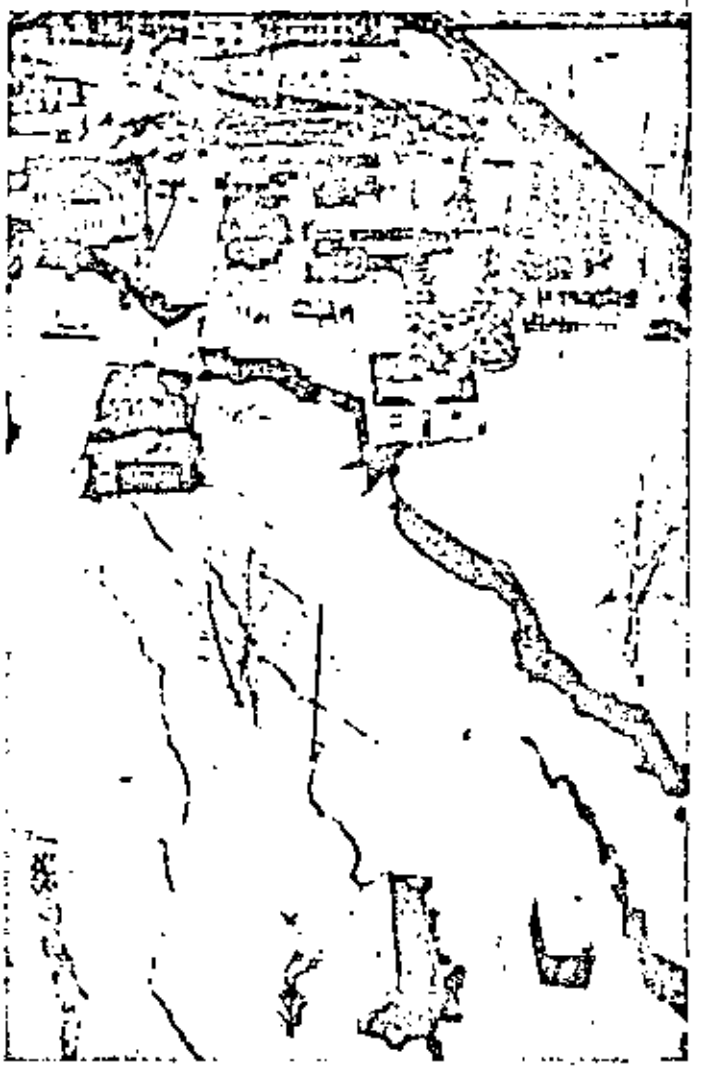

Fig 2. Area de Graben en Anchorage (1964)

(National Geographic Magazine)

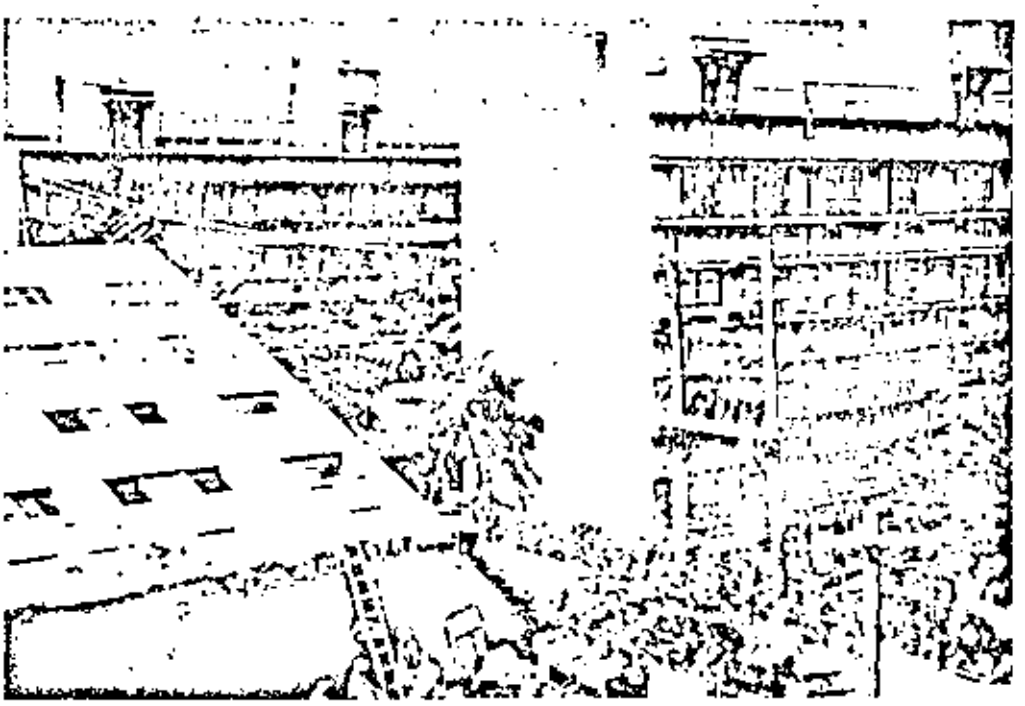

Fig 3. Inclinación de edificios durante el temblor de Niigata (1964)

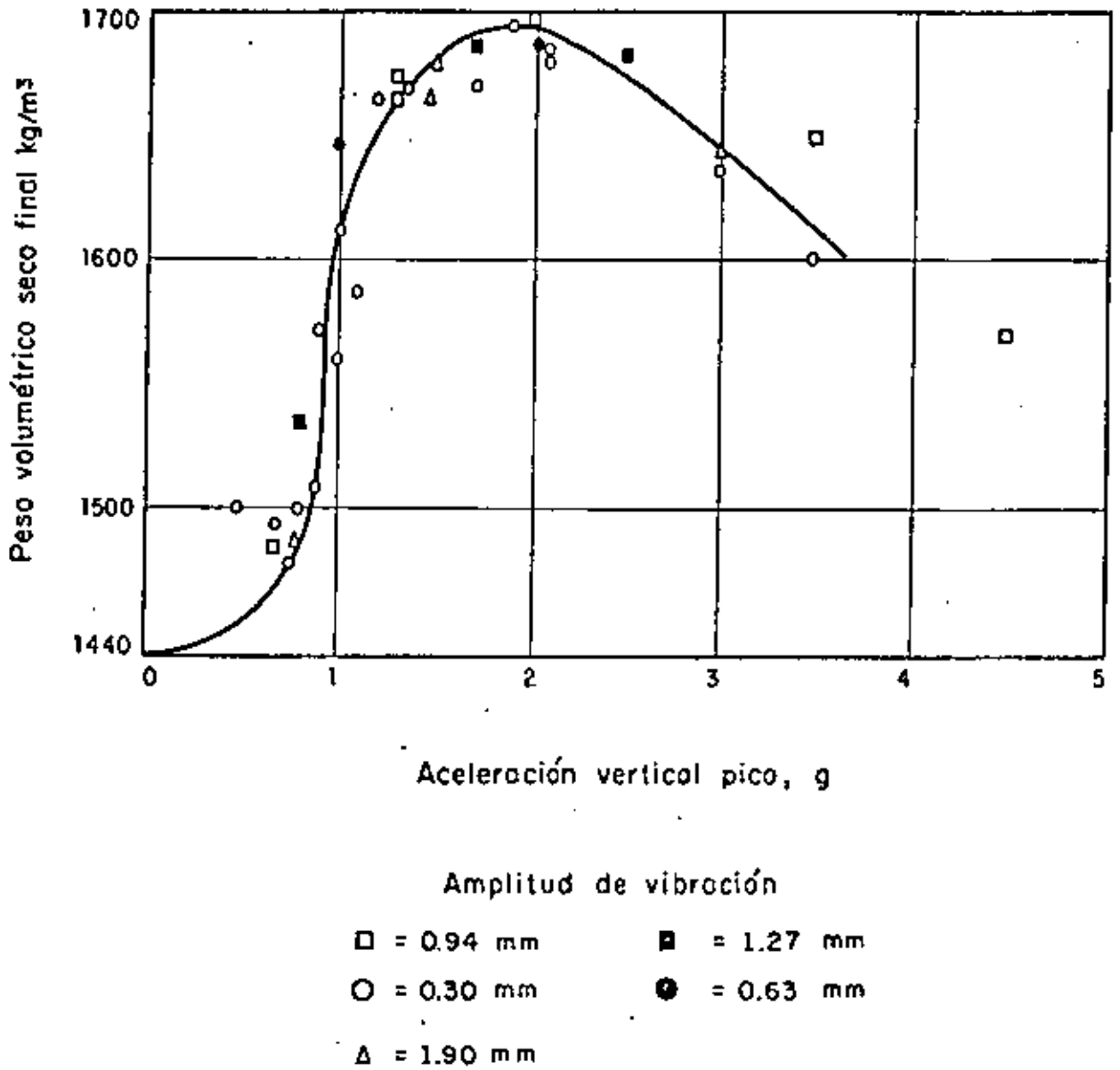

Fig 4 Efecto de la intensidad de aceleración vertical sobre la densificación de la arena en pruebas de mesa vibradora. (D'Appolonia y D'Appolonia, 1967)

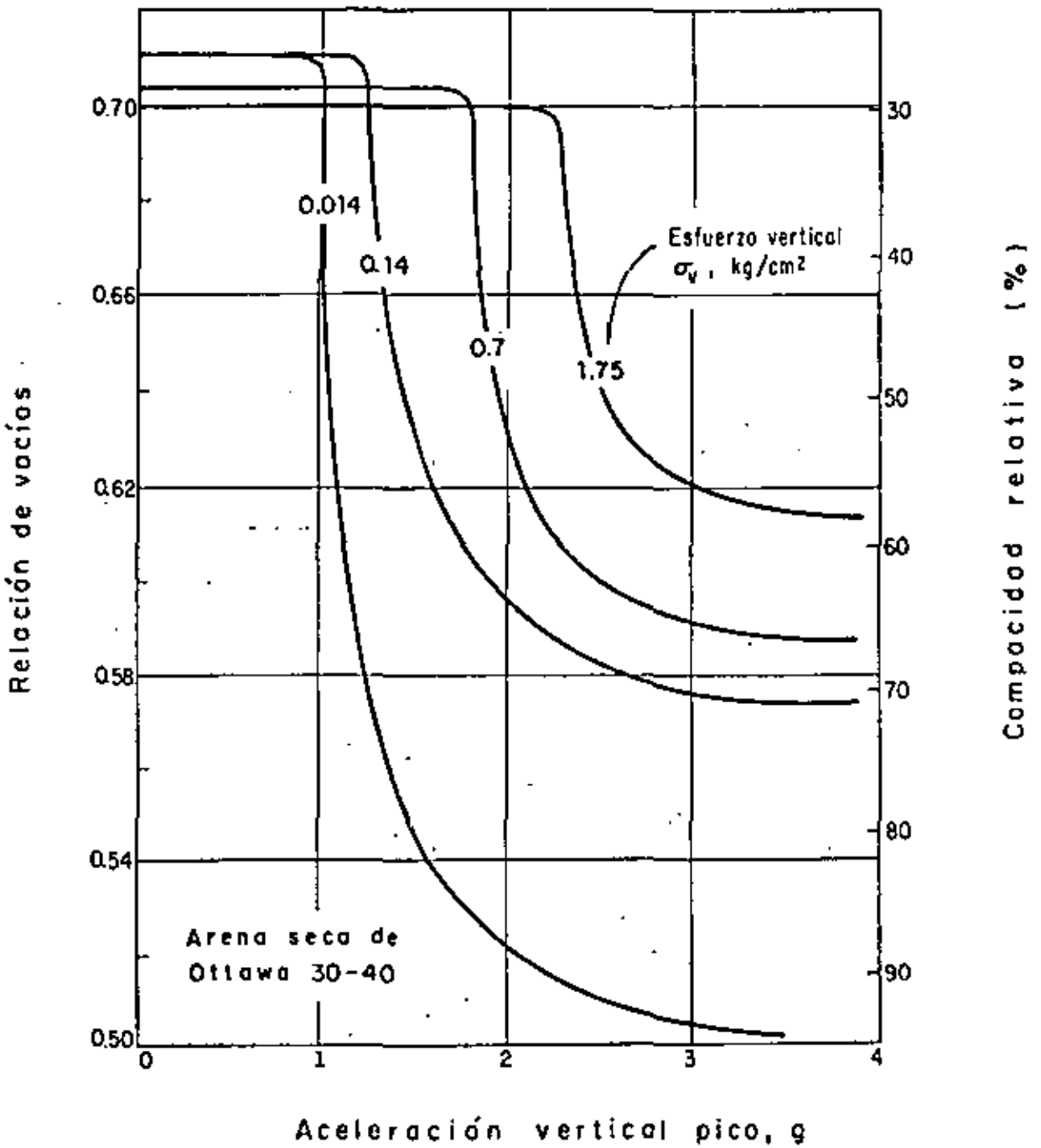

Fig 5 Efectos de la intensidad de aceleración vertical y esfuerzo de confinamiento sobre la densificación de arena seca de Ottawa en pruebas de mesa vibradora.
(Whitman y Ortegosa, 1968)

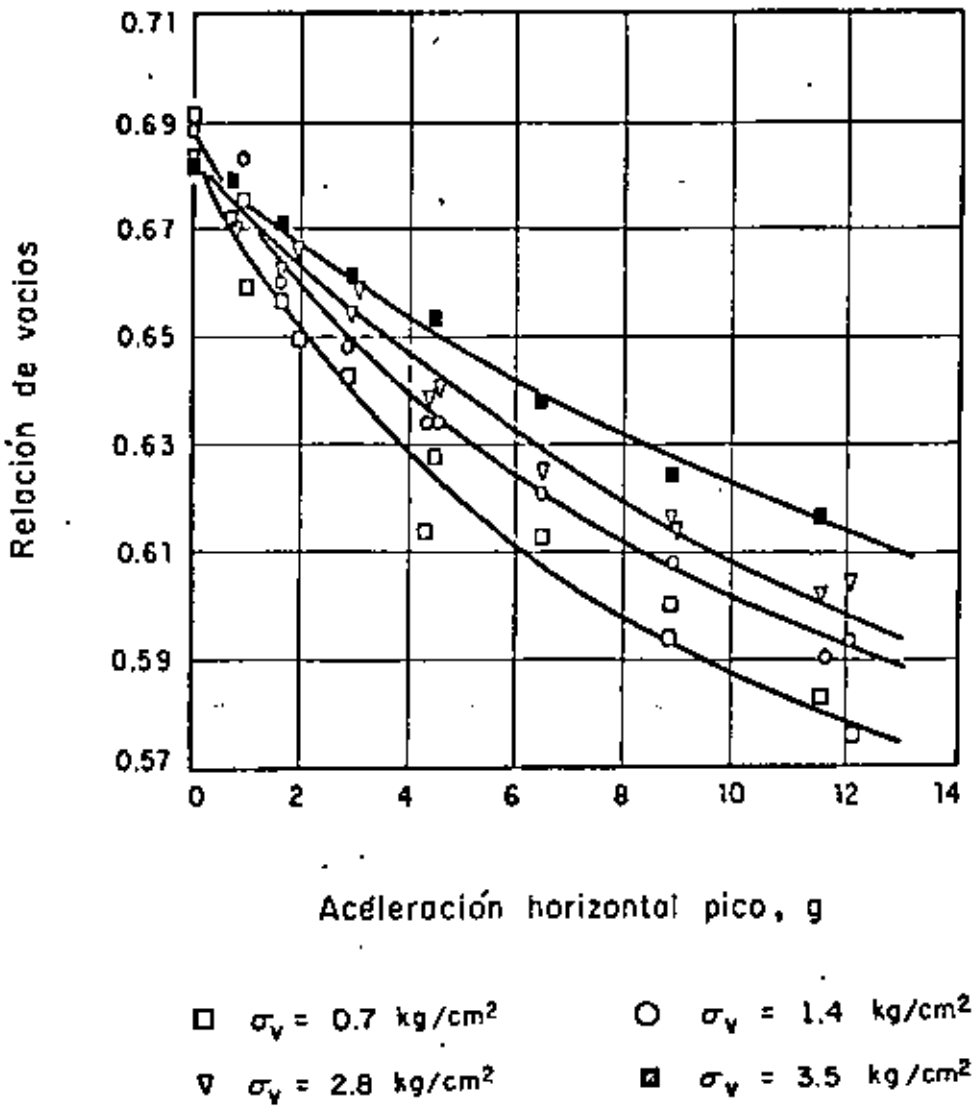

Fig 6 Efectos de la intensidad de aceleración y es fuerzo de confinamiento sobre la relación de vacíos de arena seca de Ottawa en pruebas de vibración cortante, (Youd , 1970)

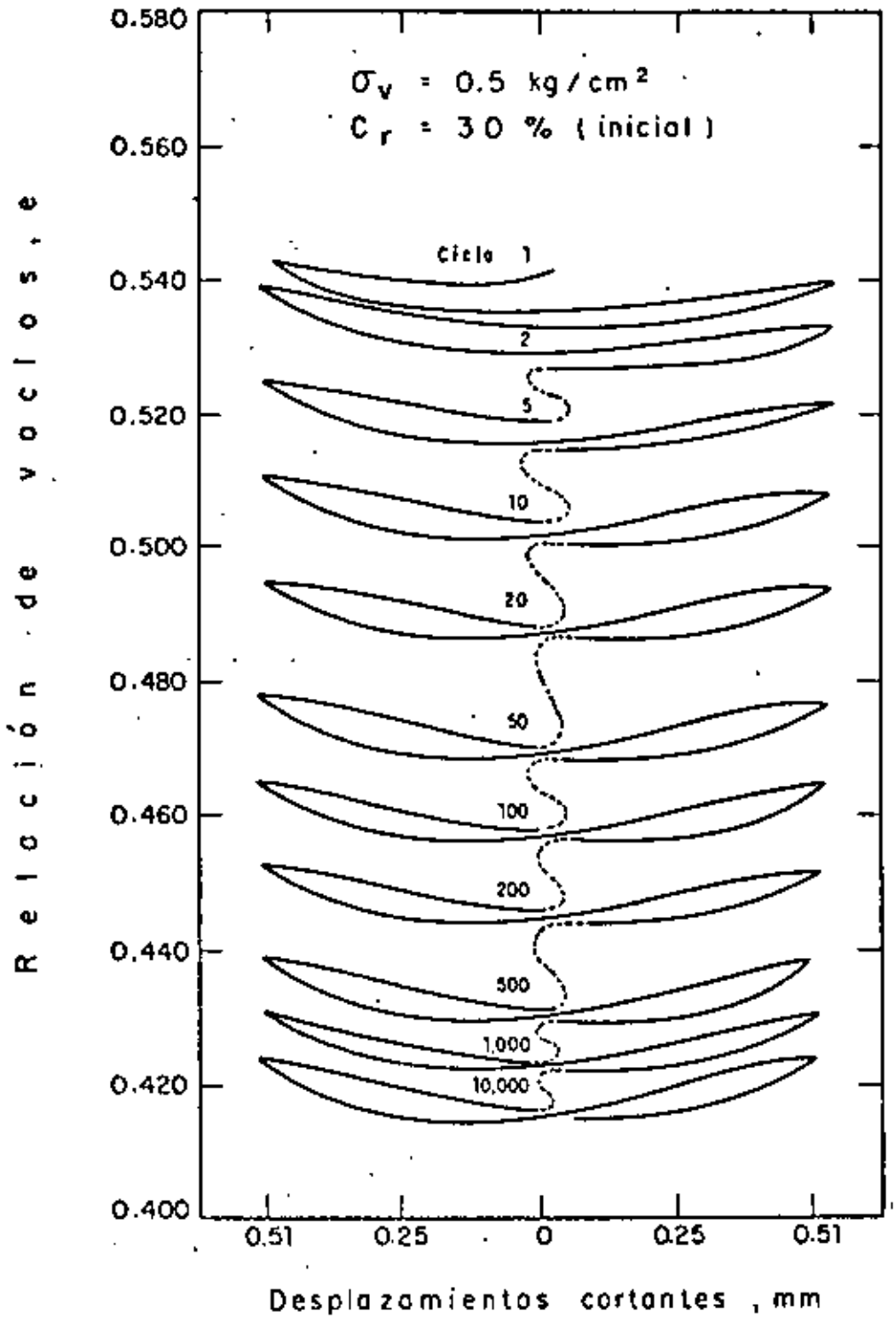

Fig 7 Compactación vs. historia esfuerzo-deformación en una prueba drenada de esfuerzo cortante cíclico sobre arena de Ottawa C-109, (Youd, 1972)

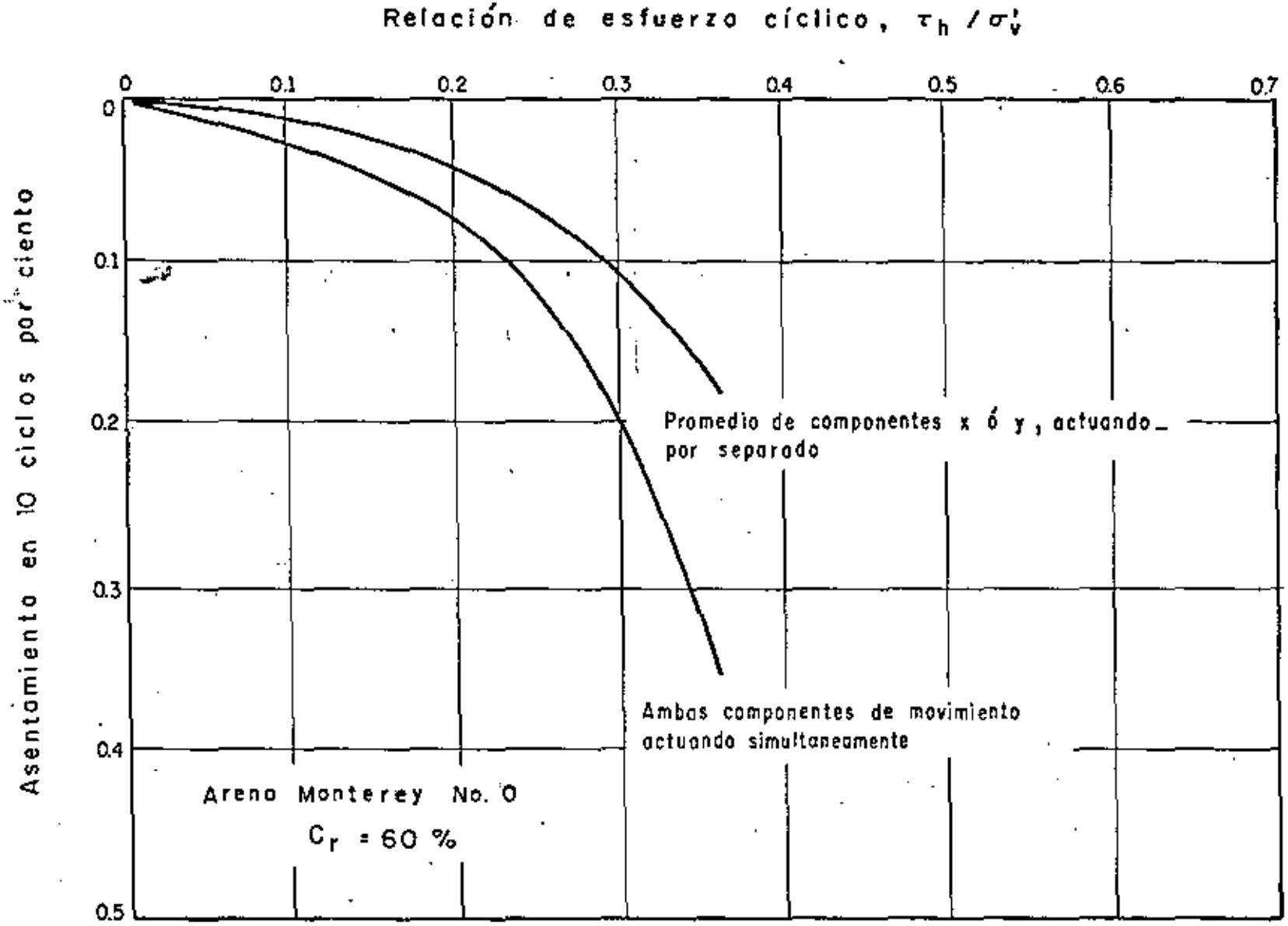

Fig 8 Asentamiento de arena seca bajo movimiento unidireccional y multidireccional, (Seed, Pyke y Martin, 1975)

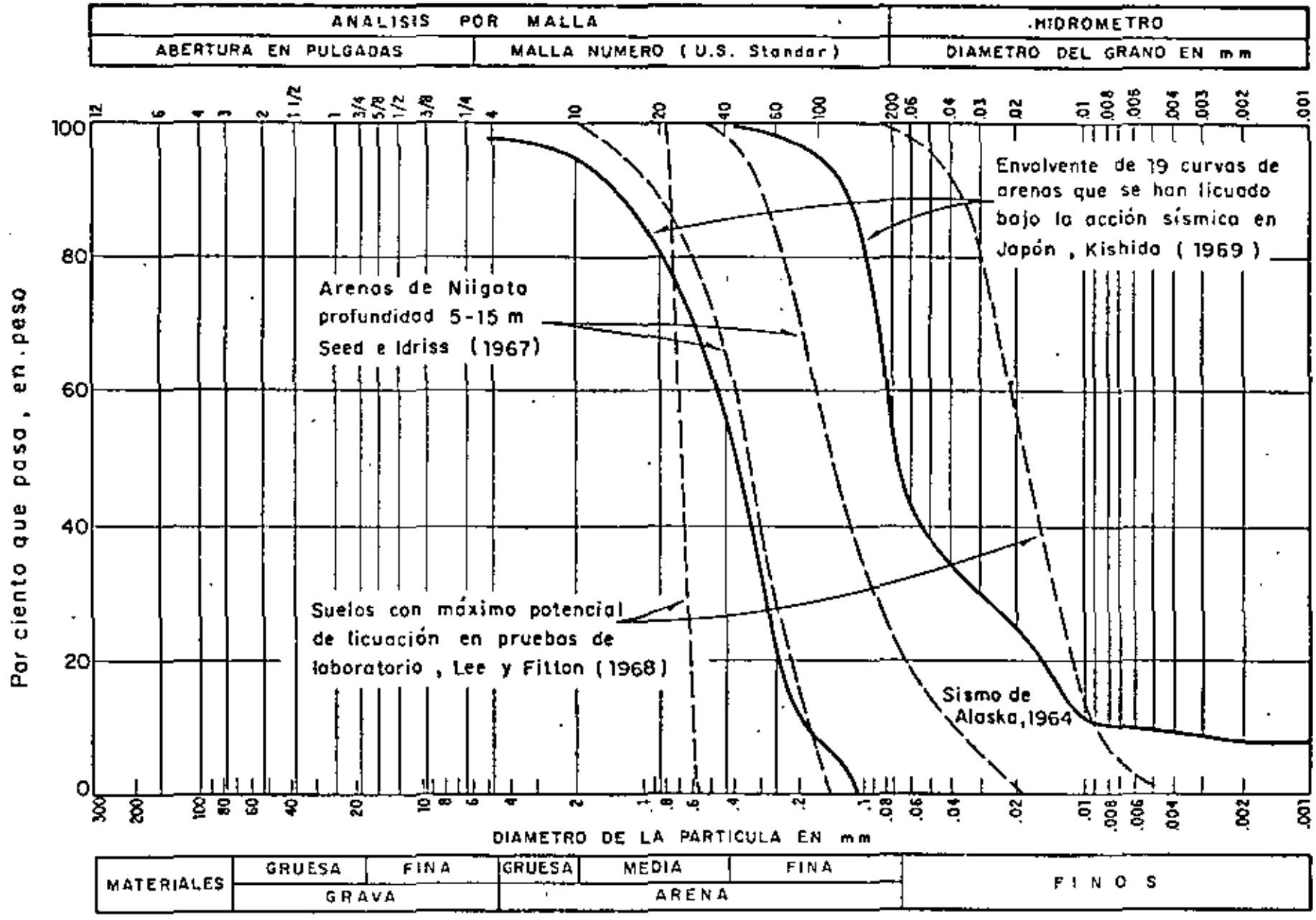

Fig 9 Granulometrías de algunos suelos que se han licuado

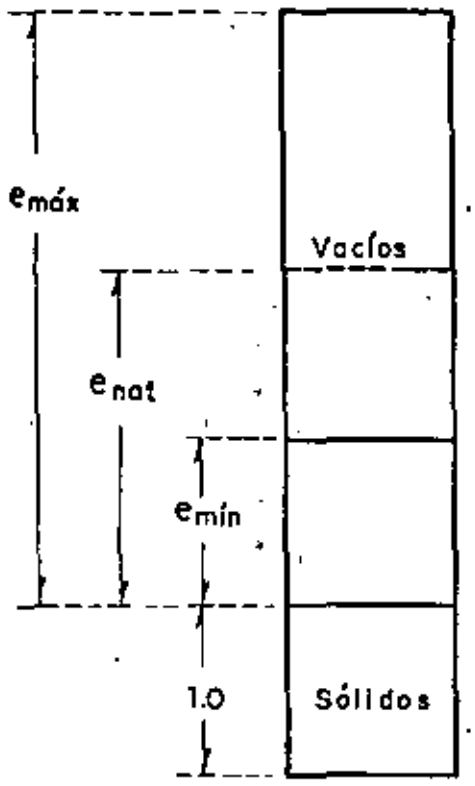

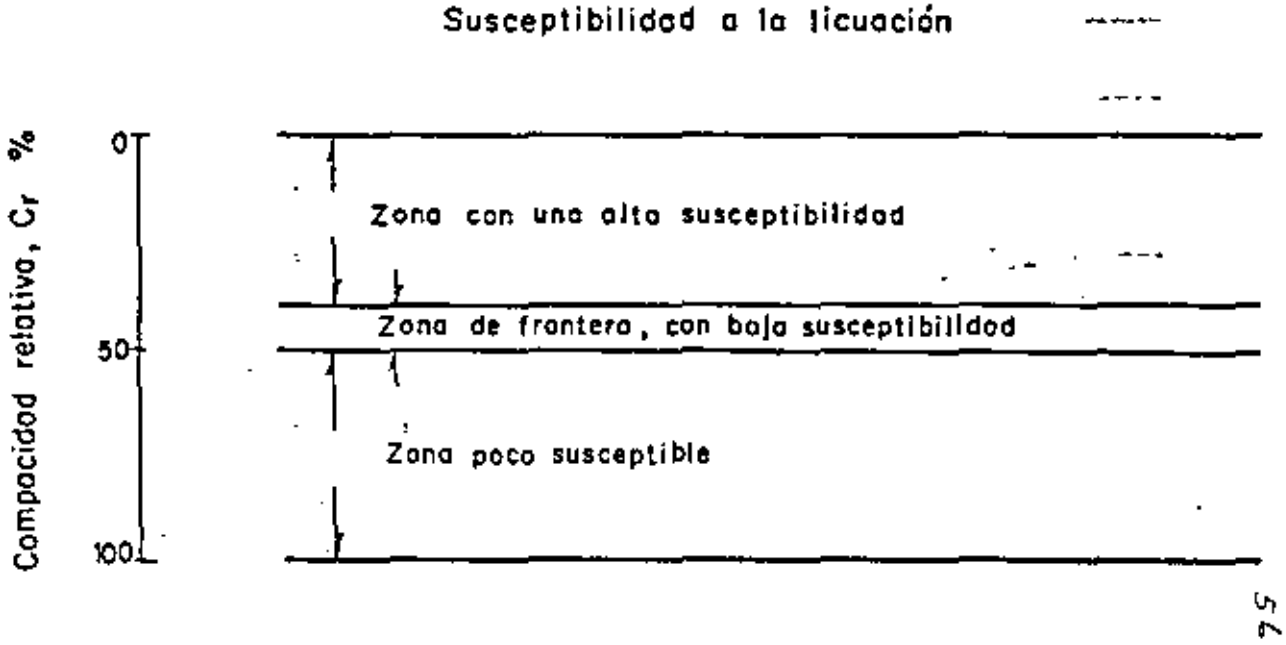

$$\text{Compacidad relativa } C_r\ (\%) = \frac{e_{máx} - e_{nat}}{e_{máx} - e_{mín}} \times 100$$

Fig 10 Concepto de compacidad relativa

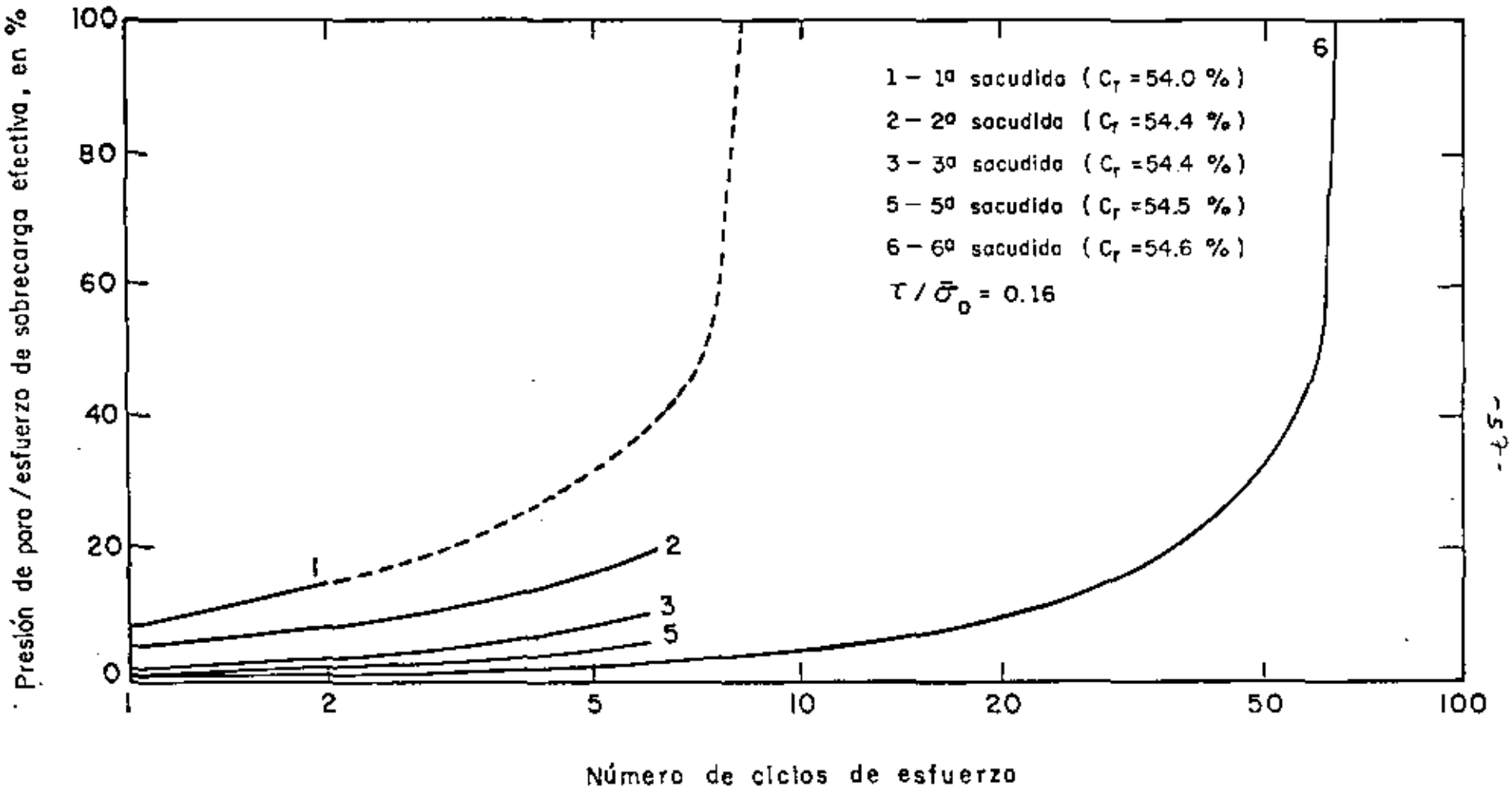

Fig 11 Efecto de la historia sísmica sobre las características de licuación de una arena

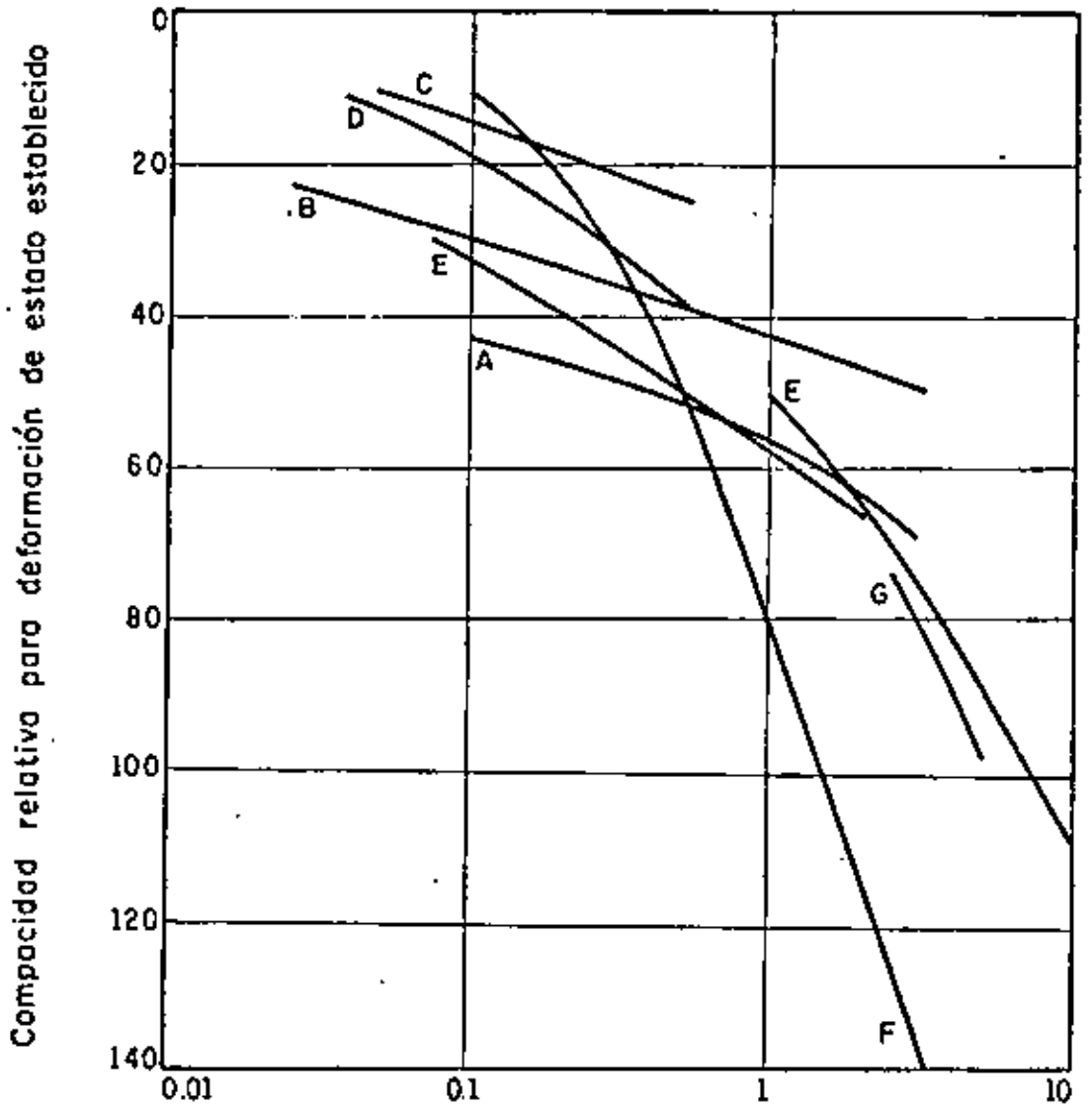

Fig 12 Curvas de estado crítico (líneas e) de arenas descritas en Castro (1972).

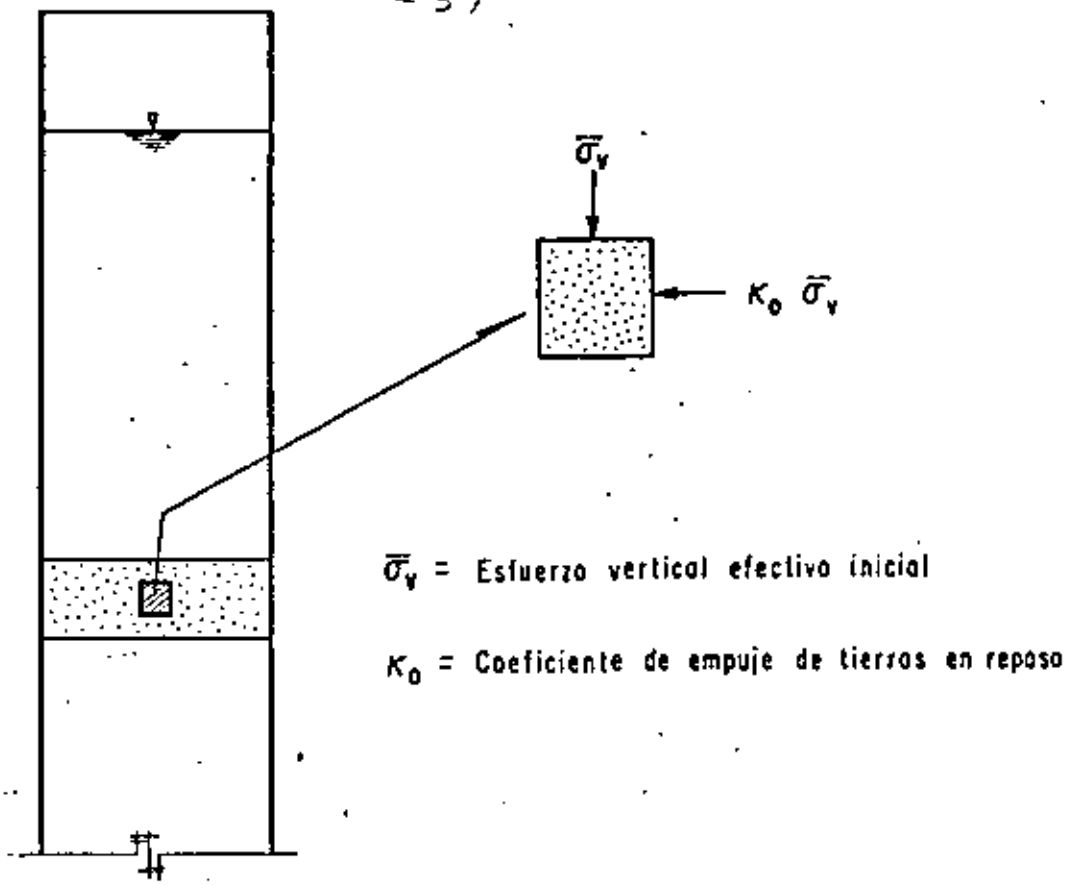

a) Localización del elemento

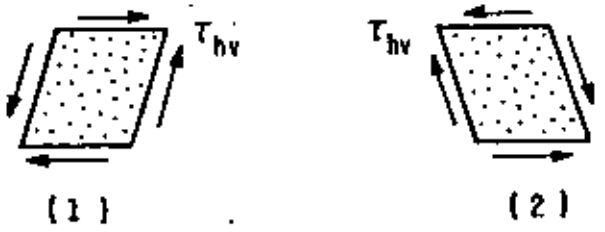

b) Esfuerzos inducidos en el elemento

Fig 13. Condición de esfuerzos para un elemento de suelo sujeto a un sismo.

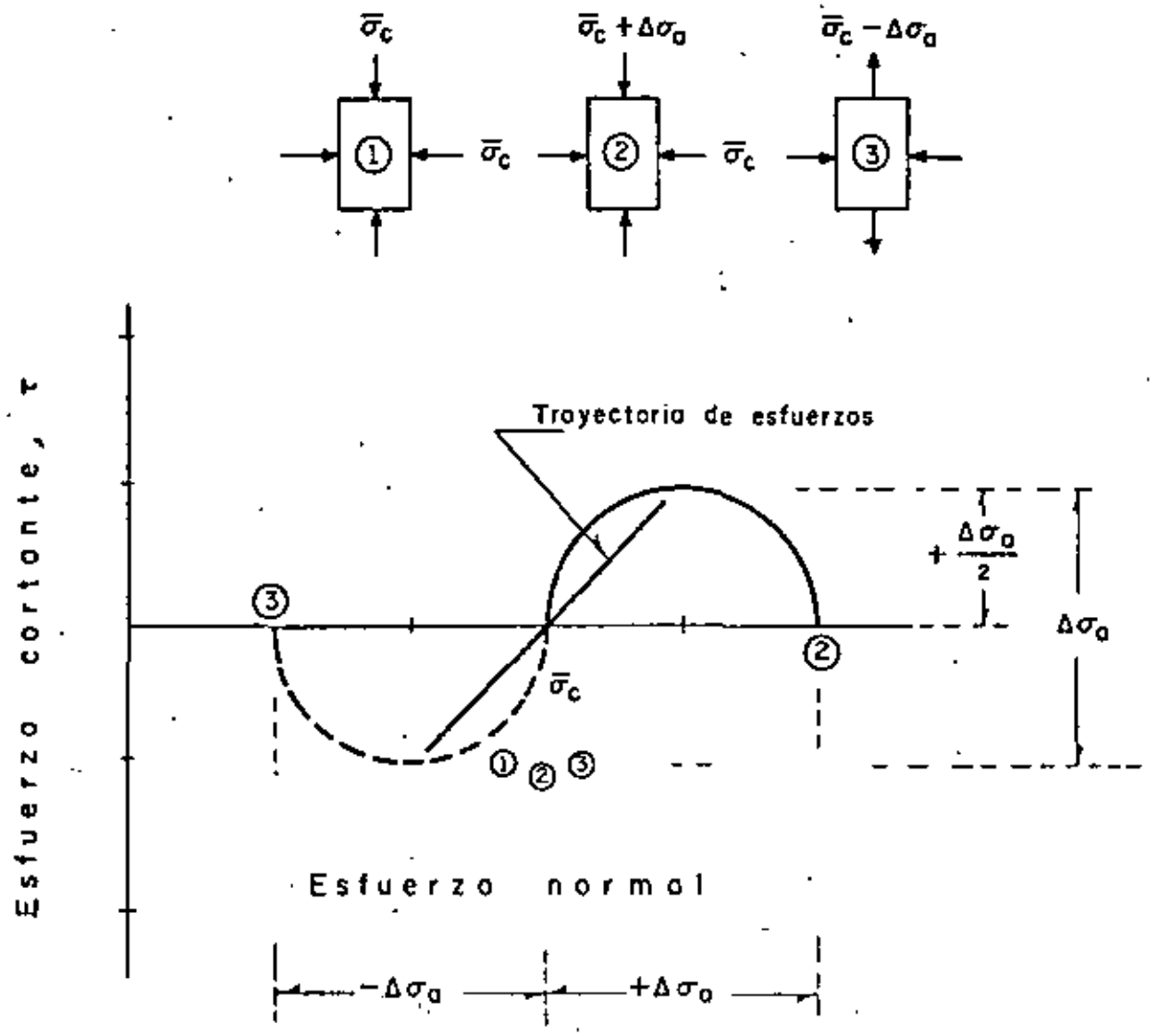

Fig 14 Círculo de Mohr en función de esfuerzos totales de un ensaye triaxial cíclico para un espécimen isotrópicamente consolidado

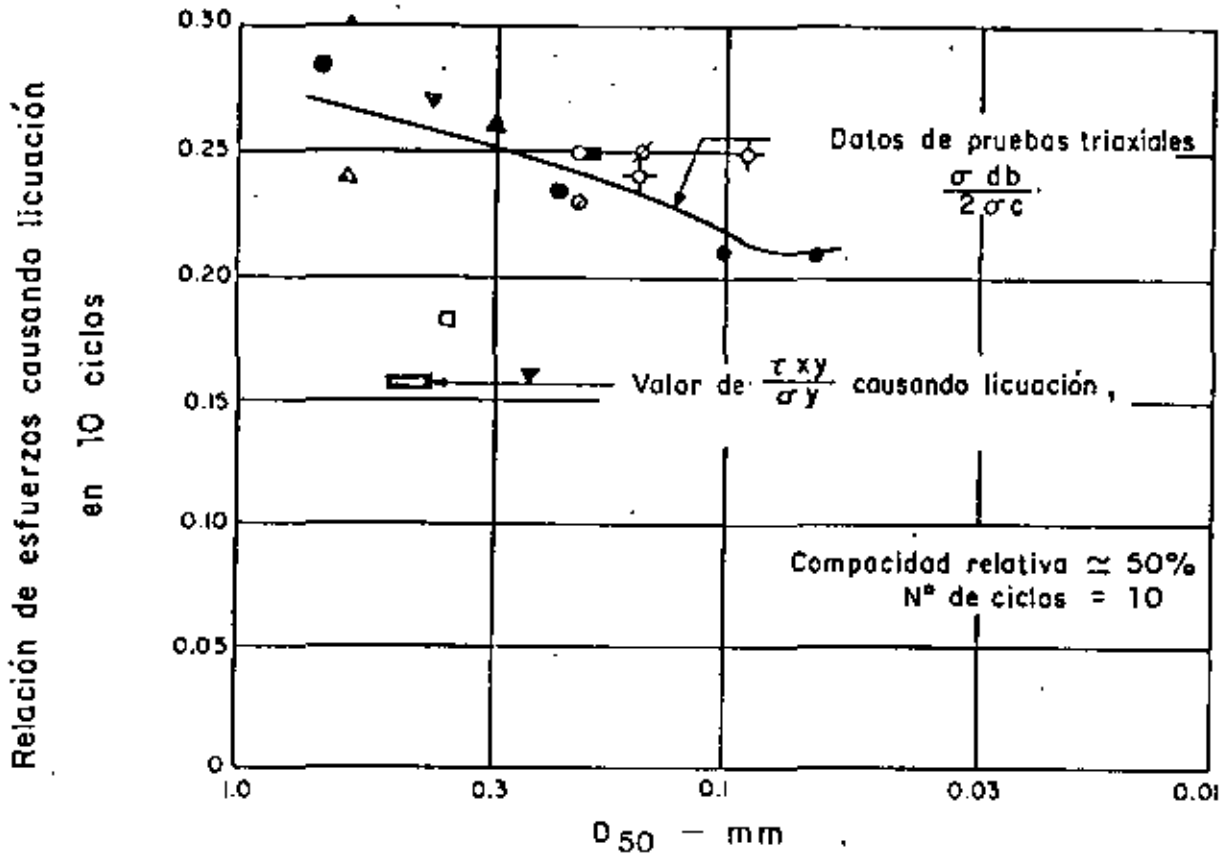

Fig 14 Condiciones de esfuerzo causando licuación de arenas en 10 ciclos

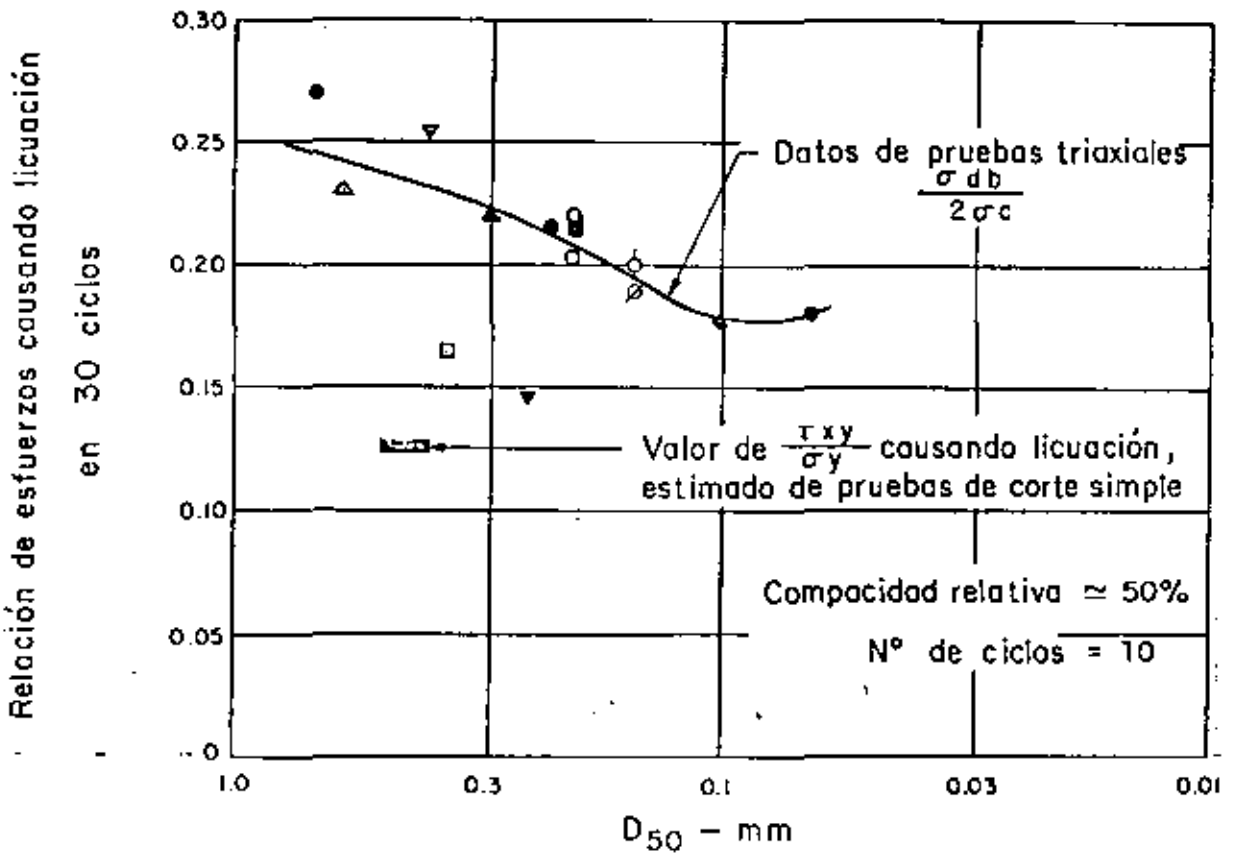

Fig. 15 Condiciones de esfuerzo causando licuación de arenas en 30 ciclos

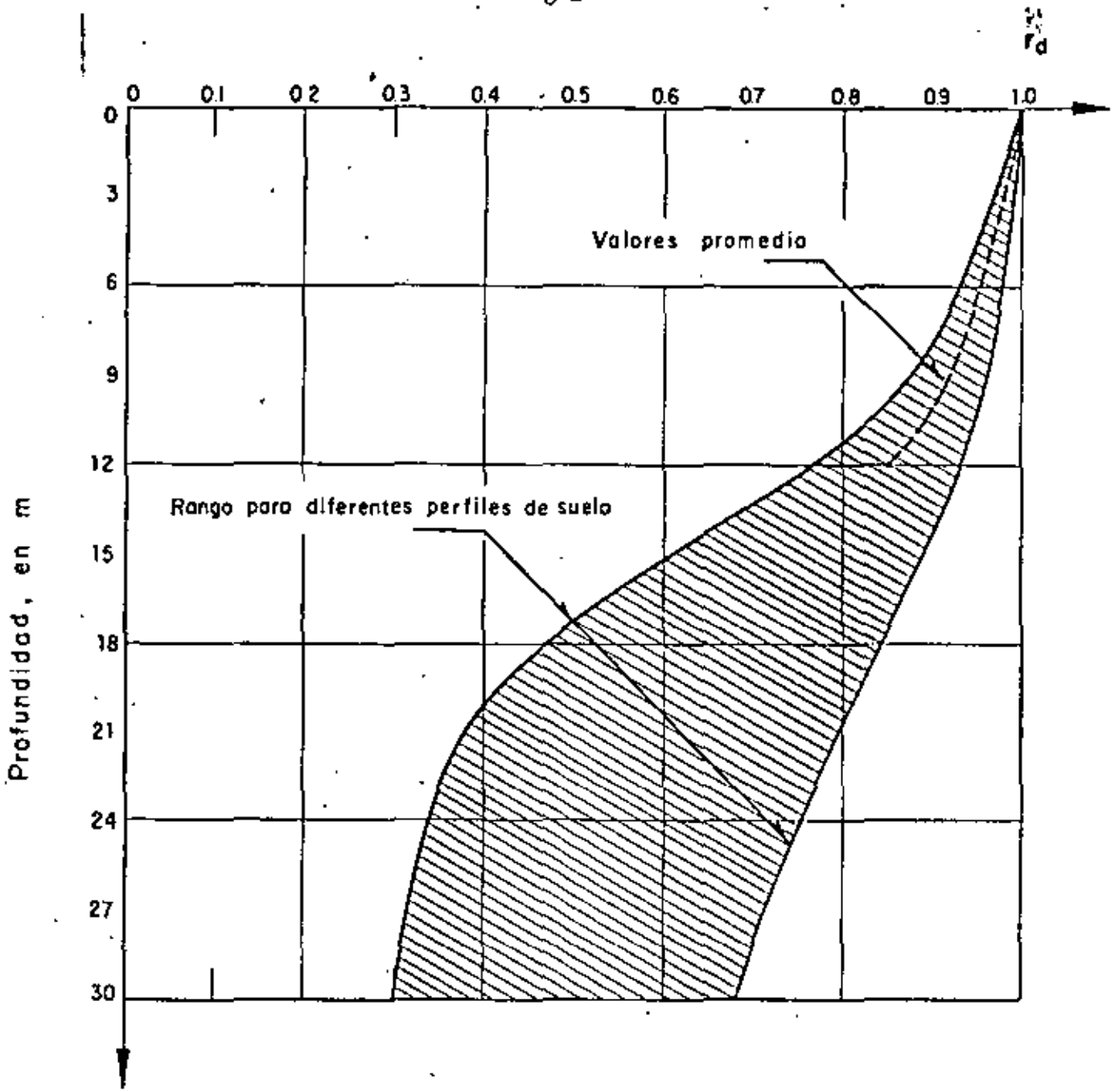

Fig 16 Rango de valores de r_d para diferentes perfiles de suelo

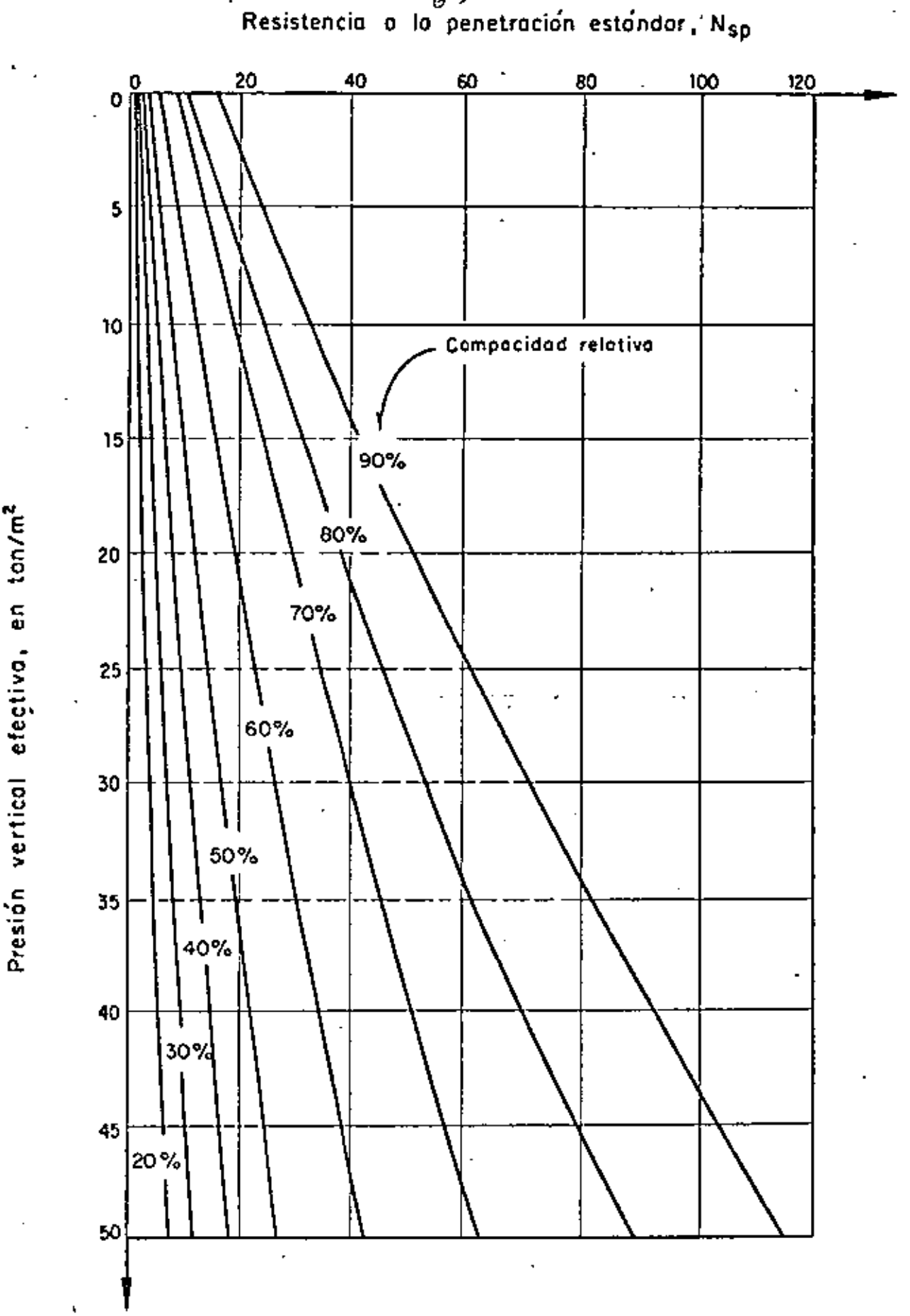

Fig 17 Relación entre la resistencia a la penetración, compacidad - relativa y presión vertical (Seed e Idress, 1970 b)

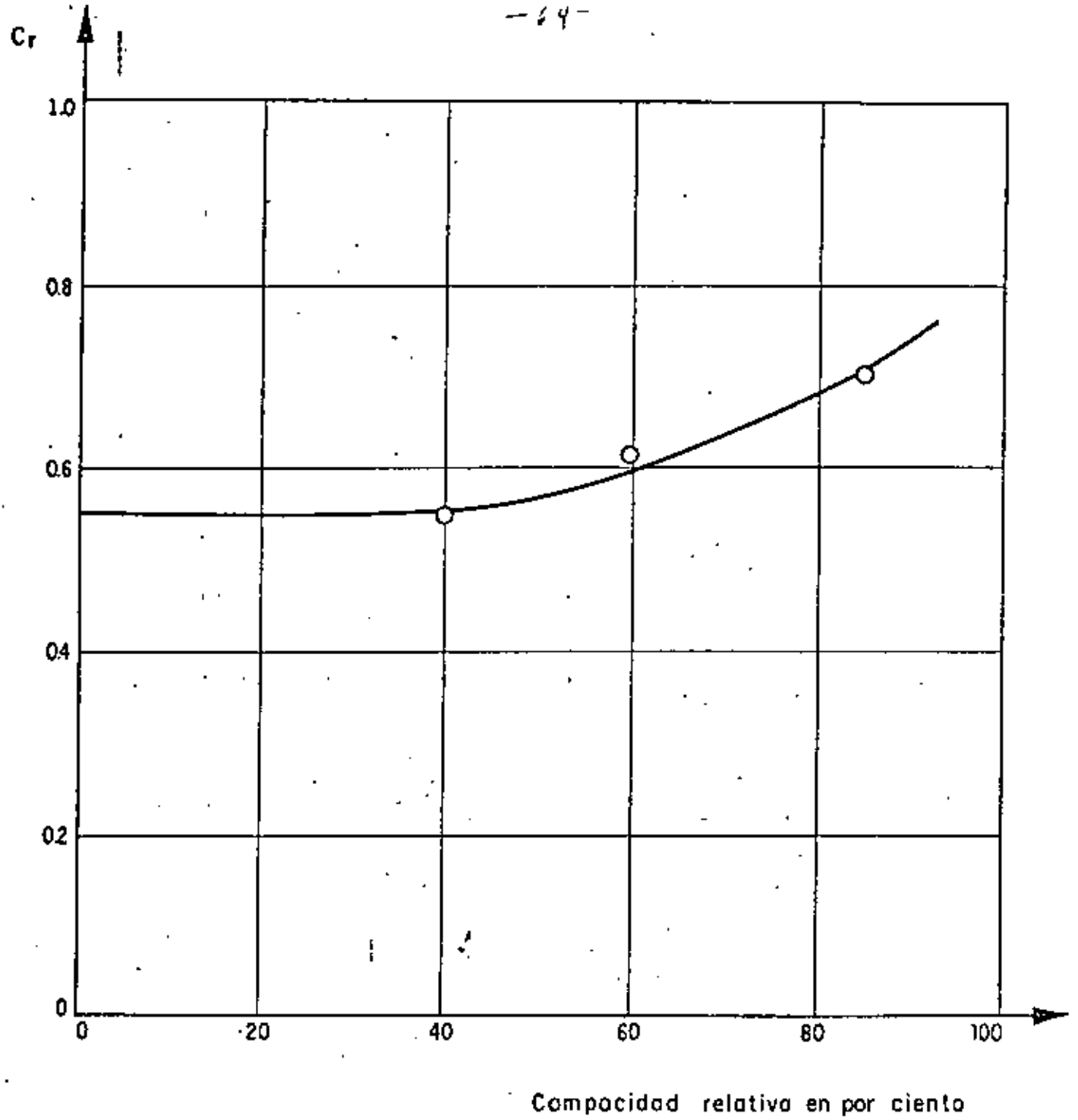

Fig 20 Relación entre d_0 y la compacidad relativa
(Seed e Idress , 1970 b)

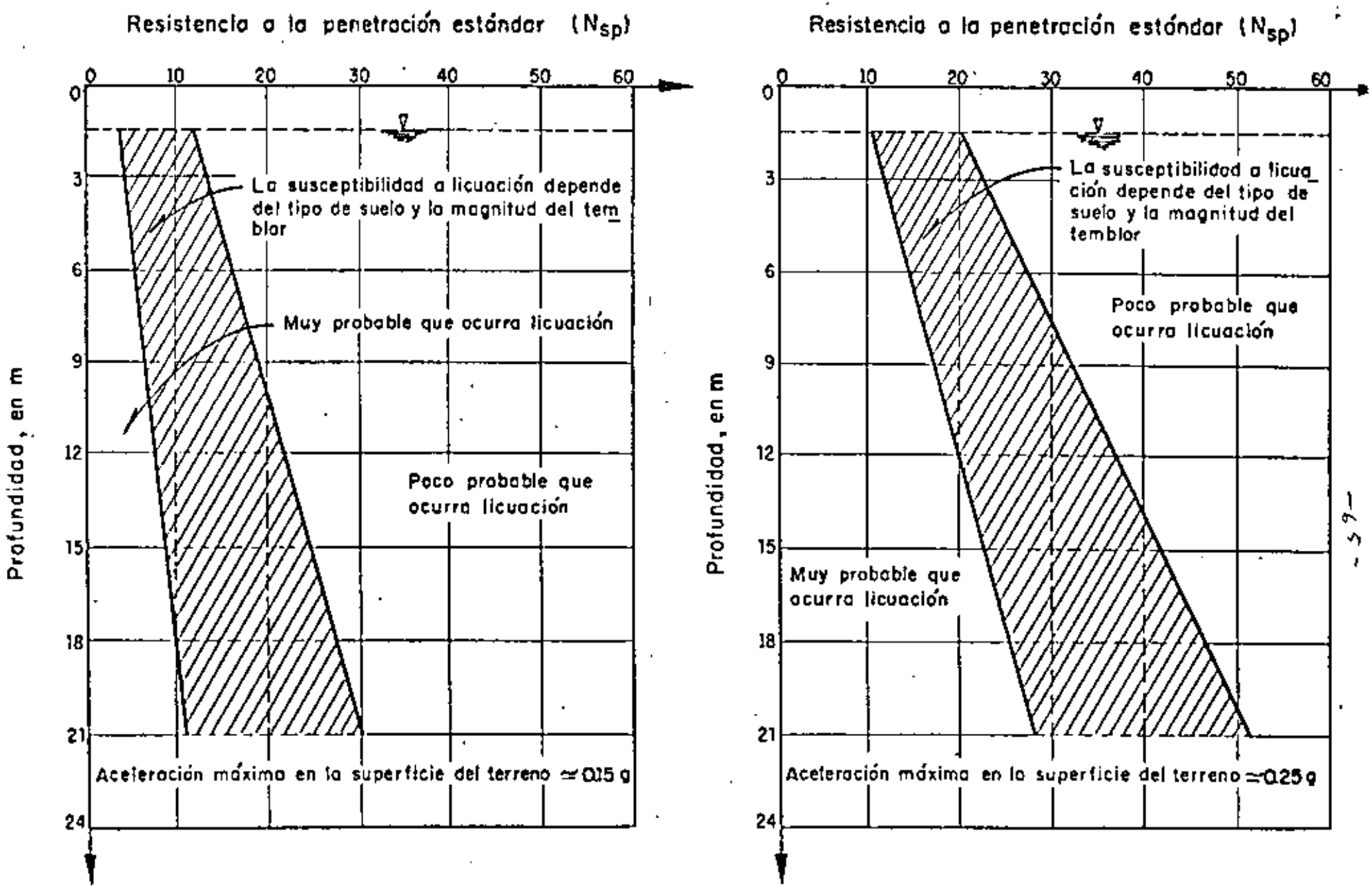

Fig 21 Gráficas para evaluar la susceptibilidad a licuación de arenas con el nivel freático a una profundidad aproximada de 1.5 m (Seed e Idress , 1970 b)

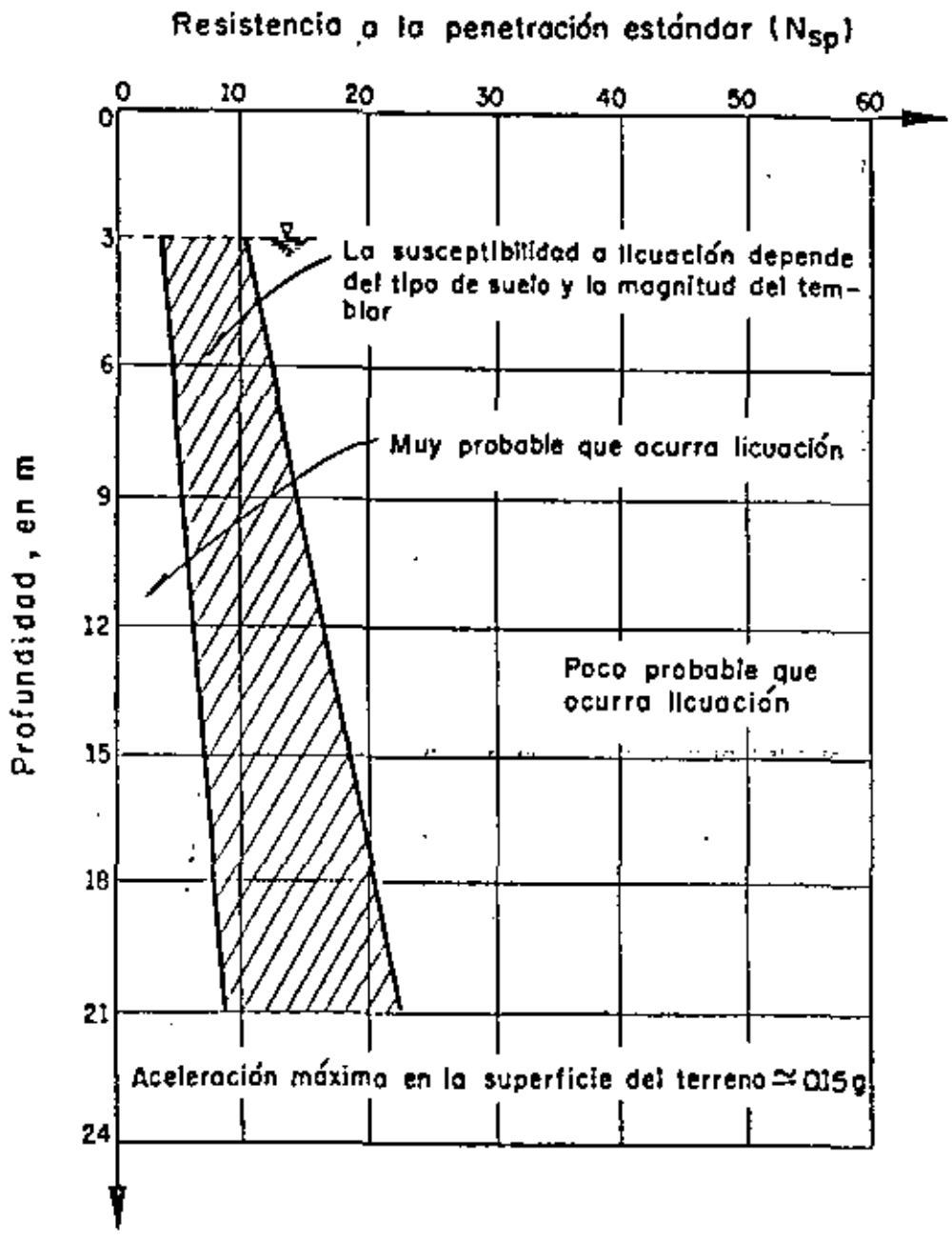

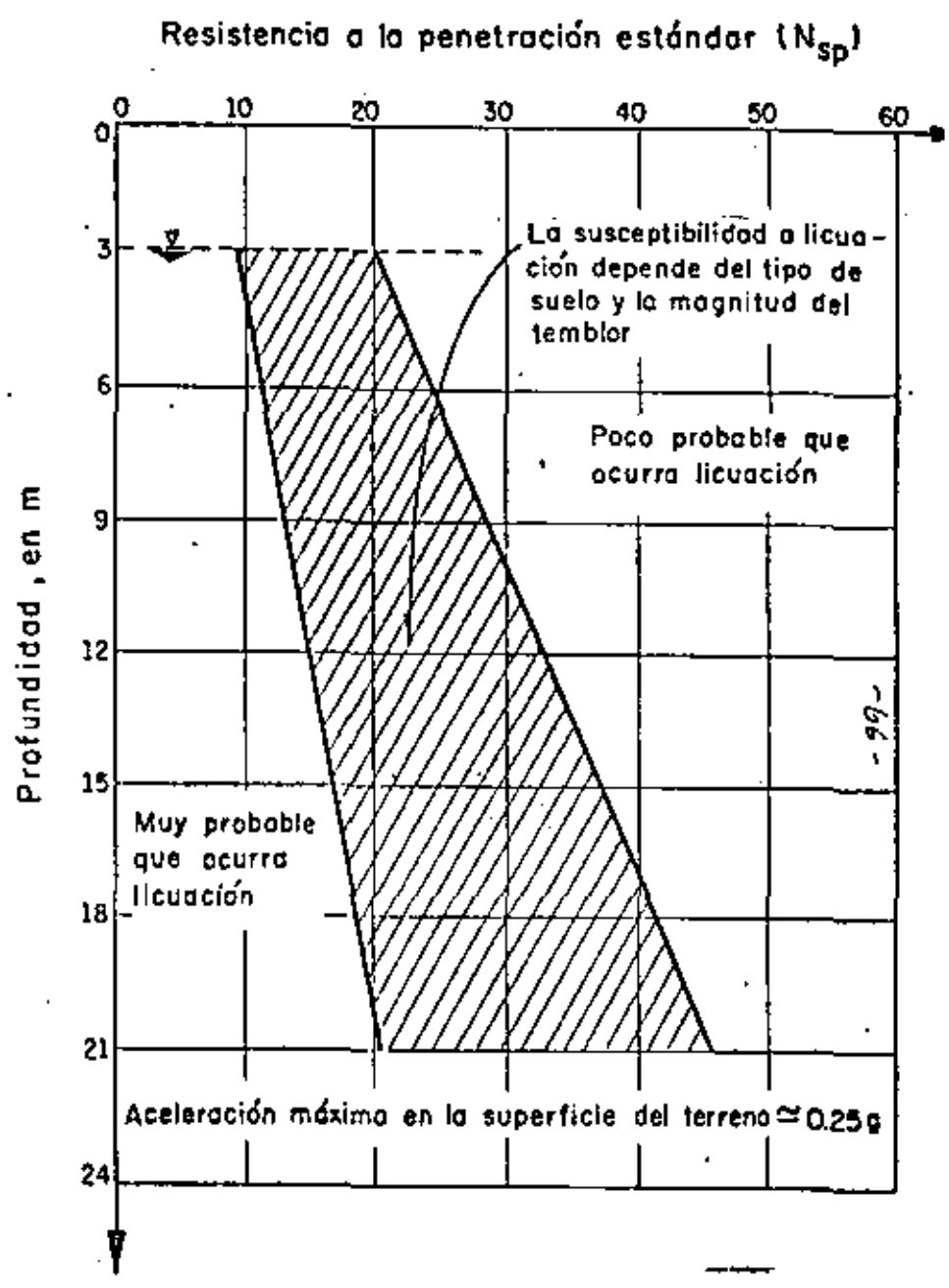

Fig 22 Gráficas para evaluar la susceptibilidad a licuación de arenas con el nivel freático a una profundidad aproximada de 3.0 m (Seed e Idress, 1970 b)

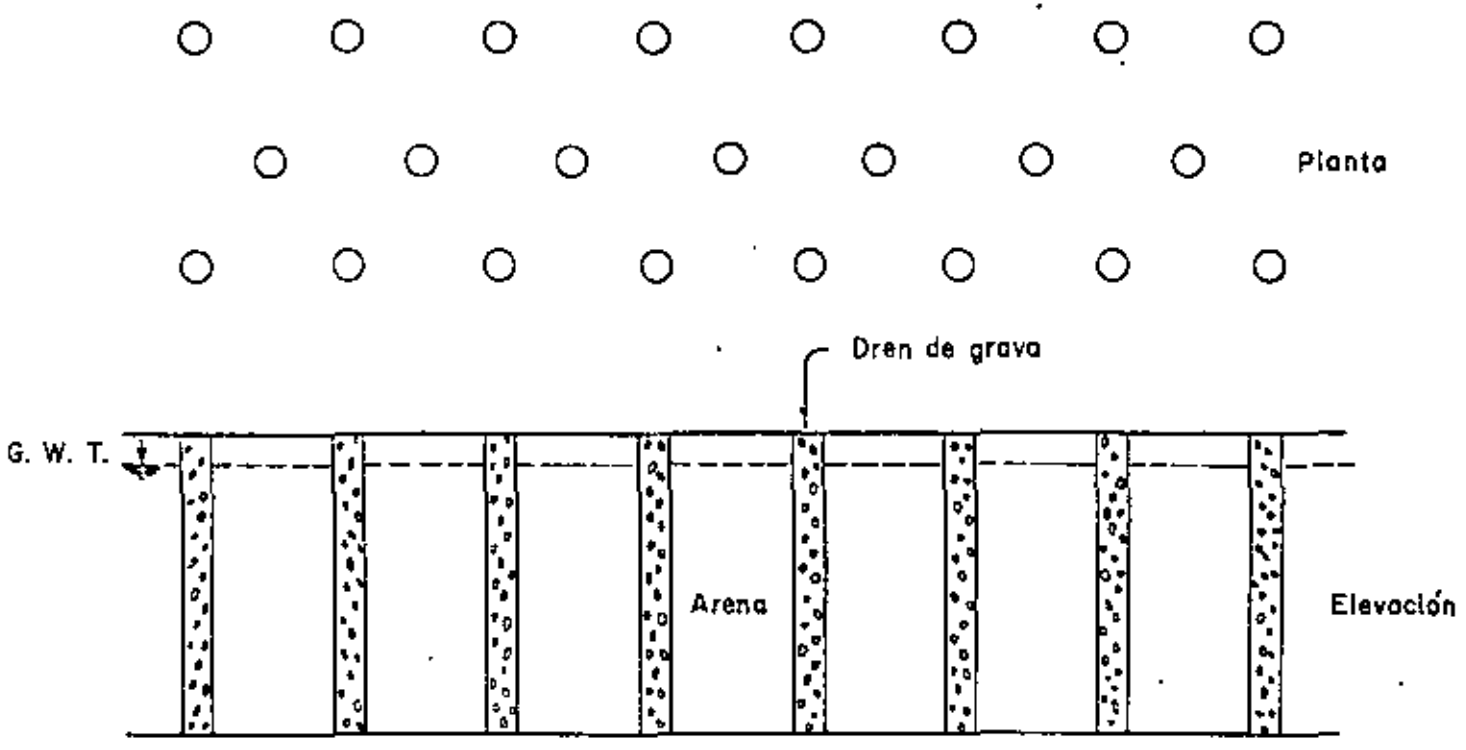

Fig 24 (a) Sistema de drenes de grava

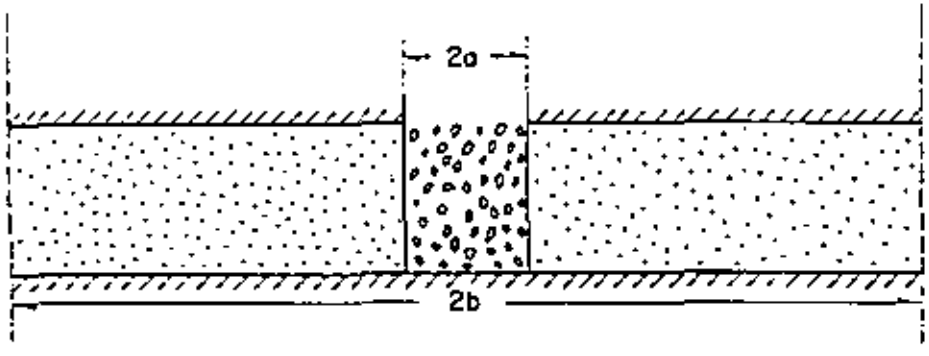

Fig 24 (b) Dren de grava con drenaje radial únicamente

centro de educación continua
división de estudios de posgrado
facultad de ingeniería unam

VI CURSO INTERNACIONAL DE INGENIERIA SISMICA

SISMOLOGIA Y SISMICIDAD

FUNDAMENTOS DE LA TEORIA DE PROBABILIDADES

DR. OCTAVIO A. RASCON CHAVEZ

JULIO, 1980

FUNDAMENTOS DE LA TEORIA DE PROBABILIDADES

NOTA

ESTOS APUNTES SON PARTE DE LA PUBLICACION "INTRODUCCION A LA TEORIA DE PROBABILIDADES", POR O. A. RASCON, PUBLICADO POR LA DIVISION DE ESTUDIOS DE POSGRADO, FACULTAD DE INGENIERIA, UNAM

SE RUEGA A LOS ASISTENTES AL CURSO QUE ESTUDIEN HASTA LA PAGINA 17, INCLUSIVE, ANTES DE LA CLASE DEL DIA 17 DE JULIO.

SIMBOLOS DE DESIGUALDADES

$<$ menor que

$\leq$ menor o igual que

$>$ mayor que

$\geq$ mayor o igual que

$\neq$ diferente de

TEORIA DE CONJUNTOS

UN *CONJUNTO* ES UNA COLECCION BIEN DEFINIDA DE OBJETOS.

NOTACION: LOS CONJUNTOS SE DENOTAN USUALMENTE CON LETRAS MAYUSCULAS, Y SUS ELEMENTOS SE ANOTAN DENTRO DE UN PAR DE LLAVES O CORCHETES.

EJEMPLOS

A) EL CONJUNTO DE NUMEROS ANOTADOS EN UN DADO ES

$S = \{1, 2, 3; 4, 5, 6\}$

B) EL CONJUNTO DE LOS NUMEROS ENTEROS MENORES QUE 5 ES

$S = \{-\infty, \ldots, -3, -2, -1, 0, 1, 2, 3, 4\}$

o $S = \{x: x \text{ ES ENTERO Y } x \leq 4\}$

C) EL CONJUNTO DE LOS NUMEROS ENTEROS POSITIVOS MENORES QUE 5 ES

$E = \{0, 1, 2, 3, 4\}$

$E = \{x: \text{ES ENTERO Y } 0 \leq x \leq 4\}$

D) EL CONJUNTO DE LOS CONTINENTES ES

$C = \{\text{ASIA, EUROPA, AMERICA, AFRICA, OCEANIA}\}$

E) EL CONJUNTO DE MARCAS QUE TIENE UNA MONEDA ES

$M = \{\text{CARA, CRUZ}\}$

F) EL CONJUNTO DE NUMEROS MAYORES DE 5 PERO MENORES O IGUALES QUE 10

$S_1 = \{x: 5 < x \leq 10\}$

CONJUNTOS

- *FINITOS.-* CUANDO TIENEN UN NUMERO FINITO DE ELEMENTOS
- *INFINITOS.-* CUANDO TIENEN UN NUMERO INFINITO DE ELEMENTOS

SUBCONJUNTOS

PARA EXPRESAR QUE UN ELEMENTO *PERTENECE* A UN CONJUNTO SE USA EL SIMBOLO ϵ. PARA EXPRESAR QUE *NO PERTENECE* SE USA EL SIMBOLO $\notin$.

EJEMPLO

SI $S_1 = \{X: 5<X\leq 10\}$, ENTONCES.

$3 \notin S_1$; $5 \notin S_1$; $8 \epsilon S_1$; $10 \epsilon S_1$

PARA EXPRESAR QUE UN CONJUNTO *ESTA CONTENIDO* EN OTRO SE USA EL SIMBOLO C; SI *NO ESTA CONTENIDO* SE USA EL SIMBOLO $\not\subset$.

PARA QUE UN CONJUNTO ESTE CONTENIDO EN OTRO SE REQUIERE QUE *TODOS* SUS ELEMENTOS LO ESTEN, ES DECIR, QUE TODOS SUS ELEMENTOS PERTENEZCAN A AMBOS CONJUNTOS.

EJEMPLO

SEAN E={3,5}; F={3,8}; G={7,9}. $E \not\subset S_1$; $F \not\subset S_1$; $G \subset S_1$

SI UN CONJUNTO, B, ESTA CONTENIDO EN OTRO, S, SE DICE QUE B ES *SUBCONJUNTO* DE S.

EJEMPLO

$B = \{X: 3\leq X\leq 8\}$ Y $S_1=\{X: 5<X\leq 10\}$

EN ESTE CASO:

$G \subset S_1 \rightarrow$ G ES SUBCONJUNTO DE S_1.

$B \not\subset S_1 \rightarrow$ B NO ES SUBCONJUNTO DE S_1

SE DICE QUE DOS CONJUNTOS SON IGUALES CUANDO CONTIENEN LOS MISMOS ELEMENTOS (NO IMPORTA EL ORDEN EN QUE ESTOS SE ESCRIBAN)

EJEMPLO

SEAN $A=\{1,3,5,7\}$, $B=\{7,5,1,3\}$ Y $C=\{7,5,1\}$

EN TAL CASO, $A = B \neq C$

CONJUNTO VACIO

DE LA MISMA MANERA QUE EXISTE EL CERO EN LOS NUMEROS, EN LA TEORIA DE CONJUNTOS EXISTE EL *CONJUNTO VACIO*, EL CUAL *NO* TIENE ELEMENTOS. USUALMENTE SE DENOTA $\emptyset$.

EJEMPLO

¿CUAL ES EL CONJUNTO DE ELEMENTOS, X, TALES QUE $2X=7$ Y X ES ENTERO?

SOLUCION :- ES EL CONJUNTO VACIO, $\emptyset$.

A $\emptyset$ SE LE CONSIDERA COMO SUBCONJUNTO DE CUALQUIER CONJUNTO. ASI, POR EJEM, TODOS LOS SUBCONJUNTOS DEL CONJUNTO

$S =\{2,5,10\}$ SON: $\{2\};\{5\};\{10\};\{2,5\};\{2,10\};\{5,10\};\{2,5,10\}$ Y $\emptyset$.

ESPACIO DE EVENTOS.

ASOCIADO A UN EXPERIMENTO SIEMPRE HAY UN CONJUNTO DE RESULTADOS POSIBLES; A DICHO CONJUNTO SE LE LLAMA *ESPACIO DE EVENTOS*.

EJEMPLOS

EL ESPACIO DE EVENTOS ASOCIADO AL EXPERIMENTO DE LANZAR UN DADO Y ANOTAR LA CARA QUE QUEDA HACIA ARRIBA ES

$S =\{1,2,3,4,5,6\}$

EL ESPACIO DE EVENTOS CORRESPONDIENTE AL EXPERIMENTO DE LANZAR DOS DADOS Y ANOTAR LOS NUMEROS QUE QUEDAN HACIA ARRIBA ES

$$S=\left\{\begin{array}{l}(1,1),(1,2),(1,3),(1,4),(1,5),(1,6)\\(2,1),(2,2),(2,3),(2,4),(2,5),(2,6)\\(3,1),(3,2),(3,3),(3,4),(3,5),(3,6)\\(4,1),(4,2),(4,3),(4,4),(4,5),(4,6)\\(5,1),(5,2),(5,3),(5,4),(5,5),(5,6)\\(6,1),(6,2),(6,3),(6,4),(6,5),(6,6)\end{array}\right\}.$$

SI EN ESTE EXPERIMENTO LA OBSERVACION DE INTERES FUESE LA SUMA DE LOS DOS NUMEROS OBSERVADOS, ENTONCES EL ESPACIO DE EVENTOS DEL EXPERIMENTO SERIA

$$S=\{2,3,4,5,6,7,8,9,10,11,12\}$$

A TODO SUBCONJUNTO DE UN ESPACIO DE EVENTOS SE LE LLAMA *EVENTO*. A LOS EVENTOS QUE TIENEN UN SOLO ELEMENTO DEL ESPACIO SE LES LLAMA *EVENTOS SIMPLES*.

SI AL REALIZAR UN EXPERIMENTO SE OBSERVA UN ELEMENTO DEL EVENTO A, ENTONCES SE DICE QUE *OCURRIO* O *SE VERIFICO* EL EVENTO A. POR EJEMPLO, SI A={2,4} Y AL LANZAR UN DADO SE OBSERVA EL 2 O 4, SE DICE QUE OCURRIO EL EVENTO A; SI SE OBSERVA CUALQUIER OTRO NUMERO, ENTONCES SE DICE QUE *NO* OCURRIO A.

ESPACIOS DE EVENTOS

- *DISCRETOS*:- SI SUS ELEMENTOS PUEDEN NUMERARSE O CONTARSE. TIENEN UN NUMERO FINITO O INFINITO NUMERABLE DE ELEMENTOS.
- *CONTINUOS*:- SI SUS ELEMENTOS *NO* PUEDEN ENUMERARSE. TIENEN UN NUMERO INFINITO NO NUMERABLE DE ELEMENTOS

EJEMPLO

LOS ESPACIOS DE EVENTOS S_1={CARA, CRUZ}; S_2={1,2,3,4,5,6,}; S_3={VERDE, ROJO} SON DISCRETOS. LOS ESPACIOS DE EVENTOS S_4={X: $-\infty<X\leq 0$}; S_5={Z: $Z\geq 3$}; S_6={Y: $3\leq Y\leq 80$} SON CONTINUOS.

EJEMPLO

¿QUE TIPOS DE ESPACIOS DE EVENTOS CORRESPONDEN A LOS SIGUIENTES EXPERIMENTOS?

A) CONTEO DEL NUMERO DE GRANOS DE UNA MAZORCA DE MAIZ

S={0,1,2,3,...,∞}, ES DISCRETO E INFINITO

B) MEDICION DE LA LONGITUD DE UNA ESPIGA DE TRIGO

S={X: $0<X<\infty$},X EN CM, ES CONTINUO E INFINITO

C) MEDICION DEL EFECTO DE UNA VACUNA, EN TERMINOS DE "EXITO" O "FRACASO"

S={EXITO, FRACASO} ES DISCRETO Y FINITO.

D) MEDICION DEL CONTENIDO DE UN ANTIBIOTICO EN UNA CAPSULA

S={Y: $0\leq Y<\infty$}, Y en mg, ES CONTINUO E INFINITO.

COMPLEMENTO DE UN EVENTO

EL *COMPLEMENTO* DE UN EVENTO A ES OTRO EVENTO QUE CONTIENE TODOS LOS ELEMENTOS DEL ESPACIO DE EVENTOS CORRESPONDIENTE QUE NO ESTAN EN A. USUALMENTE SE DENOTA CON UNA TILDE SOBRE EL SIMBOLO QUE CORRESPONDE AL EVENTO QUE COMPLEMENTA, $\bar{A}$.

EJEMPLOS

SI S={1,2,3,4,5,6} Y A={1,3,5} ENTONCES $\bar{A}$={2,4,6}.

SI S={X: $0\leq X\leq 58$} Y A={X: $3<X\leq 17$}, ENTONCES $\bar{A}$={X: $0\leq X\leq 3$, $17<X\leq 58$}

EVENTOS MUTUAMENTE EXCLUSIVOS

CUANDO DOS O MAS EVENTOS NO PUEDEN OCURRIR SIMULTANEAMENTE AL REALIZAR UNA SOLA VEZ UN EXPERIMENTO, SE DICE QUE ESTOS SON *MUTUAMENTE EXCLUSIVOS*, ES DECIR, DOS EVENTOS SON MUTUAMENTE EXCLUSIVOS CUANDO NO TIENEN NI UN SOLO ELEMENTO EN COMUN.

EJEMPLO

A) CUALQUIER EVENTO Y SU COMPLEMENTO SON MUTUAMENTE EXCLUSIVOS.

B) ¿SON $E=\{Y: 0 \leq Y \leq 25\}$ Y $A=\{2,50,100\}$ MUTUAMENTE EXCLUSIVOS?
NO, PORQUE TIENEN EL ELEMENTO 2 EN COMUN.

OPERACIONES CON EVENTOS

UNION

LA *UNION* DE DOS EVENTOS ES OTRO EVENTO CUYOS ELEMENTOS SON TODOS LOS DE AMBOS. LA OPERACION DE UNION SE DENOTA CON EL SIMBOLO U.

EJEMPLOS

A) SI $A=\{2,4,6\}$ Y $B=\{1,6,12\}$, ENTONCES
$G=AUB=\{1,4,6,12,2\}$

B) ¿SON A Y B MUTUAMENTE EXCLUSIVOS? NO PORQUE TIENEN EL 6 EN COMUN.

C) SI $D=\{Y: 0 \leq Y \leq 13\}$ Y $E=\{Y: 20 \leq Y \leq 50\}$,
ENTONCES
$DUE=\{Y: 0 \leq Y \leq 13,\ 20 \leq Y \leq 50\}$

D) SI $F=\{Y: 8 \leq Y \leq 20\}$, ENTONCES
$DUF=\{Y;\ 0 \leq Y \leq 20\}$.

E) SI $G=\{Y: 3 \leq Y \leq 10\}$, ENTONCES
$DUG=\{Y: 0 \leq Y \leq 13\}=D$; OBSERVESE QUE EN ESTE CASO GCD. EN GENERAL, SI ACB, ENTONCES AUB=B.

EN GENERAL, LA UNION DE VARIOS EVENTOS ES OTRO EVENTO CUYOS ELEMENTOS SON TODOS LOS DE LOS EVENTOS QUE SE UNEN.

EJEMPLO

AUBUF = K = {1,2,4,6, y: 8≤ y ≤20}

INTERSECCION

LA *INTERSECCION* DE DOS EVENTOS ES EL CONJUNTO DE ELEMENTOS QUE PERTENECEN SIMULTANEAMENTE A AMBOS. PARA DENOTAR LA OPERACION DE INTERSECCION SE USA EL SIMBOLO ∩ .

EJEMPLOS

A) A = {2,3,6} Y B = {2,6,10} ENTONCES A∩B = C = {2,6}

B) D = {Y: 4≤Y≤5}, ENTONCES A∩D = ∅.

OBSERVESE QUE EN ESTE EJEMPLO A Y D SON MUTUAMENTE. EXCLUSIVOS, YA QUE *NO* TIENEN NINGUN ELEMENTO EN COMUN. SIEMPRE QUE DOS EVENTOS SON MUTUAMENTE EXCLUSIVOS, SU INTERSECCION ES EL CONJUNTO VACIO.

EN GENERAL, LA *INTERSECCION* DE VARIOS EVENTOS ES EL CONJUNTO DE ELEMENTOS QUE TODOS ELLOS TIENEN EN COMUN.

EJEMPLO

SI A = {2,3,6,8}; B={2,3,10,100}; C={Y: 0≤Y≤5} Y D={Y: 2≤Y≤4}, ENTONCES

A∩B∩C∩D = E ={2,3}

AUBUCUD = F ={Y: 0≤Y≤5, 6,8,10,100}

LA OCURRENCIA DE UN EVENTO "Y" OTRO IMPLICA LA OCURRENCIA DE AMBOS A LA VEZ, ES DECIR, QUE SE VERIFIQUE LA *INTERSECCION*. LA OCURRENCIA DE UN EVENTO "O" ALGUN OTRO, IMPLICA LA OCURRENCIA DE CUALQUIERA DE ELLOS, ES DECIR DE LA *UNION*.

DIAGRAMAS DE VENN

UNA MANERA DE ILUSTRAR GRAFICAMENTE LAS OPERACIONES CON CONJUNTOS ES MEDIANTE LOS *DIAGRAMAS DE VENN*. EN ESTOS, CADA CONJUNTO SE REPRESENTA POR UNA CURVA CERRADA QUE ENCIERRA LOS ELEMENTOS QUE LE CORRESPONDEN.

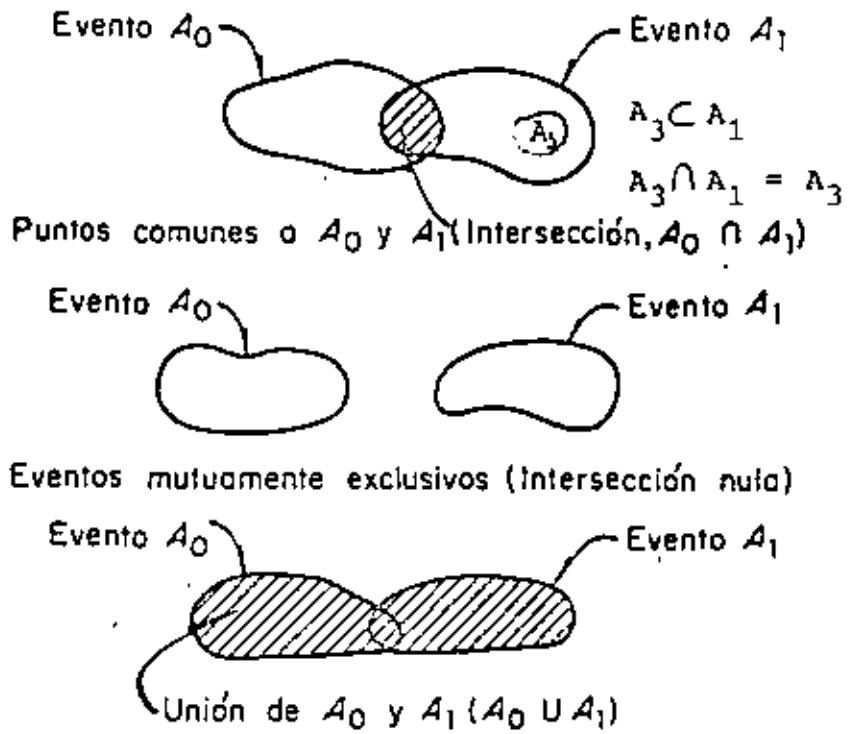

Diagramas de Venn (unión e intersección de eventos)

EVENTOS COLECTIVAMENTE EXHAUSTIVOS

SE DICE QUE LOS EVENTOS B_1, B_2, ..., B_n SON COLECTIVAMENTE EXHAUSTIVOS CUANDO LA UNION DE TODOS ELLOS ES IGUAL AL ESPACIO DE EVENTOS, ES DECIR, SI

$$B_1 \cup B_2 \cup \ldots \cup B_N = S$$

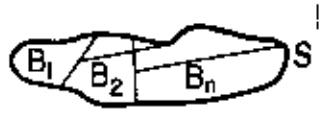

TEORIA DE PROBABILIDADES

AL LANZAR UNA MONEDA NO PODEMOS PREDECIR CON CERTEZA CUAL CARA QUEDARA HACIA ARRIBA. LO UNICO QUE SE PUEDE ASEGURAR, SI LA MONEDA NO ESTA CARGADA, ES QUE AMBAS CARAS TIENEN LA MISMA OPORTUNIDAD DE SALIR, ES DECIR, QUE LOS EVENTOS SIMPLES (CARA) Y (CRUZ) TIENEN LA MISMA PROBABILIDAD DE OCURRIR.

COMO YA SE DIJO, LA PROBABILIDAD DE QUE OCURRA UN EVENTO ES UNA MEDIDA DEL GRADO DE CONFIANZA QUE SE TIENE DE QUE ESTE OCURRA AL REALIZAR EL EXPERIMIENTO CORRESPONDIENTE.

AXIOMAS DE LA TEORIA DE PROBABILIDADES

LAS PROBABILIDADES QUE SE ASIGNAN A LOS DIFERENTES EVENTOS RELACIONADOS CON UN FENOMENO ALEATORIO DEBEN CUMPLIR CON LOS SIGUIENTES TRES AXIOMAS:

AXIOMA 1: LA PROBABILIDAD DE OCURRENCIA DE UN EVENTO A ES UN NUMERO, P(A), QUE SE LE ASIGNA A DICHO EVENTO, CUYO VALOR QUEDA EN EL INTERVALO

$$0 \leq P(A) \leq 1$$

AXIOMA 2: SI S ES UN ESPACIO DE EVENTOS, ENTONCES

$$P(S) = 1$$

AXIOMA 3: LA PROBABILIDAD, P(C), DE LA UNION, C, DE DOS EVENTOS MUTUAMENTE EXCLUSIVOS, A Y B, ES IGUAL A LA SUMA DE LAS PROBABILIDADES DE ESTOS, ES DECIR,

$$P(A \cup B) = P(C) = P(A) + P(B)$$

LEY GENERAL DE LA ADICION

SI TODOS LOS EVENTOS E_i SON MUTUAMENTE EXCLUSIVOS ENTRE SI, EL AXIOMA 3 SE GENERALIZA A:

$$P(E_1 \cup E_2 \cup \ldots \cup E_k) = P(E_1) + P(E_2) + \ldots + P(E_k)$$

ASIGNACION DE PROBABILIDADES

EXISTEN POR LO MENOS CUATRO MANERAS DE ASIGNARLE UNA PROBABILIDAD A UN EVENTO:

1. APLICANDO LA DEFINICION CLASICA DE PROBABILIDADES.
2. EN TERMINOS DE LOS RESULTADOS DE REPETIR VARIAS VECES UN EXPERIMENTO (METODO FRECUENCIAL).
3. CON BASE EN UN MODELO MATEMATICO (PROBABILISTICO) DEL FENOMENO DE QUE SE TRATE.
4. MADIANTE UN ANALISIS SUBJETIVO DEL PROBLEMA.

DEFINICION CLASICA DE PROBABILIDADES

SI M(A) ES EL NUMERO DE MANERAS *IGUALMENTE PROBABLES* EN QUE PUEDE OCURRIR EL EVENTO A Y M ES EL NUMERO TOTAL DE ELEMENTOS DEL ESPACIO DE EVENTOS CORRESPONDIENTE, ENTONCES LA PROBABILIDAD DE A ES

$$P(A) = \frac{M(A)}{M}$$

EJEMPLOS

A) SI EN UNA URNA SE TIENEN 5 BOLAS BLANCAS Y 15 NEGRAS, Y SE VA A SELECCIONAR UNA AL AZAR, ¿CUAL ES LA PROBABILIDAD DE QUE SEA BLANCA(A={BLANCA})?:

$M = 5+15=20$; $M(A)=5 \Rightarrow P(A)=\frac{5}{20}=\frac{1}{4}$

B) SI SE LANZAN DOS DADOS, ¿CUAL ES LA PROBABILIDAD DE QUE

1. SALGA UN 2 Y UN 5 (EVENTO B)?
2. LA SUMA SEA 7 (EVENTO A)

PARA EL INCISO 1 EL ESPACIO DE EVENTOS ES:

$$S = \begin{Bmatrix} (1,1) & (1,2) & (1,3) & (1,4) & (1,5) & (1,6) \\ (2.1) & (2,2) & (2,3) & (2,4) & (2,5) & (2,6) \\ (3,1) & (3,2) & (3,3) & (3,4) & (3,5) & (3,6) \\ (4,1) & (4,2) & (4,3) & (4,4) & (4,5) & (4,6) \\ (5,1) & (5,2) & (5,3) & (5,4) & (5,5) & (5,6) \\ (6,1) & (6,2) & (6,3) & (6,4) & (6,5) & (6,6) \end{Bmatrix}$$

SI EL DADO NO ESTA CARGADO, CADA PAREJA DE NUMEROS ES IGUALMENTE PROBABLE. EN TAL CASO, $M=36$ y $M(B)=2$ (APARECE (2,5) O (5,2)) $\Rightarrow P(B)=2/36=1/18$.

PARA EL INCISO 2 EL ESPACIO DE EVENTOS ES

$S_1=\{2,3,4,5,6,7,8,9,10,11,12\}$

PERO NO TODOS LOS ELEMENTOS (EVENTOS SIMPLES) SON IGUALMENTE PROBA-

BLES, YA QUE, POR EJEMPLO, EL 2 SOLO APARECERA SI SE OBSERVA LA PAREJA (1,1), EN CAMBIO EL 3 APARECERA SI OCURREN LAS PAREJAS - (1,2) O (2,1), ES DECIR, EL 3 TIENE EL DOBLE DE PROBABILIDAD QUE EL 2. POR ESTO, PARA CALCULAR LA PROBABILIDAD DE QUE LA SUMA - SEA 7 ES NECESARIO TRABAJAR CON EL ESPACIO S Y CONTAR LAS MANERAS POSIBLES DE QUE LA SUMA SEA 7, LO CUAL OCURRE SI SE OBSERVA CUALQUIERA DE LAS PAREJAS (6,1), (5,2), (4,3), (3,4), (2,5) o - (1,6), ES DECIR, HAY 6 MANERAS IGUALMENTE PROBABLES DE QUE OCURRA EL EVENTO A. POR LO TANTO

$$P(A) = \frac{M(A)}{M} = \frac{6}{36} = \frac{1}{6}$$

PROCEDIENDO DE ESTA MANERA SE PUEDEN CALCULAR LAS PROBABILIDADES DE QUE LA SUMA SEA 2,3,4, ETC. LOS RESULTADOS SON:

$$\left.\begin{array}{l} P(\{2\}) = \frac{1}{36};\ P(\{3\}) = \frac{2}{36};\ P(\{4\}) = \frac{3}{36};\ P(\{5\}) = \frac{4}{36}; \\ P(\{6\}) = \frac{5}{36};\ P(\{7\}) = \frac{6}{36};\ P(\{8\}) = \frac{5}{36};\ P(\{9\}) = \frac{4}{36}; \\ P(\{10\}) = \frac{3}{36};\ P(\{11\}) = \frac{2}{36} \text{ y } P(\{12\}) = \frac{1}{36} \end{array}\right\} \text{DISTRIBUCION DE PROBABILIDADES}$$

OBSERVESE QUE $\sum_{i=2}^{12} P(\{i\}) = 1$.

METODO FRECUENCIAL

SI N(A) ES EL NUMERO DE VECES QUE SE OBSERVA EL EVENTO A (LA FRECUENCIA DE A) AL REALIZAR N VECES UN EXPERIMENTO, LA FRECUENCIA RELATIVA DE A, DEFINIDA COMO N(A)/N, SE CONSIDERA COMO ESTIMACION DE LA PROBABILIDAD DE A, ES DECIR:

$$P(A) = \frac{N(A)}{N}$$

YA QUE, EN EL LIMITE, $P(A) = \lim_{N \to \infty} \frac{N(A)}{N}$.

EJEMPLO

DE UNA URNA QUE CONTIENE BOLAS ROJAS, BLANCAS Y AZULES, SE SACO UNA BOLA, SE ANOTO SU COLOR Y SE REGRESO A LA URNA. SI ESTE EXPERIMENTO SE REPITE 20 VECES Y LOS RESULTADOS SON

b,b,a,r,r,r,a,b,r,a,b,b,a,r,b,r,r,a,r,a, DONDE

r = ROJA, b = BLANCA, a = AZUL.

¿QUE PROBABILIDADES LE ASIGNARIA A LOS EVENTOS B = {b}, A = {a}, y R = {r}, DE ACUERDO CON EL METODO FRECUENCIAL?

EN ESTA MUESTRA SE TIENE QUE N(B)=6, N(A)=6, N(R)=8, N=20

POR LO QUE $P(B) = \frac{6}{20} = \frac{3}{10}$; $P(A) = \frac{6}{20} = \frac{3}{10}$; $P(R) = \frac{8}{20} = \frac{4}{10}$.

NOTESE QUE LOS EVENTOS B, A Y R SON MUTUAMENTE EXCLUSIVOS, YA QUE SON EVENTOS SIMPLES, Y QUE

$$P(B) + P(A) + P(R) = \frac{3}{10} + \frac{3}{10} + \frac{4}{10} = 1 = P(S)$$

EN DONDE S = {r,b,a,}.

EJEMPLO

EN UN LABORATORIO SE PROBARON 100 VIGAS DE CONCRETO REFORZADO NOMINALMENTE IDENTICAS, Y SE ANOTARON LAS CARGAS CON LAS CUALES FALLO CADA UNA. DE ESTA SUCESION DE EXPERIMENTOS SE ASIGNARON, EN TERMINOS DE LAS FRECUENCIAS RELATIVAS CORRESPONDIENTES, LAS SIGUIENTES PROBABILIDADES, CON N(A) = 17, N(B) = 24, N(C) = 27, N(D) = 13, N(E) = 11, N(F) = 8, Y N = 100:

SI A = {X: $0<X\leq 20$ ton}; P (A) = 0.17 (17/100)

SI B = {X: $20<X\leq 40$ ton}; P (B) = 0.24 (24/100)

SI C = {X: $40<X\leq 60$ ton}: P (C) = 0.27 (27/100)

SI D = {X: $60<X\leq 80$}; P (D) = 0.13 (13/100)

SI E = {X: $80<X\leq 100$}; P (E) = 0.11 (11/100)

SI F = {X: $100\leq X$}; P (F) = 0.08 (8/100)

$\Sigma P(.) = 1.00$

SI SE REALIZA UNA VEZ MAS EL EXPERIMENTO, CALCULEMOS LAS SIGUIENTES PROBABILIDADES:

A) QUE LA RESISTENCIA SEA MENOR O IGUAL QUE 80 TON. PUESTO QUE G = {X: $0<X\leq 80$ ton} SE TIENE QUE G= AUBUCUD, POR LO QUE

$P(G) = P(A) + P(B) + P(C) + P(D) = 0.17 + 0.24 + 0.27 + 0.13 = 0.81$

B) LA PROBABILIDAD QUE RESISTA MAS DE 60 TONS. PUESTO QUE

H = {X: $60<X\leq\infty$} O H={X: $X>60$} SE TIENE QUE H = DUEUF, POR LO QUE $P(H) = P(D) + P(E) + P(F) = 0.13 + 0.11 + 0.08 = 0.32$

C) LA PROBABILIDAD QUE RESISTA MAS DE 40 TON, PERO CUANDO MUCHO 100 TON.

PUESTO QUE $I = \{X: 40<X\leq 100$ SE TIENE QUE I = CUDUE

POR LO QUE $P(I) = P(C) + P(D) + P(E) = 0.27 + 0.13 + 0.11 = 0.51$

ASIGNACION DE PROBABILIDADES MEDIANTE UN MODELO MATEMATICO

MEDIANTE ESTE METODO LAS PROBABILIDADES SE ASIGNAN A PARTIR DE UN MODELO MATEMATICO QUE INVOLUCRE TODOS LOS FACTORES POSIBLES QUE INTERVIENEN EN LA ALEATORIEDAD DEL FENOMENO.

ASIGNACION DE PROBABILIDADES MEDIANTE UN ANALISIS SUBJETIVO DEL PROBLEMA.

EN ESTE CASO LAS PROBABILIDADES SE ASIGNAN DE MANERA SUBJETIVA, CON BASE EN LA EXPERIENCIA QUE SE TENGA SOBRE UN PROBLEMA SEMEJANTE, PROPIA O AJENA, DE CARACTER TEORICO O EXPERIMENTAL.

TEOREMAS

DOS TEOREMAS IMPORTANTES QUE SE DEDUCEN A PARTIR DE LOS AXIOMAS SON:

TEOREMA 1.

SI A ES UN EVENTO DEL ESPACIO S, ENTONCES $P(\bar{A}) = 1-P(A)$

DEMOSTRACION

PUESTO QUE A Y $\bar{A}$ SON MUTUAMENTE EXCLUSIVOS

Y ADEMAS $A \cup \bar{A} = S$, ENTONCES $P(S) = P(A) + P(\bar{A}) = 1$

$\Rightarrow P(\bar{A}) = 1-P(A)$

CASO PARTICULAR: PUESTO QUE $P(\bar{S})=1-P(S)=0$ Y $S=\emptyset$, SE TIENE QUE $P(\emptyset) = 0$.

TEOREMA 2.

SI A Y B SON DOS EVENTOS CUALQUIERA DE S, ENTONCES

$$P(A \cup B) = P(A) + P(B) - P(A \cap B)$$

DEMOSTRACION

SEA EL DIAGRAMA DE VENN:

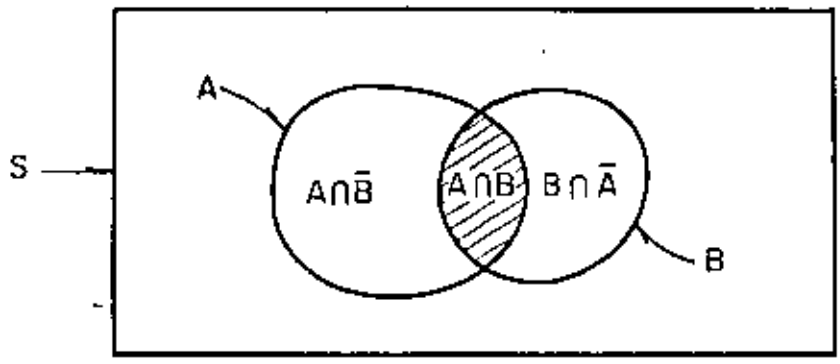

$A \cup B = (A \cap B) \cup (A \cap \bar{B}) \cup (B \cap \bar{A})$. PUESTO QUE $A \cap B$, $A \cap \bar{B}$ Y $B \cap \bar{A}$ SON MUTUAMENTE EXCLUSIVOS, SE TIENE QUE $P(A \cup B) = P(A \cap B) + P(A \cap \bar{B}) + P(B \cap \bar{A})$.

SUMANDO Y RESTANDO $P(A \cap B)$ Y AGRUPANDO TERMINOS SE OBTIENE

$$P(A \cup B) = [P(A \cap B) + P(A \cap \bar{B})] + [P(A \cap B) + P(B \cap \bar{A})] - P(A \cap B)$$

PERO $A = (A \cap \bar{B}) \cup (A \cap B) \Rightarrow P(A \cap B) + P(A \cap \bar{B}) = P(A)$

Y $B = (A \cap B) \cup (B \cap \bar{A}) \Rightarrow P(A \cap B) + P(B \cap \bar{A}) = P(B)$, POR LO QUE FINALMENTE

$$P(A \cup B) = P(A) + P(B) - P(A \cap B).$$

TEOREMA DE LA PROBABILIDAD TOTAL

SE DICE QUE UN GRUPO DE EVENTOS ES *COLECTIVAMENTE EXHAUSTIVO* SI LA UNION DE TODOS ELLOS ES EL ESPACIO DE EVENTOS CORRESPONDIENTE.

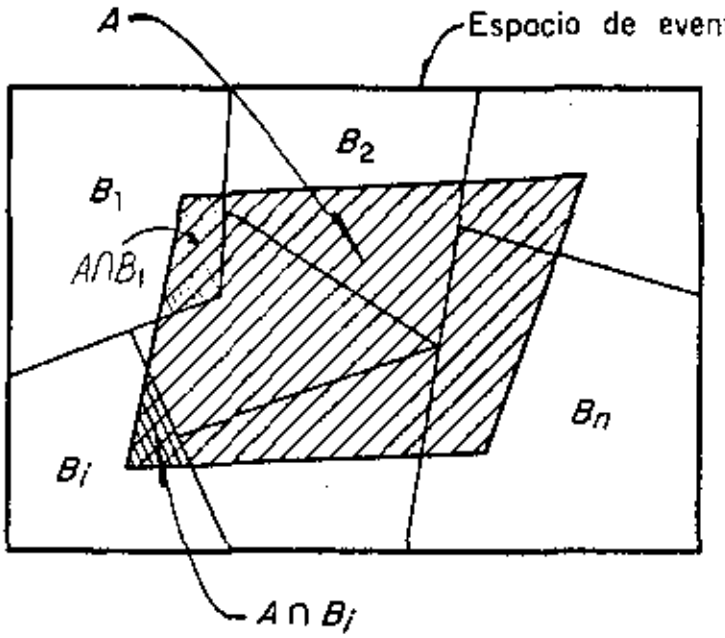

$B_1 \cup B_2 \cup \ldots \cup B_n = S$

EN UN GRUPO DE EVENTOS COLECTIVAMENTE EXHAUSTIVOS Y MUTUAMENTE EXCLUSIVOS, $B_1, B_2, \ldots, B_n$, SI A ES UN EVENTO CUALQUIERA DEFINIDO EN EL MISMO ESPACIO, ENTONCES, APLICANDO EL AXIOMA 3, RESULTA

$$P(A) = P(A \cap B_1) + P(A \cap B_2) + \ldots + P(A \cap B_n) = \sum_{i=1}^{i=n} P(A \cap B_i)$$

YA QUE LOS EVENTOS $A \cap B_i$ SON MUTUAMENTE EXCLUSIVOS Y $(A \cap B_1) \cup (A \cap B_2) \cup \ldots = A$

TOMANDO EN CUENTA QUE $P(A \cap B_i) = P(B_i)P(A|B_i)$, SE OBTIENE FINALMENTE LA ECUACION

$$P(A) = \sum_{i=1}^{i=n} P(B_i)P(A|B_i)$$

CON LA CUAL SE DEFINE EL LLAMADO *TEOREMA DE LA PROBABILIDAD TOTAL.*

TEOREMA DE BAYES

CONSIDERANDO QUE $P(B_j \cap A) = P(A \cap B_j)$, SE TIENE QUE

$$P(B_j|A) = \frac{P(B_j \cap A)}{P(A)} = \frac{P(A \cap B_j)}{P(A)}$$

DE DONDE

$$P(B_j|A) = \frac{P(B_j)P(A|B_j)}{\sum_{i=1}^{i=n} P(B_i)P(A|B_i)}$$

ESTE RESULTADO SE CONOCE COMO *TEOREMA DE BAYES*. A LAS PROBABILIDADES $P(B_j)$ QUE SE ASIGNAN A LOS EVENTOS B_j ANTES DE OBSERVAR EL EVENTO A, SE LES DENOMINA A *PRIORI O PREVIAS;* A LAS PROBABILIDADES $P(B_j|A)$ QUE SE OBTIENEN DESPUES DE OBSERVAR EL EVENTO A, SE LES LLAMA A *POSTERIORI O POSTERIORES.*

EJEMPLO

EN UNA FABRICA SE RECIBEN REGULADORES DE VOLTAJE DE DOS PROVEEDORES, B_1 Y B_2, EN PROPORCION DE 3 A 1; ES DECIR, LA PROBABILIDAD DE QUE UN REGULADOR TOMADO AL AZAR PROVENGA DEL PROVEEDOR B_1 ES $P(B_1)=3/4$, Y DEL B_2 ES $P(B_2)=1/4$.

SUPONGAMOS ADEMAS QUE EL CONTROL DE CALIDAD DEL PROVEEDOR B_1 ES MEJOR QUE EL DE B_2, DE MANERA QUE EL 95% DE LOS REGULADORES DE B_1 TRABAJAN BIEN, Y SOLO EL 80% DE LOS DE B_2 FUNCIONAN CORRECTAMENTE. CALCULEMOS LA PROBABILIDAD DE QUE UN REGULADOR TOMADO AL AZAR FUNCIONE BIEN (EVENTO A):

$$P(A|B_1) = 0.95;\ P(A|B_2) = 0.80$$

DEL TEOREMA DE LA PROBABILIDAD TOTAL:

$$P(A) = P(A|B_1)P(B_1)+P(A|B_2)P(B_2)$$

$$= 0.95 \times \frac{3}{4} + 0.80 \times \frac{1}{4} = 0.9125$$

EJEMPLO

SUPONGAMOS AHORA QUE LA PREGUNTA DEL PROBLEMA SE CAMBIA A: ¿CUAL ES LA PROBABILIDAD DE QUE UN REGULADOR TOMADO AL AZAR PROVENGA DEL PROVEEDOR B_1, SI SE HIZO UNA PRUEBA DEL REGULADOR Y SE OBSERVO QUE FUNCIONA CORRECTAMENTE?

APLICANDO EL TEOREMA DE BAYES:

$$P(B_1|A) = \frac{P(B_1)\ P(A|B_1)}{P(B_1)P(A|B_1)+P(B_2)P(A|B_2)} \; ; \; P(B_1) = \frac{3}{4} \; , \; P(B_2) = \frac{1}{4}$$

$$= \frac{\frac{3}{4} \times 0.95}{\frac{3}{4} \times 0.95 + \frac{1}{4} \times 0.80} = \frac{2.85}{3.65} = 0.78$$

ADEMAS

$$P(B_2|A) = \frac{P(B_2)\ P(A|B_2)}{\frac{3.65}{4}} = \frac{\frac{1}{4} \times 0.80}{\frac{3.65}{4}} = 0.22$$

OBSERVESE QUE

$$P(B_1|A) + P(B_2|A) = 0.78 + 0.22 = 1.00$$

EJEMPLO

SUPONGASE QUE UNA PRUEBA PARA DETECTAR DIABETES TIENE UNA EFICIENCIA DEL 95%, ES DECIR, SOLO EN EL 95% DE LOS CASOS SE DETECTA CON ELLA LA DIABETES EN UNA PERSONA QUE LA PADECE. SUPONGASE TAMBIEN QUE EL 2% DE LAS PRUEBAS QUE RESULTAN POSITIVAS SON DE GENTE SANA, Y QUE EL 3 % DE LA POBLACION DE UNA REGION DE MEXICO PADECE ESTA ENFERMEDAD.

a) ¿CUAL ES LA PROBABILIDAD DE QUE UNA PERSONA SELECCIONADA AL - AZAR PUEDA SER DECLARADA DIABETICA POR LA PRUEBA?

b) SI LA PRUEBA DICE QUE SI ES DIABETICA, ¿CUAL ES LA PROBABILIDAD DE QUE REALMENTE LO SEA?

SOLUCION

B_1 = {TIENE DIABETES}; B_2 = {NO TIENE DIABETES}; $S = \{B_1, B_2\}$

E = {LA PRUEBA DETECTA DIABETES}

$P(B_1) = 0.03$, $P(B_2) = 0.97$

$P(E|B_1) = 0.95$, $P(E|B_2) = 0.02$

a) $P(E) = P(E|B_1)P(B_1) + P(E|B_2)P(B_2)$

$= 0.95 \times 0.03 + 0.02 \times 0.97 = 0.0479$

b) $$P(B_1|E) = \frac{P(B_1)P(E|B_1)}{P(B_1)P(E|B_1)+P(B_2)P(E|B_2)}$$

$$= \frac{0.03 \times 0.95}{0.03 \times 0.95 + 0.97 \times 0.02} = 0.59$$

EJEMPLO

TRES MAQUINAS A, B Y C PRODUCEN EL 50, 20 Y 30 %, RESPECTIVAMENTE, DEL TOTAL DE ARTICULOS QUE PRODUCE UNA FABRICA. LOS PORCENTAJES DE DEFECTUOSOS QUE CADA MAQUINA ELABORA SON 1, 3 Y 5, RESPECTIVAMENTE. SI SE SELECCIONO UN ARTICULOS AL AZAR Y RESULTO DEFECTUOSO, CALCULAR LAS PROBABILIDADES DE QUE HAYA SIDO PRODUCIDO POR CADA UNA DE LAS MAQUINAS.

Solución

Sea D= {ARTICULOS DEFECTUOSOS}; ENTONCES

$$P(A|D) = \frac{P(A)\ P(D|A)}{P(A)\ \ P(D|A) + P(B)\ \ P(D|B) + P(C)\ P(D|C)}$$

CON $P(A)= 0.5$, $P(B)= 0.2$, $P(C)= 0.3$, $P(D|A)= 0.01$,

$P(D|B)= 0.03$ Y $P(D|C)= 0.05$

SE OBTIENE

$$P(A|D) = \frac{0.5 \times 0.01}{0.5 \times 0.01 + 0.2 \times 0.03 + 0.3 \times 0.05} = \frac{0.005}{0.026} = 0.19$$

ANALOGAMENTE,

$$P(B|D) = \frac{0.2 \times 0.03}{0.026} = \frac{0.006}{0.026} = 0.23$$

$$P(C|D) = \frac{0.3 \times 0.05}{0.026} = \frac{0.015}{0.026} = 0.58$$

OBSERVESE QUE

$$P(A|D) + P(B|D) + P(C|D) = 0.19 + 0.23 + 0.58 = 1.00$$

VARIABLES ALEATORIAS

CLASIFICACION DE VARIABLES

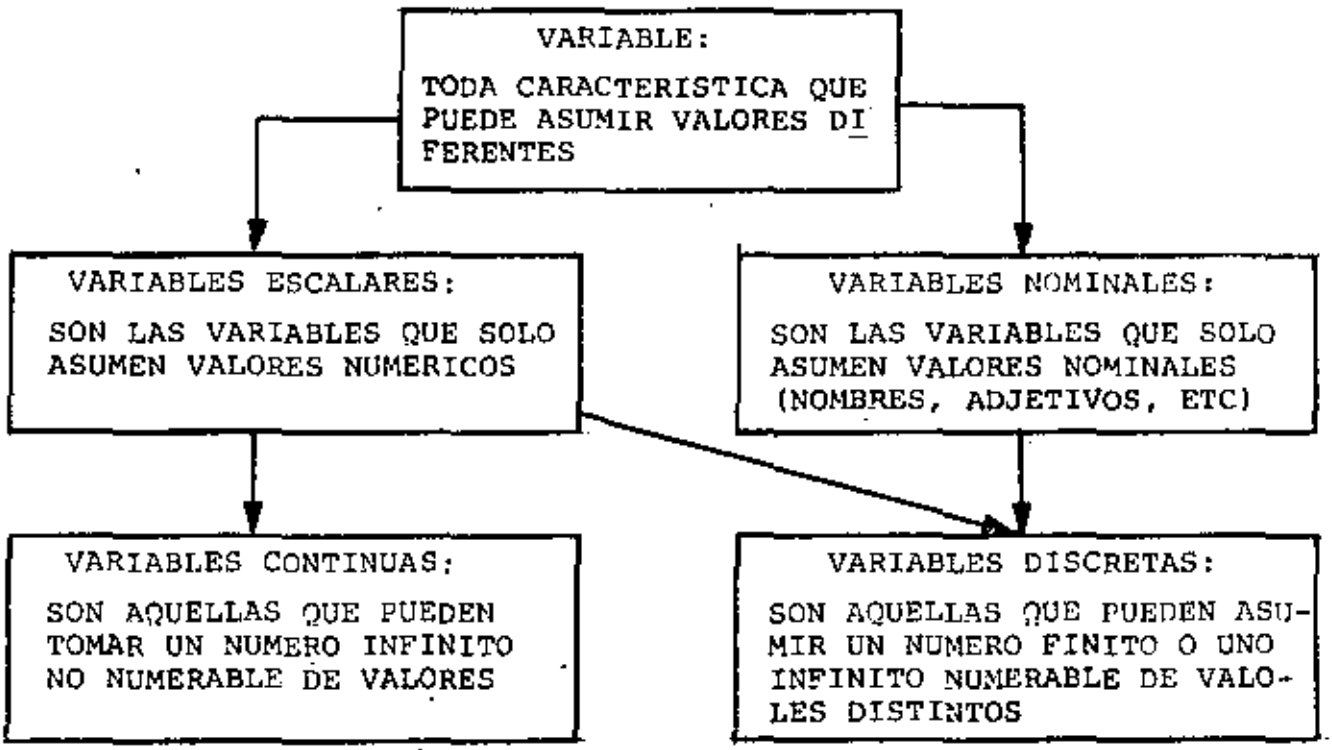

UNA *VARIABLE ALEATORIA* ES UNA VARIABLE TAL QUE NO PUEDE PREDECIRSE CON CERTEZA EL VALOR QUE ASUMIRA AL REALIZAR UN EXPERIMENTO. POR EJEMPLO, LA RESISTENCIA O CARGA DE FALLA DE UNAS VIGAS ES UNA VARIABLE ALEATORIA, YA QUE ANTES DE ROMPER UNA VIGA TOMADA AL AZAR NO SE PUEDE PRECISAR CUAL SERA SU RESISTENCIA. EN LA SIGUIENTE TABLA SE PRESENTAN LOS RESULTADOS EXPERIMENTALES CON 15 VIGAS DE CONCRETO REFORZADO, OBSERVANDOSE QUE ESTOS VARIAN DE UNAS A OTRAS DE MANERA ALEATORIA.

PRUEBAS DE VIGAS DE CONCRETO REFORZADO

Número de la viga	Carga de agrietamiento, en kg , X	Carga de falla, en kg , Y
1	4 700	4 700
2	3 840	4 220
3	3 270	4 360
4	2 310	4 680
5	2 950	4 270
6	4 810	4 810
7	2 720	4 590
8	2 720	4 490
9	4 310	4 310
10	2 950	4 630
11	4 220	4 220
12	2 720	4 340
13	2 720	4 340
14	2 630	4 770
15	2 950	4 630

A TODO EXPERIMENTO SE LE PUEDE ASOCIAR AL MENOS UNA VARIABLE ALEATORIA, DEPENDIENDO ESTA DEL PROBLEMA QUE SE TENGA PLANTEADO. POR EJEMPLO, EN EL CASO DE LA RESISTENCIA DE LAS VIGAS DE VARIABLE ALEATORIA PUEDE SER DIRECTAMENTE DICHA RESISTENCIA, EN CUYO CASO SU ESPACIO DE EVENTOS SERIA

$$S_1 = \{X: 0<X<\infty\}$$

LA VARIABLE TAMBIEN PUDO HABER SIDO UNA CUYO ESPACIO DE EVENTOS FUERA

$$S_2 = \{\text{EXITO, FRACASO}\}$$

EN DONDE EL EXITO OCURRIRIA SI LA VIGA RESISTIERA MAS DE CIERTA CANTIDAD, POR EJEMPLO 4600 KG, Y EL FRACASO OCURRIRIA SI RESISTIERA MENOS, ES DECIR:

EXITO: SI $X \geq 4600$ KG

FRACASO: SI $X < 4600$ KG

LEYES DE PROBABILIDADES

EL COMPORTAMIENTO DE UNA VARIABLE ALEATORIA SE DESCRIBE MEDIANTE SU *LEY DE PROBABILIDADES*, LA CUAL PUEDE ESPECIFICARSE DE DIFERENTES FORMAS. LA MANERA MAS COMUN DE HACERLO ES MEDIANTE SU *DISTRIBUCION O DENSIDAD DE PROBABILIDADES.*

A FIN DE EVITAR CONFUSION, SE EMPLEARA UNA LETRA MAYUSCULA PARA DENOTAR UNA VARIABLE ALEATORIA, Y LA MINUSCULA CORRESPONDIENTE PARA LOS VALORES QUE PUEDE ASUMIR. SI LA VARIABLE ALEATORIA X ES DISCRETA Y PUEDE ASUMIR LOS VALORES x_i, SU DENSIDAD DE PROBABILIDADES, $f_X(x)$ SERA EL CONJUNTO DE LAS PROBABILIDADES

$$P_X(x_i) = P(X = x_i) \qquad i = 1,2,\ldots,n$$

LA CUAL SE LEE "PROBABILIDAD DE QUE $X = x_i$". ESTO ES

$$f_X(x) = (P_X(x_i)) \qquad i = 1,2,\ldots n$$

PARA QUE UNA DENSIDAD DE PROBABILIDADES SATISFAGA LOS TRES AXIOMAS DE LA TEORIA DE PROBABILIDADES, SE DEBEN CUMPLIR LOS SIGUIENTES REQUISITOS

A) $0 \leq P_X(x_i) \leq 1$ PARA TODA x_i

B) $\sum_{i=1}^{n} P_X(x_i) = 1$, DONDE n ES EL NUMERO TOTAL DE VALORES QUE PUEDE ASUMIR X

C) $P(x_m \leq X \leq x_r) = \sum_{i=m}^{i=r} P_X(x_i)$; $m \leq r$, DONDE LAS x_i ESTAN ORDENADAS EN FORMA CRECIENTE, ES DECIR,

$$x_1 < x_2 < x_3 < \ldots < x_n$$

DISTRIBUCION DE PROBABILIDADES ACUMULADAS O FUNCION DE DISTRIBUCION

OTRA FORMA DE ESPECIFICAR LA LEY DE PROBABILIDADES DE UNA VARIABLE ALEATORIA ES MEDIANTE LA DISTRIBUCION DE PROBABILIDADES ACUMULADAS, $F_X(x)$, QUE SE DEFINE COMO EL CONJUNTO DE LAS SUMAS PARCIALES DE LAS PROBABILIDADES, $P_X(x_i)$, CORRESPONDIENTES A TODOS LOS VALORES DE X MENORES O IGUALES QUE x_i. POR LO TANTO, ESTA FUNCION DA LAS PROBABILIDADES DE QUE LA VARIABLE ALEATORIA TOME VALORES MENORES O IGUALES QUE x_m PARA CUALQUIER m, ES DECIR

$$F_X(x) = (F_X(x_m)) \quad ; \quad m = 1,2,\ldots,n$$

EN DONDE

$$F_X(x_m) = \sum_{i=1}^{i=m} P_X(x_i) = P(X \leq x_m) \; ; \; m=1,2,\ldots,n$$

EJEMPLO

SEA X LA VARIABLE ALEATORIA DISCRETA "NUMERO TOTAL DE CARROS QUE SE DETIENEN EN UNA ESQUINA DEBIDO A LA LUZ ROJA DE UN SEMAFORO". SI LAS PROBABILIDADES ASOCIADAS A CADA VALOR, DETERMINADAS POR EL METODO FRECUENCIAL, SON

$$P_X(x) = \begin{cases} 0.1 & \text{SI } x = 0 \\ 0.2 & \text{SI } x = 1 \\ 0.3 & \text{SI } x = 2 \\ 0.2 & \text{SI } x = 3 \\ 0.1 & \text{SI } x = 4 \\ 0.1 & \text{SI } x = 5 \\ 0 & \text{SI } x \geq 6 \end{cases}$$

LA DISTRIBUCION DE PROBABILIDADES Y LA DE PROBABILIDADES ACUMULADAS CORRESPONDIENTES SERAN

x	$f_X(x)$	$F_X(x)$
<0	0	0
0	0.1	0.1
1	0.2	0.3
2	0.3	0.6
3	0.2	0.8
4	0.1	0.9
5	0.1	1.0
≥ 6	0	1.0

O SEA

$$F_X(x) = \begin{cases} 0, & \text{SI } x < 0 \\ 0.1, & \text{SI } 0 \leq x < 1 \\ 0.3, & \text{SI } 1 \leq x < 2 \\ 0.6, & \text{SI } 2 \leq x < 3 \\ 0.8, & \text{SI } 3 \leq x < 4 \\ 0.9, & \text{SI } 4 \leq x < 5 \\ 1.0, & \text{SI } 5 \leq x \end{cases}$$

LAS GRAFICAS DE ESTAS DISTRIBUCIONES SE PRESENTAN EN LA FIGURA DE LA SIGUIENTE HOJA.

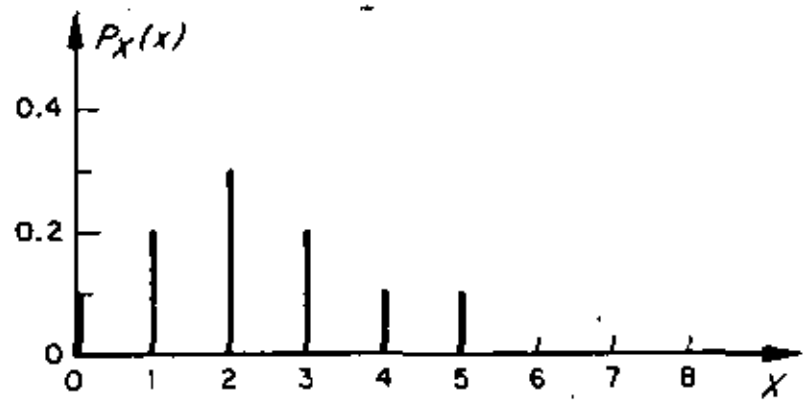

a) Distribución de probabilidades

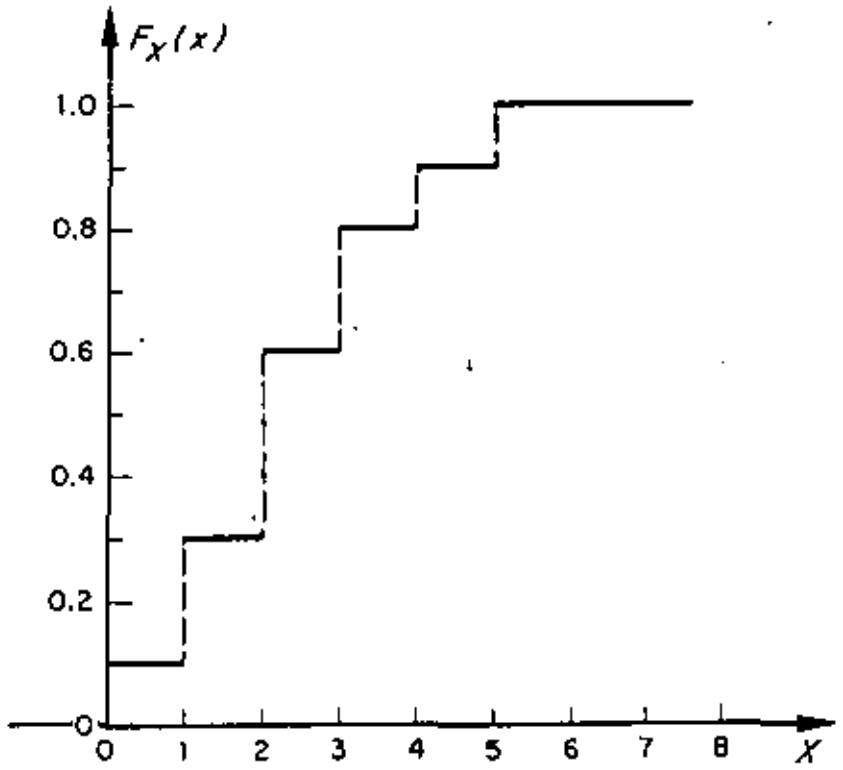

b) Función de distribución

Ley de probabilidades del ejemplo del tráfico

EJEMPLO

SEA LA VARIABLE ALEATORIA X DEFINIDA POR LA SUMA DE LOS DOS NUMEROS QUE QUEDEN HACIA ARRIBA AL LANZAR DOS DADOS. EN ESTE CASO EL ESPACIO DE EVENTOS ES

$$S = \{2,3,4,5,6,7,8,9,10,11,12\}$$

Y LA DENSIDAD DE PROBABILIDADES ES

$$f_X(x) = \{\frac{1}{36}, \frac{2}{36}, \frac{3}{36}, \frac{4}{36}, \frac{5}{36}, \frac{6}{36}, \frac{5}{36}, \frac{4}{36}, \frac{3}{36}, \frac{2}{36}, \frac{1}{36}\}$$

EN ESTE CASO $X_1=2$, $X_2=3,\ldots,X_{11}=12$

$$Y \quad f_X(2) = \frac{1}{36},\ f_X(3) = \frac{2}{36},\ldots,f_X(12) = \frac{1}{36}$$

ESTAS PROBABILIDADES FUERON CALCULADAS EN UN EJEMPLO PREVIO SOBRE PROBABILIDADES DE EVENTOS .

CON ESTAS PROBABILIDADES SE PUEDE OBTENER LA FUNCIÓN DE DISTRIBUCION O DE PROBABILIDADES ACUMULADAS, DE LA SIGUIENTE MANERA:

x	$f_x(x)$	$F_x(x)$
<2	0	0
2	1/36	1/36
3	2/36	3/36
4	3/36	6/36
5	4/36	10/36
6	5/36	15/36
7	6/36	21/36
8	5/36	26/36
9	4/36	30/36
10	3/36	33/36
11	2/36	35/36
12	1/36	36/36=1
>12	0	1
	Σ=1	

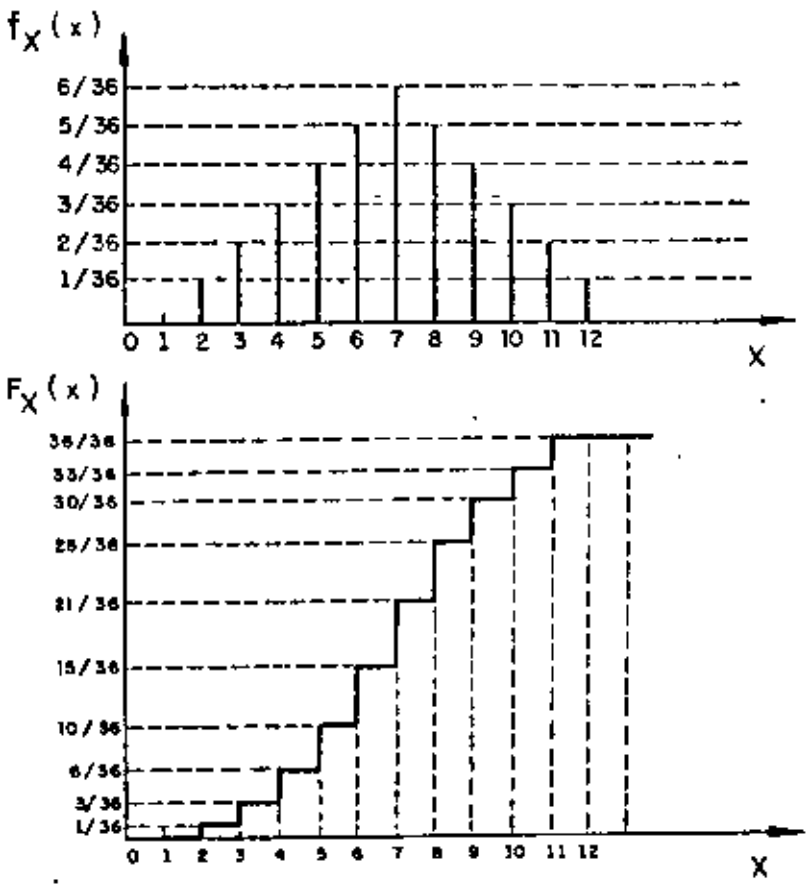

EN EL CASO DE UNA VARIABLE ALEATORIA CONTINUA, X, LA PROBABILIDAD DE QUE ESTA TOME UN VALOR COMPRENDIDO ENTRE x Y x + dx ESTA DADA POR $f_X(x)dx$, DONDE $f_X(x)$ ES LA DENSIDAD DE PROBABILIDADES DE X. POR LO TANTO, LA PROBABILIDAD DE QUE X ASUMA VALORES COMPRENDIDOS EN EL INTERVALO $x_1 \leq X \leq x_2$ ES

$$P(x_1 \leq X \leq x_2) = \int_{x_1}^{x_2} f_X(x)\, dx$$

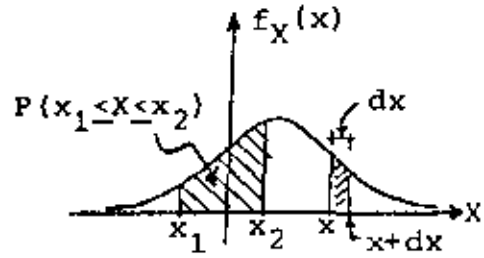

LA INTERPRETACION GRAFICA DE ESTA PROBABILIDAD ES QUE CORRESPONDE AL AREA BAJO LA CURVA DE $f_X(x)$ COMPRENDIDA ENTRE x_1 Y x_2.

PUESTO QUE $F_X(x) = P(X \leq x) = P(-\infty \leq X \leq x)$, Y EN VIRTUD DE LA ECUACION ANTERIOR SE TIENE QUE LA FUNCION DE DISTRIBUCION ES:

$$F_X(x) = \int_{-\infty}^{x} f_X(U)dU$$

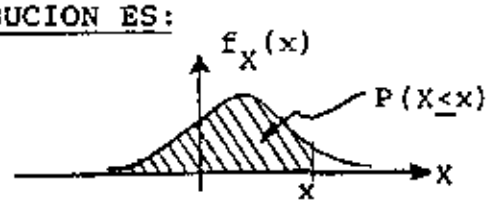

DONDE U ES SOLO UNA VARIABLE MUDA DE INTEGRACION. EL VALOR DE ESTA INTEGRAL ES IGUAL AL AREA BAJO LA CURVA DE $F_X(x)$ A LA IZQUIERDA DE x. DE ESTA ECUACION SE CONCLUYE QUE

$$\frac{dF_X(x)}{dx} = \frac{d}{dx}\left(\int_{-\infty}^{x} f_X(U)dU\right) = f_X(x)$$

ALGUNAS PROPIEDADES DE $F_X(x)$ SON:

$$0 \leq F_X(x) \leq 1$$

$$F_X(-\infty) = 0$$

$$F_X(\infty) = 1$$

$$F_X(x + \varepsilon) \geq F_X(x), \text{ SI } \varepsilon \geq 0$$

$$F_X(x_2) - F_X(x_1) = P(x_1 \leq X \leq x_2)$$

PARA SATISFACER LOS AXIOMAS DE LA TEORIA DE PROBABILIDADES SE NECESITA QUE

$$f_X(x) \geq 0 \text{ PARA TODA } x$$

$$\int_{-\infty}^{\infty} f_X(x)\, dx = 1$$

EJEMPLO

UN INGENIERO ESTA INTERESADO EN DISEÑAR UNA TORRE QUE RESISTA LAS CARGAS DEBIDAS AL VIENTO. DE UNA SERIE DE OBSERVACIONES DE LA MAXIMA VELOCIDAD ANUAL DEL VIENTO CERCA DEL SITIO DE INTERES, SE ENCUENTRA QUE EL HISTOGRAMA PUEDE AJUSTARSE RAZONABLEMENTE, DESDE UN PUNTO DE VISTA ESTADISTICO, MEDIANTE UNA *DISTRIBUCION DE PROBABILIDADES EXPONENCIAL* DE LA FORMA

$$f_X(x) = Ke^{-\lambda x} \; ; \; x \geq 0 \quad Y \quad f_X(x) = 0; \; x < 0$$

DONDE X ES LA MAXIMA VELOCIDAD DEL VIENTO, λ ES UNA CONSTANTE Y K ES OTRA CONSTANTE TAL QUE OBLIGA A QUE EL AREA BAJO LA CURVA DE $f_X(x)$ SEA IGUAL A UNO. POR TANTO,

$$\int_0^{\infty} Ke^{-\lambda x}\, dx = \frac{-K}{\lambda}\left[e^{-\lambda x}\right]_0^{\infty} = \frac{K}{\lambda} = 1$$

DE DONDE

$$K = \lambda$$

POR TANTO

$$f_X(x) = \lambda e^{-\lambda x} \; ; \; x \geq 0$$

LA FUNCION DE DISTRIBUCION SERA

$$F_X(x) = \int_0^x f_X(u)\, du = \int_0^x \lambda e^{-\lambda u}\, du = \left[-e^{-\lambda u}\right]_0^x = 1 - e^{-\lambda x} \; ; \; x \geq 0$$

EL VALOR DE λ SE PUEDE TOMAR, POR EJEMPLO, DE MANERA QUE $F_X(x)$ SE AJUSTE PARA QUE COINCIDA CON UN VALOR EMPIRICO. ASI, SI LA FRECUENCIA RELATIVA DEL EVENTO A = {X≤70 KM/H} ES 0.9, ENTONCES

$$P(0 \leq X \leq 70) = F_X(70) = 0.9$$

DE DONDE

$$0.9 = 1 - e^{-70\lambda}$$

POR LO CUAL $\lambda = 0.033$.

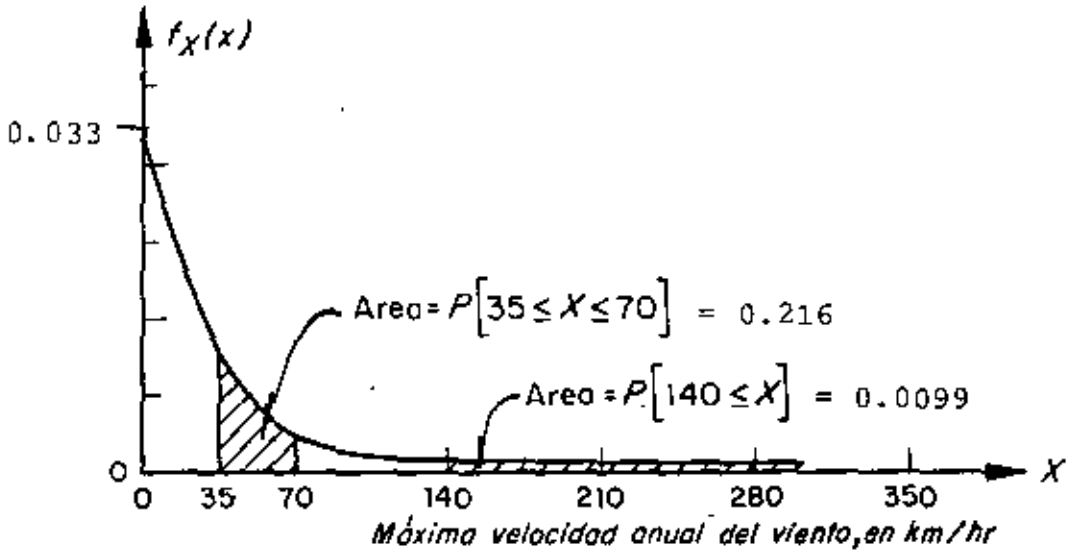

a) Densidad de probabilidades de X

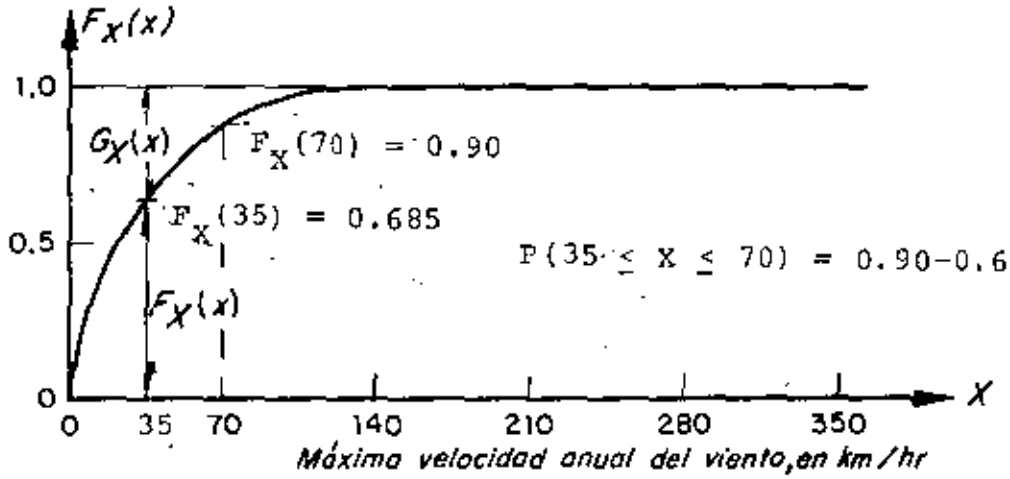

b) Función de distribución de X

Ley de probabilidades correspondiente al ejemplo de la máxima velocidad anual del viento

SI SE DESEA CALCULAR, POR EJEMPLO, LA PROBABILIDAD DE QUE LA VELOCIDAD MAXIMA DEL VIENTO EN UN AÑO DADO ESTE ENTRE 35 Y 70 KM/H, SE TENDRA:

$$P(35<X<70) = \int_{35}^{70} 0.033e^{-0.033x}dx = \left[-e^{-0.033x}\right]_{35}^{70} =$$

$$= -e^{-0.033x70} - (-e^{-0.033x35}) = -e^{-2.31} + e^{-1.155} =$$

$$= -0.099 + 0.315 = 0.216$$

EN TERMINOS DE $F_X(x)$ ESTA PROBABILIDAD QUEDA DADA POR

$$P(35 \leq X \leq 70) = F_X(70) - F_X(35) = 0.90 - (1 - e^{-1.155}) = 0.90 - 0.685$$

$$= 0.215$$

FUNCION DE DISTRIBUCION COMPLEMENTARIA

EL COMPLEMENTO, $G_X(x)$, DE LA DISTRIBUCION DE PROBABILIDADES ACUMULADAS SU UTILIZA CUANDO LAS DECISIONES SE TOMAN CON BASE EN PROBABILIDADES DE QUE SE EXCEDA UN VALOR DADO DE LA VARIABLE. LA FUNCION DE DISTRIBUCION COMPLEMENTARIA SE DEFINE COMO

$$G_X(x) = P\ (X>x) = 1 - F_X(x)$$

EJEMPLO

PARA EL PROBLEMA ANTERIOR DE LA VELOCIDAD MAXIMA ANUAL DEL VIENTO, CALCULEMOS LA PROBABILIDAD DE QUE ESTA SEA MAYOR DE 140 KM/H:

$$G_X(140) = P(X>140) = \int_{140}^{\infty} 0.33e^{-0.033x}dx = 0.0099$$

O, ALTERNATIVAMENTE

$$P(X\geq 140) = 1-F_X(140) = G_X(140) = 1-(1-e^{-0.033x140}) = e^{-4.62} = 0.0099$$

ESPERANZAS

LA ESPERANZA DE UNA FUNCION $g(X)$, DE UNA VARIABLE ALEATORIA DISCRETA, X, ES, POR DEFINICION

$$E(g(X)) = \sum_{i=1}^{i=n} g(x_i) P_X(x_i)$$

O PARA UNA VARIABLE CONTINUA

$$E(g(X)) = \int_{-\infty}^{\infty} g(x) f_X(x)\,dx$$

EJEMPLOS

1. SI $g(X)$ = CONSTANTE = c

$$E(c) = c \int_{-\infty}^{\infty} f_X(x)\,dx = c$$

2. SI $g(X) = x$

$$E[x] = \int_{-\infty}^{\infty} x f_X(x)\,dx$$

3. SI $g(X) = a + bx$

$$E[a + bx] = a \int_{-\infty}^{\infty} f_X(x)\,dx + b \int_{-\infty}^{\infty} x f_X(x)\,dx = a + bE[X]$$

4. SI $g(X) = g_1(X) + g_2(X)$

$$E[g_1(X) + g_2(X)] = \int_{-\infty}^{\infty} g_1(x) f_X(x)\,dx + \int_{-\infty}^{\infty} g_2(x) f_X(x)\,dx$$

$$= E[g_1(X)] + E[g_2(X)]$$

5. SI $g(X) = \frac{x - c}{d} = \frac{1}{d} x - \frac{c}{d}$

$$E\left(\frac{x-c}{d}\right) = \frac{1}{d} E(x) - \frac{c}{d} = \frac{E(x) - c}{d}$$

6. SI $g(X) = ax^2$

$$E(ax^2) = a \int_{-\infty}^{\infty} x^2 f_X(x)\,dx = a\,E(x^2)$$

EJEMPLO

SI X ES UNA VARIABLE ALEATORIA CON DENSIDAD DE PROBABILIDADES EXPONENCIAL, CALCULAR LA ESPERANZA DE LA FUNCION

$$g(X) = X^2$$

EN ESTE CASO SE TIENE QUE

$$f_X(x) = \lambda e^{-\lambda x}, \text{ SI } 0 \leq X \leq \infty, \text{ Y } \quad f_X(x) = 0, \text{ SI } X<0$$

POR LO QUE

$$E(X^2)=E[g(X)]= \int_{-\infty}^{\infty} g(x) f_X(x)\,dx = \lambda \int_{-\infty}^{\infty} x^2 e^{-\lambda x}\,dx$$

$$=\lambda\left[\frac{-x^2 e^{-\lambda x}}{\lambda}\right]_0^{\infty} + \frac{2\lambda}{\lambda}\int_0^{\infty} x e^{-\lambda x}\,dx = \frac{-2}{\lambda^2}\left[e^{-\lambda x}(1+\lambda x)\right]_0^{\infty} = \frac{2}{\lambda^2}$$

EN GENERAL, A LA ESPERANZA DE X^2 SE LE DENOMINA *VALOR MEDIO CUADRATICO*.

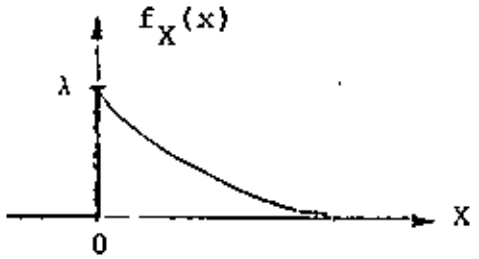

EN EL CASO DE LA VELOC. ANUAL MAXIMA DEL VIENTO

$$E(X^2) = \frac{2}{(0.033)^2} = 1836.55 \left(\frac{km}{h}\right)^2$$

MOMENTOS DE OREDEN n

a) RESPECTO AL ORIGEN, CUANDO $g(X) = X^n$

$$E(X^n) = E[g(X)] = \int_{-\infty}^{\infty} x^n f_x(x)\,dx$$

EJEMPLO: $E(X^2)$ = MOMENTO DE 2° ORDEN RESPECTO AL ORIGEN

b) RESPECTO A LA MEDIA, cuando $g(X) = [X - E(X)]^n$

$$E[X - E(X)]^n = \int_{-\infty}^{\infty} [X - E(X)]^n f_x(x)\,dx$$

EJEMPLO: $E[X - E(X)]^2$ = MOMENTO DE 2° ORDEN RESPECTO A LA MEDIA.

MEDIDAS DE TENDENCIA CENTRAL

LA MEDIA O ESPERANZA, $E[X]$, DE UNA VARIABLE ALEATORIA, X, SE CALCULA CON LAS ECUACIONES ANTERIORES PARA EL CASO EN QUE $g(X)=X$. DE ESTA MANERA, SI LA VARIABLE ES DISCRETA, SU ESPERANZA QUEDA DADA POR

$$E(X) = \sum_{i=1}^{i=n} x_i \, P_X(x_i)$$

DONDE n ES EL TOTAL DE VALORES QUE X PUEDE ASUMIR.

PARA EL CASO DE UNA VARIABLE ALEATORIA CONTINUA, LA MEDIA ES

$$\mu_X = m_x = E(X) = \int_{-\infty}^{\infty} x \, \delta_X(x) \, dx$$

OTRAS MEDIDAS USUALES DE TENDENCIA CENTRAL DE UNA VARIABLE ALEATORIA SON LA MEDIANA Y EL MODO. LA PRIMERA SE DEFINE COMO EL VALOR DE LA VARIABLE AL CUAL CORRESPONDE UNA PROBABILIDAD ACUMULADA DE 50%, Y LA SEGUNDA, COMO EL VALOR DE LA VARIABLE AL CUAL CORRESPONDE LA MAYOR PROBABILIDAD O EL MAXIMO DE LA DENSIDAD DE PROBABILIDADES, SEGUN SE TRATE DE UNA VARIABLE DISCRETA O DE UNA CONTINUA, RESPECTIVAMENTE.

EJEMPLO

SI LA DENSIDAD DE PROBABILIDADES DE LA VARIABLE ALEATORIA X CORRESPONDIENTE A LOS ERRORES EN UNA NIVELACION, ES LA DE LA SEGUNDA COLUMNA DE LA SIGUIENTE TABLA, LA MEDIA DE DICHA VARIABLE RESULTA SER 4 167 LA MEDIANA 4000 Y EL MODO 4000 MICRAS. LOS CALCULOS CORRESPONDIENTES SE LOCALIZAN EN LA TERCERA COLUMNA.

x_i, EN MICRAS	$P_X(x_i)$	$x_i P_X(x_i)$, EN MICRAS	$F_X(x_i)$
0	6/60	0	6/60
1 000	2/60	2 000/60	8/60
2 000	4/60	8 000/60	12/60
3 000	8/60	24 000/60	20/60
4 000	13/60	52 000/60	33/60≥0.5
5 000	12/60	60 000/60	45/60
6 000	7/60	42 000/60	52/60
7 000	4/60	28 000/60	56/60
8 000	2/60	16 000/60	58/60
9 000	2/60	18 000/60	60/60
TOTAL: $E[X]$ = 250 000/60=4 167 MICRAS			

LA MAXIMA PROBABILIDAD ES 13/60, POR LO QUE EL MODO VALE 4000 MICRAS. POR OTRA PARTE LA PROBABILIDAD ACUMULADA DEL 50 POR CIENTO SE EXCEDE EN x_i = 4000, POR LO QUE LA MEDIANA VALE TAMBIEN 4000 MICRAS.

EJEMPLO

CALCULAR LA ESPERANZA DE UNA VARIABLE ALEATORIA CUYA DENSIDAD DE PROBABILIDADES ES TRIANGULAR DADA POR

$$f_Y(Y) = \frac{1}{6}Y + \frac{1}{3} \qquad \text{SI } -2 \leq y \leq 0$$

$$f_Y(y) = \frac{-1}{12}Y + \frac{1}{3} \qquad \text{SI } 0 \leq y \leq 4$$

$$f_Y(y) = 0 \qquad \text{SI } y \leq -2 \text{ O } y \geq 4$$

$$E(Y) = \int_{-\infty}^{\infty} y f_Y(y)dy = \int_{-2}^{0} y\left(\frac{Y}{6} + \frac{1}{3}\right)dy + \int_{0}^{4} y\left(\frac{-Y}{12} + \frac{1}{3}\right)dy$$

$$= \left[\frac{Y^3}{18} + \frac{Y^2}{6}\right]_{-2}^{0} + \left[\frac{-Y^3}{36} + \frac{Y^2}{6}\right]_{0}^{4} = \frac{2}{3}$$

EL MAXIMO DE ESTA DENSIDAD DE PROBABILIDADES SE PRESENTA EN Y = 0, POR LO QUE

MODO = 0

POR OTRA PARTE EL 50 POR CIENTO DE PROBABILIDAD ACUMULADA SE COMPLETA EN EL VALOR DE Y QUE CUMPLE CON

$$F_Y(y) = 0.5 = \frac{1}{3} - \frac{Y^2}{24} + \frac{Y}{3}$$

RESOLVIENDO ESTA ECUACION DE SEGUNDO GRADO SE ENCUENTRA:

MEDIANA = 0.536

EJEMPLO

CALCULAR LA ESPERANZA DE UNA VARIABLE ALEATORIA CON DENSIDAD DE PROBABILIDADES EXPONENCIAL

$$f_X(x) = \lambda e^{-\lambda x}$$

$$E(X) = \int_{-\infty}^{\infty} x f_X(x)dx = \lambda \int_0^{\infty} x e^{-\lambda x}dx = \lambda\left[\frac{-e^{-\lambda x}}{\lambda^2}(1+\lambda x)\right]_0^{\infty} = \frac{1}{\lambda}$$

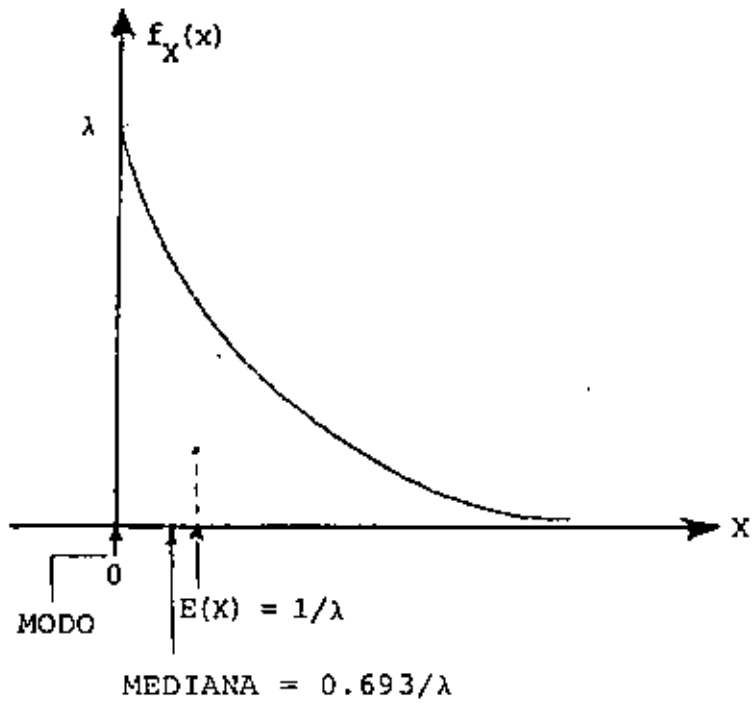

EL MAXIMO DE $f_X(x)$ ESTA EN x=0, POR LO QUE

MODO = 0

EL 50 POR CIENTO DE LA PROBABILIDAD ACUMULADA SE COMPLETA EN EL VALOR DE X QUE CUMPLE CON $F_X(x) = 0.5 = 1 - e^{-\lambda x}$

DE DONDE

$$\text{MEDIANA} = \frac{-\ell n\ 0.5}{\lambda} = \frac{0.693}{\lambda}$$

DONDE ℓn ES LOGARITMO NATURAL.

MEDIDAS DE DISPERSION

UNA MEDIDA MUY COMUN DE LA DISPERSION O VARIABILIDAD DE LOS VALORES QUE PUEDE ASUMIR UNA VARIABLE ALEATORIA ES LA VARIANCIA, LA CUAL SE DENOTA COMO $\sigma^2(X)$ O VAR (X), LA CUAL SE DEFINE COMO LA ESPERANZA DE LA FUNCION $g(X) = [X-E(X)]^2$. ASI, PARA UNA VARIABLE ALEATORIA DISCRETA

$$\sigma^2(X) = VAR(X) = \sum_{i=1}^{i=n} (x_i - E(X))^2 P_X(x_i)$$

Y PARA UNA CONTINUA

$$\sigma^2(X) = VAR(X) = \int_{-\infty}^{\infty} (x - E(X))^2 f_X(x)dx$$

DESARROLLANDO EL INTEGRANDO DE ESTA ULTIMA ECUACION:

$$\sigma^2(X) = \int_{-\infty}^{\infty} (x^2 - 2xE(X) + E^2(X)) f_X(x)dx$$

$$= \int_{-\infty}^{\infty} x^2 f_X(x)dx - 2E(X)\int_{-\infty}^{\infty} x f_X(x)dx + E^2(X)\int_{-\infty}^{\infty} f_X(x)dx = E[X^2] - E^2[X]$$

ES DECIR, LA VARIANCIA SE PUEDE CALCULAR COMO LA DIFERENCIA DEL VALOR MEDIO CUADRATICO Y EL CUADRADO DE LA MEDIA DE X.

OTRAS MEDIDAS DE DISPERSION DE LA VARIABLE ALEATORIA X SON LA DESVIACION ESTANDAR, $\sigma(X)$, LA CUAL ES IGUAL A LA RAIZ CUADRADA DE LA VARIANCIA, Y EL COEFICIENTE DE VARIACION QUE SE DEFINE COMO

$$v(X) = \sigma(X)/E(X) \quad , \text{ SI } E(X) \neq 0$$

EJEMPLO

EN LA SIGUIENTE TABLA SE CALCULA LA VARIANCIA DE LA VARIABLE ALEATORIA CUYA DENSIDAD DE PROBABILIDADES SE PRESENTO EN EL EJEMPLO ANTERIOR ($E(x) = 4167$ MICRAS)

$x_i - E(X)$ EN MICRAS	$(x_i - E(x))^2$ MICRAS^2	$P_X(x_i)$	$(x_i - E(X))^2 P_X(x_i)$, EN MICRAS
-4 167	17 363 889	6/60	1 736 388
-3 167	10 029 889	2/60	334 329
-2 167	4 695 889	4/60	313 059
-1 167	1 361 889	8/60	181 585
- 167	27 889	13/60	6 042
833	693 889	12/60	138 777
1 833	3 359 889	7/60	391 987
2 833	8 025 889	4/60	535 059
3 833	14 691 889	2/60	489 729
4 833	23 357 889	2/60	778 596
		TOTAL:	4 405 551 MICRAS^2 $= \sigma^2(X)$

LA DESVIACION ESTANDAR Y EL COEFICIENTE DE VARIACION DE ESTA VARIABLE ALEATORIA SON, RESPECTIVAMENTE,

$$\sigma(X) = \sqrt{4\ 405\ 551} = 2\ 215 \text{ MICRAS, Y } v(X) = \sigma(X)/E(X) = \frac{2\ 215}{4\ 167} = 0.531$$

EJEMPLO

SI X ES UNA VARIABLE ALEATORIA CON DISTRIBUCION DE PROBABILIDADES EXPONENCIAL, CALCULAR SU VARIANCIA, DESVIACION ESTANDAR Y COEFICIENTE DE VARIACION:

$$\sigma^2(X) = E(X-E[X])^2 = \int_{-\infty}^{\infty}(x-E[X])^2\lambda e^{-\lambda x}dx = \lambda \int_0^{\infty}(x^2-2xE[X]+E^2[X])e^{-\lambda x}dx$$

$$= \lambda \int_0^{\infty}x^2e^{-\lambda x}dx - 2E[X]\lambda\int_0^{\infty}xe^{-\lambda x}dx + E^2[X] \int_0^{\infty}\lambda e^{-\lambda x}dx$$

$$= \frac{2}{\lambda^2} - 2\,\frac{1}{\lambda}\,\frac{1}{\lambda} + \frac{1}{\lambda^2} = \frac{1}{\lambda^2}$$

YA QUE $E(X) = 1/\lambda$ Y $E[x^2] = 2/\lambda^2$.

USANDO LA FORMULA $\sigma^2(X) = E[X^2] - E^2[X]$, Y TOMANDO EN CUENTA QUE $E[X^2] = 2/\lambda^2$ SE OBTIENE:

$$\sigma^2(X) = 2/\lambda^2 - 1/\lambda^2 = 1/\lambda^2$$

EN CONSECUENCIA, LA DESVIACION ESTANDAR ES

$$\sigma(X) = \sqrt{1/\lambda^2} = 1/\lambda$$

Y EL COEFICIENTE DE VARIACION

$$v(X) = \sigma(X)/E(X) = \frac{\frac{1}{\lambda}}{\frac{1}{\lambda}} = 1$$

EJEMPLO

SEA Y UNA VARIABLE ALEATORIA CON DENSIDAD DE PROBABILIDADES TRIANGULAR DADA POR

$$f_Y(y) = \frac{1}{6}\,y + \frac{1}{3} \qquad \text{SI} \quad -2 \le y \le 0$$

$$f_Y(y) = \frac{-1}{12}\,y + \frac{1}{3} \qquad \text{SI} \quad 0 \le y \le 4$$

$$f_Y(y) = 0 \qquad \text{SI} \quad y \le -2 \text{ O } y \ge 4$$

CALCULAR LA VARIANCIA, LA DESVIACION ESTANDAR Y EL COEFICIENTE DE VARIACION.

CALCULAREMOS PRIMERO EL VALOR MEDIO CUADRATICO PARA LUEGO APLICAR LA ECUACION $\sigma^2(Y) = E(Y^2) - E^2(Y)$

$$E[Y^2] = \int_{-2}^{0} y^2\left(\frac{1}{6}\,y + \frac{1}{3}\right)dy + \int_{0}^{4} y^2\left(-\frac{y}{12} + \frac{1}{3}\right)dy = \left[\frac{y^4}{24} + \frac{y^3}{9}\right]_{-2}^{0} + \left[\frac{-y^4}{48} + \frac{y^3}{9}\right]_{0}^{4} = 2$$

$$\sigma^2(Y) = 2 - (2/3)^2 = 14/9$$

$$\sigma(Y) = 1.25\ (\sqrt{14/9})$$

$$v(Y) = 1.25/(2/3) = 1,88$$

EJEMPLO

SI SE HACE LA TRANSFORMACION $Y = ax$, ¿CUANTO VALE LA VARIANCIA DE Y EN TERMINOS DE LA DE X?

DE LO VISTO ANTERIORMENTE, $E(Y) = aE(x)$ Y $E(Y^2) = a^2E(X^2)$

$$\sigma^2(Y) = E(Y^2) - E^2(Y) = a^2E(x^2) - a^2E^2(x) = a^2[E(x^2) - E^2(x)] = a^2\sigma^2(x)$$

DISTRIBUCIONES PARTICULARES

VARIABLES ALEATORIAS DISCRETAS

DISTRIBUCION BINOMIAL O DE BERNOULLI

LA DISTRIBUCION BINOMIAL O DE BERNOULLI SE EMPLEA COMO DENSIDAD DE PROBABILIDADES DE VARIABLES ALEATORIAS DISCRETAS ASOCIADOS A EXPERIMENTOS EN LOS QUE SOLO HAY (O SOLO IMPORTAN) DOS RESULTADOS POSIBLES, UNO DE LOS CUALES USUALMENTE SE DENOMINA "EXITO" Y, EL OTRO, "FRACASO". (S = {EXITO, FRACASO}).

SEAN p= PROBABILIDAD DE OBSERVAR "EXITO" AL REALIZAR UNA VEZ EL EXPERIMENTO

q= PROBABILIDAD DE "FRACASO" = 1-p

X= VARIABLE ALEATORIA "NUMERO DE EXITOS OBSERVADOS AL REPETIR n VECES EL EXPERIMENTO "CON REEMPLAZO"

LA DISTRIBUCION DE PROBABILIDADES BINOMIAL ES

$$f(x) = \frac{n!}{x!(n-x)!} p^x q^{n-x} \quad : \quad x = 0, 1, \ldots, n$$

SE PUEDE DEMOSTRAR QUE LOS PARAMETROS DE ESTA DISTRIBUCION SON

$$E(X) = np \ , \quad \sigma^2(X) = npq$$

REFERENCIA: W. BEYER, "HANDBOOK OF TABLES FOR PROBABILITY AND STATISTICS", THE CHEMICAL RUBBER, CO. (1966).

DEMOSTRACION

SI $n=2$, ENTONCES X PUEDE ASUMIR LOS VALORES 0, 1 y 2, ES DECIR $S=\{0,1,2\}$. EL ESPACIO DE EVENTOS DEL EXPERIMENTO ES

$$S_1 = \{\underbrace{(\text{FRACASO, FRACASO})}_{X=0}, \underbrace{(\text{EXITO, FRACASO})}_{X=1}, \underbrace{(\text{FRACASO, EXITO})}_{X=1},$$

$$\underbrace{(\text{EXITO, EXITO})}_{X=2}\}$$

$$f_X(x) = \{f_X(0), f_X(1), f_X(2)\}$$

OBSERVESE QUE $x=0$ OCURRE DE UNA MANERA, $x=1$, DE DOS, Y $x=2$, DE UNA. ESTOS RESULTADOS SE PUEDEN OBTENER PERMUTANDO DOS GRUPOS, UNO CON x Y EL OTRO CON n-x ELEMENTOS:

$x=0$: $\quad {}_2P_{0,2} = \frac{2!}{0!x2!} = 1 \; ; \; P(\{0\}) = q \times q = q^2 = p^0q^2$

$x=1$: $\quad {}_2P_{1,1} = \frac{2!}{1!x1!} = 2 \; ; \; P(\{1\}) = 2pq$

$x=2$: $\quad {}_2P_{2,0} = \frac{2!}{2!x0!} = 1 \; ; \; P(\{2\}) = pxp = p^2 = p^2q^0$

$$\sum_{i=0}^{2} P(\{i\}) = q^2+2pq+p^2 = (p+q)^2 = 1$$

(OBSERVESE QUE LOS ELEMENTOS DE S_1 NO SON IGUALMENTE PROBABLES, A MENOS QUE $p = q = 1/2$.)

SI n = 3, $S = \{0,1,2,3\}$, e = EXITO Y f = FRACASO, ENTONCES

S_1= {(f,f,f), (e,f,f), (f,e,f), (f,f,e), (e,e,f), (e,f,e), (f,e,e), (e,e,e)}

x = 0: $_3P_{0,3} = \frac{3!}{0!x3!} = 1$; $P(\{0\}) = 1\ p^0q^3 = q^3$

x = 1: $_3P_{1,2} = \frac{3!}{1!x2!} = 3$; $P(\{1\}) = 3\ pq^2$

x = 2: $_3P_{2,1} = \frac{3!}{2!x1!} = 3$; $P(\{2\}) = 3p^2q$

x = 3: $_3P_{3,0} = \frac{3!}{3!x0!} = 1$; $P(\{3\}) = 1p^3q^0 = p^3$

$\sum_{i=0}^{3} P(\{i\}) = (p+q)^3 = 1$

PASANDO AL CASO GENERAL DE CUALQUIER VALOR DE n, LA PROBABILIDAD DE QUE OCURRAN x EXITOS Y n-x FRACASOS *EN UN ORDEN DETERMINADO* ES

$$P(X=x) = p^x q^{n-x}$$

EN VIRTUD DE LA LEY GENERAL DE MULTIPLICACION.

UN ORDEN POSIBLE SERIA, POR EJEMPLO,

$$\underbrace{\text{EXITO, EXITO,..., EXITO}}_{x}, \underbrace{\text{FRACASO,..., FRACASO}}_{n-x}$$

AHORA BIEN, LOS x EXITOS PUEDEN OCURRIR EN $_nP_{x,n-x}$ ORDENES DISTINTOS, CADA UNO CON PROBABILIDAD p^xq^{n-x}. POR LO TANTO, EN VIRTUD DE LA LEY GENERAL DE ADICION, LA DISTRIBUCION DE PROBABILIDADES DE X RESULTA SER

$$f_X(x) = \frac{n!}{x!(n-x)!}\ p^x q^{n-x} \quad ; \quad x = 0,1,\ldots,n$$

LA CUAL SE CONOCE CON EL NOMBRE DE *BINOMIAL O DE BERNOULLI.*

LA ESPERANZA DE LA DISTRIBUCION DE BERNOULLI ES

$$E(X) = \sum_{x=0}^{n} x \frac{n!}{x!(n-x)!} p^x q^{n-x} = \sum_{x=1}^{n} x \frac{n!}{x!(n-x)!} p^x q^{n-x}$$

$$= np \underbrace{\sum_{x=1}^{n} \frac{(n-1)!}{(x-1)!(n-x)!} p^{x-1} q^{n-x}}_{(p+q)^{n-1}} = np(p+q)^{n-1} = np$$

LA VARIANCIA DE LA DISTRIBUCION BINOMIAL ES

$$\sigma^2(X) = E[(X-E(X))^2] = E[(X-np)^2]$$

PERO $E[(X-np)^2] = E(X^2-2npX + n^2p^2) = E[X + X(X-1) - 2npX + n^2p^2]$

$$= E[(1-2np)X] + E[X(X-1)] + E(n^2p^2)$$

$$= (1-2np)np + n^2p^2 + \sum_{x=0}^{n} \frac{n!}{x!(n-x)!} p^x q^{n-x} x(x-1)$$

$$= np - n^2p^2 + \sum_{x=2}^{n} n(n-1) \frac{(n-2)!}{(x-2)!(n-x)!} p^2 p^{x-2} q^{n-x}$$

$$= np - n^2p^2 + n(n-1)p^2 \sum_{x=2}^{n} \frac{(n-2)!}{(x-2)!(n-x)!} p^{x-2} q^{n-x}$$

$$= np - n^2p^2 + n(n-1)p^2(p+q)^{n-2} = np - np^2 = np(1-p) = npq$$

EN RESUMEN, PARA LA DISTRIBUCION BINOMIAL,

$$E(X) = np \quad ; \quad \sigma^2(X) = npq \; ; \; \sigma(X) = \sqrt{npq}$$

EJEMPLO

SI CON BASE EN LA EXPERIENCIA DE MUCHO TIEMPO SE SABE QUE UNA MAQUINA IMPRIME COLORES DEFECTUOSOS EN UN 5 POR CIENTO DE LAS VECES, CALCULAR LA PROBABILIDAD DE QUE DE 10 IMPRESIONES SE OBTENGA:

a. NINGUNA DEFECTUOSA
b. UNA DEFECTUOSA
c. MAS DE UNA DEFECTUOSA

ASIMISMO, CALCULAR LA MEDIA Y LA DESVIACION ESTANDAR DEL NUMERO DE DEFECTUOSAS.

Solución

SEA EXITO = IMPRESION DEFETUOSA
EN TAL CASO $p = 0.05$ Y $q = 1-0.05 = 0.95$

a. NINGUNA DEFECTUOSA ES LO MISMO

QUE $X = 0$; ENTONCES $n-x = 10-0=10$ Y:

$$P(x=0) = f_x(0) = \frac{n!}{x!\ (n-x)!} = \frac{10!}{0!\ (10-0)!}\ (0.05)^0(0.95)^{10}$$

$$= \frac{10!}{10!}\ (0.95)^{10} = 0.599 = 59.9\%$$

b. UNA DEFECTUOSA ES LO MISMO
QUE $X = 1$; ENTONCES $n-x = 10-1 = 9$ Y:

$$P(x = 1) = f_x(1) = \frac{10!}{1!\ 9!}\ (0.05)^1(0.95)^9$$

$$= \frac{10 \times 9!}{9!}\ (0.05)(0.6302) = 0.315$$

c. MAS DE UNA DEFECTUOSA ES LO MISMO
QUE $x > 1$

$$P(X > 1) = 1-P(X \leq 1) = 1-[P(x = 0)+P(x = 1)]$$

$$= 1-(0.599+0.315) = 0.086$$

$$E(x) = np = 10x0.05 = 0.5$$

$$\sigma^2(x) = npq = 10 \times 0.05 \times 0.95 = 0.0475$$

$$\sigma(x) = \sqrt{0.0475} = 0.2179$$

EJEMPLO

RESOLVER AHORA EL INCISO b. DEL EJEMPLO ANTERIOR, PARA EL CASO EN QUE $p = 0.1$

$$P(x = 1) = \frac{10!}{1!\ 9!}(0.10)^1(0.90)^9 = 0.3874 = 38.74\%$$

USANDO LAS TABLAS DE LA DISTRIBUCION BINOMINAL:

$$\{X = x\} \cup \{X \leq x-1\} = \{X \leq x\}$$

POR LO TANTO $P\{X = x\} + P\{X \leq x-1\} = P\{X \leq x\}$

Y $P\{X = x\} = P\{X \leq x\} - P\{X \leq x-1\}$

EN ESTE EJEMPLO $x = 1$ y $x-1=0$, POR LO QUE

$$P(X=1) = P(X\leq 1) - P(X \leq 0)$$

$$= 0.7361 - 0.3487 = 0.3874$$

DISTRIBUCION DE POISSON

UNA DISTRIBUCION DE PROBABILIDADES PARA UNA VARIABLE ALEATORIA DISCRETA, X, DE LA FORMA

$$f_X(x) = \frac{\lambda^x e^{-\lambda}}{x!} \; ; \; x = 0, 1, 2, \ldots$$

SE LLAMA DISTRIBUCION DE POISSON; EN ESTA ECUACION λ ES UNA CONSTANTE. SE PUEDE DEMOSTRAR QUE LA MEDIA Y LA VARIANCIA PARA ESTA DISTRIBUCION QUEDAN DADAS POR

$$E(X) = \sum_{x=0}^{\infty} x \frac{\lambda^x e^{-\lambda}}{x!} = \lambda$$

$$\sigma^2(x) = \sum_{x=0}^{\infty} (x-\lambda)^2 \frac{\lambda^x e^{-\lambda}}{x!} = \lambda$$

UNA VEZ CONOCIDA λ, CON ESTA DISTRIBUCION SE PUEDEN CALCULAR LAS PROBABILIDADES DE QUE UN EVENTO OCURRA x VECES.

ES POSIBLE DEMOSTRAR QUE LA DISTRIBUCION DE POISSON PUEDE EMPLEARSE COMO UNA PROXIMACION DE LA DE BERNOULLI, TOMANDO $\lambda = np$, CUANDO n ES GRANDE Y p PEQUEÑA, PERO DE TAL MANERA QUE $npq > 1$. AL RESPECTO, SI $n=20$ y $p=0.05$, ENTONCES EL ERROR QUE SE TIENE AL USAR DICHA APROXIMACION ES MENOR DE 3 POR CIENTO PARA VALORES DE X MENORES DE 3; PARA $X=4$ y $X=5$ LOS ERRORES RESPECTIVOS SON 15 Y 41 POR CIENTO, DEBIDO A QUE NO SE CUMPLE CON LA CONDICION DE QUE npq SEA MAYOR DE UNO, YA QUE $npq = 20 \times 0.05 \times 0.95 = 0.95$

EJEMPLO

SI LA PROBABILIDAD DE QUE FALLE UNA VARILLA DE ACERO AL APLICARLE UNA DETERMINADA FUERZA DE TENSION ES DE 0.001, ¿CUAL ES LA PROBABILIDAD DE QUE DE 2000 VARILLAS PROBADAS FALLEN A) TRES, B) MAS DE DOS?

CON $\lambda = 2000 \times 0.001 = 2$ Y CONSIDERANDO QUE $npq = 1.9 > 1$, SE PUEDE USAR LA DISTRIBUCION DE POISSON COMO APROXIMACION DE LA BINOMIAL:

a) $$P[X = 3] = \frac{\lambda^3 e^{-\lambda}}{3!}$$

$$P[X = 3] = \frac{2^3 e^{-2}}{3!} = 0.18$$

CON LAS TABLAS: $P[X=3] = 0.857 - 0.677 = 0.18$

EN ESTE CASO LA DISTRIBUCION BINOMIAL DA COMO RESULTADO

$$P[X=3] = \frac{2000!}{3! \times 1997!} (0.001)^3 (0.999)^{1997} = 0.184$$

b) $$P[X > 2] = 1 - P[X \leq 2] = 1 - F_X(2) = 1 - \left\{P[X = 0] + P[X = 1] + P[X = 2]\right\} = 1 - \frac{2^0 e^{-2}}{0!} - \frac{2^1 e^{-2}}{1!} - \frac{2^2 e^{-2}}{2!} =$$

$$= 1 - \frac{1}{e^2} - \frac{2}{e^2} - \frac{2}{e^2} = 1 - \frac{5}{e^2} = 0.323$$

CON LAS TABLAS: $P[X > 2] = 1 - 0.677 = 0.323$

EJEMPLO

UNA COMPAÑIA ASEGURADORA DESPUES DE MUCHOS AÑOS DE EXPERIENCIA HA HA ESTIMADO QUE EL 0.004% DE LA POBLACION FALLECE ANUALMENTE POR ACCIDENTE AUTOMOVILISTICO. SI ESTA COMPAÑIA TIENE 40,000 ASEGURADOS, ¿CUAL ES LA PROBABILIDAD DE QUE 2 DE ELLOS MUERAN EN UN AÑO POR ESTE TIPO DE ACCIDENTE?

SEA X EL NUMERO DE PERSONAS QUE MUEREN ANUALMENTE DE ENTRE LOS ASEGURADOS, POR ACCIDENTE, LA MEDIA DE X ES

$$E[X] = 0.00004 \times 40{,}000 = 1.6 = \lambda$$

ADEMAS, TOMANDO EN CUENTA QUE npq>1, SE PUEDE USAR SIN GRAN ERROR LA DISTRIBUCION DE POISSON:

$$P[X=x] = \frac{\lambda^x e^{-\lambda}}{x!} = \frac{(1.6)^x e^{-1.6}}{x!} \; ; \; x=0,\ 1,\ 2,\ldots$$

POR LO QUE

$$P[X=2] = \frac{(1.6)^2 e^{-1.6}}{2!} = \frac{0.2019 \times 2.56}{2} = 0.26$$

LA DISTRIBUCION DE PROBABILIDADES PARA ESTA VARIABLE ALEATORIA ES:

x	0	1	2	3	4	5	6	...
$f_X(x)$	0.202	0.323	0.258	0.138	0.055	0.018	0.005	...

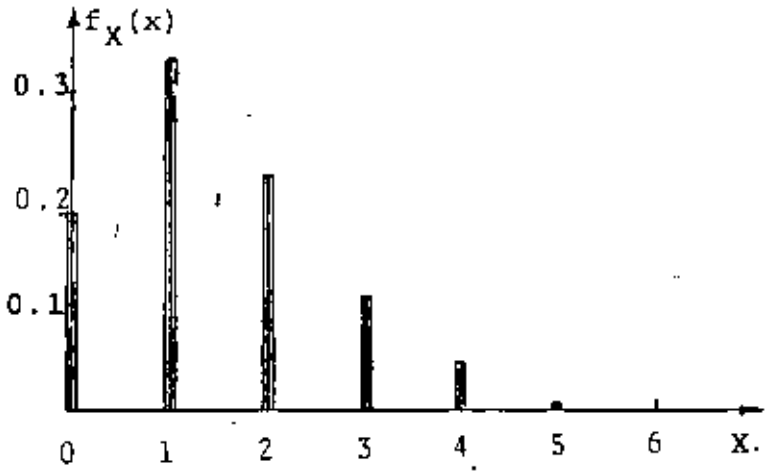

EJEMPLO

EN LA AMPLIACION DEL CARRIL PARA DAR VUELTA A LA IZQUIERDA EN UNA AVENIDA, SOLO HAY CAPACIDAD PARA 3 AUTOS COMO MAXIMO ESPERANDO LA FLECHA LUMINOSA DEL SEMAFORO. EN UN ESTUDIO ESTADISTICO DEL TRANSITO EN ESE LUGAR SE ENCONTRO QUE EN CADA CICLO DE LUCES DEL SEMAFORO HAY EN PROMEDIO 6 AUTOS QUE VAN A DAR VUELTA. ¿CUAL ES LA PROBABILIDAD DE QUE EN UN CICLO DEL SEMAFORO, TOMADO AL AZAR, SE CONGESTIONE EL TRANSITO POR EXCEDERSE LA CAPACIDAD DEL CARRIL?

$$G(3) = P[X>3] = ?$$

SI $A=\{X>3\}$, $\bar{A}=\{X\leq 3\}$

$P(\bar{A}) = 1-P(A)$ O $P(A)= 1-P(\bar{A})$. CON $\lambda=6$,

$$P(\bar{A}) = P[X\leq 3] = \sum_{x=0}^{x=3} f_X(x) = \sum_{x=0}^{x=3} \frac{e^{-6}6^x}{x!}$$

$$P(\bar{A}) = e^{-6}\left(1 + 6 + \frac{6^2}{2} + \frac{6^3}{6}\right) = 61e^{-6} = 0.151$$

$$P[A] = P[X>3] = 1-0.151 = 0.849$$

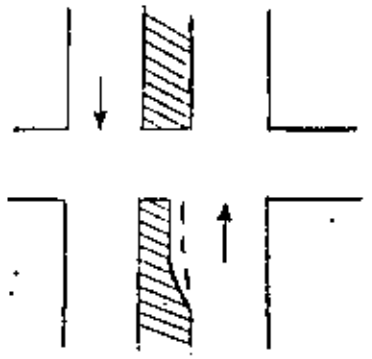

DE LAS TABLAS:

$P[X>3]= 1-P[X\leq 3]= 1-0.151=0.849$

PROCESO ESTOCASTICO DE POISSON

CON BASE EN LA DISTRIBUCION DE POISSON SE PUEDE DEDUCIR QUE LA DISTRIBUCION DE PROBABILIDADES DEL NUMERO DE OCURRENCIAS DE UN EVENTO DURANTE UN PERIODO t QUEDA DADA POR

$$f_X(x) = P[X = x \text{ EN UN LAPSO } t]$$

$$f_X(x) = \frac{(\lambda t)^x e^{-\lambda t}}{x!} \; ; \; x = 0, 1, 2, \ldots$$

DONDE

λ = NUMERO MEDIO DE OCURRENCIAS POR UNIDAD DE TIEMPO.

LA ESPERANZA Y LA VARIANCIA DE ESTE PROCESO, PARA UN LAPSO t, SON

$$E(X) = \lambda t$$

$$\sigma^2(X) = \lambda t$$

PARA QUE ESTA DISTRIBUCION SE APLIQUE SE REQUIERE QUE EL EVENTO OCURRA CADA VEZ DE MANERA INDEPENDIENTE DE LAS OCURRENCIAS PREVIAS, Y QUE λ SEA CONSTANTE. A λ SE LE CONOCE COMO INTENSIDAD DEL PROCESO; A SU RECIPROCO, $1/\lambda$ SE LE DENOMINA *PERIODO DE RECURRENCIA.*

t_i = tiempo de ocurrencia de iésimo evento

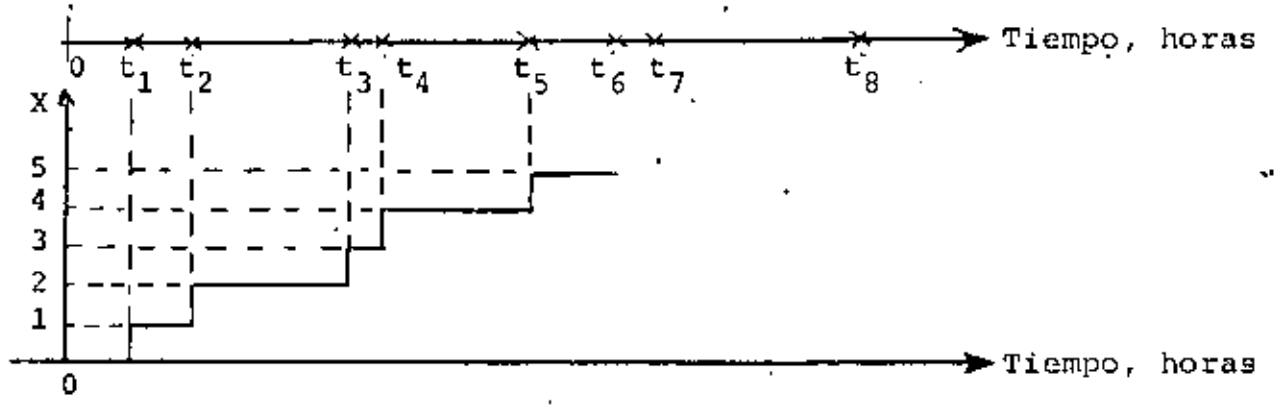

EJEMPLO

EN UNA CENTRAL DE COMUNICACIONES SE TIENE UNA DEMANDA MEDIA DEL SERVICIO DE 8 LLAMADAS CADA MINUTO. CALCULAR LAS PROBABILIDADES DE QUE EN 2 MINUTOS NO SE SOLICITE EL SERVICIO, DE QUE SE SOLICITE SOLO UNA VEZ, Y MAS DE UNA VEZ.

$$f_X(0) = P[X=0] = \frac{(\lambda t)^0 e^{-8x2}}{0!} = e^{-16} = 0.00004$$

$$f_X(1) = \frac{16^1 e^{-16}}{1!} = 0.00064$$

$$P[X>1] = 1 - (0.00004 + 0.00064) = 0.99932$$

EJEMPLO

MEDIANTE UN ESTUDIO ESTADISTICO SOBRE LA OCURRENCIA DE MAREMOTOS EN LA COSTA MEXICANA DEL OCEANO PACIFICO SE ESTIMO QUE UNA OLA DE 4m DE ALTURA O MAYOR SOBRE EL NIVEL DE LA MAREA TIENE UN PERIODO DE RECURRENCIA DE 100 AÑOS. CALCULAR LAS PROBABILIDADES DE QUE EN LOS PROXIMOS 10, 50 y 100 AÑOS NO OCURRA NINGUN MAREMOTO EN DICHA REGION CUYA OLA MAXIMA EXCEDE DE 4m, SUPONIENDO QUE LA OCURRENCIA DE LOS MAREMOTOS SE PUEDE MODELAR MEDIANTE UN PROCESO ESTOCASTICO DE POISSON.

LA DISTRIBUCION DE PROBABILIDADES DE LA VARIABLE ALEATORIA X=NUMERO DE MAREMOTOS CUYA OLA MAXIMA ES MAYOR DE 4m, CON $\lambda=1/100=0.01$ ES

$$f_X(x) = \frac{(\lambda t)^x e^{-\lambda t}}{x!} = \frac{(0.01t)^x e^{-0.01t}}{x!}$$

POR LO TANTO, PARA t=10, 50 Y 100 AÑOS, SE TIENE, RESPECTIVAMENTE, QUE:

a) $f_X(0) = \frac{(0.01\times10)^0 e^{-0.01\times10}}{0!} = e^{-0.1} = 0.905$

b) $f_X(0) = \frac{(0.01\times50)^0 e^{-0.01\times50}}{0!} = e^{-0.5} = 0.607$

c) $f_X(0) = \frac{(0.01\times100)^0 e^{-0.01\times100}}{0!} = e^{-1} = 0.368$

PARA ESTE MISMO PROBLEMA, LAS PROBABILIDADES DE QUE OCURRA AL MENOS UN MAREMOTO CON OLA MAXIMA MAYOR DE 4m SON, RESPECTIVAMENTE,

a) $P[X \geq 1] = 1 - f_X(0) = 1 - 0.905 = 0.095$

b) $P[X \geq 1] = 1 - 0.607 = 0.393$

c) $P[X \geq 1] = 1 - 0,368 = 0,632$

EJEMPLO

SE SABE QUE UNA MAQUINA QUE PRODUCE PAPEL PARA DIBUJO, LO HACE CON UN DEFECTO POR CADA 100 M FABRICADOS

a. ¿CUAL ES LA PROBABILIDAD DE TENER CERO DEFECTOS EN UN PLIEGO DE 20 M?

$\lambda = 1/100 = 0.01$ DEFECTOS /METRO

$$P(X = 0) = \frac{(\lambda t)^0 e^{-\lambda t}}{x!} = \frac{(0.01x20)^0 e^{-0.01x20}}{0!} =$$

$$\frac{(0.2)^0 e^{-0.2}}{0!} = 0.820$$

(EN ESTE CASO t = LONGITUD)

b. ¿CUAL ES LA PROBABILIDAD DE TENER UN DEFECTO EN 20m?

$$P(X = 1) = \frac{(0.2)^1 e^{-0.2}}{1!} = 0.164$$

c. ¿CUAL ES LA PROBABILIDAD DE TENER UNO O CERO DEFECTOS?

$P(0 \leq x \leq 1) = P(X = 0) + P(X = 1) = 0.820 + 0.164 = 0.984$

d. ¿CUAL ES LA PROBABILIDAD DE TENER MAS DE UN DEFECTO?

$P(X > 1) = 1 - P(X \leq 1) = 1 - 0.984 = 0.016$

EJEMPLO

SE SABE QUE EN CIERTA ZONA GEOGRAFICA SE LOCALIZA UNA ESPECIE ANIMAL RARA A RAZON DE 2 EJEMPLARES POR 100 KM^2. SI SE TOMA UNA FOTOGRAFIA AEREA QUE ABARQUE 120 KM^2, ¿CUAL ES LA PROBABILIDAD DE LOCALIZAR 5 ANIMALES?

$$\text{CON } \lambda = \frac{2}{100} = 0.02 \text{ ANIMALES/KM}^2$$

$$P(X = 5) = \frac{(\lambda t)^5 e^{-\lambda t}}{X!} = \frac{(0.02 \times 120)^5 e^{-0.02 \times 120}}{5!} =$$

$$\frac{2.4^5 e^{-2.4}}{5!} = \frac{79.626}{120 \times 10.943} = 0.061$$

(EN ESTE CASO t= AREA)

¿CUAL ES LA PROBABILIDAD DE LOCALIZAR UN ANIMAL?

$$P(X = 1) = \frac{2.4^1 e^{-2.4}}{1!} = 0.219$$

¿CUAL ES LA PROBABILIDAD DE NO LOCALIZAR NINGUNO?

$$P(X = 0) = \frac{(2.4)^0 e^{-2.4}}{0!} = 0.091$$

¿CUAL ES LA PROBABILIDAD DE LOCALIZAR MAS DE UNO?

$$P(X > 1) = 1 - P(X \leq 1) = 1 - (0.219 + 0.091) = 0.690$$

SE PUEDE DEMOSTRAR QUE:
CUANDO UN EVENTO OCURRE SIGUIENDO UN PROCESO DE POISSON, LA VARIABLE ALEATORIA "TIEMPO ENTRE UNA OCURRENCIA CUALQUIERA Y LA SIGUIENTE" TIENE UNA DISTRIBUCION DE PROBABILIDADES EXPONENCIAL.

EJEMPLO

SI LOS MAREMOTOS QUE SE REGISTRAN EN UN PUNTO DE LA COSTA MEXICANA DEL OCEANO PACIFICO OCURREN SIGUIENDO UN PROCESO DE POISSON CON $\lambda = 0.01$, CALCULAR LA PROBABILIDAD DE QUE ENTRE UN MAREMOTO Y EL SIGUIENTE TRANSCURRA UN TIEMPO

a. MAYOR DE 100 AÑOS
b. ENTRE 50 Y 100 AÑOS

$$a.\ P(t > 100) = \int_{100}^{\infty} \lambda\, e^{-\lambda t} dt = e^{-0.01 \times 100} = e^{-1} = 36.79\%$$

$$b.\ P(50 \leq t \leq 100) = \int_{50}^{100} 0.01\, e^{-0.01\, t} dt = F(100) - F(50)$$

$$= (1 - e^{-0.01 \times 100}) - (1 - e^{-0.01 \times 50}) = e^{-0.5} - e^{-1} =$$

$$0.6065 - 0.3679 = 0,2386$$

VARIABLES ALEATORIAS CONTINUAS

DISTRIBUCION UNIFORME

SE DICE QUE UNA VARIABLE ALEATORIA CONTINUA, X, TIENE *DISTRIBUCION UNIFORME* ENTRE X = a Y X = b(b>a) SI

$$f_X(x) = \text{CONSTANTE} = \frac{1}{b - a} \quad ; \quad a \leq X \leq b$$

LO QUE SIGNIFICA QUE LA PROBABILIDAD DE OBTENER UN VALOR ENTRE x Y x + dx ES LA MISMA PARA CUALQUIER x COMPRENDIDA ENTRE a Y b. LA GRAFICA DE DICHA DISTRIBUCION ES

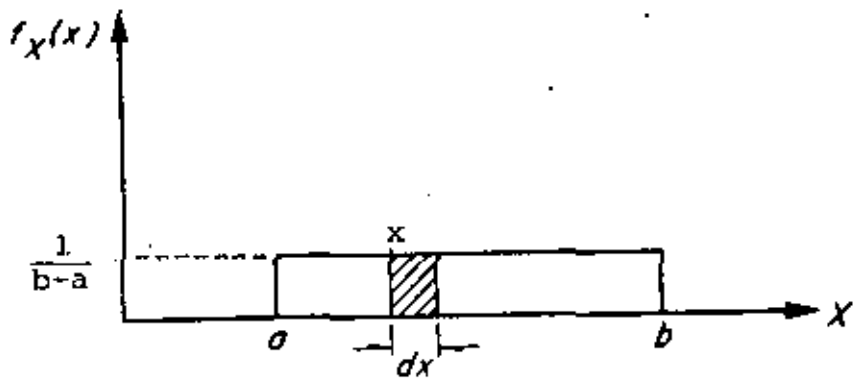

Distribución uniforme de una variable aleatoria continua

LA ESPERANZA Y LA VARIANCIA DE LA DISTRIBUCION UNIFORME SE CALCULAN DE LA SIGUIENTE MANERA:

$$E[X] = \int_a^b x \frac{1}{b-a}\,dx = \left[\frac{x^2}{2(b-a)}\right]_a^b = \frac{b^2 - a^2}{2(b-a)} = (b + a)/2$$

$$\sigma^2(X) = \int_a^b (x - E[X])^2 \frac{1}{b-a}\,dx = \int_a^b \frac{x^2}{b-a}\,dx + \int_a^b \frac{(E[X])^2}{b-a}\,dx -$$

$$- \int_a^b \frac{2xE[X]}{a-b}\,dx$$

$$= \left[\frac{x^3}{3(b-a)}\right]_a^b + \left[\frac{(E[X])^2}{b-a}\,x\right]_a^b - \left[\frac{2\,E[X]}{b-a}\,\frac{x^2}{2}\right]_a^b =$$

$$= \frac{b^3 - a^3}{3(b-a)} + (E[X])^2 - E[X](b + a) = \frac{(b-a)^2}{12}$$

LA DISTRIBUCION DE PROBABILIDADES ACUMULADAS ES

$$F_X(x) = \int_a^x f_X(u)\,du = \int_a^x \frac{1}{b-a}\,du = \frac{x-a}{b-a}, \quad a \leq x \leq b$$

LA GRAFICA DE ESTA FUNCION ES UNA LINEA RECTA DE a A b:

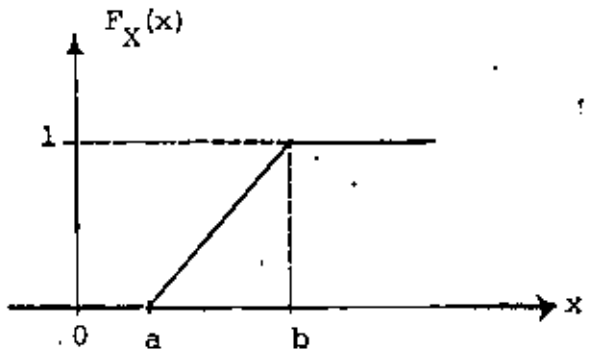

EJEMPLO

¿CUANTO VALE LA PROBABILIDAD DE QUE X SEA MENOR QUE 1/3, SI ES UNA VARIABLE ALEATORIA CON DISTRIBUCION UNIFORME EN EL INTERVALO 0-1?

$$F_X\left(\frac{1}{3}\right) = \frac{x - a}{b - a} = \frac{\frac{1}{3} - a}{b - a}$$

PARA a = 0 Y b = 1 NOS QUEDA

$$F_X\left(\frac{1}{3}\right) = \frac{\frac{1}{3} - 0}{1 - 0} = \frac{1}{3}$$

DISTRIBUCION NORMAL

UNA DE LAS DISTRIBUCIONES DE VARIABLES ALEATORIAS CONTINUAS MAS UTIL ES LA *DISTRIBUCION NORMAL* O DE *GAUSS*, DEFINIDA POR LA ECUACION

$$f_X(x) = \frac{1}{\sigma\sqrt{2\pi}}\, e^{-(x-\mu)^2/2\sigma^2}$$

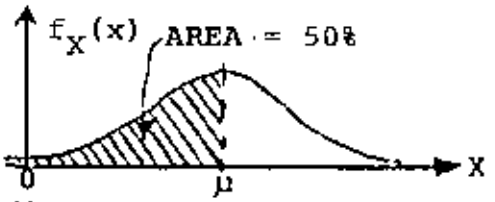

DONDE μ ES LA MEDIA Y σ LA DESVIACION ESTANDAR DE X.

SI SE HACE LA TRANSFORMACION

$$Z = (X-\mu)/\sigma \quad \left(E(Z) = E\left[\frac{x-\mu}{\sigma}\right] = \frac{E(x)-\mu}{\sigma} = 0;\ \sigma^2(Z)\ \frac{\sigma^2(x)}{\sigma^2} = 1\right)$$

ENTONCES LA ECUACION ANTERIOR SE REDUCE A LA LLAMADA *FORMA ESTANDAR*, CUYA ECUACION ES

$$f_Z(z) = \frac{1}{\sqrt{2\pi}}\, e^{-z^2/2} \ ;\ F_Z(z) = \int_{-\infty}^{z} \frac{1}{\sqrt{2\pi}}\, e^{-z^2/2}\, dz$$

EN ESTE CASO LA VARIABLE ALEATORIA Z TIENE DISTRIBUCION NORMAL CON *MEDIA IGUAL A CERO Y VARIANCIA IGUAL A UNO.*

EXISTEN TABLAS PARA CALCULAR LAS PROBABILIDADES DE UNA VARIABLE ASOCIADA A UNA DISTRIBUCION NORMAL ESTANDAR. EN LA SIGUIENTE FIGURA SE MUESTRA LA FORMA DE CAMPANA DE ESTA DISTRIBUCION, OBSERVANDOSE LA SIMETRIA RESPECTO A Z=E(Z)=0 Y QUE ES ASINTOTICA AL EJE Z.

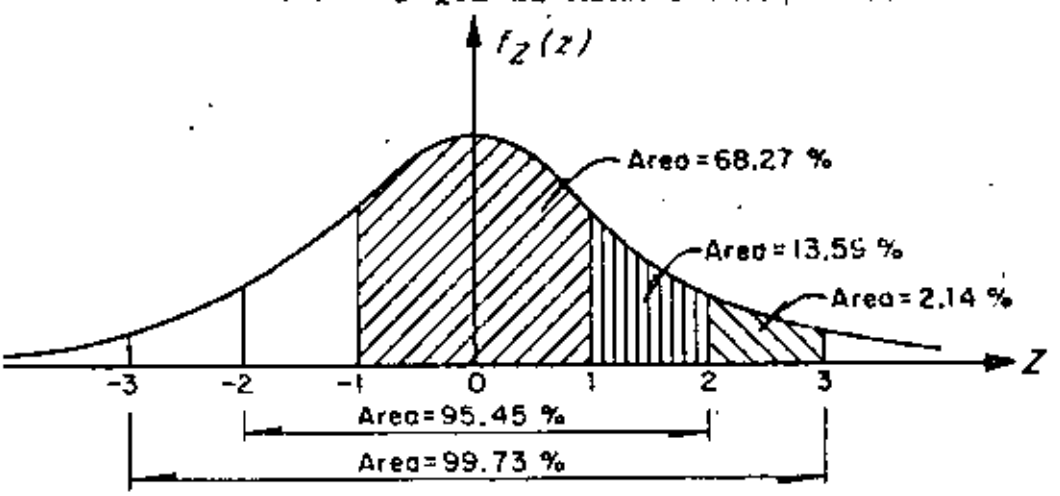

Distribución normal de una variable aleatoria continua

LA UTILIDAD DE LA DISTRIBUCION NORMAL ESTANDAR RADICA EN QUE

$$P[x_1 \leq X \leq x_2] = \int_{x_1}^{x_2} f_X(x)dx = P[z_1 \leq Z \leq z_2] = \int_{z_1}^{z_2} f_Z(z)dz$$

DONDE

$$z_1 = \frac{z_{1-\mu}}{\sigma} \quad Y \quad z_2 = \frac{x_{2-\mu}}{\sigma}$$

TABLA 3

FUNCION DE DISTRIBUCION NORMAL ESTANDAR

$$F_Z(z) = \int_{-\infty}^{z} \frac{1}{\sqrt{2\pi}} e^{-u^2/2}\, du$$

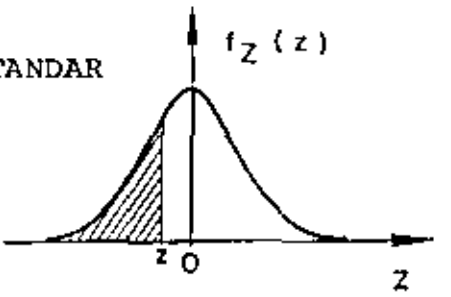

z	0	1	2	3	4	5	6	7	8	9
−3.	.0013									
−2.9	.0019	.0018	.0017	.0017	.0016	.0016	.0015	.0015	.0014	.0014
−2.8	.0026	.0025	.0024	.0023	.0023	.0022	.0021	.0021	.0020	.0019
−2.7	.0035	.0034	.0033	.0032	.0031	.0030	.0029	.0028	.0027	.0026
−2.6	.0047	.0045	.0044	.0043	.0041	.0040	.0039	.0038	.0037	.0036
−2.5	.0062	.0060	.0059	.0057	.0055	.0054	.0052	.0051	.0049	.0048
−2.4	.0082	.0080	.0078	.0075	.0073	.0071	.0069	.0068	.0066	.0064
−2.3	.0107	.0104	.0102	.0099	.0096	.0094	.0091	.0089	.0087	.0084
−2.2	.0139	.0136	.0132	.0129	.0125	.0122	.0119	.0116	.0113	.0110
−2.1	.0179	.0174	.0170	.0166	.0162	.0158	0154	.0150	.0146	.0143
−2.0	.0227	.0222	.0217	.0212	.0207	.0202	.0197	.0192	.0188	.0183
−1.9	.0287	.0281	.0274	.0268	.0262	.0256	.0250	.0244	.0239	.0233
−1.8	.0359	.0351	.0344	.0336	.0329	.0322	.0314	.0307	.0300	.0294
−1.7	.0446	.0436	.0427	.0418	.0409	.0401	.0392	.0384	.0375	.0367
−1.6	.0548	.0537	.0526	.0516	.0505	.0495	.0485	.0475	.0465	.0455
−1.5	.0668	.0655	.0643	.0630	.0618	.0606	.0594	.0582	.0571	.0559
−1.4	.0808	.0793	.0778	.0764	.0749	.0735	0721	.0708	.0694	.0681
−1.3	.0968	.0951	.0934	.0918	.0901	.0885	.0869	.0853	.0838	.0823
−1.2	.1151	.1131	.1112	.1093	.1075	.1056	.1038	.1020	.1003	.0985
−1.1	.1357	.1335	.1314	.1292	.1271	.1251	.1230	.1210	.1190	.1170
−1.0	.1587	.1562	.1539	.1515	.1492	.1469	.1446	.1423	.1401	.1379
−.9	.1841	.1814	.1788	.1762	.1736	.1711	.1685	.1660	.1635	.1611
−.8	.2119	.2090	.2061	.2033	.2005	.1977	.1949	.1921	.1894	.1867
−.7	.2420	.2389	.2358	.2326	.2297	.2266	.2236	.2206	.2177	.2148
−.6	.2743	.2709	.2676	.2643	.2611	.2578	.2546	.2514	.2483	.2451
−.5	.3085	.3050	.3015	.2981	.2946	.2912	.2877	.2843	.2810	.2776
−.4	.3446	.3409	.3372	.3336	.3300	.3264	.3228	.3192	.3156	.3121
−.3	.3821	.3783	.3745	.3707	.3669	.3632	.3594	.3557	.3520	.3483
−.2	.4207	.4168	.4129	.4090	.4052	.4013	.3974	.3936	.3897	.3859
−.1	.4602	.4562	.4522	.4483	.4443	.4404	.4364	.4325	.4286	.4247
−.0	.5000	.4960	.4920	.4880	.4840	.4801	.4761	.4721	.4681	.4641

TABLA 3 (continuación)

FUNCION DE DISTRIBUCION NORMAL ESTANDAR

$$F_Z(z) = \int_{-\infty}^{z} \frac{1}{\sqrt{2\pi}} e^{-u^2/2}\, du$$

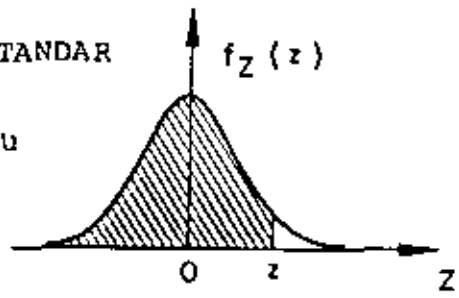

z	0	1	2	3	4	5	6	7	8	9
.0	.5000	.5040	.5080	.5120	.5160	.5199	.5239	.5279	.5319	.5359
.1	.5398	.5438	.5478	.5517	.5557	.5596	.5636	.5675	.5714	.5753
.2	.5793	.5832	.5871	.5910	.5948	.5987	.6026	.6064	.6103	.6141
.3	.6179	.6217	.6255	.6293	.6331	.6368	.6406	.6443	.6480	.6517
.4	.6554	.6591	.6628	.6664	.6700	.6736	.6772	.6808	.6844	.6879
.5	.6915	.6950	.6985	.7019	.7054	.7088	.7123	.7157	.7190	.7224
.6	.7257	.7291	.7324	.7357	.7389	.7422	.7454	.7486	.7517	.7549
.7	.7580	.7611	.7642	.7673	.7704	.7734	.7764	.7794	.7823	.7852
.8	.7881	.7910	.7939	.7967	.7995	.8023	.8051	.8079	.8106	.8133
.9	.8159	.8186	.8212	.8238	.8264	.8289	.8315	.8340	.8365	.8389
1.0	.8413	.8438	.8461	.8485	.8508	.8531	.8554	.8577	.8599	.8621
1.1	.8643	.8665	.8686	.8708	.8729	.8749	.8770	.8790	.8810	.8830
1.2	.8849	.8869	.8888	.8907	.8925	.8944	.8962	.8980	.8997	.9015
1.3	.9032	.9049	.9066	.9082	.9099	.9115	.9131	.9147	.9162	.9177
1.4	.9192	.9207	.9222	.9236	.9251	.9265	.9279	.9292	.9306	.9319
1.5	.9332	.9345	.9357	.9370	.9382	.9394	.9406	.9418	.9429	.9441
1.6	.9452	.9463	.9474	.9484	.9495	.9505	.9515	.9525	.9535	.9545
1.7	.9554	.9564	.9573	.9582	.9591	.9599	.9608	.9616	.9625	.9633
1.8	.9641	.9649	.9656	.9664	.9671	.9678	.9686	.9693	.9700	.9706
1.9	.9713	.9719	.9726	.9732	.9738	.9744	.9750	.9756	.9761	.9767
2.0	.9773	.9778	.9783	.9788	.9793	.9798	.9803	.9808	.9812	.9817
2.1	.9821	.9826	.9830	.9834	.9838	.9842	.9846	.9850	.9854	.9857
2.2	.9861	.9864	.9868	.9871	.9875	.9878	.9881	.9884	.9887	.9890
2.3	.9893	.9896	.9898	.9901	.9904	.9906	.9909	.9911	.9913	.9916
2.4	.9918	.9920	.9922	.9925	.9927	.9929	.9931	.9932	.9934	.9936
2.5	.9939	.9940	.9941	.9943	.9945	.9946	.9948	.9949	.9951	.9952
2.6	.9953	.9955	.9956	.9957	.9959	.9960	.9961	.9962	.9963	.9964
2.7	.9965	.9966	.9967	.9968	.9969	.9970	.9971	.9972	.9973	.9974
2.8	.9974	.9975	.9976	.9977	.9977	.9978	.9979	.9979	.9980	.9981
2.9	.9981	.9982	.9982	.9983	.9984	.9984	.9985	.9985	.9986	.9986
3.	.9987									

EJEMPLO

COMO RESULTADO DE UNA LARGA SERIE DE EXPERIMENTOS PROBANDO A COMPRESION SIMPLE CILINDROS DE CONCRETO, SE HA ESTIMADO QUE LA ESPERANZA DE LA RESISTENCIA ES DE 240 KG/CM^2 Y LA DESVIACION ESTANDAR DE 30 KG/CM^2.

A) ¿CUAL ES LA PROBABILIDAD DE QUE OTRO CILINDRO TOMADO AL AZAR RESISTA MENOS DE 240 KG/CM^2?

B. ¿CUAL ES LA PROBABILIDAD DE QUE RESISTA MAS DE 330 KG/CM^2?

C) ¿CUAL ES LA PROBABILIDAD DE QUE SU RESISTENCIA ESTE EN EL INTERVALO DE 210 A 240 KG/CM^2?

SUPONGASE QUE LA DISTRIBUCION DE PROBABILIDADES ES NORMAL.

SOLUCION

A) PARA EMPLEAR LAS TABLAS DE DISTRIBUCION NORMAL ES NECESARIO ESTANDARIZAR LA VARIABLE X, EMPLEANDO $\mu=240$ Y $\sigma=30$, CON $x_1=240$:

$$z_1 = \frac{240 - 240}{30} = 0$$

RECURRIENDO A LA TABLA DE LA DISTRIBUCION NORMAL SE OBTIENE

$$P[X \leq 240] = P[Z \leq 0] = 0.5$$

O SEA, LA PROBABILIDAD QUE CORRESPONDE AL AREA SOMBREADA DE LA SIGUIENTE FIGURA:

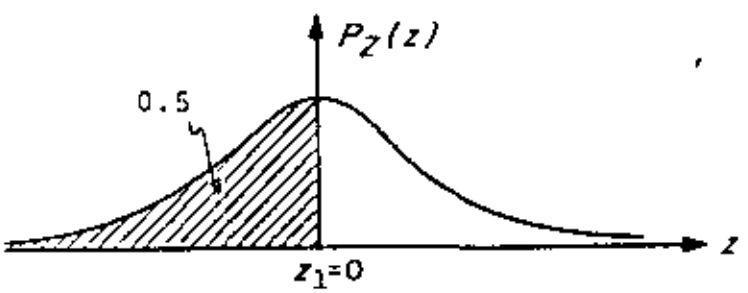

Distribución normal correspondiente al inciso c del ejemplo

B) EL VALOR ESTANDARIZADO DE LA VARIABLE, PARA x_1=330 KG/CM^2, ES

$$z_1 = \frac{330 - 240}{30} = 3$$

POR LO QUE

$$P[X \geq 330] = P[Z \geq 3] = 1-0.9987 = 0.0013$$

QUE ES EL AREA SOMBREADA DE LA SIGUIENTE FIGURA:

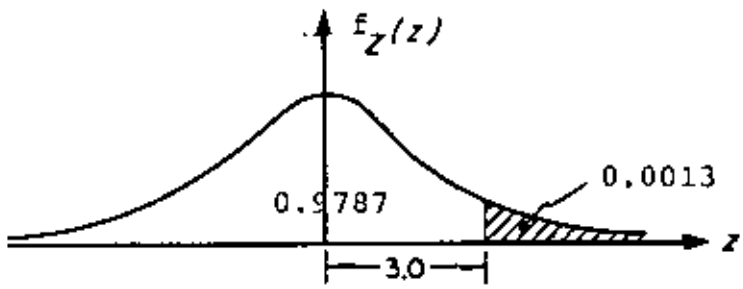

Distribución normal correspondiente al inciso b del ejemplo

C) LOS VALORES ESTANDARIZADOS DE LA VARIABLE, PARA x_1=210 Y x_2=240 SON:

$$z_1 = \frac{210 - 240}{30} = -1$$

$$z_2 = \frac{240 - 240}{30} = 0$$

POR LO QUE

$$P[210 \leq X \leq 240] = P[-1 \leq Z \leq 0] = 0.3413$$

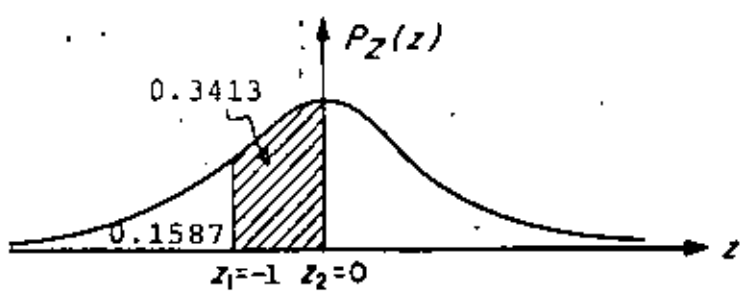

Distribución normal correspondiente al inciso c del ejemplo

EJEMPLO

SE HA ENCONTRADO QUE LA VARIABLE ALEATORIA "ERROR EN LA MEDICION DE LAS DISTANCIAS ENTRE DOS PUNTOS" TIENE DISTRIBUCION NORMAL CON MEDIA CERO. SI SE SABE QUE EL TAMAÑO VERDADERO DE UNA LINEA ES DE 2 M Y QUE LA VARIANCIA DE SUMEDICION ES $9CM^2$, CALCULAR LA PROBABILIDAD DE QUE EN UNA MEDICION LA LONGITUD QUE SE REGISTRE SEA

a. MENOR DE 195 CM
b. MAYOR DE 203 CM
c. COMPRENDIDO ENTRE 198 Y 202 CM.

a. $P(X < 195) = ?$ CON $\mu = 200$ CM Y $\sigma = \sqrt{9} = 3$ CM

$$Z = \frac{195-200}{3} = \frac{-5}{3} = -1.67$$

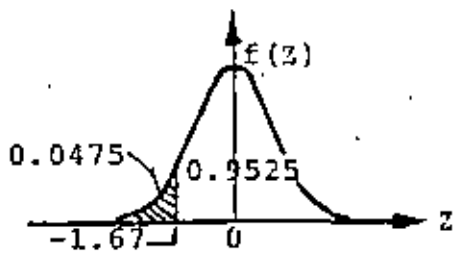

$P(X < 195) = P(Z < -1.67) = 0.0475 = 4.75\%$

b. $$Z = \frac{203 - 200}{3} = 1$$

$P(X > 203) = 1 - P(X \leq 203) = 1 - P(Z < 1) = 1 - 0.8413 = 0.1587 = 15.87\%$

c. $P(198 < X < 202) = ?$

$$Z_1 = \frac{198 - 200}{3} = -0.67, \quad Z_2 = \frac{202 - 200}{3} = 0.67$$

$P(198 < X < 202) = P(-0.67 < Z < 0.67) = 2 \times 0.2486 = 0.4972 = 49.72\ \%$

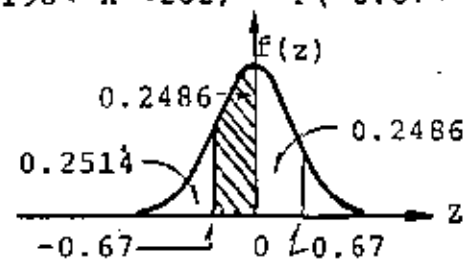

TEOREMA CENTRAL DEL LIMITE

SEAN LAS VARIABLES ALEATORIAS $X_1, X_2, \ldots, X_k$, CON DENSIDADES DE PROBABILIDADES ARBITRARIAS, CUYA SUMA SE DENOTARA COMO W, ES DECIR

$$W = X_1 + X_2 + \ldots + X_k$$

ES POSIBLE DEMOSTRAR EL TEOREMA DENOMINADO *TEOREMA CENTRAL DEL LIMITE*, CUYO ENUNCIADO INDICA QUE CONFORME AUMENTA EL NUMERO DE VARIABLES INVOLUCRADAS EN LA SUMA ANTERIOR (AL AUMENTAR k), LA DENSIDAD DE PROBABILIDADES DE W TIENDE A SER LA DISTRIBUCION NORMAL. ADEMAS SE PUEDE DEMOSTRAR QUE SI TODAS LAS VARIABLES $X_1, X_2, \ldots, X_k$ TIENEN DISTRIBUCION NORMAL, ENTONCES, RIGUROSAMENTE, W TAMBIEN LA TIENE, INDEPENDIENTEMENTE DEL NUMERO DE VARIABLES QUE APAREZCAN EN LA SUMA.

A PARTIR DEL TEOREMA DEL LIMITE CENTRAL SE DEMUESTRA QUE LA DISTRIBUCION DE BERNOULLI SE PUEDE APROXIMAR MEDIANTE LA NORMAL CUANDO EL NUMERO DE REPETICIONES DEL EXPERIMENTO ES GRANDE (30 O MAS), CON LO CUAL SE LOGRA UN AHORRO CONSIDERABLE DE LABOR NUMERICA EN LA SOLUCION DE ALGUNOS PROBLEMAS. PARA MEJORAR ESTA APROXIMACION, CONVIENE EFECTUAR UNA CORRECCION POR CONTINUIDAD, LA CUAL SE JUSTIFICA POR USAR UNA DISTRIBUCION CONTINUA EN VEZ DE UNA DISCRETA, SUMANDO O RESTANDO, SEGUN SEA EL CASO, 0.5 AL VALOR DE X QUE SE USE. POR EJEMPLO, SI SE DESEA CUANTIFICAR LA PROBABILIDAD DE QUE DE 2000 ENSAYES SE LOGREN DE 3 A 6 EXITOS, LOS LIMITES REALES QUE SE DEBEN USAR AL APLICAR LA DISTRIBUCION CONTINUA SON $x_1=2.5$ Y $x_2=6.5$.

centro de educación continua
división de estudios de posgrado
facultad de ingeniería unam

VI CURSO INTERNACIONAL DE INGENIERIA SISMICA

SISMOLOGIA Y SISMICIDAD

GEOLOGY AND PROBABILITY IN THE ASSESSMENT OF SEISMIC RISK

DR. LUIS ESTEVA MARABOTO

JULIO, 1980

RESUMEN

Se presenta un criterio para la evaluación probabilística de riesgo sísmico cuando se cuenta con información geotectónica y sismológica. Los procedimientos sugeridos se basan en el empleo de la evidencia geológica para la formulación de un conjunto de hipótesis alternativas sobre los modelos analíticos de sismicidad. Se asigna una distribución de probabilidades a dicho conjunto y se introduce la evidencia estadística para juzgar la validez de cada hipótesis y modificar la probabilidad asignada inicialmente a ella.

ABSTRACT

A criterion is presented for the probabilistic evaluation of seismic risk when geotectonic and seismological information is available. The procedures suggested rely on use of geological evidence for the formulation of a set of alternate hypotheses concerning analytical models of seismicity. A probability distribution is assigned to that set and statistical evidence is introduced in order to assess the probable validity of each hypothesis and to modify the initial probability initially assigned to it.

1. INTRODUCTION

Rational formulation of engineering decisions in seismic areas requires probabilistic assessment of the maximum intensities that may occur at a site in given time intervals. Unlike variables that are relevant in many other decision problems, where probabilities are estimated almost exclusively on the basis of relative frequencies of the outcomes of repetitions of a given experiment, seismic risk estimates should make use of information stemming from sources of different nature, some of which, while being the object of probabilistic evaluations, can not be interpreted in terms of relative frequencies. Thus, geologists talk of the maximum magnitude that may be generated in a given area, by looking at the dimensions of the gological accidents and by extrapolating the observations of other regions which available evidence allows to brand as similar to the one of interest. Following nearly parallel lines, some geophysicists estimate the energy that can be liberated by a single shock in a given area by making quantitative

assumptions about source dimensions, dislocation amplitude and stress drop, consistent with tectonic models of the region and, again, with comparisons with areas of similar tectonic characteristics. Statisticians, on the other hand, are prone to base their predictions of the future exclusively on the basis of observations on a sample, however scanty that sample may be.

None of these approaches, by itself, suffices to provide a satisfactory answer to the requirements of decision makers: purely statistical analysis is unacceptable because it neglects a wealth of relevant information, and it is not clear that bounds can always be assigned to magnitudes in given areas, or that, when this is feasible, those bounds are sufficiently low that designing for them is economically sound, even if they are not very likely to occur in the near future. In fact, some studies relating source dimensions, stress drop and magnitude show that, considering not unusually high stress drops, it does not take very large source dimensions to get magnitudes 8.0 and greater.

A criterion for combining the above approaches in the probabilistic assessment of seismic risk is presented in this paper. Its philosophy consists in using the geological, geophysical or any other non-statistical evidence for producing a set of alternate assumptions concerning a mathematical (stochastic process) model of seismicity in a given source area. An initial, or prior, probability is assigned to each hypothesis, and the statistical information is then used for improving that probability assignment. The criterion is based on application of Bayes theorem, also called the theorem of the probabilities of the hypotheses. A previous formulation (1) has

evolved through the interaction of multidisciplinary groups in the development of seismic risk studies performed in the last few years in Mexico (2-4). Since estimates of risk depend on conceptual models of the geophysical process involved, and these are little known at present, more questions are raised here than solutions given.

2. MEASURES OF SEISMIC RISK

Let y be a measure of earthquake intensity. According to the problem at hand, y may be peak ground acceleration, velocity, spectral ordinate for a given natural period, or, shortly, any variable that determines the response of the system under study. This means that a relation can be established between the intensity of a given earthquake and the corresponding loss D(y).

A commonly applied criterion assumes that seismic risk should be measured by the highest intensity that can be caused at the site by the largest-magnitude earthquake that can be generated at any of the potential seismic sources in the vicinity. However, engineering systems cannot always be designed for the worst possible condition to be expected. Instead, decisions have to be based on cost-benefit studies. When designing for earthquakes, a significant cost term is made of the value of the expected actualized cost of damage or failure, as given by the following equation:

$$E[F] = \int_0^{\infty} \delta_t e^{-\gamma t} dt. \qquad (1)$$

Here, $e^{-\gamma t}$ is a compound interest actualization function, γ the interest rate and δ_t the expected cost of damage or failure per unit time at instant t. Its value can be obtained from Eq 2, where $\nu_t(y)$ (in general a function of t) is the mean number of earthquakes per unit time whose intensity is greater than y and D(y) is defined above*

$$\delta_t = \int_0^\infty - \frac{\partial \nu_t(y)}{\partial y} D(y)\, dy \qquad (2)$$

From Eqs 1 and 2 and the corresponding cost-benefit studies, it is concluded that evaluation of seismic risk for engineering purposes implies the definition of function $\nu_t(y)$ (henceforth called regional seismicity). This can be done as shown in the sequel.

3. MAGNITUDES, INTENSITIES AND FREQUENCY FUNCTIONS

With the possible exception of the rare cases where the record of intensities at a site suffices for producing reliable estimates of $\nu_t(y)$, evaluation of seismic risk should include the following steps:

a) Identifying the potential sources of activity
b) Formulating mathematical models of local seismicity for each source
c) Obtaining the contribution of each source to $\nu_t(y)$ and adding up contributions of the various sources.

---

* Eqs. 1 and 2 imply that every time that some damage or failure occurs the system is repaired or rebuilt in such a manner that the function D(y) remains unchanged. Corresponding expressions can be obtained for more general conditions (19). In general they require no more information about the mathematical model of seismicity.

This section deals with step c). The rest of the paper is devoted to the more difficult problems relevant to steps a) and b).

Let $\lambda_t(M)$ (also a function of time, as is regional seismicity) be the mean number of earthquakes with magnitude greater than M generated per unit volume and per unit time in a given seismic source. If a deterministic relationship M(y, X) holds between magnitude M, intensity y at a site, and focal coordinates X of an earthquake, $\nu_t(y)$ and $\lambda_t(M)$ can be related as follows:

$$\nu_t(y) = \int_{vol} \lambda_t(M(y,X))\, dV \qquad (3a)$$

Unless some information is available concerning systematic effects related to a given origin and a given site (attributable either to local soil or to propagation path properties), the influence of X is a function only of distance R, either to the instrumental focus or to the causative fault. Eq 3 then becomes:

$$\nu_t(y) = \int_{vol} \lambda_t(M(y,R))\, dV \qquad (3b)$$

A number of empirical or semi-empirical expressions relating M, R and y have been proposed. A summary of them is given in Ref 5. The author has made use of information in Refs 6-8 in order to derive expressions relating magnitude, hypocentral distance and various measures of intensity on firm ground, such as peak ground acceleration and of velocity (respectively a, v, $\bar{A}$ and $\bar{V}$) (9). These expressions are of the form

$$y = b_1 e^{b_2 M} R'^{-b_3} \qquad (4)$$

where $R' = R + R_0$; R must be given in kilometers and b_1, b_2, b_3 and R_0 are given in Table 1, which also shows the mean m and the standard deviation σ of the natural logarithm of the ratio of observed to computed intensities.

TABLE 1. EXPRESSIONS RELATING MAGNITUDE, INTENSITY AND HYPOCENTRAL DISTANCE

Expression for:	b_1	b_2	b_3	R_0	m	σ
v (cm/sec)	32	1.0	1.7	25	0.124	0.74
a (cm/sec^2)	5 600	0.8	2.0	40	0.04	0.64
$\overline{V}$ (cm/sec)	250	1.0	1.7	60	0.058	0.64
$\overline{A}$ (cm/sec^2)	69 600	0.8	2.0	70	0	0.75

The significant dispersion of these expressions, implied by the high values of σ, is due mainly to their having been obtained from data of earthquakes originating in different sources and having different mechanisms and propagation paths. The form of Eq 4 gives place, moreover, to a faster variation of intensities with respect to magnitudes in the near field than what occurs in nature because the liberation of energy is distributed throughout volumes whose dimensions can be significant with respect to the site-to-source distance. This relatively low sensitivity of y with respect to M in the near field has been verified in practice at least for earthquakes produced by a strike-slip mechanism (10, 11). This effect can be represented by expressions as simple as Eq 4, if b_2 is taken, for instance, of the form $b_2 = A + BR/(C + R)$.

For wide zones in the earth's crust, $\lambda(M)$, the average value of $\lambda_t(M)$ over long time intervals, can be approximated as follows,

$$\lambda(M) = \alpha_1 e^{-\beta_1 M} \quad \text{for } M \leq M_1$$
$$\lambda(M) = \alpha_2 e^{-\beta_2 M} \quad \text{for } M > M_1 \qquad (5)$$

where $\beta_2 \geq \beta_1$, M_1 is a magnitude beyond which there is a higher rate of decrease of $\lambda(M)$ with magnitude; continuity at M_1 requires that α_2 equal $\alpha_1 \exp((\beta_2 - \beta_1) M_1)$.

As a result of the statistical dispersion in the expressions relating M, X and y, Eq 3 has to be changed to the following:

$$\nu(y) = \int_{vol} \lambda [M(y,X)] \varphi (y, X) \, dV \qquad (6)$$

where $\varphi(y, X)$ is a corrective function that can be computed as described in Ref 21.

4. ANALYTICAL MODELS OF SEISMICITY

As has been pointed out, when engineering decisions concerning construction in seismic areas have to be made, it does not suffice to express local seismicity in terms of an upper bound for magnitudes, the probability of whose excedance is arbitrarily assumed to be negligibly small. Instead, it should be expressed in terms of the probability distribution of the maximum magnitude that can be generated at given sources during given time periods. These probabilities depend on the following functions:

a) Frequency-magnitude relations for small volumes of the earth's crust
b) Statistical correlation functions of the process of earthquake generation in time and space.

The analytical models of local seismicity postulated in this paper are stochastic processes of the renewal type: the time interval between occurrence of successive earthquakes having magnitudes greater than a given value are mutually independent random variables. Let T be any such time interval. Its probability density function will be assumed of the gamma type:

$$f_T(t) = \frac{\nu}{(k-1)!} (\nu t)^{k-1} e^{-\nu t} \qquad (7)$$

Here, ν and k are two positive numbers and a! is the factorial function of a. This distribution was adopted because a wide number of distributions can be approximated by it, if parameters ν and k are properly chosen (17). ν and k are related with the first two moments of the probability density function of T:

$$E(T) = k/\nu, \; V(T) = 1/\sqrt{k} \qquad (8)$$

where E means expectation and V coefficient of variation.

The probability density function of the wainting time T_1, from the origin to the occurrence of the first event, differs from Eq 7, since the time elapsed between the last prior event is usually unknown. The distribution of T_1 coincides with that of the excess life in a renewal process at an arbitrary value of t that tends to infinity. The corresponding probability density function has been shown to be (18)

$$f_{T_1}(t) = \frac{1}{E(T)} [1 - F_T(t)] \qquad (9)$$

where $F_T(t)$ is the probability distribution function of the time between successive events.

An important function in decisions under seismic hazard conditions is the conditional distribution of the additional time to next event, when it is known that there have been no events for a time t_0. If t_0 is measured from the instant just following the occurrence of an event and if $\tau = (T - t_0)/E(T)$ and $u_0 = t_0/E(T)$, then

$$f_\tau(u \mid T > t_0) = \frac{f_{T/E(T)}(u + u_0)}{1 - F_{T/E(T)}(u_0)} \qquad (10)$$

The Poisson process is the particular case of the gamma process for which $k = 1$. In that instance, Eqs 7, 9 and 10 lead to

$$f_T(t) = f_{T_1}(t) = f_{T-t_0}(t \mid T > t_0) = f_{T_1-t_0}(t \mid T_1 > t_0) = \nu e^{-\nu t} \qquad (11)$$

which reflect the non-informative property of Poisson process: at any given instant the conditional probability density function of the time to next event does not depend on the time elapsed since the last one.

Explicit expressions for evaluation of the conditional and the unconditional probability density functions of T and T_1 for the general gamma process are given in the appendix.

The Poisson process assumption is ordinarily adopted in probabilistic seismic risk studies. It is difficult either to substantiate it or to reject it in general on the basis of statistical data alone, since these are scanty,

particularly in small areas or for large magnitudes. After consideration of the geophysical processes in play it is reasonable to conclude, however, that if strain energy stored in a region grows in a more or less systematic manner, the risk function should grow with the time elapsed since the last event. Preliminary statistical analysis of the waiting times between earthquakes with magnitudes 6.5 or 7.0 and greater in some seismic provinces in the southern coast of Mexico shows that if shocks occurred in the same seismic province within a few months of each other are lumped together as single events, the resulting distribution of waiting times can be approximated by a gamma function with $k = 2$. However, results have not been uniform. Reliable evaluations of alternate assumptions concerning k will have to rest partially on simulation of the process of storage and liberation of strain energy.

According to Eqs 1 and 2, the actualized value of the expected cost of damage or failure is a function of $\nu_i(y)$, which is a function not only of $\lambda(M)$ in the neighbouring seismic sources, but also of the probability distribution of $T/E(T)$. The possible significance of the value of k in the variables that affect seismic design decisions can be inferred from Table 2, which compares the initial and the conditional expected values of the time to next event, as well as the actualized values of the expected cost of failure for the Poisson and the gamma processes. These quantities were computed by means of the expressions developed in the appendix. The actualized value of the expected cost of failure was obtained from the expression that follows.

$$\frac{E[F]}{D} = \int_0^{\infty} f_T(t+t_o \mid T \geq t_o)\, e^{-\gamma t}\, dt \qquad (12)$$

This expression is consistent with the assumptions that a structure fails when a given intensity with return period E(T) is exceeded, that the cost of that failure is D, and that the system is not rebuilt after failure. k was taken as 2, and two values of $\gamma E(T)$ were considered: 10 and 100.

TABLE 2. COMPARISON OF POISSON AND GAMMA PROCESSES

	GAMMA PROCESS, k = 2				POISSON PROCESS		
			E(F)/D			E(F)/D	
t_o	$E(\tau \mid T \geq t_o)$	$E(\tau_1 \mid T \geq t_o)$	$\gamma E(T)=10$	$\gamma E(T)=100$	$E(\tau \mid T \geq t_o) = E(\tau_1 \mid T \geq t_o)$	$\gamma E(T)=10$	$\gamma E(T)=100$
0	1.0	0.75	0.0278	0.0004			
0.1	0.92	0.73	0.0511	0.0036			
0.2	0.86	0.71	0.0675	0.0059			
0.5	0.75	0.67	0.0973	0.0100			
1	0.67	0.63	0.120	0.0132	1.0	0.0909	0.0099
2	0.60	0.58	0.139	0.0158			
5	0.54	0.54	0.154	0.0179			
10	0.52	0.52	0.160	0.0187			
∞	0.50	0.50	0.167	0.0196			

This table shows very significant differences between the expected cost of failure for both processes. At small values of t_o, E(F)/D for the Poisson process is greater than that for the gamma process, but as time goes on and no earthquakes occur, E(F)/D grows gradually for the gamma process, until the actualized risk for the latter becomes nearly twice that for the Poisson process. Clearly, the problem is significant when making engineering decisions.

Improved analytical models of seismicity should also cover those observed cases where the sources of large shocks move systematically along faults. This can be done by means of Markov process models, but extensive seismological and geophysical studies are required before the range of applicability of those models can be established and their parameters estimated.

5. ELEMENTS IN THE ESTIMATION OF LOCAL SEISMICITY

Only exceptionally can frequency-magnitude relations for small volumes of the earth's crust and statistical correlation functions of the process of earthquake generation be derived exclusively from statistical analysis of recorded shocks. In most cases this information is too limited for that purpose and it often seems to contradict geological evidence. Since the latter, as well as its connection with seismicity, is beset with wide margins of uncertainty, information of a different nature has to be evaluated, its uncertainty analysed, and conclusions reached that are consistent with all pieces of information. A probabilistic criterion that accomplishes this is presented here: on the basis of geotectonic information and of conceptual models of the physical processes involved, a set of alternate assumptions can be made concerning the functions in question (frequency-magnitude, time and space correlation) and an initial probability distribution assigned to it; statistical information is used to judge about the likelihood of each assumption, and a posterior probability distribution is obtained. How statistical information contributes to the posterior probabilities of the alternate assumptions depends on the extent of that information and on the degree of uncertainty implied by the

initial probabilities. Thus, if the geological evidence supports confidence in a particular assumption or range of assumptions, statistical information should not greatly modify the initial probabilities. If, on the other hand, a long and reliable statistical record is available, it may practically determine the form and parameters of the mathematical model selected to represent local seismicity.

Analysis of geological information must consider local details as well as general structure and evolution. In some areas it is clear that all potential earthquake sources can be identified by surface faults, and their displacements in recent geological times measured. When mean displacements per unit time can be estimated, the order of magnitude of creep and of energy liberated by shocks and hence of the frequency-magnitude law can be established (12, 13), the corresponding uncertainty evaluated, and the initial probability distribution assigned. The fact that frequency-magnitude relations are only weakly correlated with the size of recent displacements is reflected in large uncertainties (14).

Application of the criterion described in the foregoing paragraph may be unfeasible or inadequate in many practical problems, as in areas where the abundance of faults of different sizes, ages and activity, and the insufficient accuracy with which focal coordinates are determined preclude a differentiation of all sources. Regional seismicity may then be evaluated under the assumption that at least part of the seismic activity is distributed in a given volume rather than concentrated in faults of different importance. The same situation would be faced when dealing with active

zones where surface evidence of motions does not exist. Hence, consideration of the overall behaviour of complex geological structures is in general more significant than the study of local details.

To the authors's knowledge, not much work has been done in the analysis of the overall behaviour of large geological structures with respect to the energy that can be expected to be liberated per unit volume and per unit time in given portions of those structures. Important research and applications should be expected, however, since, as a result of the contribution of modern plate tectonics theory to the understanding of large scale tectonic processes, the numerical values of some of the variables correlated with energy liberation are being determined, and can be used at least to obtain orders of magnitude of expected activity along plate boundaries. Far less understood are the occurrence of shocks in apparently inactive regions of continental shields and the behaviour of complex continental blocks or regions of intense folding, but even there some progress is contemplated in the study of accumulation of stresses in the crust (15).

Knowledge of the geological structure can serve to formulate initial probability distributions of seismicity even when quantitative use of geophysical information seems beyond reach. Initial probability distribution of local seismicity parameters α, β, M_1 (Eq 5) of the relatively small volumes of the earth's crust that contribute significantly to the seismic risk at a site can be assigned by comparison with the average seismicity observed in wider areas of similar tectonic characteristics or where the extent and completeness of

statistical information warrant reliable estimates of frequency-magnitude curves (1). In this manner we can, for instance, use the information about the average distribution of the depths of earthquakes of different magnitudes throughout a seismic province in order to estimate the corresponding distribution in an area of that province where activity has been low during the observation interval even though there might be no apparent geophysical reason for the difference. Likewise, the expected value and the coefficient of variation of $\lambda(M)$ in a given area of moderate or low seismicity (like a continental shield) can be obtained from the statistics of the motions originated at all the supposedly stable or aseismic regions in the world (16).

Fig. 1 illustrates the kind of concepts that one has to consider when trying to use all available information for the quantitative probabilistic analysis of seismic risk. The southern coast of Mexico is one of the regions of highest activity in the world. Large shallow shocks are produced by the interaction of the continental mass and the ocean bottom's plate (Cocos plate) that underthrusts it. Seismological data shows significant gaps of activity along the coast during the present century and not much is known about previous history. At points along those gaps seismic risk estimates based on observed intensities would be quite low. No significant difference is evident in the geological structure of these regions with respect to the rest of the coast, with the exception of some faults transverse to the coast, that divide the continental formation into several blocks. An analysis of the locations of previous large earthquakes along

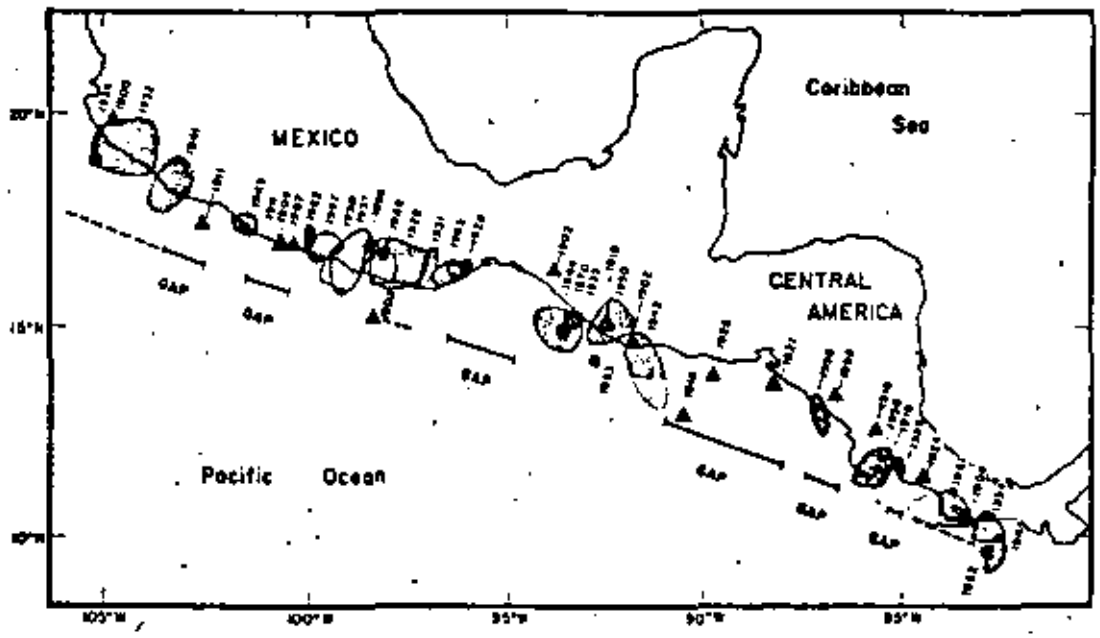

Fig. 1 Gaps of seismic activity (after Kelleher et al., Ref.20)

the coast has led Kelleher et al. (20) to conclude that those gaps are with high probability the locations of large magnitude shocks in the near future. The probabilistic evaluation of all these pices of information can be done as described in the next section.

6. SIGNIFICANCE OF STATISTICAL INFORMATION

In the proposed formulation, statistical data serve to ascertain the probable validity of each of the alternative models of local seismicity that can be postulated on the grounds of geological evidence. Any criterion that intends to weight information of different nature and different degrees of uncertainty should permit obtaining probabilistic conclusions consistent with the degree of confidence attached to each source of information. This is accomplished through use of the concepts of bayesian statistical analysis, as described in the sequel.

Let H_i, $i = 1, \ldots, n$, be a comprehensive set of mutually exclusive assumptions concerning a given, imperfectly known phenomenon and let A be the observed outcome of such a phenomenon. Suppose also that before observing outcome A we assign an initial probability $P(H_i)$ to each hypothesis. If $P(A \mid H_i)$ is the probability of A in case hypothesis H_i is true, then Bayes' theorem states the following (17):

$$P(H_i \mid A) = P(H_i) \frac{P(A \mid H_i)}{\sum_j P(H_j)\ P(A \mid H_j)} \qquad (13)$$

The first member in this equation is the (posterior) probability that assumption H_i is true, given the observed outcome A.

In the evaluation of seismic risk problems Bayes' theorem can be used to improve the initial estimates of $\lambda(M)$, β, M_1, and variation of $\lambda(M)$ with depth in a given area.

Consider $\lambda(M)$. If a model as given by Eq 7 is adopted, we start by assuming for each M and initial probability function for the actual, but unknown, value of $\lambda(M)$. If the possible assumptions concerning the values of $\lambda(M)$ for a given M constitute a continuous interval, the initial probabilities of the alternative hypotheses can be expressed in terms sumption is made concerning the form of this probability density function, only the initial values of $E(\lambda(M))$ and $V(\lambda(M))$ have to be assumed. It is advantageous to assign to $\nu = k/E(T)$ a gamma distribution. Then, if ρ and μ

are the parameters of this initial distribution of ν, if k is assumed to be known, and if the observed outcome is expressed as the time t_n elapsed between n + 1 consecutive events (earthquakes with magnitude $\geq M$), application of Eq 13 leads to the conclusion that the posterior probability function of ν is also gamma, now with parameters $\rho + nk$ and $\mu + t_n$. The initial and the posterior expected values of ν are respectively equal to ρ/μ, and to $(\rho + nk)/(\mu + t_n)$. When initial uncertainty about ν is small ρ and μ will be relatively large and the initial and the posterior expected values of ν will not differ greatly. On the other hand, if only statistical information were deemed significant, ρ and μ should be given very small values in the initial distribution, and $E(\nu)$, and hence $\lambda(M)$, would be practically defined by n, k and t_n. This means that the initial estimates of geologists should not only include expected or most probable values of the different parameters, but also statements about ranges of possible values and degrees of confidence attached to each.

In the case studied above only a portion of the statistical information was used. In most cases, especially if seismic activity has been low during the observation interval, significant information is provided by the durations of the intervals elapsed from the initiation of observations to the first of the n + 1 events considered and from the last of those events until the end of the observation period. Here, application of Eq 13 leads to expressions slightly more complicated than those obtained when only information about t_n is used.

The particular case when the statistical record reports no events during time t_0 comes up frequently in practical problems. Expressions applicable to

that situation are presented in the appendix. Here, consider their application to one of the seismic gaps in Fig 1. An initial set of assumptions and corresponding probabilities was adopted as described in the following. From previous studies referring to all the southern coast of Mexico, local seismicity in the gap area (measured in terms of λ for $M \geq 6.5$) was represented by a gamma process with $k = 2$. An initial probability density function for ν was adopted in such a manner that the expected value of $\lambda(6.5)$ for the region coincided with its average throughout the complete seismic province. Two values of ρ were considered: 2 and 10, which correspond to coefficients of variation of 0.71 and 0.32, respectively. The values in Table 3 were obtained for the ratio of the final to the initial expected values of ν, in terms of u_o, the ratio of the length of the observation interval to the initial expected value of the return perior, E(T).

TABLE 3. BAYESIAN ESTIMATES OF SEISMICITY IN ONE SEISMIC GAP

$u_o = t_o/E(T)$	$E''(\nu)/E'(\nu)$		$E''(\tau_1 \mid T_1 \geq t_o)$	
	$\rho = 2$	$\rho = 10$	$\rho = 2$	$\rho = 10$
0	1.0	1.0	0.75	0.75
0.1	0.95	0.99	0.76	0.74
0.5	0.75	0.94	0.91	0.71
1	0.58	0.87	1.14	0.73
5	0.20	0.54	3.11	1.05
10	0.11	0.36	5.47	1.55
20	0.06	0.22	10.50	2.48

The last two columns of the table contain the ratios of the computed values of $E(T_1)$ and E(T) when ν is taken equal respectively to its initial or to its

posterior expected value. This table shows that, for $\rho = 10$, that is, when uncertainty attached to the geologically based assumptions is low, the expected value of the time to next event keeps decreasing, in accordance with the conclusions of Ref 20. However, as time goes on and no events occur the statistical evidence leads to a reduction in the estimated risk, which shows in the increased conditional expected values of τ_1. For $\rho = 2$ the geological evidence is less significant and risk estimates decrease at a faster rate.

Bayesian estimation of other parameters would run along the same lines. The most important problems emerging in practical applications are related to the bayesian analysis of jointly distributed variables (21).

7. CONCLUDING REMARKS

A common difficulty encountered in the solution of problems by interdisciplinary groups is the need to establish a clear formulation of the objectives and a framework that permits unified analysis of all viewpoints. In seismic risk evaluation different especialists have in their minds different models of seismicity. However, the objetive must be the same: estimation of probabilities that given intensities are exceeded at a site in given time intervals. As suggested in this paper, those probabilities are estimated from stochastic process models of the generation of earthquakes in different seismic sources. Since neither present geophysical knowledge nor statistical data warrant adoption of a specific analytical model, decisions are based on the

consideration of a set of alternate hypotheses concerning that model, and a probability distribution attached to that set. Establishment of this distribution can be done by application of bayesian statistical theory to the processing of all relevant pieces of information.

The analytical models presented here serve only to illustrate the possibilities. More general models should be studied as they are suggested by considerations about the physical processes involved (21).

8. ACKNOWLEDGEMENT

The author wishes to recognize the valuable comments of E. Rosenblueth and R. G. Sexsmith.

9. REFERENCES

1. L. Esteva, Seismicity prediction: a bayesian approach, *Procs., 4th World Conference on Earthquake Engineering*, Santiago (1969)

2. J. L. Trigos and L. Esteva, Riesgo sísmico en Las Truchas (México), *Institute of Engineering*, National University of México (1973)

3. J. L. Trigos and L. Esteva, Riesgo sísmico en Managua, Nicaragua, *Ministry of Public Works*, México (1973)

4. J. L. Trigos and L. Esteva, Riesgo sísmico en El Sumidero (México), *Institute of Engineering*, National University of Mexico (1973)

5. N. N. Ambraseys, Dynamics and response of foundation materials in epicentral regions of strong earthquakes, *Procs., 5th World Conference on Earthquake Engineering*, Rome (1973)

6. D. E. Hudson, Analysis of strong motion earthquake accelerograms, Vol. III, Response spectra, part A, EERL, *Caltech*, Pasadena, Calif. (1972)

7. D. E. Hudson, Ed., Strong motion instrumental data on the San Fernando earthquake of February 9, 1971, EERL, *Caltech*, Pasadena, Calif. (1971)

8. D. E. Hudson, Strong motion earthquake accelerograms, digitized and plotted data, Vol. III, corrected accelerograms and integrated ground velocity and displacement curves, Part A, EERL, *Caltech*, Pasadena, Calif. (1971)

9. L. Esteva and R. Villaverde, Seismic risk, design spectra and structural reliability, *Procs., 5th World Conference on Earthquake Engineering*, Rome (1973)

10. J. H. Dietrich, A deterministic near-field source model, *Procs., 5th World Conference on Earthquake Engineering*, Rome (1973)

11. M. D. Trifunac, Characterization of response spectra by parameters governing the gross nature of the earthquake source mechanisms, *Procs., 5th World Conference on Earthquake Engineering*, Rome (1973)

12. R. E. Wallace, Earthquake recurrence intervals on the San Andreas Fault, *Bull. Geological Society of America*, Vol.81 (oct 1970)

13. G. F. Davies and J. N. Brune, Regional and global fault slip rates from seismicity, *Nature Physical Science*, Vol. 229, No 4 (jan 1971)

14. B. A. Petrushevsky, The geological fundamentals of seismic zoning, *Scientific Translation Service*, order 5032, Ann Arbor, Mich (1966)

15. E. Artyushkov (Institute of Physics of the Earth, USSR Academy of Sciences), personal communication.

16. L. Esteva, Bases para la formulación de decisiones de diseño sísmico, *Institute of Engineering*, National University of Mexico (1968)

17. H. Raiffa and R. Schlaifer, Applied statistical decision theory, *MIT Press*, Cambridge, Mass (1969)

18. E. Parzen, Stochastic processes, *Holden Day*, San Francisco (1962)

19. E. Rosenblueth, Optimum design for infrequent disturbances, submitted for publication to ASCE (1974)

20. J. Kelleher, L. Sykes and J. Oliver, Possible criteria for predicting earthquake locations and their application to major plate boundaries of the Pacific and the Caribeean, *Journal of Geophysical Research*, Vol. 78, No. 14 (may 1973)

21. L. Esteva, Probabilistic models of seismicity based on seismotectonic evidence, *Institute of Engineering*, National University of Mexico (1974)

APPENDIX 1. PARTICULAR GAMMA PROBABILITY FUNCTIONS

Explicit expressions for evaluation of some of the functions introduced in the text can be obtained in closed form when k is an integer. Some of these cases are studied here. The expressions obtained are used in the examples contained in the body of the paper.

Probability density function of T_1. Substitution of Eq 7 into Eq 9 and integration by parts lead to

$$f_{T_1}(t) = \frac{1}{k} \sum_{m=1}^{k} \frac{\nu}{(m-1)!} (\nu t)^{m-1} e^{-\nu t} \qquad (A1)$$

whose expected value is

$$E(T_1) = \frac{k+1}{2k} E(T) \qquad (A2)$$

Conditional probability density functions of T *and* T_1. The denominator of the second member of Eq 10 can be obtained in closed form when k is an integer. In that case,

$$f_r(u|T \geq t_o) = \frac{\frac{k}{(k-1)!} (k(u+u_o))^{k-1}}{\sum_{m=1}^{k} \frac{1}{(m-1)!} (k u_o)^{m-1}} e^{-ku} \qquad (A3)$$

The corresponding conditional probability density function for T_1 is

$$f_{\tau_1}(u|T_1 \geq t_o) = \frac{\sum_{m=1}^{k} \frac{k}{(m-1)!} [k(u+u_o)]^{m-1}}{\sum_{m=1}^{k} \sum_{n=1}^{m} \frac{1}{(n-1)!} (k u_o)^{n-1}} e^{-ku} \qquad (A4)$$

where $\tau_1 = (T_1 - t_o)/E(T)$.

The conditional expectations of T and T_1 can be obtained from weighting of T and T_1 with respect to the probability density functions of Eqs A3 and A4:

$$E(\tau | T \geq t_o) = (A - Bu_o)/B \qquad (A5)$$

$$E(\tau_1 | T_1 \geq t_o) = (A_1 - B_1 u_o)/B \qquad (A6)$$

where

$$A = \sum_{m=1}^{k+1} \frac{1}{(m-1)!} (k u_o)^{m-1} e^{-ku_o} \qquad (A7)$$

$$B = \sum_{m=1}^{k} \frac{1}{(m-1)!} (k u_o)^{m-1} e^{-ku_o} \qquad (A8)$$

$$A_1 = \frac{1}{k} \sum_{m=1}^{k} \sum_{n=1}^{m+1} \frac{m}{k(n-1)!} (k u_o)^{n-1} e^{-ku_o} \qquad (A9)$$

$$B_1 = \frac{1}{k} \sum_{m=1}^{k} \sum_{n=1}^{m} \frac{1}{(n-1)!} (k u_o)^{n-1} e^{-ku_o} \qquad (A10)$$

APPENDIX 2. BAYESIAN ESTIMATION OF ν WHEN $T_1 \geq t_o$

Suppose that the initial probability density function of ν in a given area is gamma with parameters ρ and μ, and that no events have occurred in the area for t_o years. The probability of this outcome given ν is equal to the probability that $T_1 \geq t_o$. From integration of Eq A1 one obtains,

$$P(T_1 > t \mid \nu, k) = \frac{1}{k} \sum_{m=1}^{k} \sum_{n=1}^{m} \frac{1}{(n-1)!} (\nu t_o)^{n-1} e^{-\nu t_o} \qquad \text{(A11)}$$

Application of Eq 13 in this case can be expressed as

$$f''(\nu \mid T_1 > t_o) = \frac{f'(\nu)\ P(T_1 \geq t_o \mid \nu, k)}{\int f'(\nu)\ P(T_1 \geq t_o \mid \nu, k)\ d\nu} \qquad \text{(A12)}$$

Here, f' and f'' stand for the initial and posterior probability density functions of ν and $f'(\nu)$ adopts the form of a gamma function with parameters ρ and μ. After performing all substitutions and integrations, the following is obtained:

$$f''(\nu \mid T_1 \geq t_o) = K^{-1} \sum_{m=1}^{k} \sum_{n=1}^{m} B_n\ g_n(\nu). \qquad \text{(A13)}$$

Here,

$$K = \sum_{m=1}^{k} \sum_{n=1}^{m} B_n \qquad \text{(A14)}$$

$$B_n = \frac{(n+\rho-2)!}{(\rho-1)!\ (n-1)!} \cdot \frac{\mu^{\rho}\, t_o^{n-1}}{(t_o+\mu)^{n+\rho-2}} \qquad \text{(A15)}$$

and $g_n(\nu)$ is the gamma probability density function with parameters $t + \mu$, $n + \rho - 1$.

MAGNITUD DE UN TEMBLOR.- Es una medida de la cantidad de energía liberada por un sismo (escala de Richter)

INTENSIDAD DE UN TEMBLOR.- Es una medida subjetiva del grado de destructividad de un temblor en una localidad dada (escala de Mercalli modificada, MM) (12 grados)

FOCO, HIPOCENTRO.- ES EL PUNTO DONDE SE INICIA LA GENERACION DE ENERGIA DEL TEMBLOR (COINCIDE CON EL PUNTO DE RUPTURA INICIAL DE LA FALLA GEOLOGICA EN QUE SE GENERA)

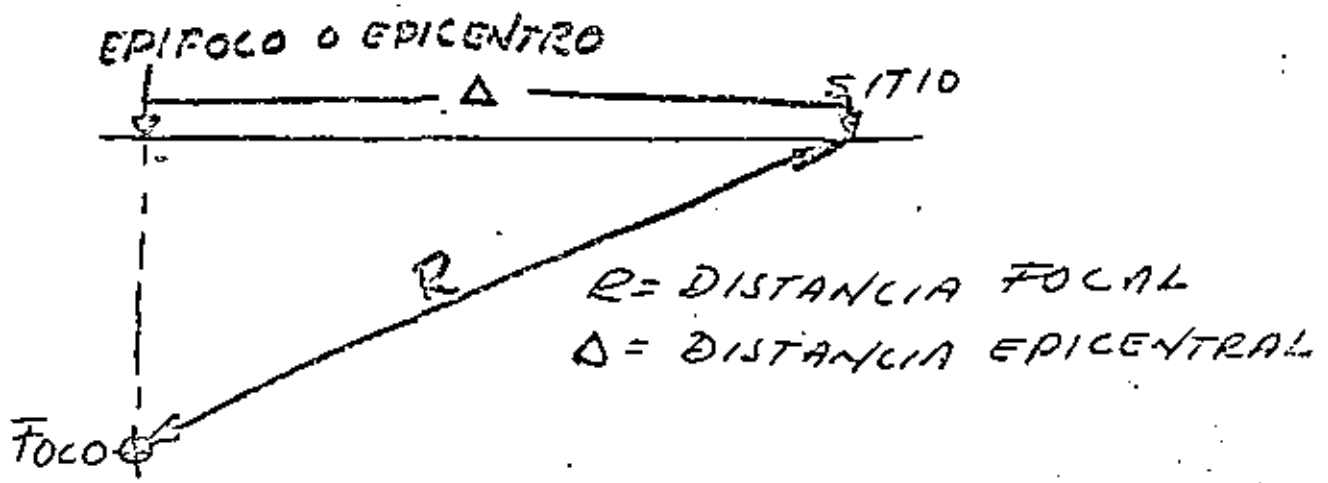

ISOSISTAS.- LINEAS QUE DELIMITAN ZONAS DE IGUAL INTENSIDAD SISMICA

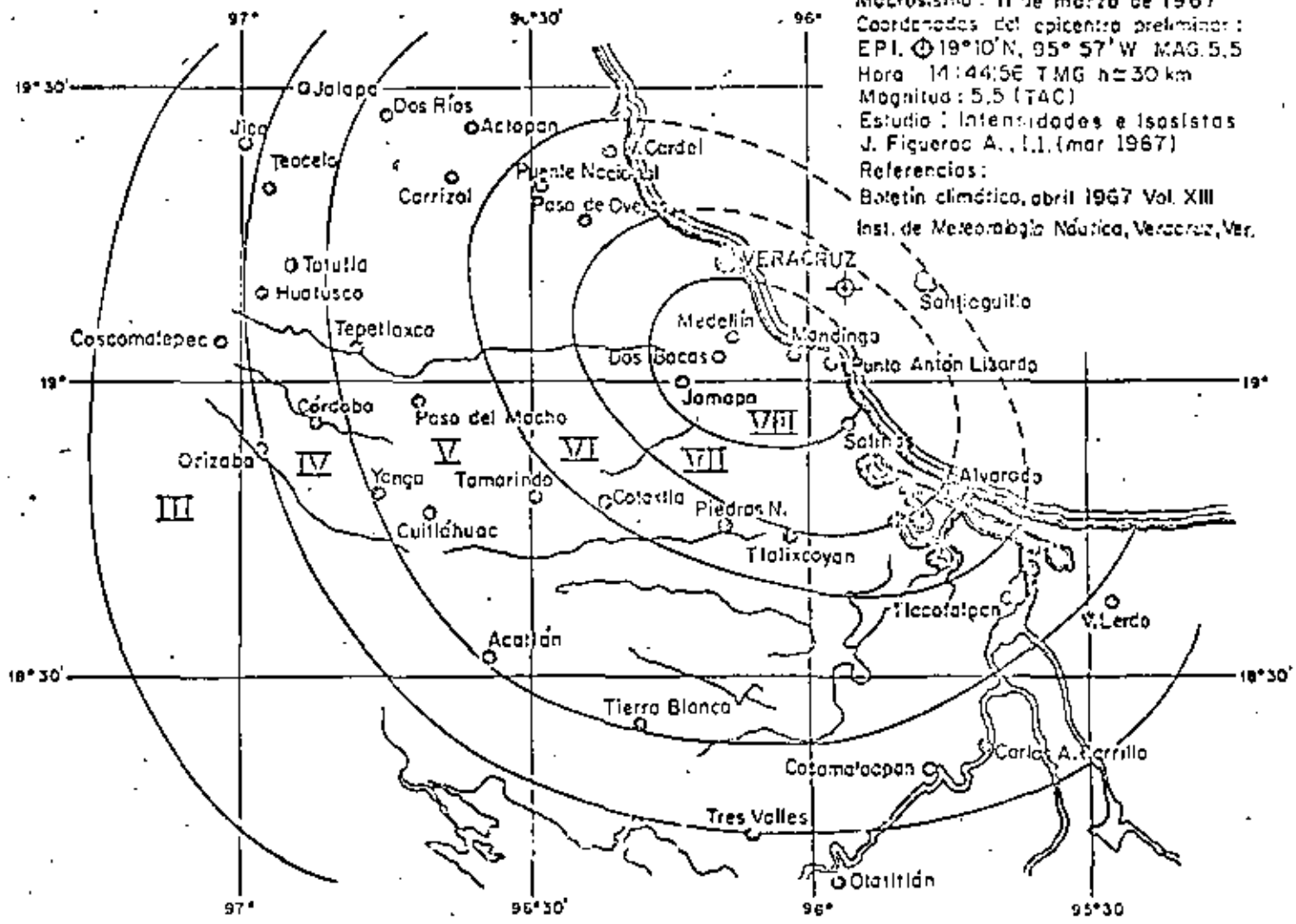
Macrosismo : 11 de marzo de 1967
Coordenadas del epicentro preliminar :
EPI. ⏻ 19°10'N, 95° 57'W MAG. 5,5
Hora 14:44:56 TMG h=30 km
Magnitud : 5,5 (TAC)
Estudio : Intensidades e Isosistas
J. Figueroa A., I.I. (mar 1967)
Referencias :
Boletín climático, abril 1967 Vol. XIII
Inst. de Meteorología Náutica, Veracruz, Ver.
97°
96°30'
96°
95°30
19°30'
19°
18°30'
Jalapa
Dos Ríos
Actopan
Jico
Teocelo
Carrizal
V. Cardel
Puente Nacional
Paso de Ovejas
VERACRUZ
Santiaguillo
Medellín
Mandinga
Punta Antón Lizardo
Totutla
Huatusco
Coscomatepec
Tepetlaxco
Dos Bocas
Jamapa
Córdoba
Paso del Macho
Orizaba
Yanga
Tamarindo
Cotaxtla
Piedras N.
Cuitláhuac
Tlalixcoyan
Alvarado
Salinas
Acatlán
Tlacotalpan
V. Lerdo
Tierra Blanca
Carlos A. Carrillo
Cosamaloapan
Tres Valles
Otatitlán
III
IV
V
VI
VII
VIII

Fig 8.

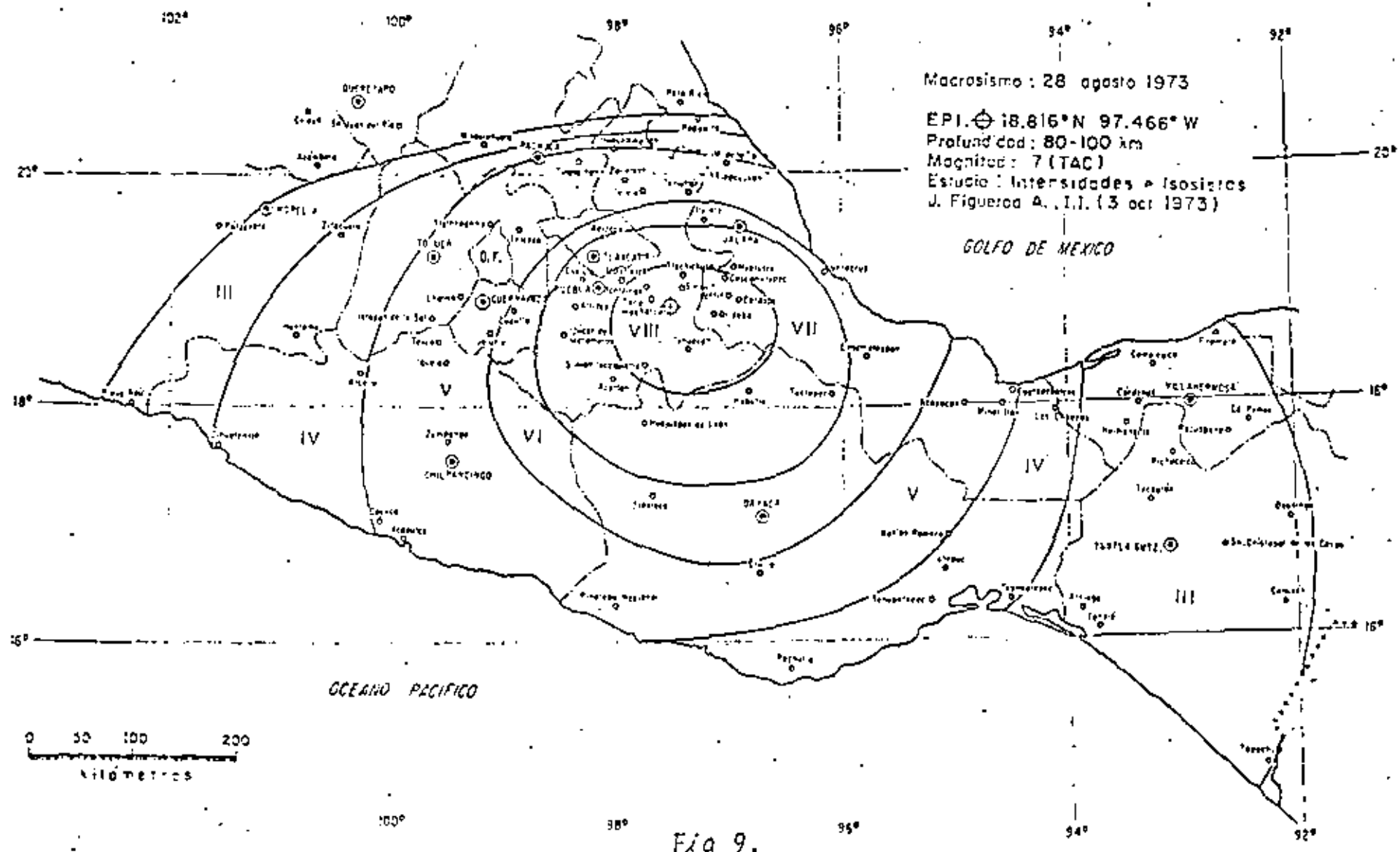
Macrosismo : 28 agosto 1973
EPI. ⊕ 18.816°N 97.466° W
Profundidad : 80-100 km
Magnitud : 7 (TAC)
Estudio : Intensidades e Isosistas
J. Figueroa A., I.I. (3 oct 1973)
GOLFO DE MEXICO
OCEANO PACIFICO
III
IV
V
VI
VII
VIII
O.F.
0 50 100 200
kilometros

Fig 9.

CORRELACIONES ENTRE

$\underline{M}$ = Magnitud (esc. Richter)
$\underline{R}$ = Distancia focal (en km)
$\underline{v_{máx}}$ = Velocidad máxima del terreno $\left(\frac{cm}{seg}\right)$
$\underline{a_{máx}}$ = Aceleración máxima del terreno $\left(\frac{cm}{seg^2}\right)$

$\underline{V_{máx}}$ = Velocidad espectral media máxima (para $\xi=0$) en $\frac{cm}{seg}$

$\underline{A_{máx}}$ = Aceleración espectral media máxima, en cm/seg^2 (para $\xi=0$)
I = Intensidad en escala de Nerelli Modificada

$$\underline{v_{máx}} = 32\, e^{M} (R+25)^{-1.7}$$

$$\underline{a_{máx}} = 5600\, e^{0.8M} (R+40)^{-2}$$

Ordenadas espectrales máximas promedio.

$$\underline{V_{máx}} = 250\, e^{M} (R+60)^{-1.7}$$

$$\underline{A_{máx}} = 69600\, e^{0.8M} (R+70)^{-2}$$

NOTA: Estas correlaciones corresponden a las componentes horizontales de los temblores

$$I = 1.45M - 5.7 \log_{10} R + 7.9 \; ; \; I = \frac{\log 14 v_{máx}}{\log 2}$$

$$I = \frac{\log 14\, v_{máx}}{\log 2}$$

$v_{máx}$ = Velocidad máxima del terreno

I = Intensidad en la escala MM

Apropiada para $I \leq 10$. Para $I > 10$ se sobrestima I.

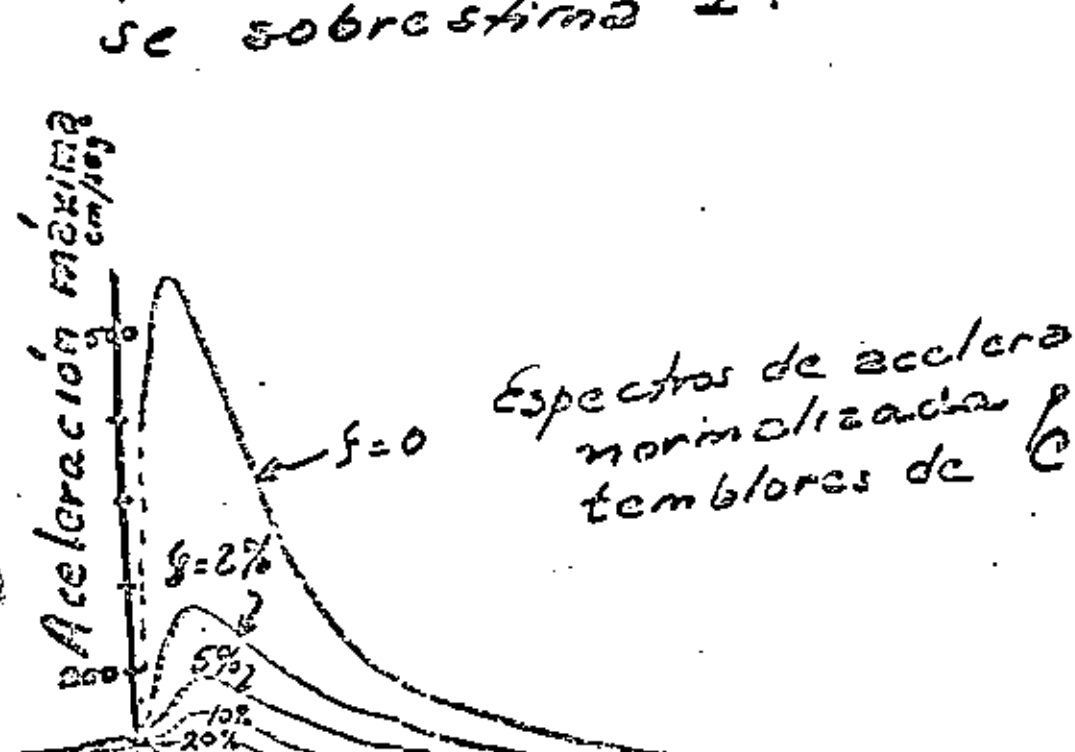

Espectros de aceleración media normalizada para los temblores de California

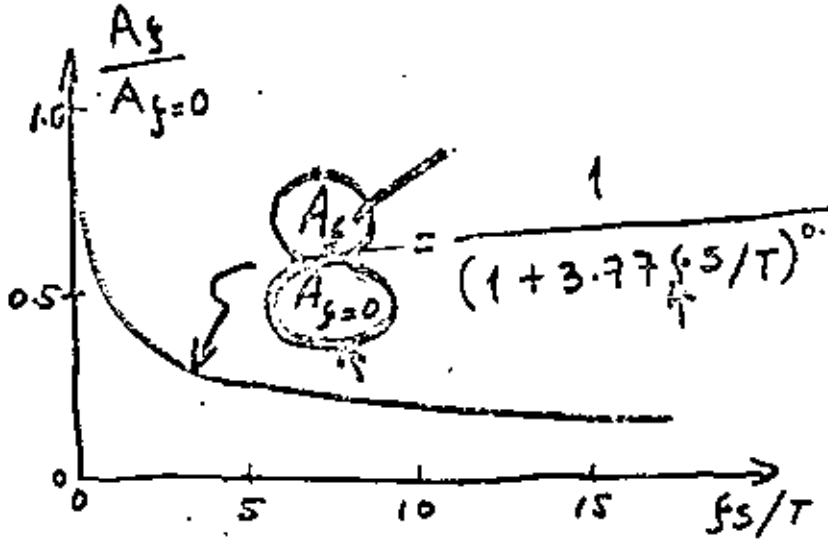

$$\frac{A_\zeta}{A_{\zeta=0}} = \frac{1}{(1+3.77(\zeta s/T)^{0.45}} \quad ; \quad 0.2 \leq T \leq 5 \text{ seg}$$

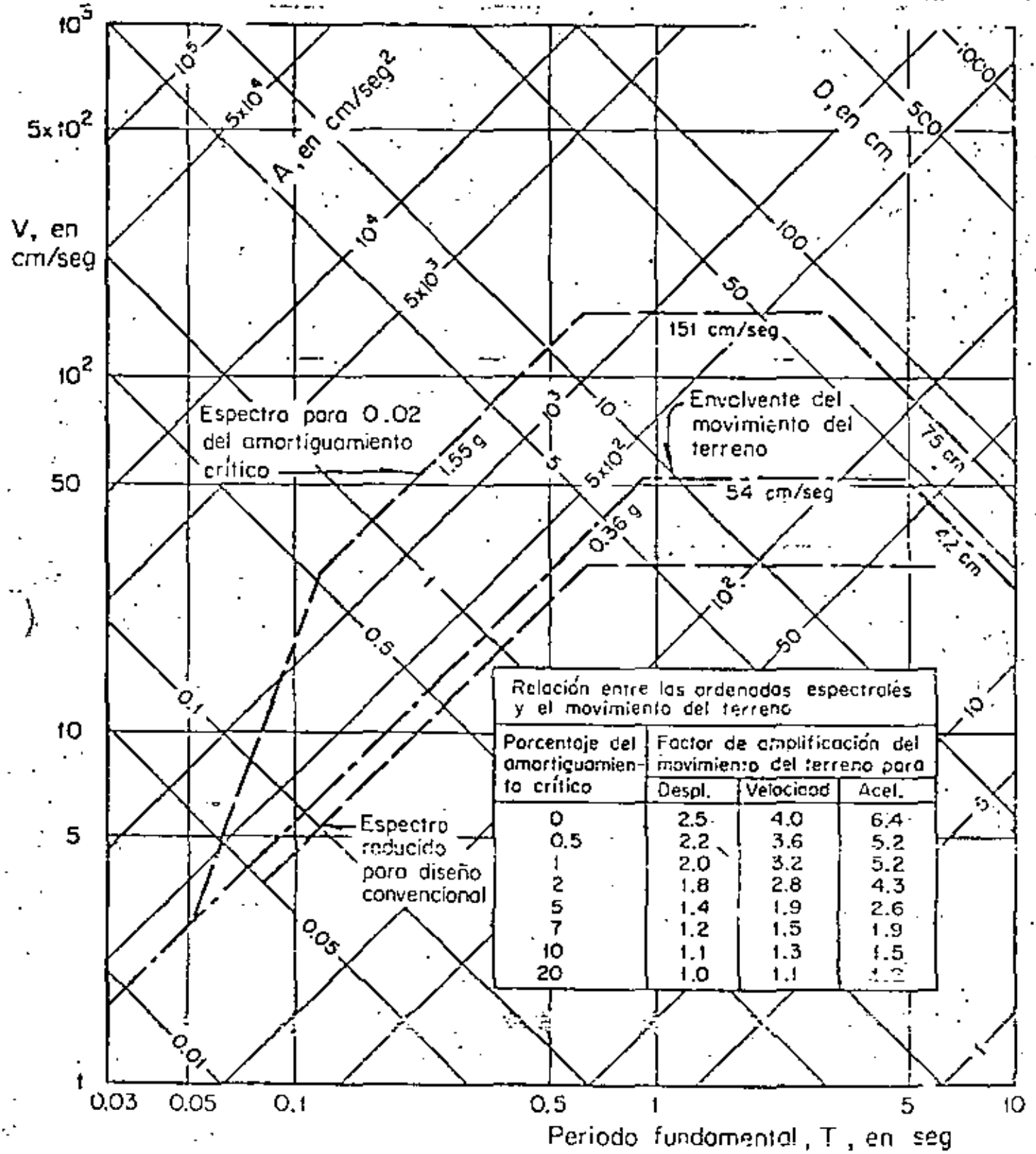

Fig 9. Construcción de espectros de diseño

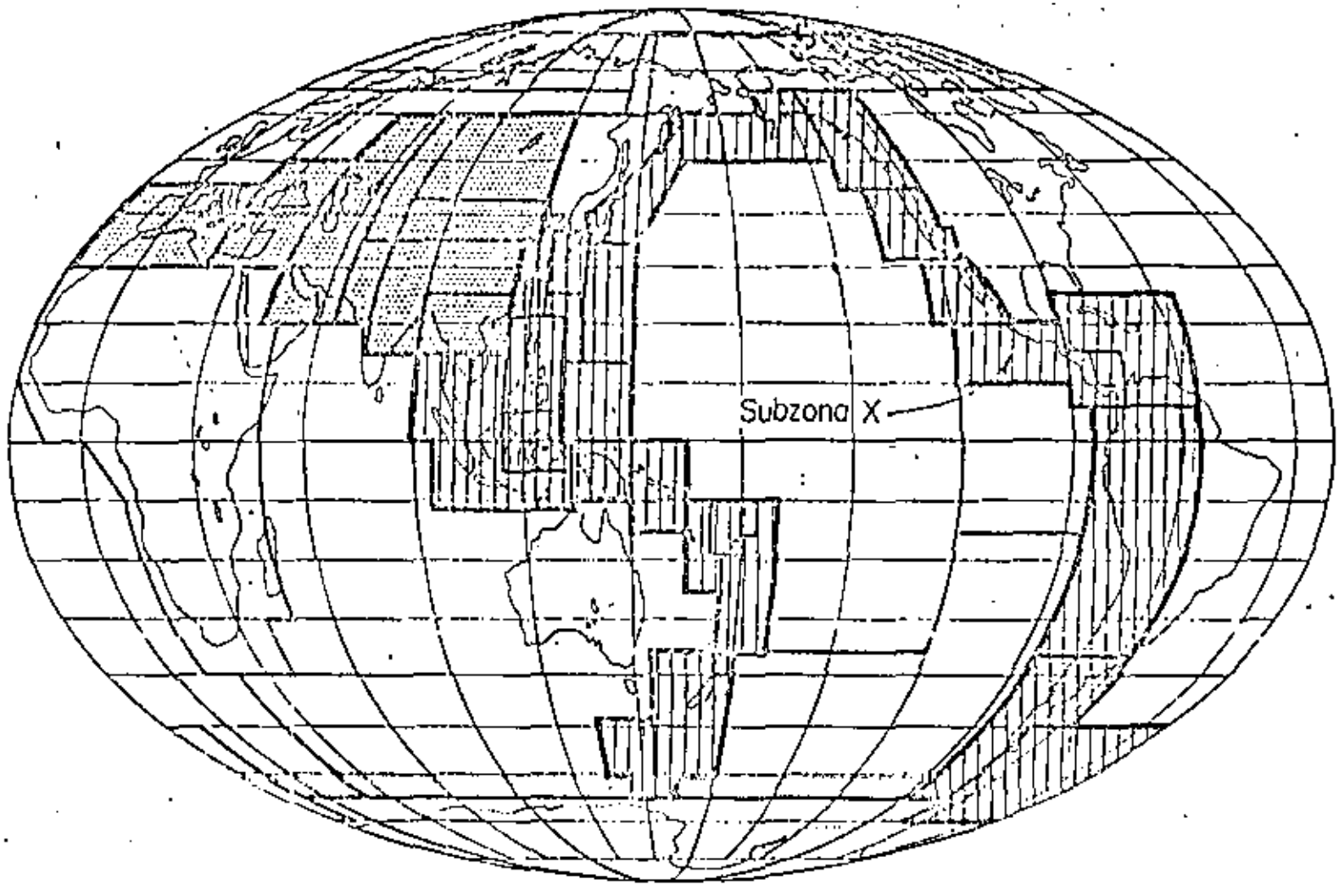

Fig. 3.3 Las tres macrozonas sísmicas del mundo

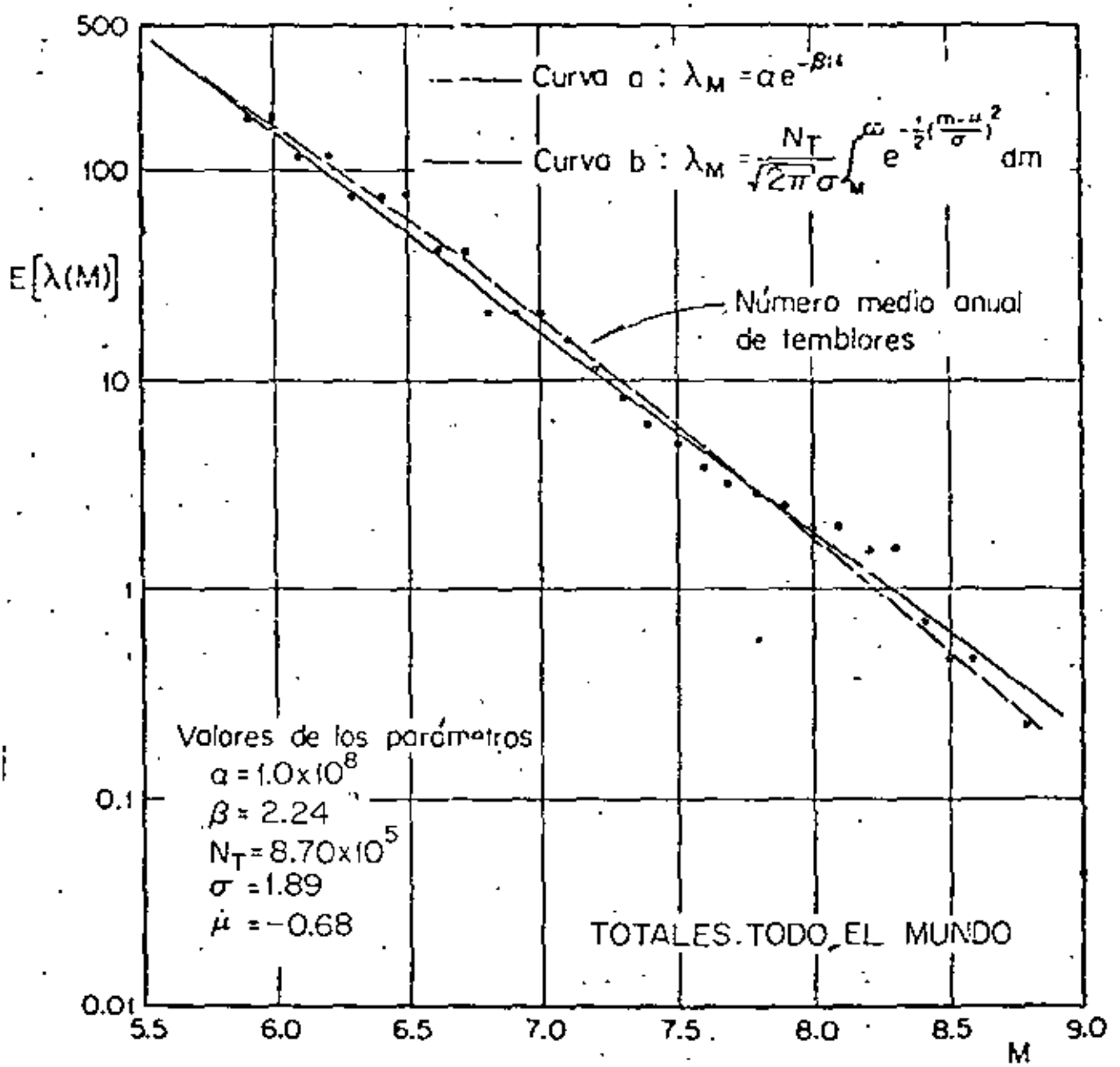

Superficiales	0.67
Intermedios	0.25
Profundos	0.08
Totales	1.00

Fig. 3.2 Números medios anuales de temblores con magnitud mayor que M

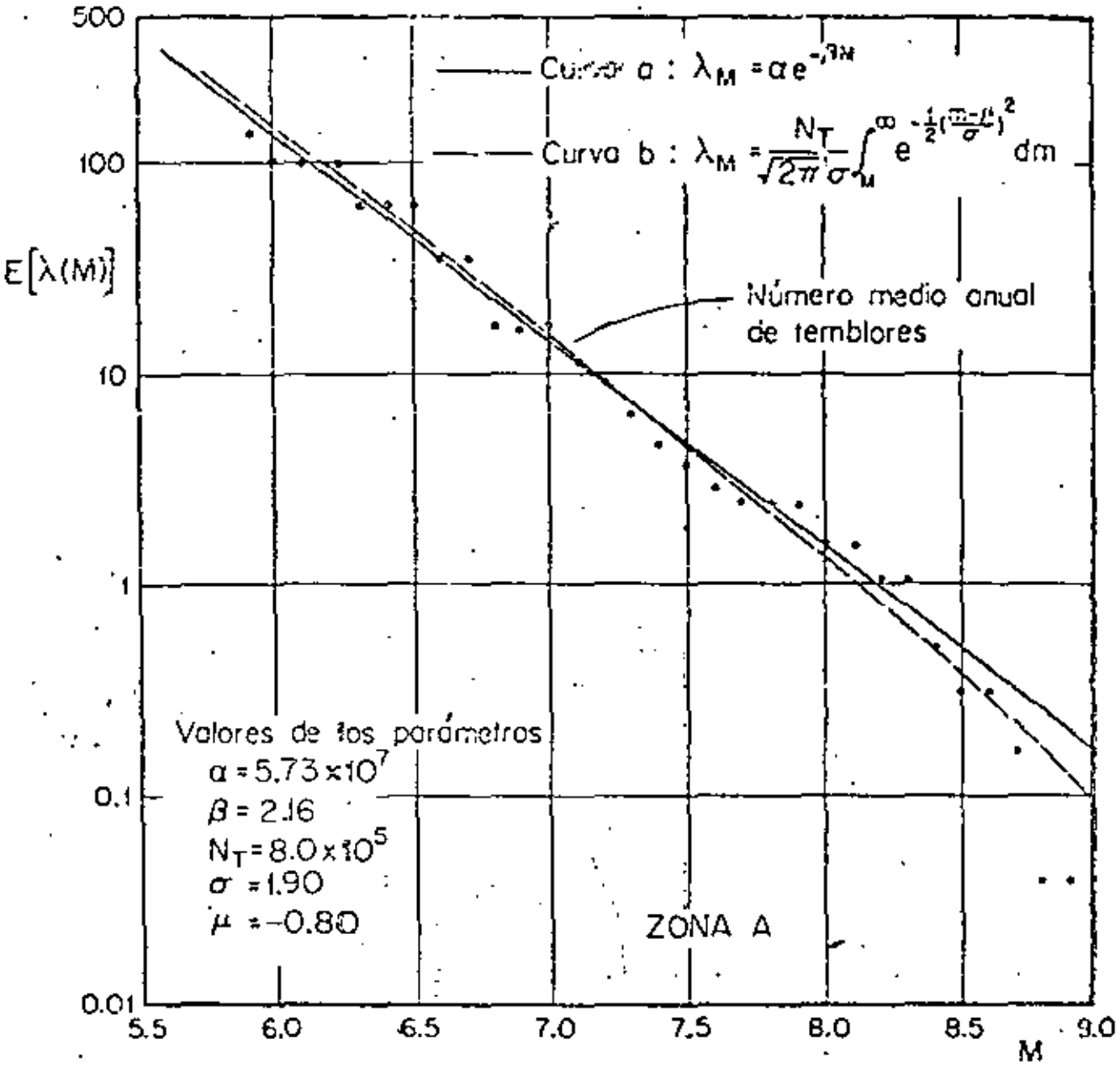

Superficioles	0.65
Intermedios	0.28
Profundos	0.07
Totales	1.00

Fig. 3.4 Números medios anuales de temblores con magnitud mayor que M
Cinturón circumpacífico

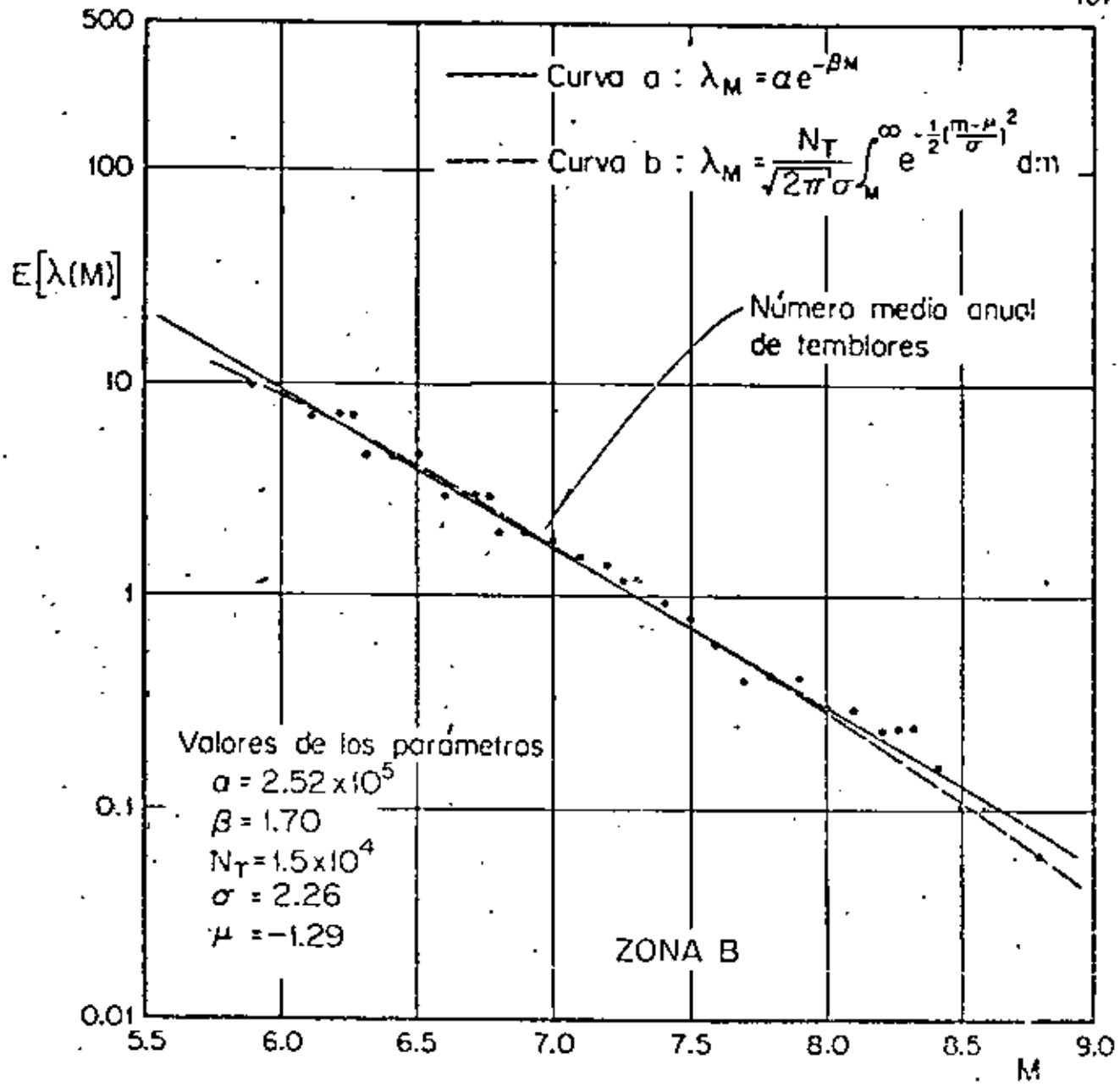

Superficiales	0.70
Intermedios	0.30
Profundos	——
Totales	1.00

Fig. 3.5 Números medios anuales de temblores con magnitud mayor que M
Cinturón alpino

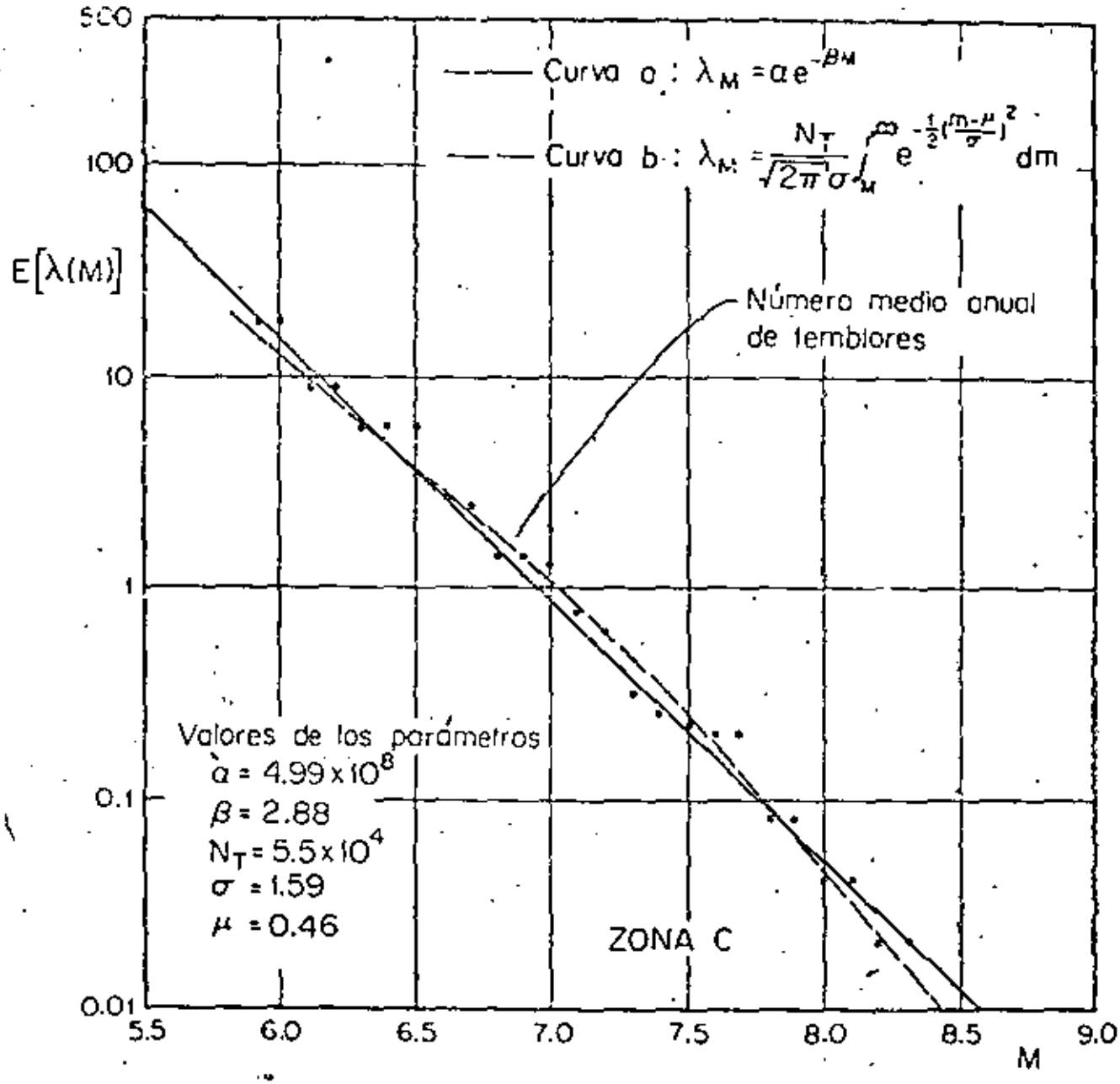

Superficiales	0.85
Intermedios	—
Profundos	0.15
Totales	1.00

Fig: 3.6 Números medios anuales de temblores con magnitud mayor que M
Zona de baja sismicidad

Directorio de Asistentes al VI Curso Internacional de Ingeniería Sísmica
SISMOLOGIA Y SISMICIDAD 1980.

1. Oscar A. Arce Villalobos
Instituto Tecnológico de Costa Rica
Director del Depto. de Ingeniería de Const.
Apdo. 159
Cartago, Costa Rica

Calle 30 # 928 Dist. 2
San José Costa Rica

2. David Ivan Barrezueta Barrezueta
Universidad Estatal de Guayaquil
Profesor
Guayaquil, Ecuador

Machala y Camilo Destrege
Bloque 4
Guayaquil, Ecuador
363241

3. Rafael Pedro Brito Ramírez
Instituto de Ingeniería
Ayudante de Investigador
UNAM
548 54 79

Huasteca 169
Col. Industrial
Z.P.14
517 18 30

4. Teresa Cecilia Codocedo Loayza
Universidad de Guadalajara
Instituto Tecnológico
Blvd. a Tlaquepaque
Guadalajara, Jal.
17 49 05

Carlos Villaseñor 751
Jardines Alcalde
Guadalajara, Jal.
23 49 81

5. Ricardo Efraín Cruz Cantú
ECA, S. A.
Pte. 146 # 911
Ind. Vallejo
México, D. F.
587 03 11

Marroquín y Rivera 20
Gpe. Insurgentes
México , D. F.
537 97 94

6. Jesús Hernán Flores Ruiz
Instituto Nacional de Investigaciones Nucleares
B. Franklin 161
México, D.F.
271 16 98

Sur 81 # 425
Col. Lorenzo Boturini
768 35 61

7. Alberto Fuentes G.
Instituto de Ingeniería
UNAM

8. Vicente González González
S A H O P
Jefe Zona Sur
Depto. Prev. Emergencias Urbanas
Av. Constituyentes 946
México D.F.
271 30 00 Ext. 411

Ret 34 Av. Genaro García 40-A-3
Jardín Balbuena
Z.P. 9
571 48 81

9. Jorge Rafael Grijalva Daza
Instituto Mexicano del Petróleo
Jefe del Departamento
Av. 100 metros No. 152
México 14, DF.
567.66.00 Ext. 2327

Edif. E -21 Depto. 32
Torres de Mixcoac
Z.P.19
593 83 76

10. Salvador Guillén Dueñas
Jalapa 291
México 7, D.F.

11. Rafael López Patiño
Escuela de Ingeniería
Universidad Autónoma de Guerrero
Chilpancingo, Gro.
2 27 41

Colegio Militar 14
Chilpancingo, Gro.

12. Leobardo López Pineda
Instituto Nacional de Investigaciones Nucleares
Bartolache 1038-4
México 12, D.F.
559 30 31

Correspondencia 153-13
México 13, D.F.
590 39 29

13. Jorge Maldonado Barrera
Instituto Nacional de Investigaciones Nucleares
Bartolache 1038 A
México 12, D.F.
559 30 31 575 08 87

Constantino 51 Depto. 201
Col. Ex-Hipódromo de P.
México 2, D.F.

14. Samuel Alberto E. Martínez Aquino
Instituto Tecnológico de Tehuacán
Sta. Ma. Coapan
Tehuacan, Pue.

Reforma Norte 306-1
Tehuacan, Pue.
2 27 50

15. José Abraham Martínez Baini
Escuela de Ingeniería Civil
Universidad Autónoma de Querétaro
Centro Universitario
Querétaro, Qro.

Guadalupe Posada 8
Col. Alcanfores
Querétaro, Qro.
2 51 89

16. José Ignacio Mejía Ordaz
Instituto Mexicano del Petróleo
Ac. Cien Metros No. 152
Mexico 14, D.F.

Fco. Martín del Campo 55
Iztapalapa
México 13, D.F.
691 55 99

17. José Enrique Rebolledo Yange
Universidad Técnica de Machala
Facultad de Ingeniería Civil
Machala, Ecuador

18. Antonio Ríos Rojas
Aseguradora Mexicana S.A.
Plaza de los Ferrocarrileros No.9
Col. San Rafael
Z.P. 4
566 52 77 Ext. 141

Horoes de Nacozari 97-201
Col.. Morelos
Z.P. 2
789 38 34

19. Virgilio Rubio Vázquez
Comisión Nacional de Seguridad Nuclear y Salvaguardías
Av. Insurgentes Sur 1806 -4 °
México 20, D.F.
534 87 88

Av. La Hda. Andador 8 # 52
Villa Coapa
México 22, D.F.
594 12 15

20. Carlos Valencia Carmona
Universidad Veracruzana

Giotto 66-201
Col., Mixcoac
Z.P. 19
598 50 67

21. Rodolfo Vázquez Zeferino
Escuela de Ingeniería
Universidad Autónoma de Guerrero
Av. Casa de la Juventud s/n
Chilpancingo, Gro.
22 7 41

Dr. Parra 9
Centro
Tlxtla, Gro.

22. Isidro Villasante Muñoz
Aseguradora Mexicana, S.A.
Plaza de los Ferrocarriles No. 9
México, D.F.
566 29 22

Abraham González 67
México 4, D.F.
566 52 77

23. Luis Zapata Baglietto
José E. Paredes 174
Pueblo Libre
Lima, Perú